APPENDICES

A Austin Community Landfill Testing Results

A.1 Austin Community Landfill Location 1

A.1.1 Downhole Seismic Testing

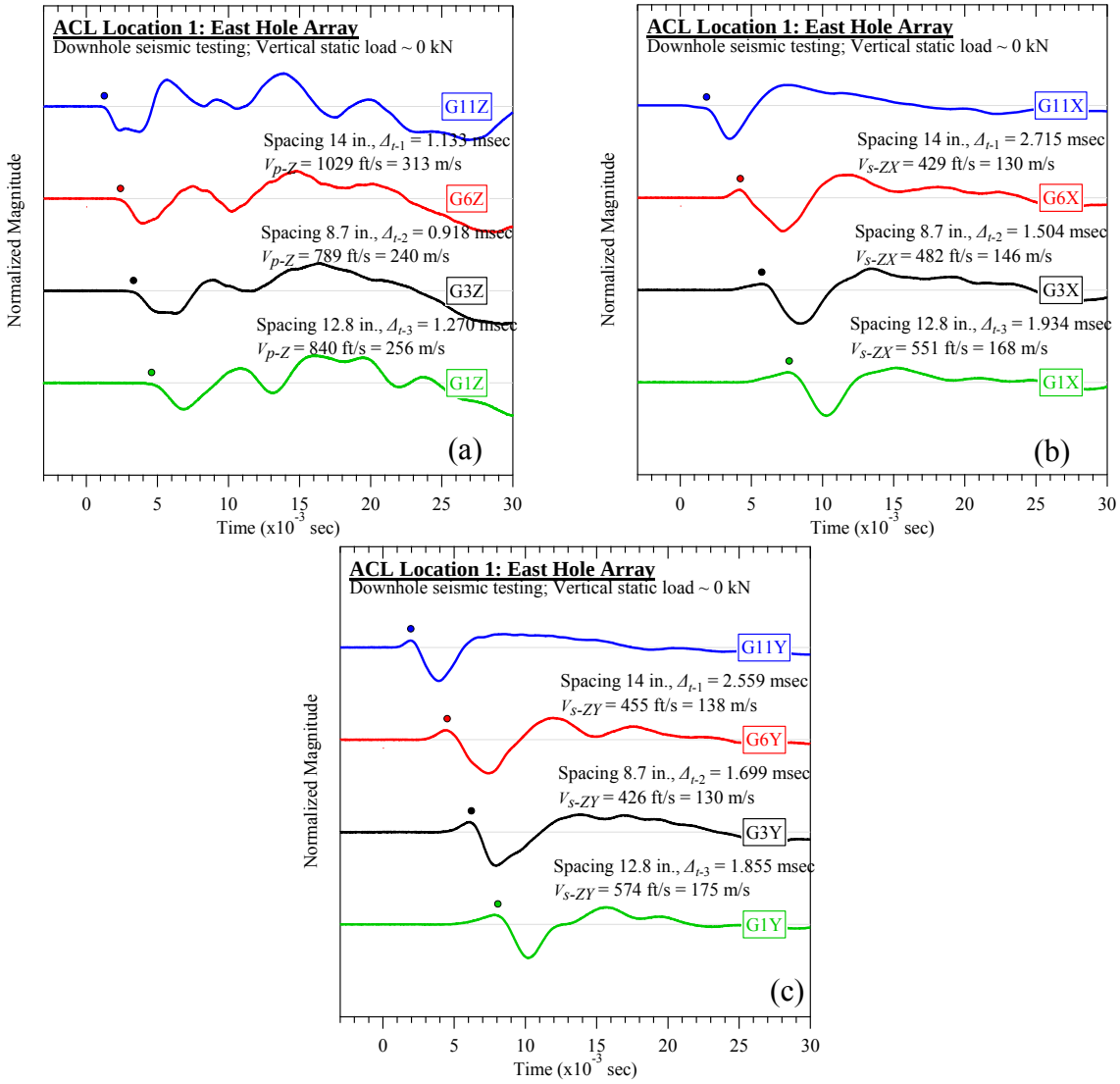

Figure A-1. Austin Community Landfill #1 (east hole): Downhole seismic testing at vertical load of 0 kN: (a) V_{p-Z}, (b) V_{s-ZX}, and (c) V_{s-ZY}.

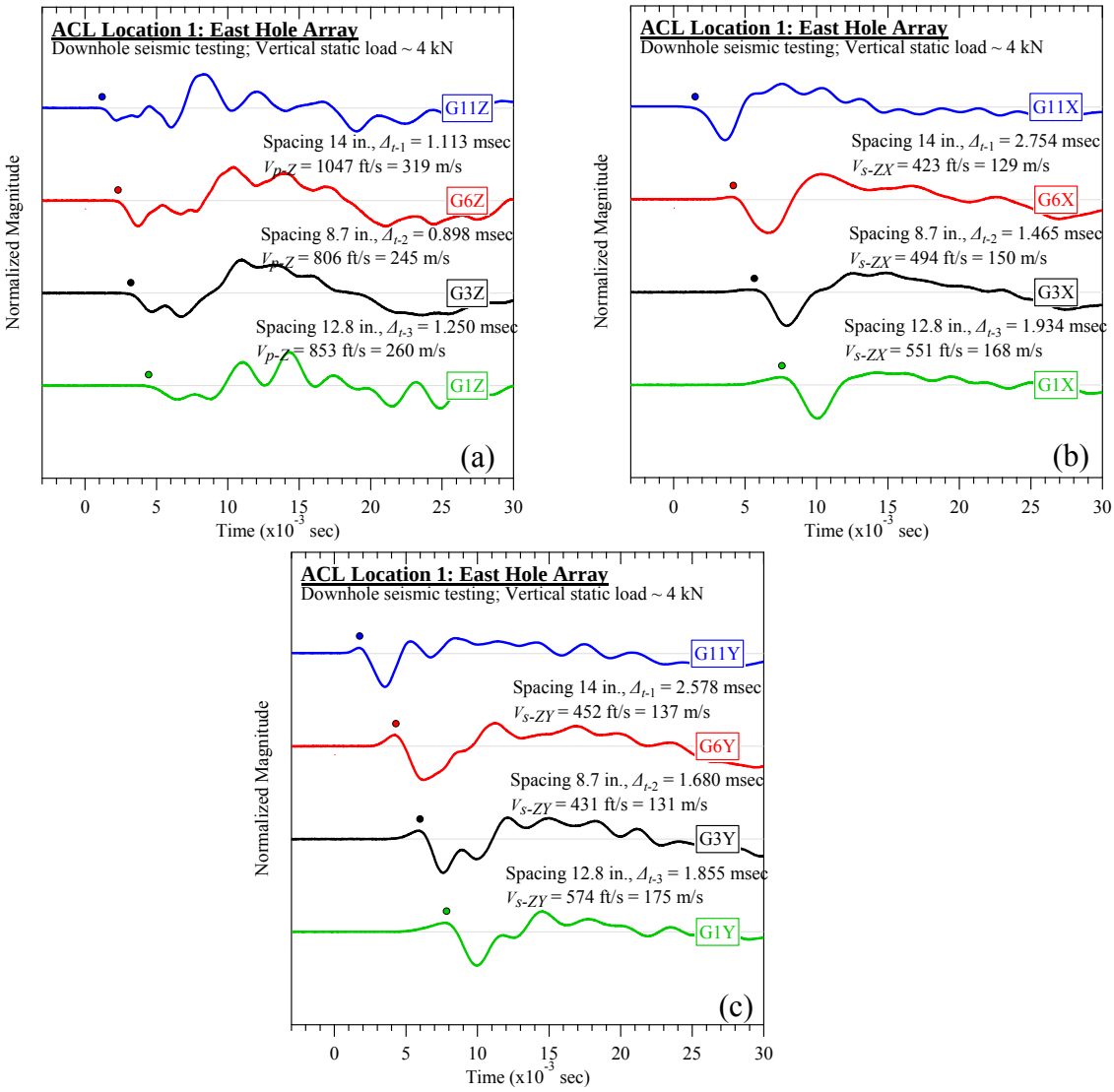

Figure A-2. Austin Community Landfill #1 (east hole): Downhole seismic testing at vertical load of 4 kN: (a) $V_{p\text{-}Z}$, (b) $V_{s\text{-}ZX}$, and (c) $V_{s\text{-}ZY}$.

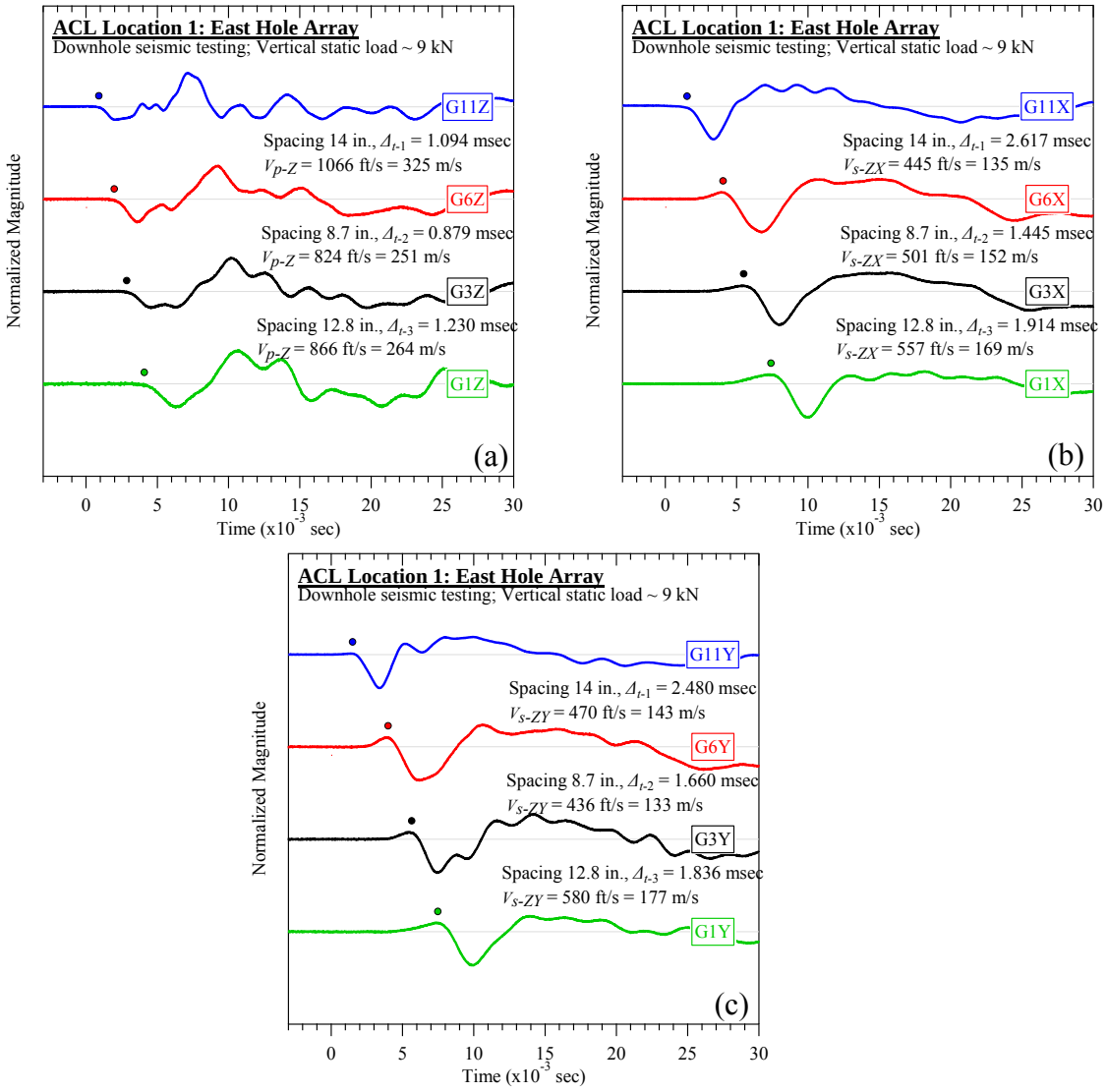

Figure A-3. Austin Community Landfill #1 (east hole): Downhole seismic testing at vertical load of 9 kN: (a) $V_{p\text{-}Z}$, (b) $V_{s\text{-}ZX}$, and (c) $V_{s\text{-}ZY}$.

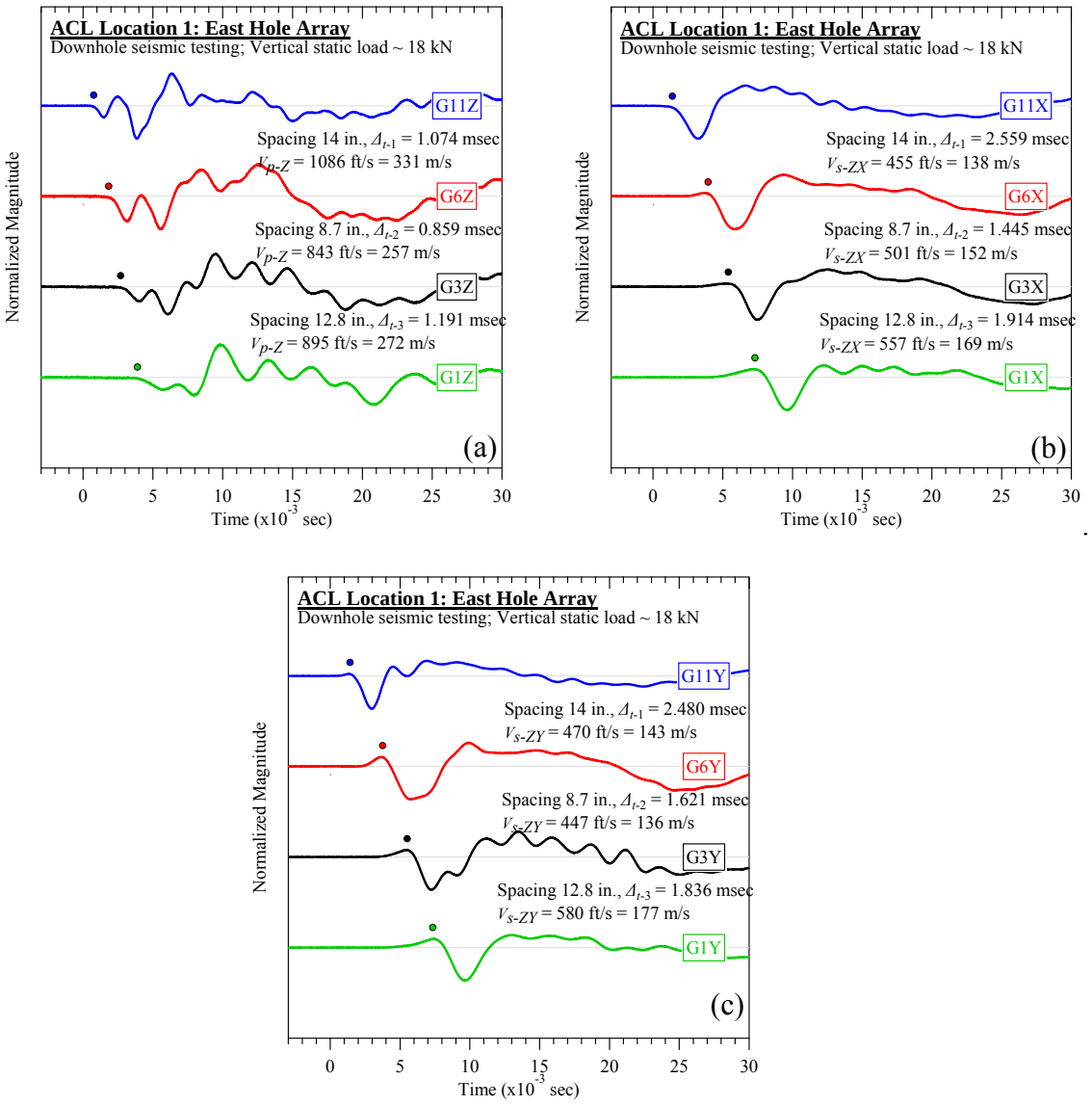

Figure A-4. Austin Community Landfill #1 (east hole): Downhole seismic testing at vertical load of 18 kN: (a) V_{p-Z}, (b) V_{s-ZX}, and (c) V_{s-ZY}.

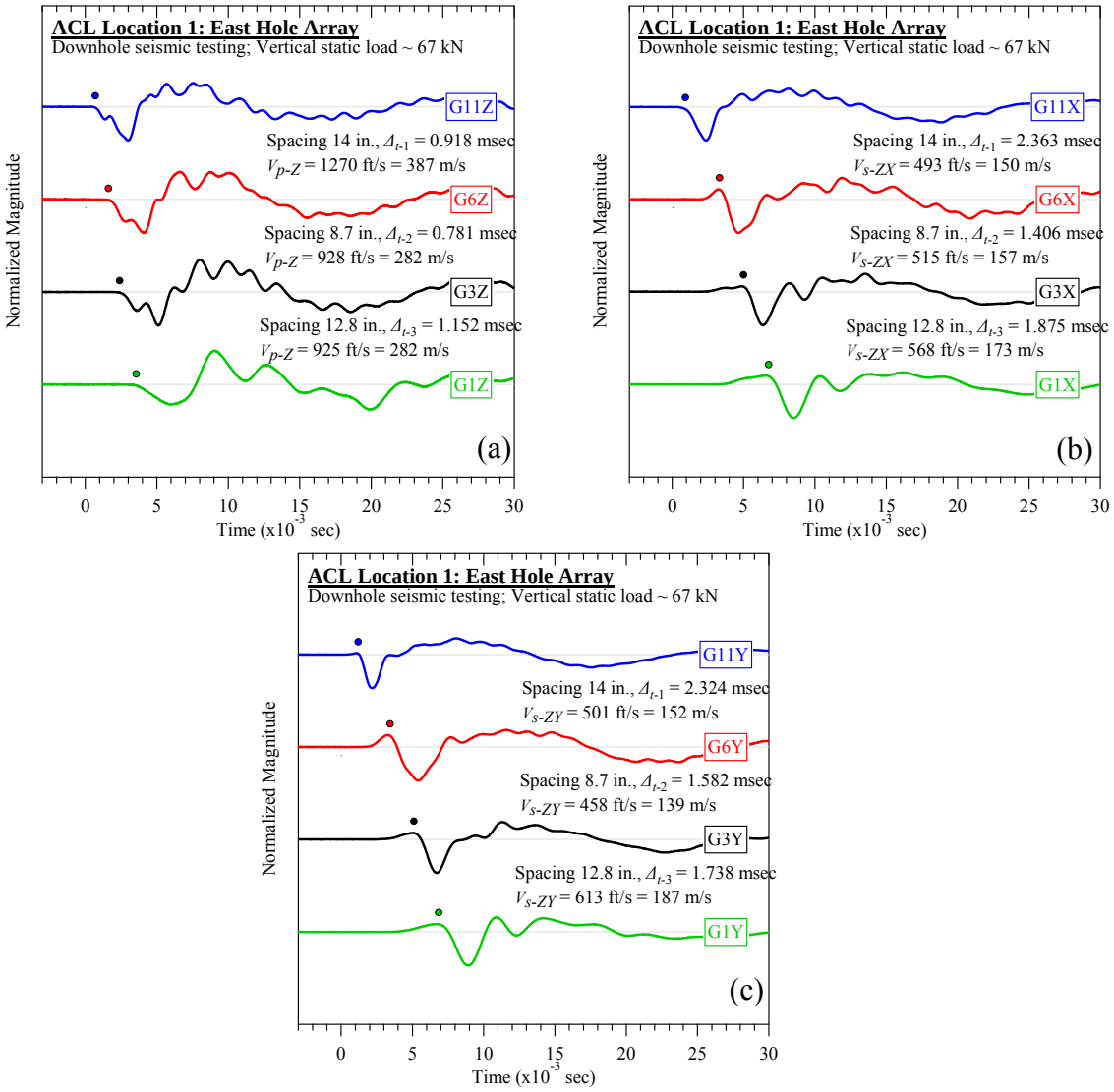

Figure A-5. Austin Community Landfill #1 (east hole): Downhole seismic testing at vertical load of 67 kN: (a) V_{p-Z}, (b) V_{s-ZX}, and (c) V_{s-ZY}.

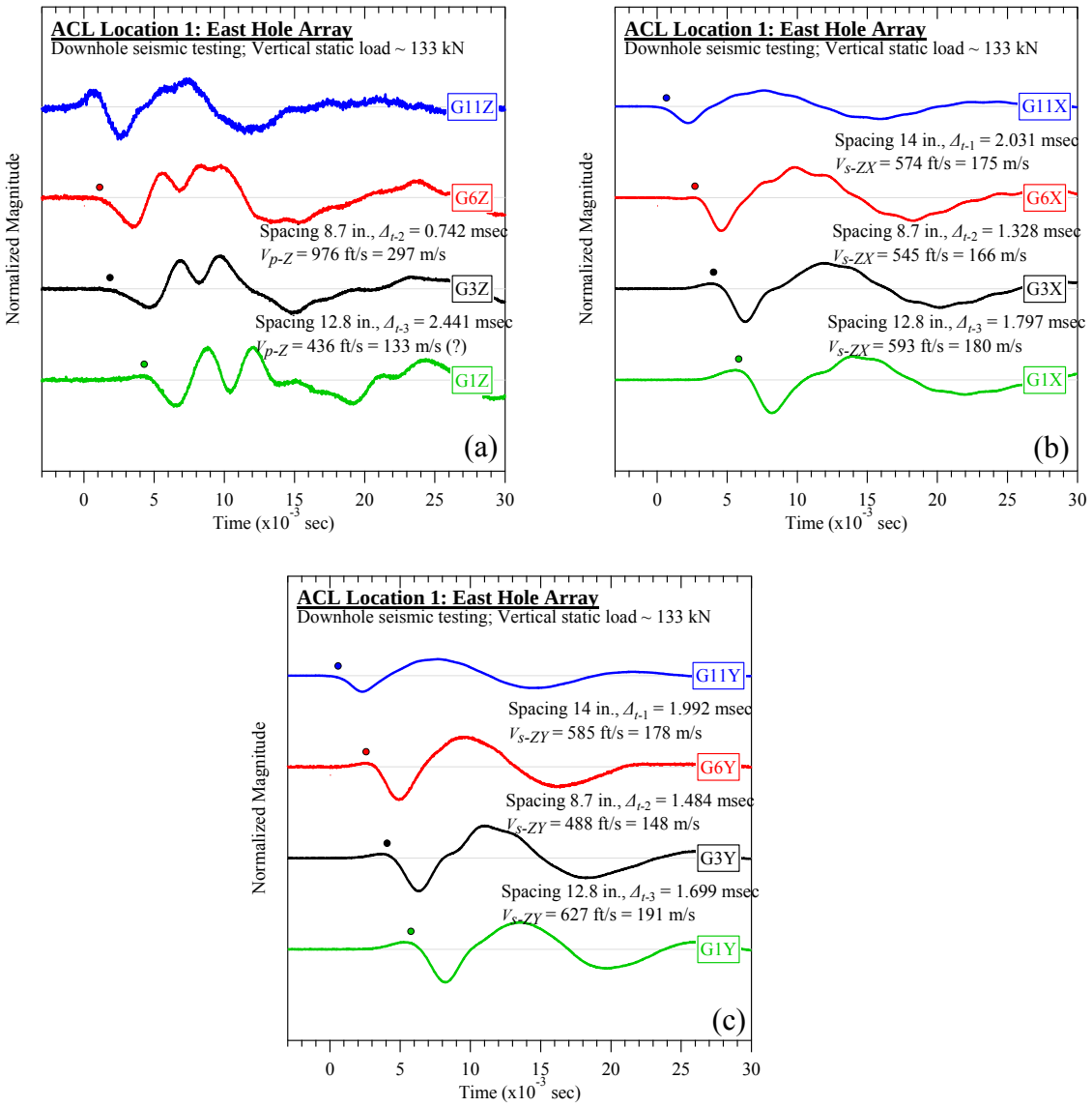

Figure A-6. Austin Community Landfill #1 (east hole): Downhole seismic testing at vertical load of 133 kN: (a) $V_{p\text{-}Z}$, (b) $V_{s\text{-}ZX}$, and (c) $V_{s\text{-}ZY}$.

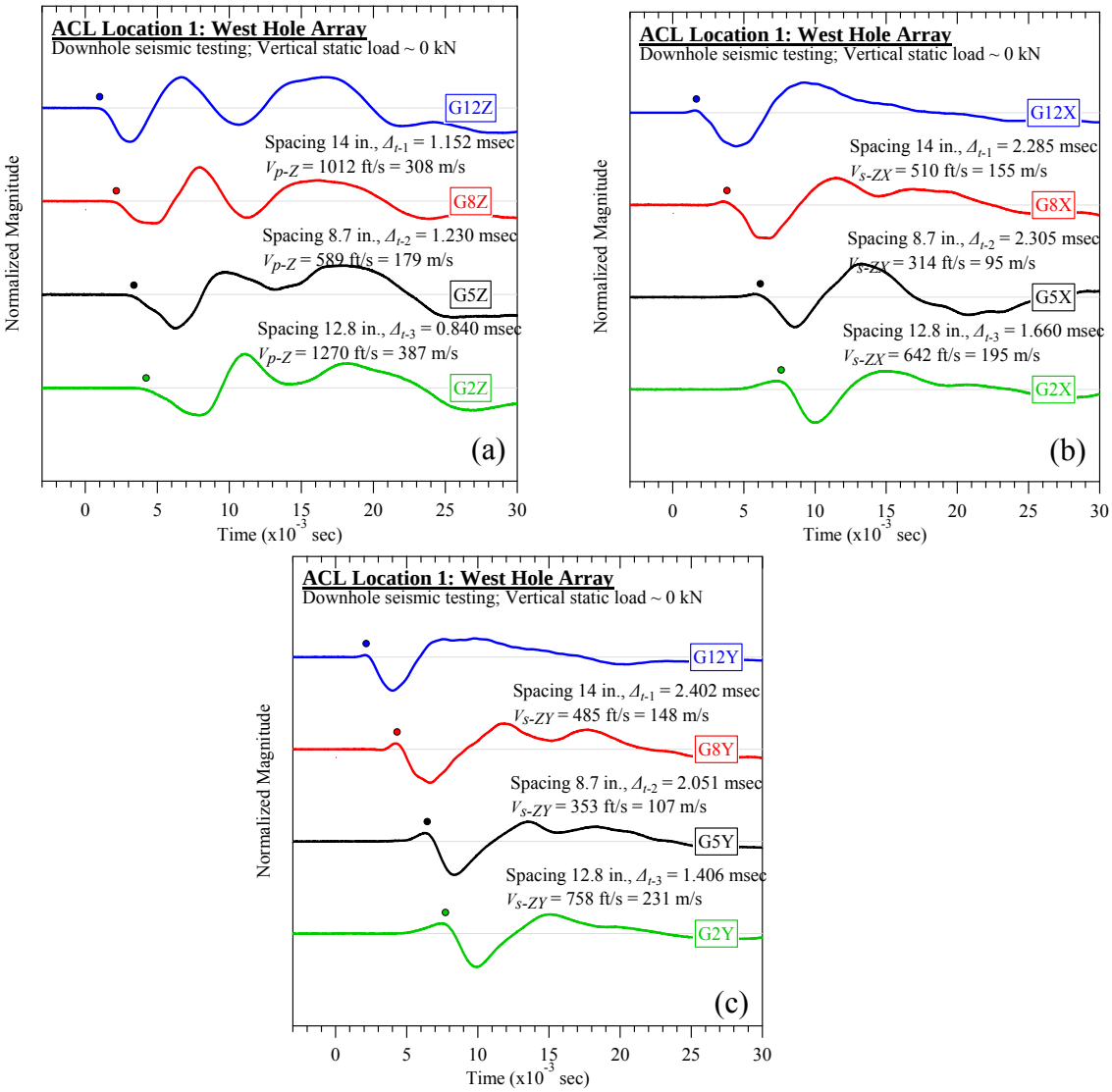

Figure A-7. Austin Community Landfill #1 (west hole): Downhole seismic testing at vertical load of 0 kN: (a) V_{p-Z}, (b) V_{s-ZX}, and (c) V_{s-ZY}.

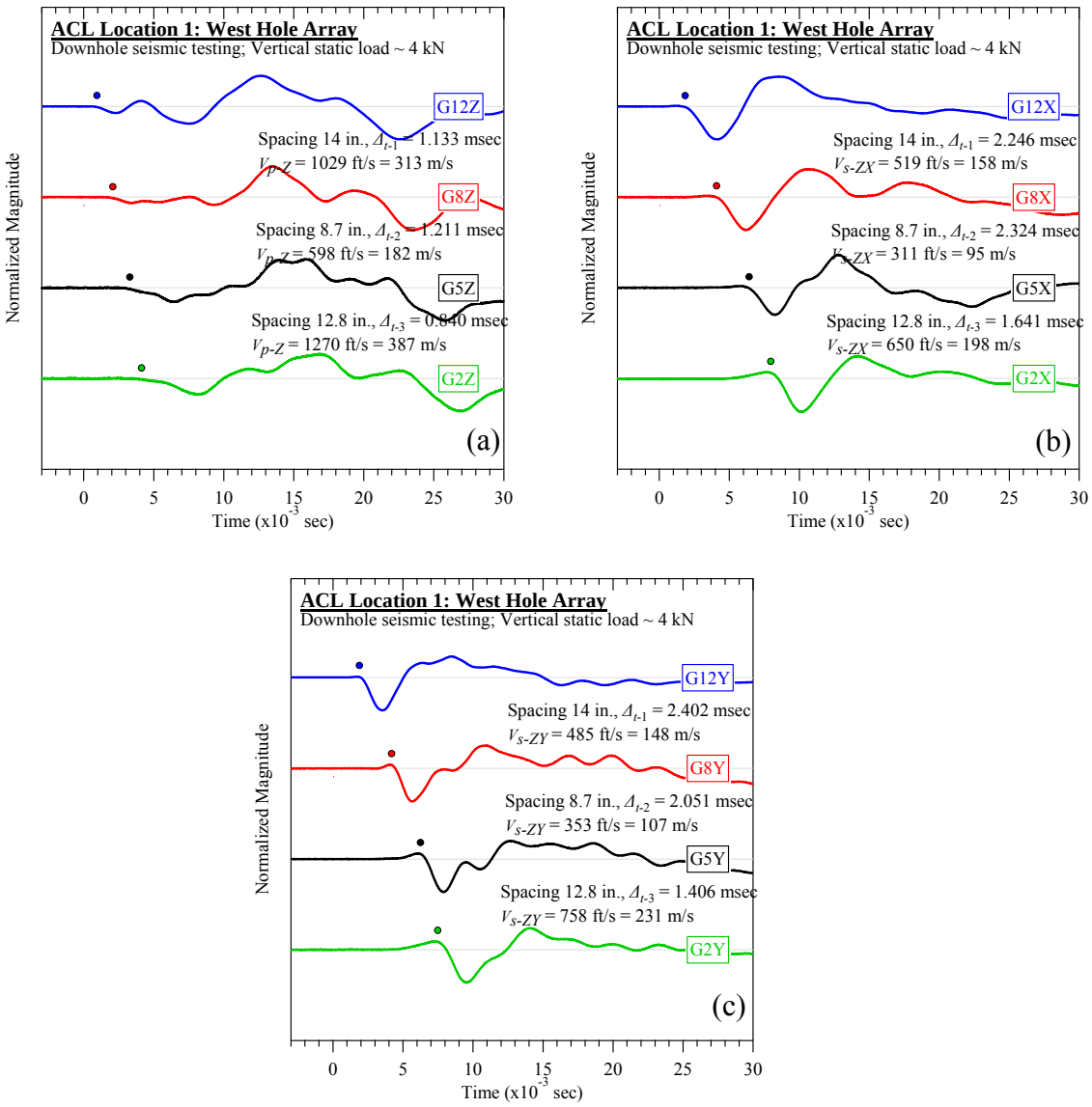

Figure A-8. Austin Community Landfill #1 (west hole): Downhole seismic testing at vertical load of 4 kN: (a) V_{p-Z}, (b) V_{s-ZX}, and (c) V_{s-ZY}.

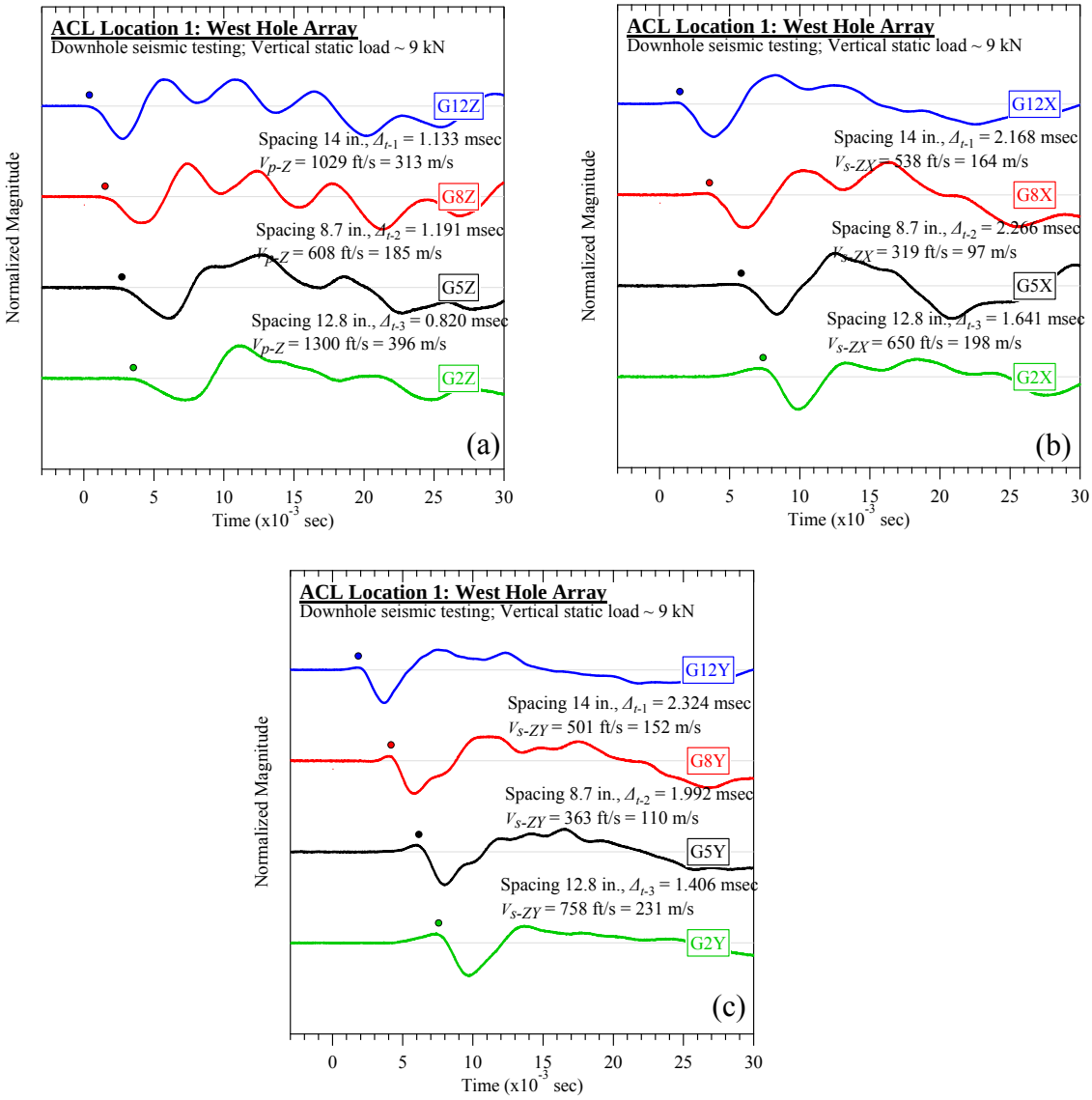

Figure A-9. Austin Community Landfill #1 (west hole): Downhole seismic testing at vertical load of 9 kN: (a) $V_{p\text{-}Z}$, (b) $V_{s\text{-}ZX}$, and (c) $V_{s\text{-}ZY}$.

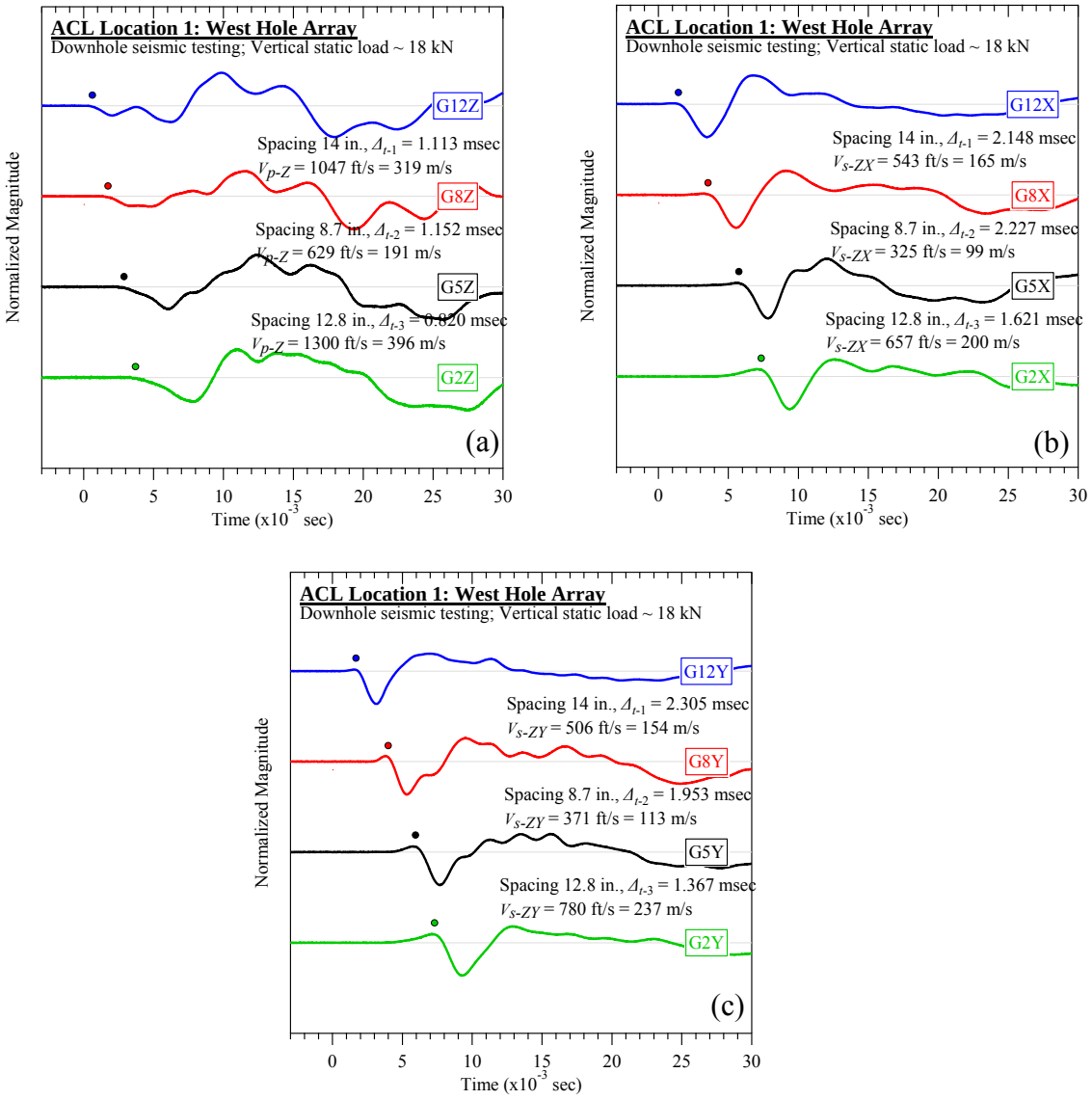

Figure A-10. Austin Community Landfill #1 (west hole): Downhole seismic testing at vertical load of 18 kN: (a) V_{p-Z}, (b) V_{s-ZX}, and (c) V_{s-ZY}.

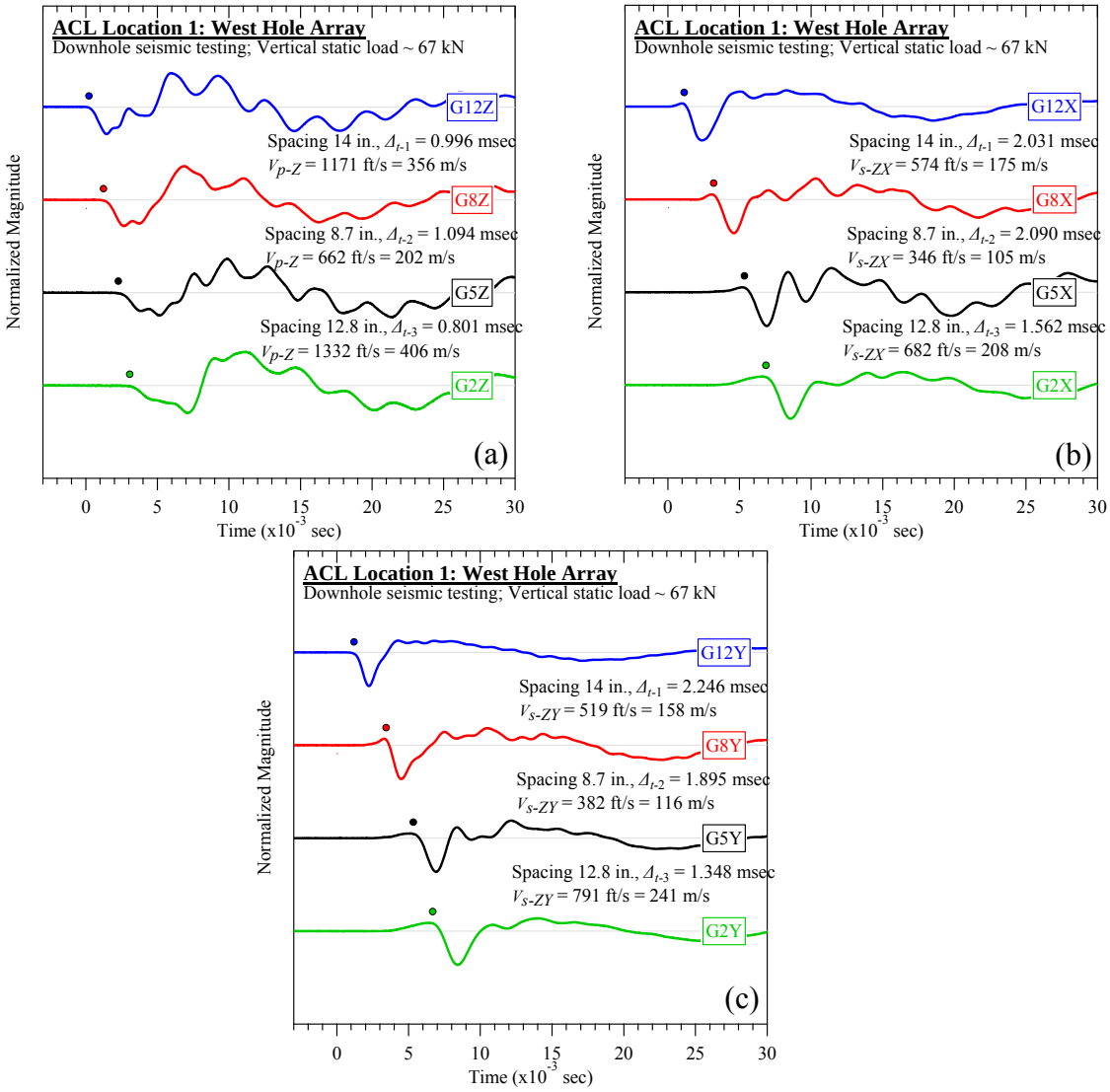

Figure A-11. Austin Community Landfill #1 (west hole): Downhole seismic testing at vertical load of 67 kN: (a) $V_{p\text{-}Z}$, (b) $V_{s\text{-}ZX}$, and (c) $V_{s\text{-}ZY}$.

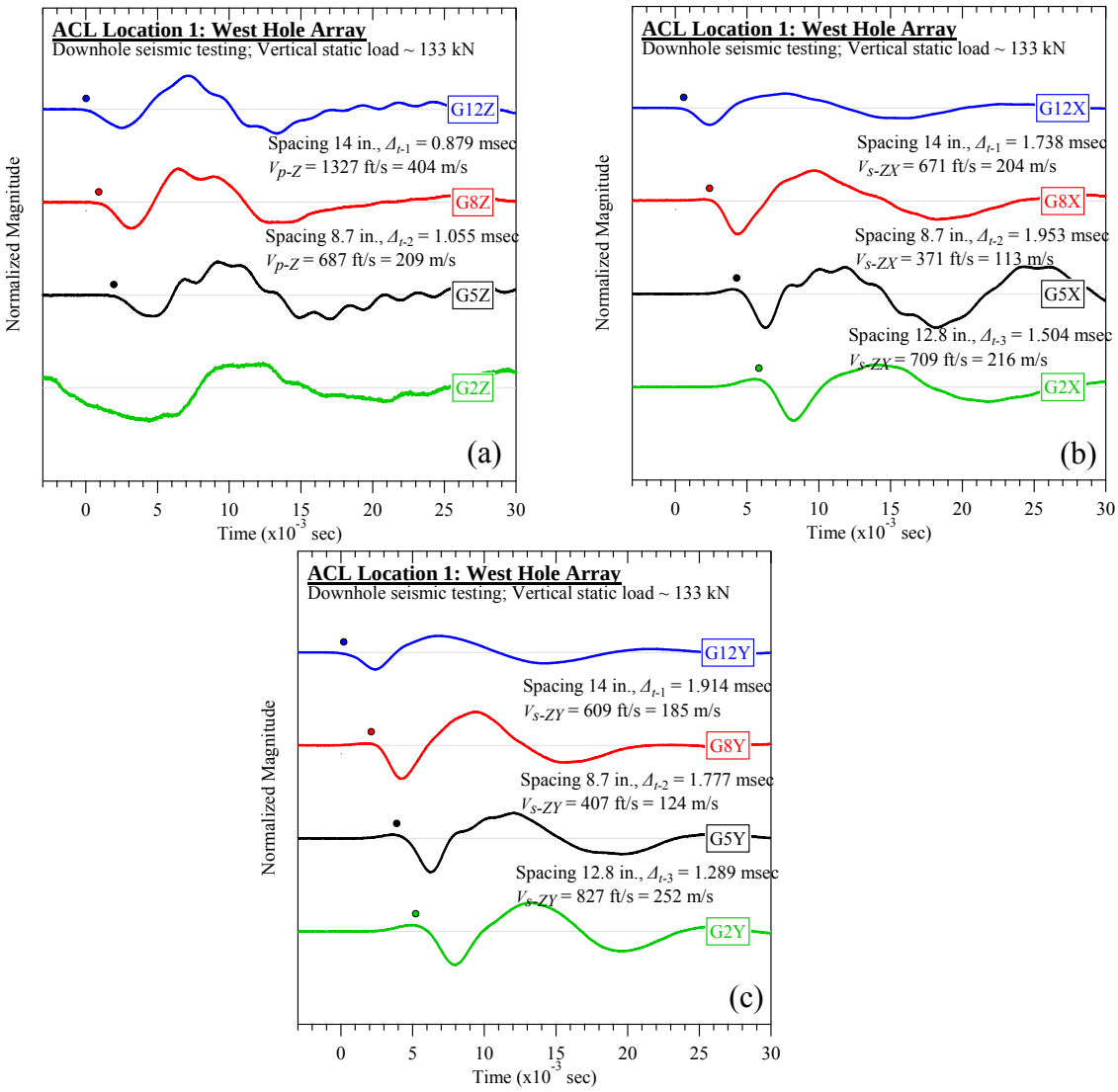

Figure A-12. Austin Community Landfill #1 (west hole): Downhole seismic testing at vertical load of 133 kN: (a) $V_{p\text{-}Z}$, (b) $V_{s\text{-}ZX}$, and (c) $V_{s\text{-}ZY}$.

A.1.2 Crosshole Seismic Testing

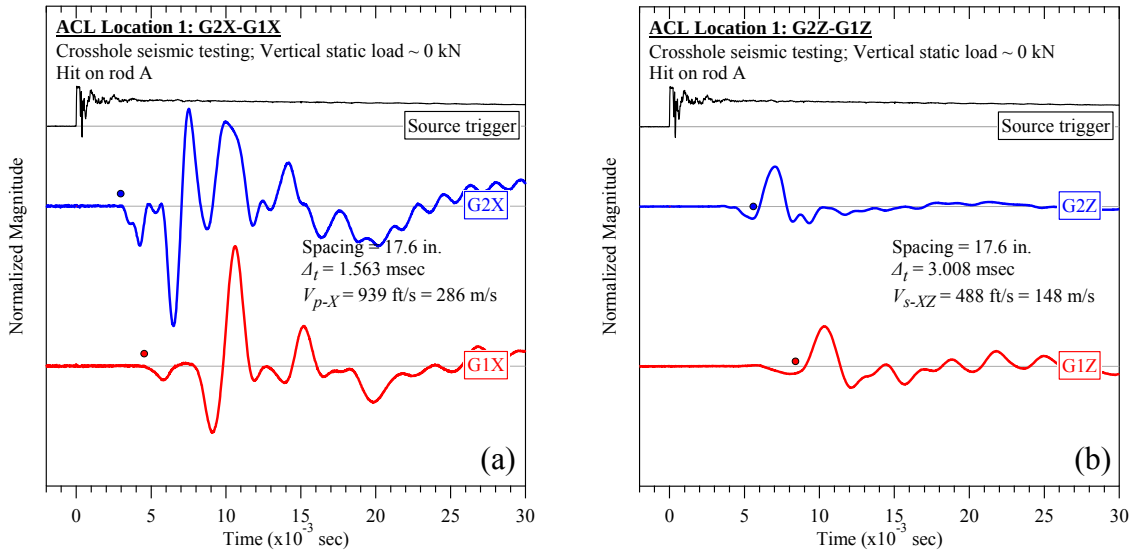

Figure A-13. Austin Community Landfill #1 (rod A): Crosshole seismic testing at vertical load of 0 kN: (a) $V_{p\text{-}X}$ and (b) $V_{s\text{-}XZ}$.

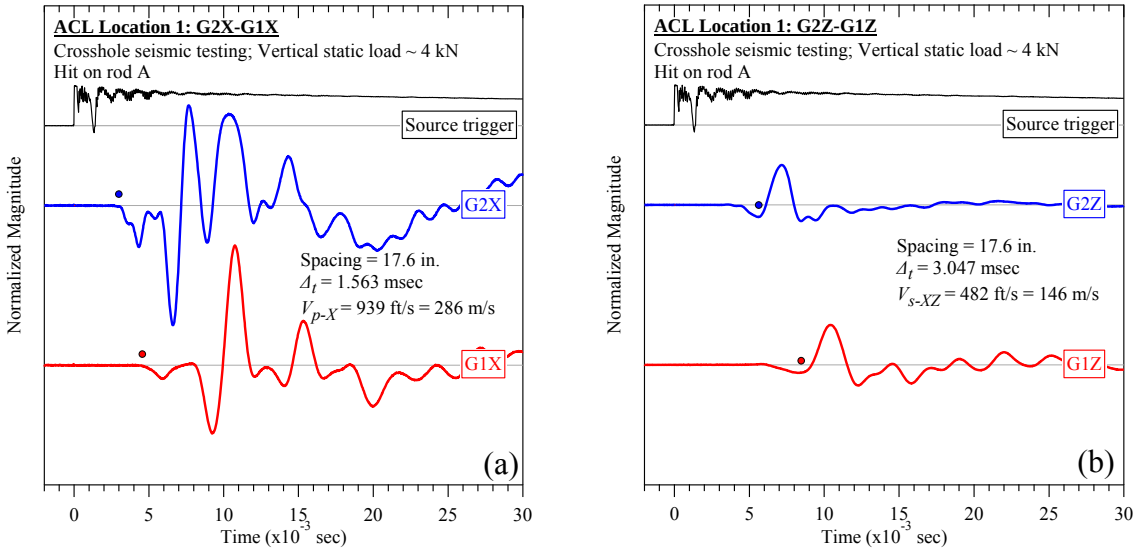

Figure A-14. Austin Community Landfill #1 (rod A): Crosshole seismic testing at vertical load of 4 kN: (a) $V_{p\text{-}X}$ and (b) $V_{s\text{-}XZ}$.

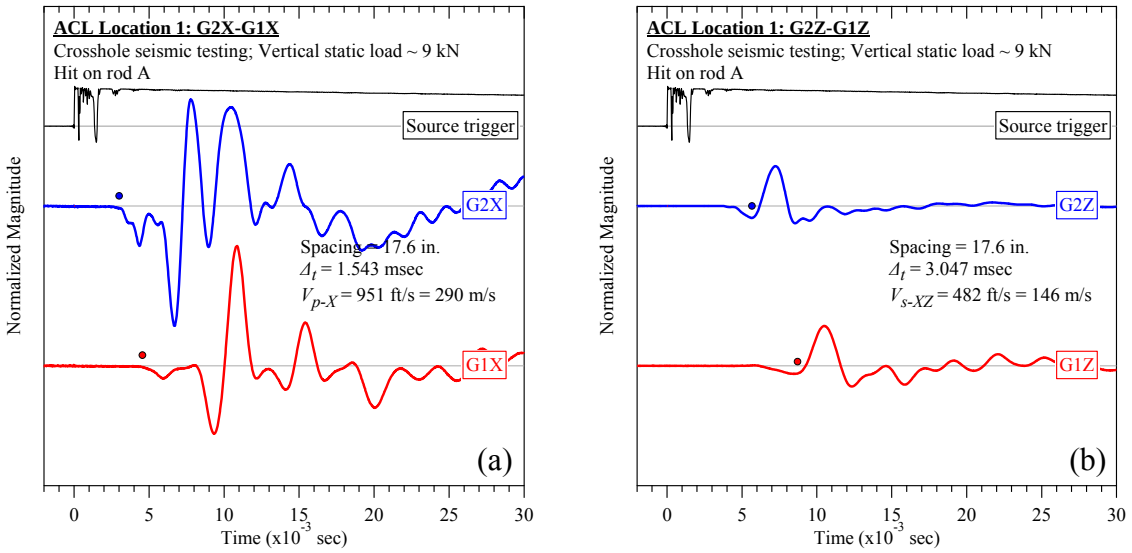

Figure A-15. Austin Community Landfill #1 (rod A): Crosshole seismic testing at vertical load of 9 kN: (a) $V_{p\text{-}X}$ and (b) $V_{s\text{-}XZ}$.

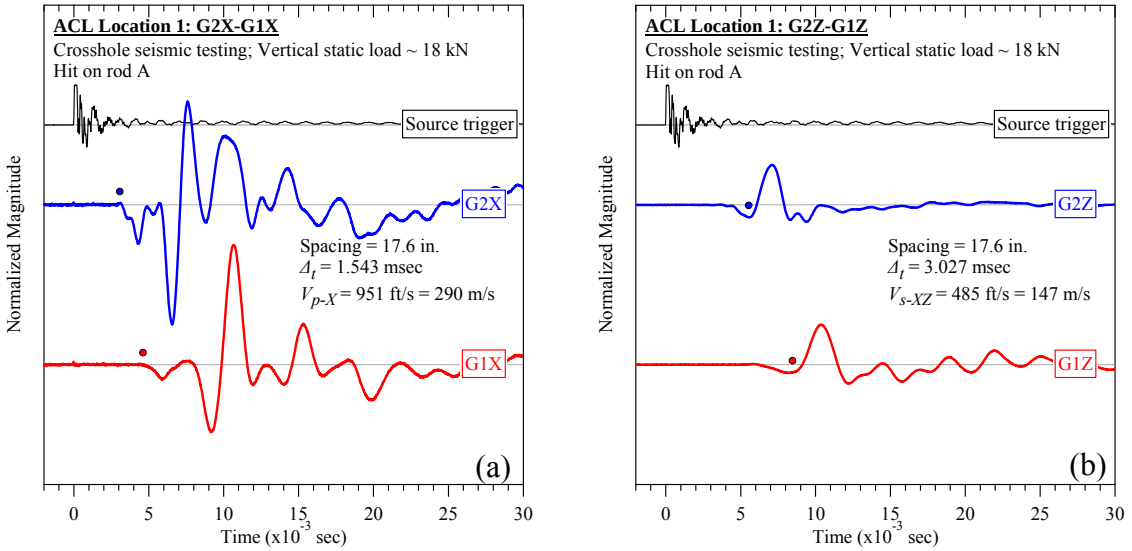

Figure A-16. Austin Community Landfill #1 (rod A): Crosshole seismic testing at vertical load of 18 kN: (a) $V_{p\text{-}X}$ and (b) $V_{s\text{-}XZ}$.

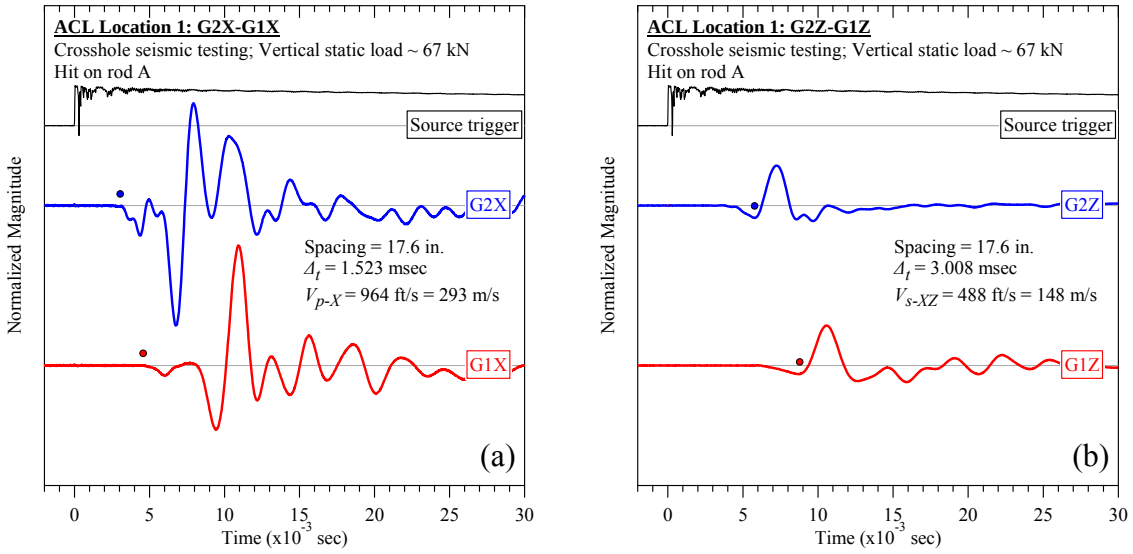

Figure A-17. Austin Community Landfill #1 (rod A): Crosshole seismic testing at vertical load of 67 kN: (a) $V_{p\text{-}X}$ and (b) $V_{s\text{-}XZ}$.

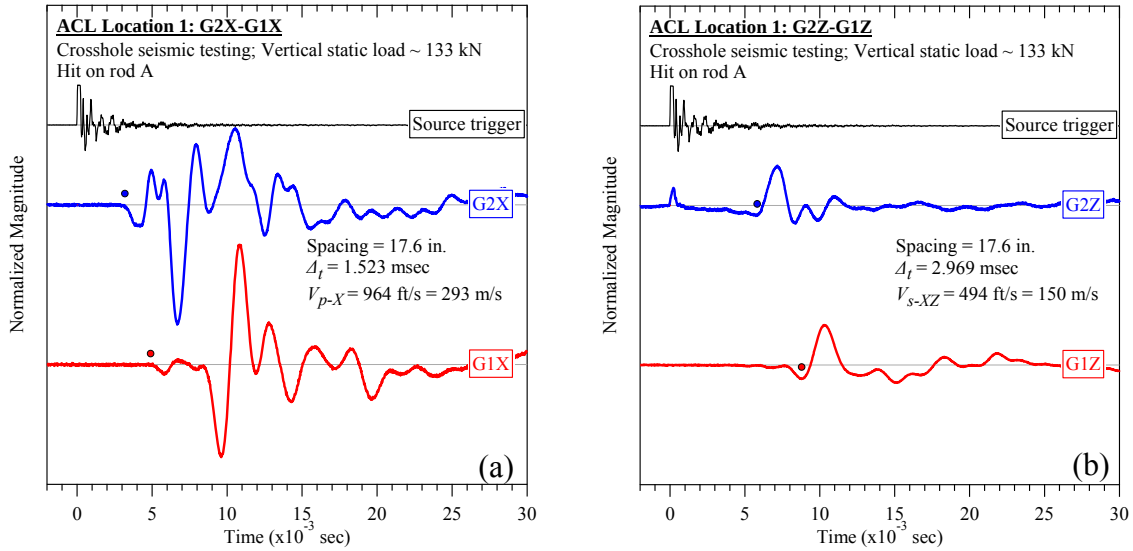

Figure A-18. Austin Community Landfill #1 (rod A): Crosshole seismic testing at vertical load of 133 kN: (a) $V_{p\text{-}X}$ and (b) $V_{s\text{-}XZ}$.

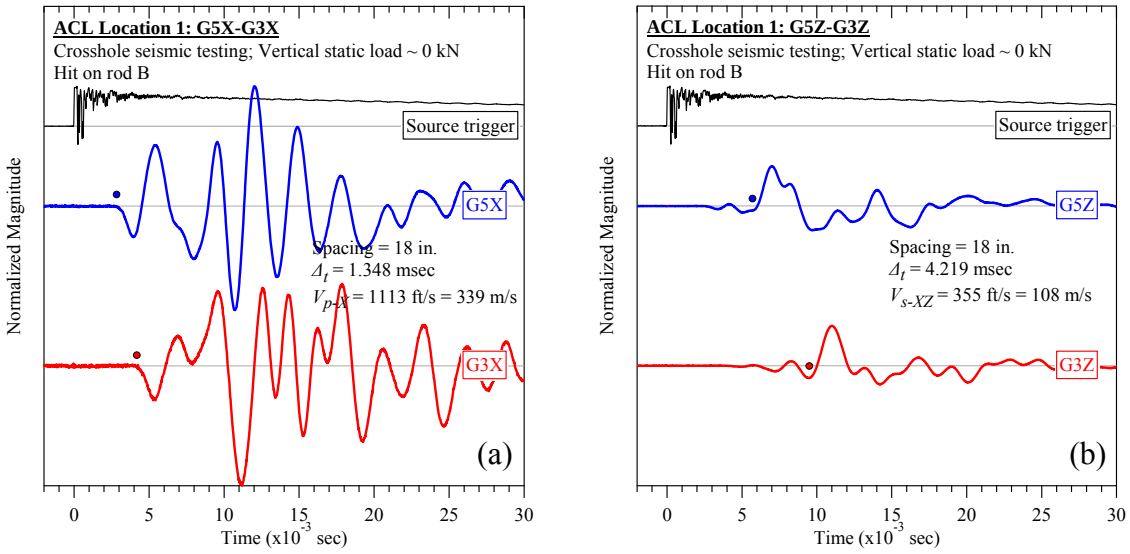

Figure A-19. Austin Community Landfill #1 (rod B): Crosshole seismic testing at vertical load of 0 kN: (a) $V_{p\text{-}X}$ and (b) $V_{s\text{-}XZ}$.

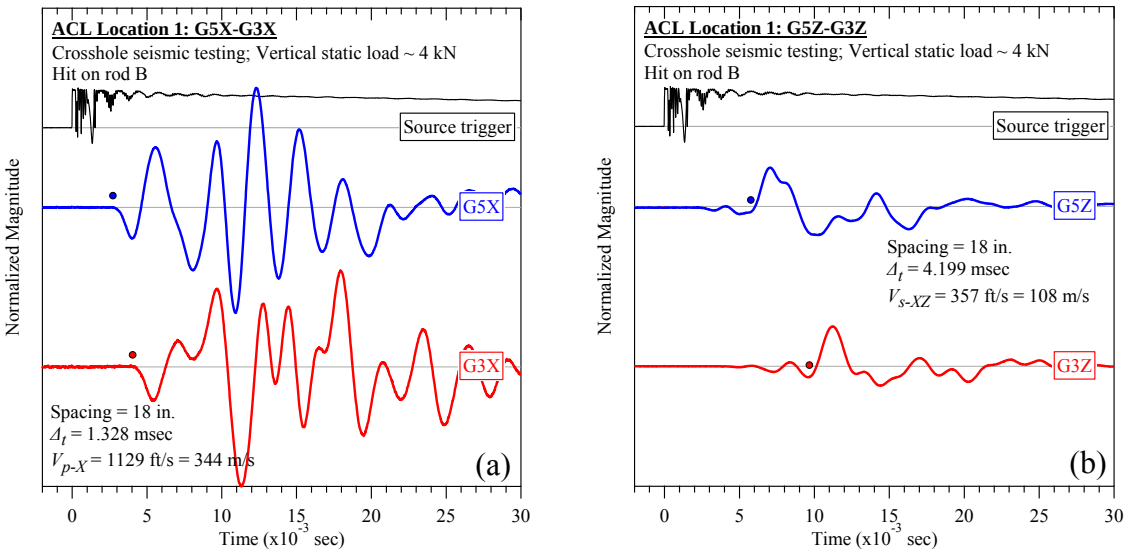

Figure A-20. Austin Community Landfill #1 (rod B): Crosshole seismic testing at vertical load of 4 kN: (a) $V_{p\text{-}X}$ and (b) $V_{s\text{-}XZ}$.

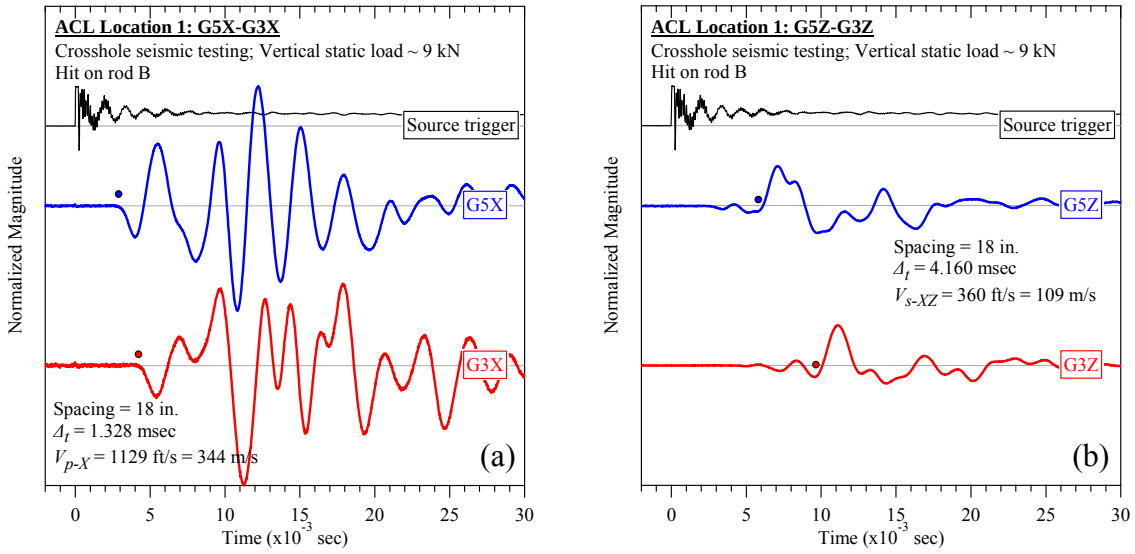

Figure A-21. Austin Community Landfill #1 (rod B): Crosshole seismic testing at vertical load of 9 kN: (a) $V_{p\text{-}X}$ and (b) $V_{s\text{-}XZ}$.

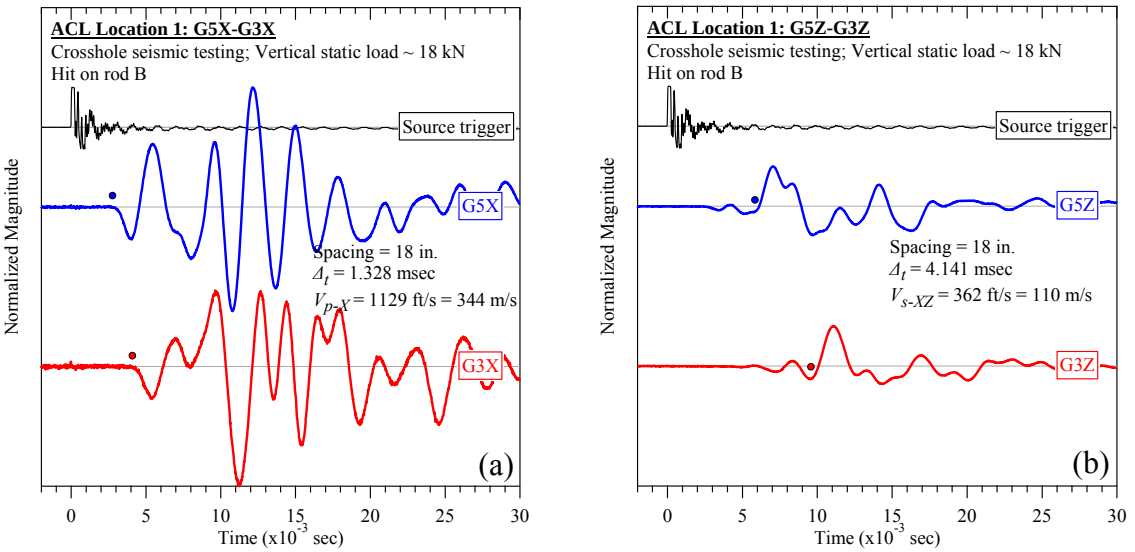

Figure A-22. Austin Community Landfill #1 (rod B): Crosshole seismic testing at vertical load of 18 kN: (a) $V_{p\text{-}X}$ and (b) $V_{s\text{-}XZ}$.

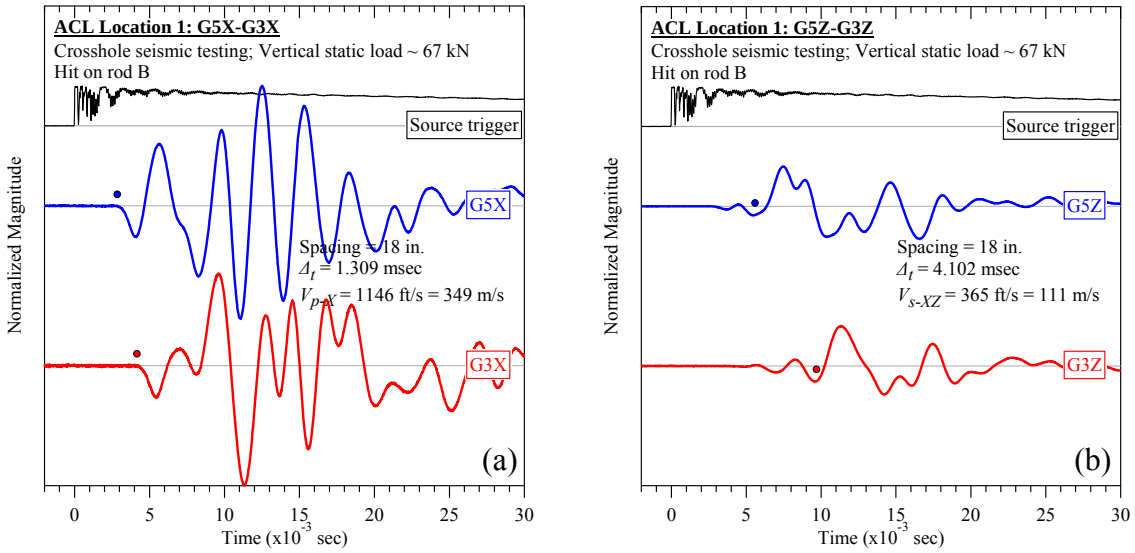

Figure A-23. Austin Community Landfill #1 (rod B): Crosshole seismic testing at vertical load of 67 kN: (a) $V_{p\text{-}X}$ and (b) $V_{s\text{-}XZ}$.

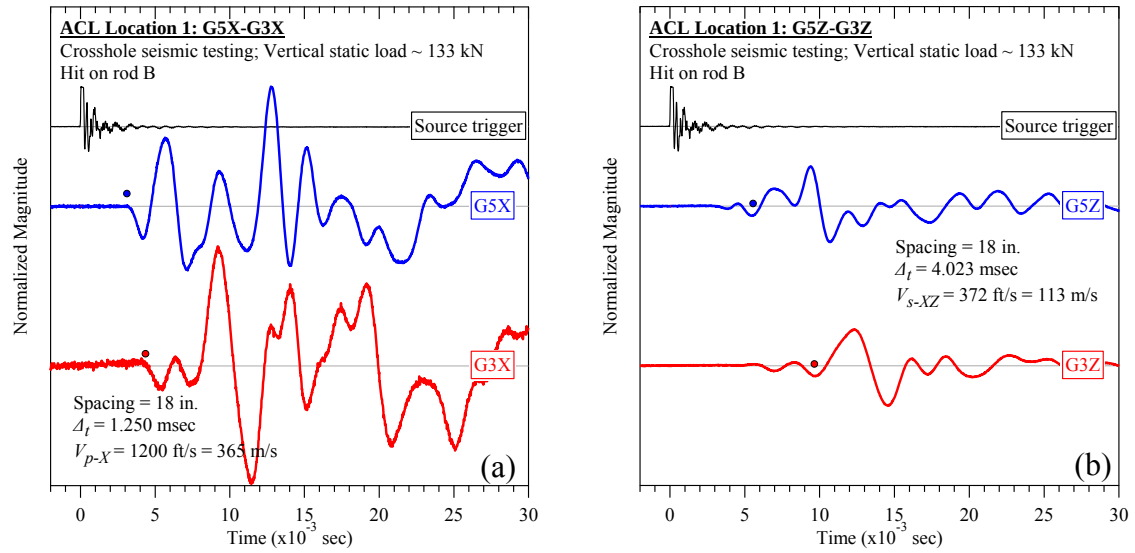

Figure A-24. Austin Community Landfill #1 (rod B): Crosshole seismic testing at vertical load of 133 kN: (a) $V_{p\text{-}X}$ and (b) $V_{s\text{-}XZ}$.

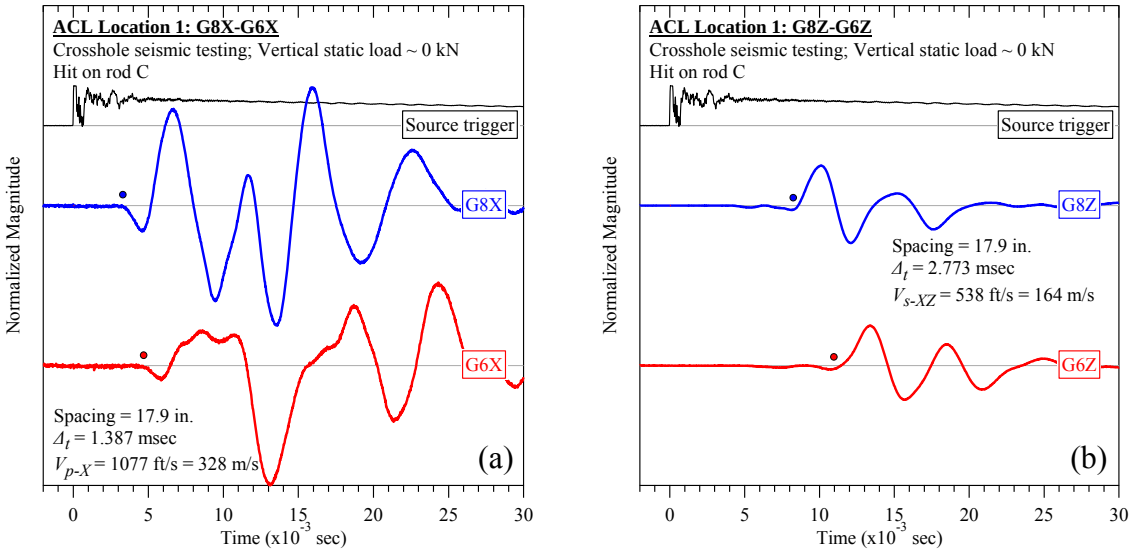

Figure A-25. Austin Community Landfill #1 (rod C): Crosshole seismic testing at vertical load of 0 kN: (a) $V_{p\text{-}X}$ and (b) $V_{s\text{-}XZ}$.

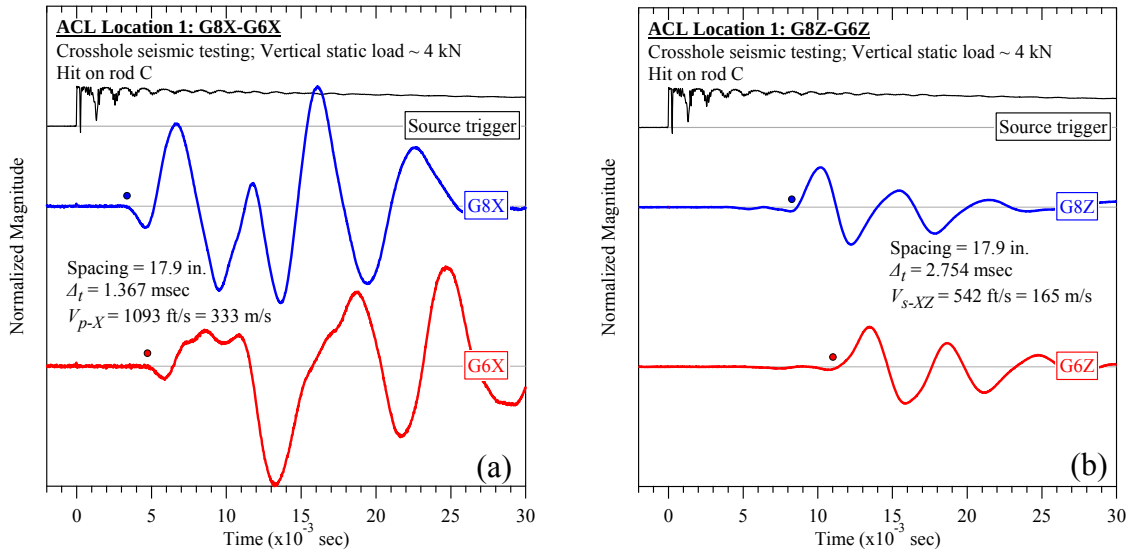

Figure A-26. Austin Community Landfill #1 (rod C): Crosshole seismic testing at vertical load of 4 kN: (a) $V_{p\text{-}X}$ and (b) $V_{s\text{-}XZ}$.

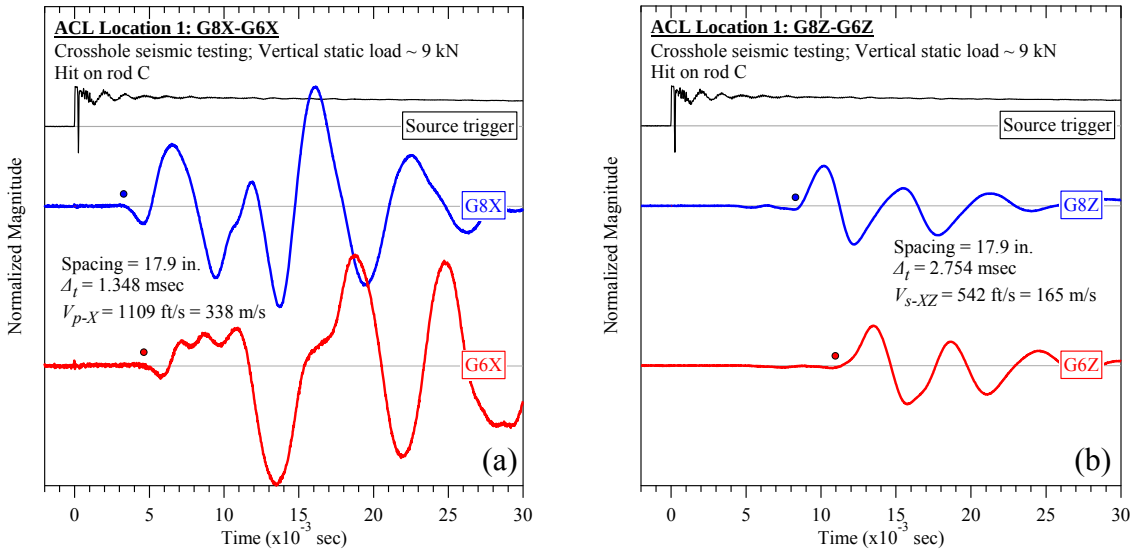

Figure A-27. Austin Community Landfill #1 (rod C): Crosshole seismic testing at vertical load of 9 kN: (a) $V_{p\text{-}X}$ and (b) $V_{s\text{-}XZ}$.

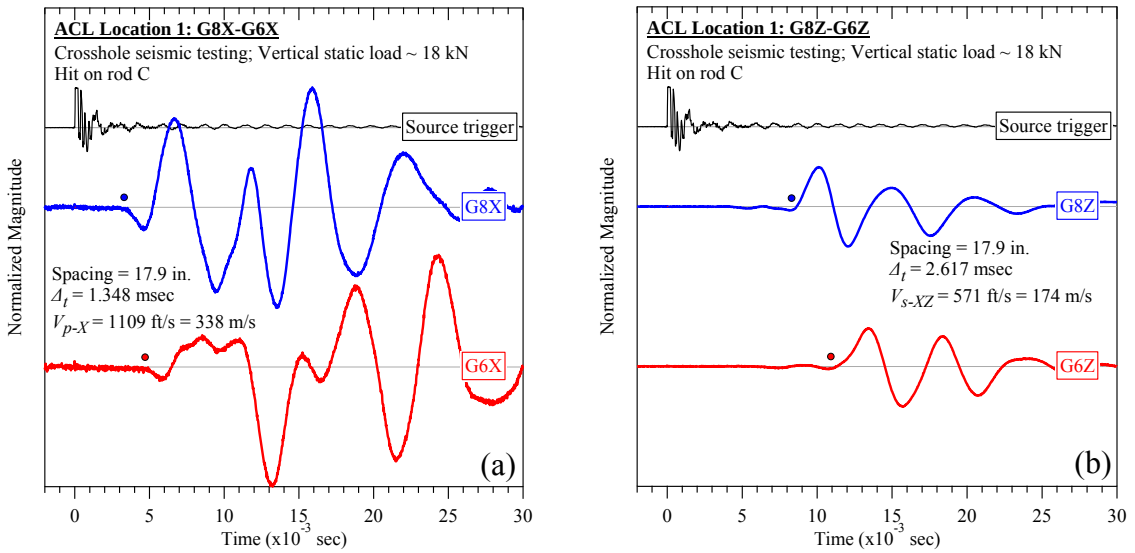

Figure A-28. Austin Community Landfill #1 (rod C): Crosshole seismic testing at vertical load of 18 kN: (a) $V_{p\text{-}X}$ and (b) $V_{s\text{-}XZ}$.

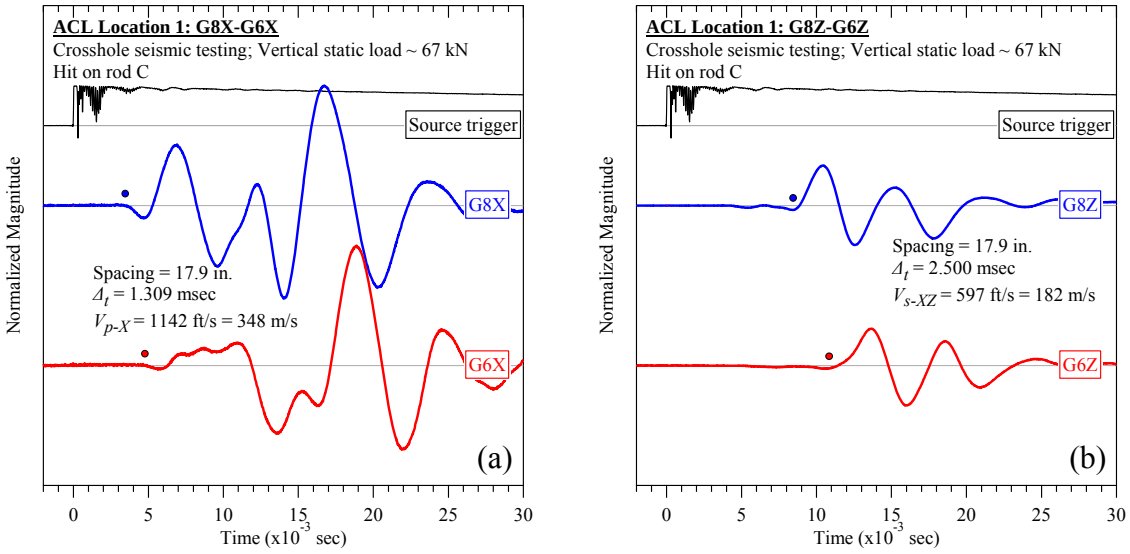

Figure A-29. Austin Community Landfill #1 (rod C): Crosshole seismic testing at vertical load of 67 kN: (a) $V_{p\text{-}X}$ and (b) $V_{s\text{-}XZ}$.

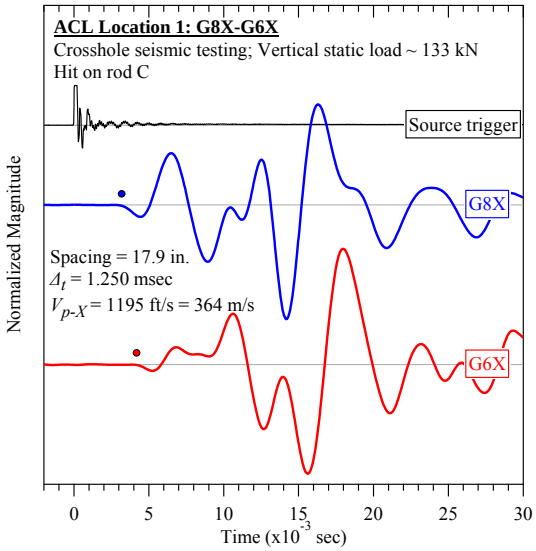

Figure A-30. Austin Community Landfill #1 (rod C): Crosshole seismic testing at vertical load of 133 kN: $V_{p\text{-}X}$.

A.1.3 Steady-state Dynamic Testing

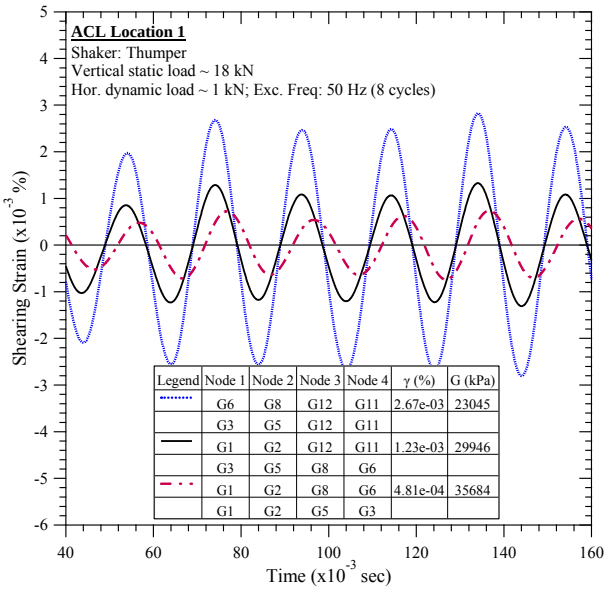

Figure A-31. Austin Community Landfill #1: Steady-state dynamic testing at vertical load of 18 kN and horizontal dynamic load of 1 kN.

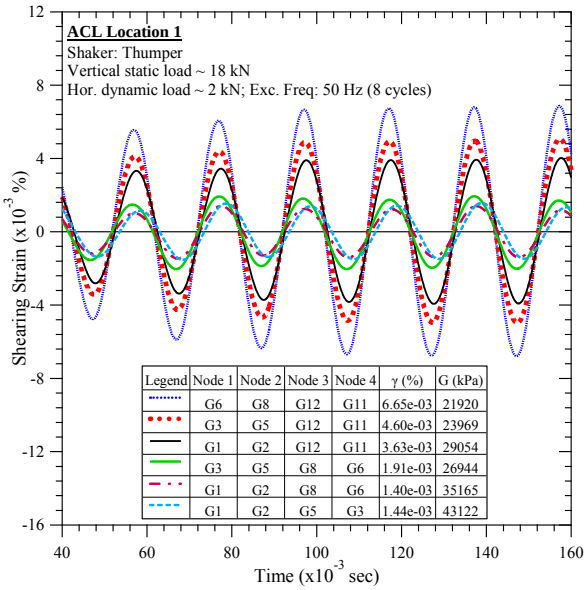

Figure A-32. Austin Community Landfill #1: Steady-state dynamic testing at vertical load of 18 kN and horizontal dynamic load of 2 kN.

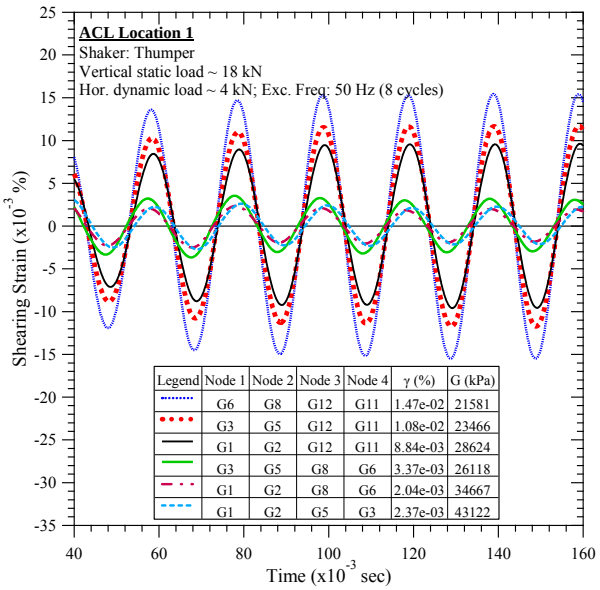

Figure A-33. Austin Community Landfill #1: Steady-state dynamic testing at vertical load of 18 kN and horizontal dynamic load of 4 kN.

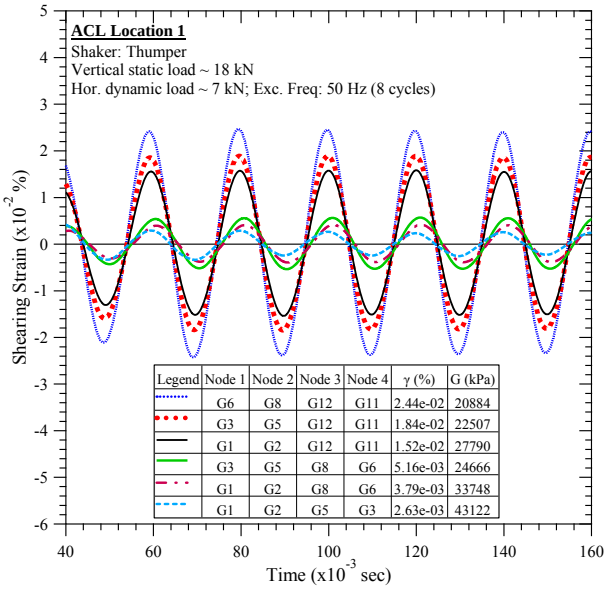

Figure A-34. Austin Community Landfill #1: Steady-state dynamic testing at vertical load of 18 kN and horizontal dynamic load of 7 kN.

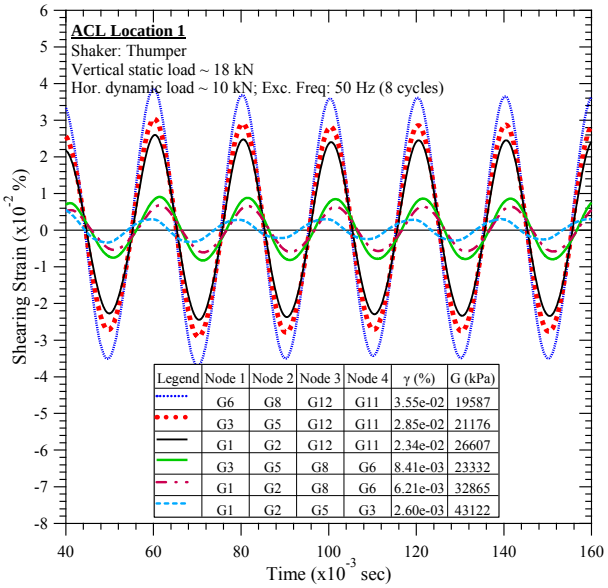

Figure A-35. Austin Community Landfill #1: Steady-state dynamic testing at vertical load of 18 kN and horizontal dynamic load of 10 kN.

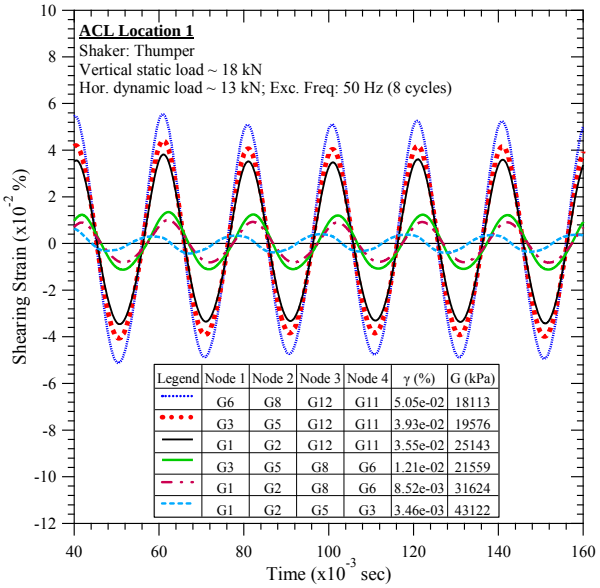

Figure A-36. Austin Community Landfill #1: Steady-state dynamic testing at vertical load of 18 kN and horizontal dynamic load of 13 kN.

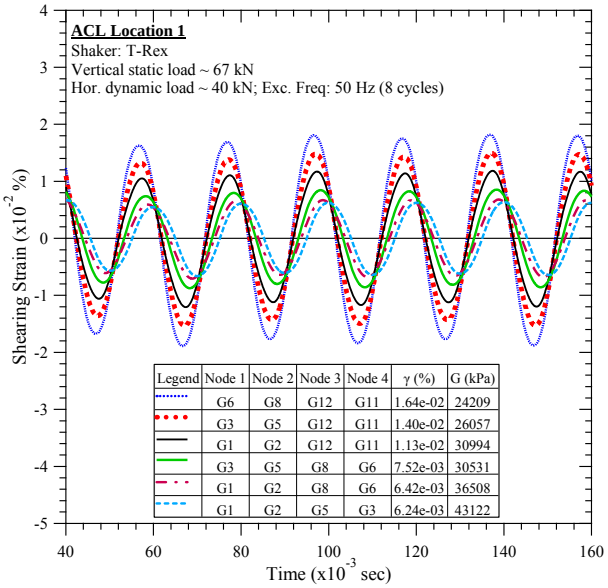

Figure A-37. Austin Community Landfill #1: Steady-state dynamic testing at vertical load of 67 kN and horizontal dynamic load of 40 kN.

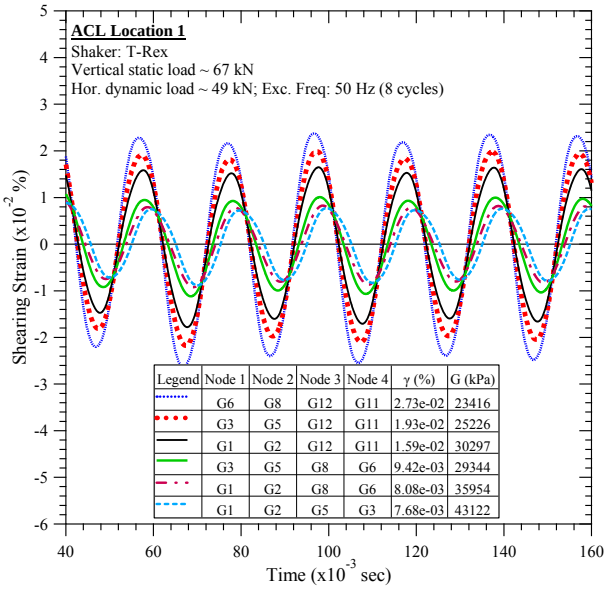

Figure A-38. Austin Community Landfill #1: Steady-state dynamic testing at vertical load of 67 kN and horizontal dynamic load of 49 kN.

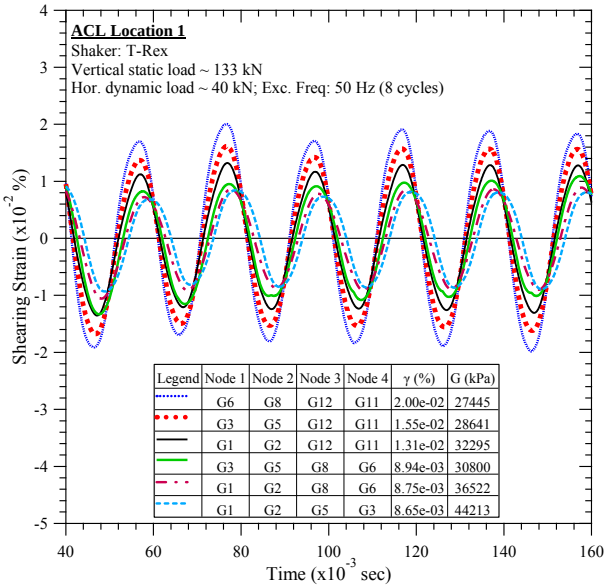

Figure A-39. Austin Community Landfill #1: Steady-state dynamic testing at vertical load of 133 kN and horizontal dynamic load of 40 kN.

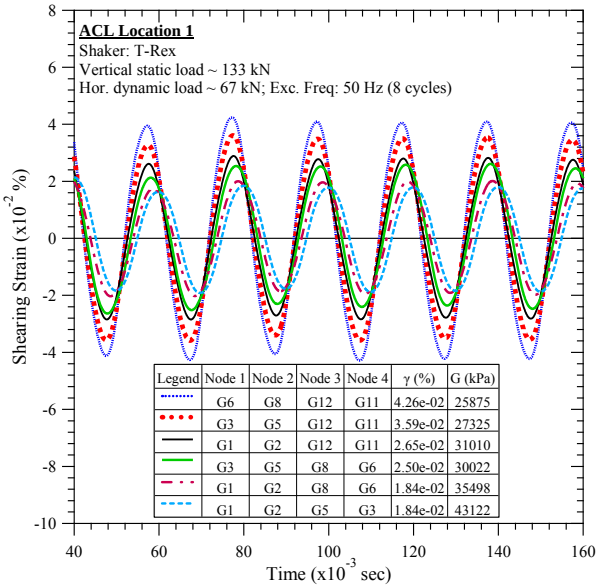

Figure A-40. Austin Community Landfill #1: Steady-state dynamic testing at vertical load of 133 kN and horizontal dynamic load of 67 kN.

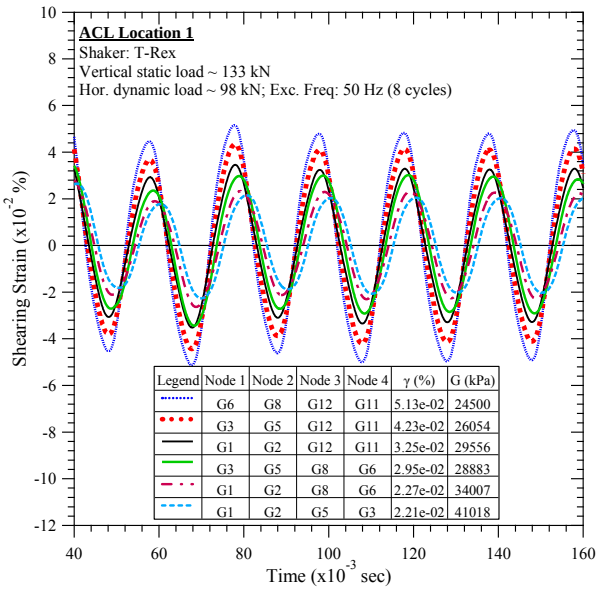

Figure A-41. Austin Community Landfill #1: Steady-state dynamic testing at vertical load of 133 kN and horizontal dynamic load of 98 kN.

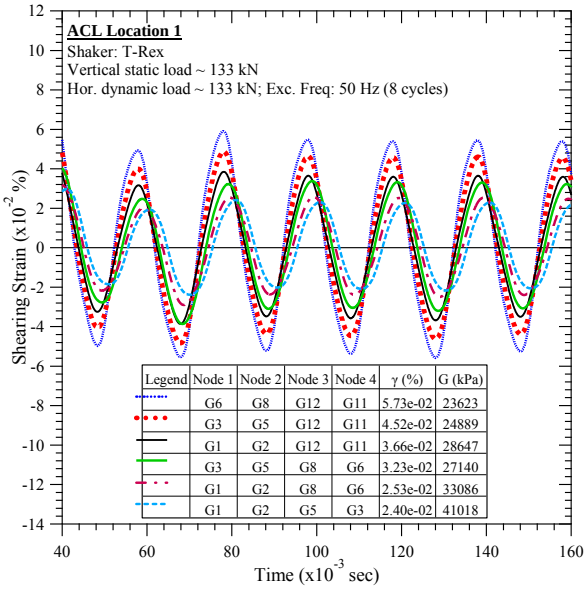

Figure A-42. Austin Community Landfill #1: Steady-state dynamic testing at vertical load of 133 kN and horizontal dynamic load of 133 kN.

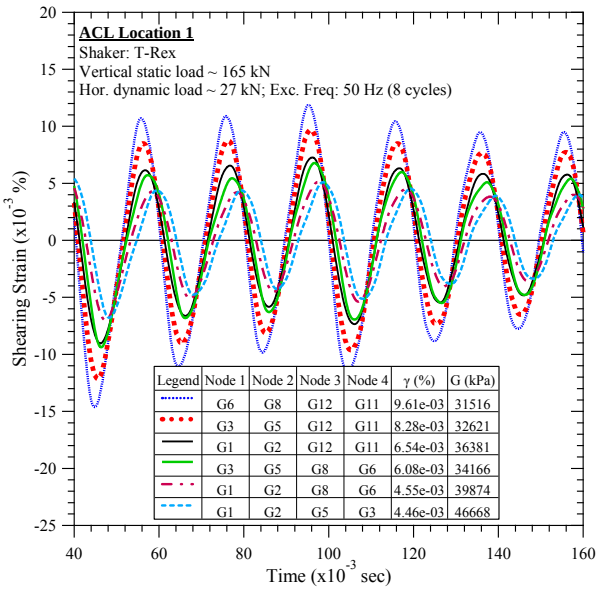

Figure A-43. Austin Community Landfill #1: Steady-state dynamic testing at vertical load of 165 kN and horizontal dynamic load of 27 kN.

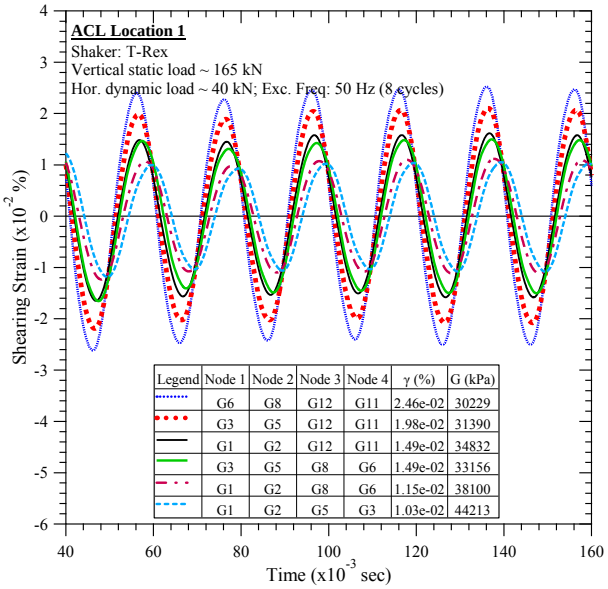

Figure A-44. Austin Community Landfill #1: Steady-state dynamic testing at vertical load of 165 kN and horizontal dynamic load of 40 kN.

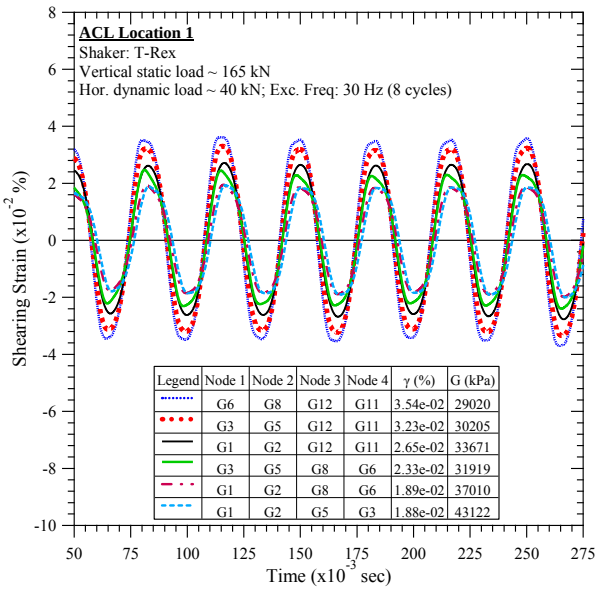

Figure A-45. Austin Community Landfill #1: Steady-state dynamic testing at vertical load of 165 kN and horizontal dynamic load of 40 kN.

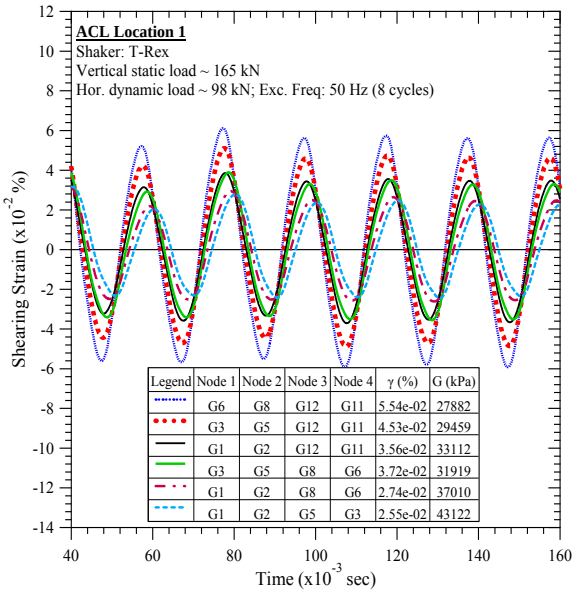

Figure A-46. Austin Community Landfill #1: Steady-state dynamic testing at vertical load of 165 kN and horizontal dynamic load of 98 kN.

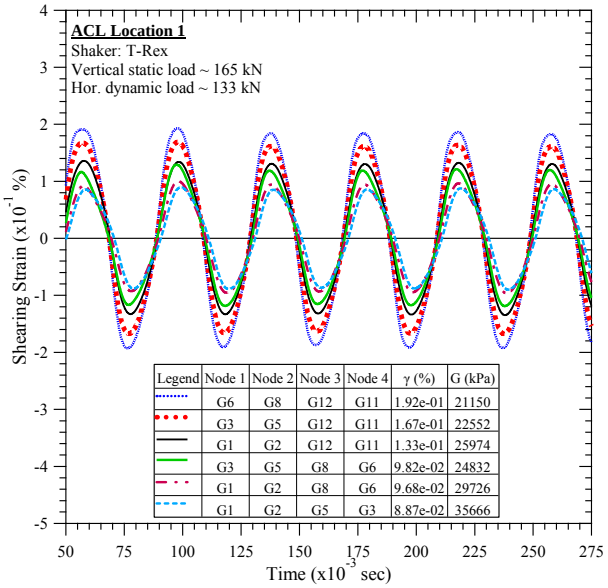

Figure A-47. Austin Community Landfill #1: Steady-state dynamic testing at vertical load of 165 kN and horizontal dynamic load of 133 kN.

A.2 Austin Community Landfill Location 2

A.2.1 Downhole Seismic Testing

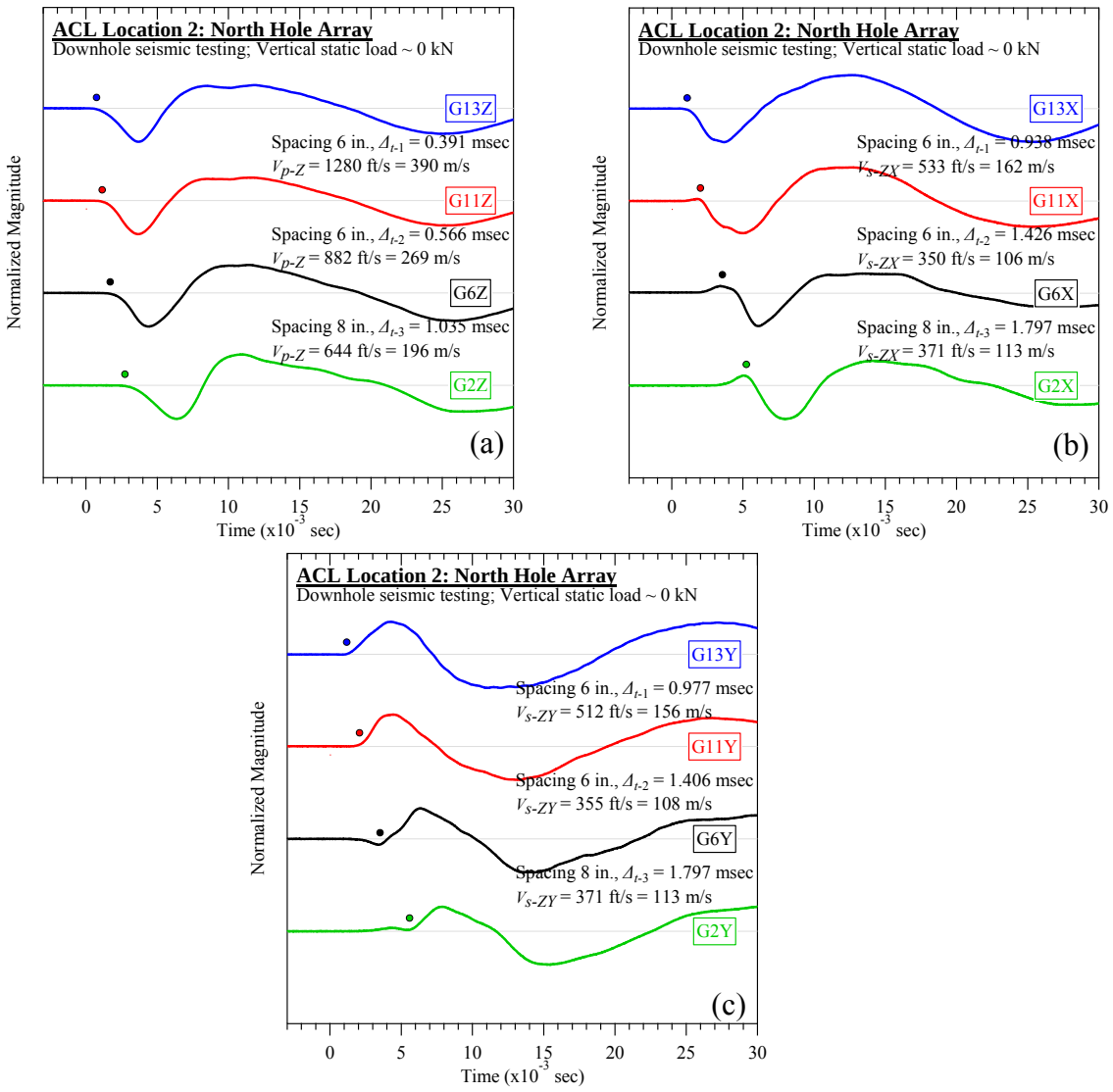

Figure A-48. Austin Community Landfill #2 (north hole): Downhole seismic testing at vertical load of 0 kN: (a) $V_{p\text{-}Z}$, (b) $V_{s\text{-}ZX}$, and (c) $V_{s\text{-}ZY}$.

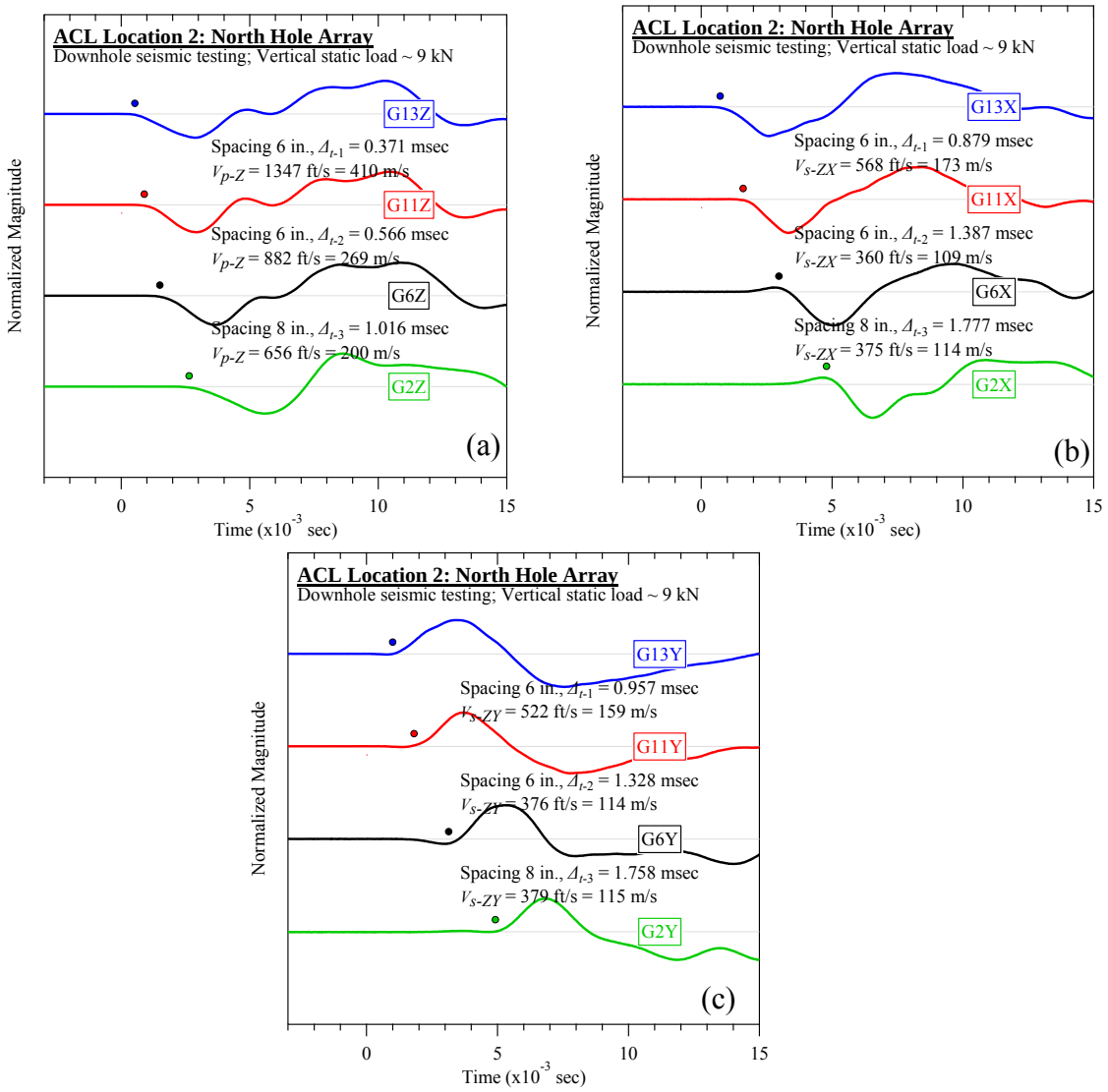

Figure A-49. Austin Community Landfill #2 (north hole): Downhole seismic testing at vertical load of 9 kN: (a) $V_{p\text{-}Z}$, (b) $V_{s\text{-}ZX}$, and (c) $V_{s\text{-}ZY}$.

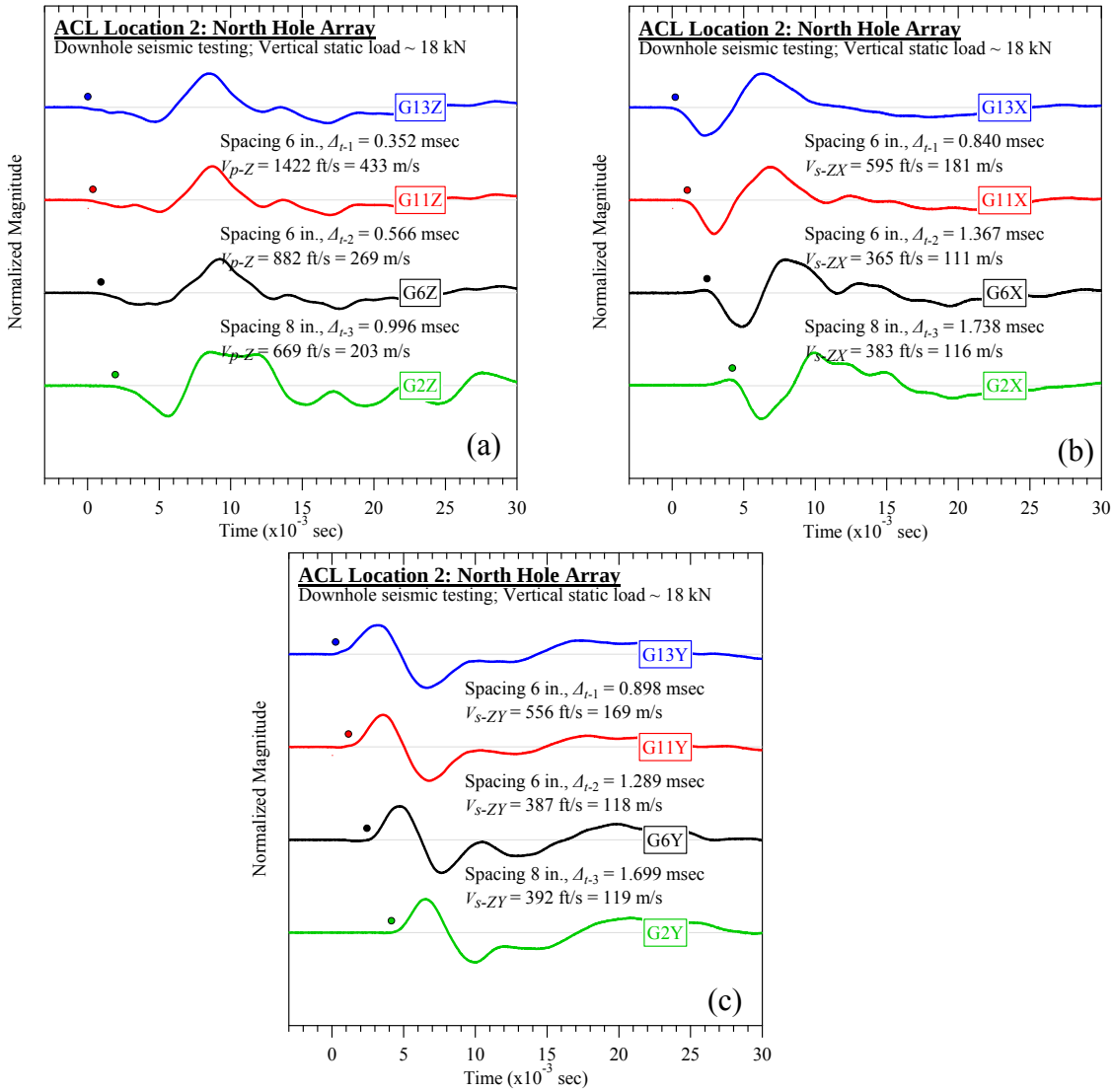

Figure A-50. Austin Community Landfill #2 (north hole): Downhole seismic testing at vertical load of 18 kN: (a) $V_{p\text{-}Z}$, (b) $V_{s\text{-}ZX}$, and (c) $V_{s\text{-}ZY}$.

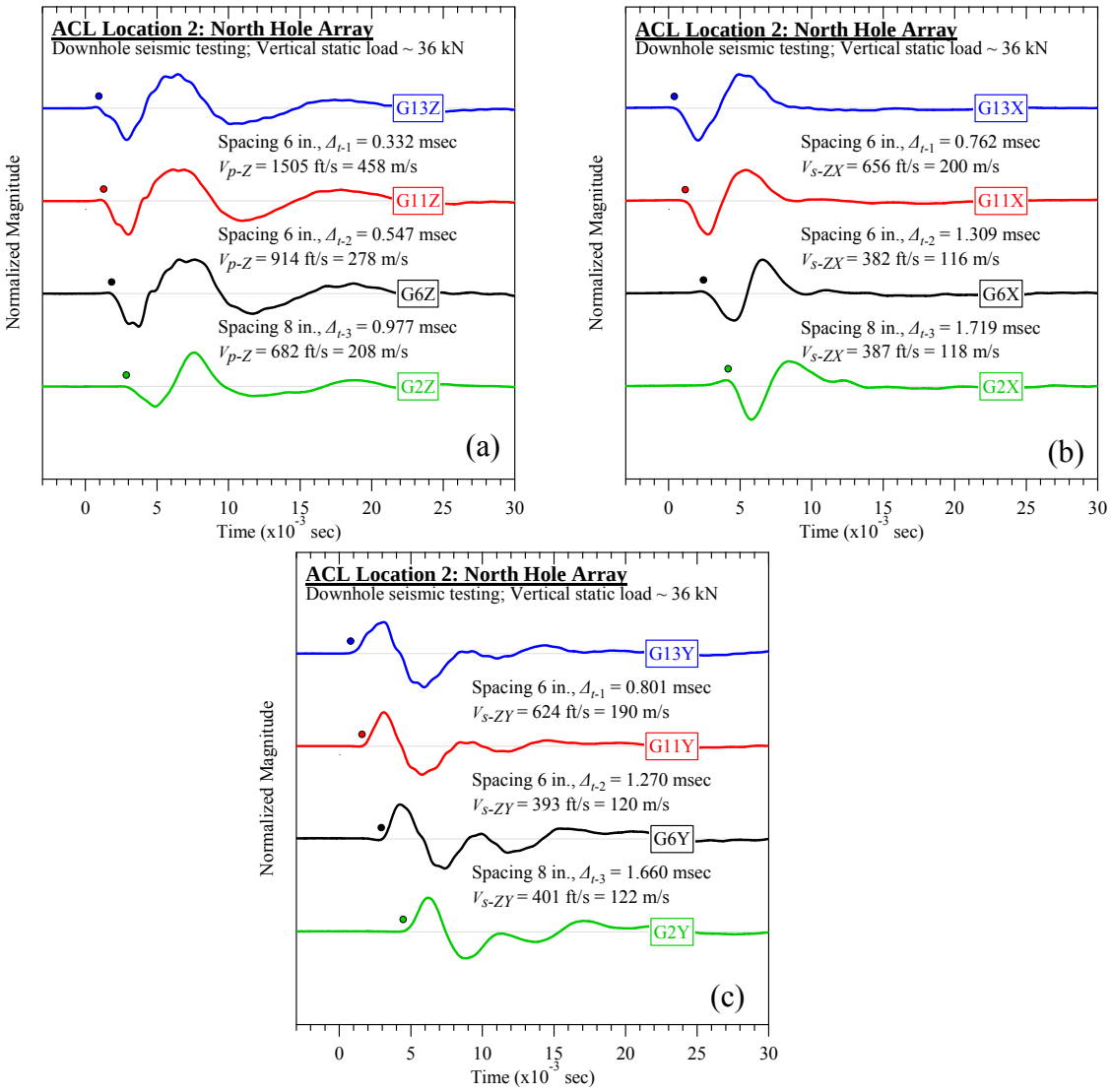

Figure A-51. Austin Community Landfill #2 (north hole): Downhole seismic testing at vertical load of 36 kN: (a) $V_{p\text{-}Z}$, (b) $V_{s\text{-}ZX}$, and (c) $V_{s\text{-}ZY}$.

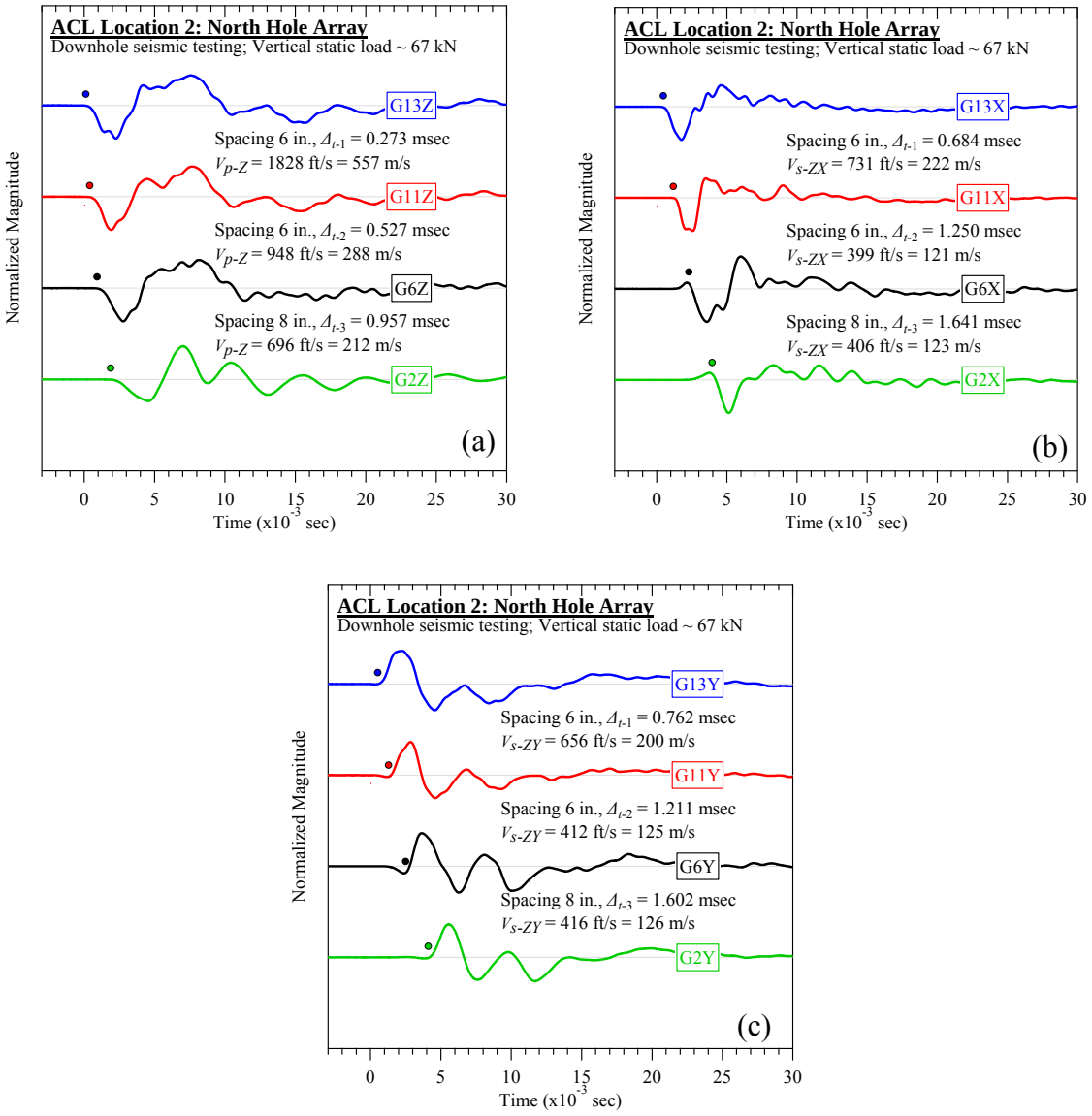

Figure A-52. Austin Community Landfill #2 (north hole): Downhole seismic testing at vertical load of 67 kN: (a) V_{p-Z}, (b) V_{s-ZX}, and (c) V_{s-ZY}.

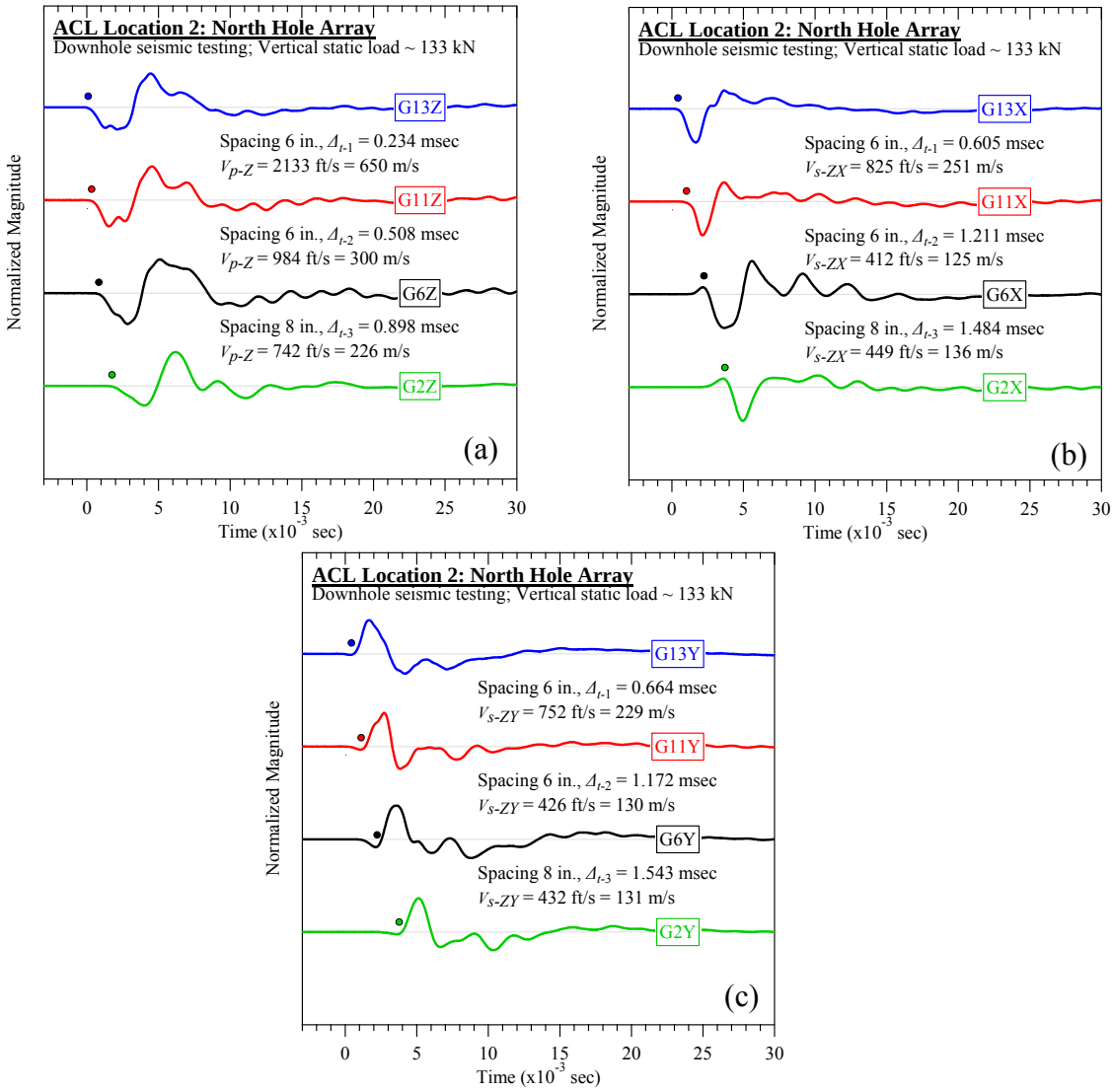

Figure A-53. Austin Community Landfill #2 (north hole): Downhole seismic testing at vertical load of 133 kN: (a) $V_{p\text{-}Z}$, (b) $V_{s\text{-}ZX}$, and (c) $V_{s\text{-}ZY}$.

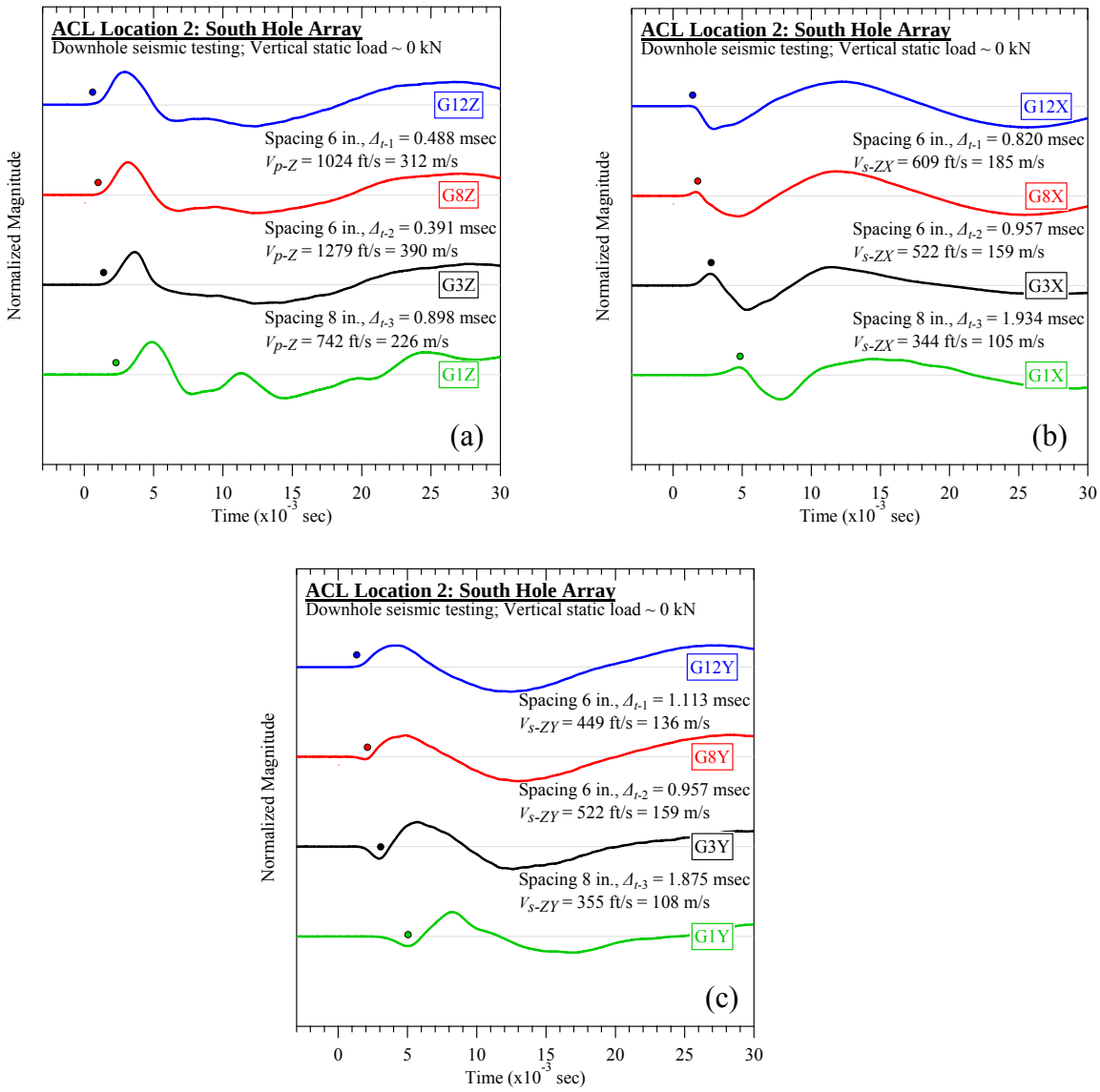

Figure A-54. Austin Community Landfill #2 (south hole): Downhole seismic testing at vertical load of 0 kN: (a) V_{p-Z}, (b) V_{s-ZX}, and (c) V_{s-ZY}.

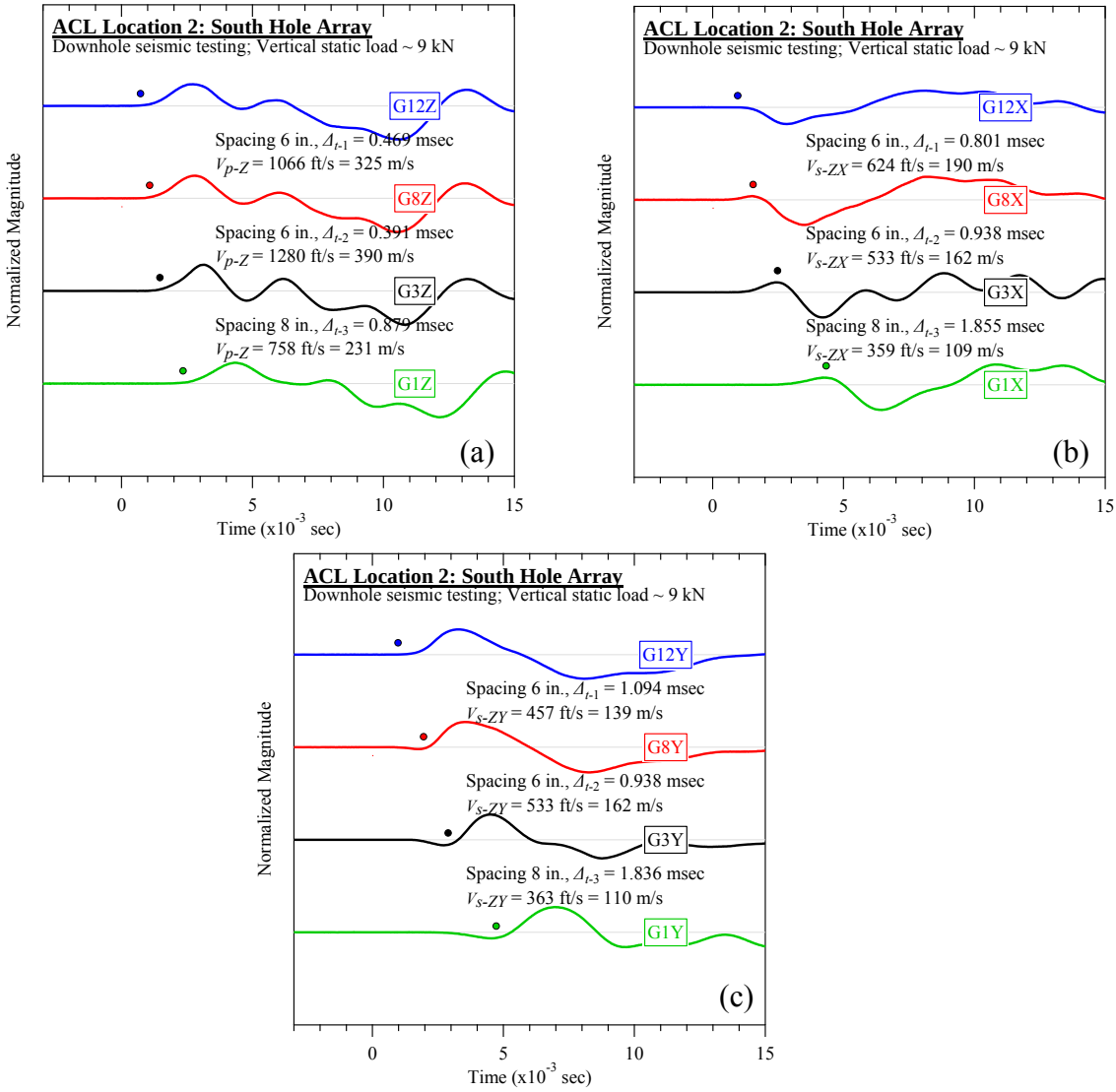

Figure A-55. Austin Community Landfill #2 (south hole): Downhole seismic testing at vertical load of 9 kN: (a) $V_{p\text{-}Z}$, (b) $V_{s\text{-}ZX}$, and (c) $V_{s\text{-}ZY}$.

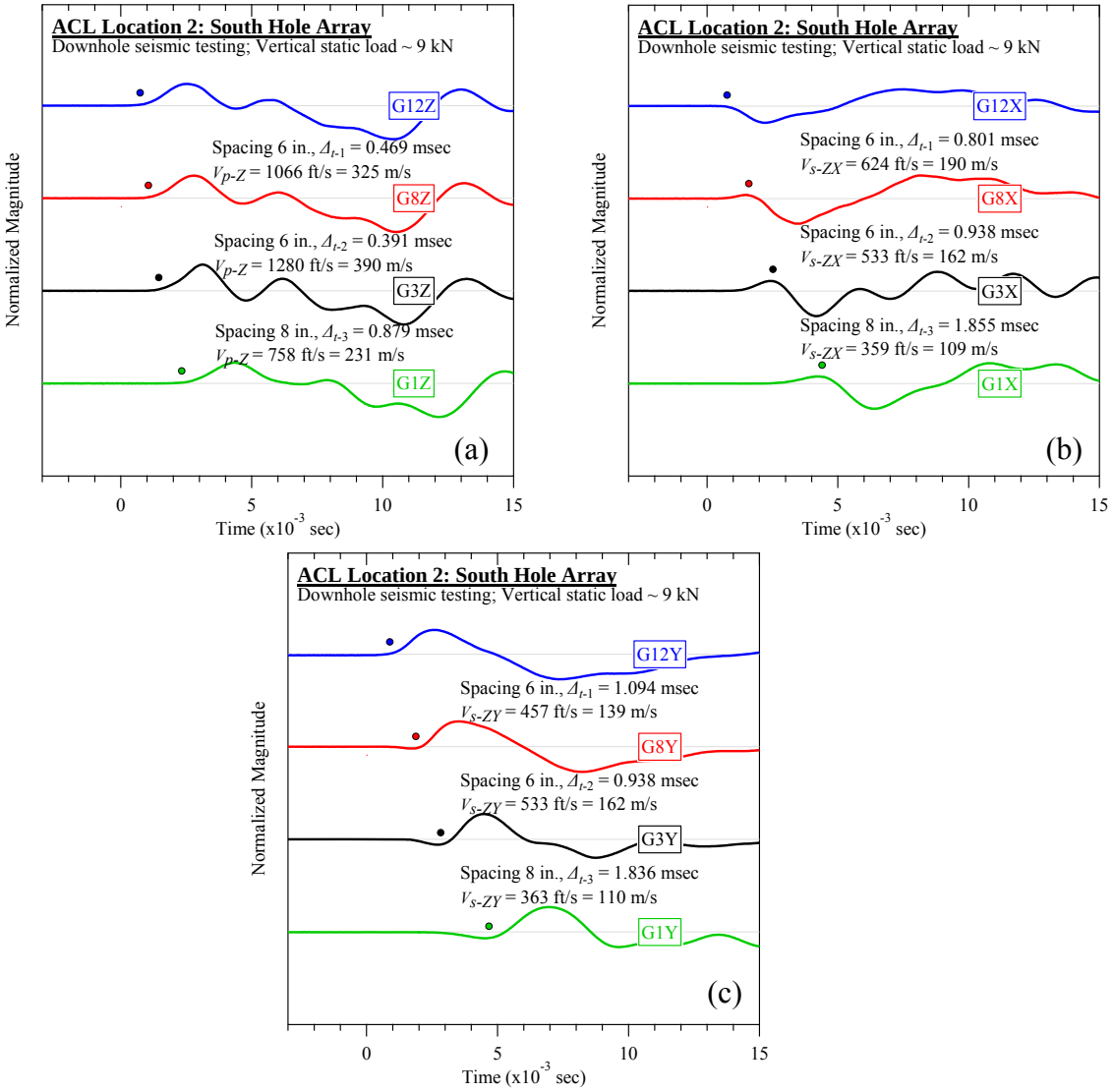

Figure A-56. Austin Community Landfill #2 (south hole): Downhole seismic testing at vertical load of 9 kN: (a) $V_{p\text{-}Z}$, (b) $V_{s\text{-}ZX}$, and (c) $V_{s\text{-}ZY}$.

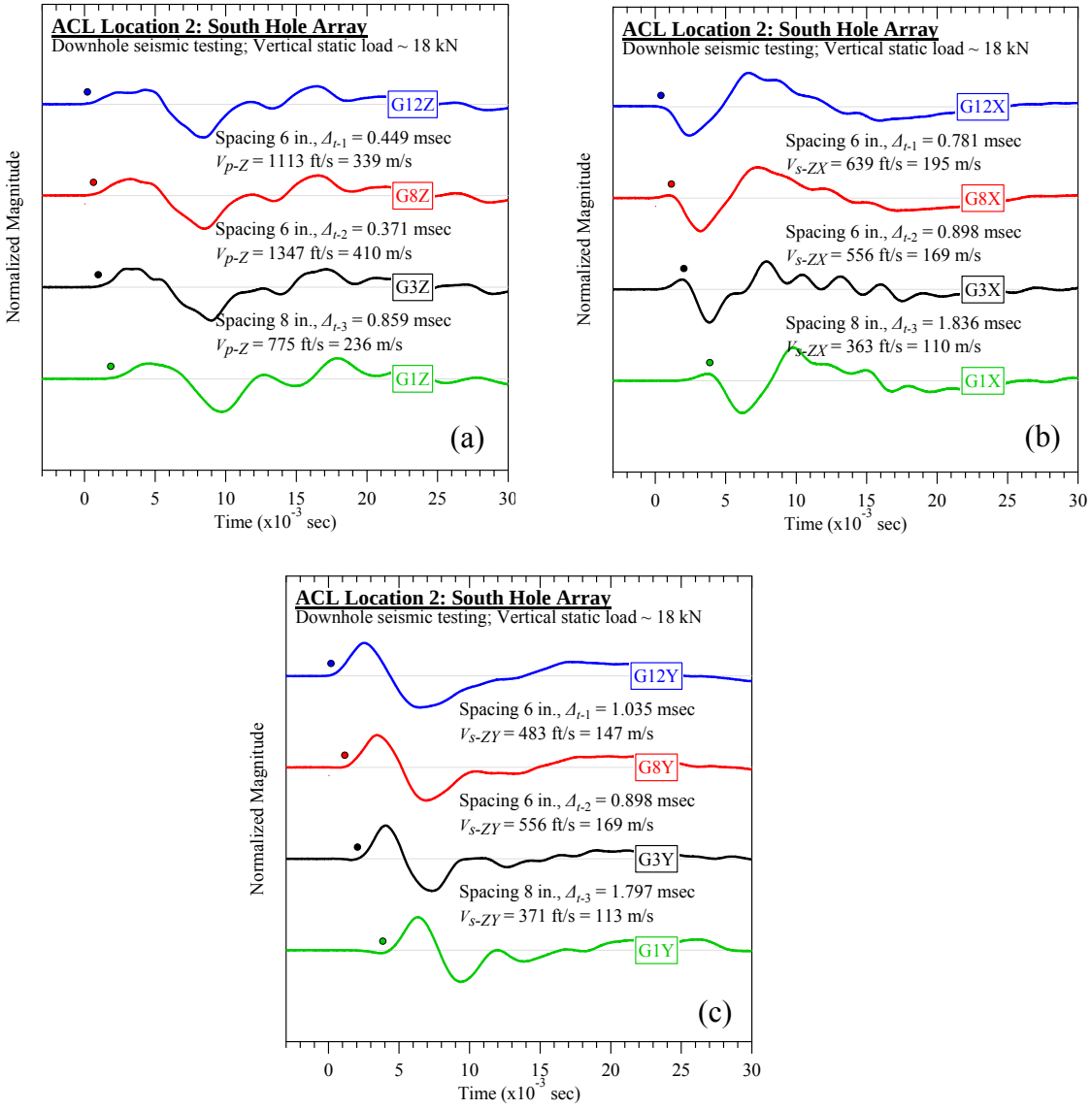

Figure A-57. Austin Community Landfill #2 (south hole): Downhole seismic testing at vertical load of 18 kN: (a) V_{p-Z}, (b) V_{s-ZX}, and (c) V_{s-ZY}.

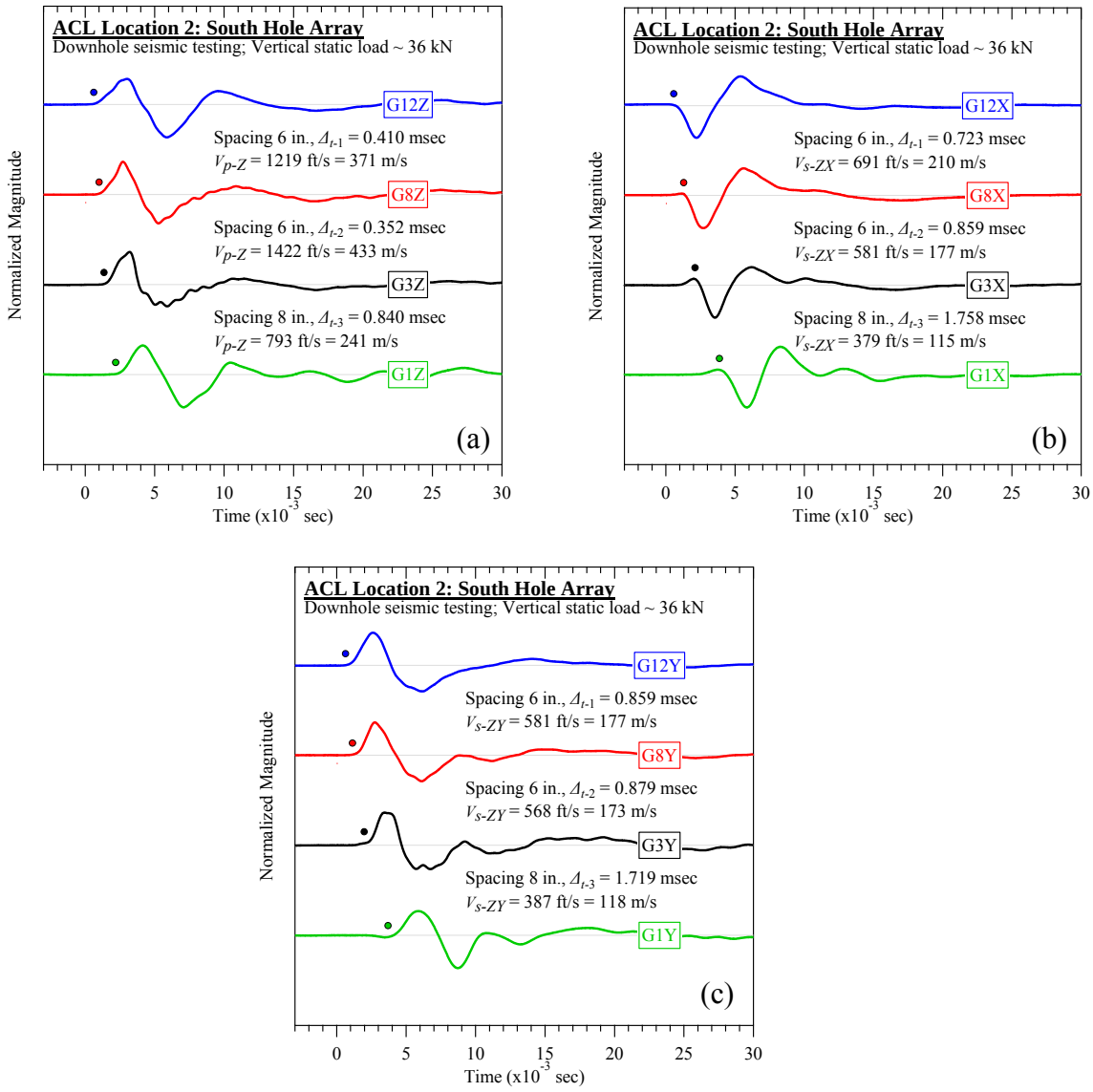

Figure A-58. Austin Community Landfill #2 (south hole): Downhole seismic testing at vertical load of 36 kN: (a) V_{p-Z}, (b) V_{s-ZX}, and (c) V_{s-ZY}.

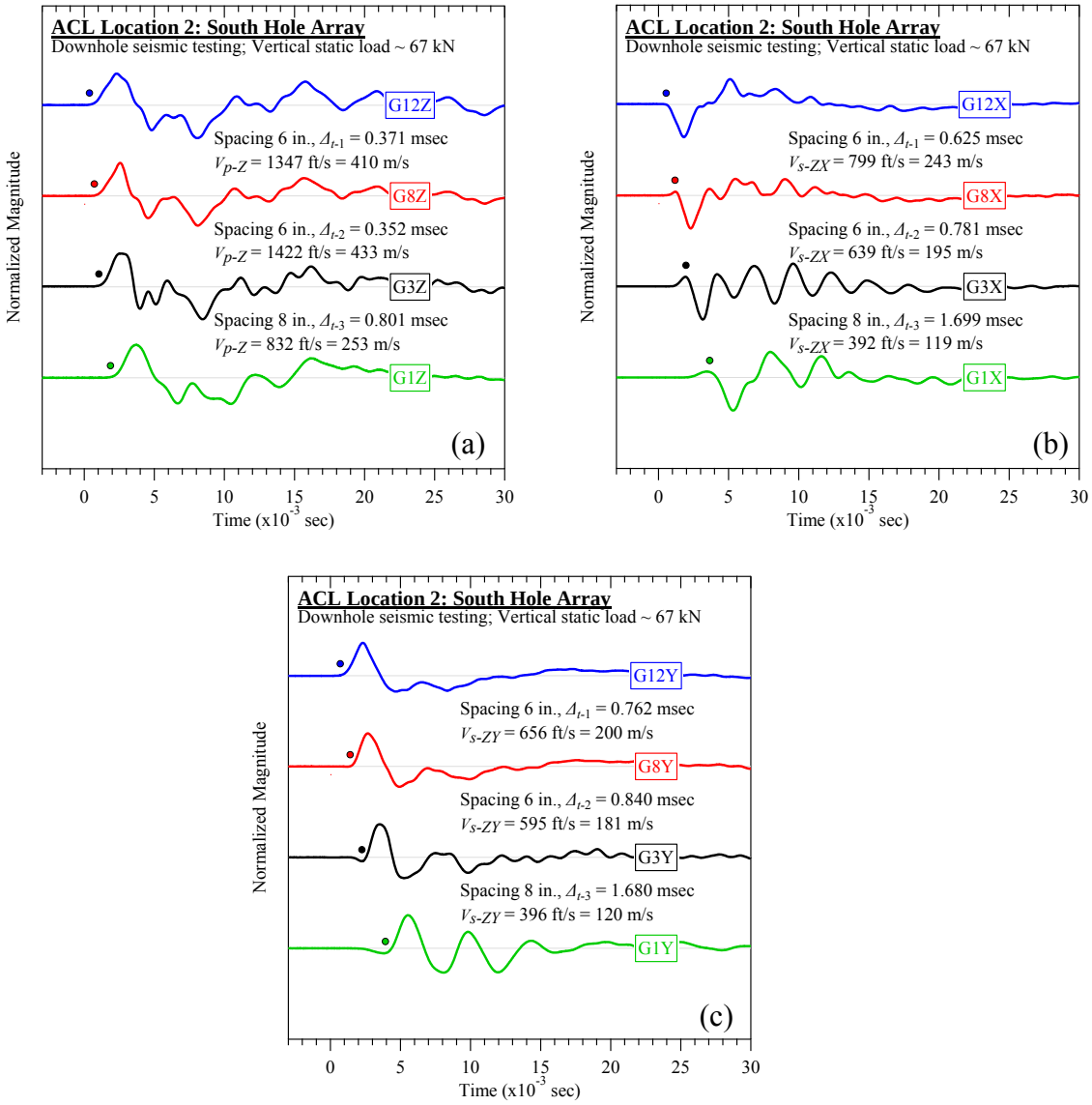

Figure A-59. Austin Community Landfill #2 (south hole): Downhole seismic testing at vertical load of 67 kN: (a) $V_{p\text{-}Z}$, (b) $V_{s\text{-}ZX}$, and (c) $V_{s\text{-}ZY}$.

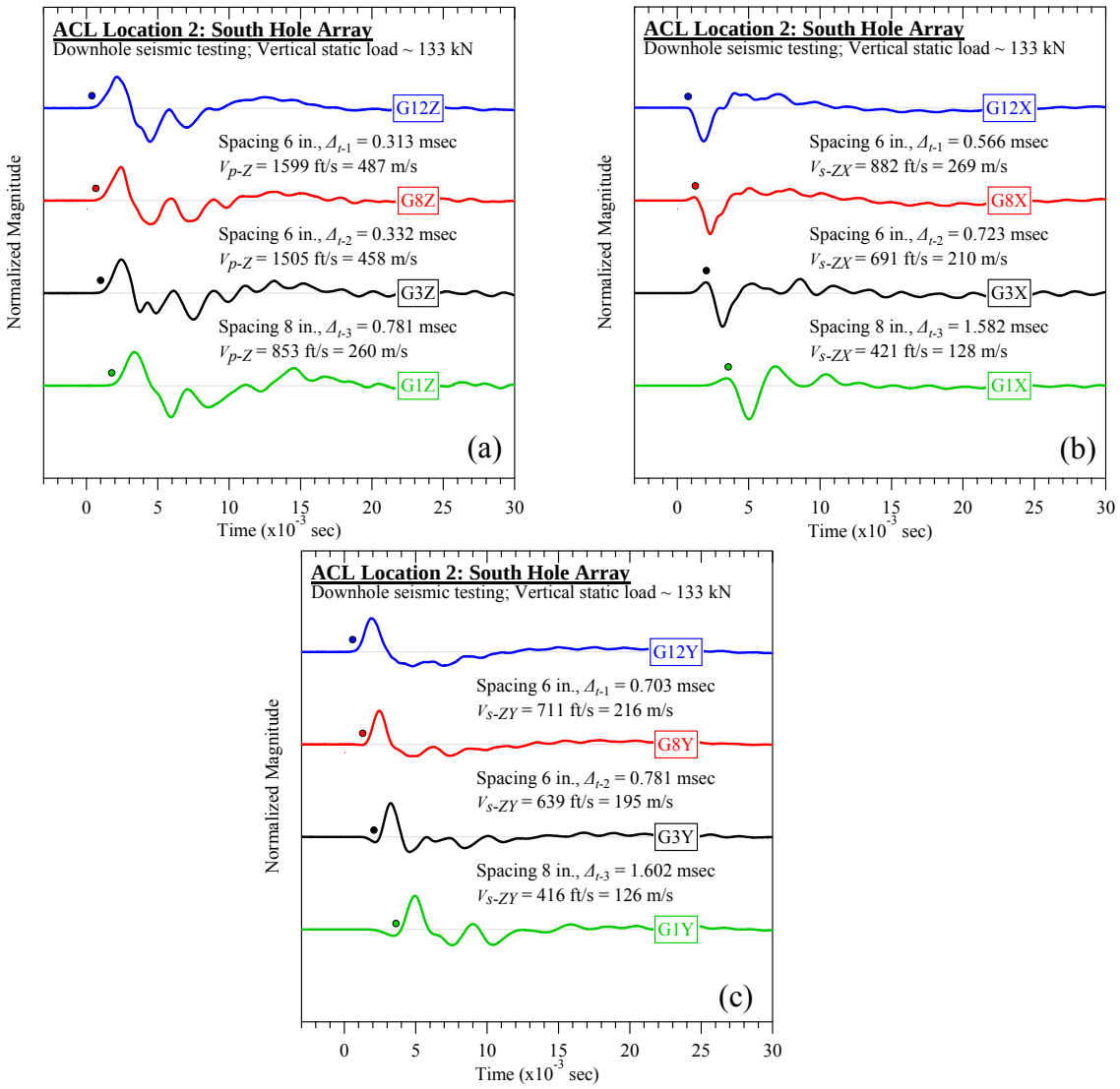

Figure A-60. Austin Community Landfill #2 (south hole): Downhole seismic testing at vertical load of 133 kN: (a) $V_{p\text{-}Z}$, (b) $V_{s\text{-}ZX}$, and (c) $V_{s\text{-}ZY}$.

A.2.2 Crosshole Seismic Testing

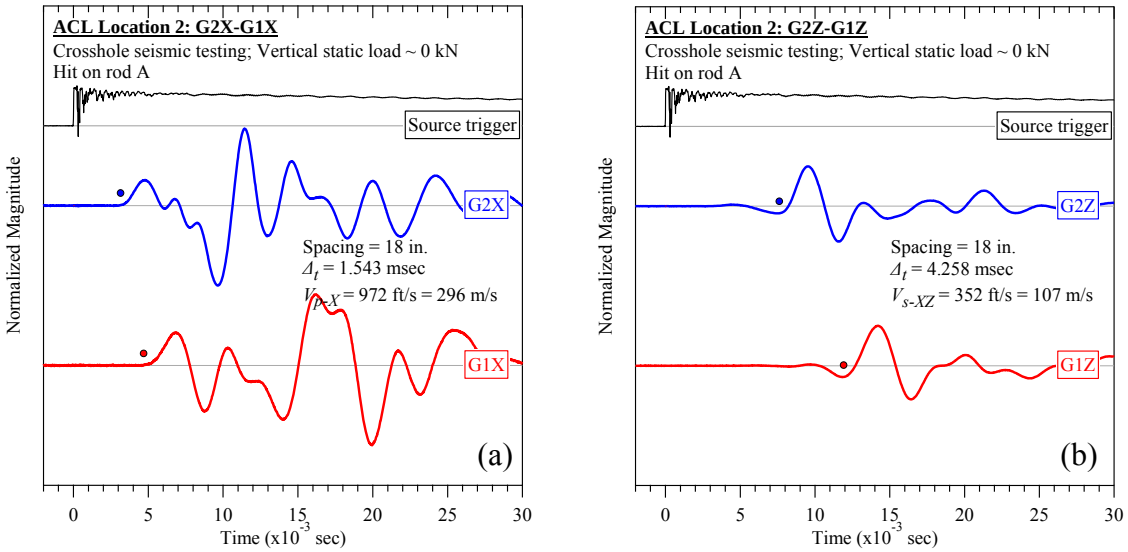

Figure A-61. Austin Community Landfill #2 (rod A): Crosshole seismic testing at vertical load of 0 kN: (a) $V_{p\text{-}X}$ and (b) $V_{s\text{-}XZ}$.

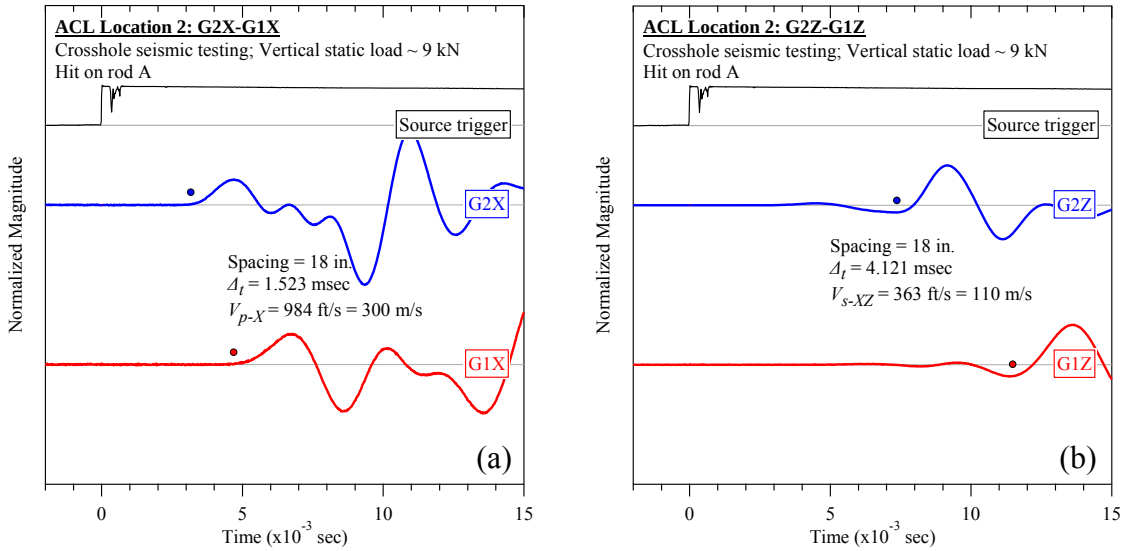

Figure A-62. Austin Community Landfill #2 (rod A): Crosshole seismic testing at vertical load of 9 kN: (a) $V_{p\text{-}X}$ and (b) $V_{s\text{-}XZ}$.

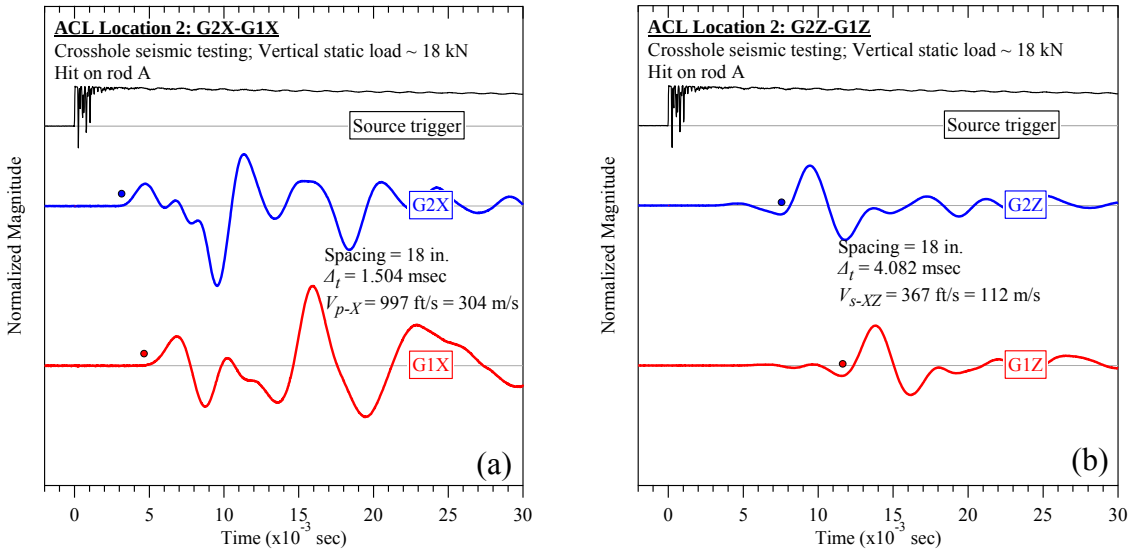

Figure A-63. Austin Community Landfill #2 (rod A): Crosshole seismic testing at vertical load of 18 kN: (a) $V_{p\text{-}X}$ and (b) $V_{s\text{-}XZ}$.

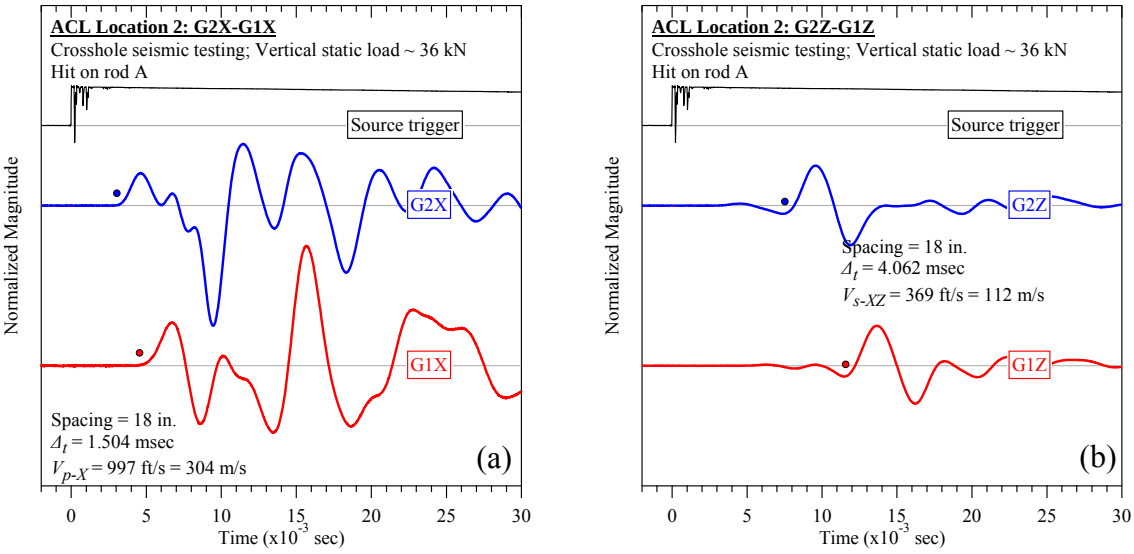

Figure A-64. Austin Community Landfill #2 (rod A): Crosshole seismic testing at vertical load of 36 kN: (a) $V_{p\text{-}X}$ and (b) $V_{s\text{-}XZ}$.

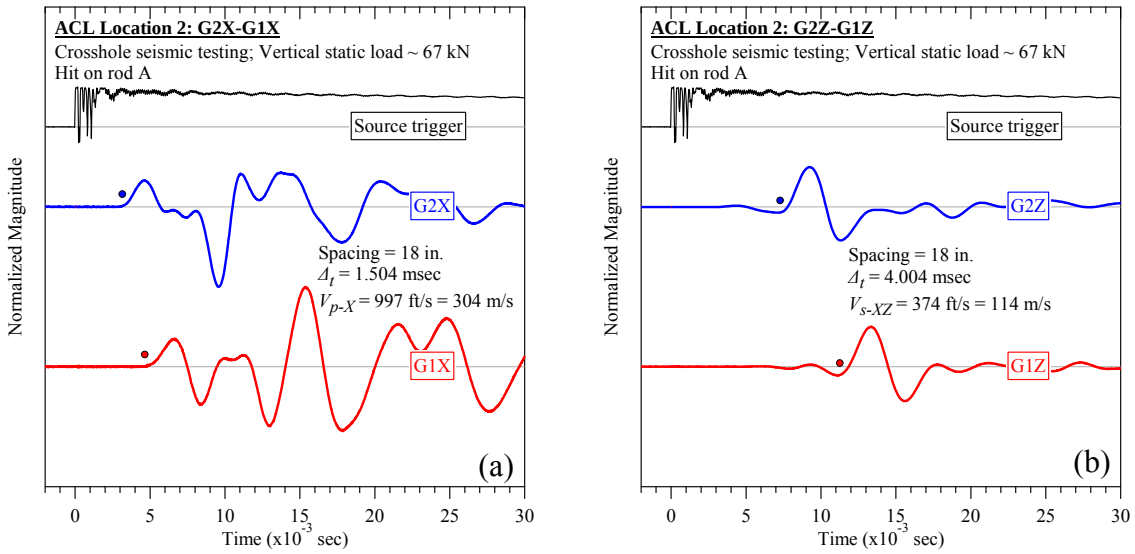

Figure A-65. Austin Community Landfill #2 (rod A): Crosshole seismic testing at vertical load of 67 kN: (a) $V_{p\text{-}X}$ and (b) $V_{s\text{-}XZ}$.

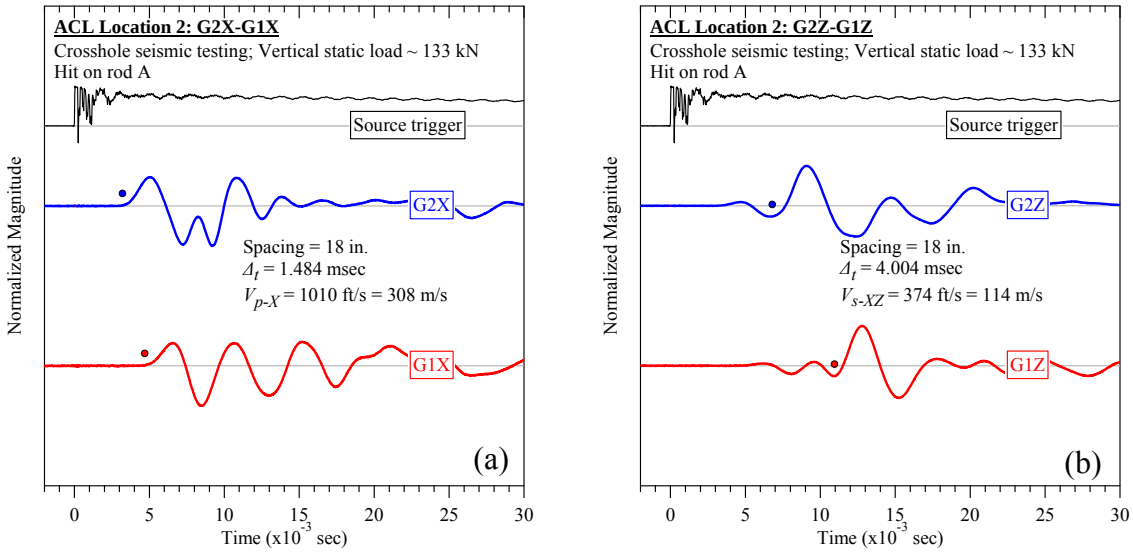

Figure A-66. Austin Community Landfill #2 (rod A): Crosshole seismic testing at vertical load of 133 kN: (a) $V_{p\text{-}X}$ and (b) $V_{s\text{-}XZ}$.

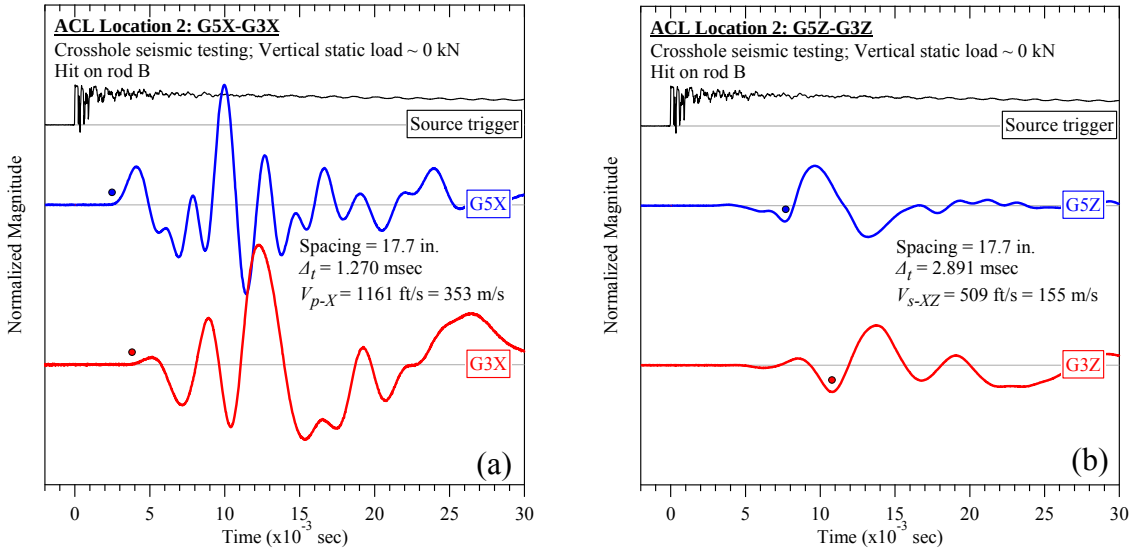

Figure A-67. Austin Community Landfill #2 (rod B): Crosshole seismic testing at vertical load of 0 kN: (a) $V_{p\text{-}X}$ and (b) $V_{s\text{-}XZ}$.

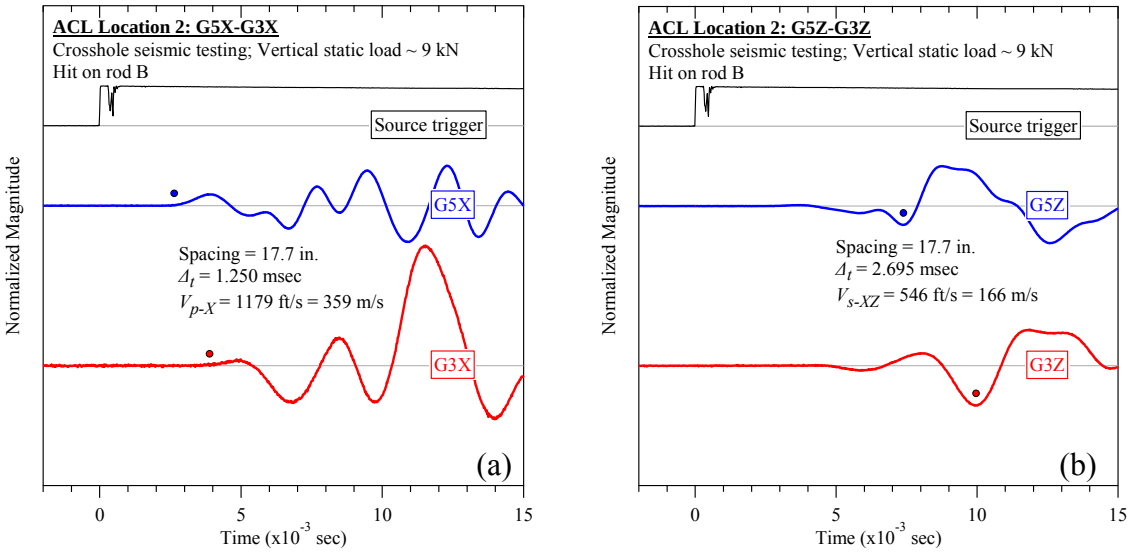

Figure A-68. Austin Community Landfill #2 (rod B): Crosshole seismic testing at vertical load of 9 kN: (a) $V_{p\text{-}X}$ and (b) $V_{s\text{-}XZ}$.

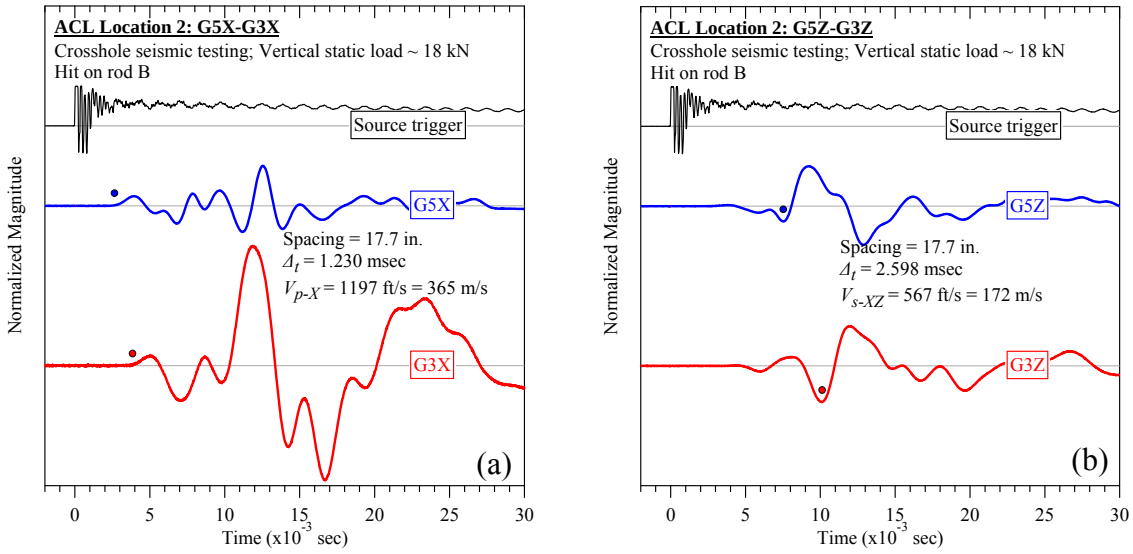

Figure A-69. Austin Community Landfill #2 (rod B): Crosshole seismic testing at vertical load of 18 kN: (a) $V_{p\text{-}X}$ and (b) $V_{s\text{-}XZ}$.

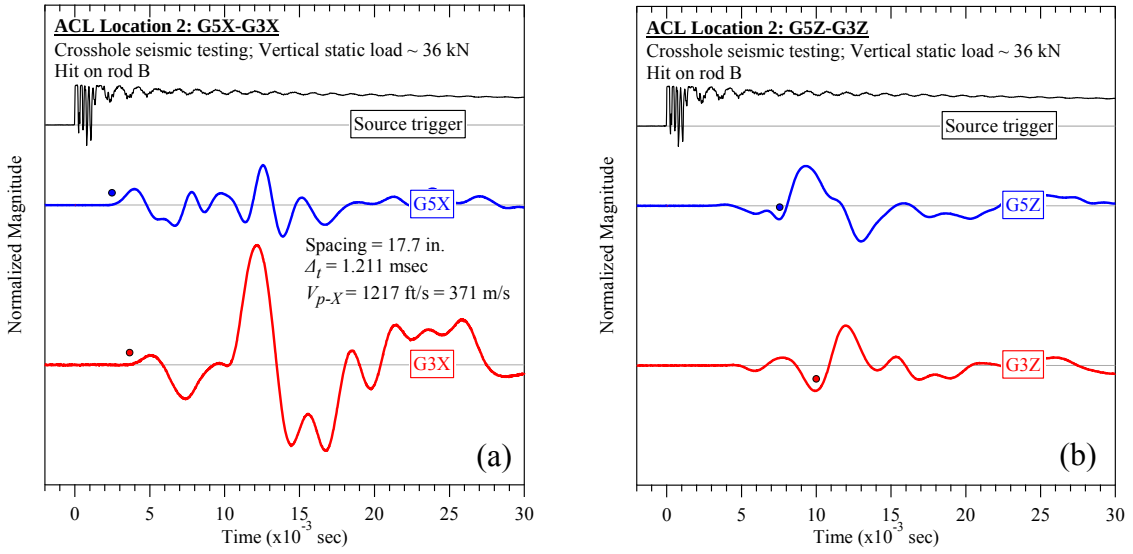

Figure A-70. Austin Community Landfill #2 (rod B): Crosshole seismic testing at vertical load of 36 kN: (a) $V_{p\text{-}X}$ and (b) $V_{s\text{-}XZ}$.

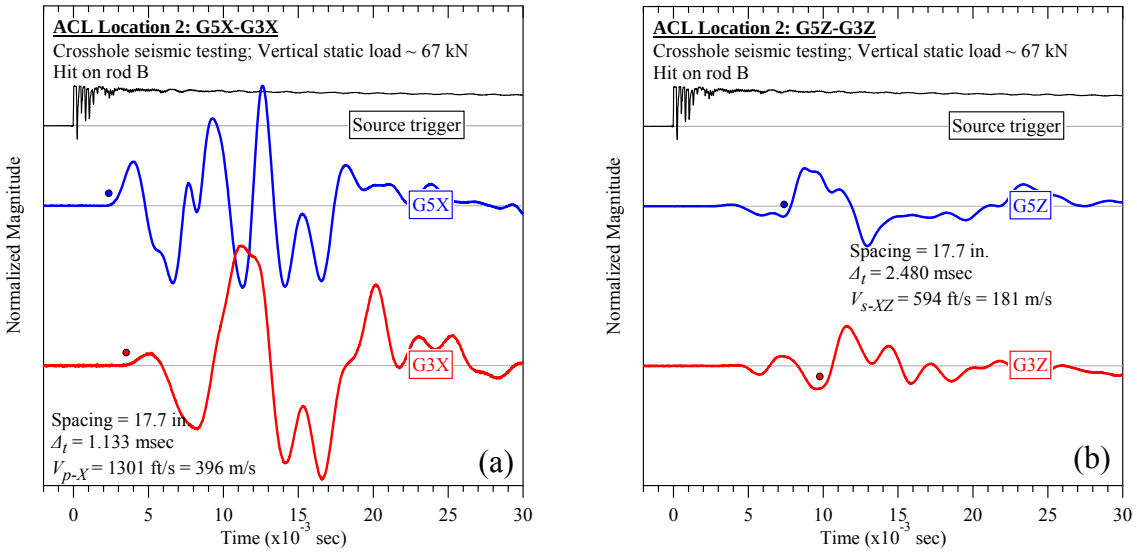

Figure A-71. Austin Community Landfill #2 (rod B): Crosshole seismic testing at vertical load of 67 kN: (a) $V_{p\text{-}X}$ and (b) $V_{s\text{-}XZ}$.

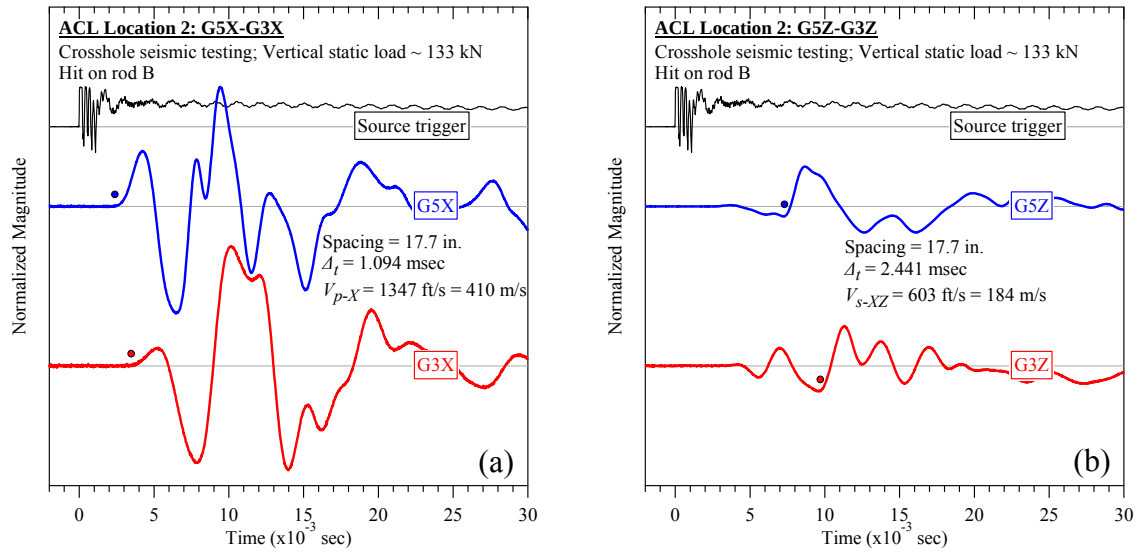

Figure A-72. Austin Community Landfill #2 (rod B): Crosshole seismic testing at vertical load of 133 kN: (a) $V_{p\text{-}X}$ and (b) $V_{s\text{-}XZ}$.

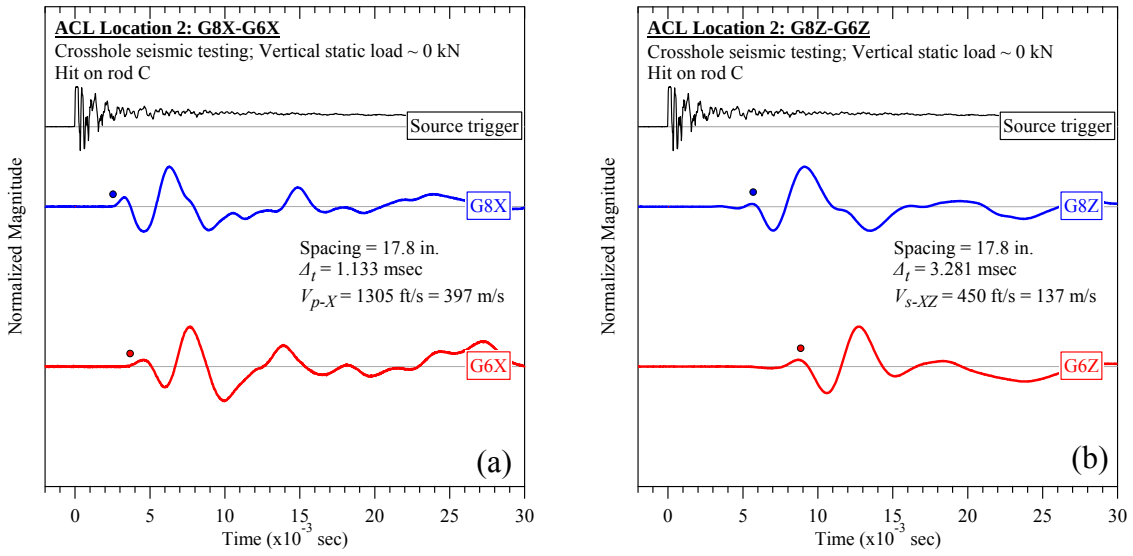

Figure A-73. Austin Community Landfill #2 (rod C): Crosshole seismic testing at vertical load of 0 kN: (a) $V_{p\text{-}X}$ and (b) $V_{s\text{-}XZ}$.

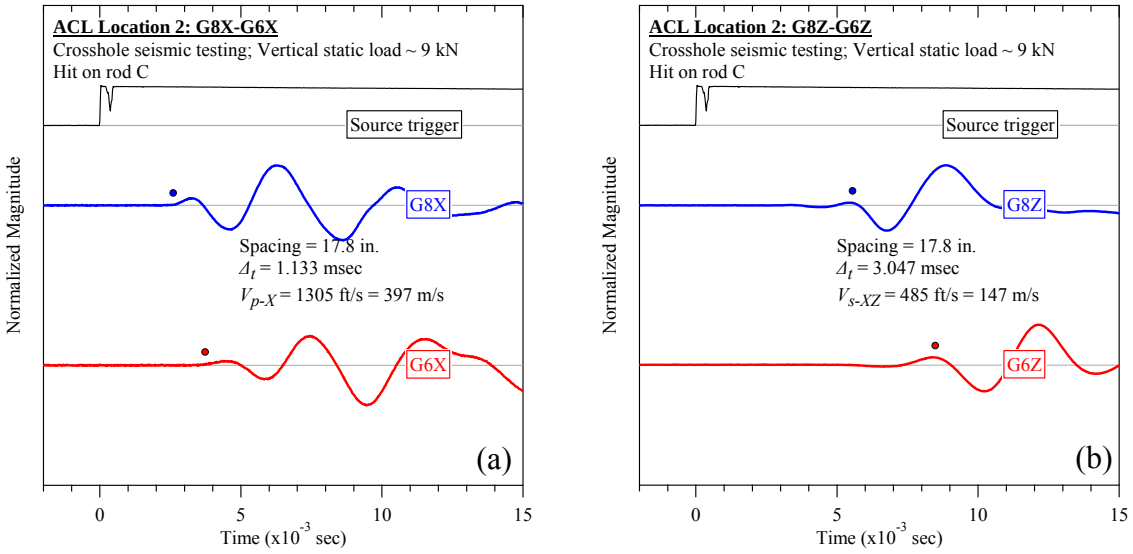

Figure A-74. Austin Community Landfill #2 (rod C): Crosshole seismic testing at vertical load of 9 kN: (a) $V_{p\text{-}X}$ and (b) $V_{s\text{-}XZ}$.

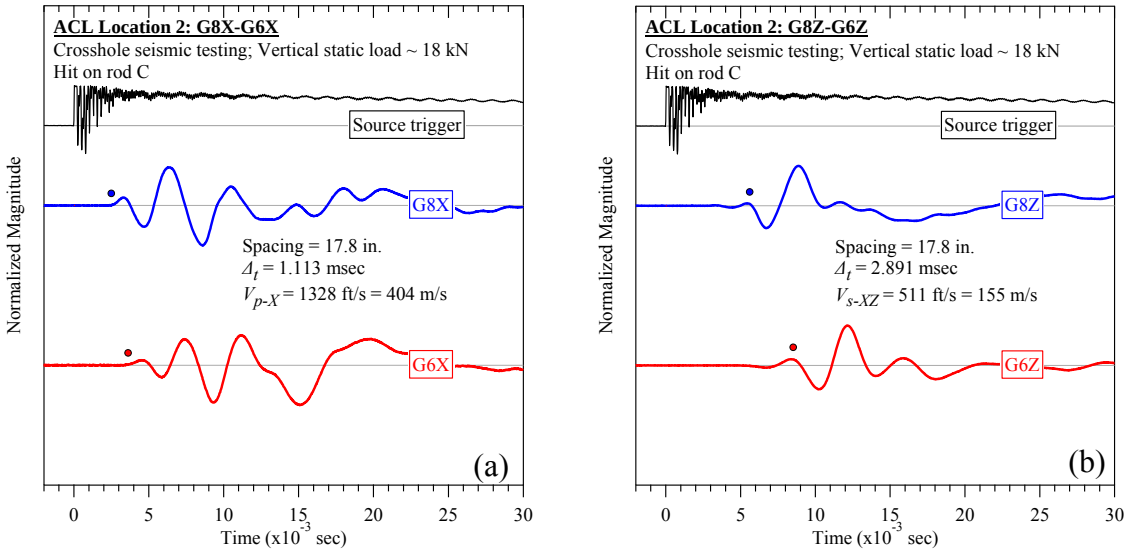

Figure A-75. Austin Community Landfill #2 (rod C): Crosshole seismic testing at vertical load of 18 kN: (a) $V_{p\text{-}X}$ and (b) $V_{s\text{-}XZ}$.

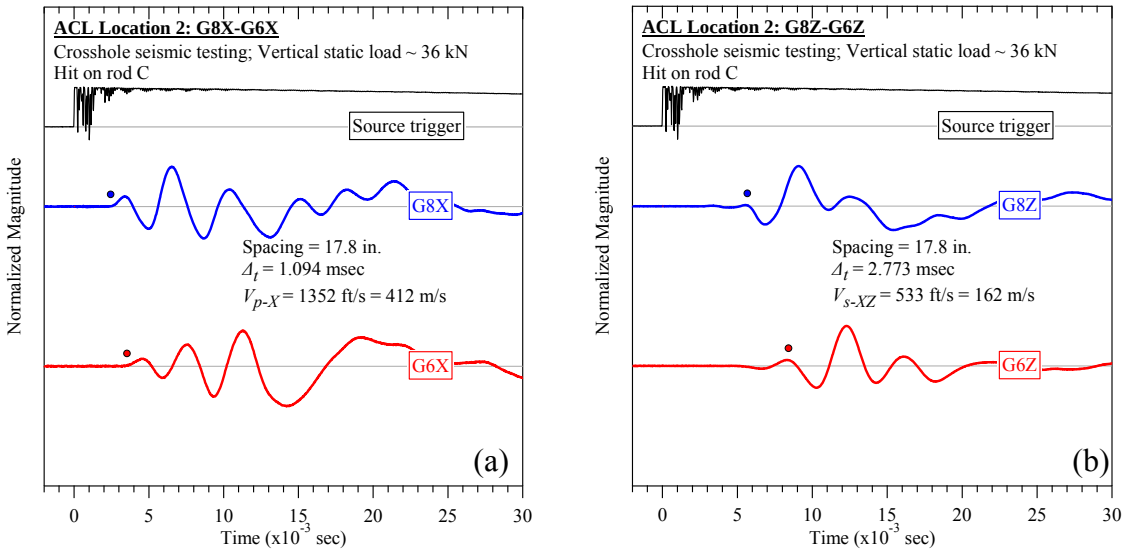

Figure A-76. Austin Community Landfill #2 (rod C): Crosshole seismic testing at vertical load of 36 kN: (a) $V_{p\text{-}X}$ and (b) $V_{s\text{-}XZ}$.

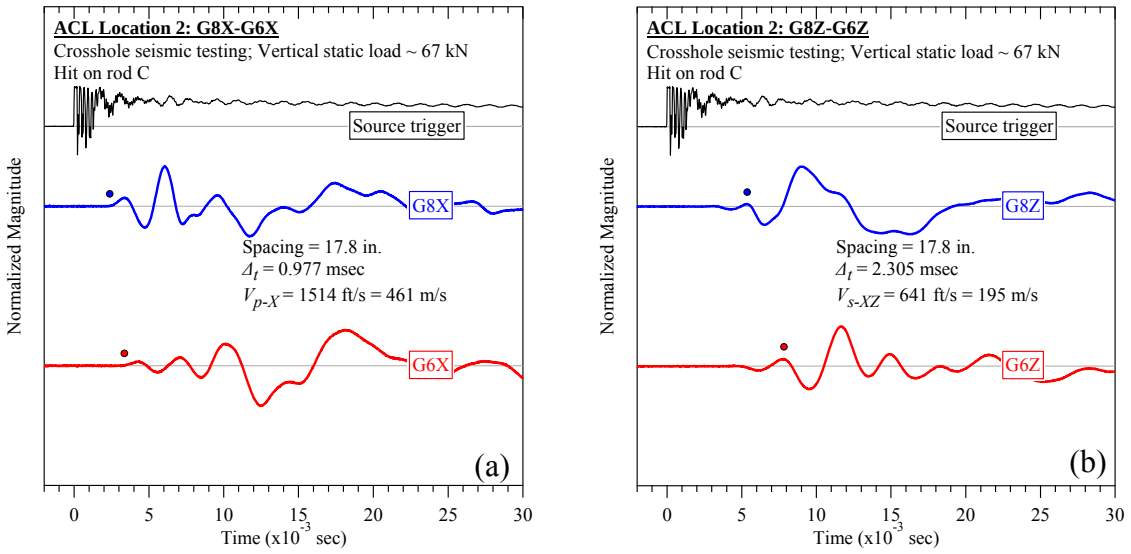

Figure A-77. Austin Community Landfill #2 (rod C): Crosshole seismic testing at vertical load of 67 kN: (a) $V_{p\text{-}X}$ and (b) $V_{s\text{-}XZ}$.

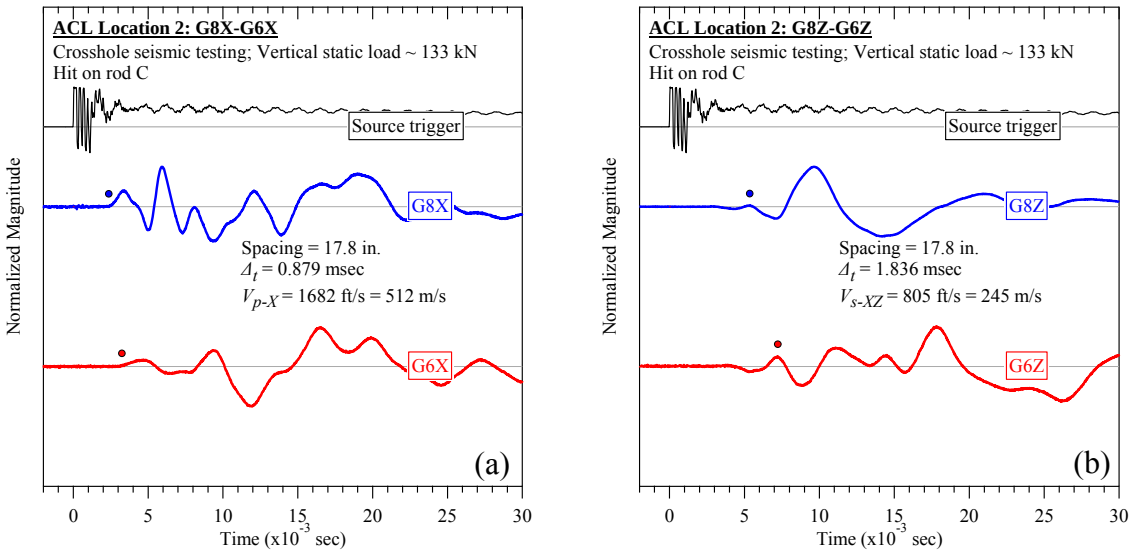

Figure A-78. Austin Community Landfill #2 (rod C): Crosshole seismic testing at vertical load of 133 kN: (a) $V_{p\text{-}X}$ and (b) $V_{s\text{-}XZ}$.

A.2.3 Steady-state Dynamic Testing

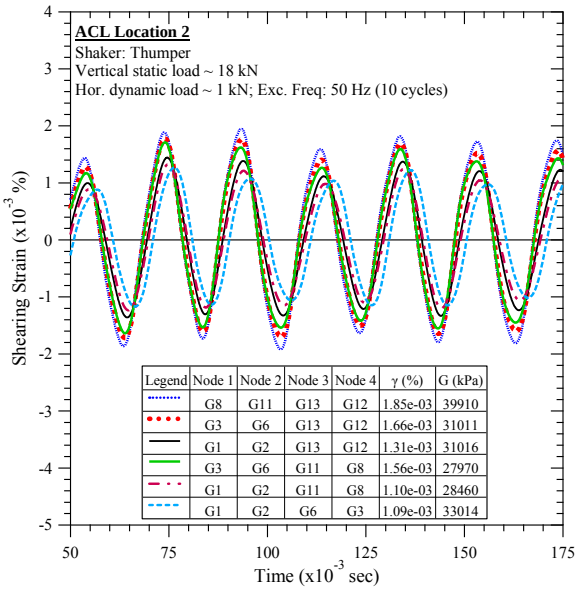

Figure A-79. Austin Community Landfill #2: Steady-state dynamic testing at vertical load of 18 kN and horizontal dynamic load of 1 kN.

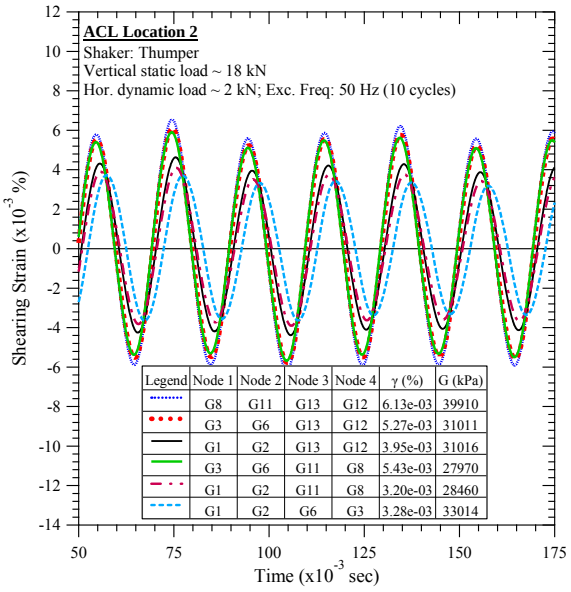

Figure A-80. Austin Community Landfill #2: Steady-state dynamic testing at vertical load of 18 kN and horizontal dynamic load of 2 kN.

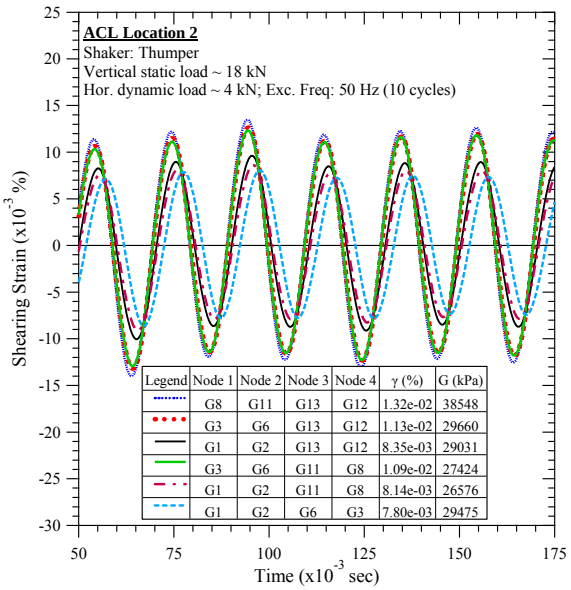

Figure A-81. Austin Community Landfill #2: Steady-state dynamic testing at vertical load of 18 kN and horizontal dynamic load of 4 kN.

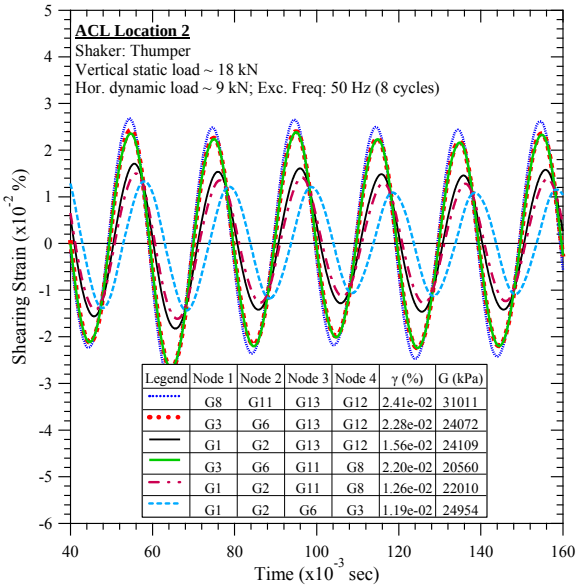

Figure A-82. Austin Community Landfill #2: Steady-state dynamic testing at vertical load of 18 kN and horizontal dynamic load of 9 kN.

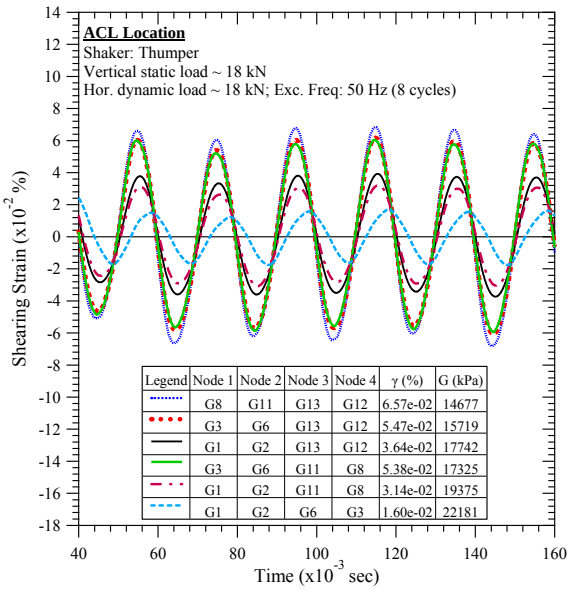

Figure A-83. Austin Community Landfill #2: Steady-state dynamic testing at vertical load of 18 kN and horizontal dynamic load of 18 kN.

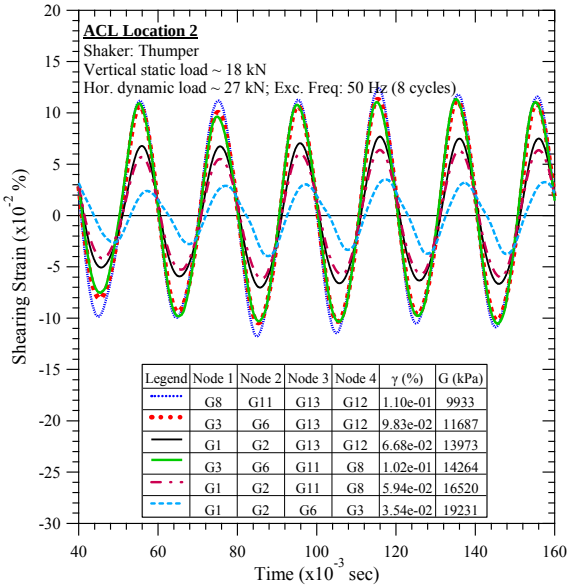

Figure A-84. Austin Community Landfill #2: Steady-state dynamic testing at vertical load of 18 kN and horizontal dynamic load of 27 kN.

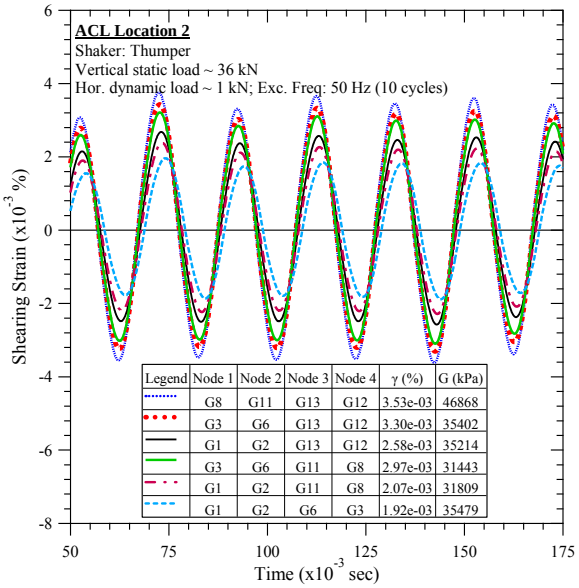

Figure A-85. Austin Community Landfill #2: Steady-state dynamic testing at vertical load of 36 kN and horizontal dynamic load of 1 kN.

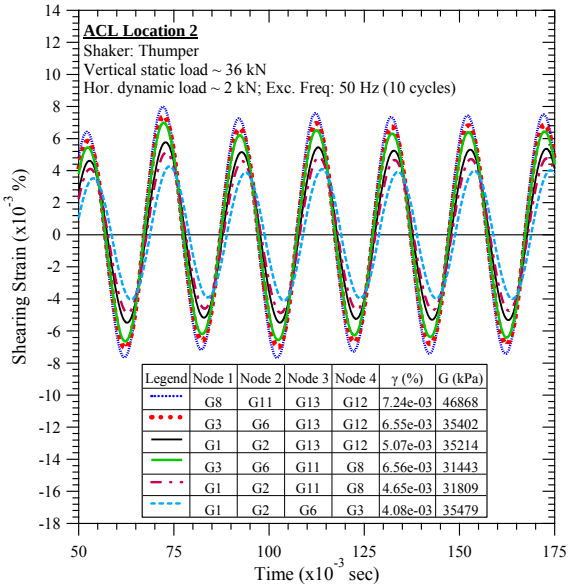

Figure A-86. Austin Community Landfill #2: Steady-state dynamic testing at vertical load of 36 kN and horizontal dynamic load of 2 kN.

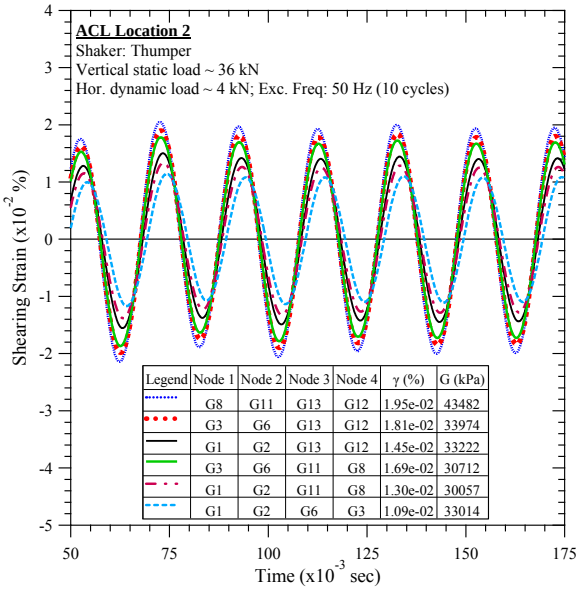

Figure A-87. Austin Community Landfill #2: Steady-state dynamic testing at vertical load of 36 kN and horizontal dynamic load of 4 kN.

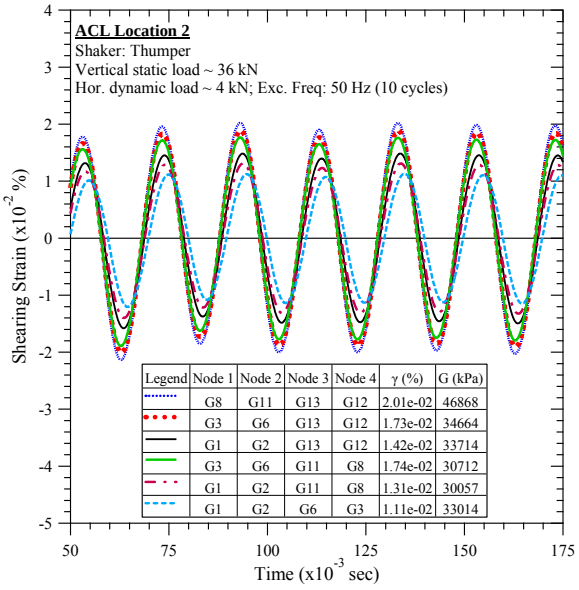

Figure A-88. Austin Community Landfill #2: Steady-state dynamic testing at vertical load of 36 kN and horizontal dynamic load of 4 kN.

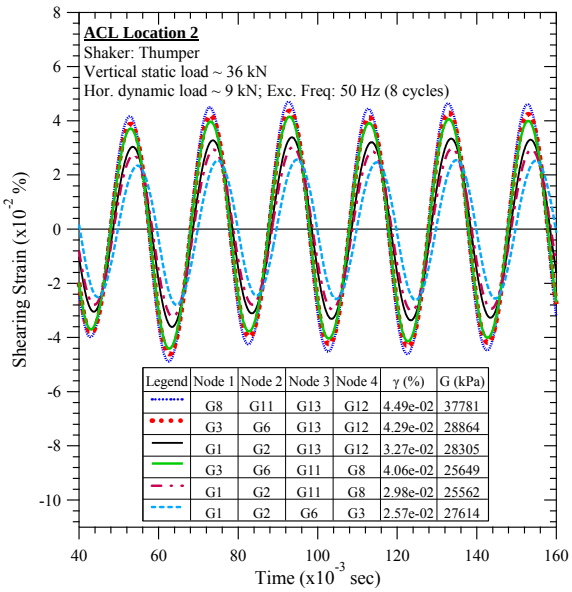

Figure A-89. Austin Community Landfill #2: Steady-state dynamic testing at vertical load of 36 kN and horizontal dynamic load of 9 kN.

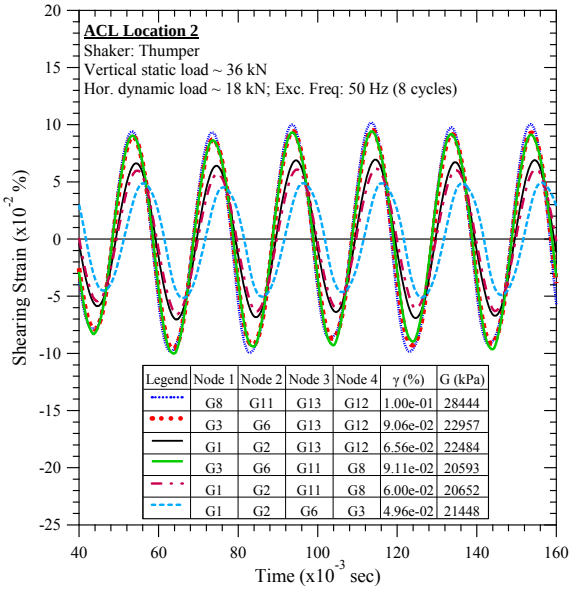

Figure A-90. Austin Community Landfill #2: Steady-state dynamic testing at vertical load of 36 kN and horizontal dynamic load of 18 kN.

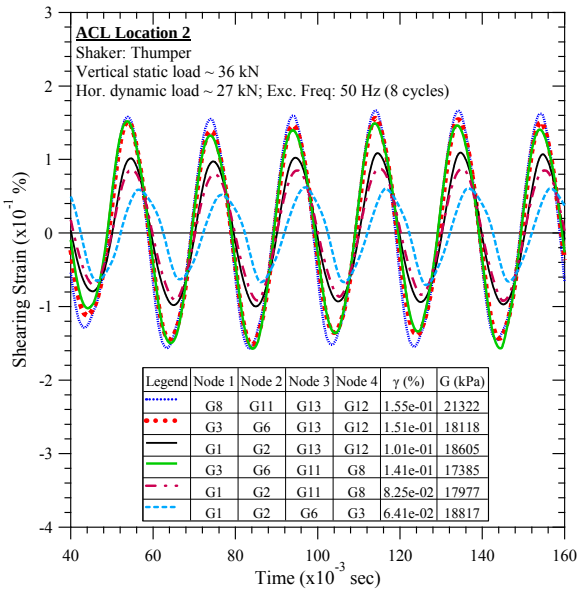

Figure A-91. Austin Community Landfill #2: Steady-state dynamic testing at vertical load of 36 kN and horizontal dynamic load of 27 kN.

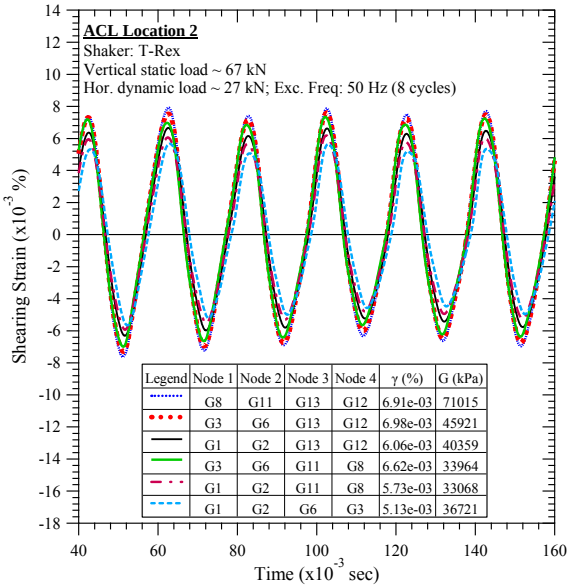

Figure A-92. Austin Community Landfill #2: Steady-state dynamic testing at vertical load of 67 kN and horizontal dynamic load of 27 kN.

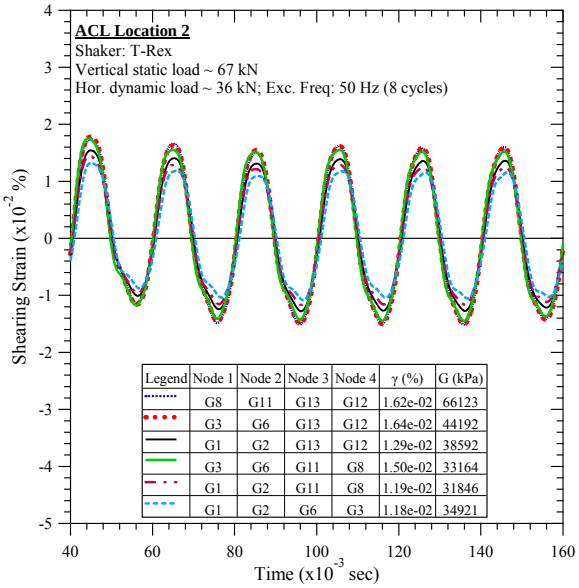

Figure A-93. Austin Community Landfill #2: Steady-state dynamic testing at vertical load of 67 kN and horizontal dynamic load of 36 kN.

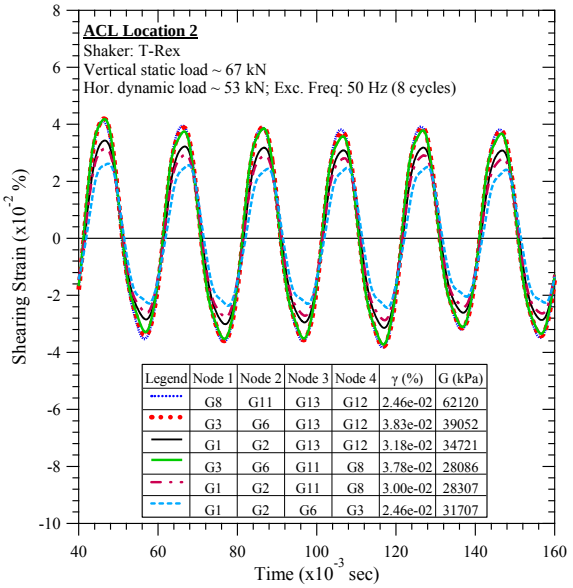

Figure A-94. Austin Community Landfill #2: Steady-state dynamic testing at vertical load of 67 kN and horizontal dynamic load of 53 kN.

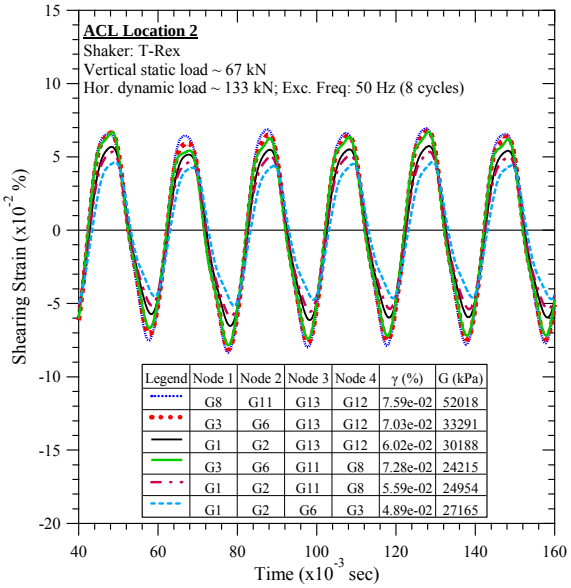

Figure A-95. Austin Community Landfill #2: Steady-state dynamic testing at vertical load of 67 kN and horizontal dynamic load of 133 kN.

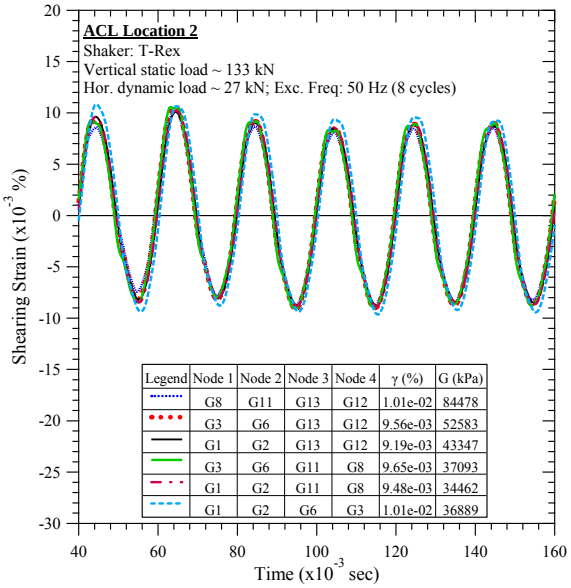

Figure A-96. Austin Community Landfill #2: Steady-state dynamic testing at vertical load of 133 kN and horizontal dynamic load of 27 kN.

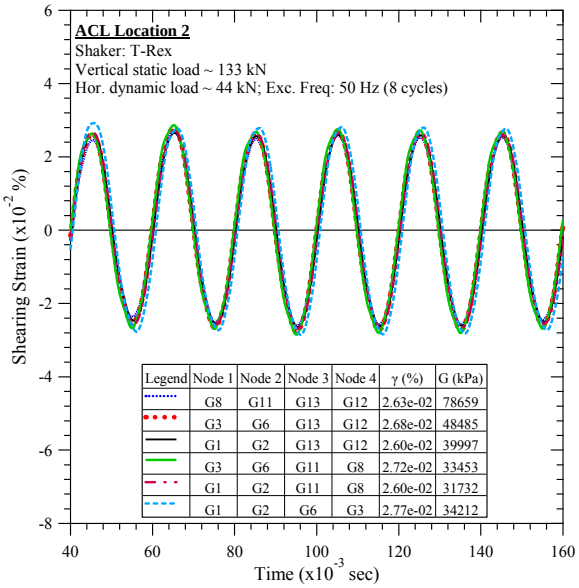

Figure A-97. Austin Community Landfill #2: Steady-state dynamic testing at vertical load of 133 kN and horizontal dynamic load of 44 kN.

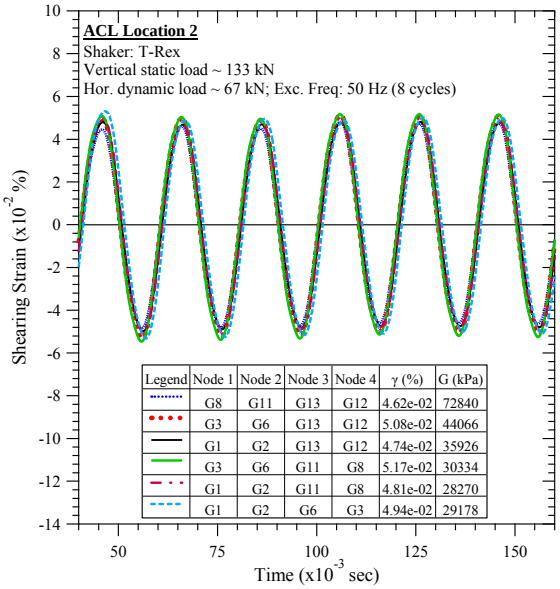

Figure A-98. Austin Community Landfill #2: Steady-state dynamic testing at vertical load of 133 kN and horizontal dynamic load of 67 kN.

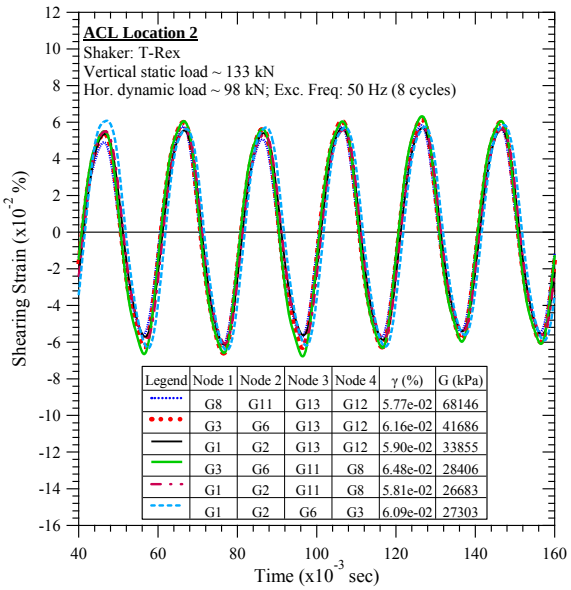

Figure A-99. Austin Community Landfill #2: Steady-state dynamic testing at vertical load of 133 kN and horizontal dynamic load of 98 kN.

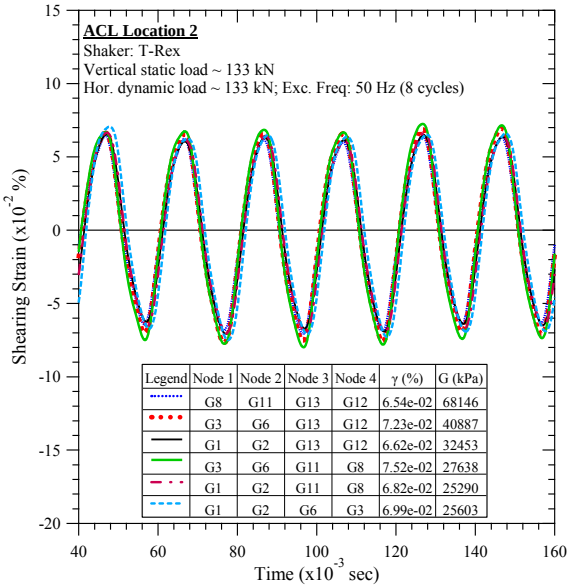

Figure A-100. Austin Community Landfill #2: Steady-state dynamic testing at vertical load of 133 kN and horizontal dynamic load of 133 kN.

B Lamb Canyon Sanitary Landfill Testing Results

B.1 Lamb Canyon Sanitary Landfill Location 1

B.1.1 Downhole Seismic Testing

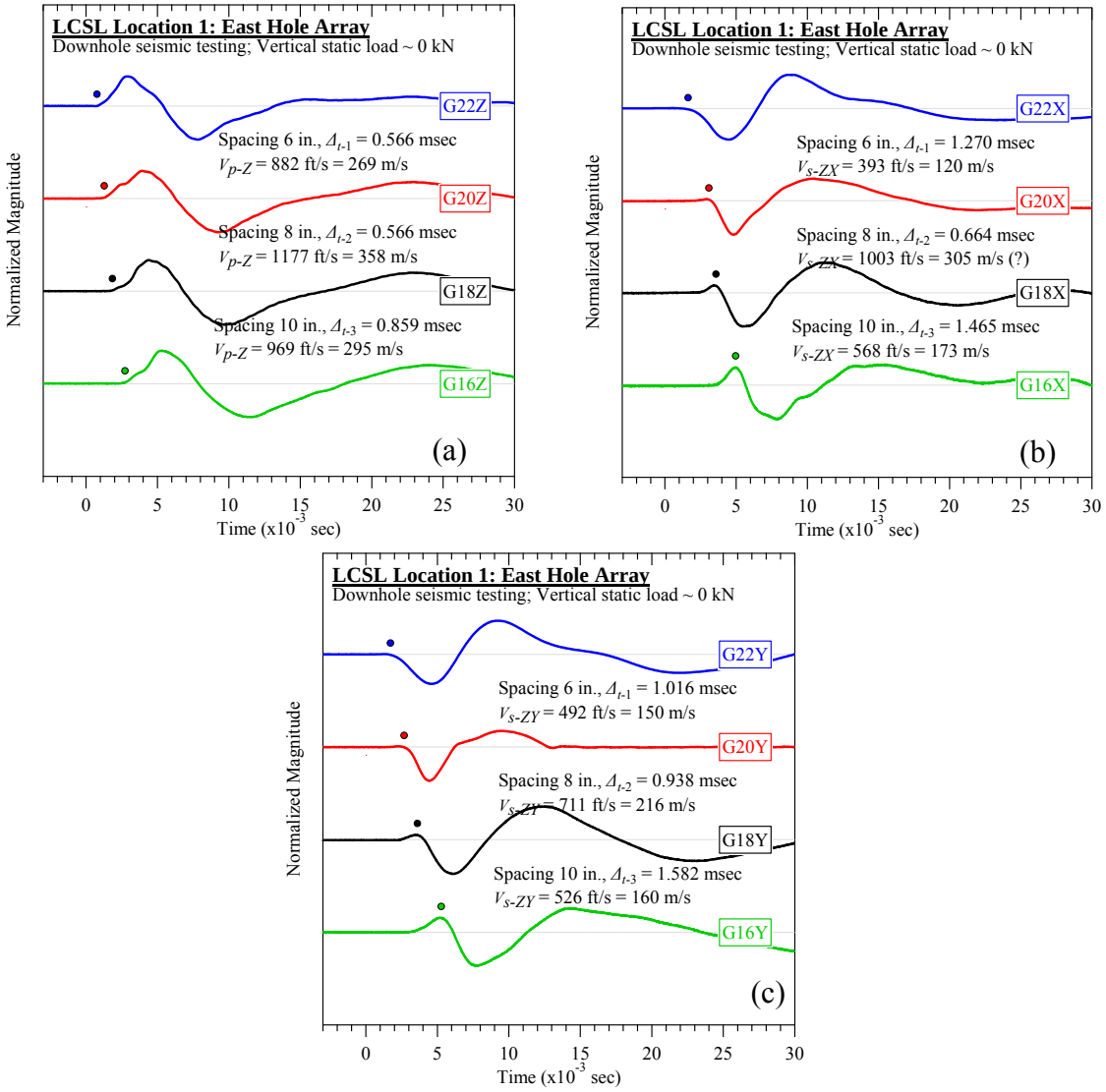

Figure B-1. Lamb Canyon Sanitary Landfill #1 (east hole): Downhole seismic testing at vertical load of 0 kN: (a) V_{p-Z}, (b) V_{s-ZX}, and (c) V_{s-ZY}.

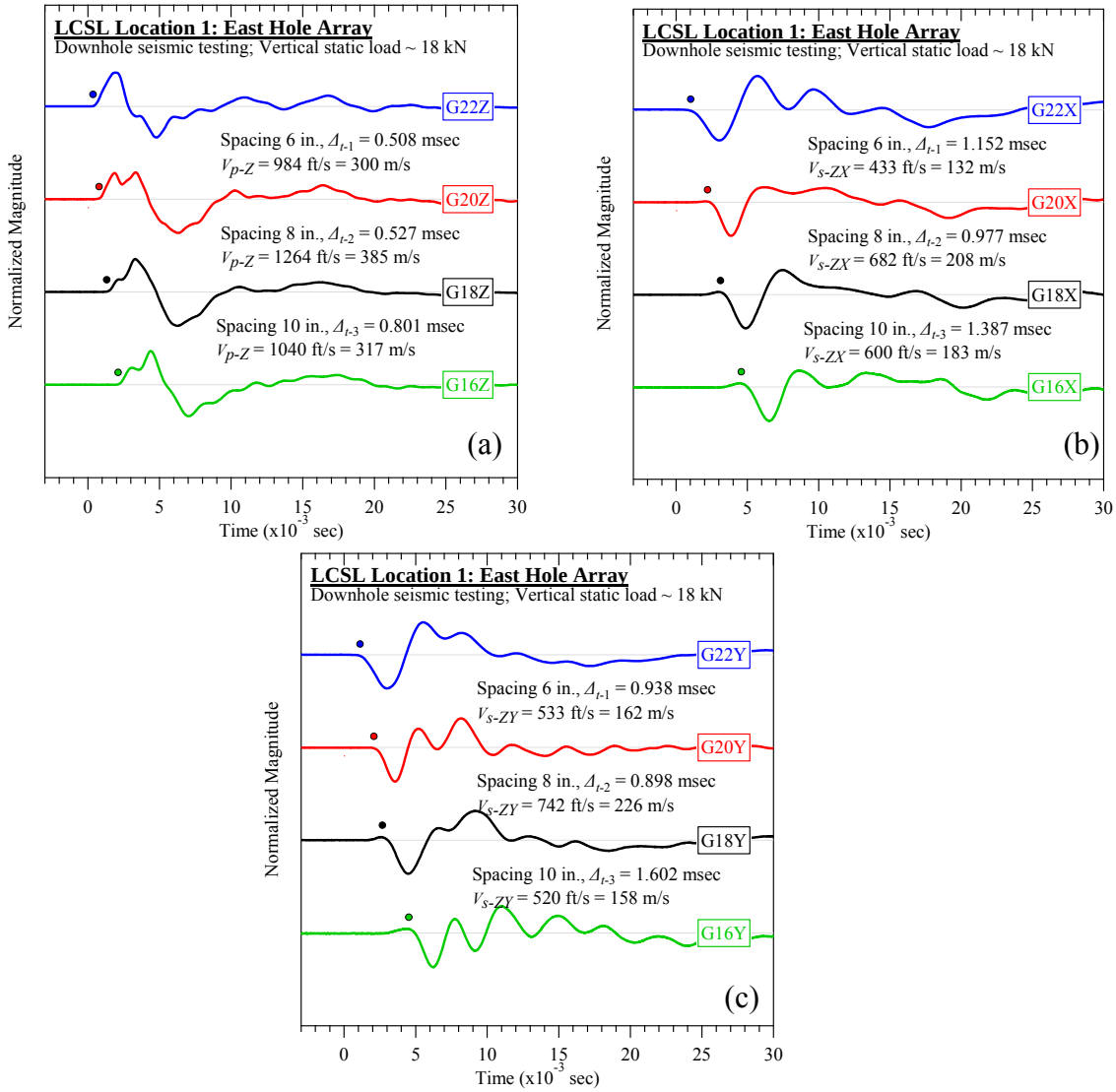

Figure B-2. Lamb Canyon Sanitary Landfill #1 (east hole): Downhole seismic testing at vertical load of 18 kN: (a) $V_{p\text{-}Z}$, (b) $V_{s\text{-}ZX}$, and (c) $V_{s\text{-}ZY}$.

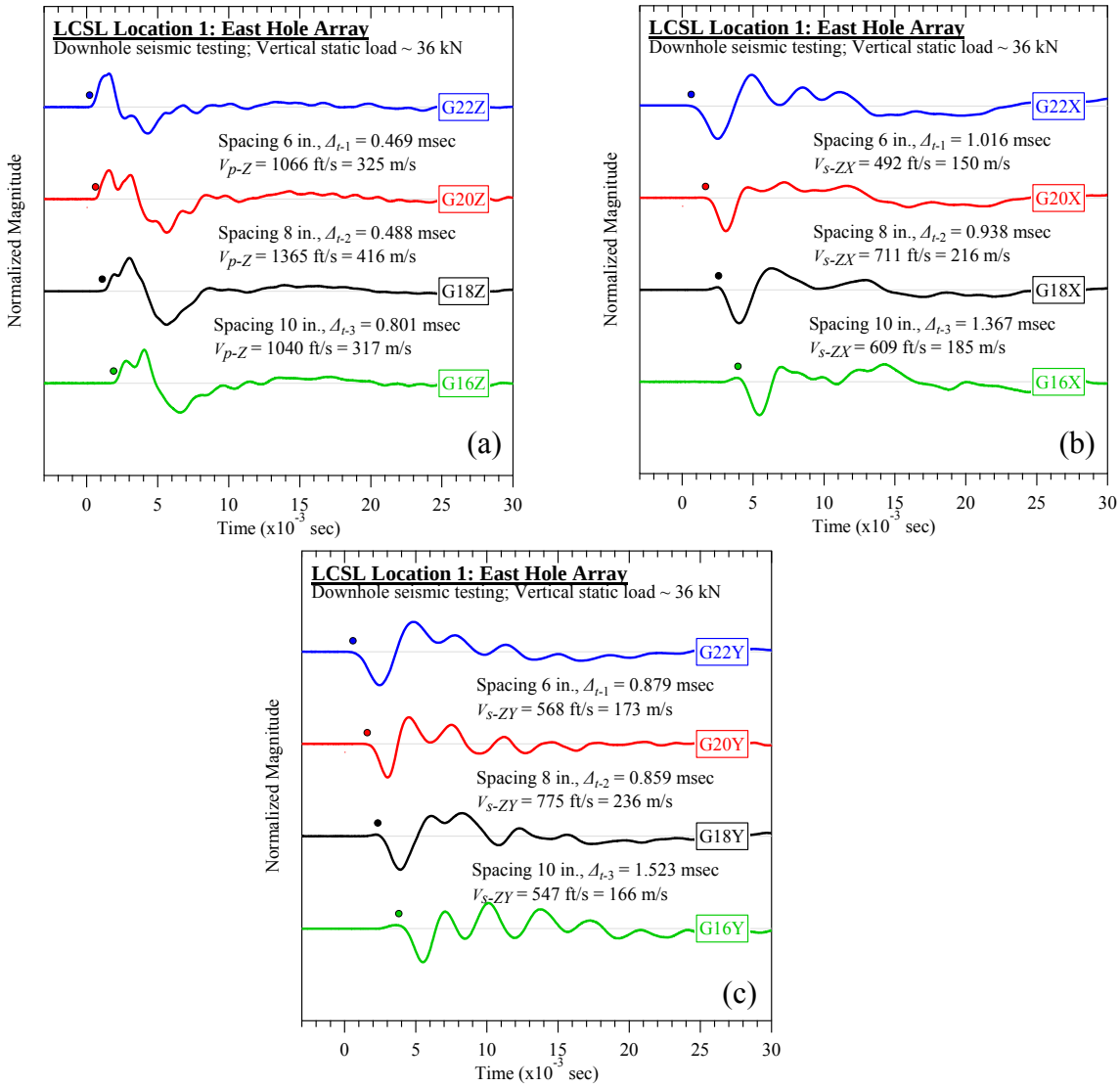

Figure B-3. Lamb Canyon Sanitary Landfill #1 (east hole): Downhole seismic testing at vertical load of 36 kN: (a) $V_{p\text{-}Z}$, (b) $V_{s\text{-}ZX}$, and (c) $V_{s\text{-}ZY}$.

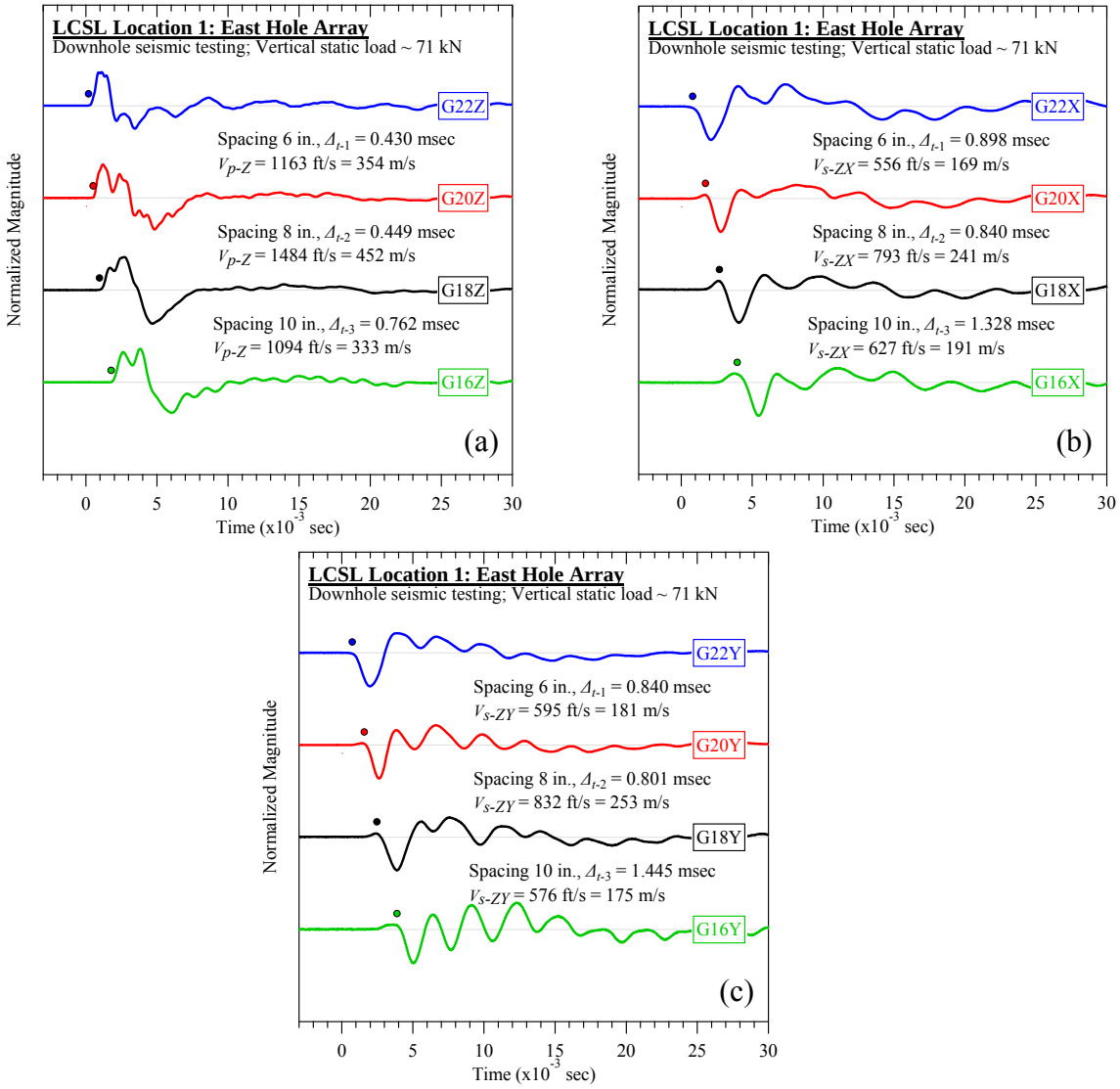

Figure B-4. Lamb Canyon Sanitary Landfill #1 (east hole): Downhole seismic testing at vertical load of 71 kN: (a) V_{p-Z}, (b) V_{s-ZX}, and (c) V_{s-ZY}.

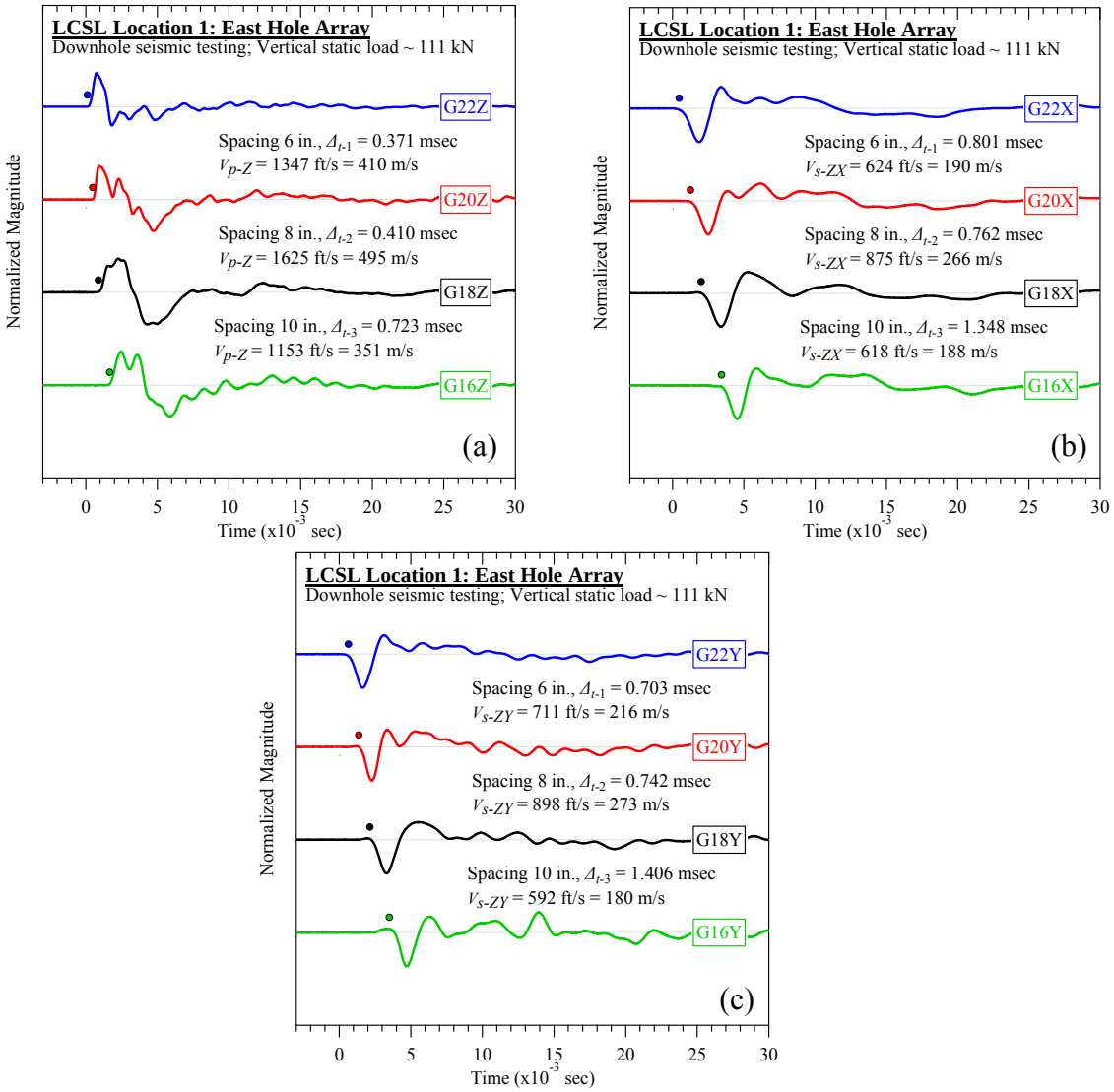

Figure B-5. Lamb Canyon Sanitary Landfill #1 (east hole): Downhole seismic testing at vertical load of 111 kN: (a) V_{p-Z}, (b) V_{s-ZX}, and (c) V_{s-ZY}.

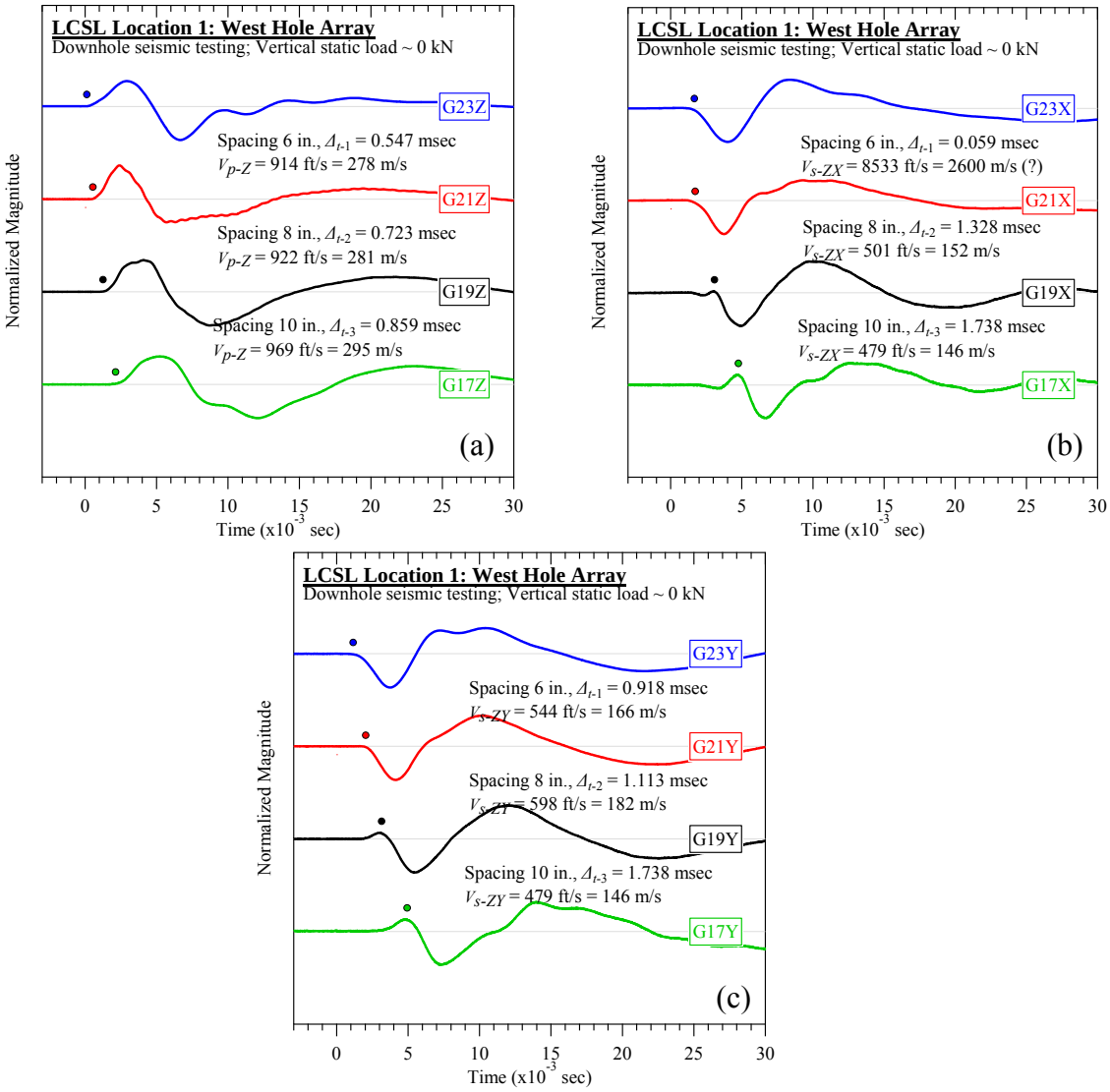

Figure B-6. Lamb Canyon Sanitary Landfill #1 (west hole): Downhole seismic testing at vertical load of 0 kN: (a) $V_{p\text{-}Z}$, (b) $V_{s\text{-}ZX}$, and (c) $V_{s\text{-}ZY}$.

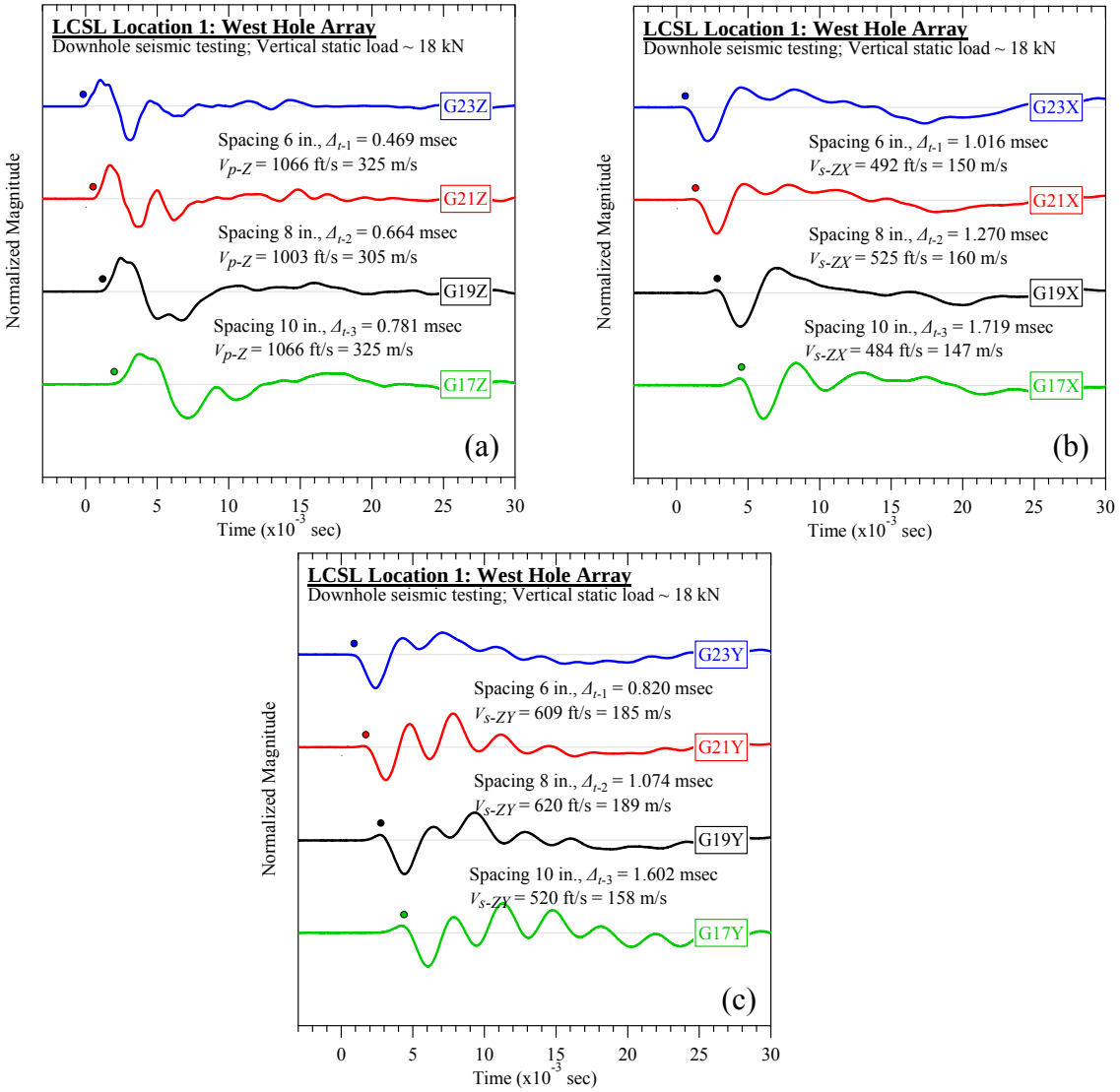

Figure B-7. Lamb Canyon Sanitary Landfill #1 (west hole): Downhole seismic testing at vertical load of 18 kN: (a) V_{p-Z}, (b) V_{s-ZX}, and (c) V_{s-ZY}.

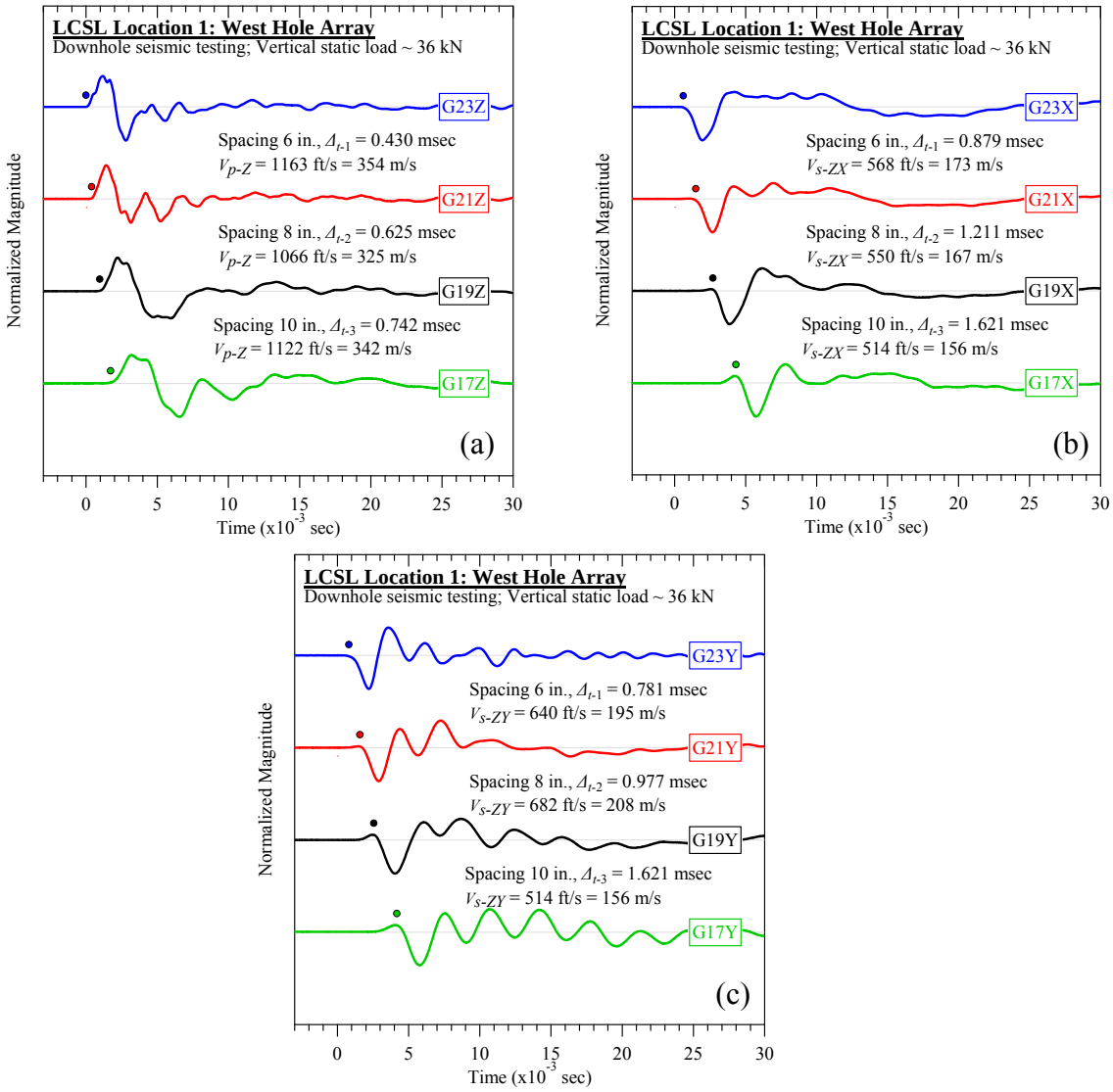

Figure B-8. Lamb Canyon Sanitary Landfill #1 (west hole): Downhole seismic testing at vertical load of 36 kN: (a) V_{p-Z}, (b) V_{s-ZX}, and (c) V_{s-ZY}.

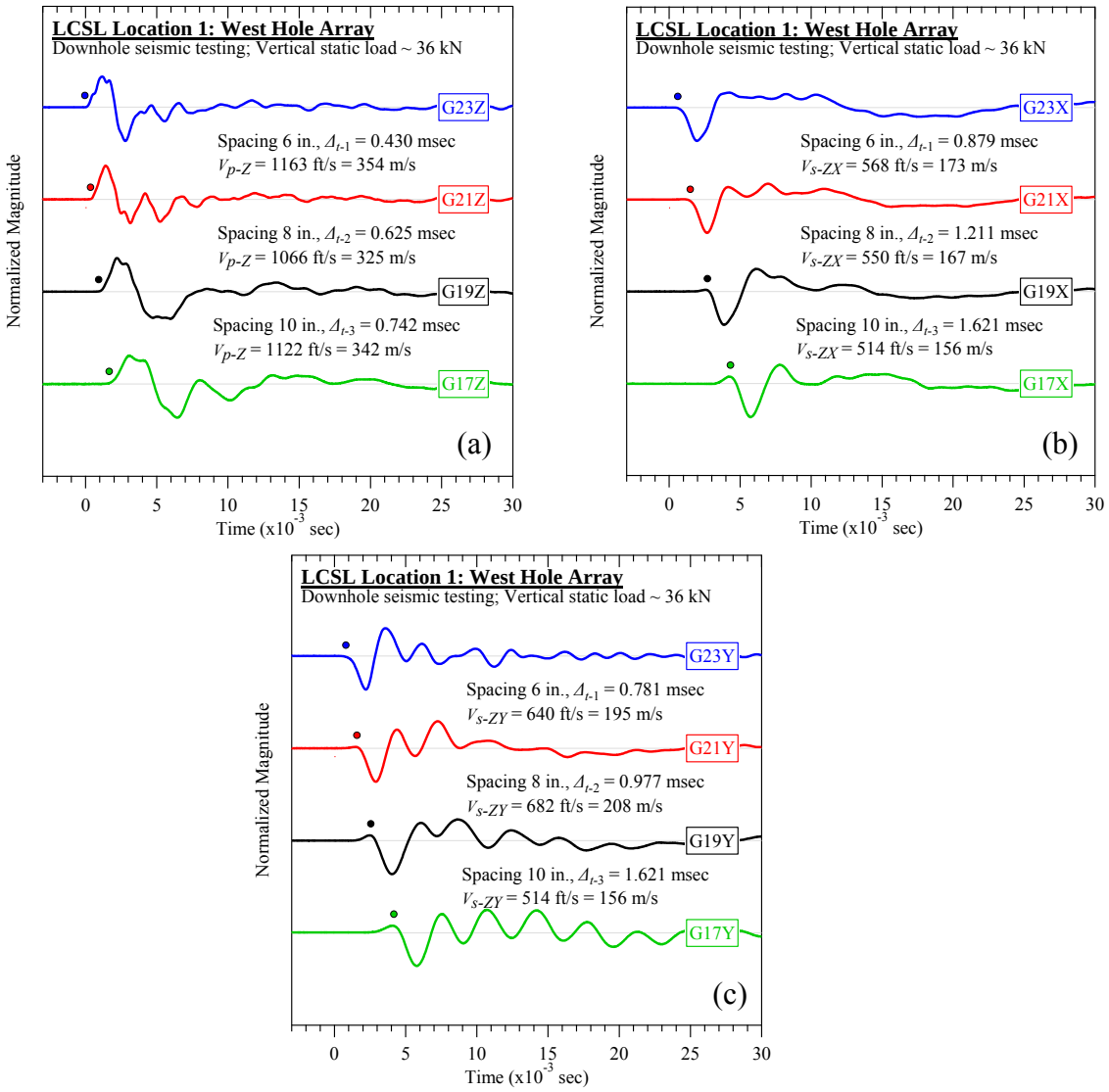

Figure B-9. Lamb Canyon Sanitary Landfill #1 (west hole): Downhole seismic testing at vertical load of 36 kN: (a) V_{p-Z}, (b) V_{s-ZX}, and (c) V_{s-ZY}.

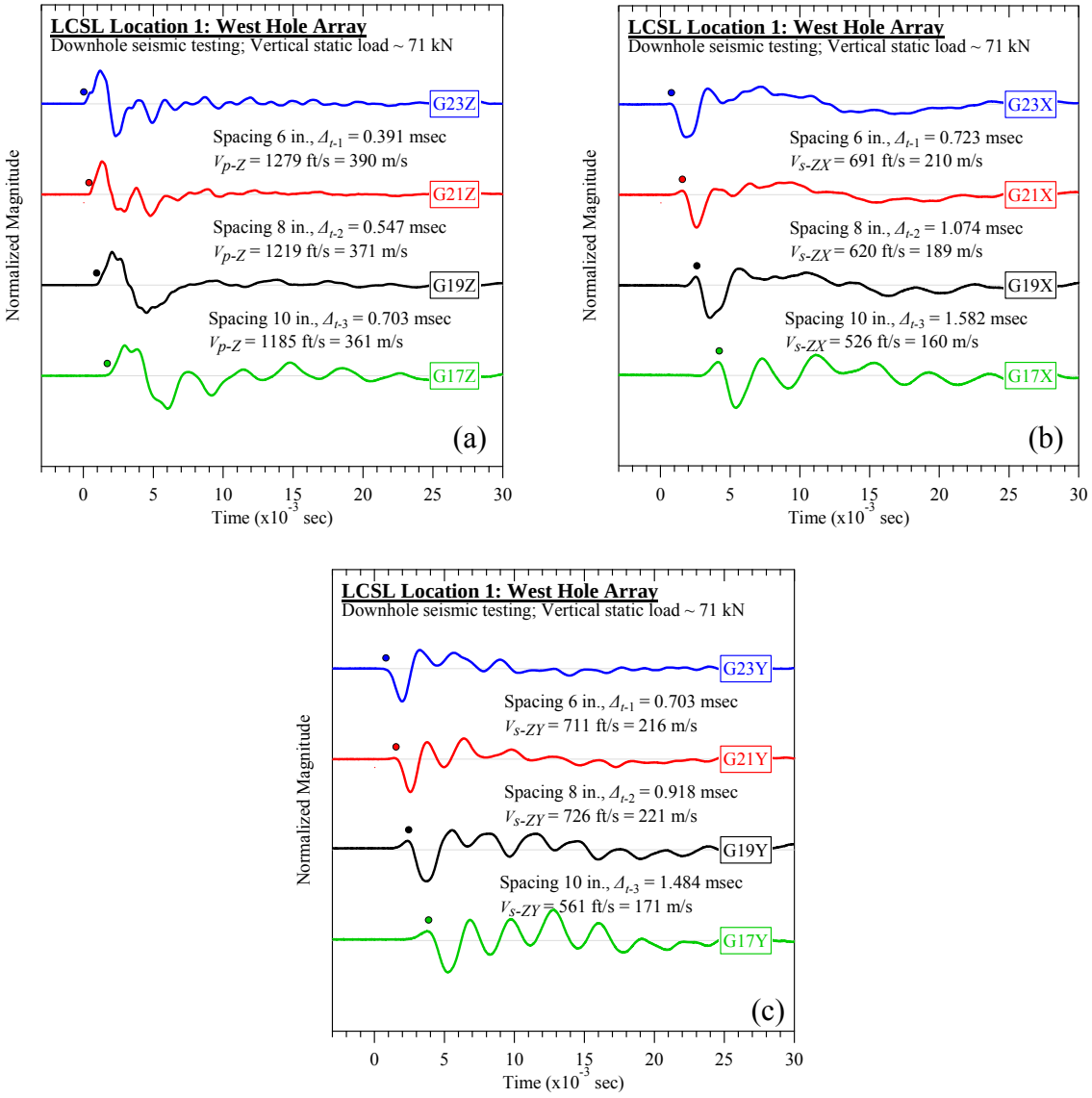

Figure B-10. Lamb Canyon Sanitary Landfill #1 (west hole): Downhole seismic testing at vertical load of 71 kN: (a) V_{p-Z}, (b) V_{s-ZX}, and (c) V_{s-ZY}.

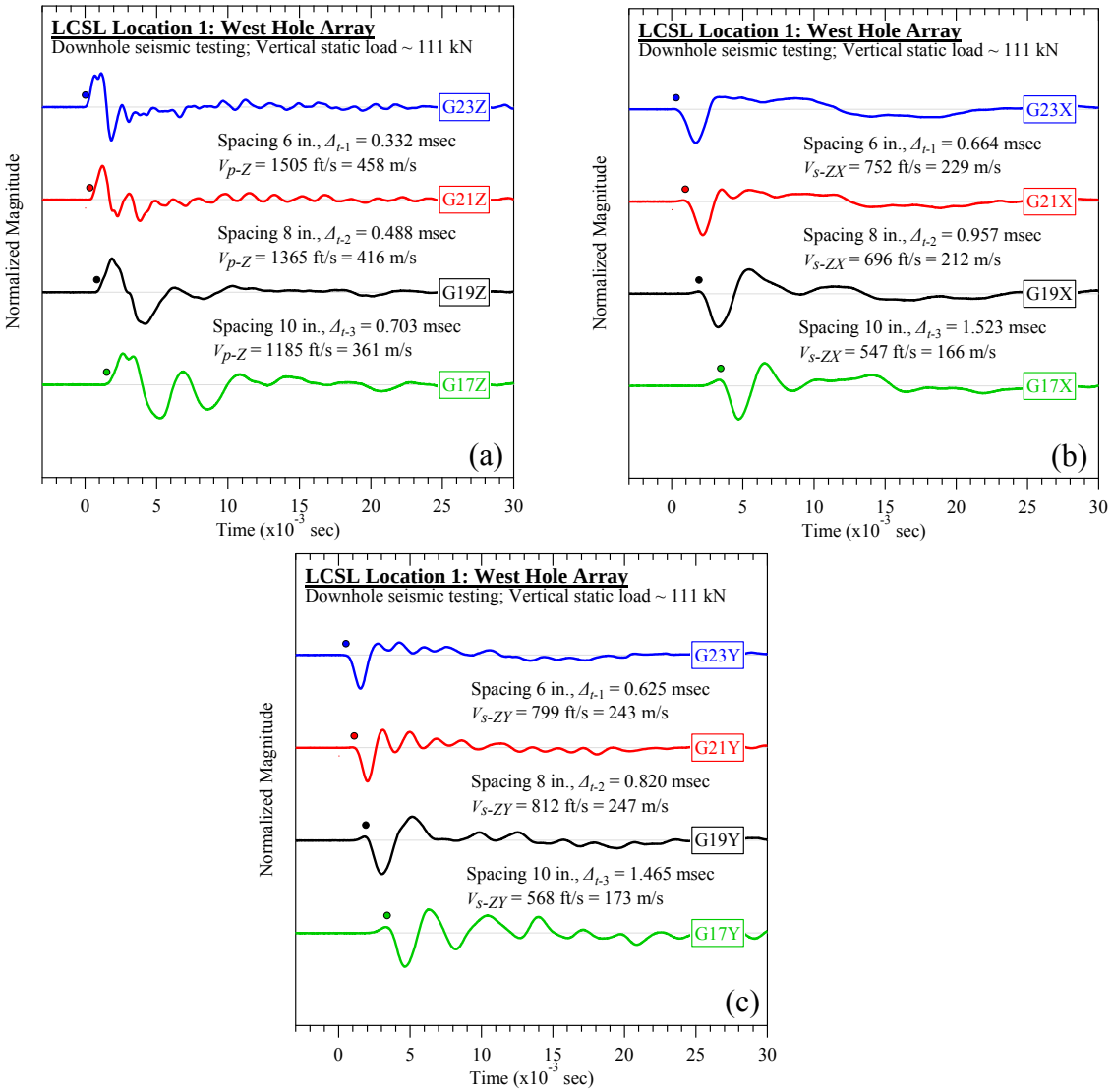

Figure B-11. Lamb Canyon Sanitary Landfill #1 (west hole): Downhole seismic testing at vertical load of 111 kN: (a) $V_{p\text{-}Z}$, (b) $V_{s\text{-}ZX}$, and (c) $V_{s\text{-}ZY}$.

B.1.2 Crosshole Seismic Testing

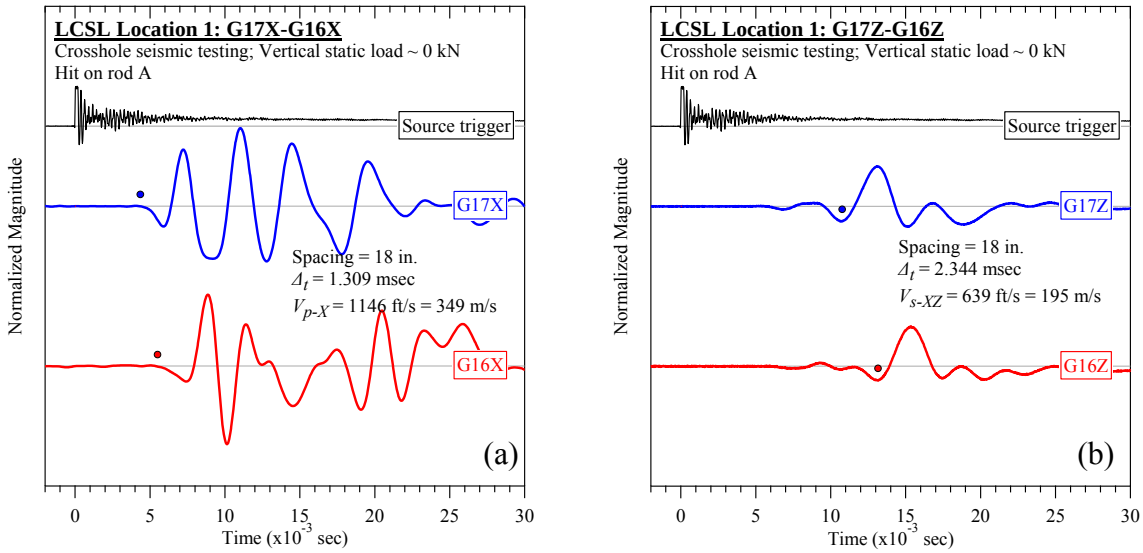

Figure B-12. Lamb Canyon Sanitary Landfill #1 (rod A): Crosshole seismic testing at vertical load of 0 kN: (a) $V_{p\text{-}X}$ and (b) $V_{s\text{-}XZ}$.

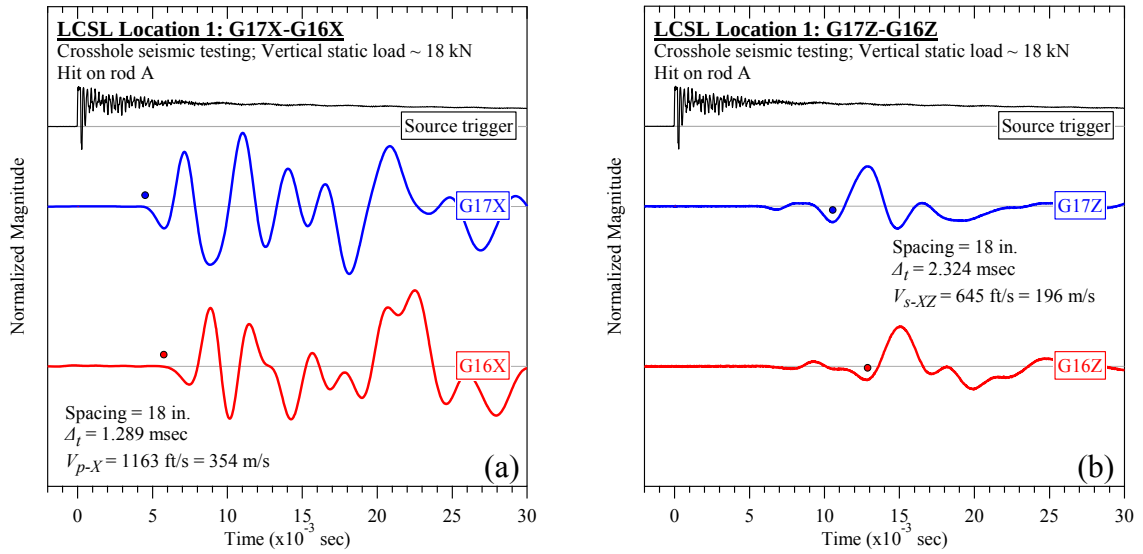

Figure B-13. Lamb Canyon Sanitary Landfill #1 (rod A): Crosshole seismic testing at vertical load of 18 kN: (a) $V_{p\text{-}X}$ and (b) $V_{s\text{-}XZ}$.

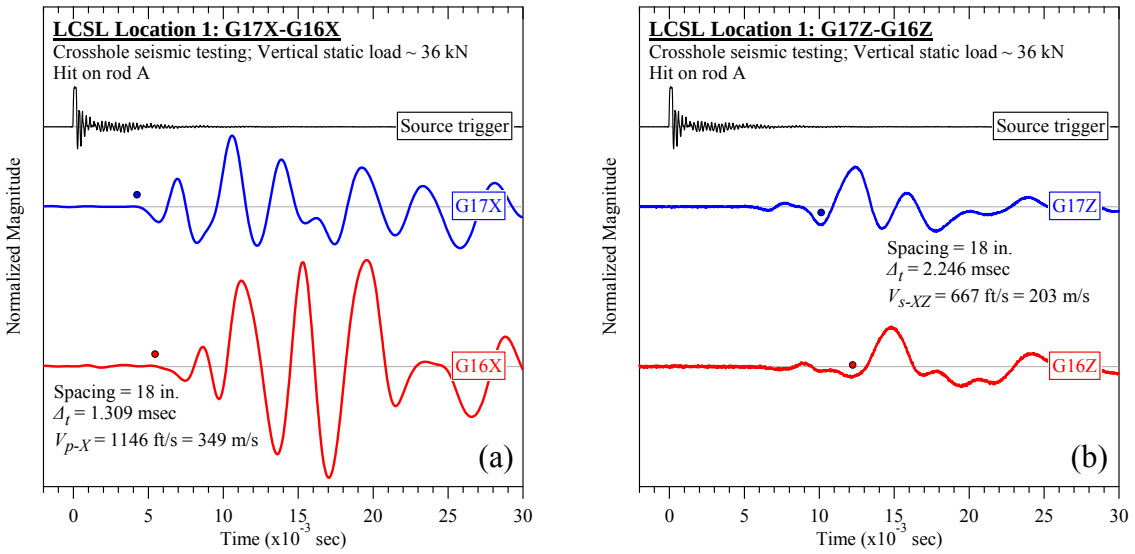

Figure B-14. Lamb Canyon Sanitary Landfill #1 (rod A): Crosshole seismic testing at vertical load of 36 kN: (a) $V_{p\text{-}X}$ and (b) $V_{s\text{-}XZ}$.

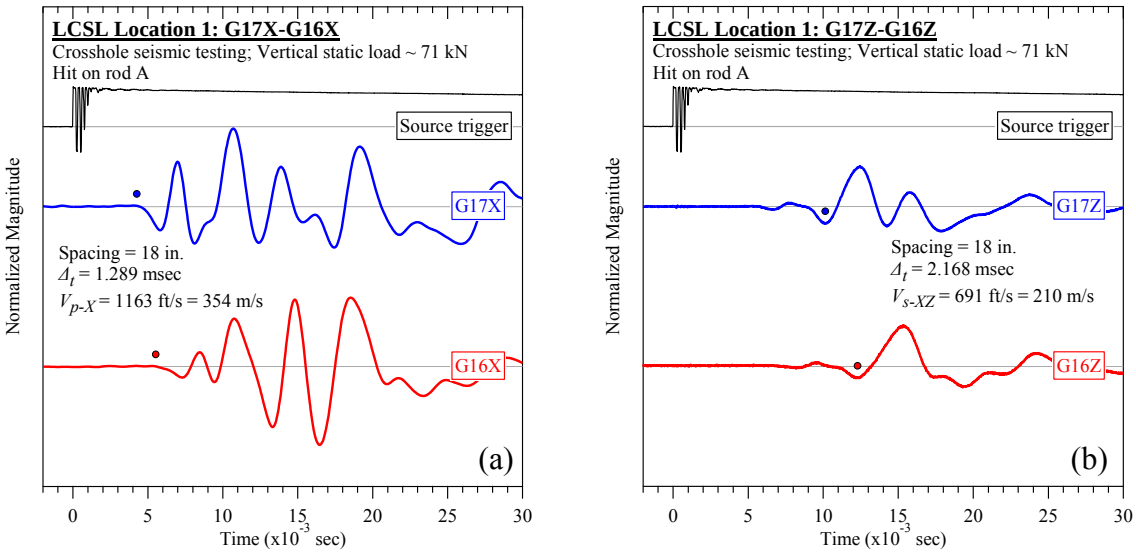

Figure B-15. Lamb Canyon Sanitary Landfill #1 (rod A): Crosshole seismic testing at vertical load of 71 kN: (a) $V_{p\text{-}X}$ and (b) $V_{s\text{-}XZ}$.

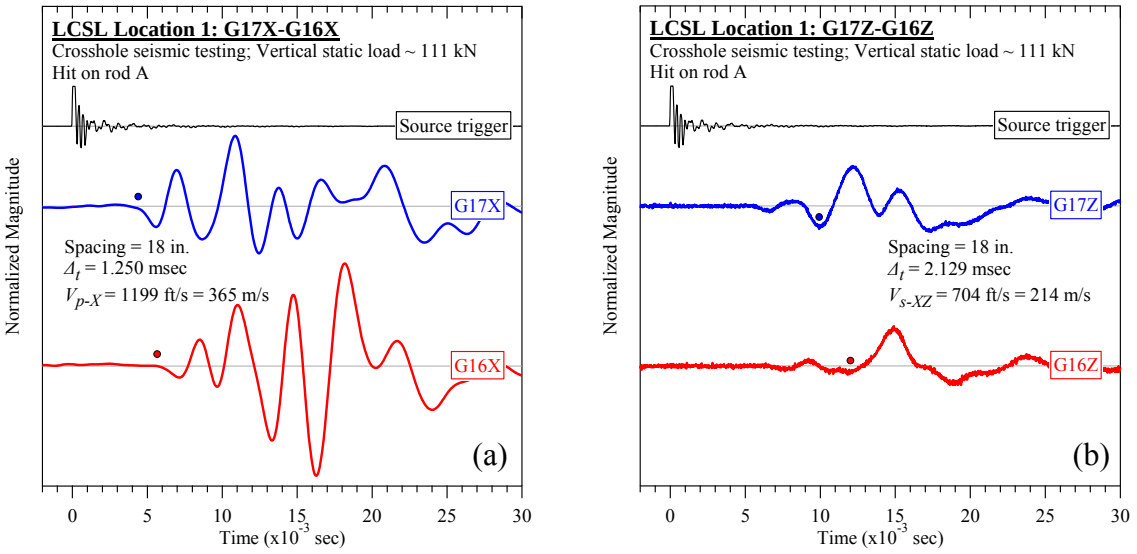

Figure B-16. Lamb Canyon Sanitary Landfill #1 (rod A): Crosshole seismic testing at vertical load of 111 kN: (a) $V_{p\text{-}X}$ and (b) $V_{s\text{-}XZ}$.

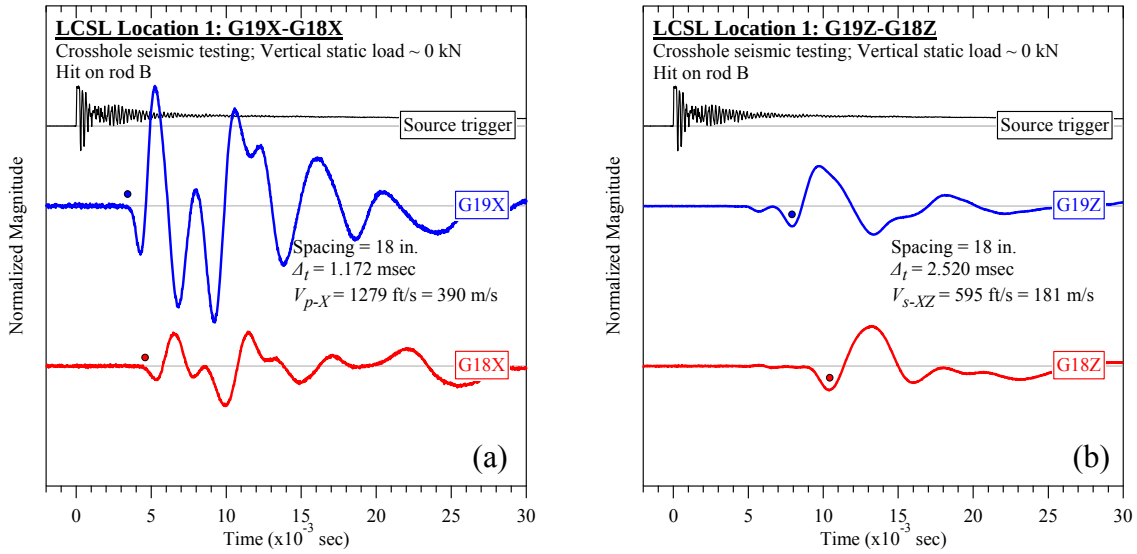

Figure B-17. Lamb Canyon Sanitary Landfill #1 (rod B): Crosshole seismic testing at vertical load of 0 kN: (a) $V_{p\text{-}X}$ and (b) $V_{s\text{-}XZ}$.

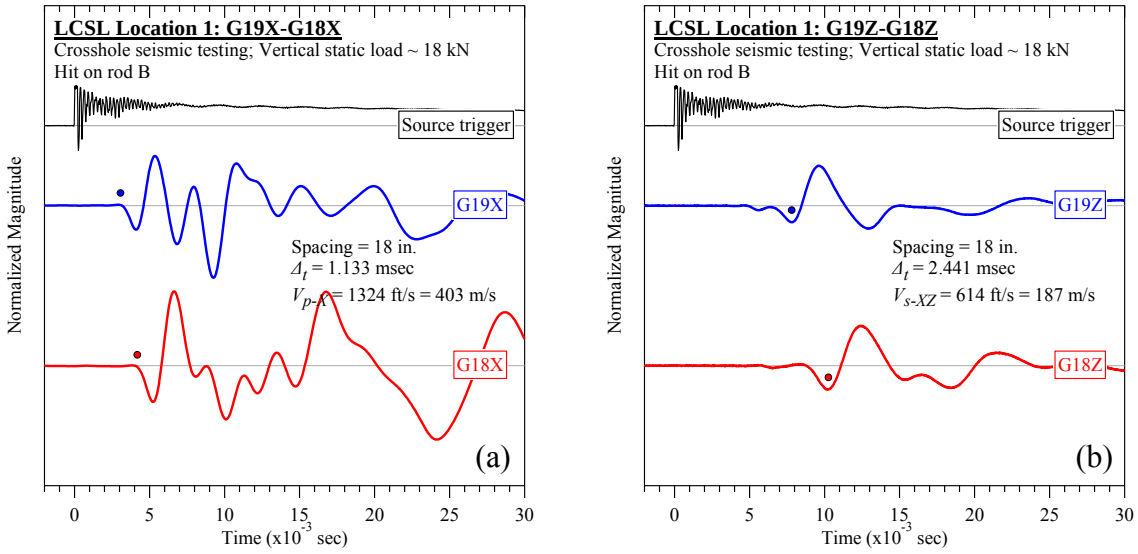

Figure B-18. Lamb Canyon Sanitary Landfill #1 (rod B): Crosshole seismic testing at vertical load of 18 kN: (a) $V_{p\text{-}X}$ and (b) $V_{s\text{-}XZ}$.

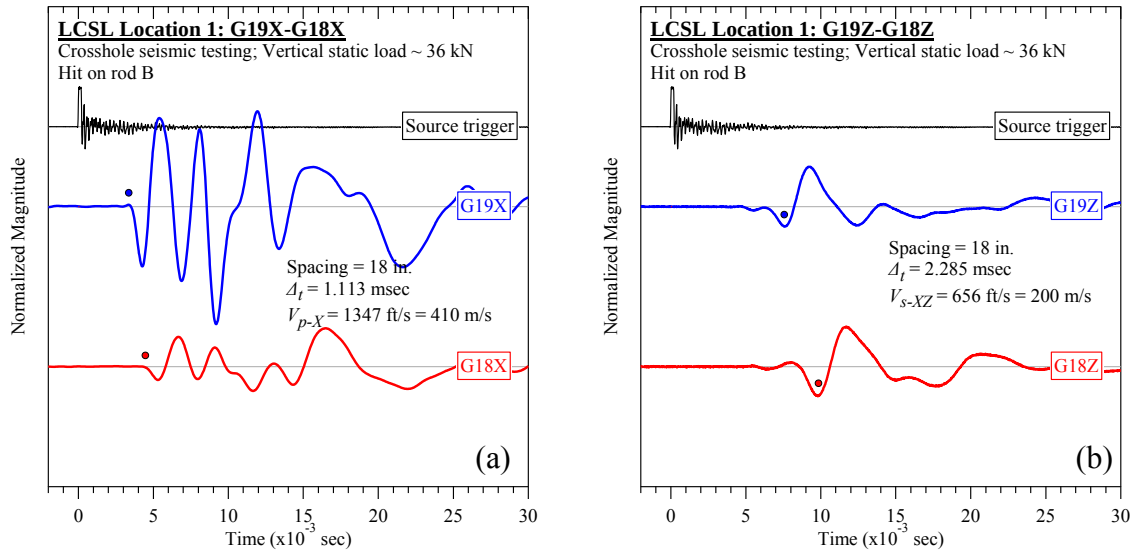

Figure B-19. Lamb Canyon Sanitary Landfill #1 (rod B): Crosshole seismic testing at vertical load of 36 kN: (a) $V_{p\text{-}X}$ and (b) $V_{s\text{-}XZ}$.

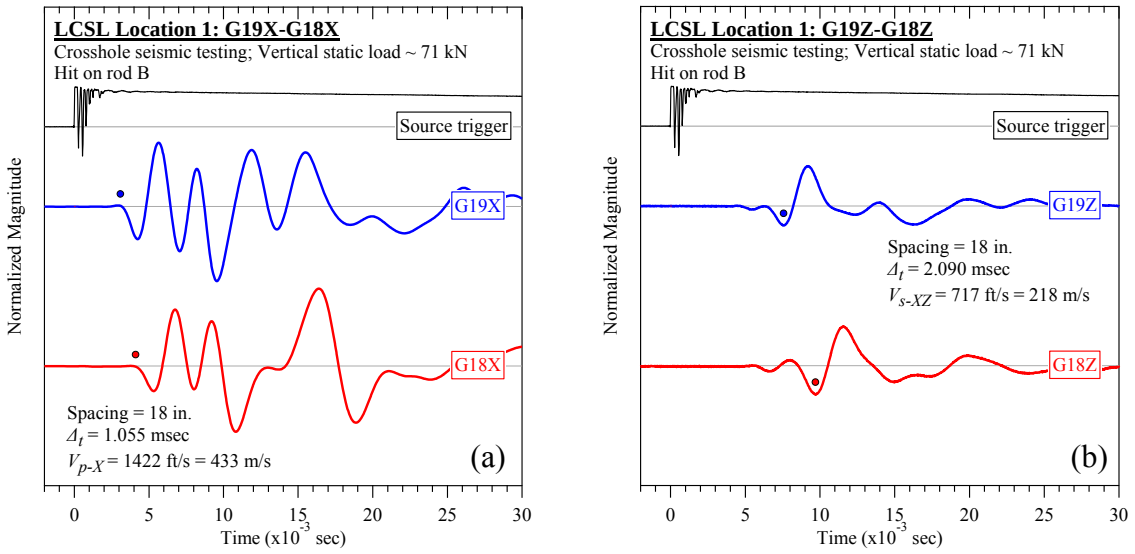

Figure B-20. Lamb Canyon Sanitary Landfill #1 (rod B): Crosshole seismic testing at vertical load of 71 kN: (a) $V_{p\text{-}X}$ and (b) $V_{s\text{-}XZ}$.

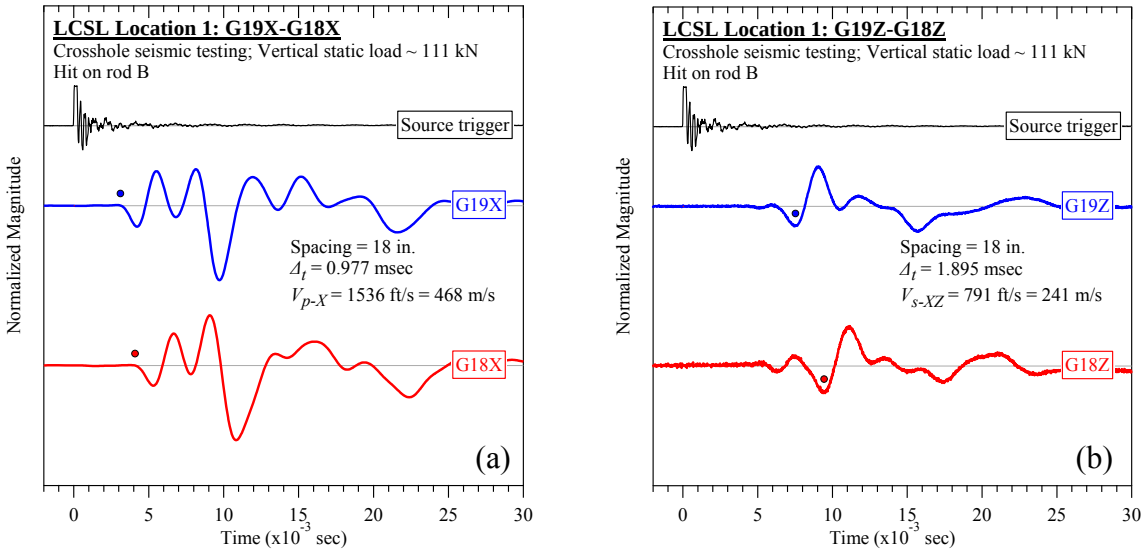

Figure B-21. Lamb Canyon Sanitary Landfill #1 (rod B): Crosshole seismic testing at vertical load of 111 kN: (a) $V_{p\text{-}X}$ and (b) $V_{s\text{-}XZ}$.

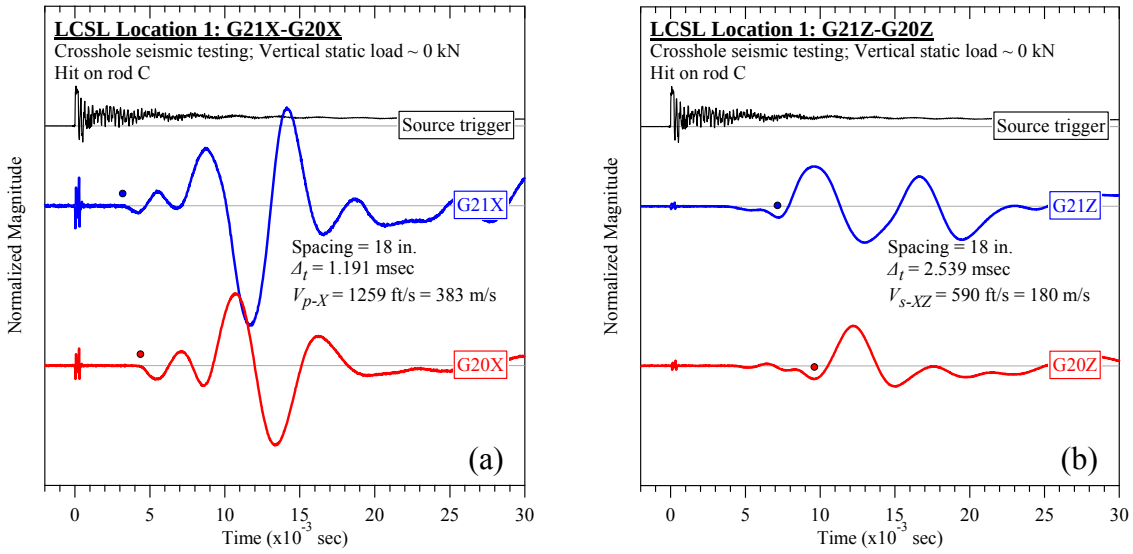

Figure B-22. Lamb Canyon Sanitary Landfill #1 (rod C): Crosshole seismic testing at vertical load of 0 kN: (a) $V_{p\text{-}X}$ and (b) $V_{s\text{-}XZ}$.

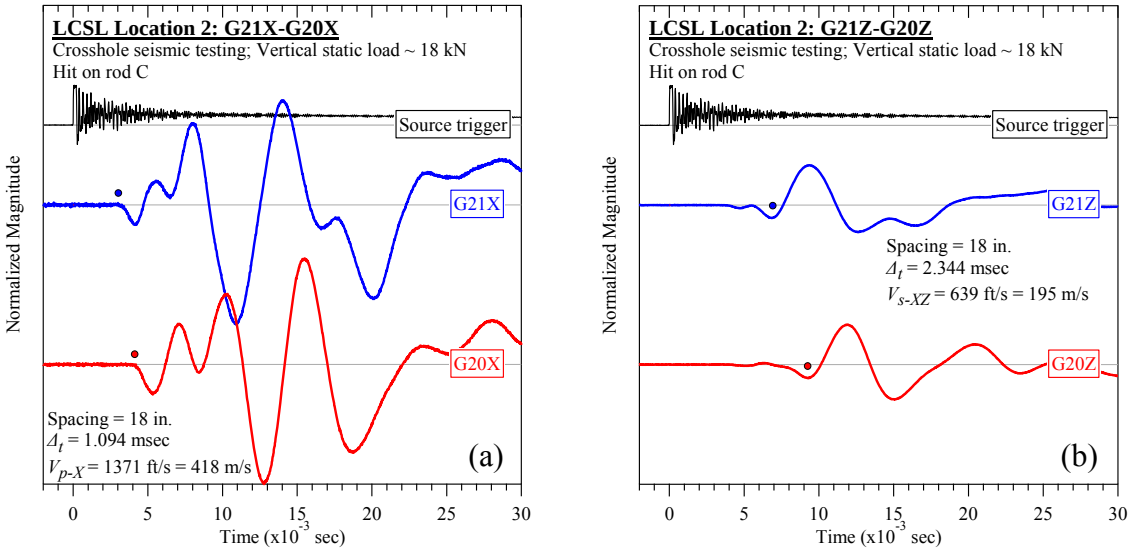

Figure B-23. Lamb Canyon Sanitary Landfill #1 (rod C): Crosshole seismic testing at vertical load of 18 kN: (a) $V_{p\text{-}X}$ and (b) $V_{s\text{-}XZ}$.

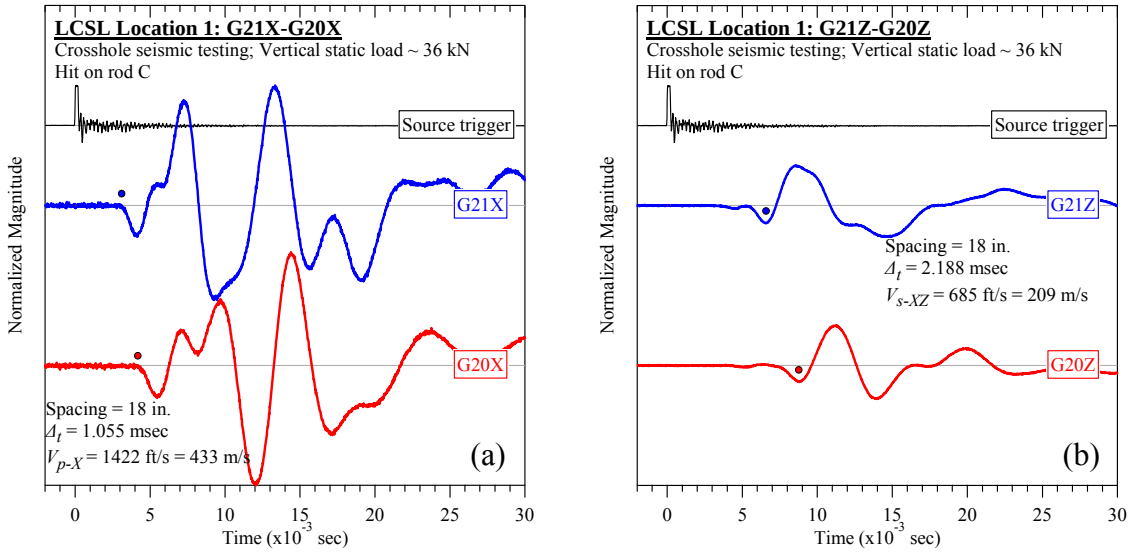

Figure B-24. Lamb Canyon Sanitary Landfill #1 (rod C): Crosshole seismic testing at vertical load of 36 kN: (a) $V_{p\text{-}X}$ and (b) $V_{s\text{-}XZ}$.

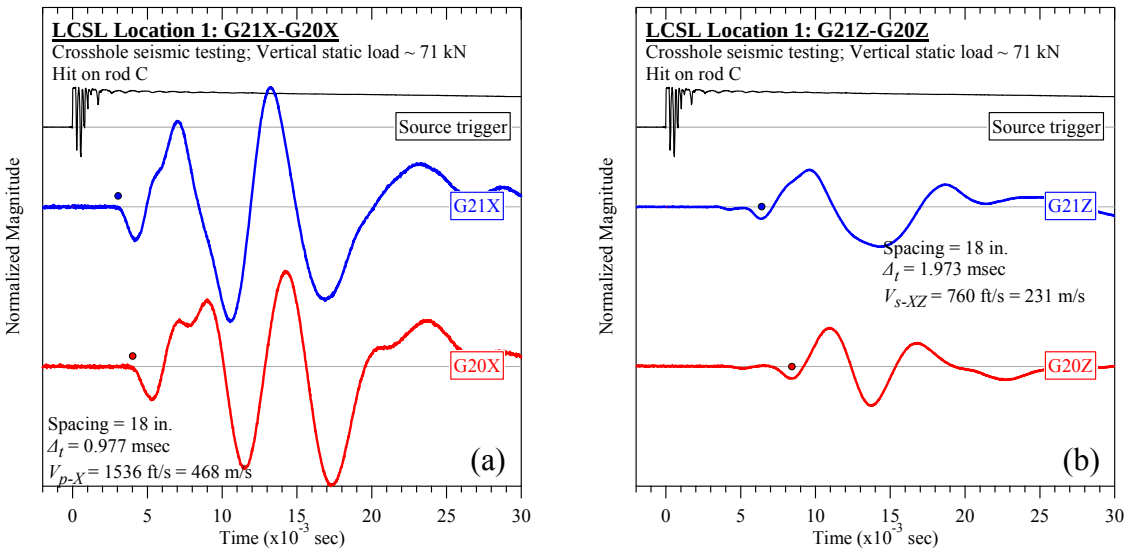

Figure B-25. Lamb Canyon Sanitary Landfill #1 (rod C): Crosshole seismic testing at vertical load of 71 kN: (a) $V_{p\text{-}X}$ and (b) $V_{s\text{-}XZ}$.

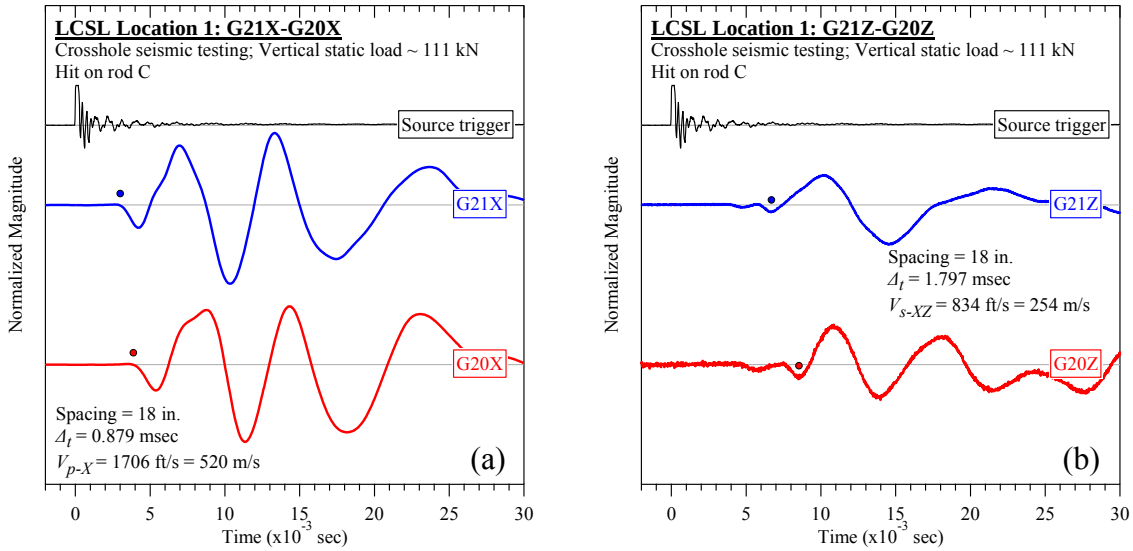

Figure B-26. Lamb Canyon Sanitary Landfill #1 (rod C): Crosshole seismic testing at vertical load of 111 kN: (a) $V_{p\text{-}X}$ and (b) $V_{s\text{-}XZ}$.

B.1.3 Steady-state Dynamic Testing

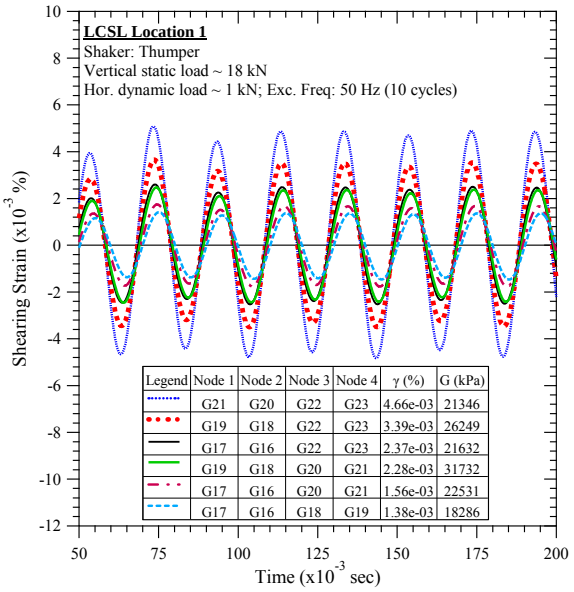

Figure B-27. Lamb Canyon Sanitary Landfill #1: Steady-state dynamic testing at vertical load of 18 kN and horizontal dynamic load of 1 kN.

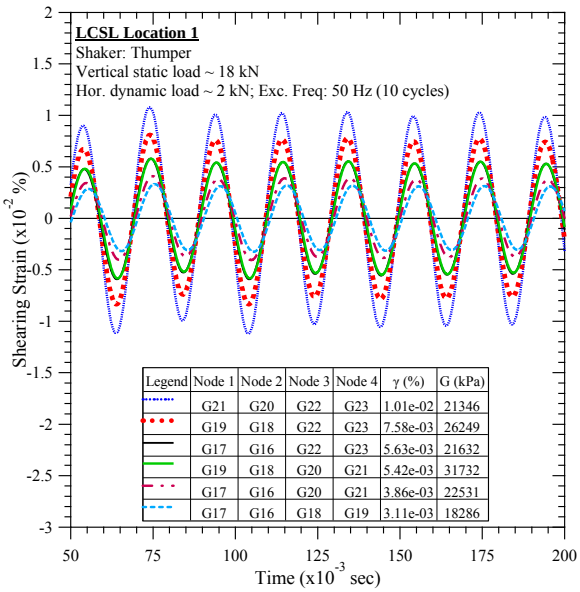

Figure B-28. Lamb Canyon Sanitary Landfill #1: Steady-state dynamic testing at vertical load of 18 kN and horizontal dynamic load of 2 kN.

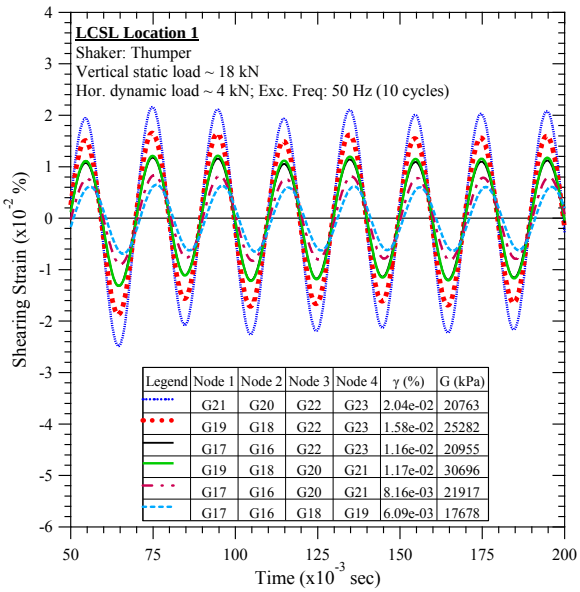

Figure B-29. Lamb Canyon Sanitary Landfill #1: Steady-state dynamic testing at vertical load of 18 kN and horizontal dynamic load of 4 kN.

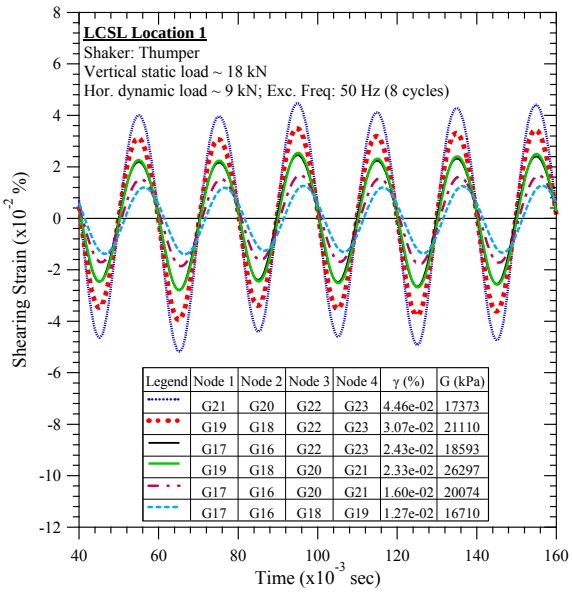

Figure B-30. Lamb Canyon Sanitary Landfill #1: Steady-state dynamic testing at vertical load of 18 kN and horizontal dynamic load of 9 kN.

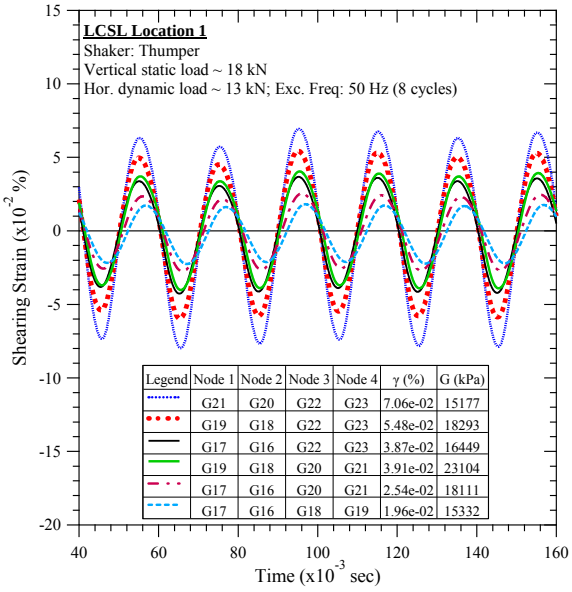

Figure B-31. Lamb Canyon Sanitary Landfill #1: Steady-state dynamic testing at vertical load of 18 kN and horizontal dynamic load of 13 kN.

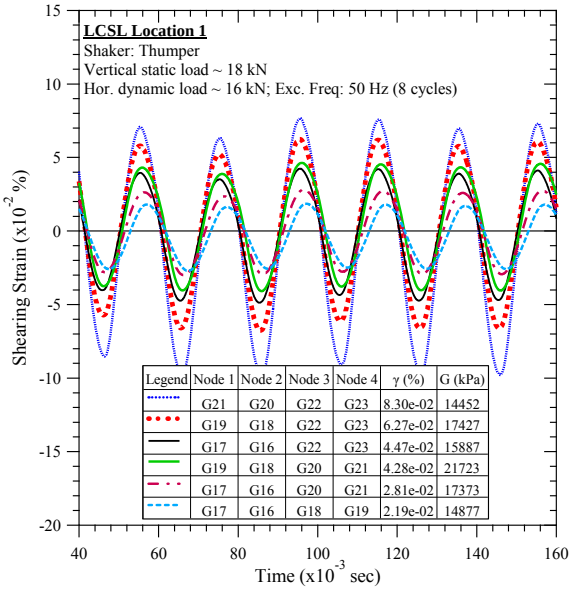

Figure B-32. Lamb Canyon Sanitary Landfill #1: Steady-state dynamic testing at vertical load of 18 kN and horizontal dynamic load of 16 kN.

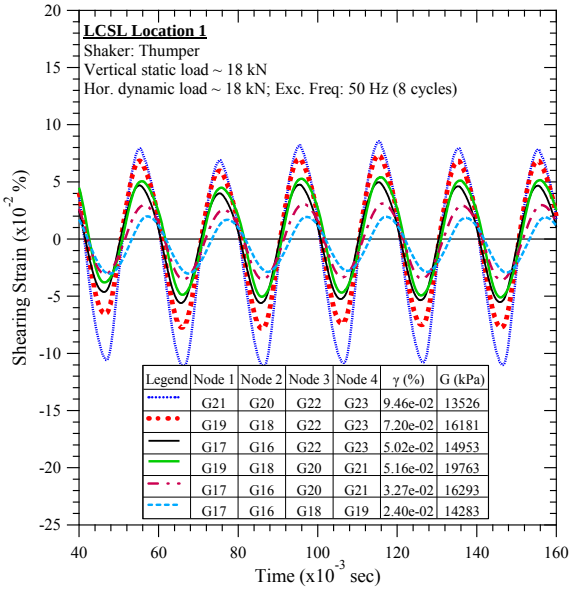

Figure B-33. Lamb Canyon Sanitary Landfill #1: Steady-state dynamic testing at vertical load of 18 kN and horizontal dynamic load of 18 kN.

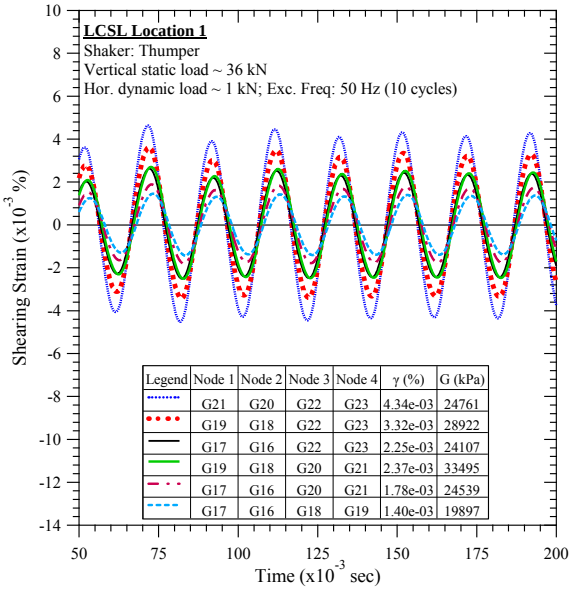

Figure B-34. Lamb Canyon Sanitary Landfill #1: Steady-state dynamic testing at vertical load of 36 kN and horizontal dynamic load of 1 kN.

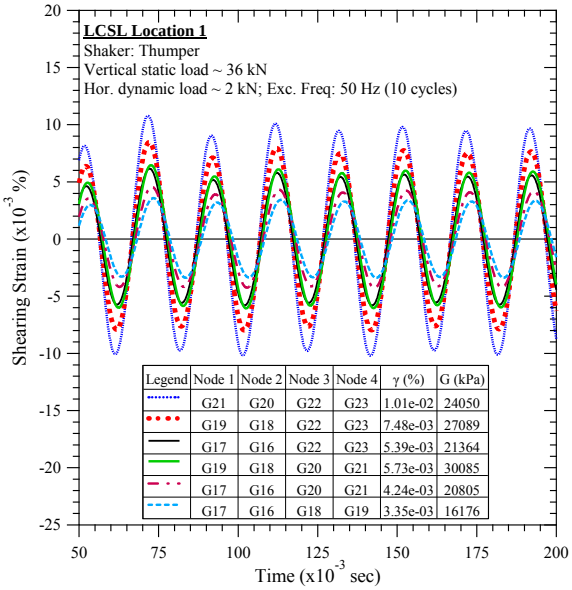

Figure B-35. Lamb Canyon Sanitary Landfill #1: Steady-state dynamic testing at vertical load of 36 kN and horizontal dynamic load of 2 kN.

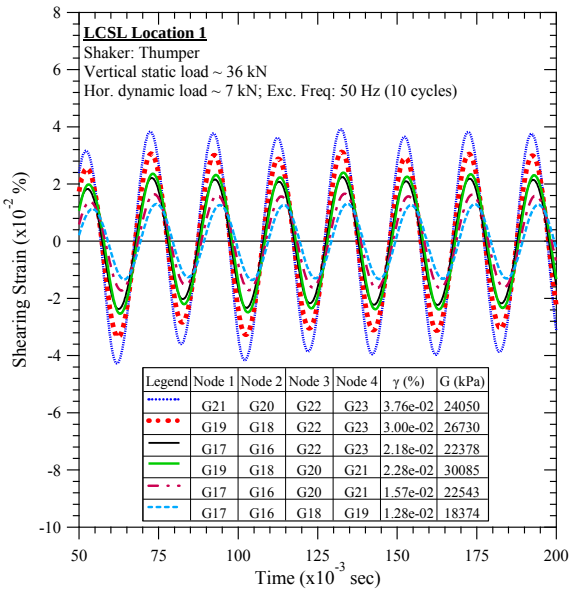

Figure B-36. Lamb Canyon Sanitary Landfill #1: Steady-state dynamic testing at vertical load of 36 kN and horizontal dynamic load of 7 kN.

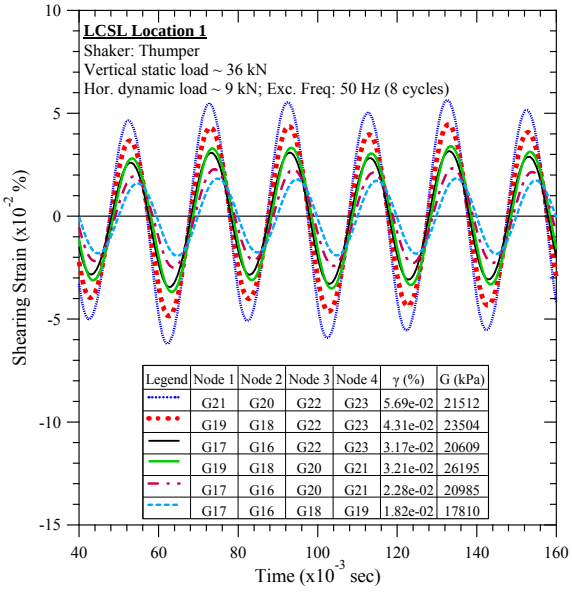

Figure B-37. Lamb Canyon Sanitary Landfill #1: Steady-state dynamic testing at vertical load of 36 kN and horizontal dynamic load of 9 kN.

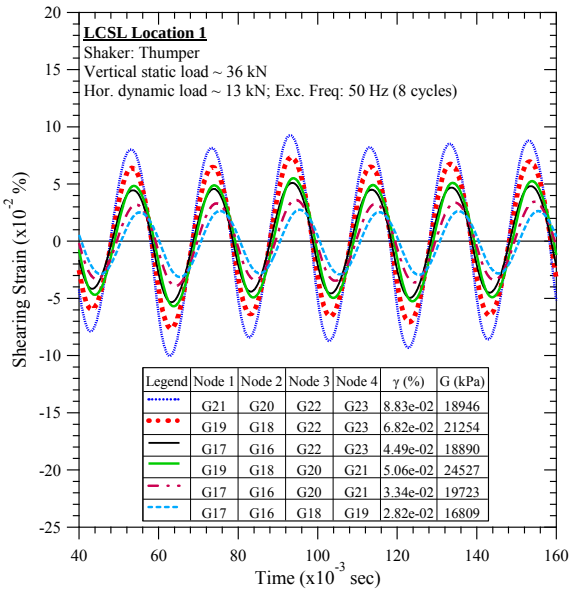

Figure B-38. Lamb Canyon Sanitary Landfill #1: Steady-state dynamic testing at vertical load of 36 kN and horizontal dynamic load of 13 kN.

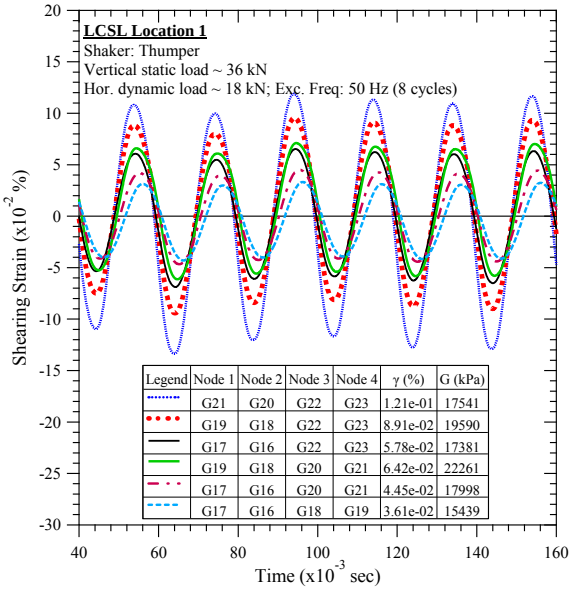

Figure B-39. Lamb Canyon Sanitary Landfill #1: Steady-state dynamic testing at vertical load of 36 kN and horizontal dynamic load of 18 kN.

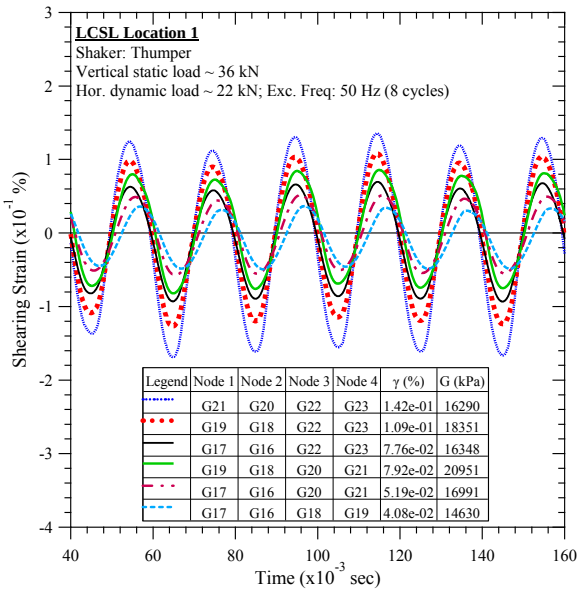

Figure B-40. Lamb Canyon Sanitary Landfill #1: Steady-state dynamic testing at vertical load of 36 kN and horizontal dynamic load of 22 kN.

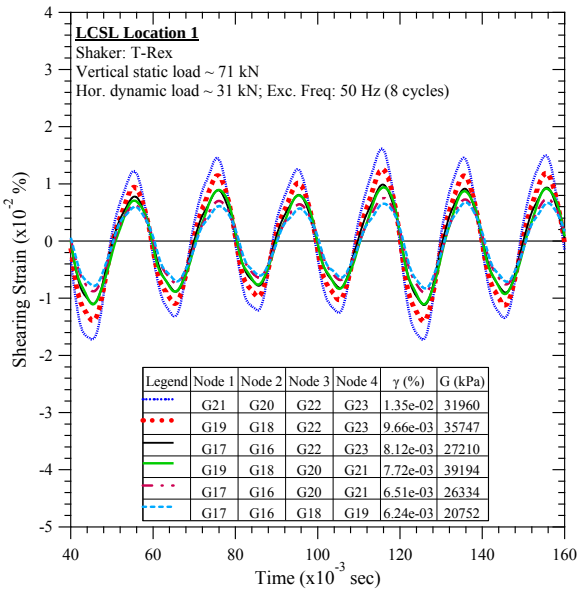

Figure B-41. Lamb Canyon Sanitary Landfill #1: Steady-state dynamic testing at vertical load of 71 kN and horizontal dynamic load of 31 kN.

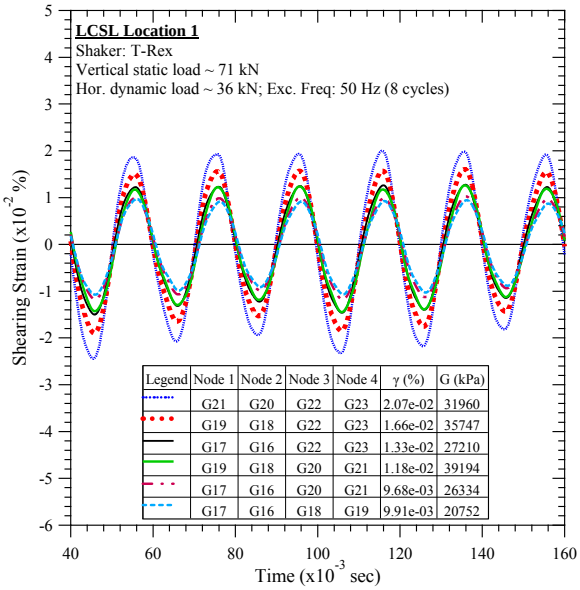

Figure B-42. Lamb Canyon Sanitary Landfill #1: Steady-state dynamic testing at vertical load of 71 kN and horizontal dynamic load of 36 kN.

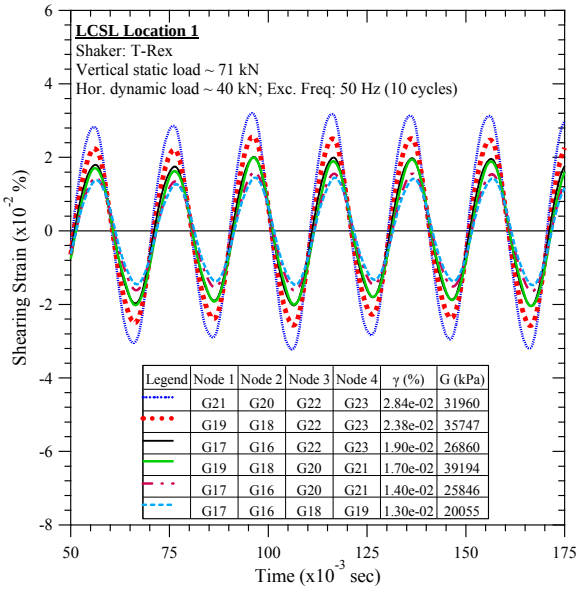

Figure B-43. Lamb Canyon Sanitary Landfill #1: Steady-state dynamic testing at vertical load of 71 kN and horizontal dynamic load of 40 kN.

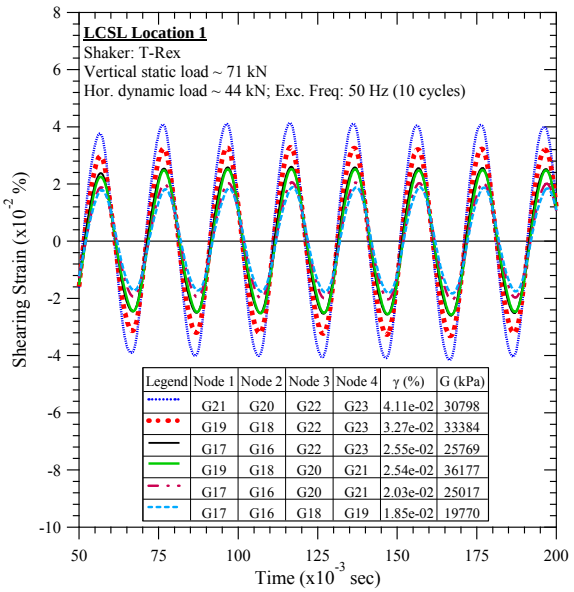

Figure B-44. Lamb Canyon Sanitary Landfill #1: Steady-state dynamic testing at vertical load of 71 kN and horizontal dynamic load of 44 kN.

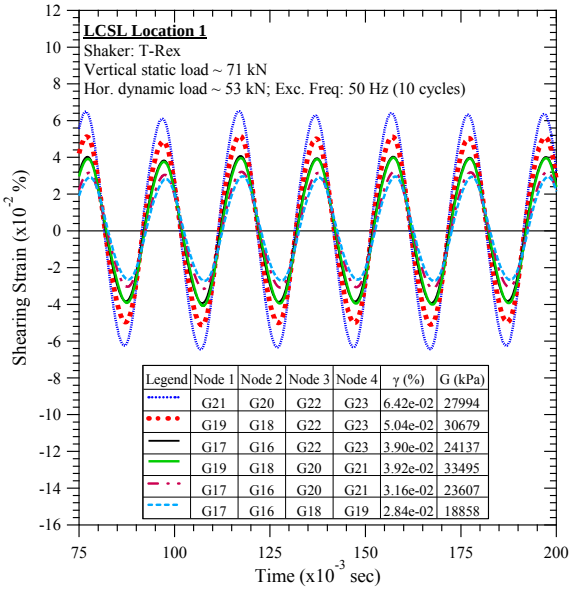

Figure B-45. Lamb Canyon Sanitary Landfill #1: Steady-state dynamic testing at vertical load of 71 kN and horizontal dynamic load of 53 kN.

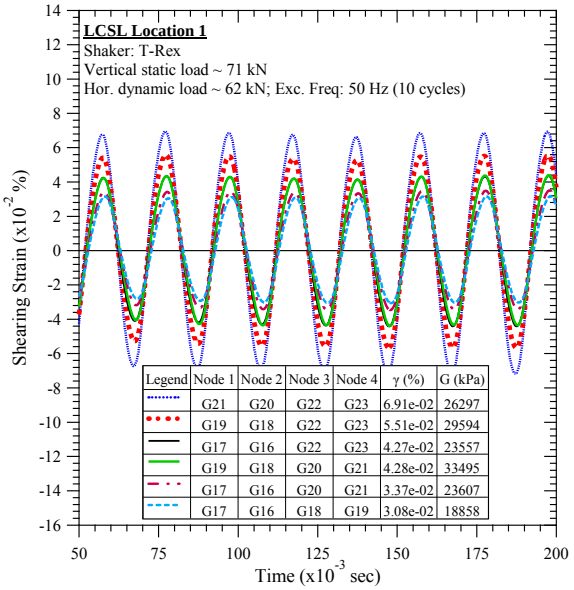

Figure B-46. Lamb Canyon Sanitary Landfill #1: Steady-state dynamic testing at vertical load of 71 kN and horizontal dynamic load of 62 kN.

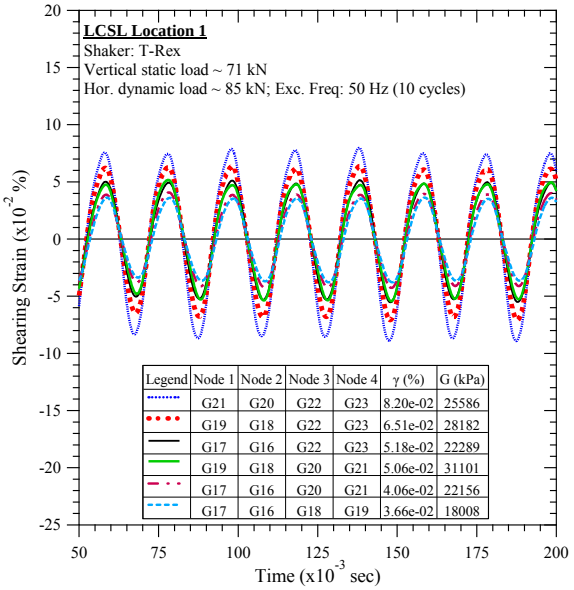

Figure B-47. Lamb Canyon Sanitary Landfill #1: Steady-state dynamic testing at vertical load of 71 kN and horizontal dynamic load of 85 kN.

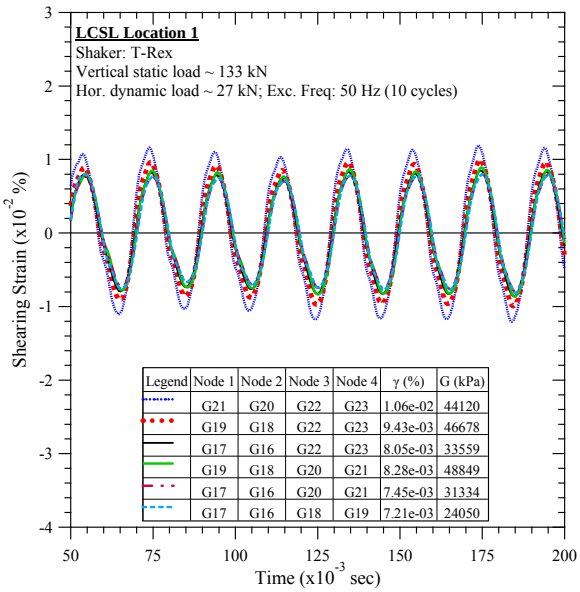

Figure B-48. Lamb Canyon Sanitary Landfill #1: Steady-state dynamic testing at vertical load of 133 kN and horizontal dynamic load of 27 kN.

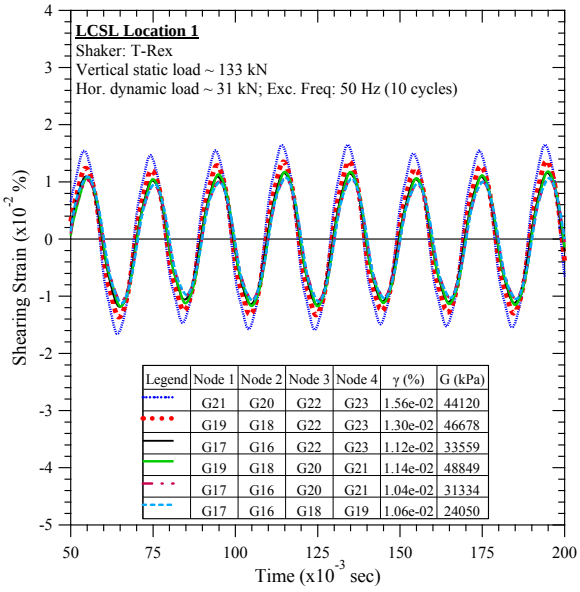

Figure B-49. Lamb Canyon Sanitary Landfill #1: Steady-state dynamic testing at vertical load of 133 kN and horizontal dynamic load of 31 kN.

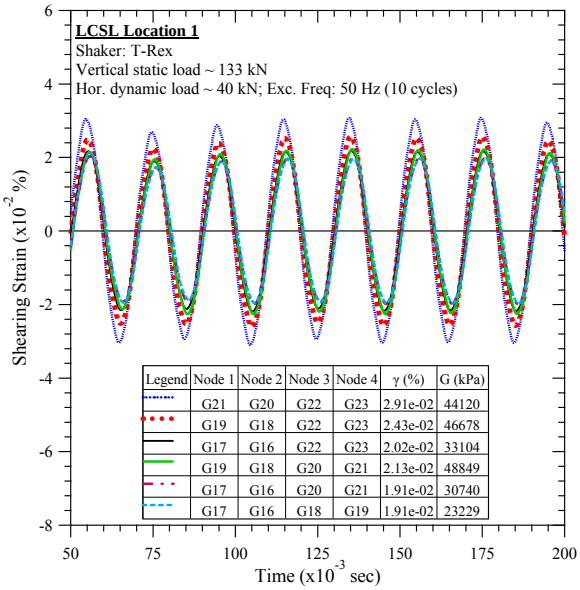

Figure B-50. Lamb Canyon Sanitary Landfill #1: Steady-state dynamic testing at vertical load of 133 kN and horizontal dynamic load of 40 kN.

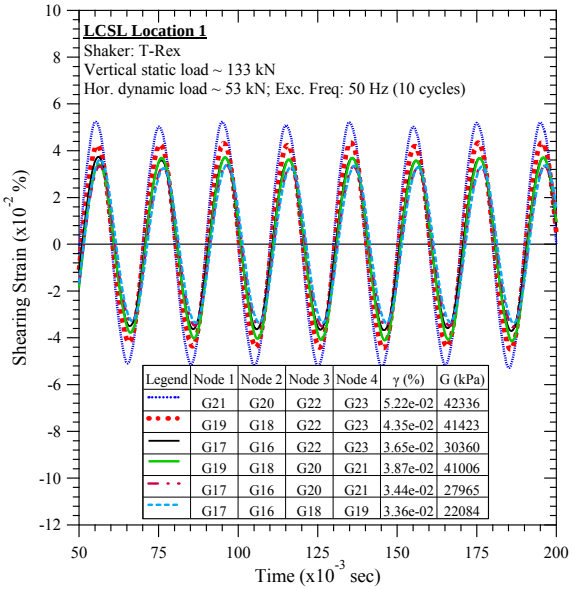

Figure B-51. Lamb Canyon Sanitary Landfill #1: Steady-state dynamic testing at vertical load of 133 kN and horizontal dynamic load of 53 kN.

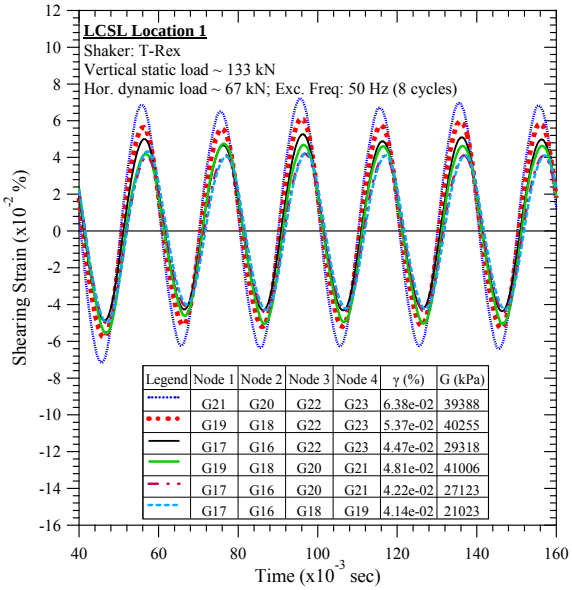

Figure B-52. Lamb Canyon Sanitary Landfill #1: Steady-state dynamic testing at vertical load of 133 kN and horizontal dynamic load of 67 kN.

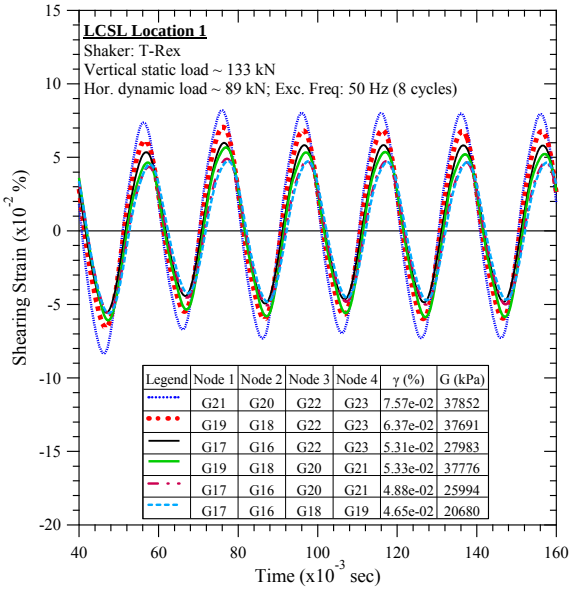

Figure B-53. Lamb Canyon Sanitary Landfill #1: Steady-state dynamic testing at vertical load of 133 kN and horizontal dynamic load of 89 kN.

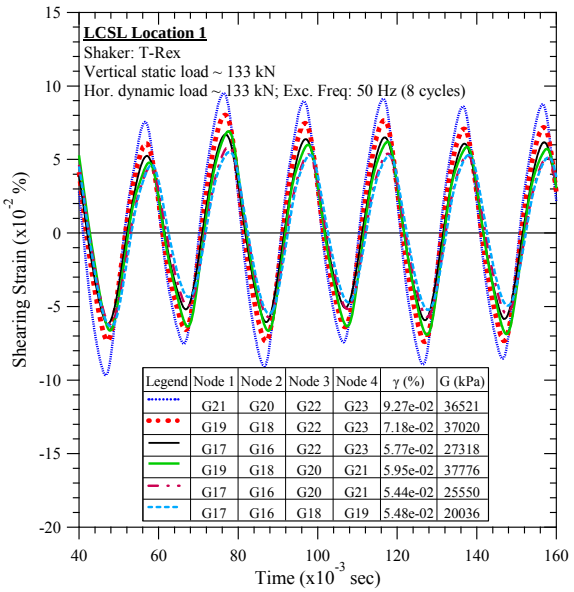

Figure B-54. Lamb Canyon Sanitary Landfill #1: Steady-state dynamic testing at vertical load of 133 kN and horizontal dynamic load of 133 kN.

B.2 Lamb Canyon Sanitary Landfill Location 2

B.2.1 Downhole Seismic Testing

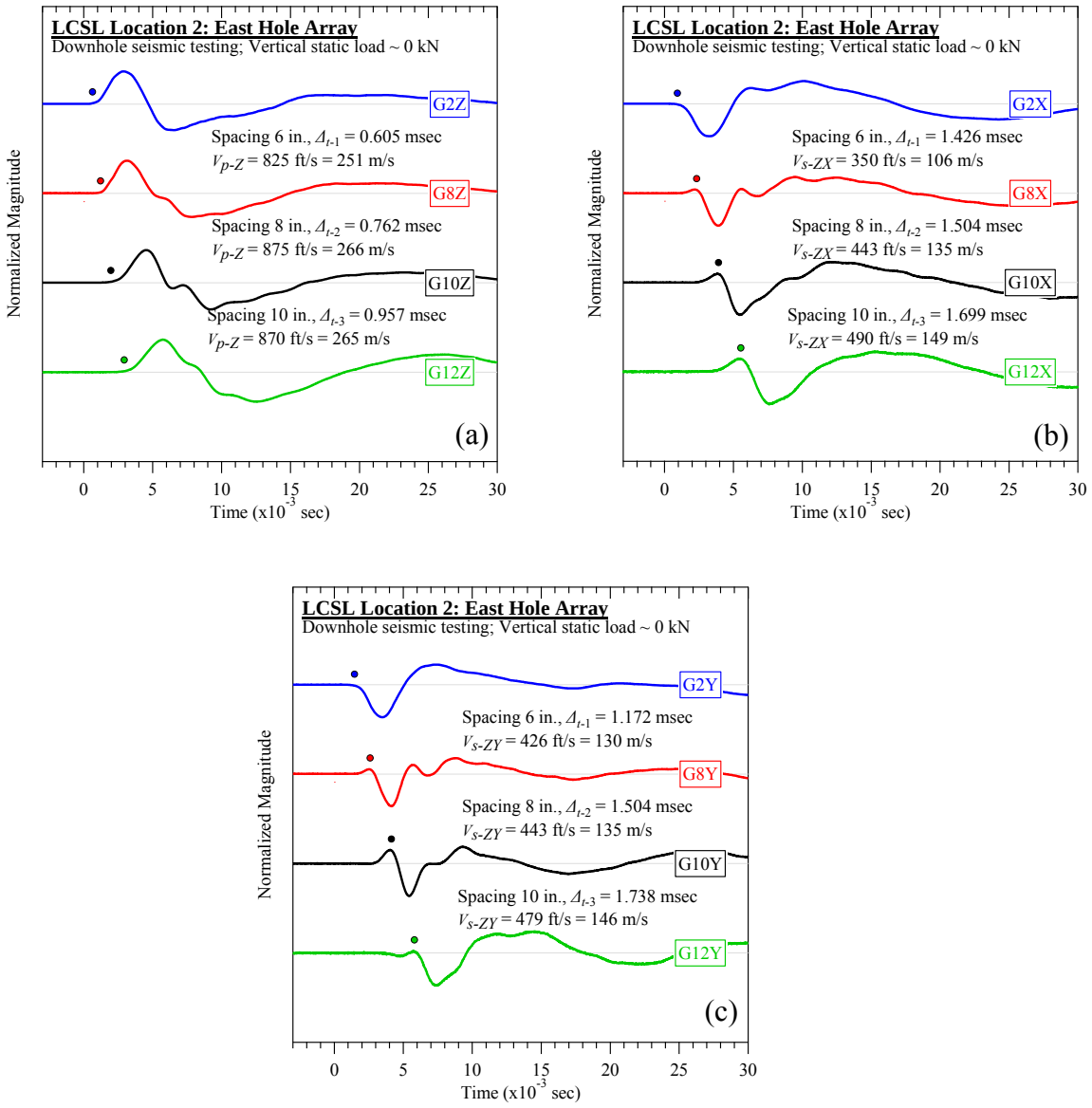

Figure B-55. Lamb Canyon Sanitary Landfill #2 (east hole): Downhole seismic testing at vertical load of 0 kN: (a) $V_{p\text{-}Z}$, (b) $V_{s\text{-}ZX}$, and (c) $V_{s\text{-}ZY}$.

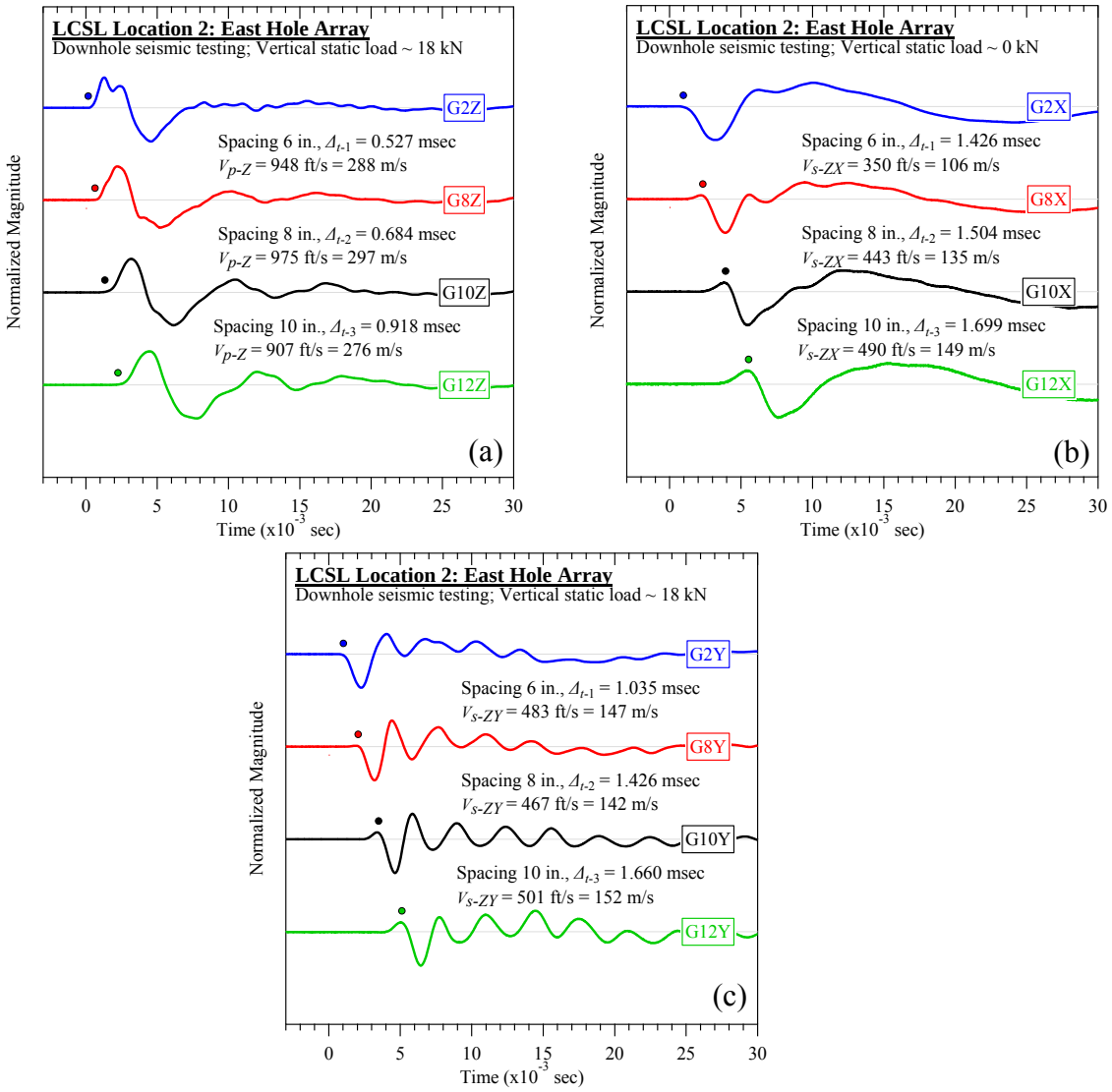

Figure B-56. Lamb Canyon Sanitary Landfill #2 (east hole): Downhole seismic testing at vertical load of 18 kN: (a) $V_{p\text{-}Z}$, (b) $V_{s\text{-}ZX}$, and (c) $V_{s\text{-}ZY}$.

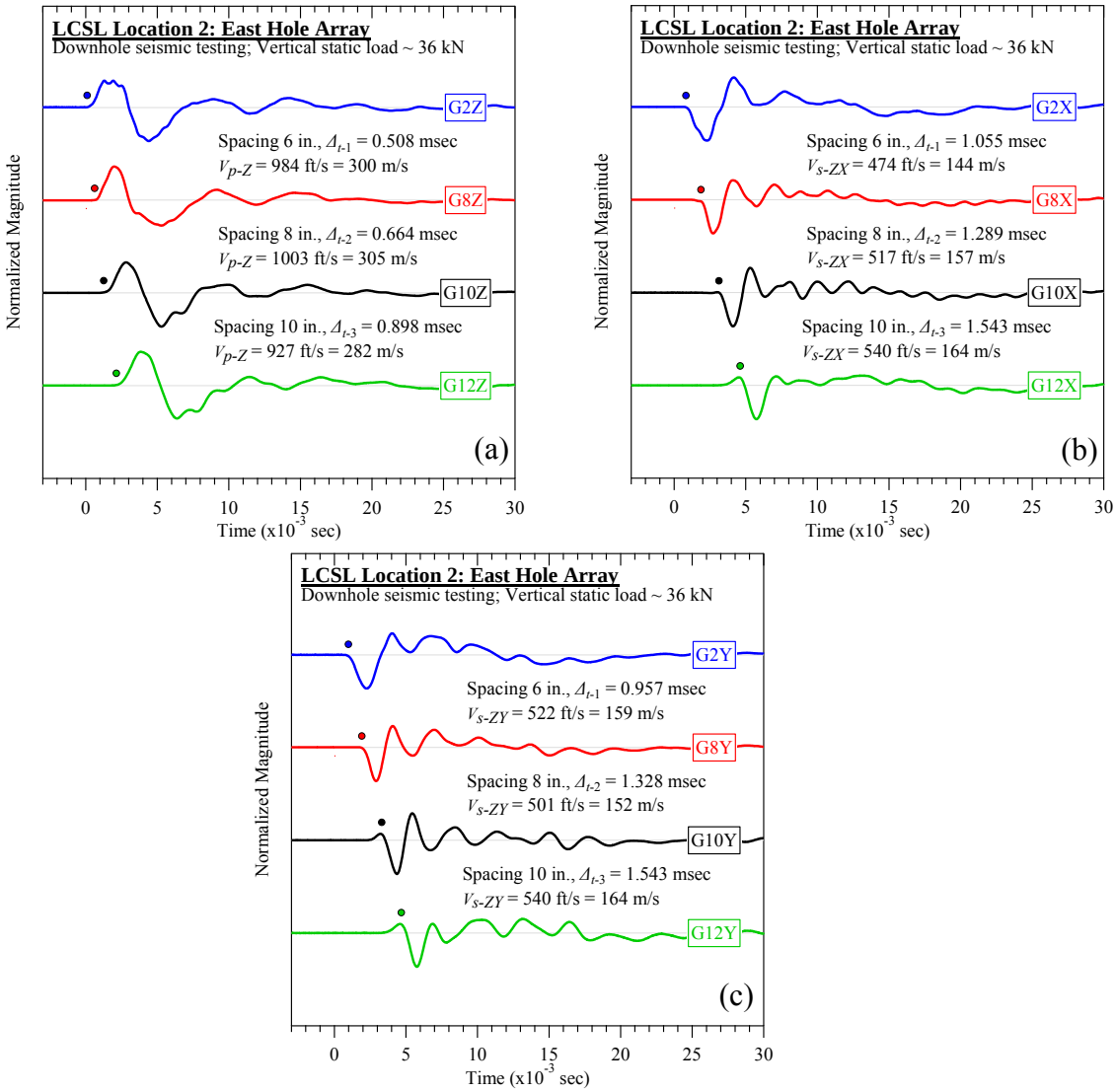

Figure B-57. Lamb Canyon Sanitary Landfill #2 (east hole): Downhole seismic testing at vertical load of 36 kN: (a) $V_{p\text{-}Z}$, (b) $V_{s\text{-}ZX}$, and (c) $V_{s\text{-}ZY}$.

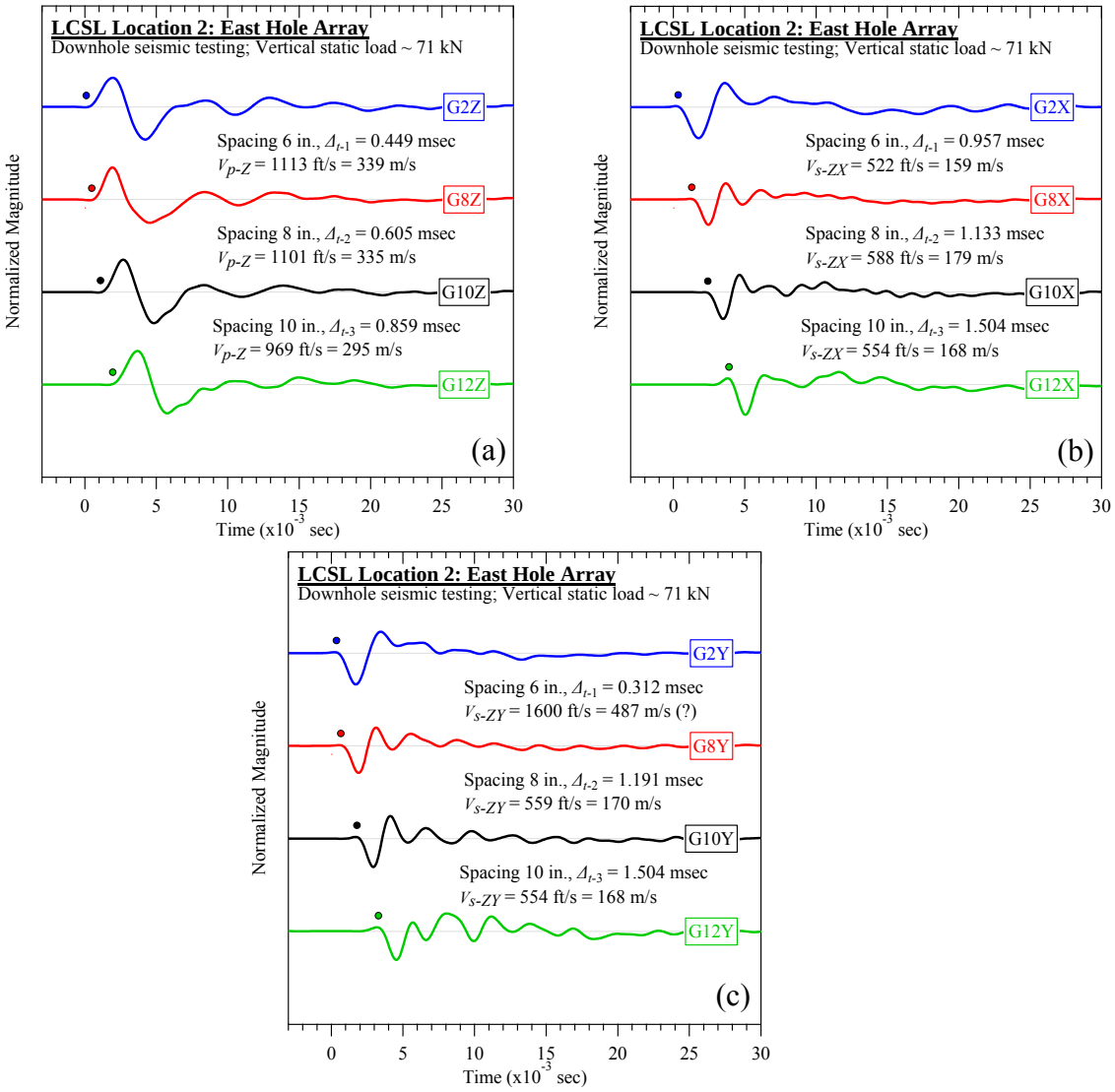

Figure B-58. Lamb Canyon Sanitary Landfill #2 (east hole): Downhole seismic testing at vertical load of 71 kN: (a) $V_{p\text{-}Z}$, (b) $V_{s\text{-}ZX}$, and (c) $V_{s\text{-}ZY}$.

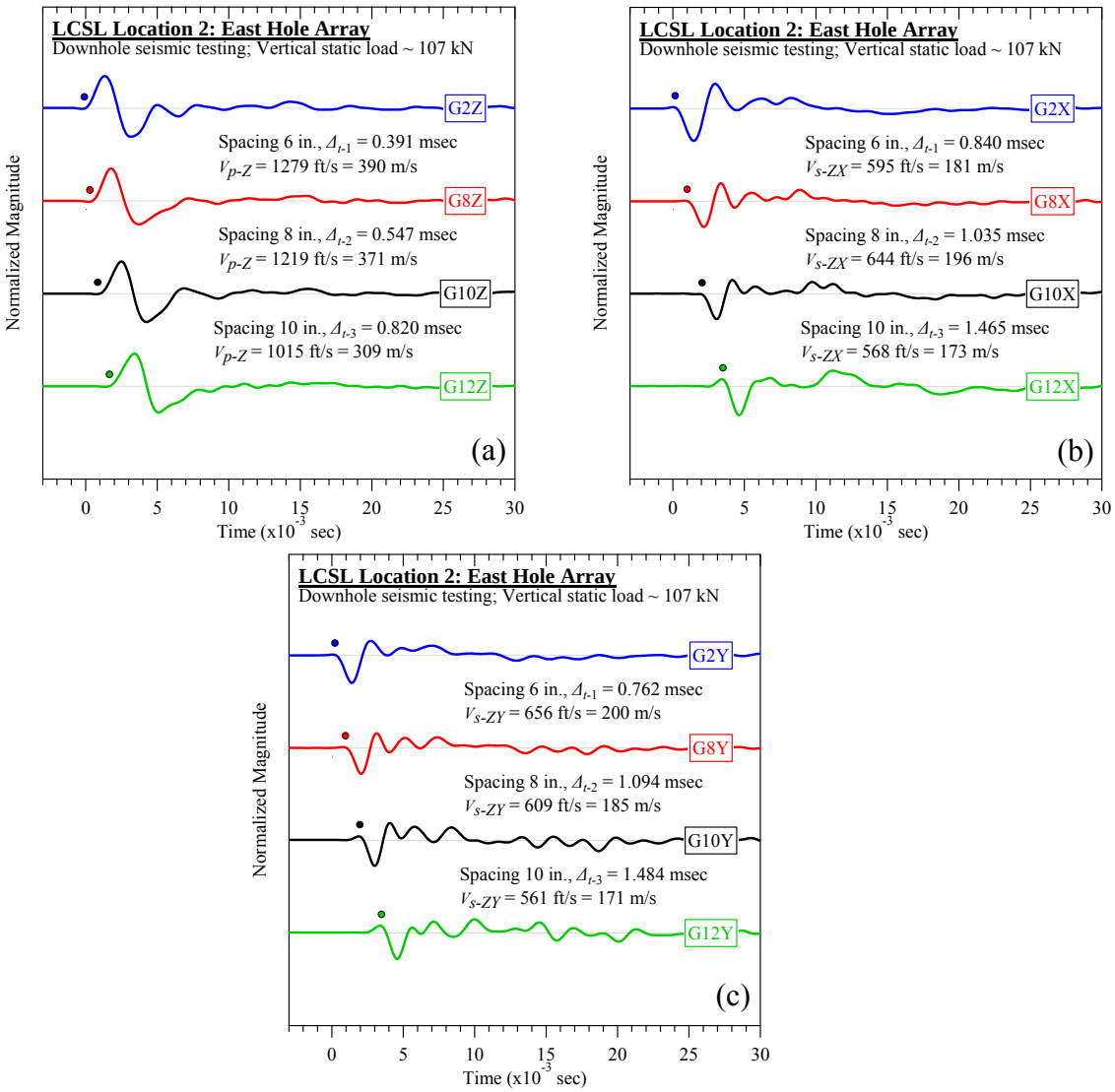

Figure B-59. Lamb Canyon Sanitary Landfill #2 (east hole): Downhole seismic testing at vertical load of 107 kN: (a) $V_{p\text{-}Z}$, (b) $V_{s\text{-}ZX}$, and (c) $V_{s\text{-}ZY}$.

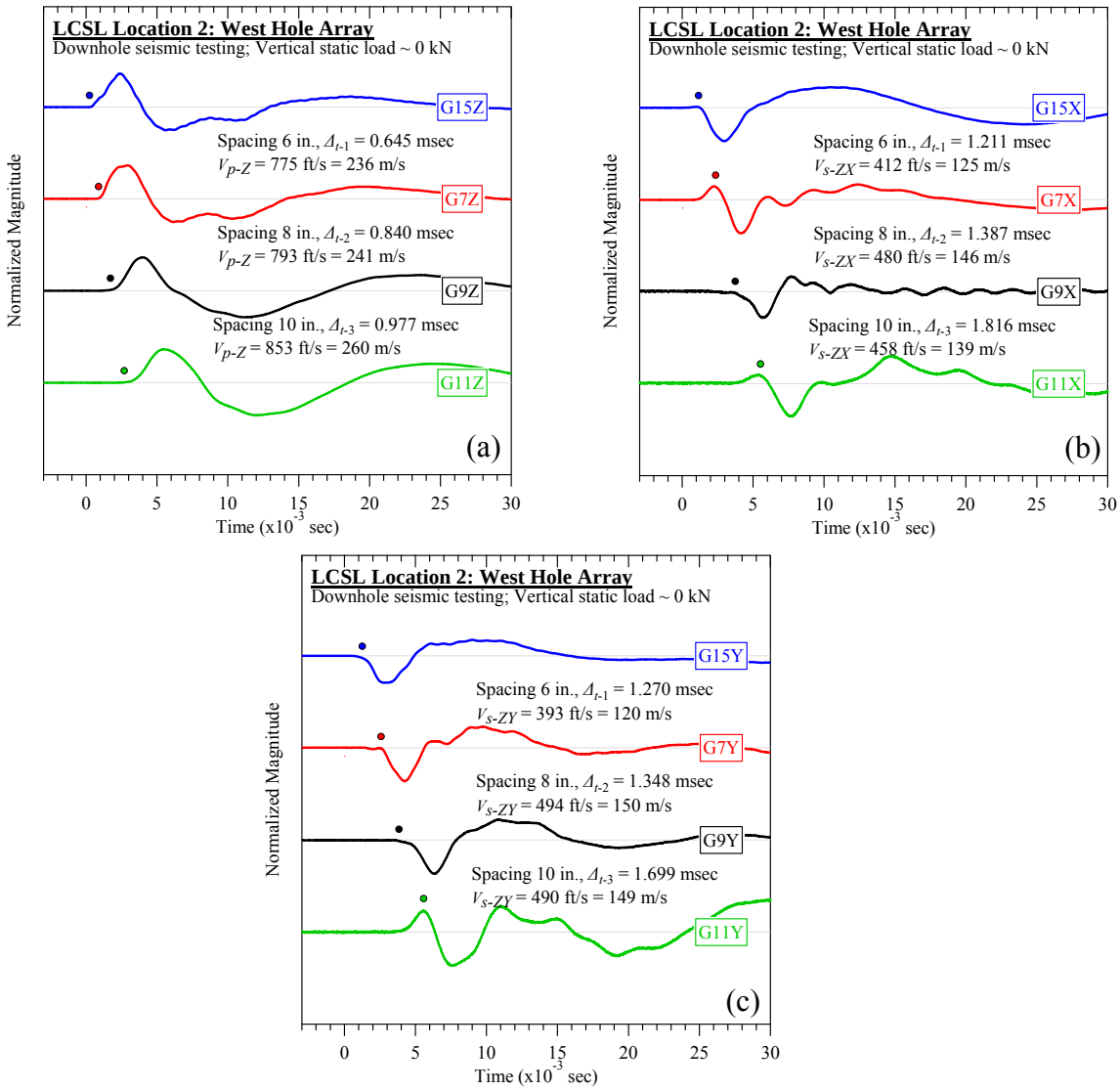

Figure B-60. Lamb Canyon Sanitary Landfill #2 (west hole): Downhole seismic testing at vertical load of 0 kN: (a) $V_{p\text{-}Z}$, (b) $V_{s\text{-}ZX}$, and (c) $V_{s\text{-}ZY}$.

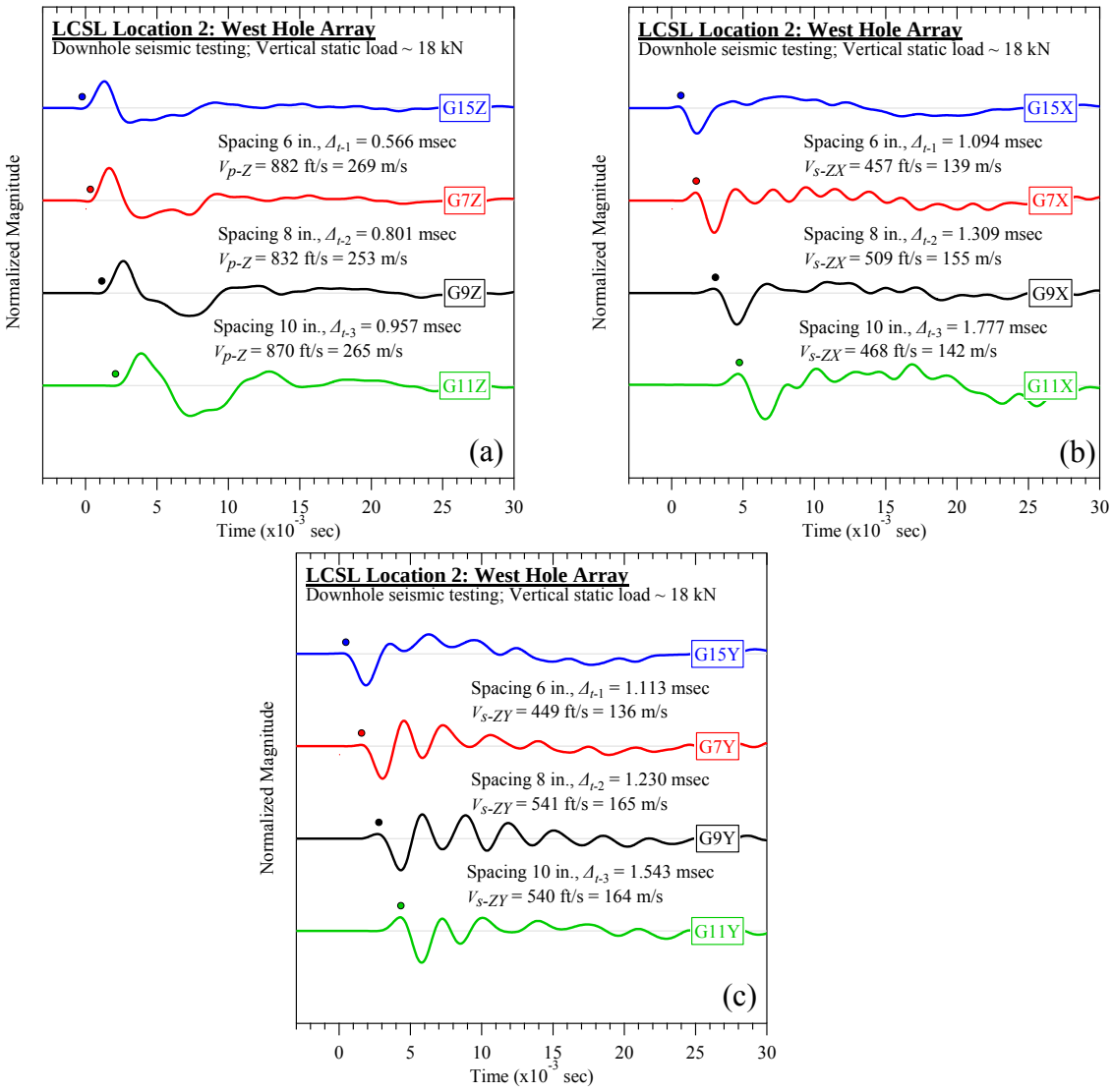

Figure B-61. Lamb Canyon Sanitary Landfill #2 (west hole): Downhole seismic testing at vertical load of 18 kN: (a) $V_{p\text{-}Z}$, (b) $V_{s\text{-}ZX}$, and (c) $V_{s\text{-}ZY}$.

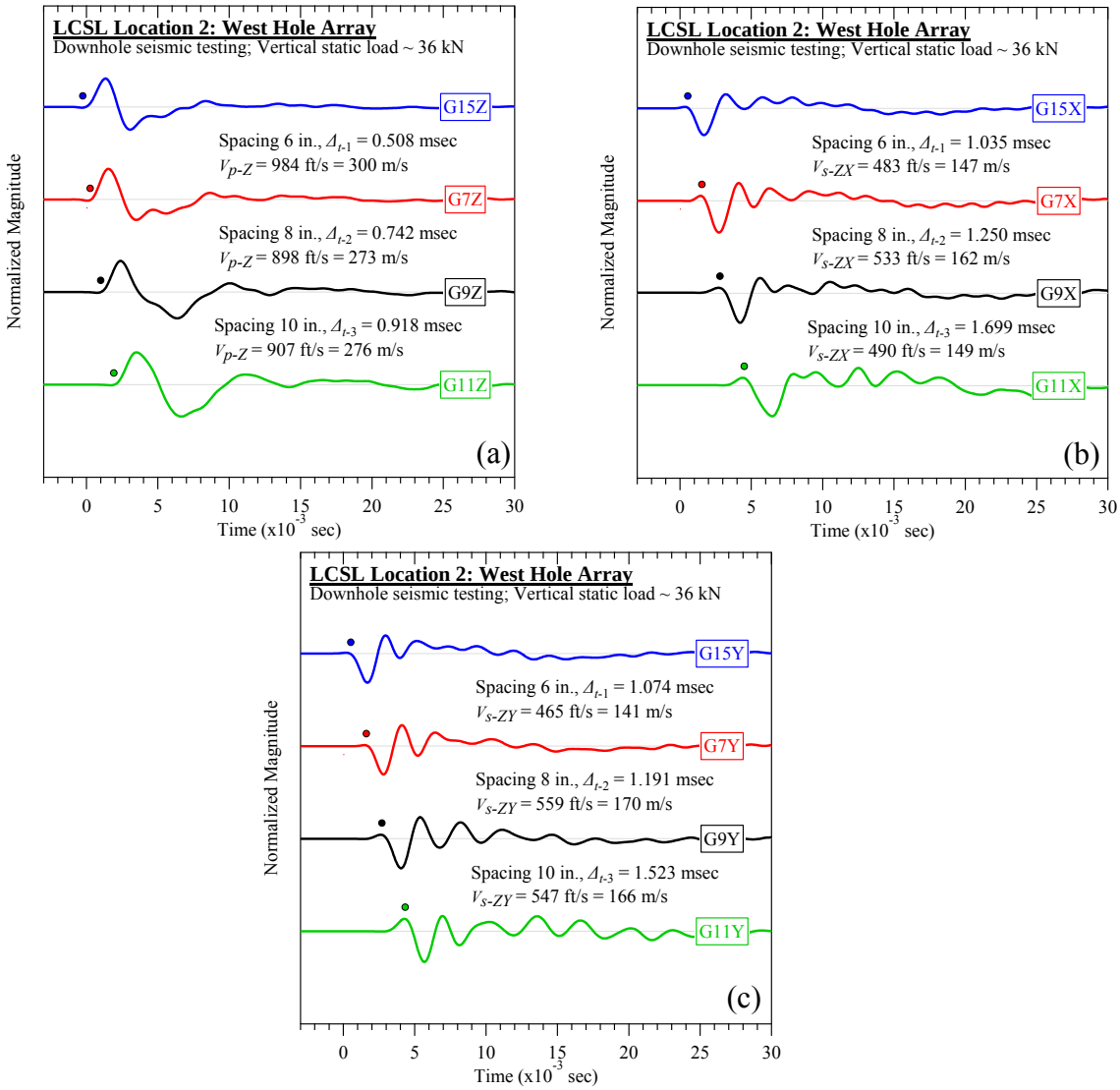

Figure B-62. Lamb Canyon Sanitary Landfill #2 (west hole): Downhole seismic testing at vertical load of 36 kN: (a) $V_{p\text{-}Z}$, (b) $V_{s\text{-}ZX}$, and (c) $V_{s\text{-}ZY}$.

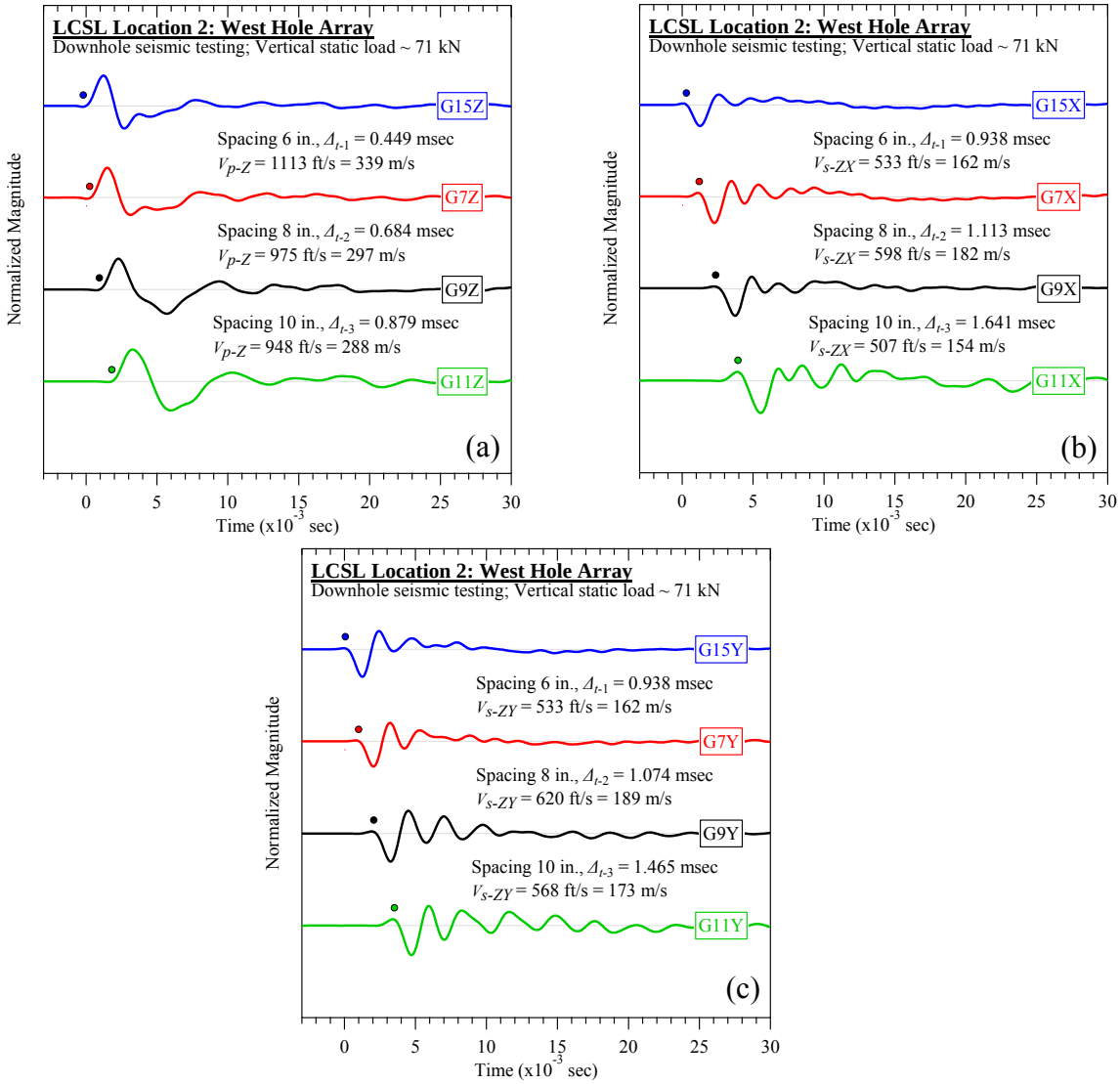

Figure B-63. Lamb Canyon Sanitary Landfill #2 (west hole): Downhole seismic testing at vertical load of 71 kN: (a) $V_{p\text{-}Z}$, (b) $V_{s\text{-}ZX}$, and (c) $V_{s\text{-}ZY}$.

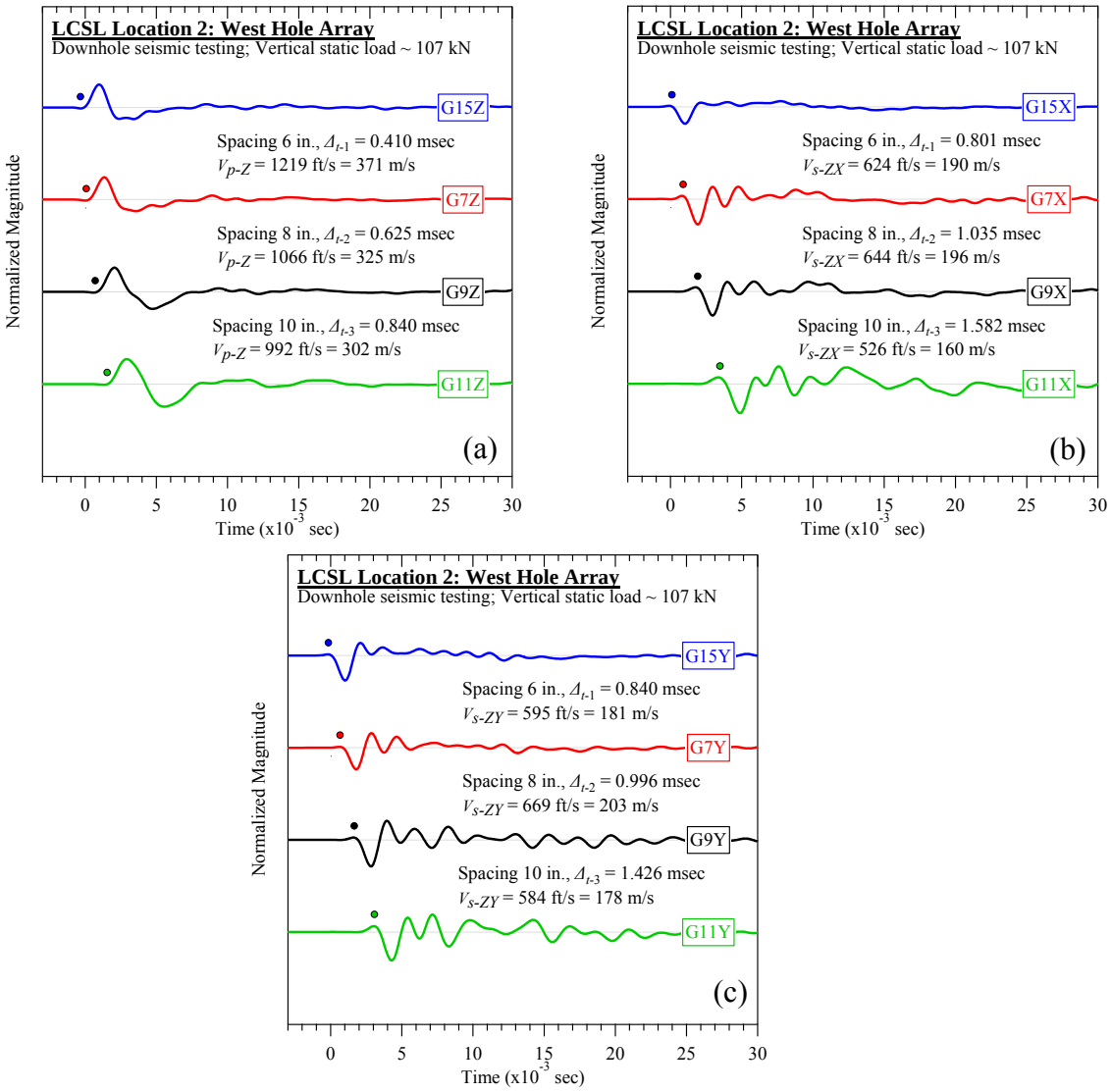

Figure B-64. Lamb Canyon Sanitary Landfill #2 (west hole): Downhole seismic testing at vertical load of 107 kN: (a) $V_{p\text{-}Z}$, (b) $V_{s\text{-}ZX}$, and (c) $V_{s\text{-}ZY}$.

B.2.2 Crosshole Seismic Testing

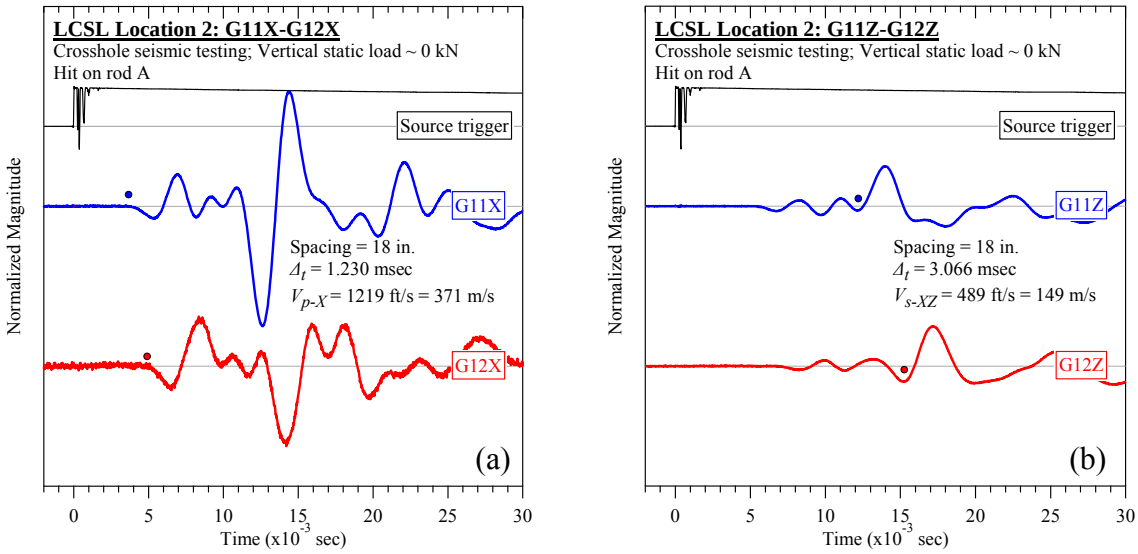

Figure B-65. Lamb Canyon Sanitary Landfill #2 (rod A): Crosshole seismic testing at vertical load of 0 kN: (a) $V_{p\text{-}X}$ and (b) $V_{s\text{-}XZ}$.

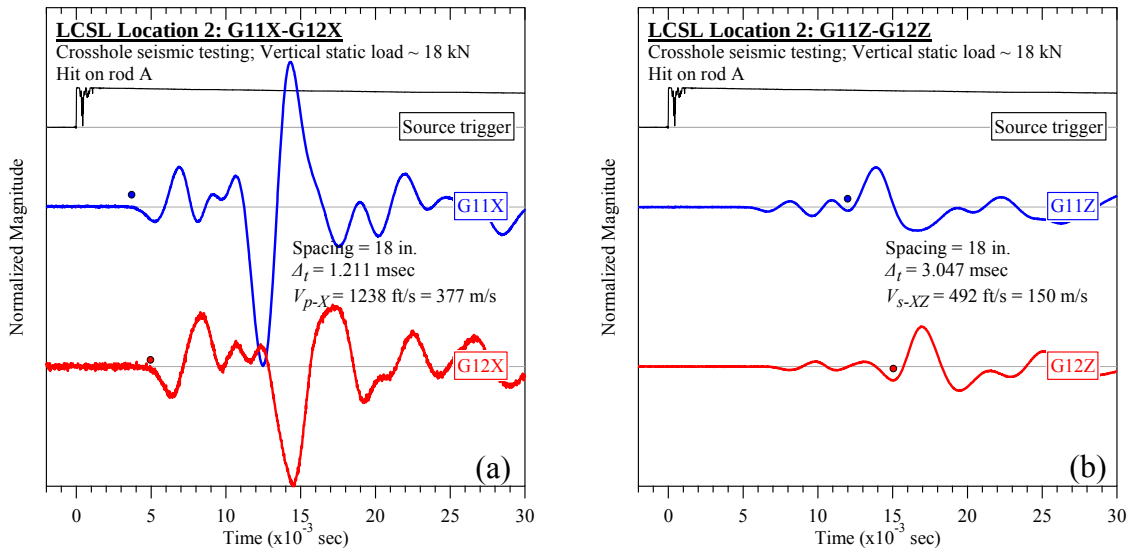

Figure B-66. Lamb Canyon Sanitary Landfill #2 (rod A): Crosshole seismic testing at vertical load of 18 kN: (a) $V_{p\text{-}X}$ and (b) $V_{s\text{-}XZ}$.

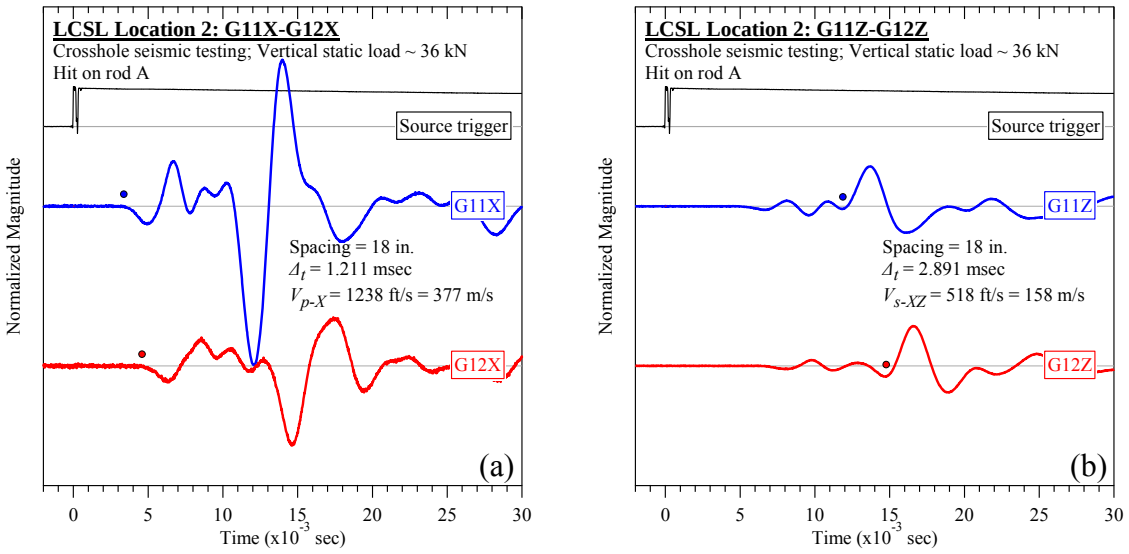

Figure B-67. Lamb Canyon Sanitary Landfill #2 (rod A): Crosshole seismic testing at vertical load of 36 kN: (a) $V_{p\text{-}X}$ and (b) $V_{s\text{-}XZ}$.

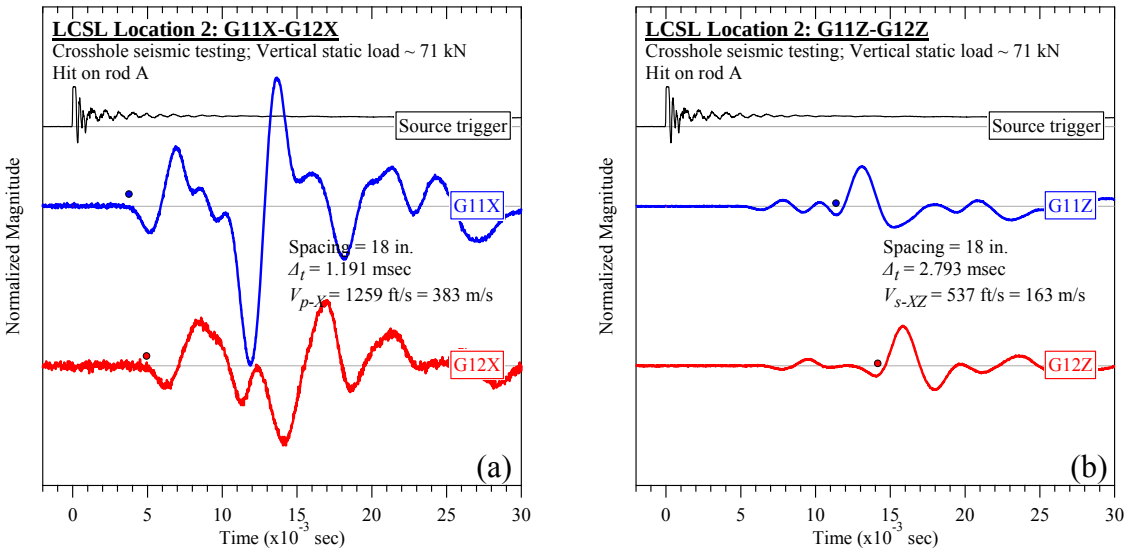

Figure B-68. Lamb Canyon Sanitary Landfill #2 (rod A): Crosshole seismic testing at vertical load of 71 kN: (a) $V_{p\text{-}X}$ and (b) $V_{s\text{-}XZ}$.

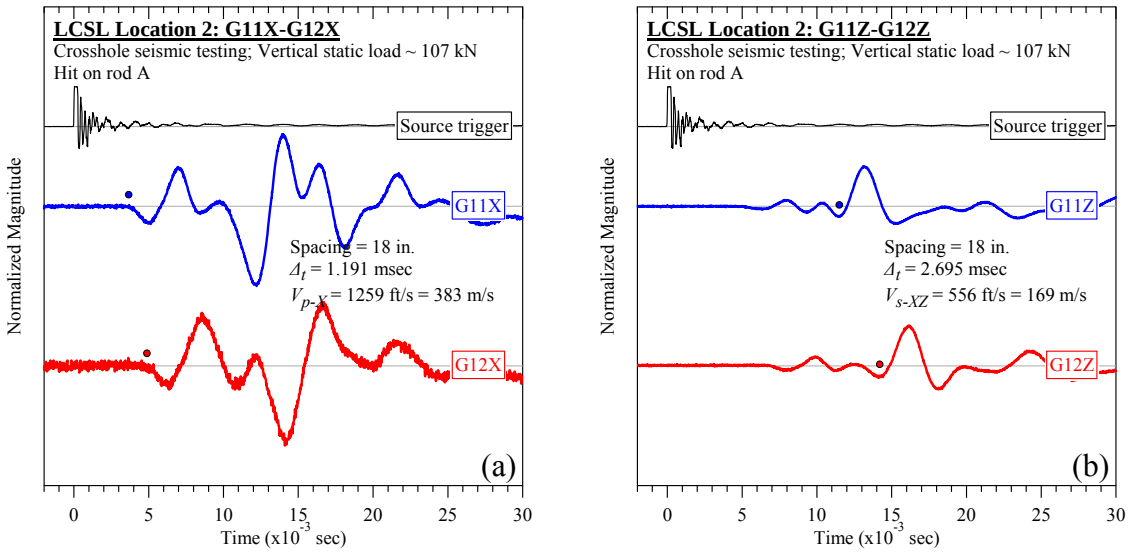

Figure B-69. Lamb Canyon Sanitary Landfill #2 (rod A): Crosshole seismic testing at vertical load of 107 kN: (a) $V_{p\text{-}X}$ and (b) $V_{s\text{-}XZ}$.

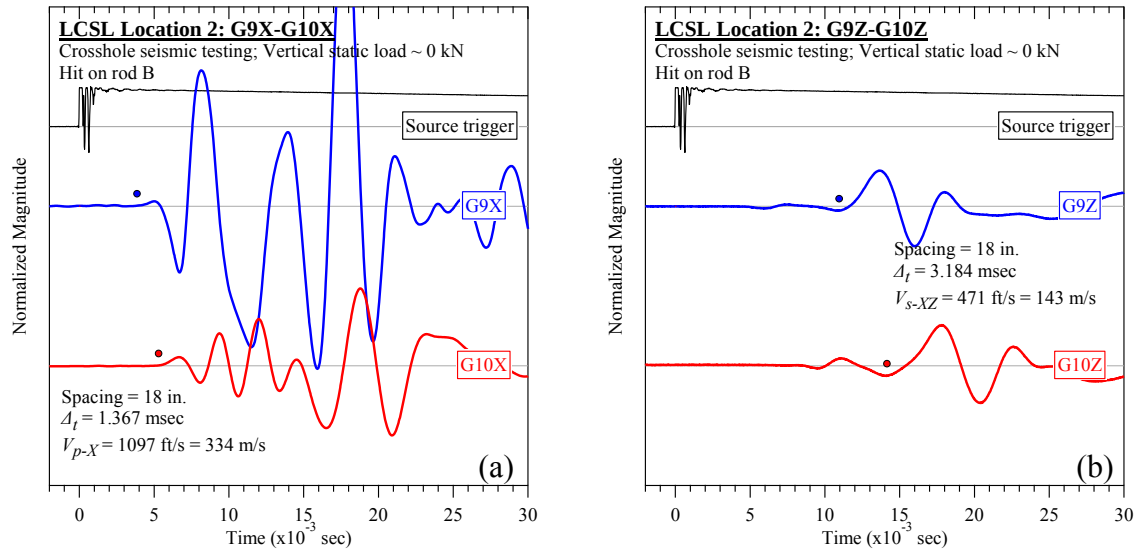

Figure B-70. Lamb Canyon Sanitary Landfill #2 (rod B): Crosshole seismic testing at vertical load of 0 kN: (a) $V_{p\text{-}X}$ and (b) $V_{s\text{-}XZ}$.

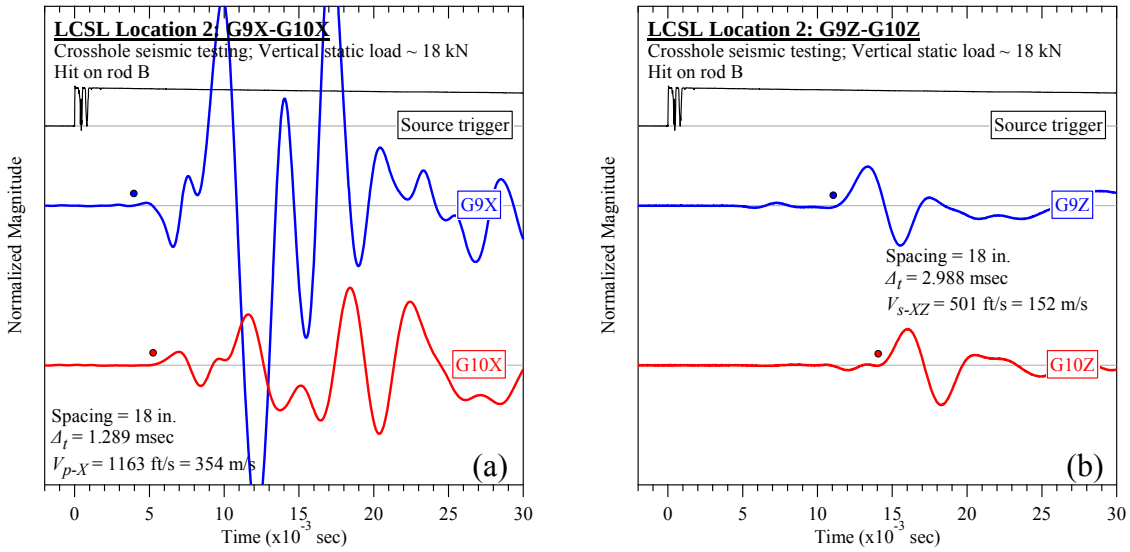

Figure B-71. Lamb Canyon Sanitary Landfill #2 (rod B): Crosshole seismic testing at vertical load of 18 kN: (a) $V_{p\text{-}X}$ and (b) $V_{s\text{-}XZ}$.

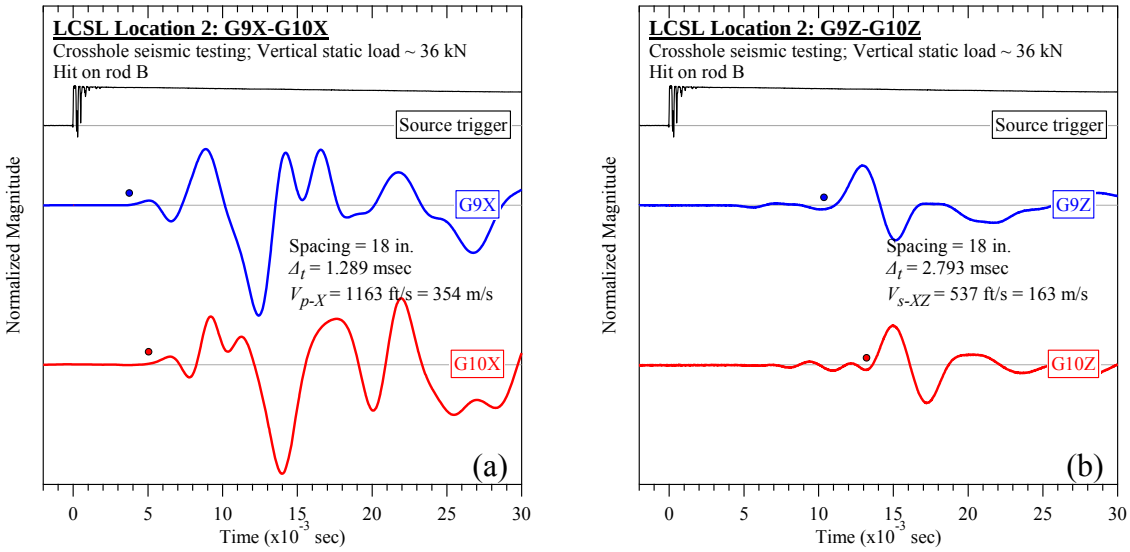

Figure B-72. Lamb Canyon Sanitary Landfill #2 (rod B): Crosshole seismic testing at vertical load of 36 kN: (a) $V_{p\text{-}X}$ and (b) $V_{s\text{-}XZ}$.

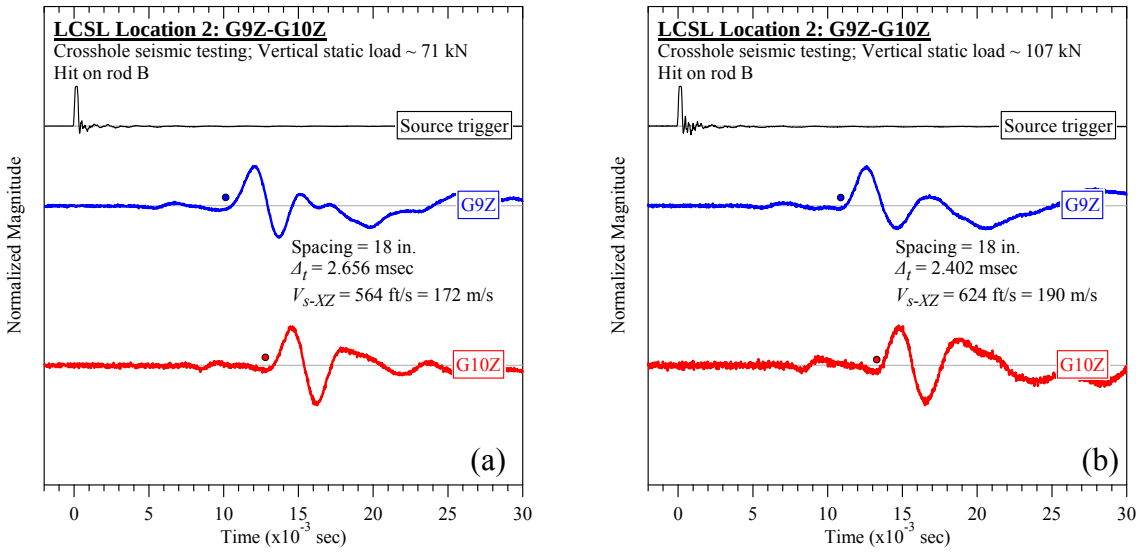

Figure B-73. Lamb Canyon Sanitary Landfill #2 (rod B): Crosshole seismic testing at vertical load of (a)71 kN and (b) 107 kN: $V_{s\text{-}XZ}$.

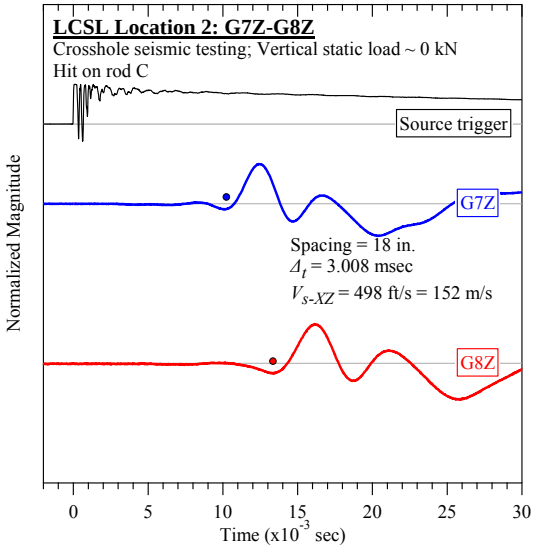

Figure B-74. Lamb Canyon Sanitary Landfill #2 (rod C): Crosshole seismic testing at vertical load of 0 kN: $V_{s\text{-}XZ}$.

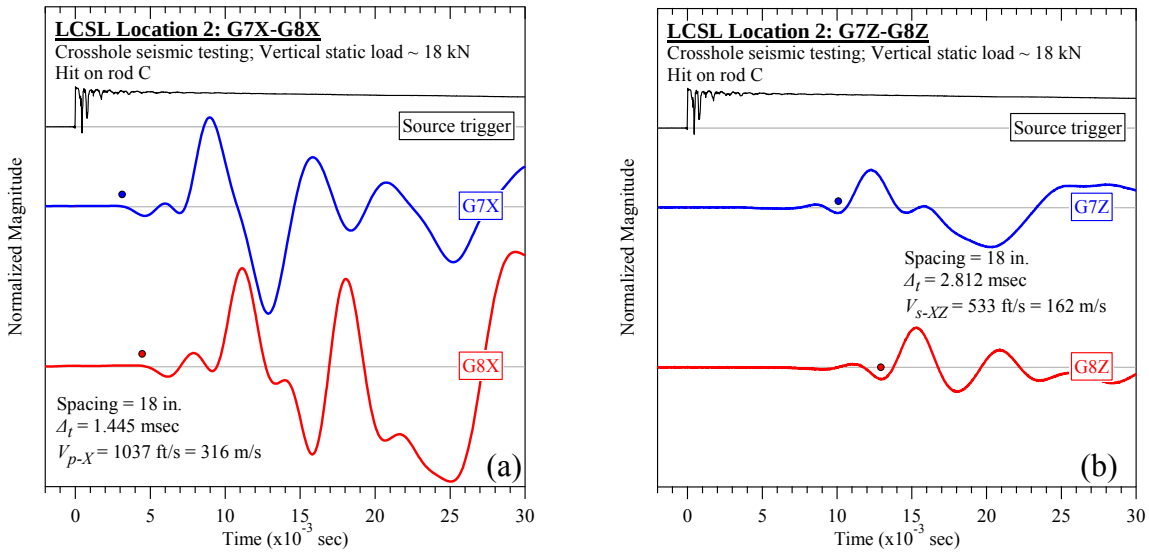

Figure B-75. Lamb Canyon Sanitary Landfill #2 (rod C): Crosshole seismic testing at vertical load of 18 kN: (a) $V_{p\text{-}X}$ and (b) $V_{s\text{-}XZ}$.

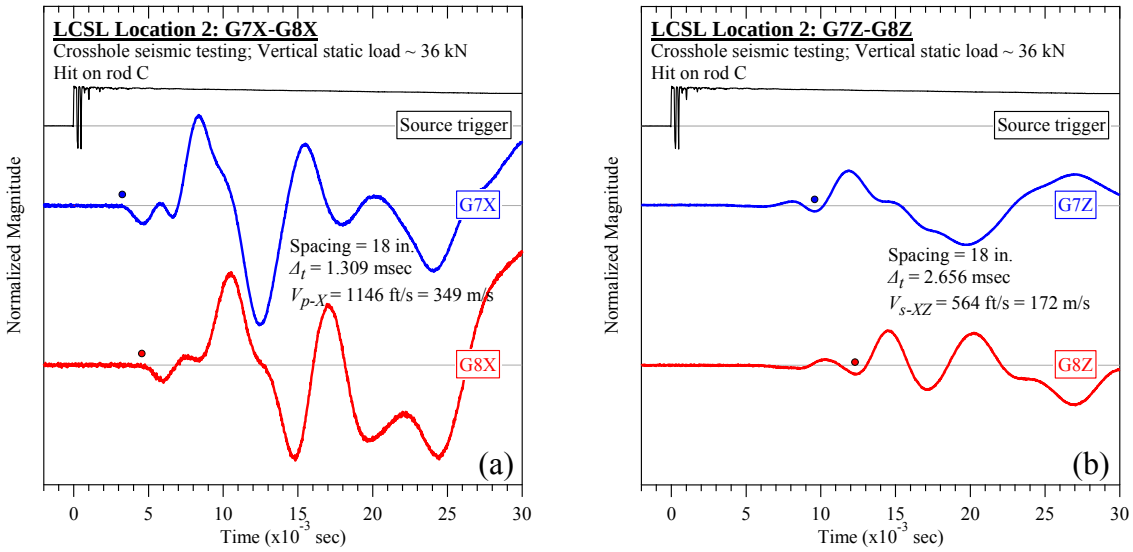

Figure B-76. Lamb Canyon Sanitary Landfill #2 (rod C): Crosshole seismic testing at vertical load of 36 kN: (a) $V_{p\text{-}X}$ and (b) $V_{s\text{-}XZ}$.

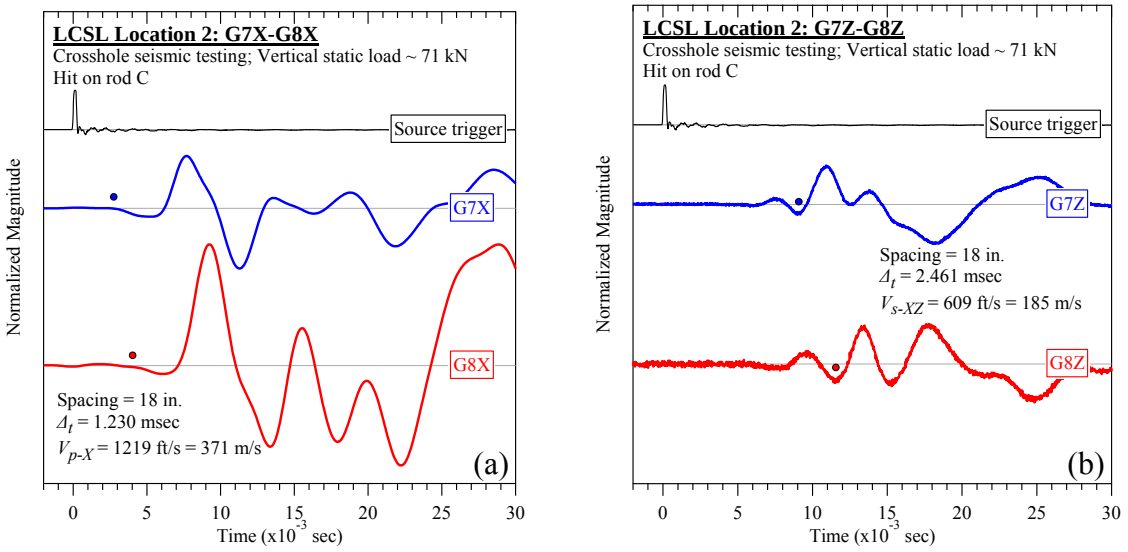

Figure B-77. Lamb Canyon Sanitary Landfill #2 (rod C): Crosshole seismic testing at vertical load of 71 kN: (a) $V_{p\text{-}X}$ and (b) $V_{s\text{-}XZ}$.

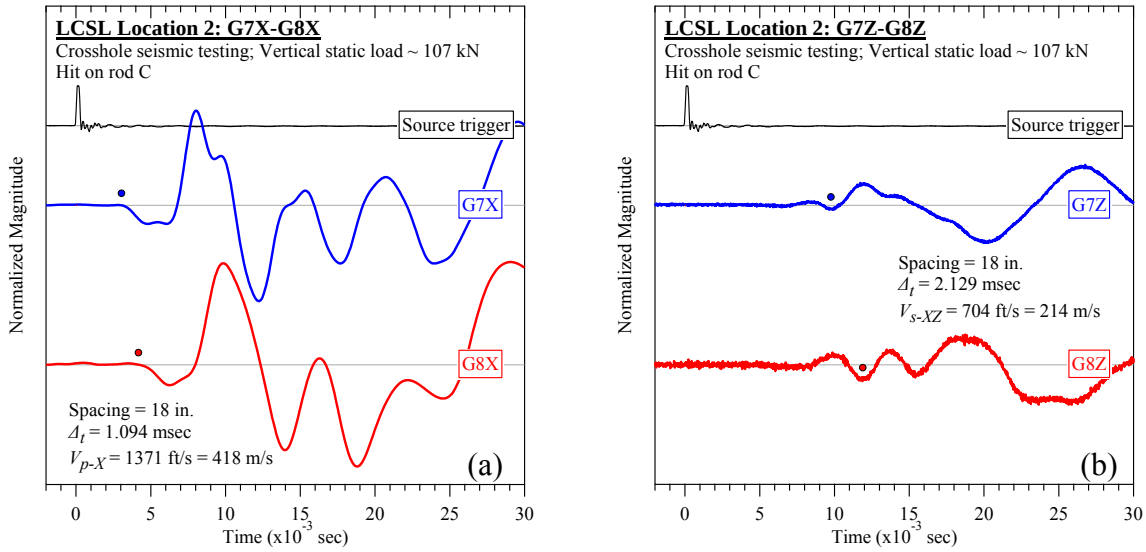

Figure B-78. Lamb Canyon Sanitary Landfill #2 (rod C): Crosshole seismic testing at vertical load of 107 kN: (a) $V_{p\text{-}X}$ and (b) $V_{s\text{-}XZ}$.

B.2.3 Steady-state Dynamic Testing

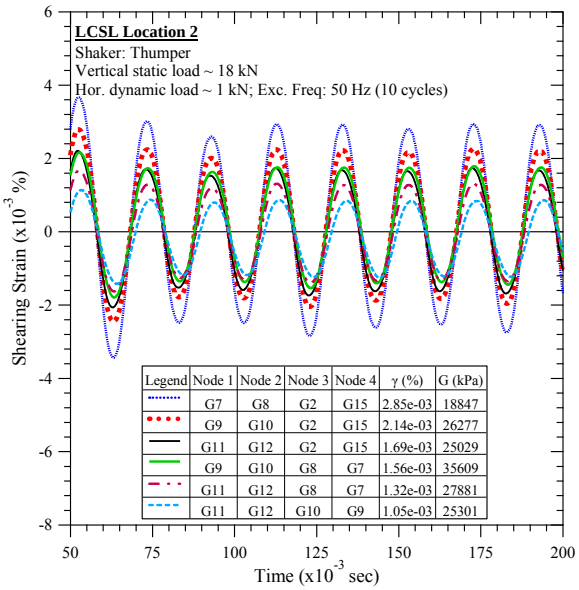

Figure B-79. Lamb Canyon Sanitary Landfill #2: Steady-state dynamic testing at vertical load of 18 kN and horizontal dynamic load of 1 kN.

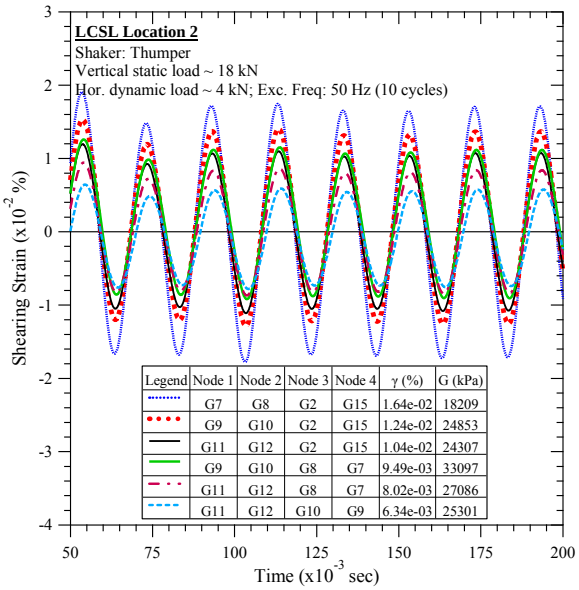

Figure B-80. Lamb Canyon Sanitary Landfill #2: Steady-state dynamic testing at vertical load of 18 kN and horizontal dynamic load of 4 kN.

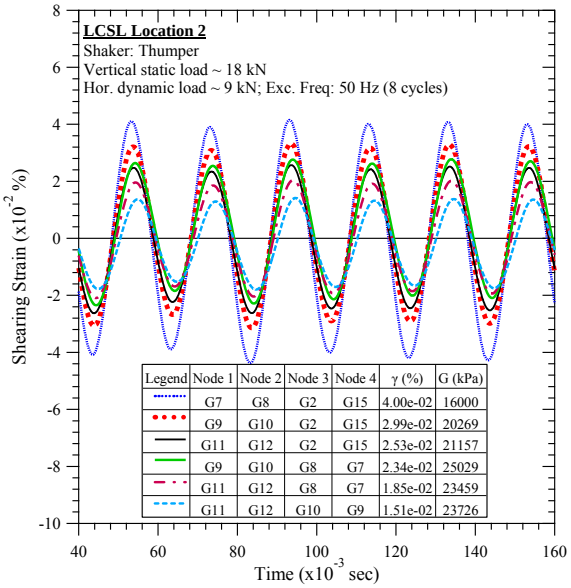

Figure B-81. Lamb Canyon Sanitary Landfill #2: Steady-state dynamic testing at vertical load of 18 kN and horizontal dynamic load of 9 kN.

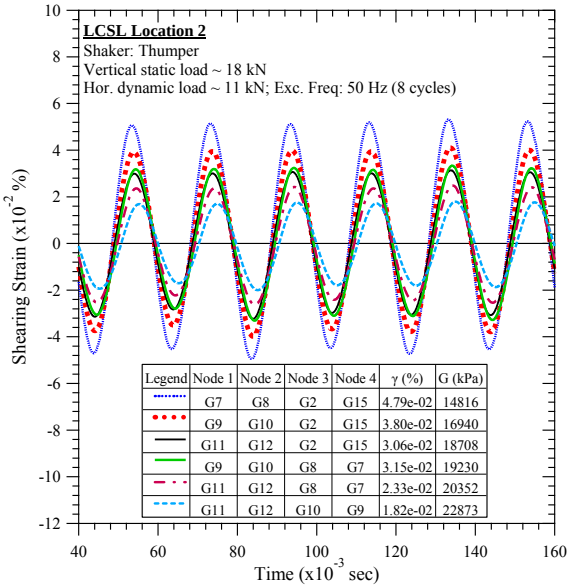

Figure B-82. Lamb Canyon Sanitary Landfill #2: Steady-state dynamic testing at vertical load of 18 kN and horizontal dynamic load of 11 kN.

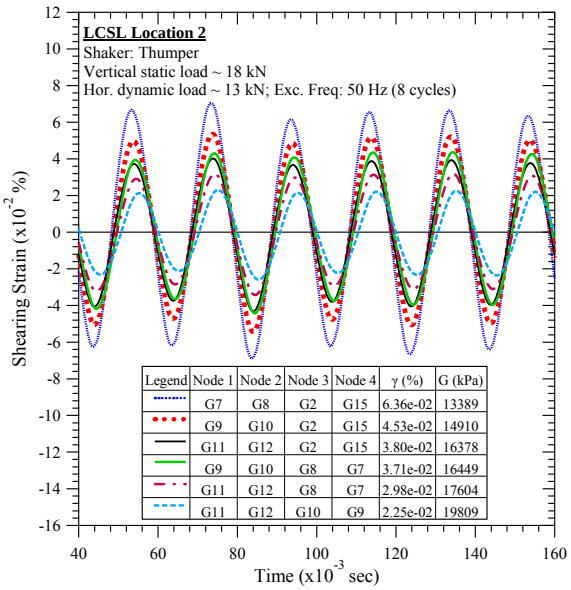

Figure B-83. Lamb Canyon Sanitary Landfill #2: Steady-state dynamic testing at vertical load of 18 kN and horizontal dynamic load of 13 kN.

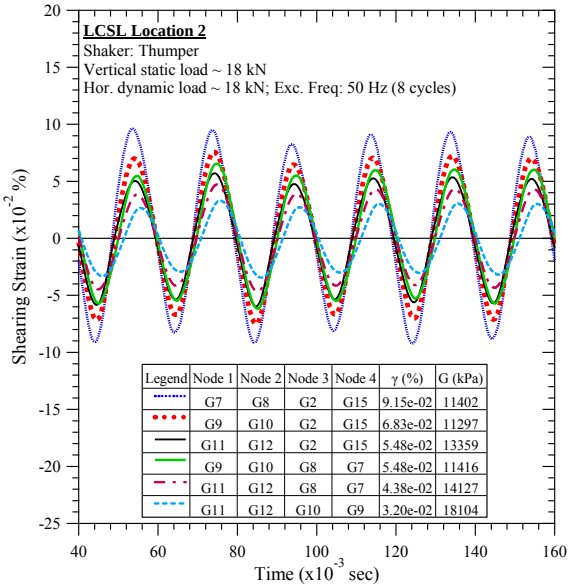

Figure B-84. Lamb Canyon Sanitary Landfill #2: Steady-state dynamic testing at vertical load of 18 kN and horizontal dynamic load of 18 kN.

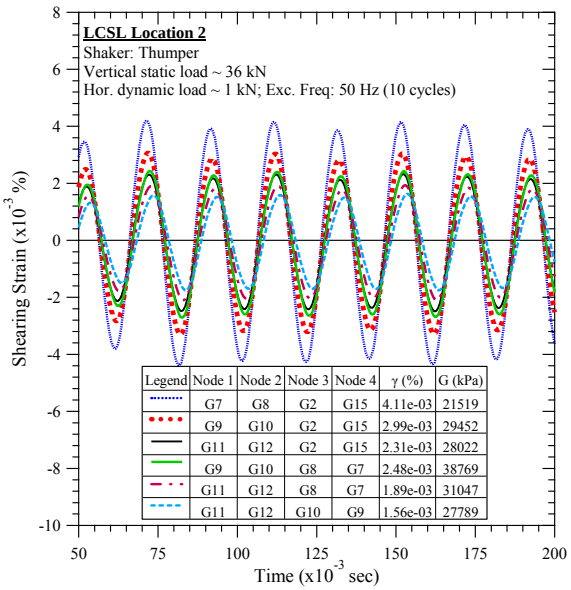

Figure B-85. Lamb Canyon Sanitary Landfill #2: Steady-state dynamic testing at vertical load of 36 kN and horizontal dynamic load of 1 kN.

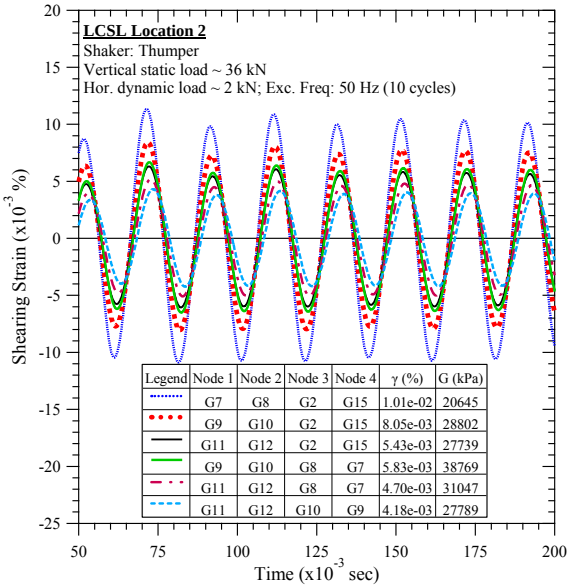

Figure B-86. Lamb Canyon Sanitary Landfill #2: Steady-state dynamic testing at vertical load of 36 kN and horizontal dynamic load of 2 kN.

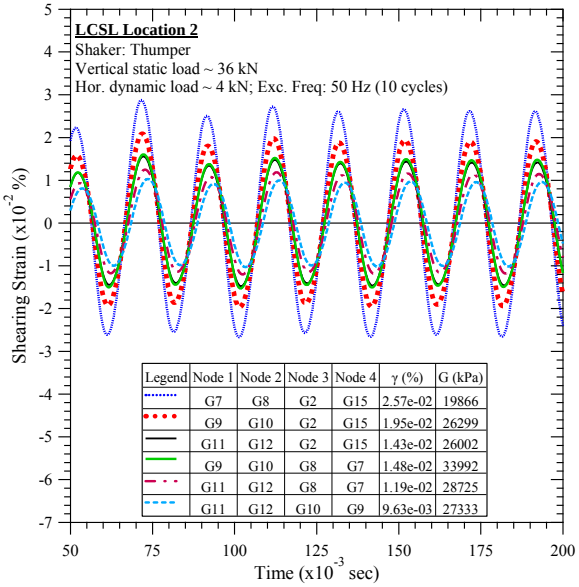

Figure B-87. Lamb Canyon Sanitary Landfill #2: Steady-state dynamic testing at vertical load of 36 kN and horizontal dynamic load of 4 kN.

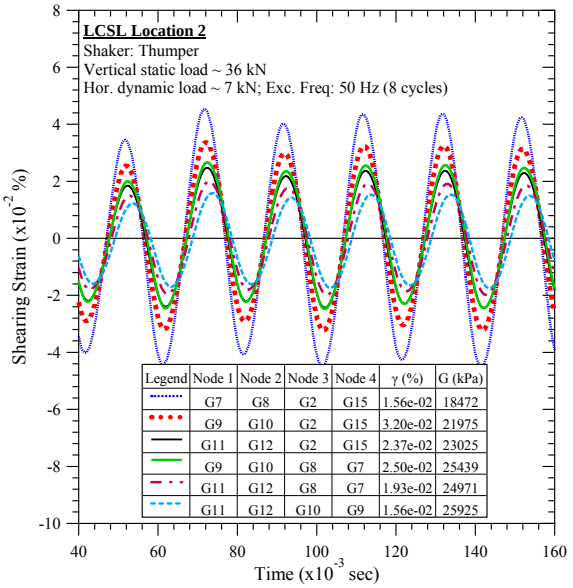

Figure B-88. Lamb Canyon Sanitary Landfill #2: Steady-state dynamic testing at vertical load of 36 kN and horizontal dynamic load of 7 kN.

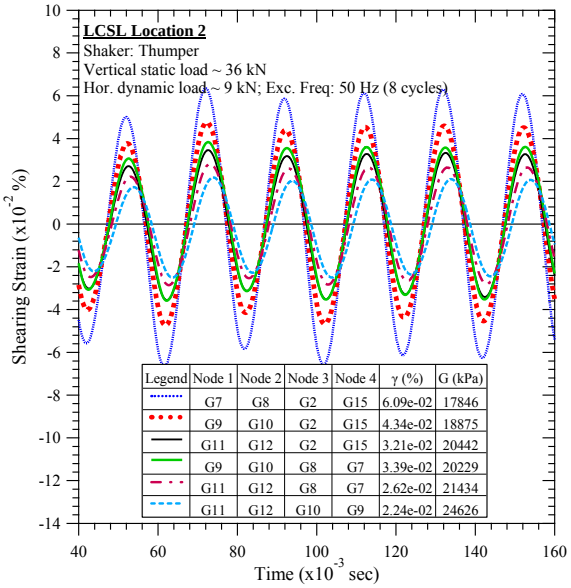

Figure B-89. Lamb Canyon Sanitary Landfill #2: Steady-state dynamic testing at vertical load of 36 kN and horizontal dynamic load of 9 kN.

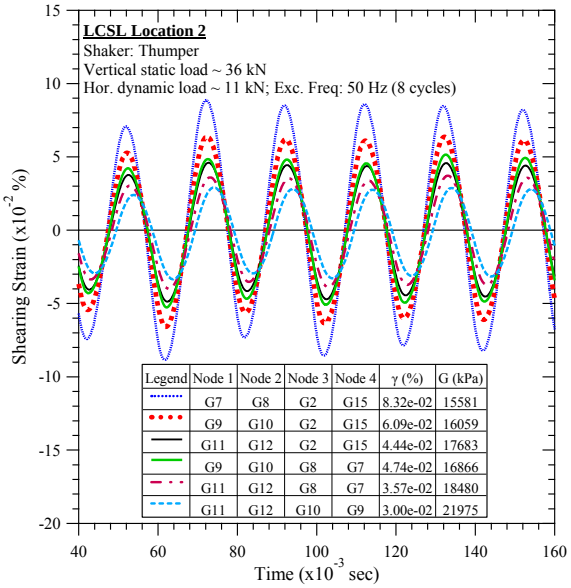

Figure B-90. Lamb Canyon Sanitary Landfill #2: Steady-state dynamic testing at vertical load of 36 kN and horizontal dynamic load of 11 kN.

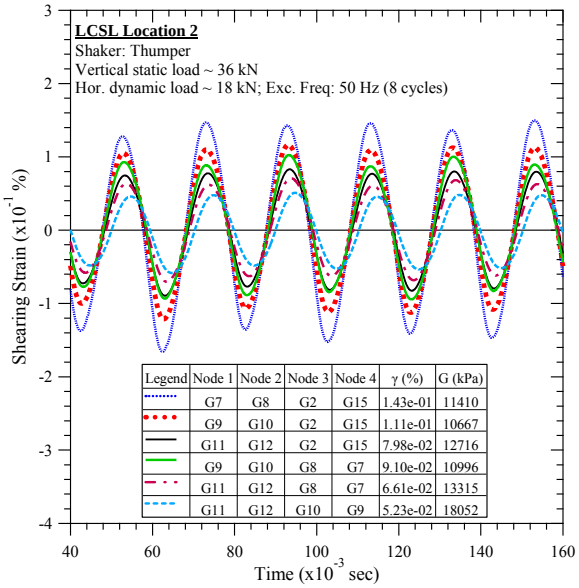

Figure B-91. Lamb Canyon Sanitary Landfill #2: Steady-state dynamic testing at vertical load of 36 kN and horizontal dynamic load of 18 kN.

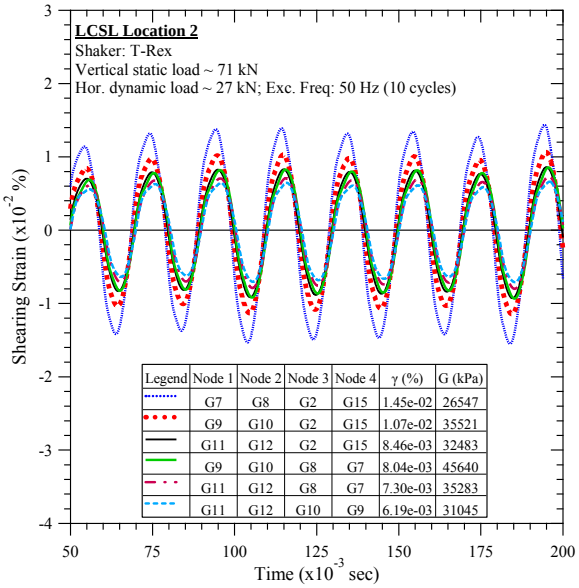

Figure B-92. Lamb Canyon Sanitary Landfill #2: Steady-state dynamic testing at vertical load of 71 kN and horizontal dynamic load of 27 kN.

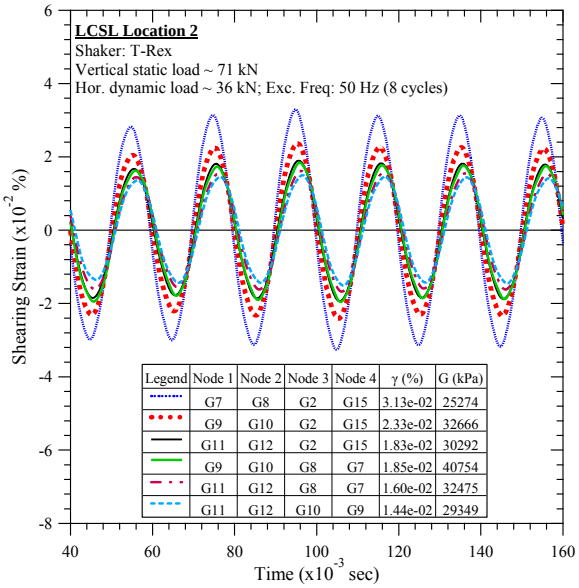

Figure B-93. Lamb Canyon Sanitary Landfill #2: Steady-state dynamic testing at vertical load of 71 kN and horizontal dynamic load of 36 kN.

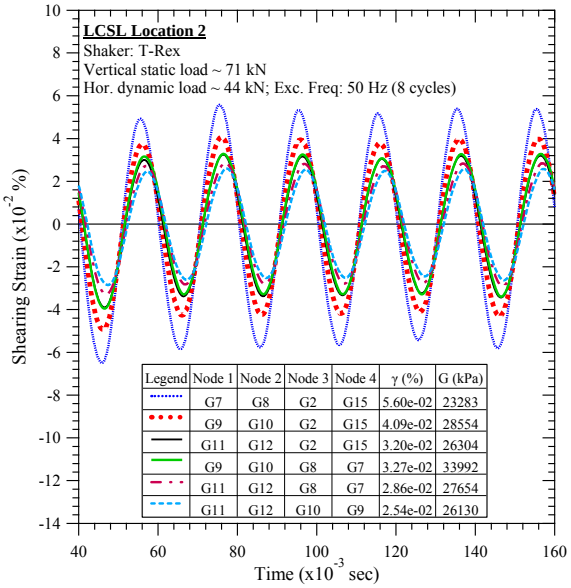

Figure B-94. Lamb Canyon Sanitary Landfill #2: Steady-state dynamic testing at vertical load of 71 kN and horizontal dynamic load of 44 kN.

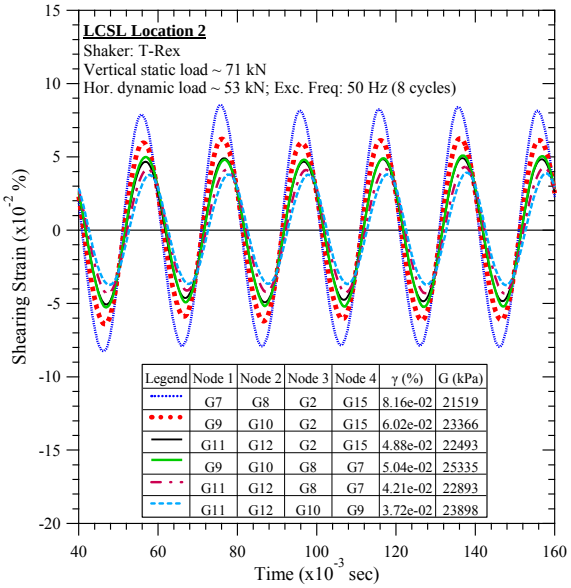

Figure B-95. Lamb Canyon Sanitary Landfill #2: Steady-state dynamic testing at vertical load of 71 kN and horizontal dynamic load of 53 kN.

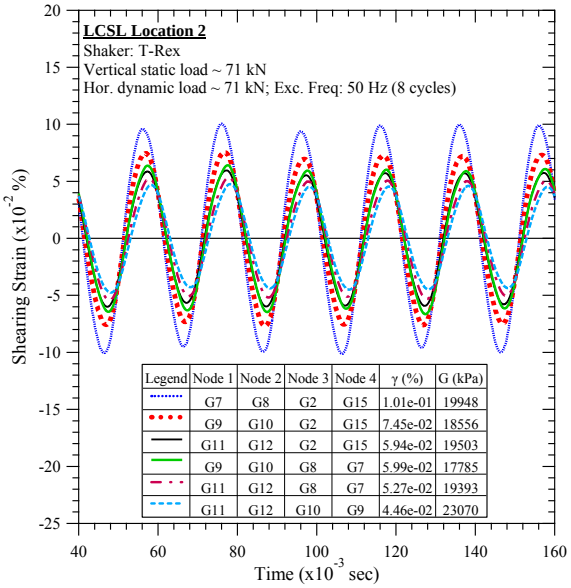

Figure B-96. Lamb Canyon Sanitary Landfill #2: Steady-state dynamic testing at vertical load of 71 kN and horizontal dynamic load of 71 kN.

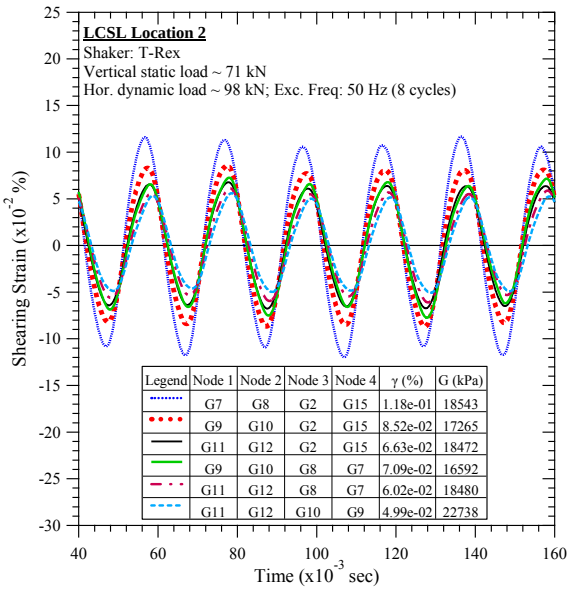

Figure B-97. Lamb Canyon Sanitary Landfill #2: Steady-state dynamic testing at vertical load of 71 kN and horizontal dynamic load of 98 kN.

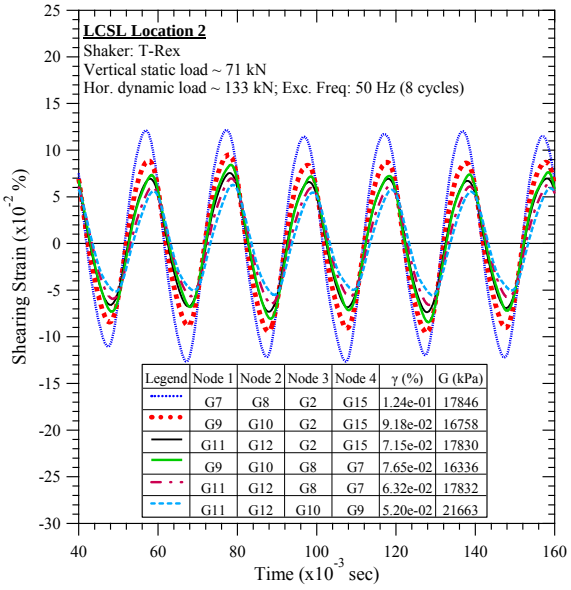

Figure B-98. Lamb Canyon Sanitary Landfill #2: Steady-state dynamic testing at vertical load of 71 kN and horizontal dynamic load of 133 kN.

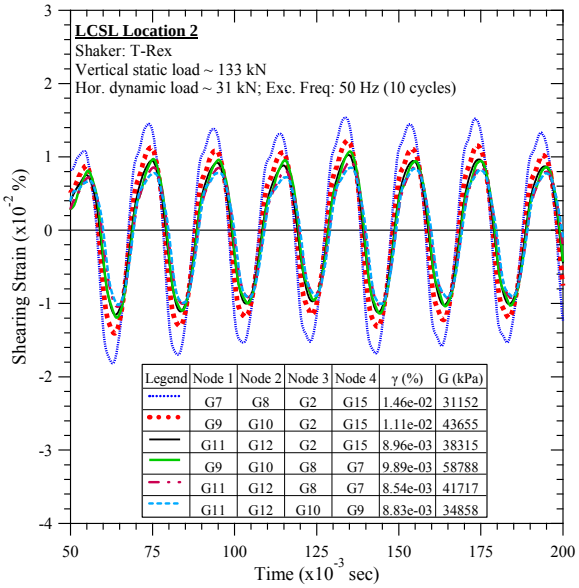

Figure B-99. Lamb Canyon Sanitary Landfill #2: Steady-state dynamic testing at vertical load of 133 kN and horizontal dynamic load of 31 kN.

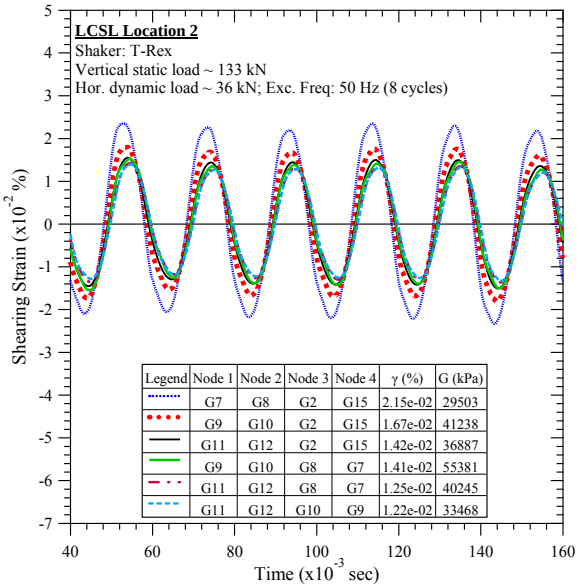

Figure B-100. Lamb Canyon Sanitary Landfill #2: Steady-state dynamic testing at vertical load of 133 kN and horizontal dynamic load of 36 kN.

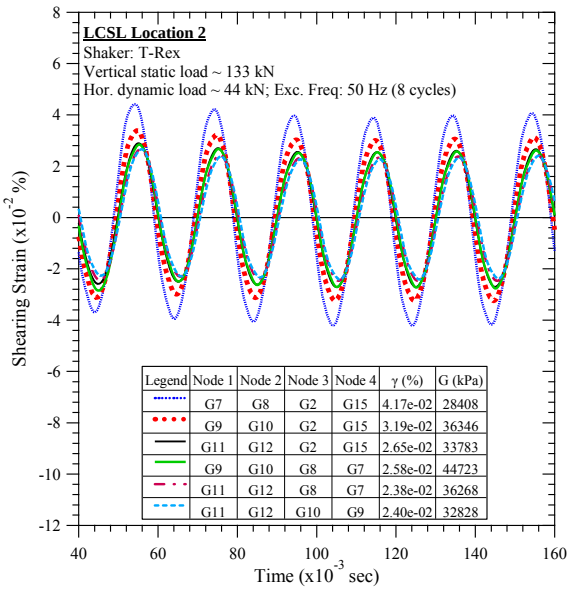

Figure B-101. Lamb Canyon Sanitary Landfill #2: Steady-state dynamic testing at vertical load of 133 kN and horizontal dynamic load of 44 kN.

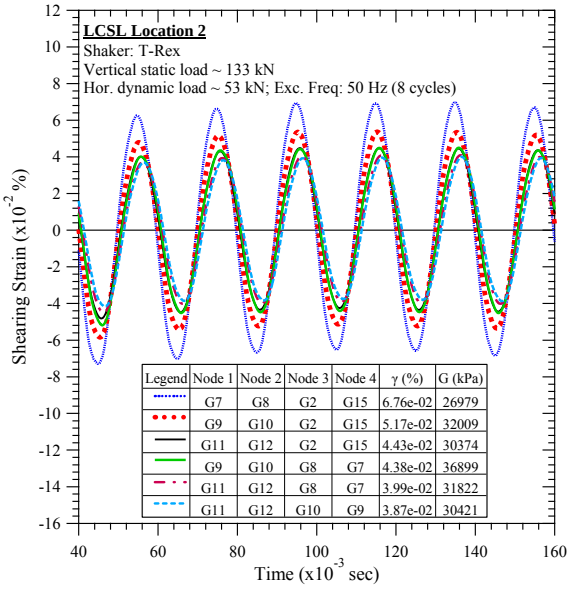

Figure B-102. Lamb Canyon Sanitary Landfill #2: Steady-state dynamic testing at vertical load of 133 kN and horizontal dynamic load of 53 kN.

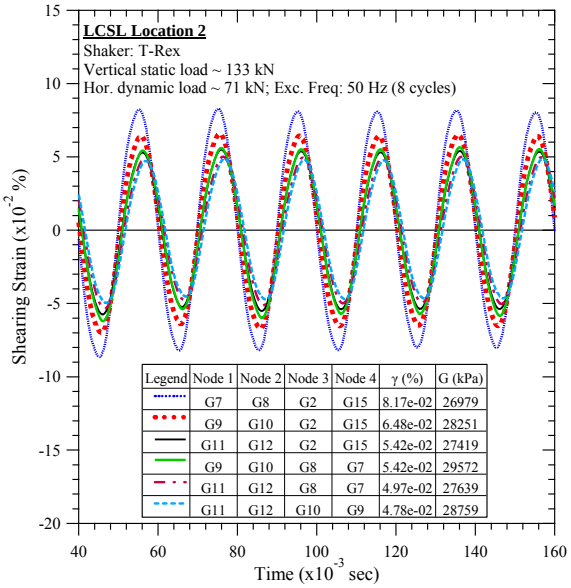

Figure B-103. Lamb Canyon Sanitary Landfill #2: Steady-state dynamic testing at vertical load of 133 kN and horizontal dynamic load of 71 kN.

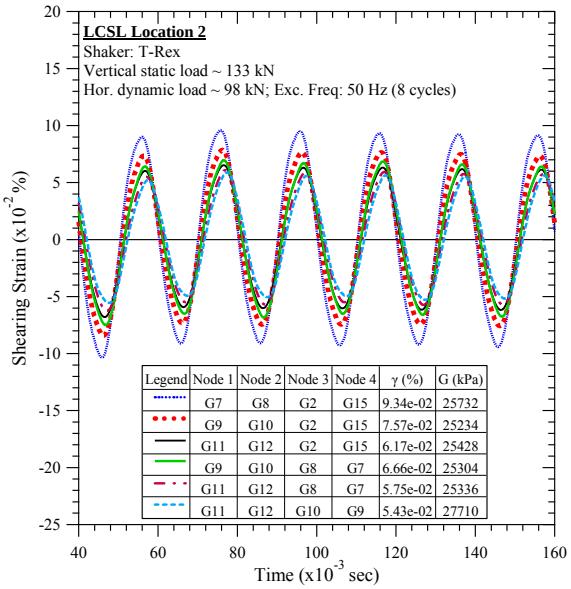

Figure B-104. Lamb Canyon Sanitary Landfill #2: Steady-state dynamic testing at vertical load of 133 kN and horizontal dynamic load of 98 kN.

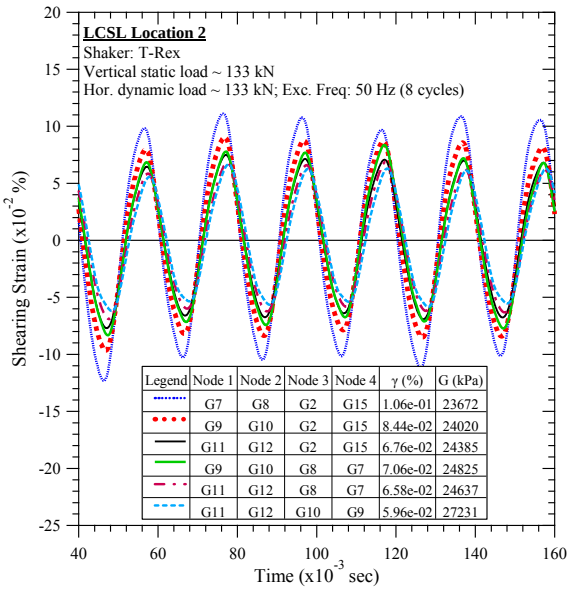

Figure B-105. Lamb Canyon Sanitary Landfill #2: Steady-state dynamic testing at vertical load of 133 kN and horizontal dynamic load of 133 kN.

B.3 Lamb Canyon Sanitary Landfill Location 3

B.3.1 Downhole Seismic Testing

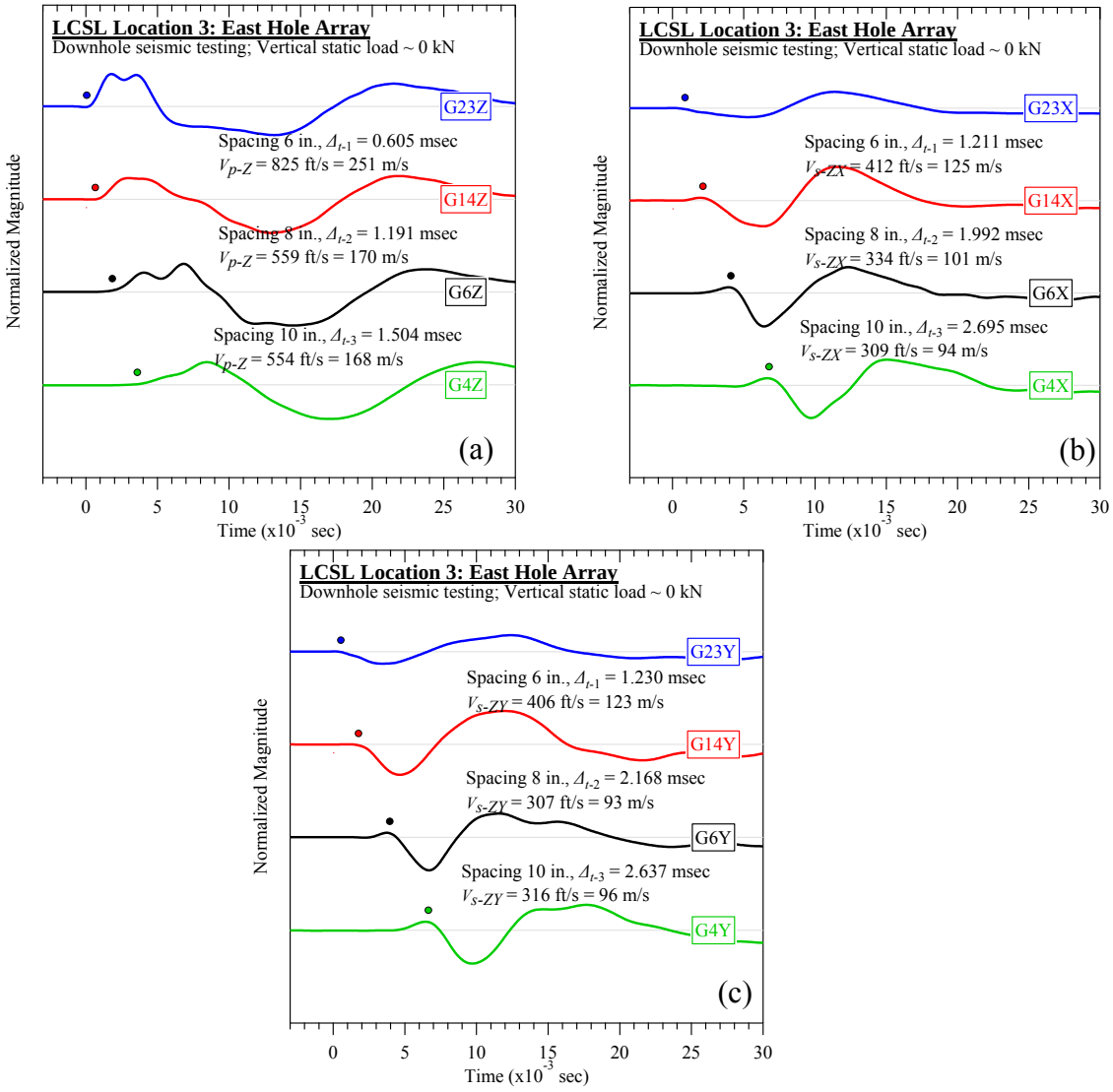

Figure B-106. Lamb Canyon Sanitary Landfill #3 (east hole): Downhole seismic testing at vertical load of 0 kN: (a) $V_{p\text{-}Z}$, (b) $V_{s\text{-}ZX}$, and (c) $V_{s\text{-}ZY}$.

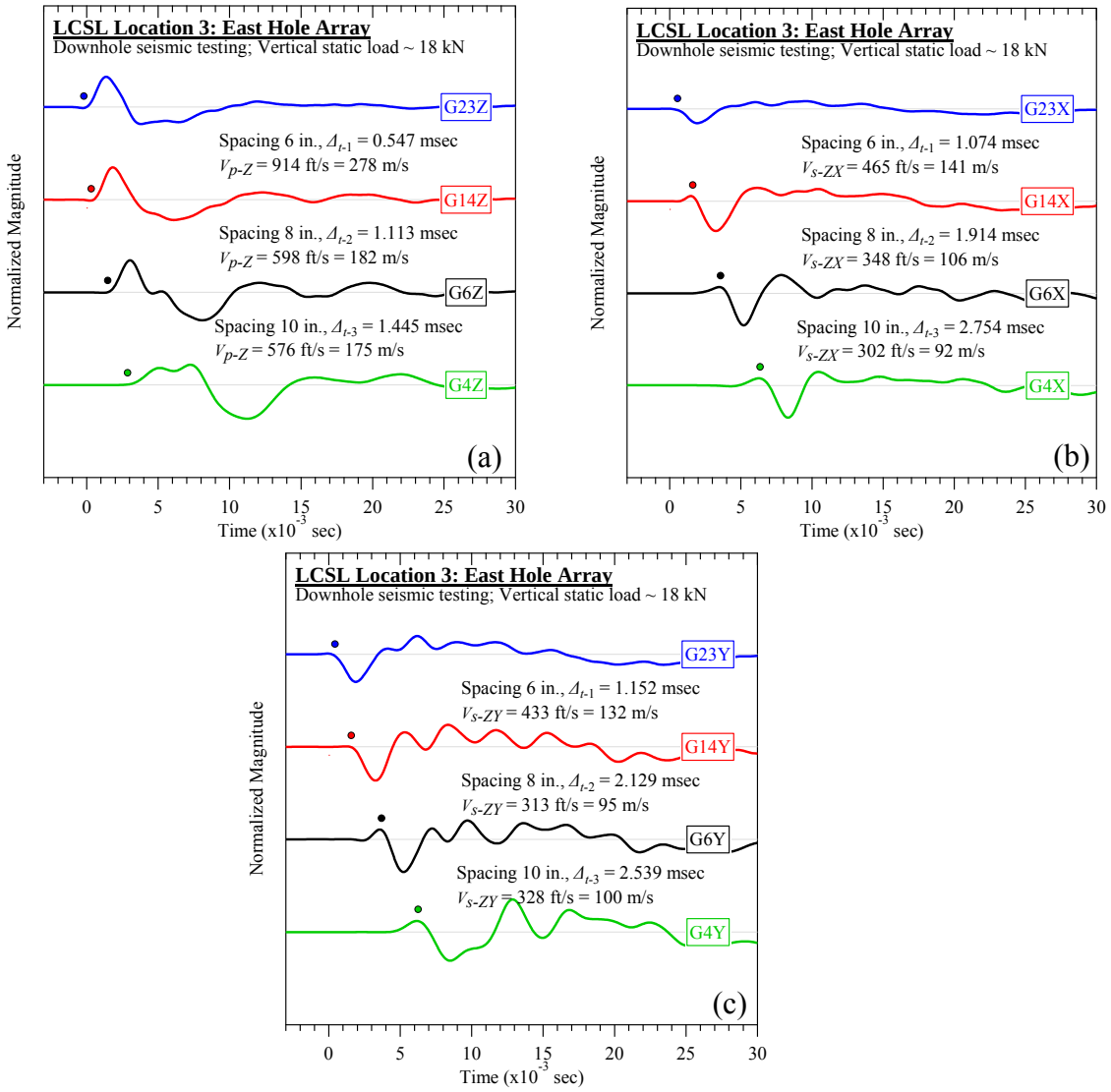

Figure B-107. Lamb Canyon Sanitary Landfill #3 (east hole): Downhole seismic testing at vertical load of 18 kN: (a) $V_{p\text{-}Z}$, (b) $V_{s\text{-}ZX}$, and (c) $V_{s\text{-}ZY}$.

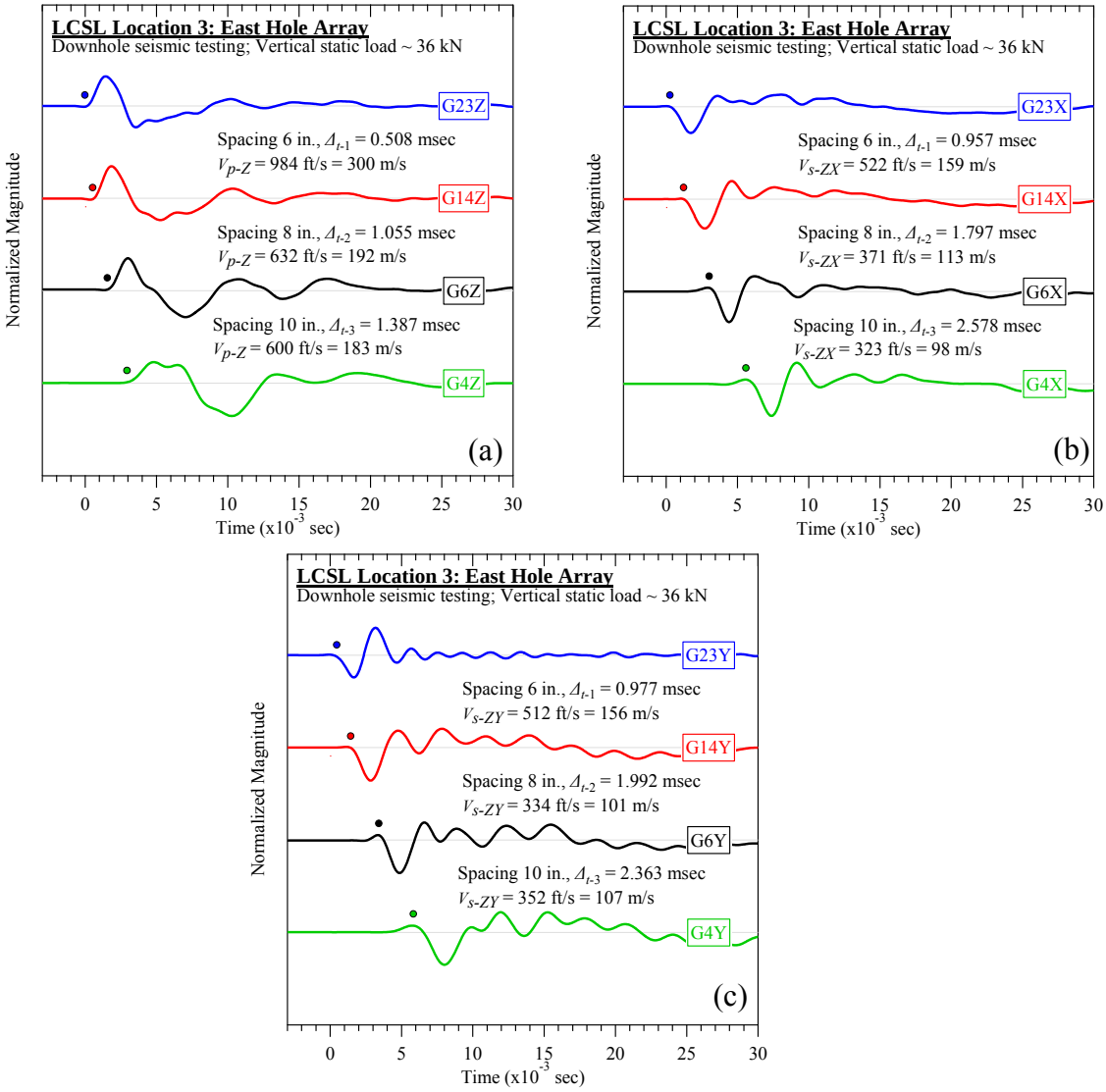

Figure B-108. Lamb Canyon Sanitary Landfill #3 (east hole): Downhole seismic testing at vertical load of 36 kN: (a) V_{p-Z}, (b) V_{s-ZX}, and (c) V_{s-ZY}.

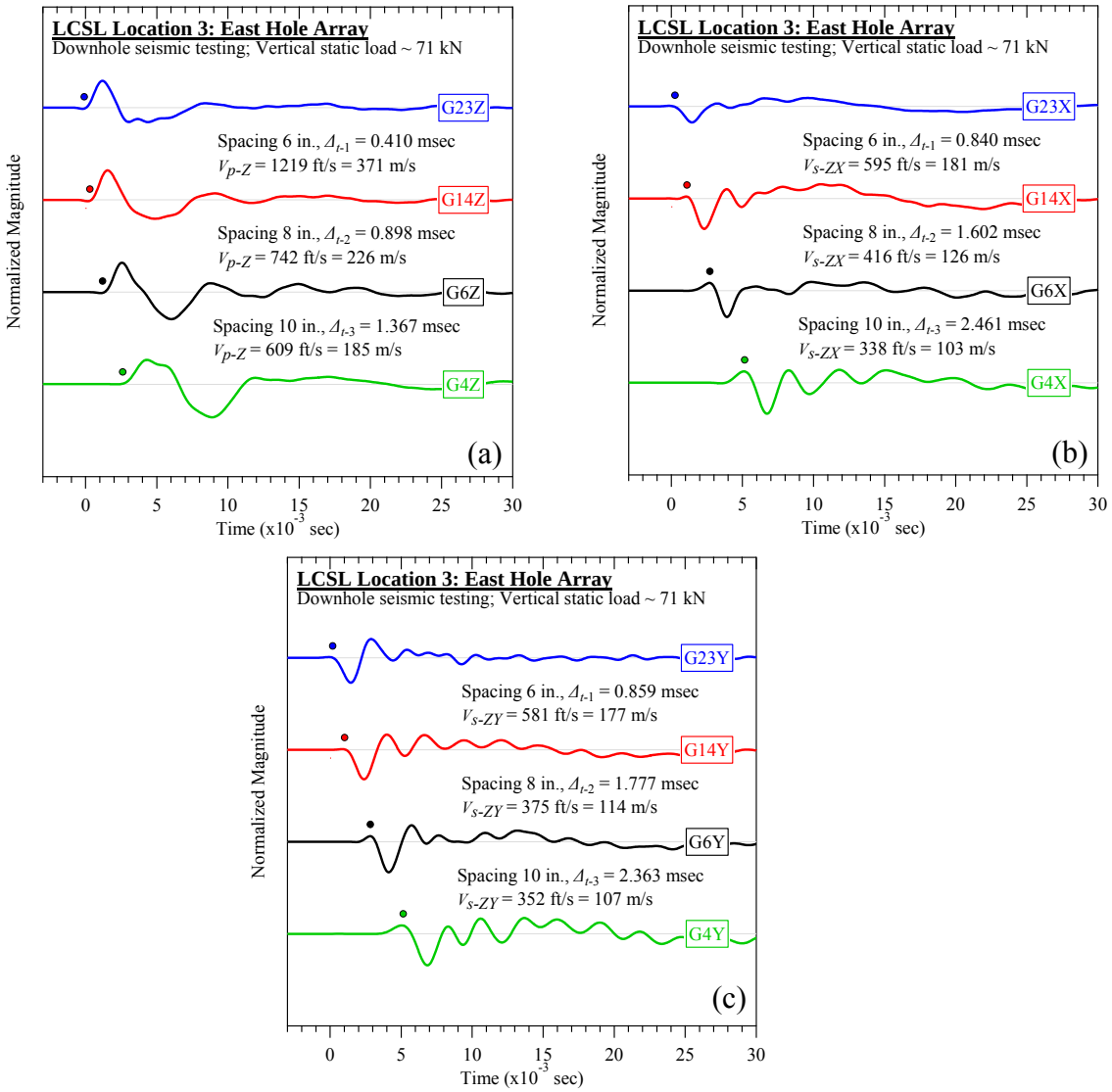

Figure B-109. Lamb Canyon Sanitary Landfill #3 (east hole): Downhole seismic testing at vertical load of 71 kN: (a) $V_{p\text{-}Z}$, (b) $V_{s\text{-}ZX}$, and (c) $V_{s\text{-}ZY}$.

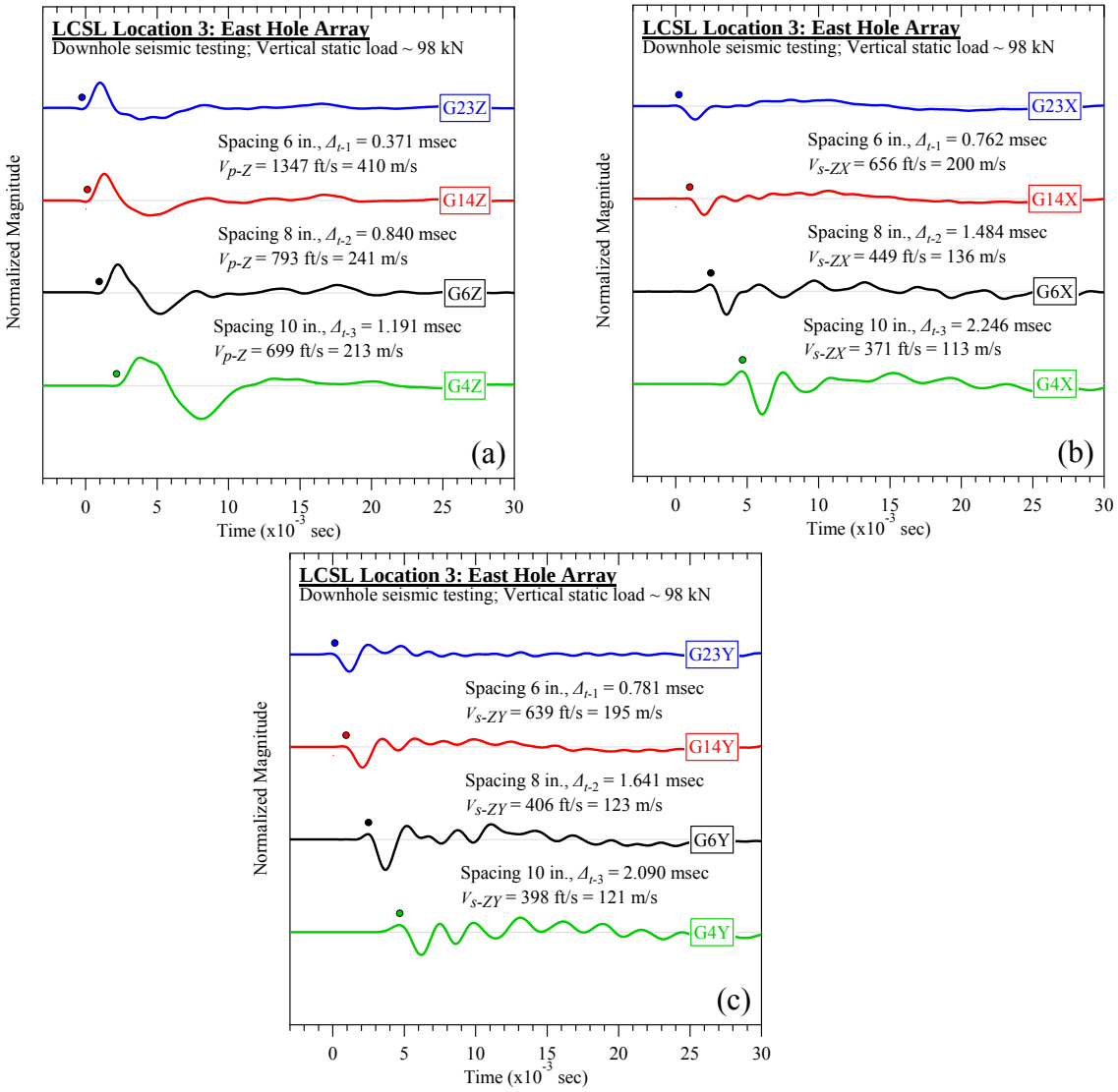

Figure B-110. Lamb Canyon Sanitary Landfill #3 (east hole): Downhole seismic testing at vertical load of 98 kN: (a) $V_{p\text{-}Z}$, (b) $V_{s\text{-}ZX}$, and (c) $V_{s\text{-}ZY}$.

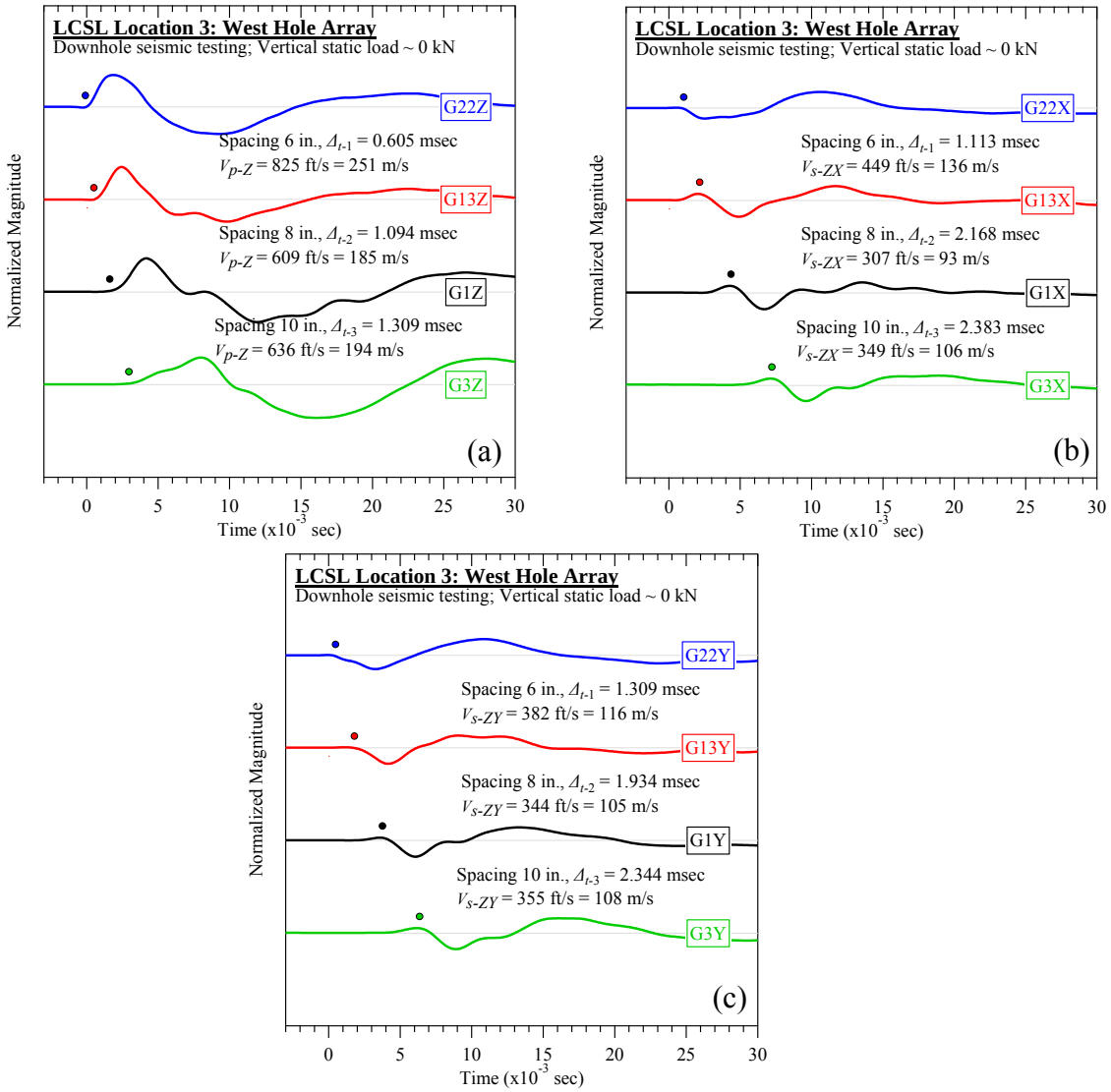

Figure B-111. Lamb Canyon Sanitary Landfill #3 (west hole): Downhole seismic testing at vertical load of 0 kN: (a) $V_{p\text{-}Z}$, (b) $V_{s\text{-}ZX}$, and (c) $V_{s\text{-}ZY}$.

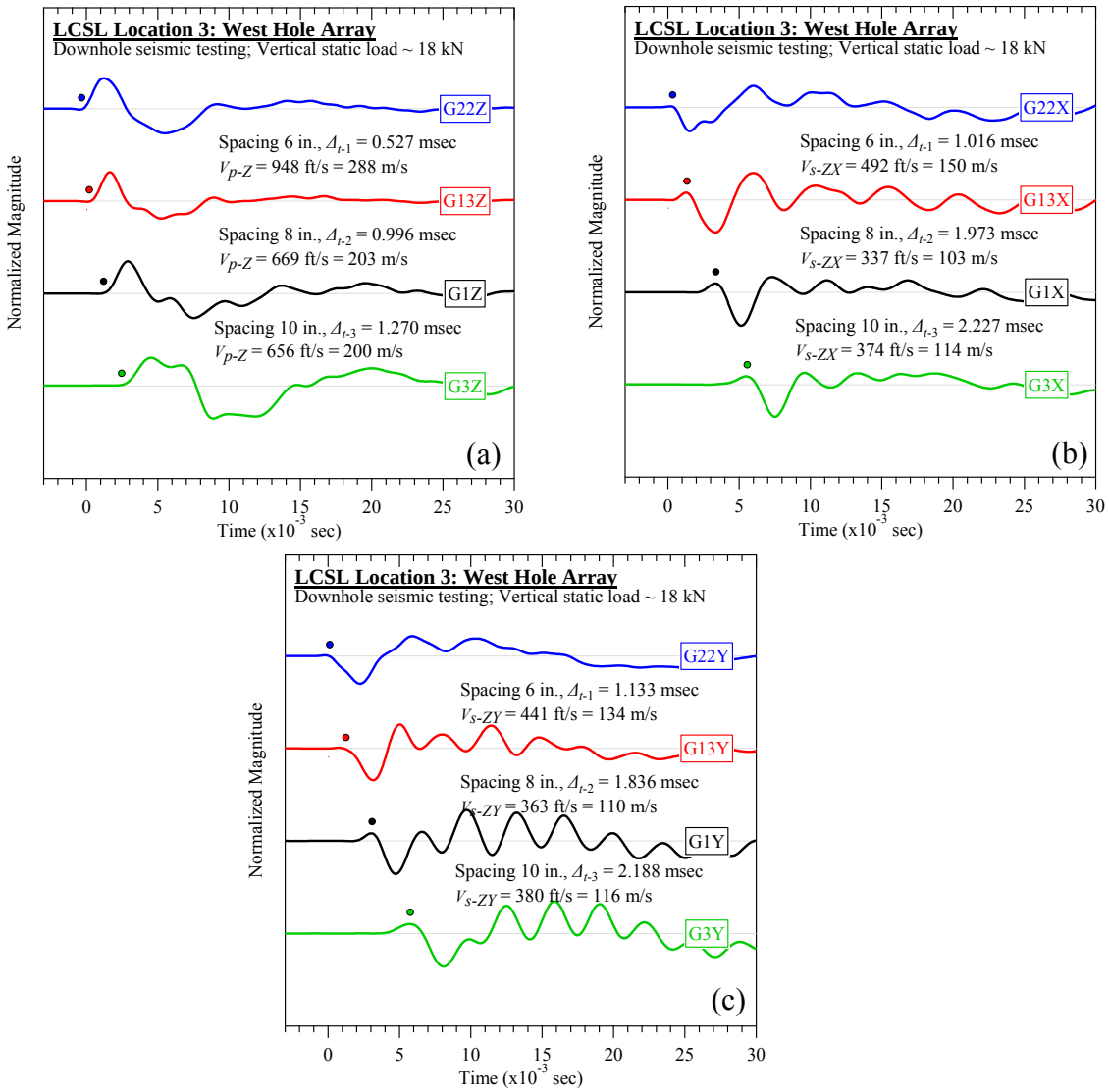

Figure B-112. Lamb Canyon Sanitary Landfill #3 (west hole): Downhole seismic testing at vertical load of 18 kN: (a) $V_{p\text{-}Z}$, (b) $V_{s\text{-}ZX}$, and (c) $V_{s\text{-}ZY}$.

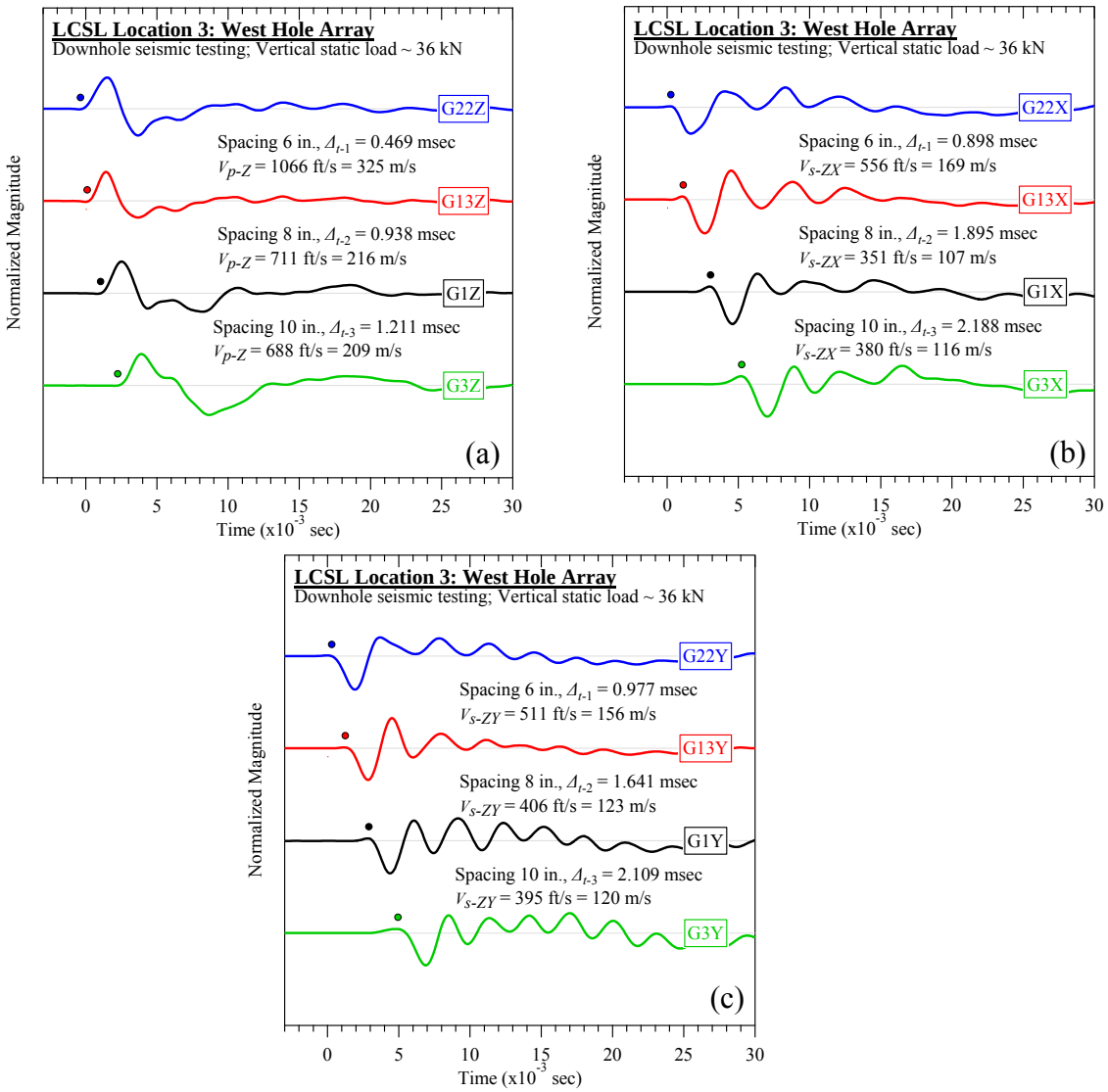

Figure B-113. Lamb Canyon Sanitary Landfill #3 (west hole): Downhole seismic testing at vertical load of 36 kN: (a) $V_{p\text{-}Z}$, (b) $V_{s\text{-}ZX}$, and (c) $V_{s\text{-}ZY}$.

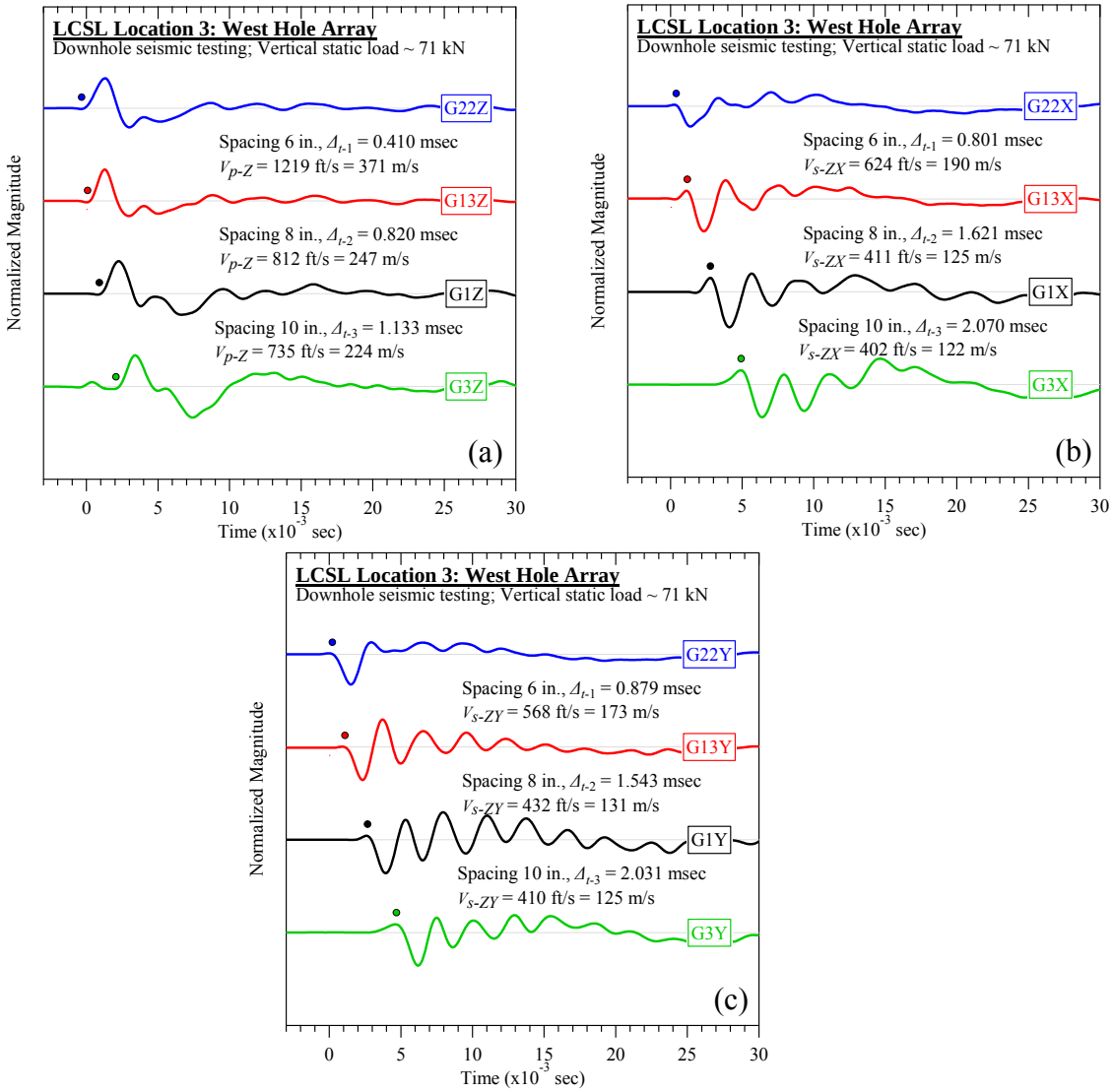

Figure B-114. Lamb Canyon Sanitary Landfill #3 (west hole): Downhole seismic testing at vertical load of 71 kN: (a) $V_{p\text{-}Z}$, (b) $V_{s\text{-}ZX}$, and (c) $V_{s\text{-}ZY}$.

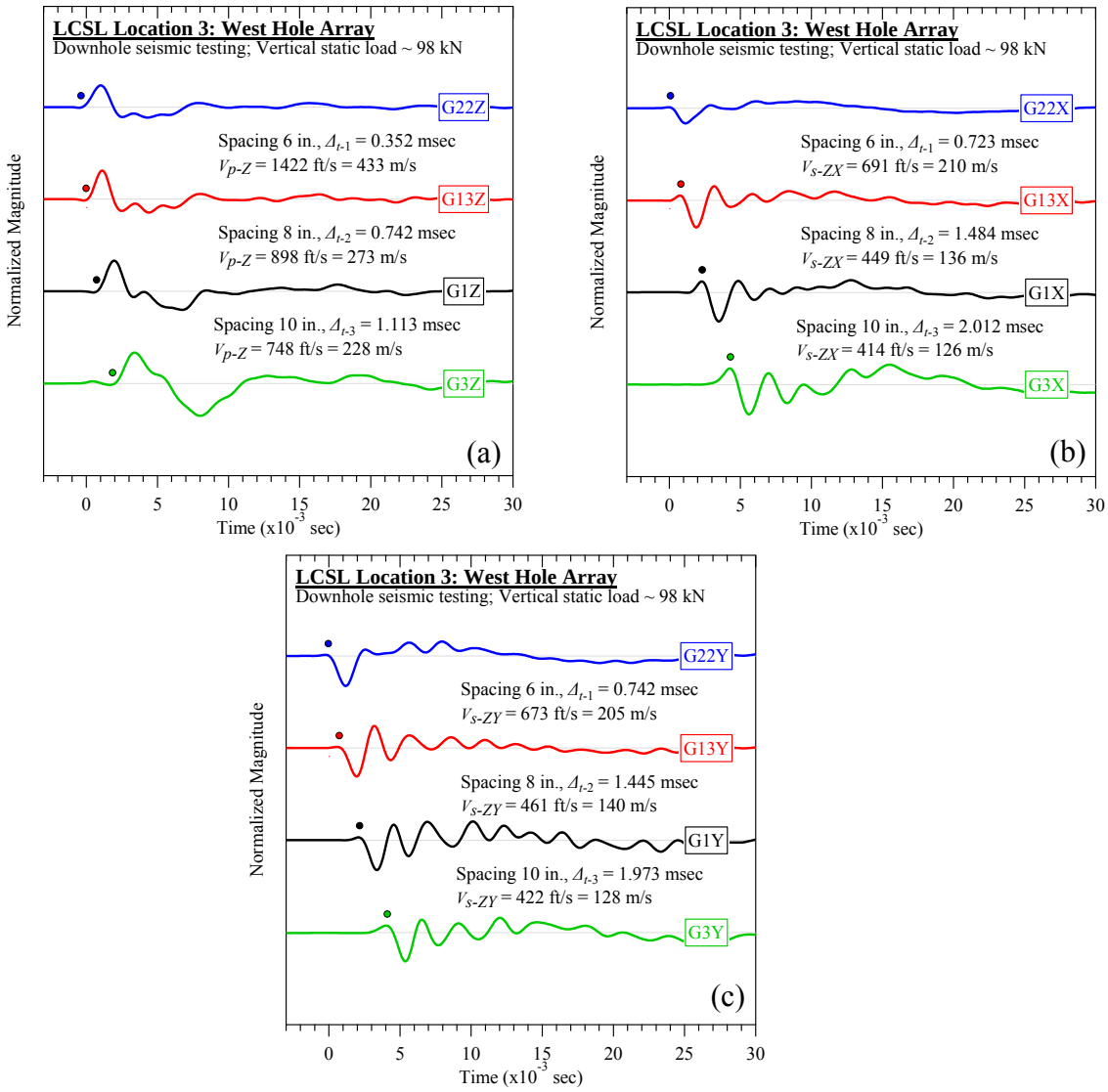

Figure B-115. Lamb Canyon Sanitary Landfill #3 (west hole): Downhole seismic testing at vertical load of 98 kN: (a) $V_{p\text{-}Z}$, (b) $V_{s\text{-}ZX}$, and (c) $V_{s\text{-}ZY}$.

B.3.2 Crosshole Seismic Testing

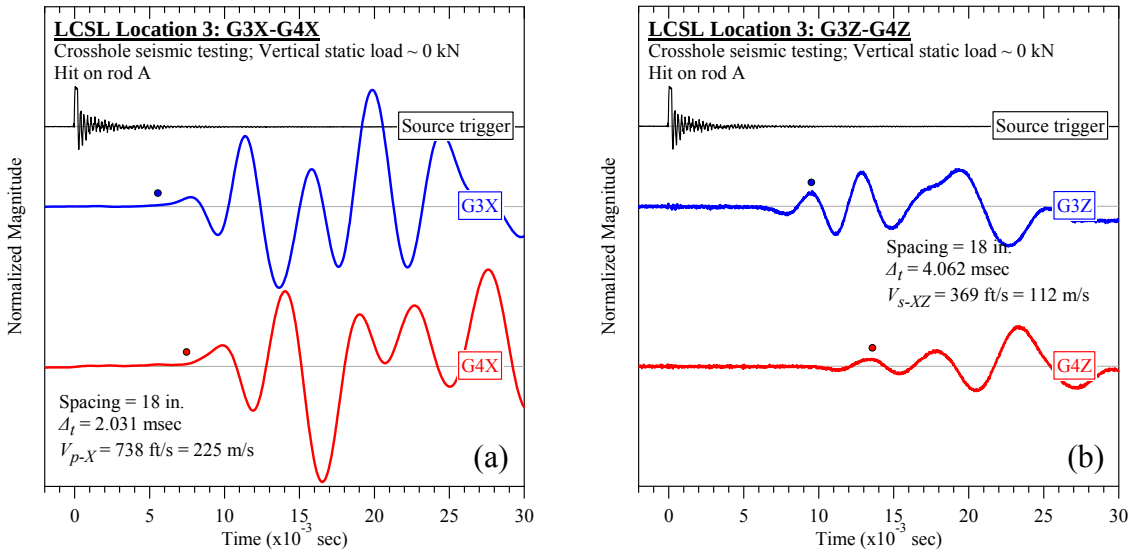

Figure B-116. Lamb Canyon Sanitary Landfill #3 (rod A): Crosshole seismic testing at vertical load of 0 kN: (a) $V_{p\text{-}X}$ and (b) $V_{s\text{-}XZ}$.

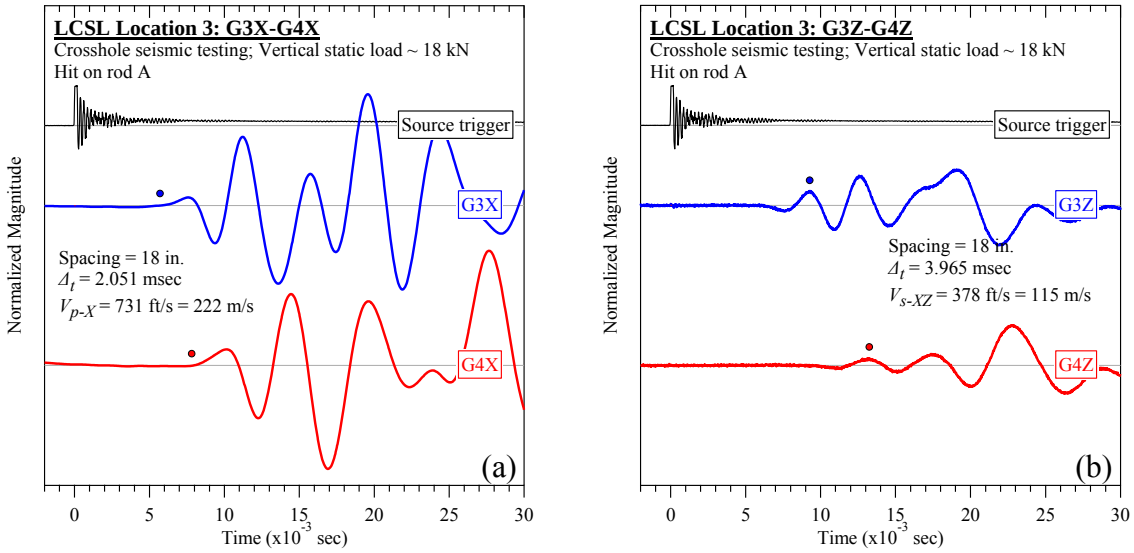

Figure B-117. Lamb Canyon Sanitary Landfill #3 (rod A): Crosshole seismic testing at vertical load of 18 kN: (a) $V_{p\text{-}X}$ and (b) $V_{s\text{-}XZ}$.

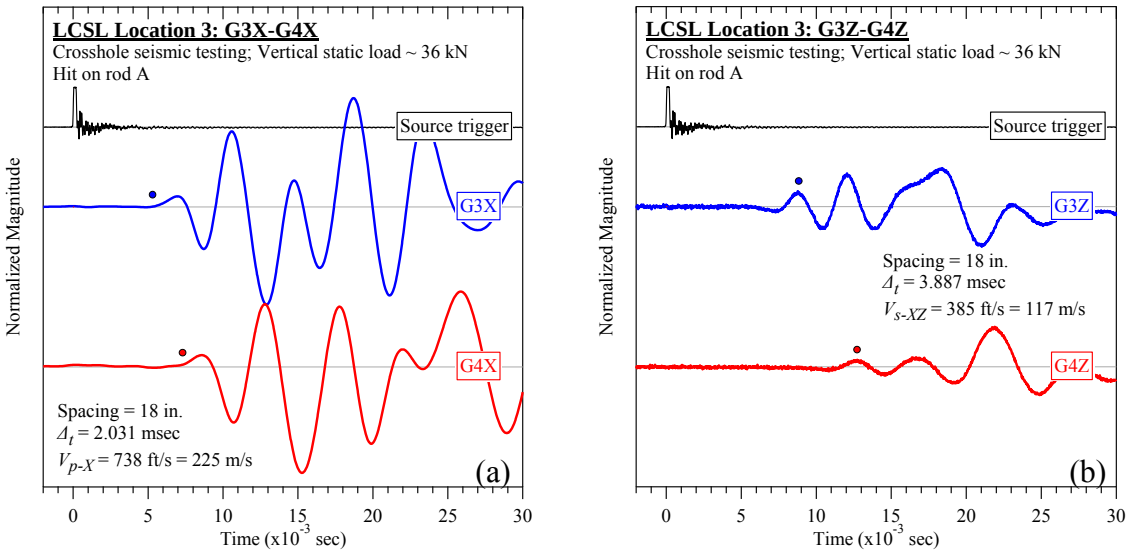

Figure B-118. Lamb Canyon Sanitary Landfill #3 (rod A): Crosshole seismic testing at vertical load of 36 kN: (a) $V_{p\text{-}X}$ and (b) $V_{s\text{-}XZ}$.

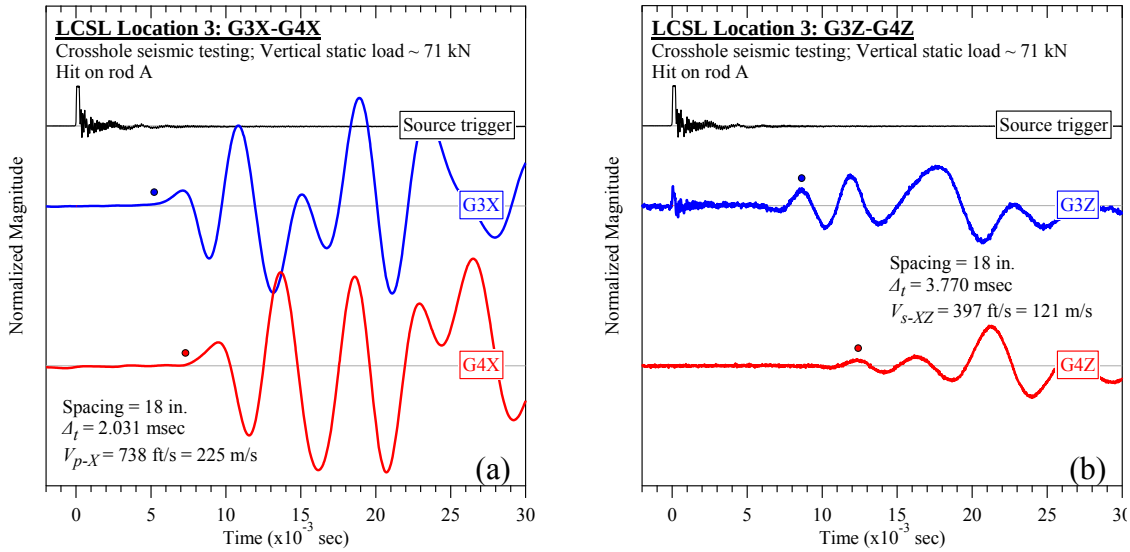

Figure B-119. Lamb Canyon Sanitary Landfill #3 (rod A): Crosshole seismic testing at vertical load of 71 kN: (a) $V_{p\text{-}X}$ and (b) $V_{s\text{-}XZ}$.

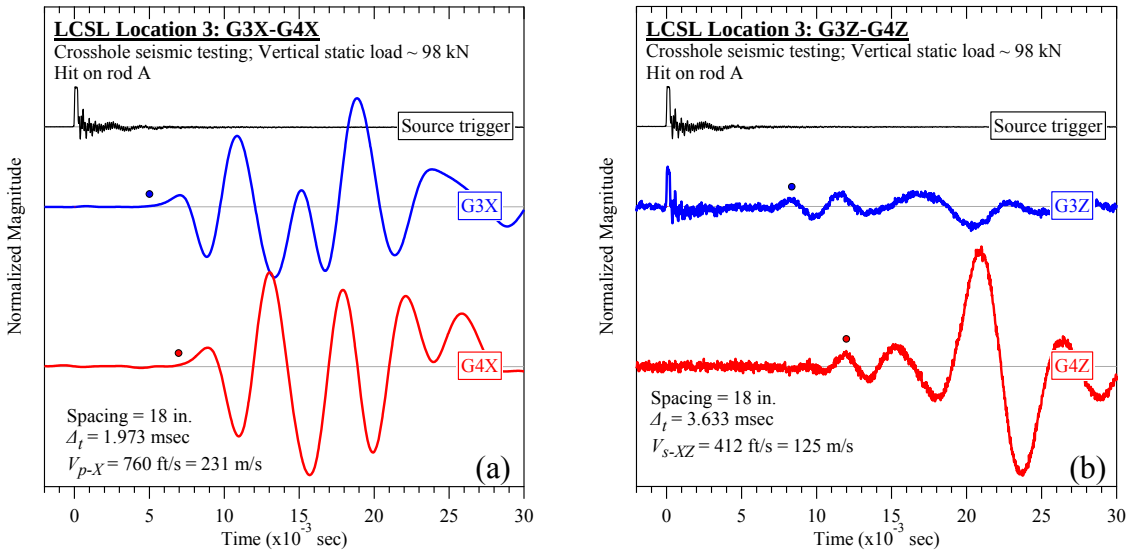

Figure B-120. Lamb Canyon Sanitary Landfill #3 (rod A): Crosshole seismic testing at vertical load of 98 kN: (a) $V_{p\text{-}X}$ and (b) $V_{s\text{-}XZ}$.

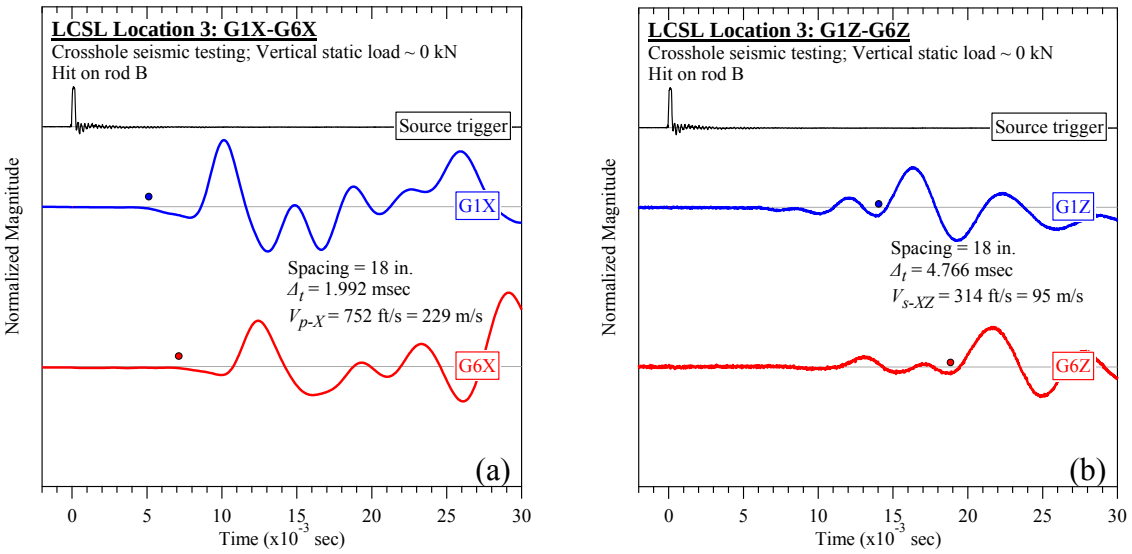

Figure B-121. Lamb Canyon Sanitary Landfill #3 (rod B): Crosshole seismic testing at vertical load of 0 kN: (a) $V_{p\text{-}X}$ and (b) $V_{s\text{-}XZ}$.

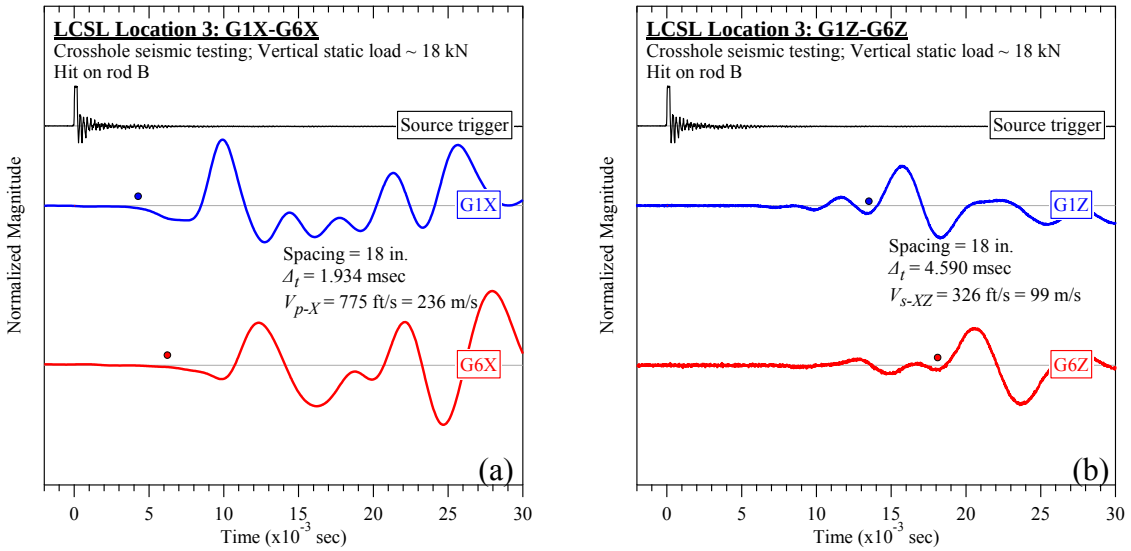

Figure B-122. Lamb Canyon Sanitary Landfill #3 (rod B): Crosshole seismic testing at vertical load of 18 kN: (a) $V_{p\text{-}X}$ and (b) $V_{s\text{-}XZ}$.

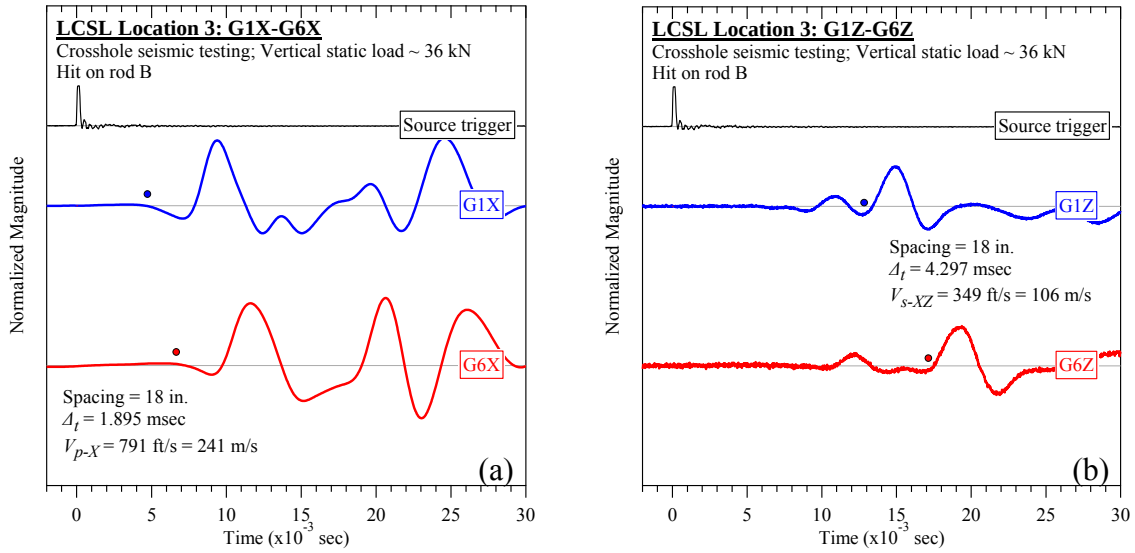

Figure B-123. Lamb Canyon Sanitary Landfill #3 (rod B): Crosshole seismic testing at vertical load of 36 kN: (a) $V_{p\text{-}X}$ and (b) $V_{s\text{-}XZ}$.

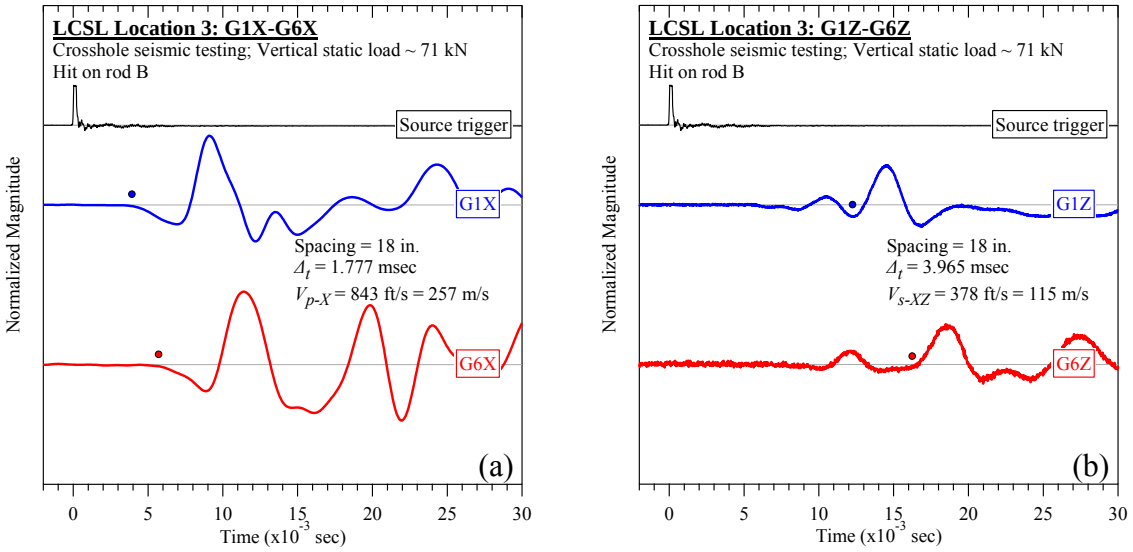

Figure B-124. Lamb Canyon Sanitary Landfill #3 (rod B): Crosshole seismic testing at vertical load of 71 kN: (a) $V_{p\text{-}X}$ and (b) $V_{s\text{-}XZ}$.

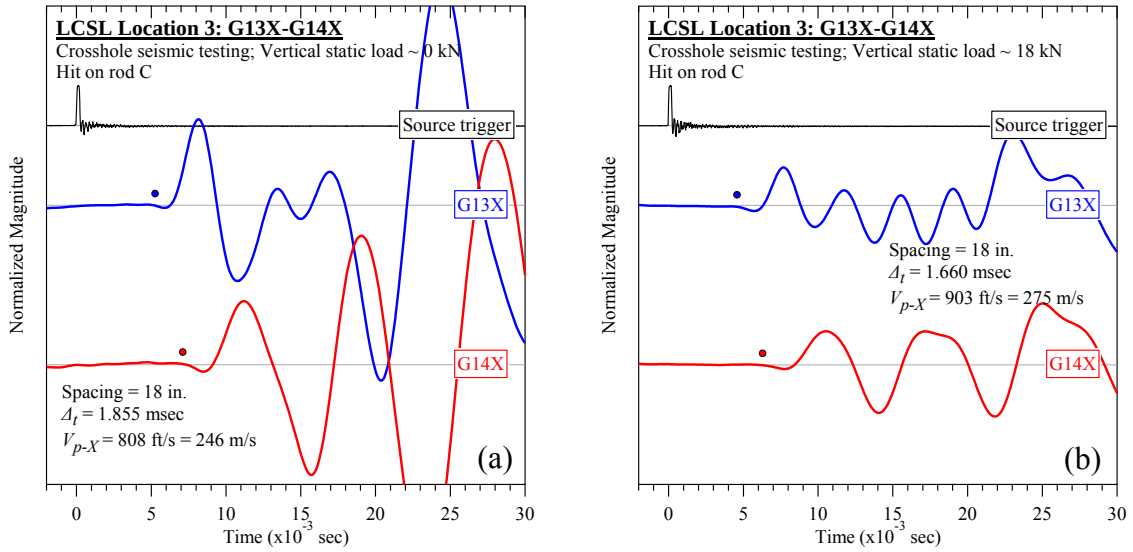

Figure B-125. Lamb Canyon Sanitary Landfill #3 (rod C): Crosshole seismic testing at vertical load of (a) 0 kN and (b) 18 kN: $V_{p\text{-}X}$.

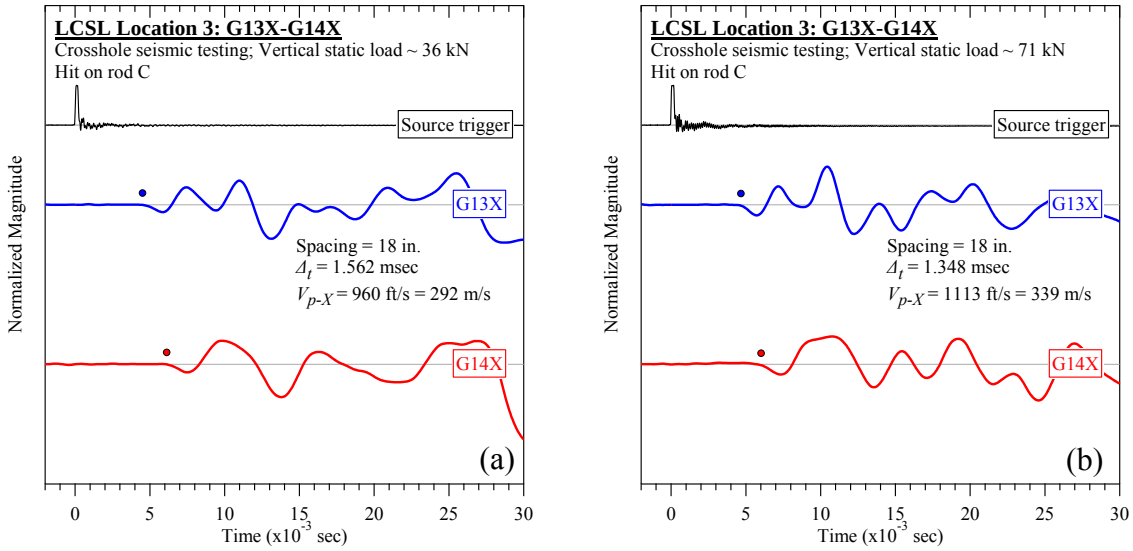

Figure B-126. Lamb Canyon Sanitary Landfill #3 (rod C): Crosshole seismic testing at vertical load of (a) 36 kN and (b) 71 kN: $V_{p\text{-}X}$.

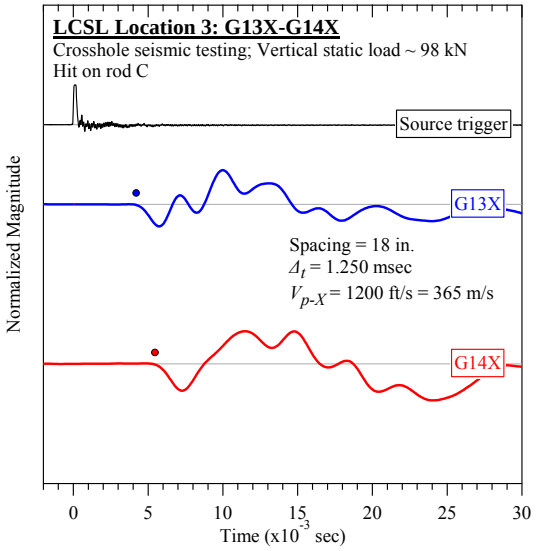

Figure B-127. Lamb Canyon Sanitary Landfill #3 (rod C): Crosshole seismic testing at vertical load of 98 kN: $V_{p\text{-}X}$.

B.3.3 Steady-state Dynamic Testing

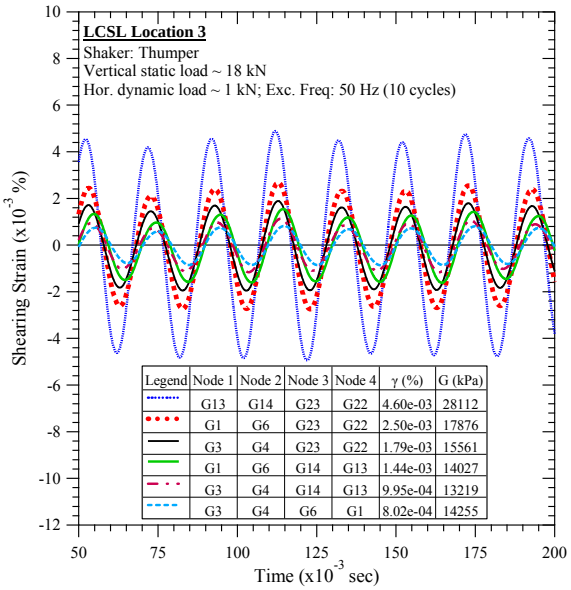

Figure B-128. Lamb Canyon Sanitary Landfill #3: Steady-state dynamic testing at vertical load of 18 kN and horizontal dynamic load of 1 kN.

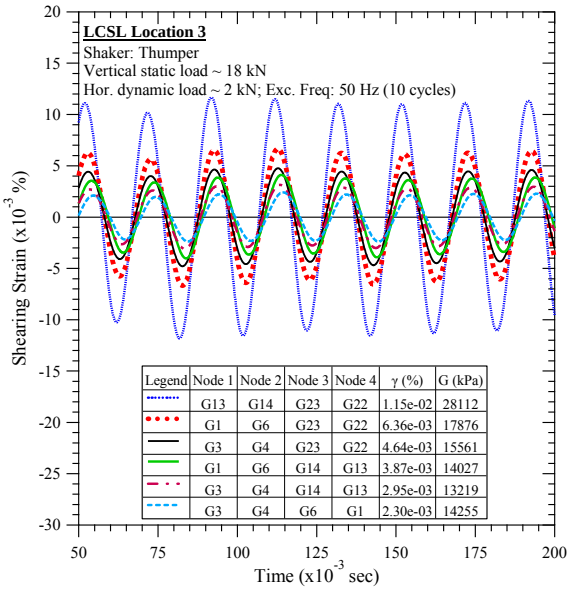

Figure B-129. Lamb Canyon Sanitary Landfill #3: Steady-state dynamic testing at vertical load of 18 kN and horizontal dynamic load of 2 kN.

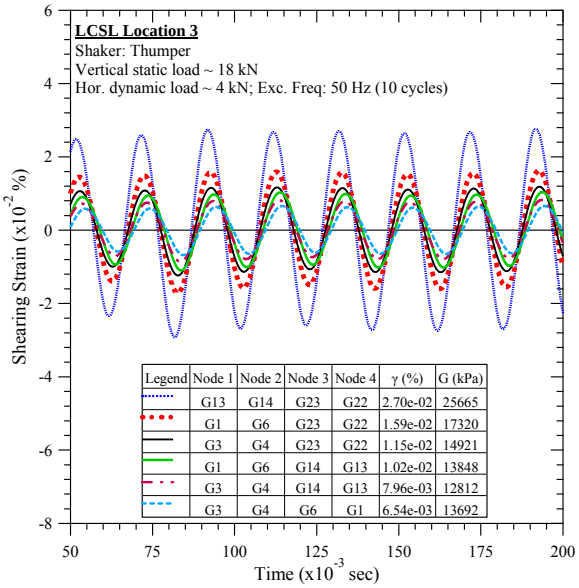

Figure B-130. Lamb Canyon Sanitary Landfill #3: Steady-state dynamic testing at vertical load of 18 kN ton and horizontal dynamic load of 4 kN.

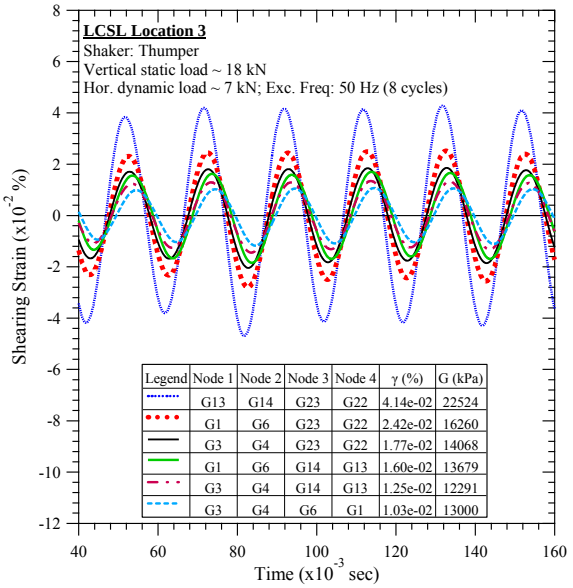

Figure B-131. Lamb Canyon Sanitary Landfill #3: Steady-state dynamic testing at vertical load of 18 kN ton and horizontal dynamic load of 7 kN.

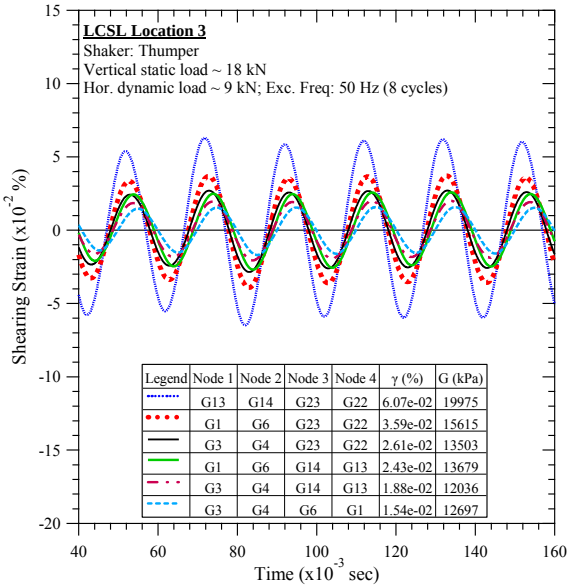

Figure B-132. Lamb Canyon Sanitary Landfill #3: Steady-state dynamic testing at vertical load of 18 kN and horizontal dynamic load of 9 kN.

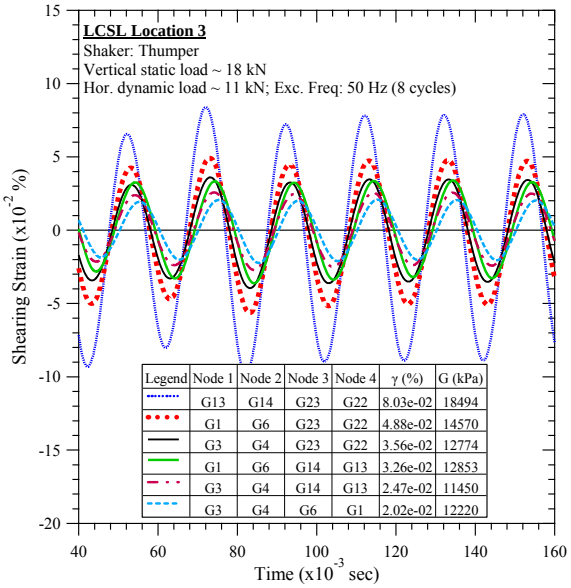

Figure B-133. Lamb Canyon Sanitary Landfill #3: Steady-state dynamic testing at vertical load of 18 kN and horizontal dynamic load of 11 kN.

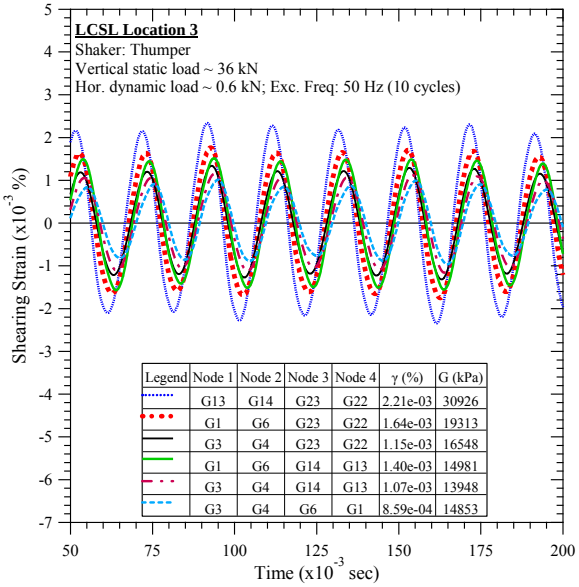

Figure B-134. Lamb Canyon Sanitary Landfill #3: Steady-state dynamic testing at vertical load of 36 kN and horizontal dynamic load of 0.6 kN.

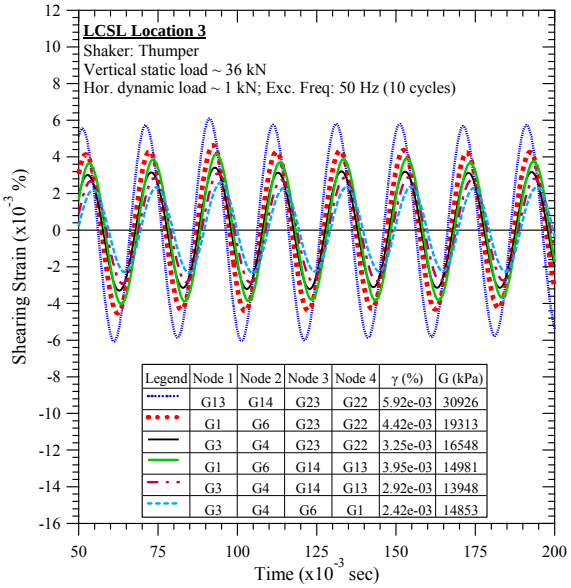

Figure B-135. Lamb Canyon Sanitary Landfill #3: Steady-state dynamic testing at vertical load of 36 kN and horizontal dynamic load of 1 kN.

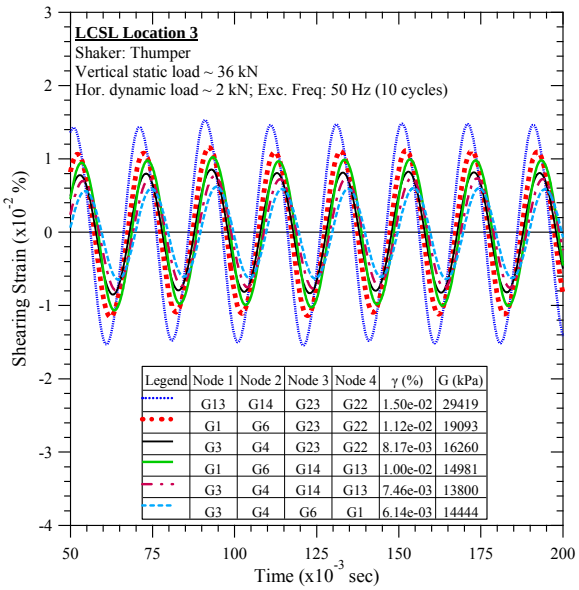

Figure B-136. Lamb Canyon Sanitary Landfill #3: Steady-state dynamic testing at vertical load of 36 kN and horizontal dynamic load of 2 kN.

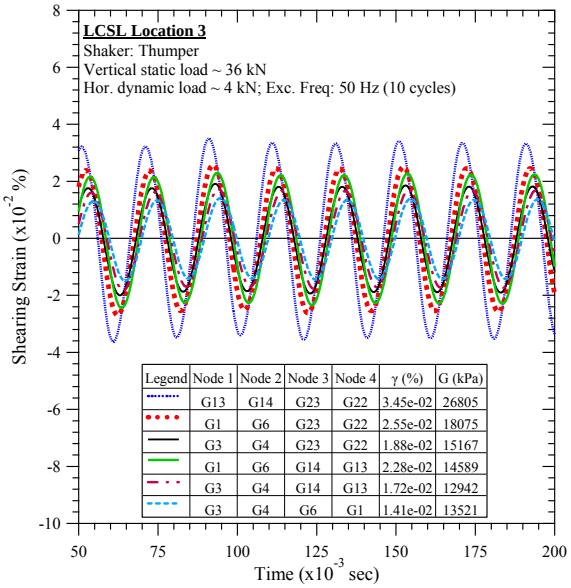

Figure B-137. Lamb Canyon Sanitary Landfill #3: Steady-state dynamic testing at vertical load of 36 kN and horizontal dynamic load of 4 kN.

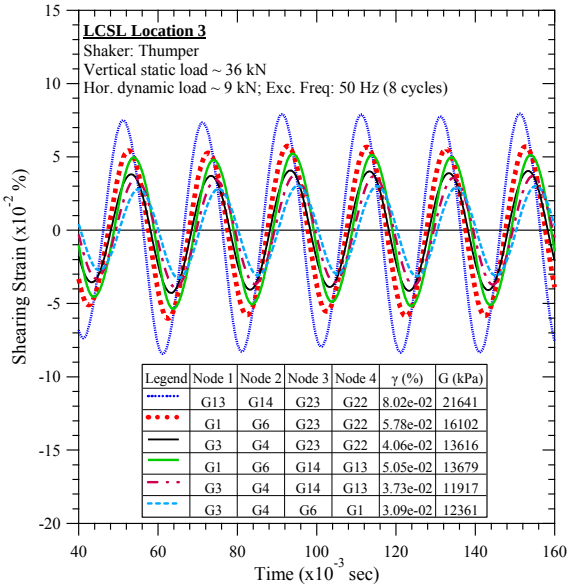

Figure B-138. Lamb Canyon Sanitary Landfill #3: Steady-state dynamic testing at vertical load of 36 kN and horizontal dynamic load of 9 kN.

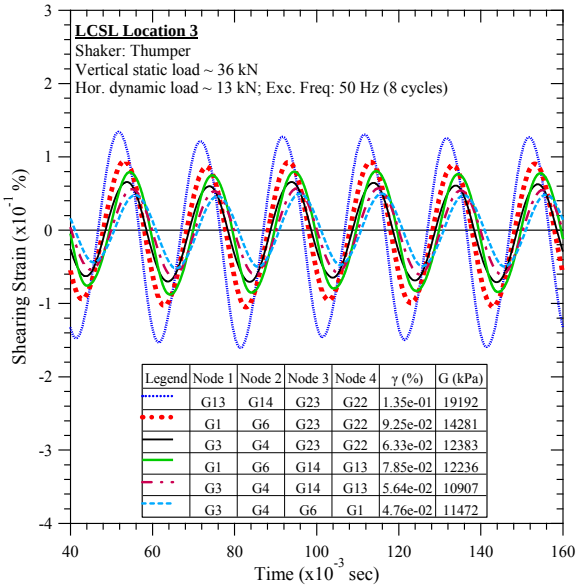

Figure B-139. Lamb Canyon Sanitary Landfill #3: Steady-state dynamic testing at vertical load of 36 kN and horizontal dynamic load of 13 kN.

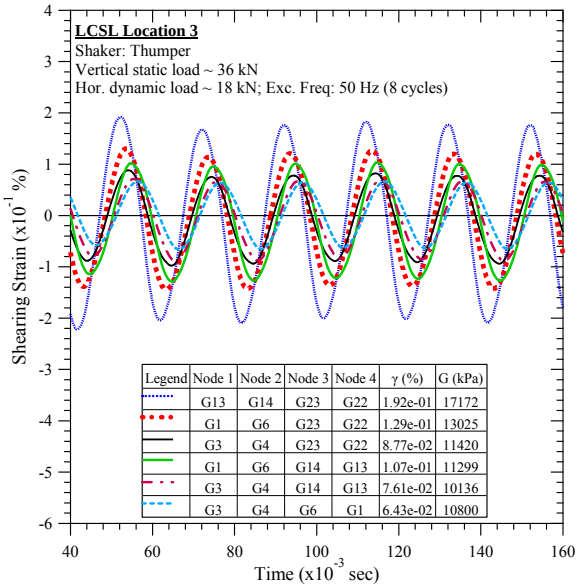

Figure B-140. Lamb Canyon Sanitary Landfill #3: Steady-state dynamic testing at vertical load of 36 kN and horizontal dynamic load of 18 kN.

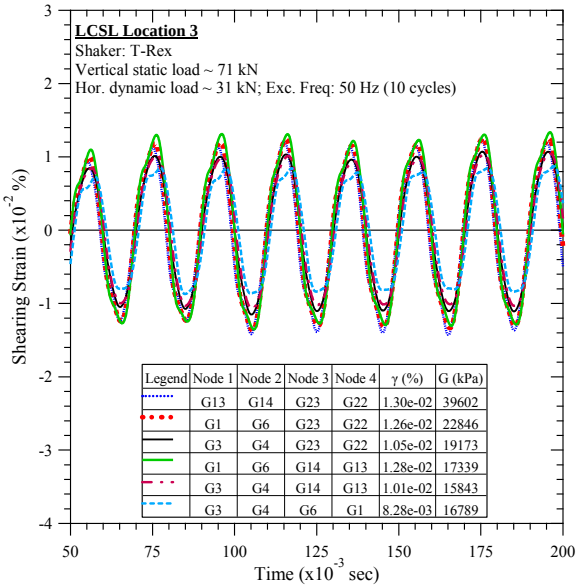

Figure B-141. Lamb Canyon Sanitary Landfill #3: Steady-state dynamic testing at vertical load of 71 kN and horizontal dynamic load of 31 kN.

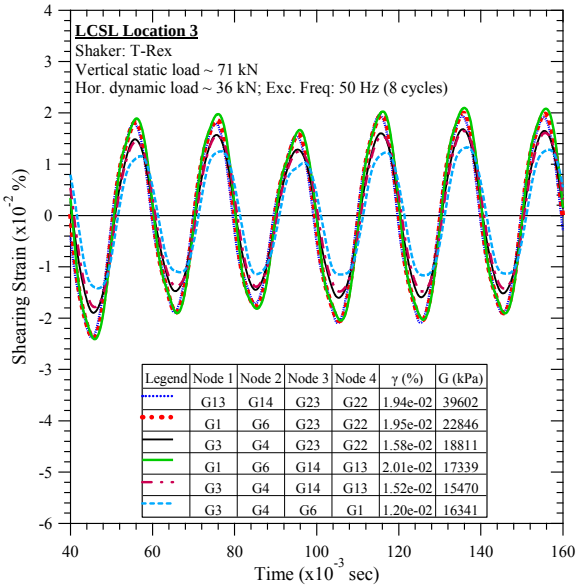

Figure B-142. Lamb Canyon Sanitary Landfill #3: Steady-state dynamic testing at vertical load of 71 kN and horizontal dynamic load of 36 kN.

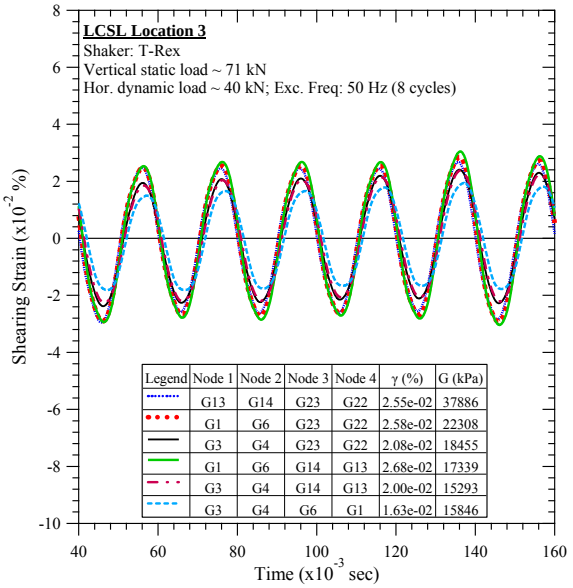

Figure B-143. Lamb Canyon Sanitary Landfill #3: Steady-state dynamic testing at vertical load of 71 kN and horizontal dynamic load of 40 kN.

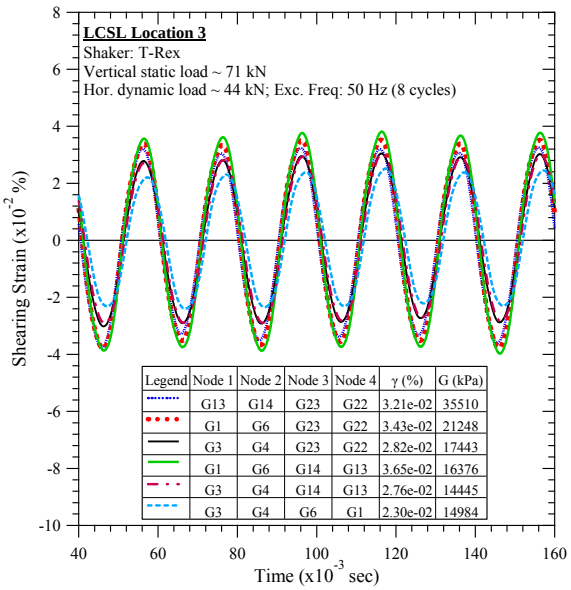

Figure B-144. Lamb Canyon Sanitary Landfill #3: Steady-state dynamic testing at vertical load of 71 kN and horizontal dynamic load of 44 kN.

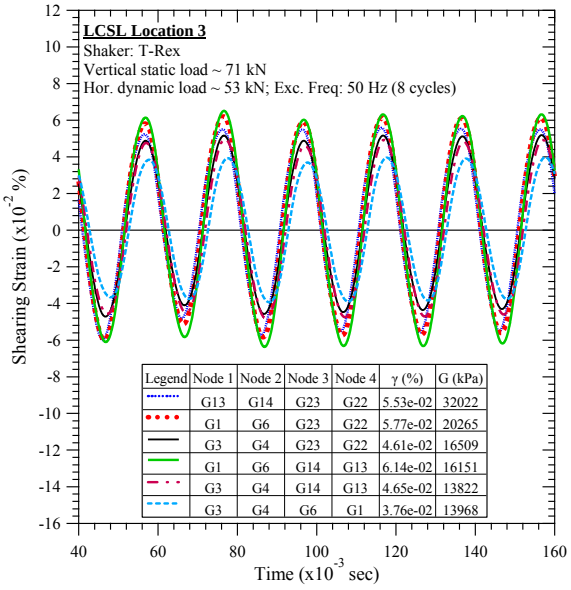

Figure B-145. Lamb Canyon Sanitary Landfill #3: Steady-state dynamic testing at vertical load of 71 kN ton and horizontal dynamic load of 53 kN.

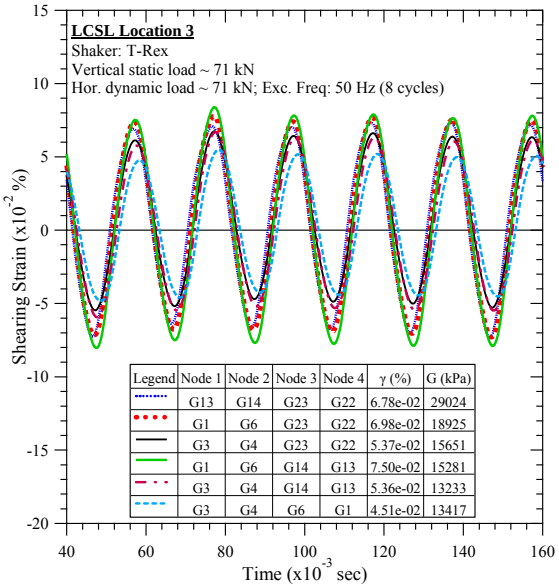

Figure B-146. Lamb Canyon Sanitary Landfill #3: Steady-state dynamic testing at vertical load of 71 kN and horizontal dynamic load of 71 kN.

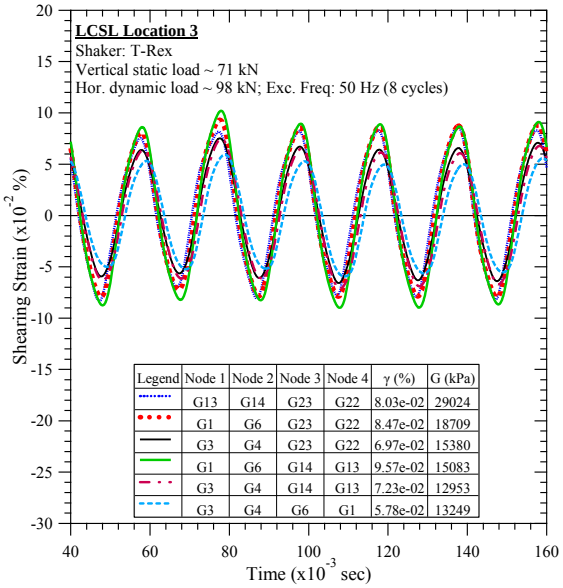

Figure B-147. Lamb Canyon Sanitary Landfill #3: Steady-state dynamic testing at vertical load of 71 kN and horizontal dynamic load of 98 kN.

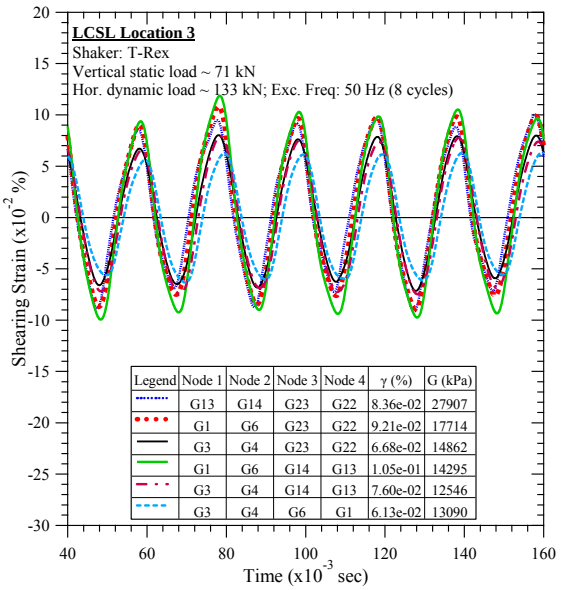

Figure B-148. Lamb Canyon Sanitary Landfill #3: Steady-state dynamic testing at vertical load of 71kN and horizontal dynamic load of 133 kN.

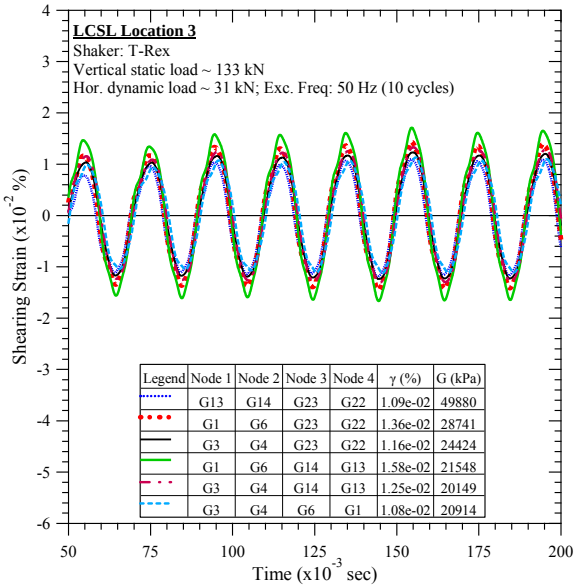

Figure B-149. Lamb Canyon Sanitary Landfill #3: Steady-state dynamic testing at vertical load of 133 kN and horizontal dynamic load of 31 kN.

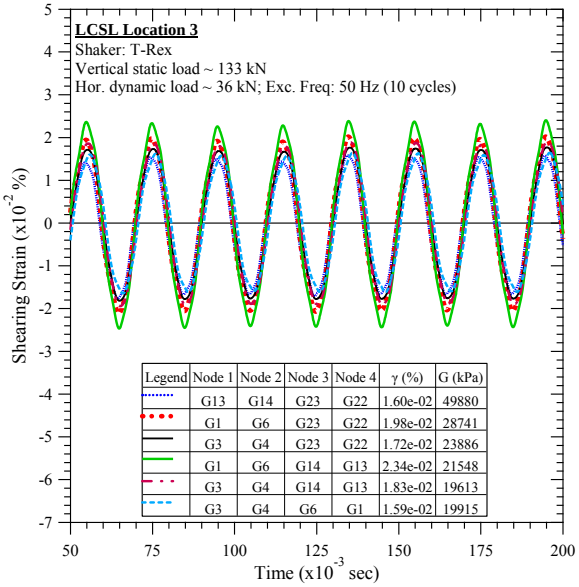

Figure B-150. Lamb Canyon Sanitary Landfill #3: Steady-state dynamic testing at vertical load of 133 kN and horizontal dynamic load of 36 kN.

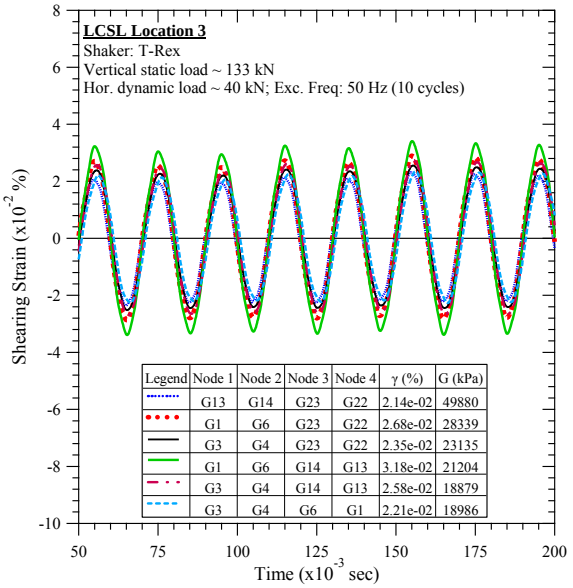

Figure B-151. Lamb Canyon Sanitary Landfill #3: Steady-state dynamic testing at vertical load of 133 kN and horizontal dynamic load of 40 kN.

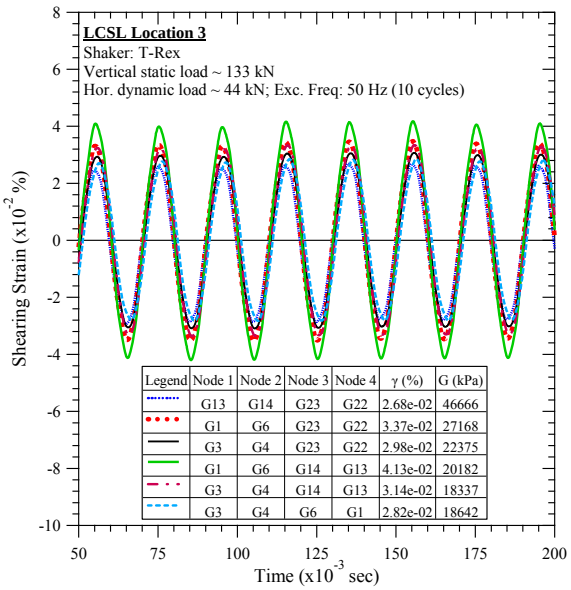

Figure B-152. Lamb Canyon Sanitary Landfill #3: Steady-state dynamic testing at vertical load of 133 kN ton and horizontal dynamic load of 44 kN.

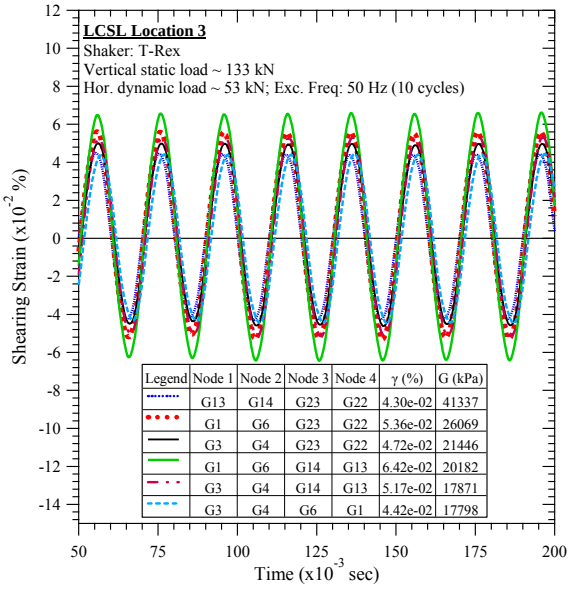

Figure B-153. Lamb Canyon Sanitary Landfill #3: Steady-state dynamic testing at vertical load of 133 kN and horizontal dynamic load of 53 kN.

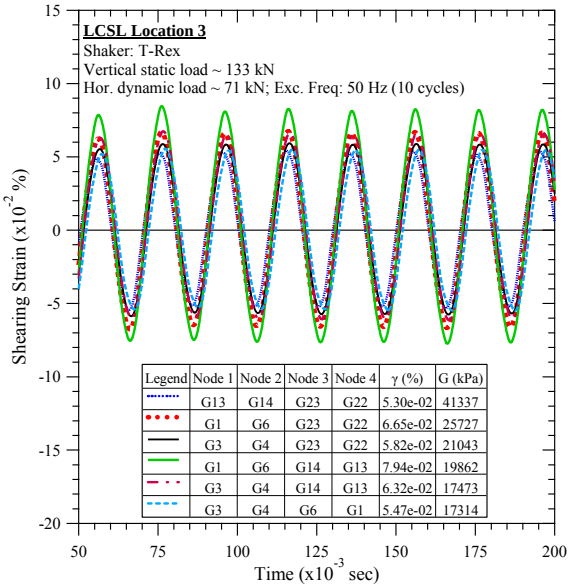

Figure B-154. Lamb Canyon Sanitary Landfill #3: Steady-state dynamic testing at vertical load of 133 kN ton and horizontal dynamic load of 71 kN.

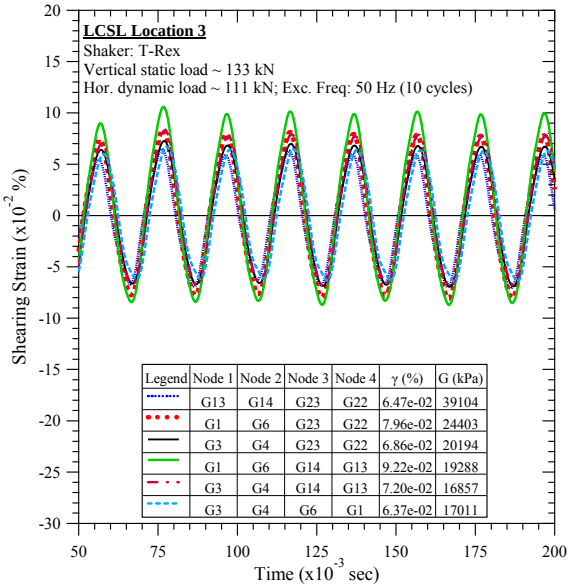

Figure B-155. Lamb Canyon Sanitary Landfill #3: Steady-state dynamic testing at vertical load of 133 kN and horizontal dynamic load of 111 kN.

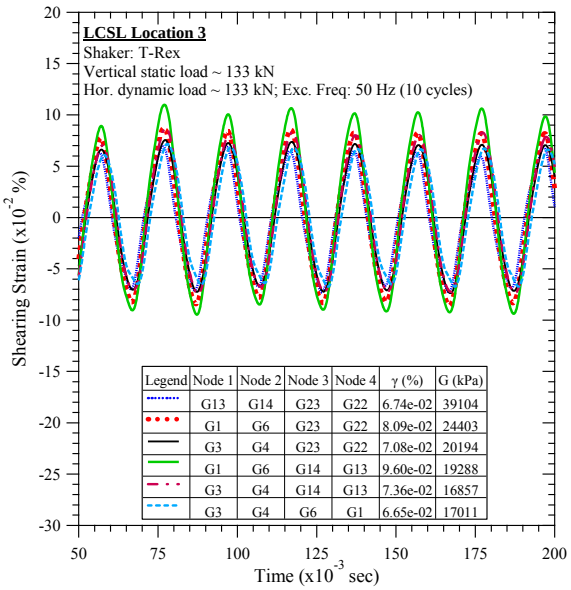

Figure B-156. Lamb Canyon Sanitary Landfill #3: Steady-state dynamic testing at vertical load of 133 kN and horizontal dynamic load of 133 kN.

C Los Reales Landfill Testing Results

C.1 Los Reales Landfill Location 1

C.1.1 Downhole Seismic Testing

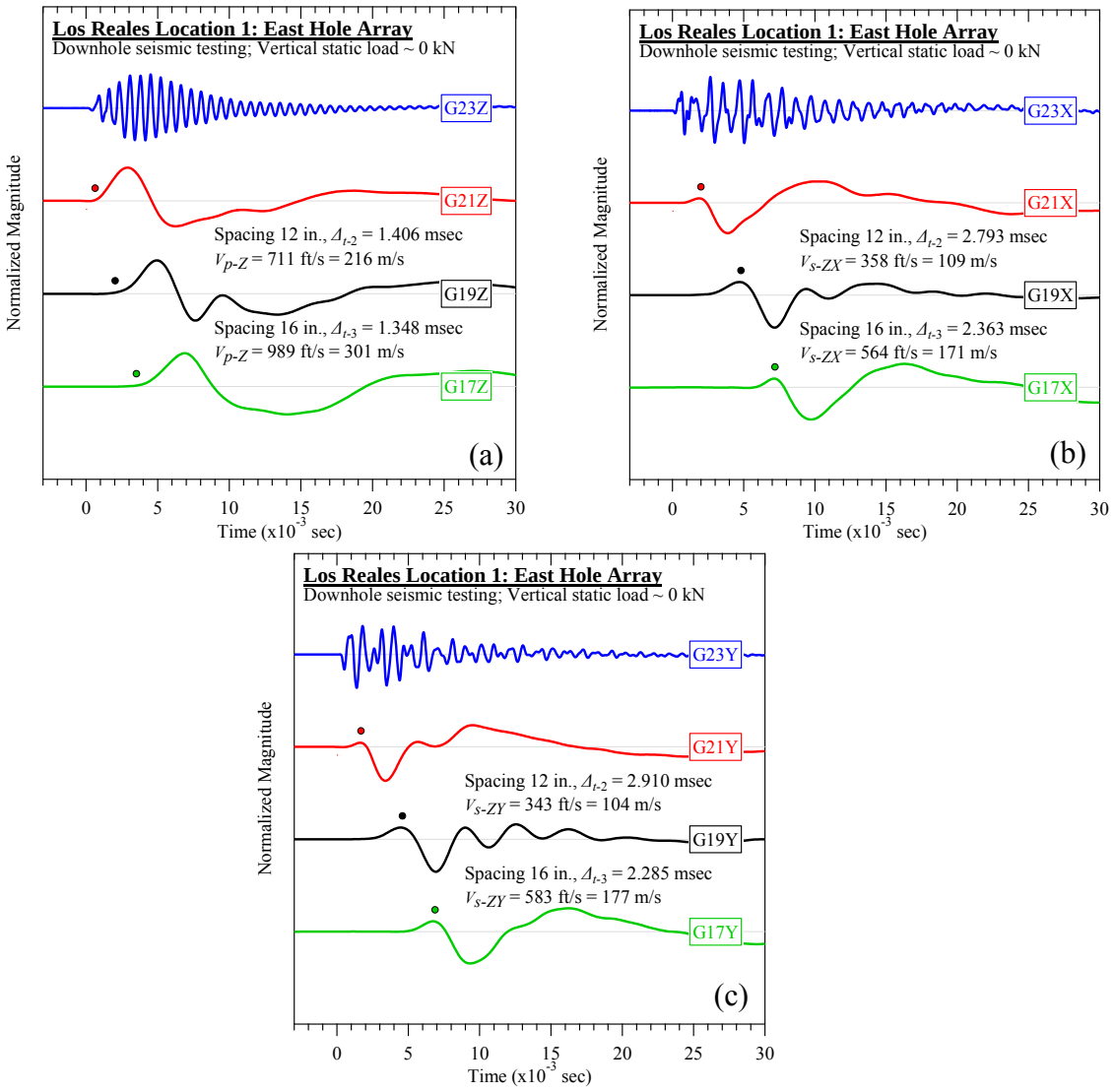

Figure C-1. Los Reales Landfill #1 (east hole): Downhole seismic testing at vertical load of 0 kN: (a) $V_{p\text{-}Z}$, (b) $V_{s\text{-}ZX}$, and (c) $V_{s\text{-}ZY}$.

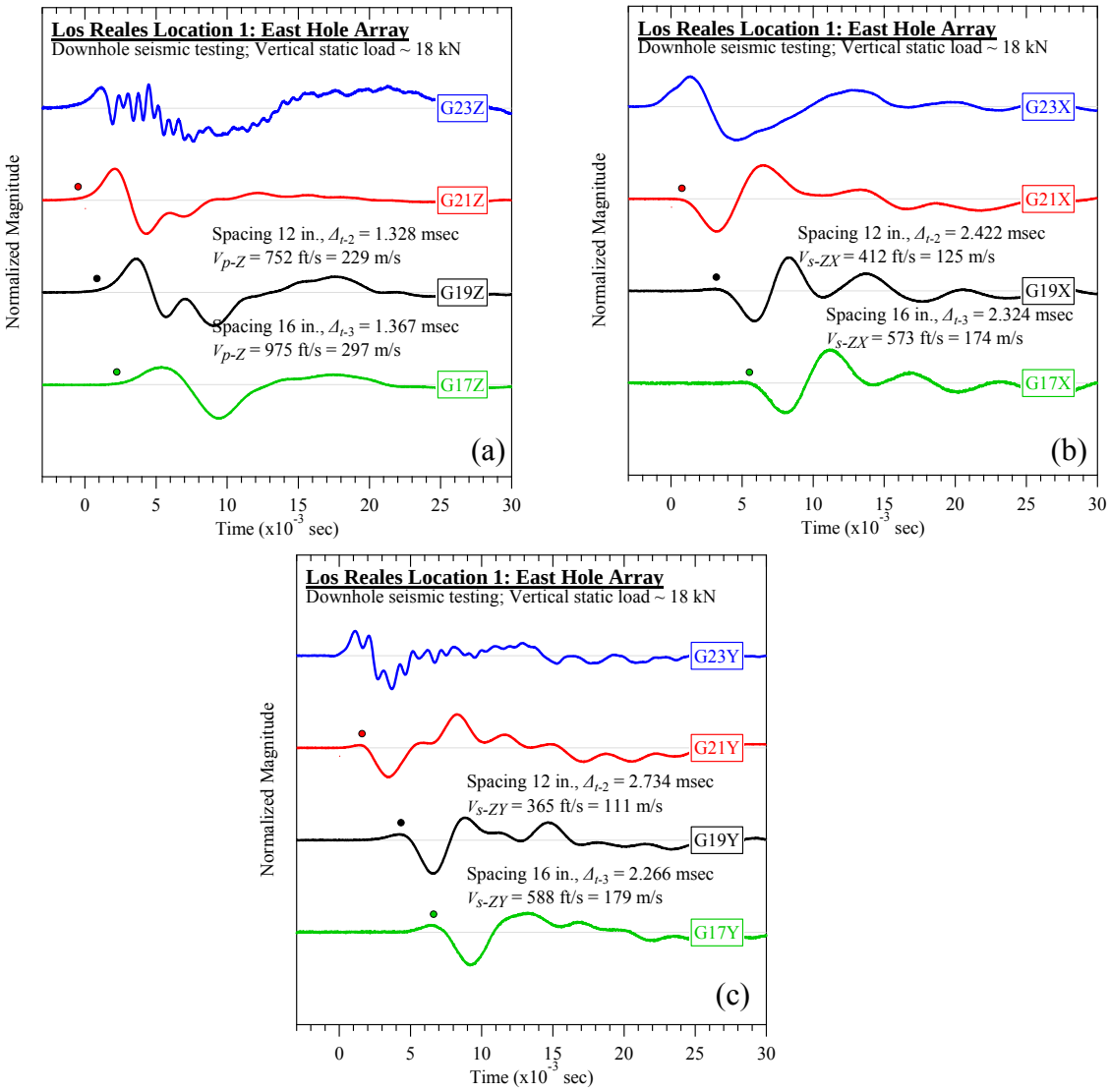

Figure C-2. Los Reales Landfill #1 (east hole): Downhole seismic testing at vertical load of 18 kN: (a) $V_{p\text{-}Z}$, (b) $V_{s\text{-}ZX}$, and (c) $V_{s\text{-}ZY}$.

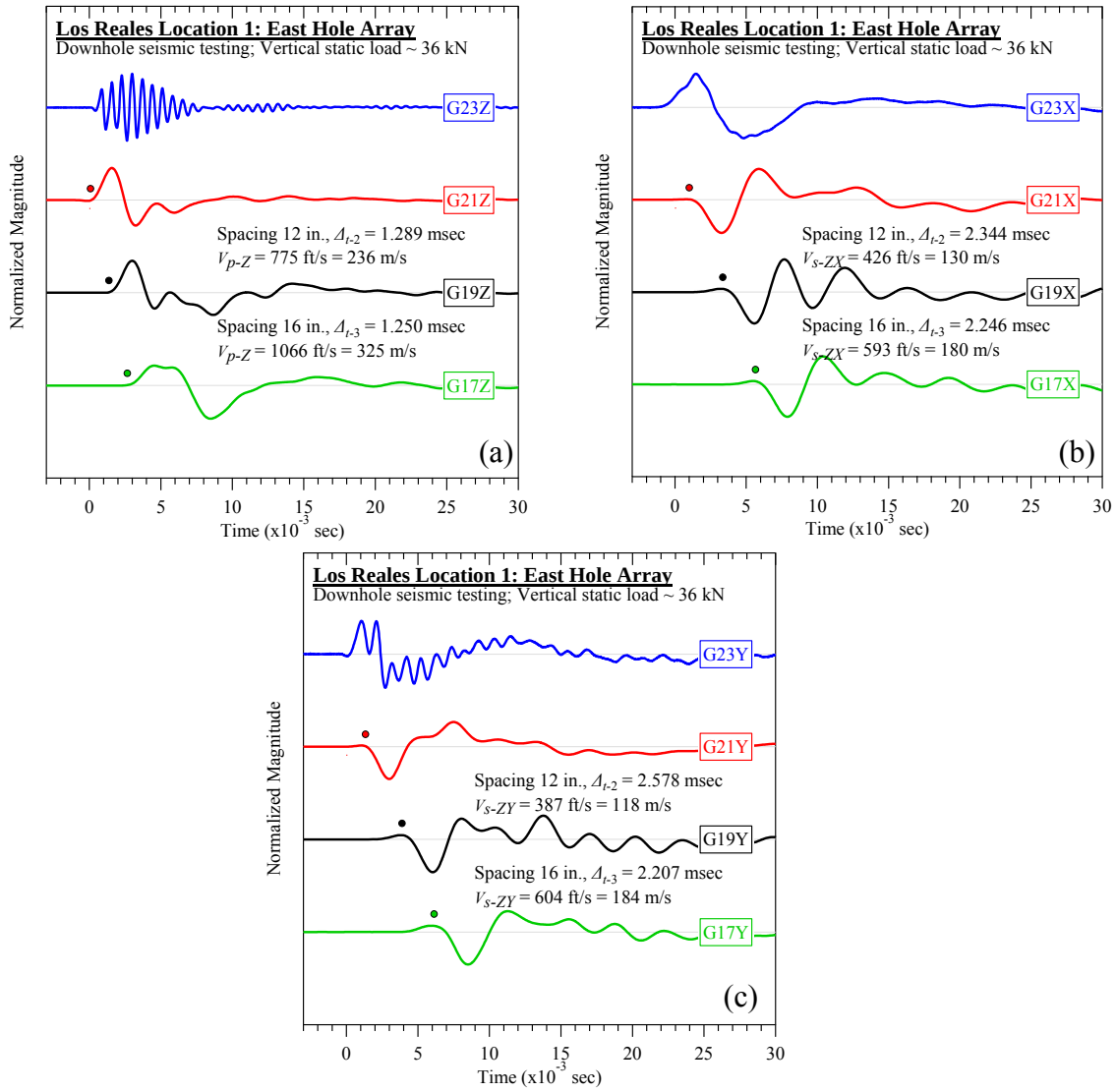

Figure C-3. Los Reales Landfill #1 (east hole): Downhole seismic testing at vertical load of 36 kN: (a) $V_{p\text{-}Z}$, (b) $V_{s\text{-}ZX}$, and (c) $V_{s\text{-}ZY}$.

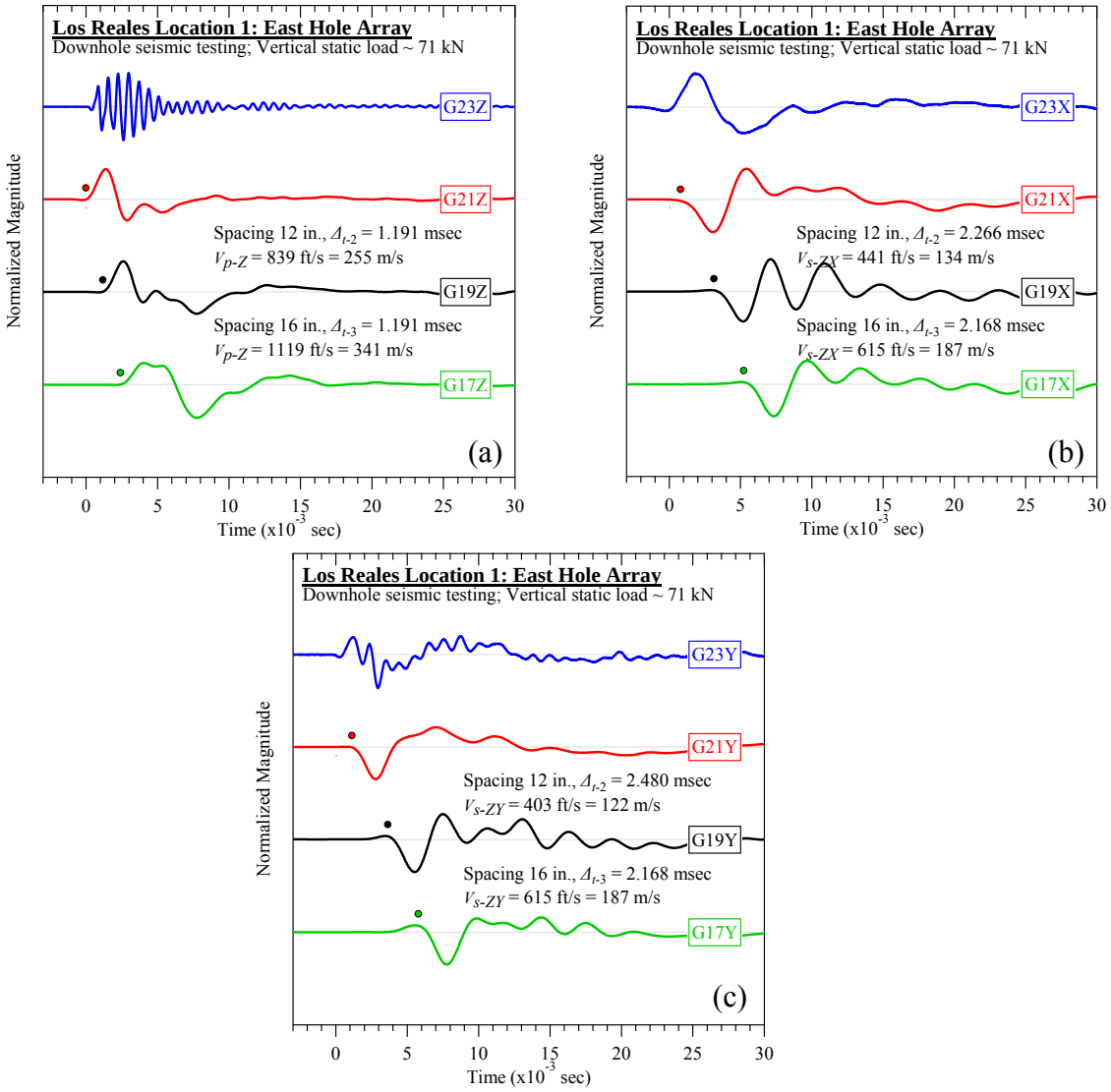

Figure C-4. Los Reales Landfill #1 (east hole): Downhole seismic testing at vertical load of 71 kN: (a) V_{p-Z}, (b) V_{s-ZX}, and (c) V_{s-ZY}.

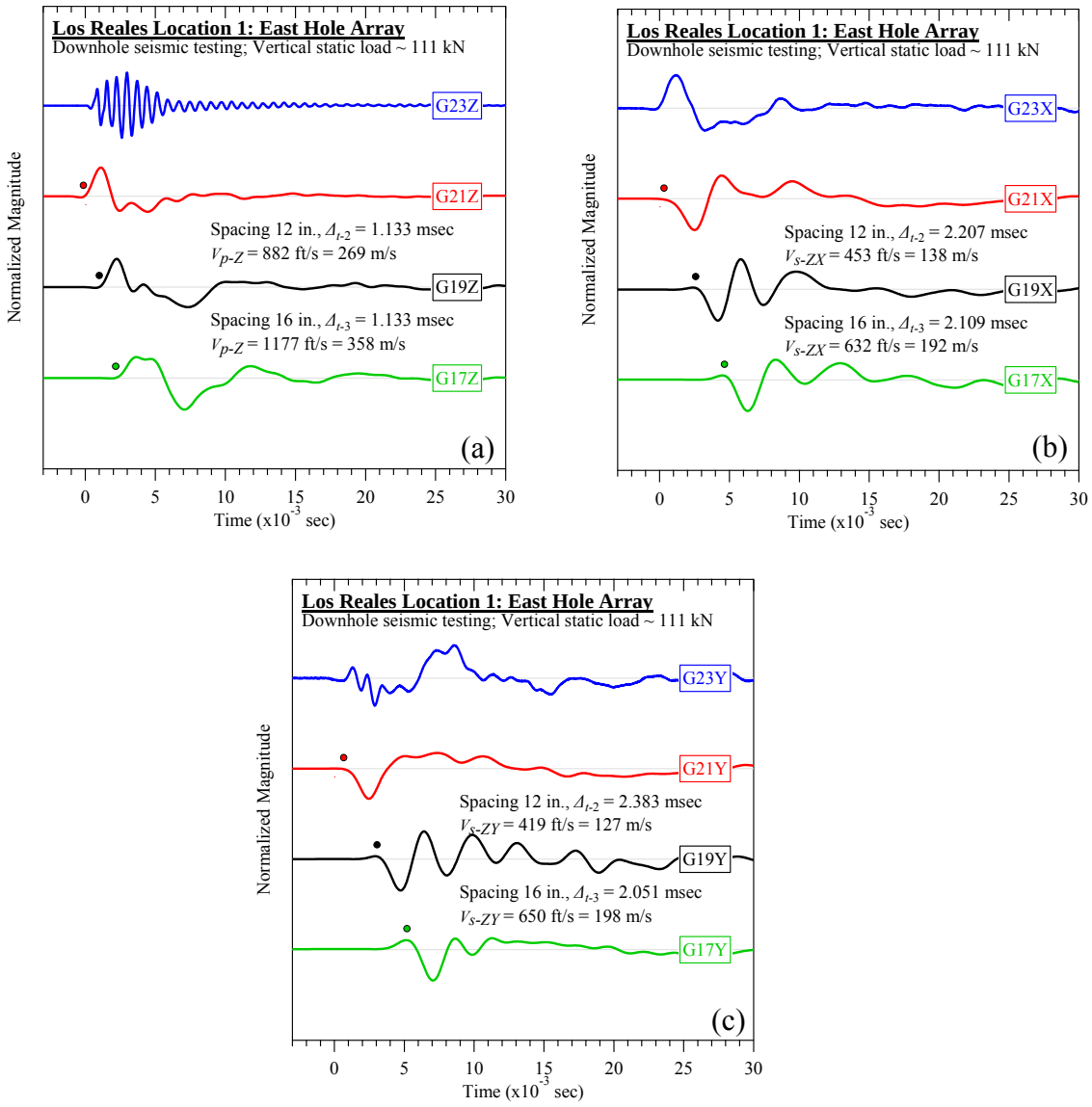

Figure C-5. Los Reales Landfill #1 (east hole): Downhole seismic testing at vertical load of 111 kN: (a) V_{p-Z}, (b) V_{s-ZX}, and (c) V_{s-ZY}.

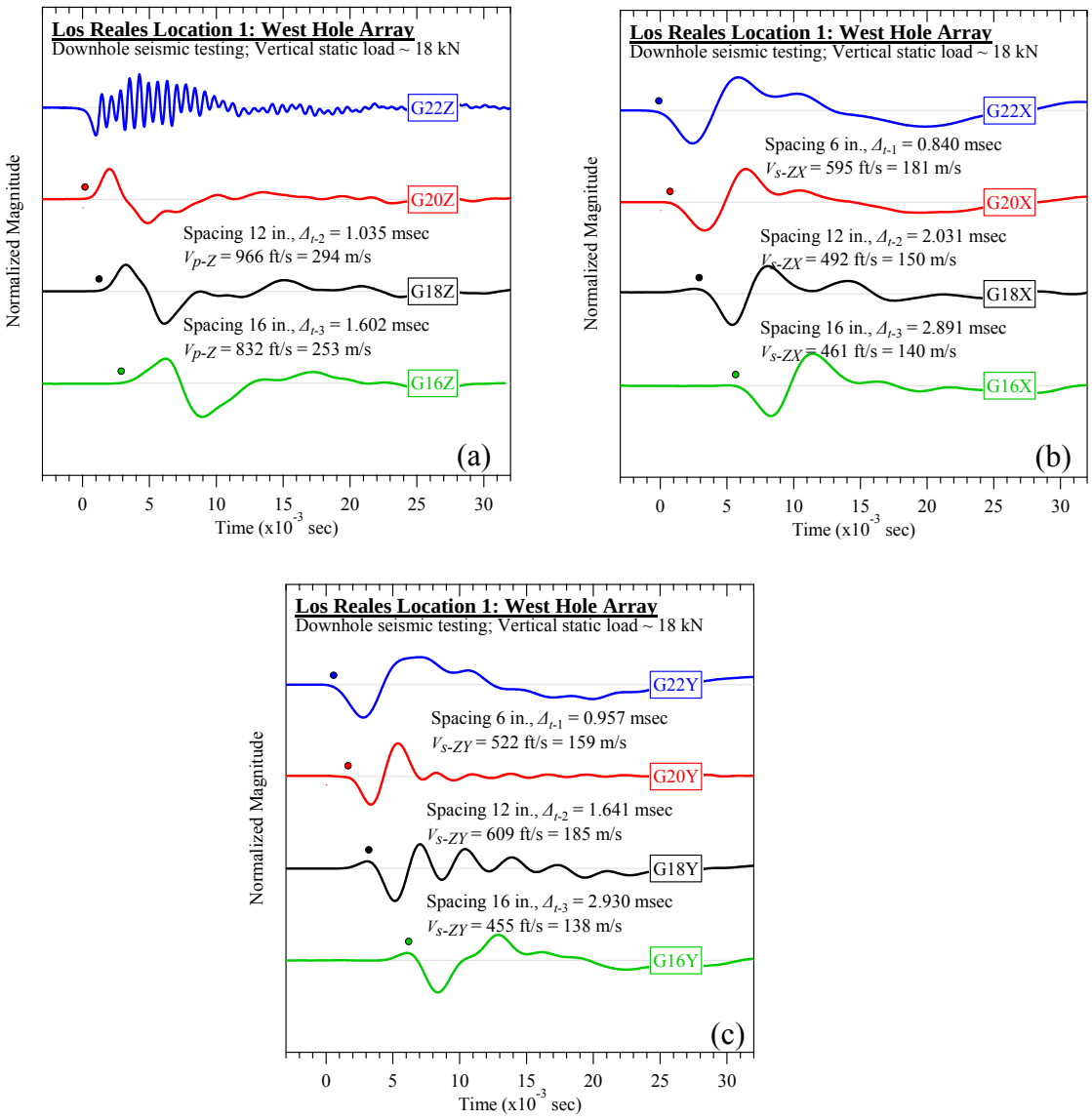

Figure C-6. Los Reales Landfill #1 (west hole): Downhole seismic testing at vertical load of 18 kN: (a) $V_{p\text{-}Z}$, (b) $V_{s\text{-}ZX}$, and (c) $V_{s\text{-}ZY}$.

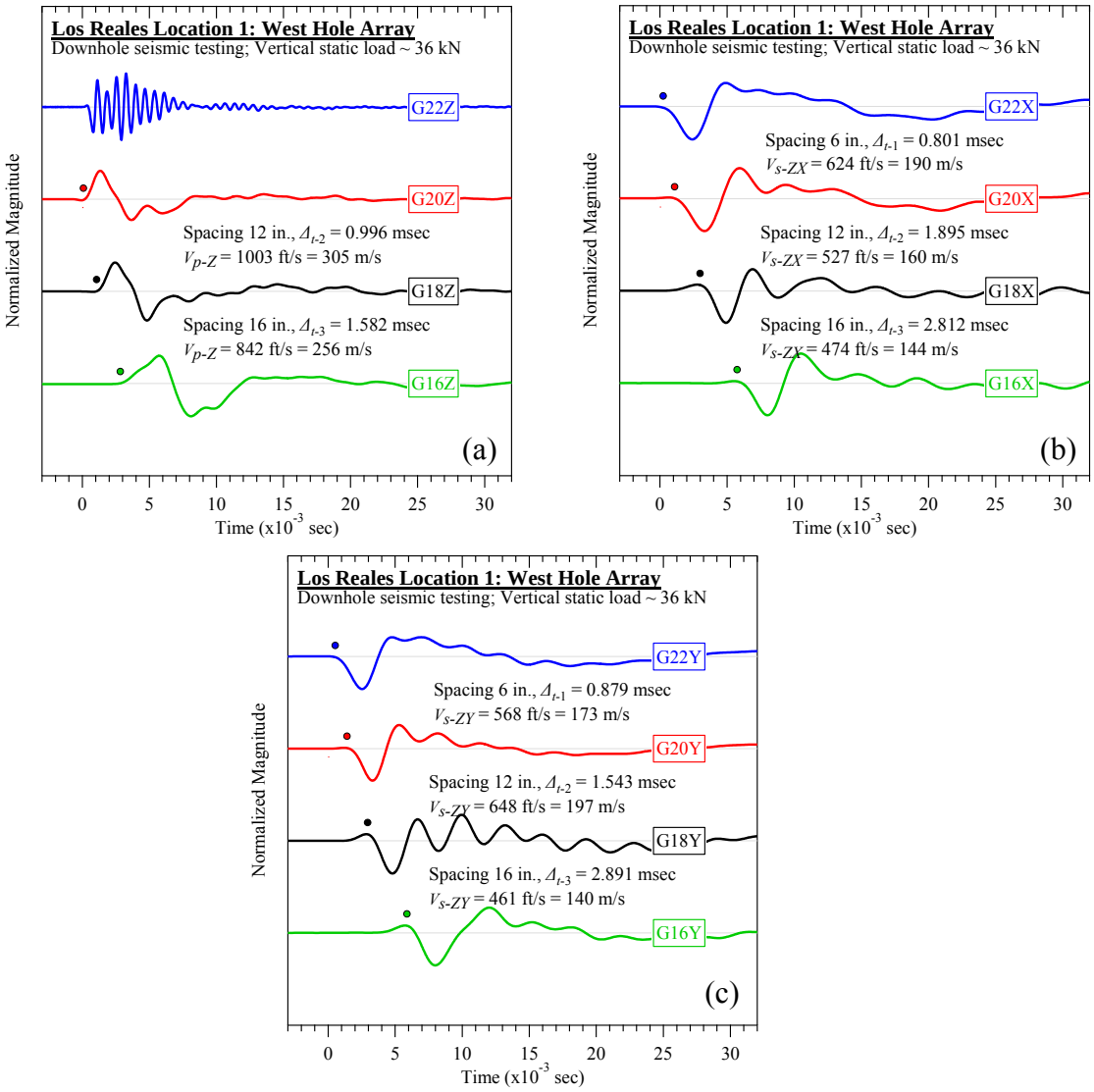

Figure C-7. Los Reales Landfill #1 (west hole): Downhole seismic testing at vertical load of 36 kN: (a) $V_{p\text{-}Z}$, (b) $V_{s\text{-}ZX}$, and (c) $V_{s\text{-}ZY}$.

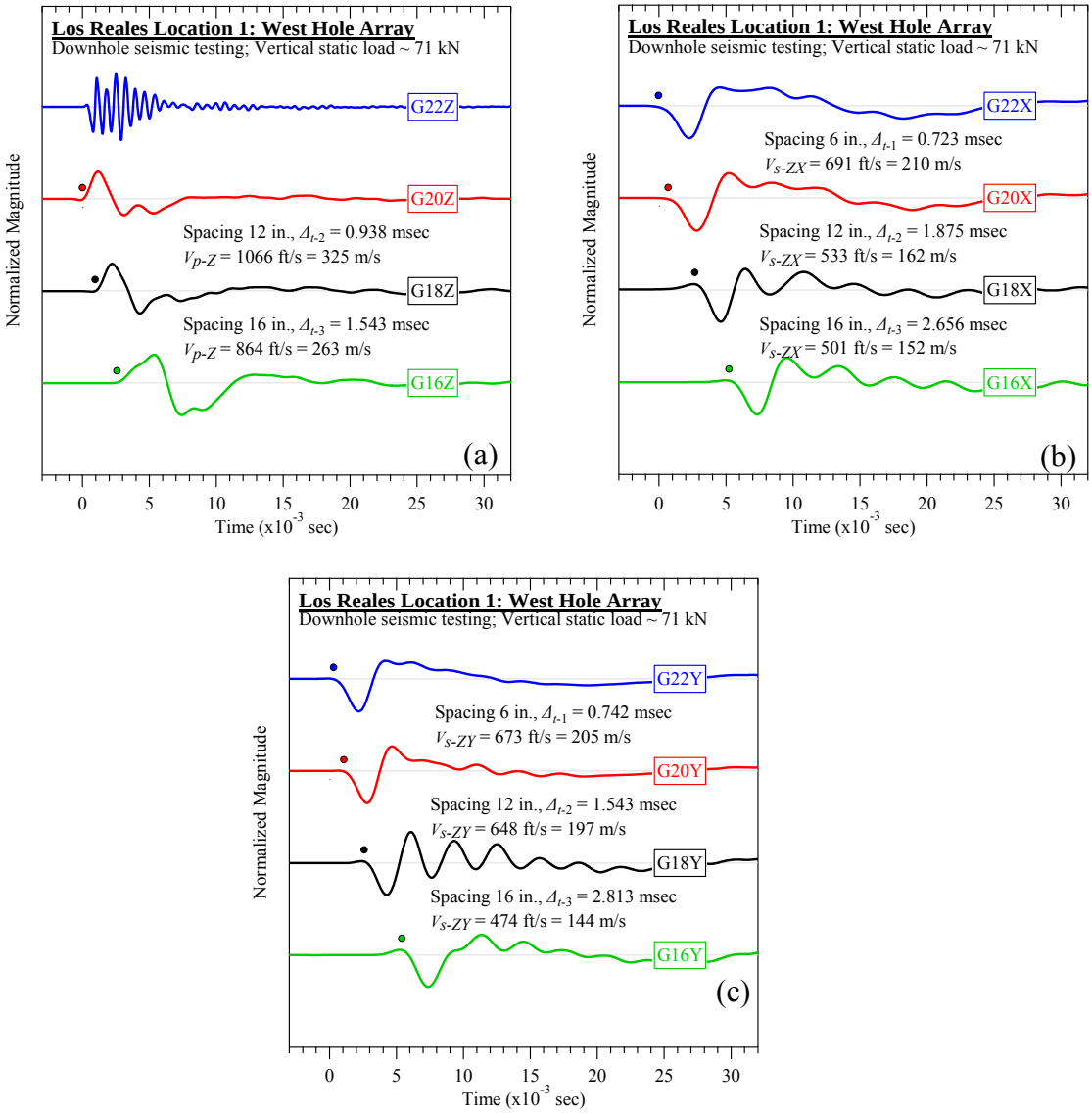

Figure C-8. Los Reales Landfill #1 (west hole): Downhole seismic testing at vertical load of 71 kN: (a) $V_{p\text{-}Z}$, (b) $V_{s\text{-}ZX}$, and (c) $V_{s\text{-}ZY}$.

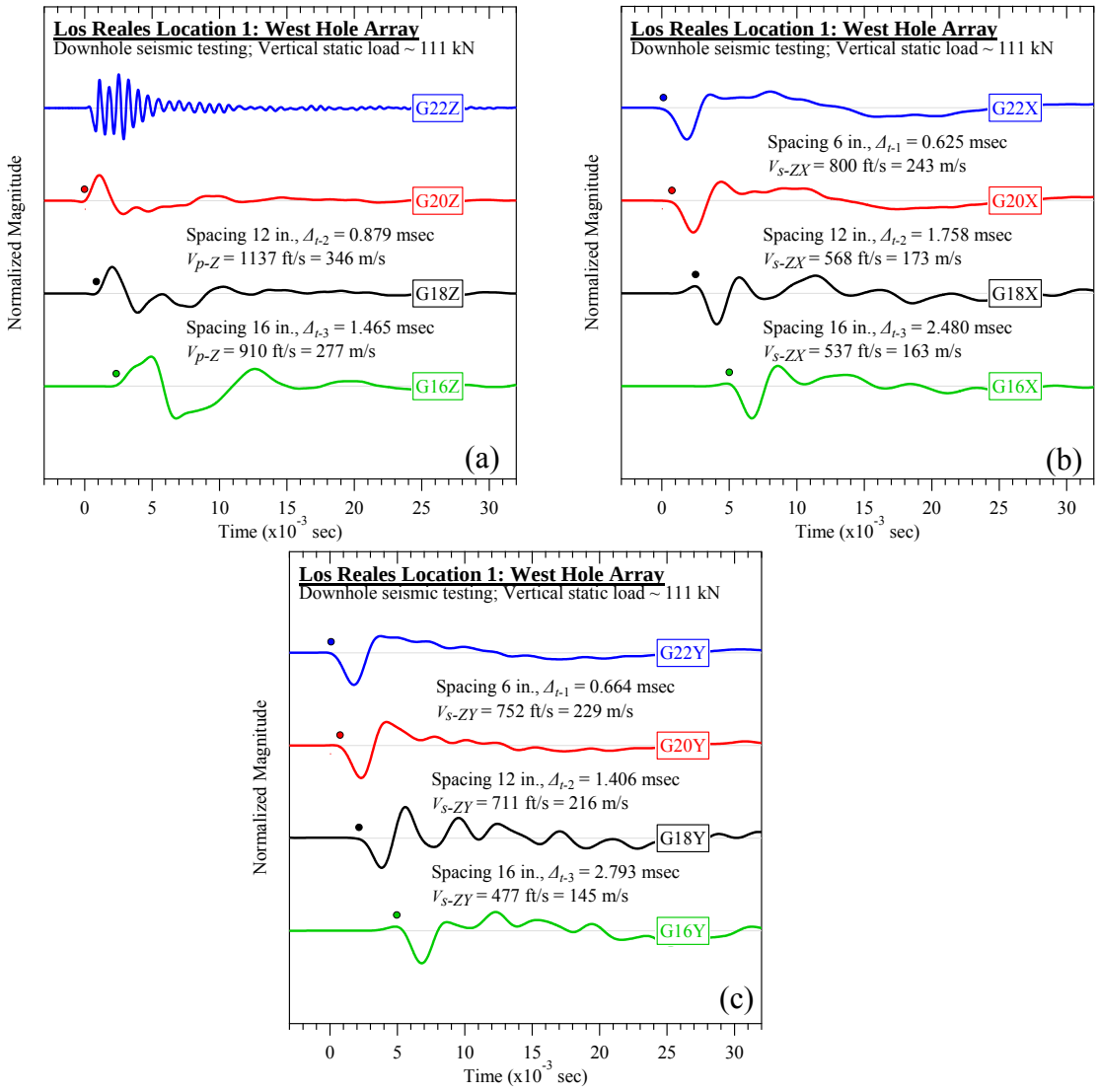

Figure C-9. Los Reales Landfill #1 (west hole): Downhole seismic testing at vertical load of 111 kN: (a) $V_{p\text{-}Z}$, (b) $V_{s\text{-}ZX}$, and (c) $V_{s\text{-}ZY}$.

C.1.2 Crosshole Seismic Testing

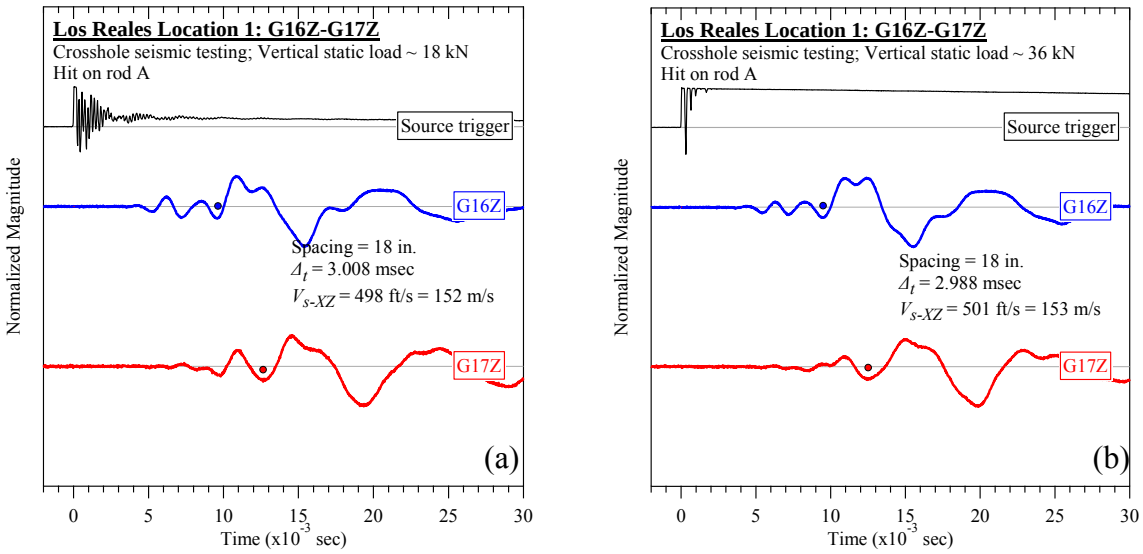

Figure C-10. Los Reales Landfill #1 (rod A): Crosshole seismic testing at vertical loads of (a) 18 kN and (b) 36 kN: $V_{s\text{-}XZ}$.

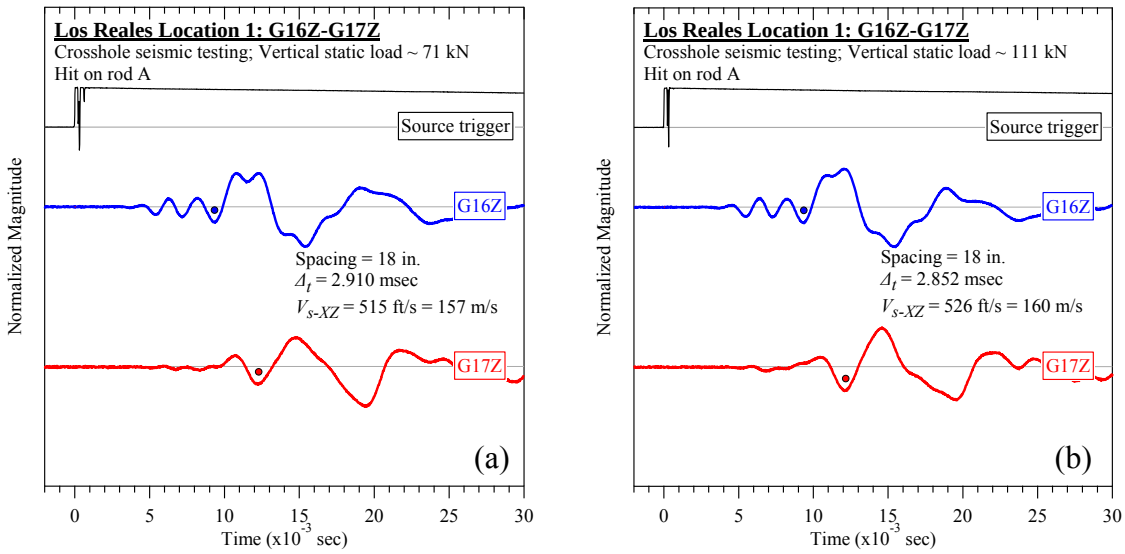

Figure C-11. Los Reales Landfill #1 (rod A): Crosshole seismic testing at vertical loads of (a) 71 kN and (b) 111 kN: $V_{s\text{-}XZ}$.

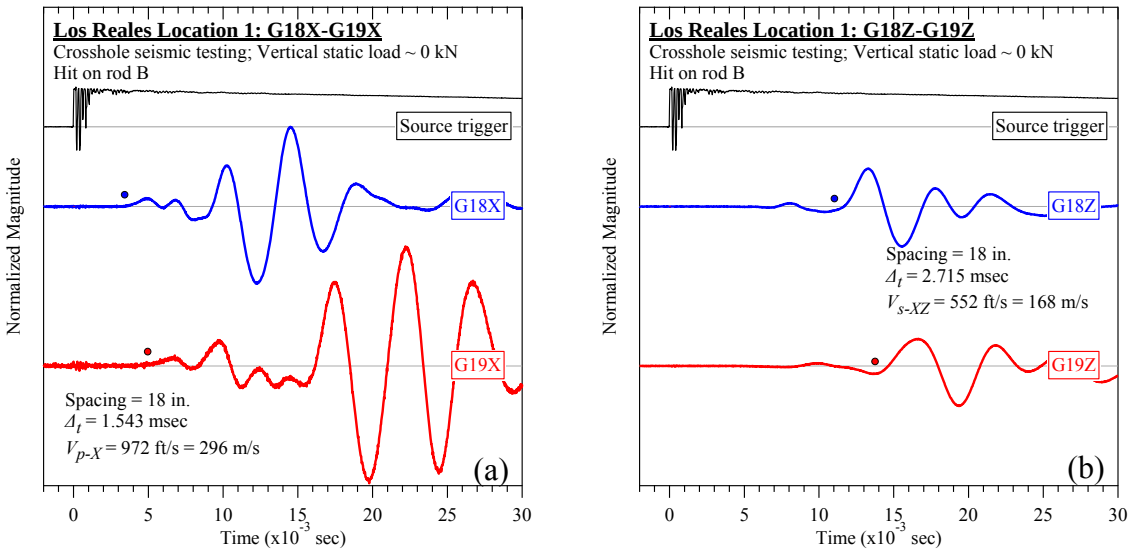

Figure C-12. Los Reales Landfill #1 (rod B): Crosshole seismic testing at vertical load of 0 kN: (a) $V_{p\text{-}X}$ and (b) $V_{s\text{-}XZ}$.

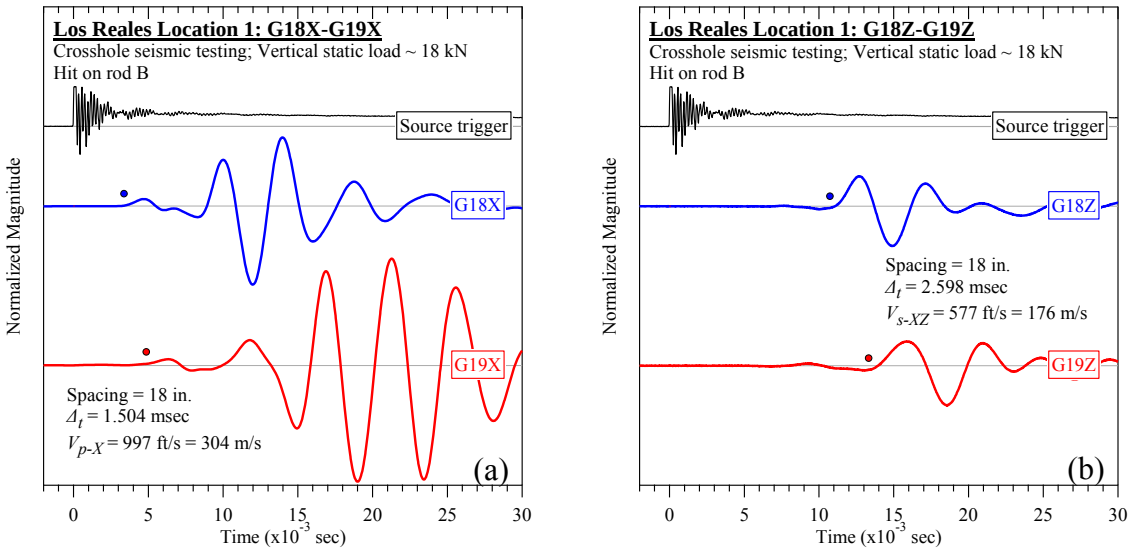

Figure C-13. Los Reales Landfill #1 (rod B): Crosshole seismic testing at vertical load of 18 kN: (a) $V_{p\text{-}X}$ and (b) $V_{s\text{-}XZ}$.

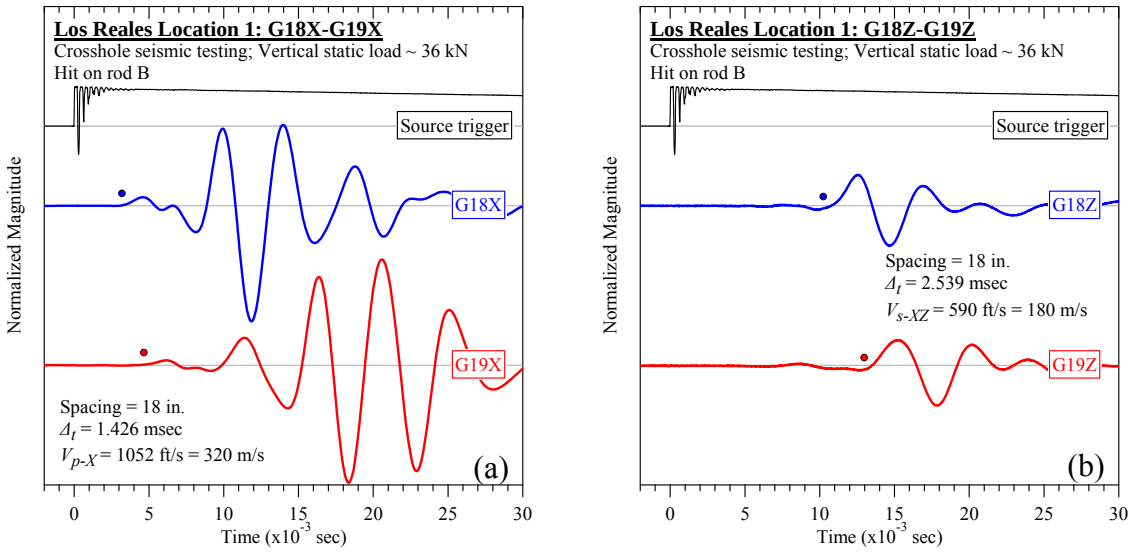

Figure C-14. Los Reales Landfill #1 (rod B): Crosshole seismic testing at vertical load of 36 kN: (a) $V_{p\text{-}X}$ and (b) $V_{s\text{-}XZ}$.

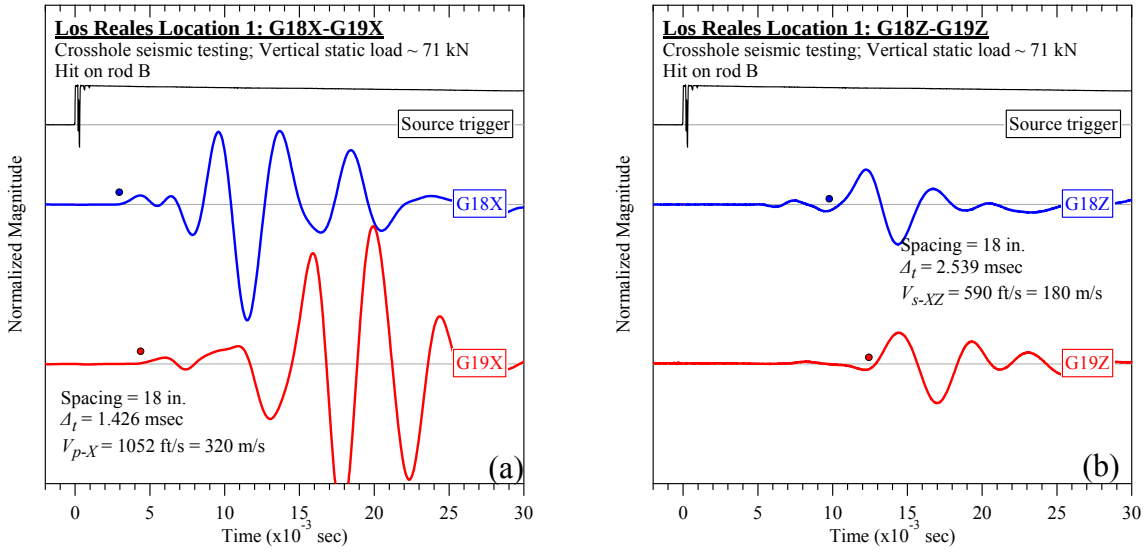

Figure C-15. Los Reales Landfill #1 (rod B): Crosshole seismic testing at vertical load of 71 kN: (a) $V_{p\text{-}X}$ and (b) $V_{s\text{-}XZ}$.

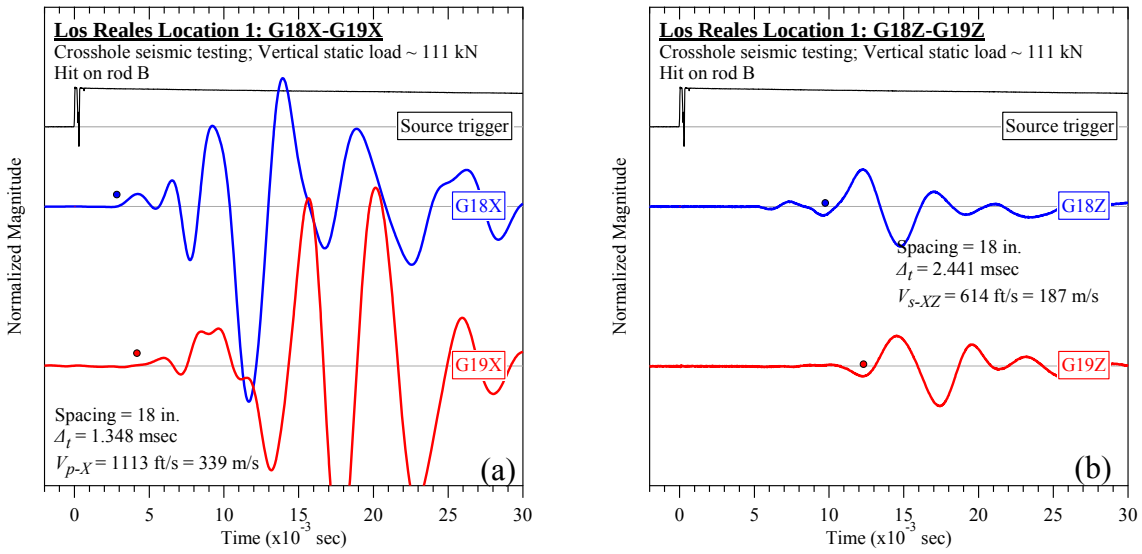

Figure C-16. Los Reales Landfill #1 (rod B): Crosshole seismic testing at vertical load of 111 kN: (a) $V_{p\text{-}X}$ and (b) $V_{s\text{-}XZ}$.

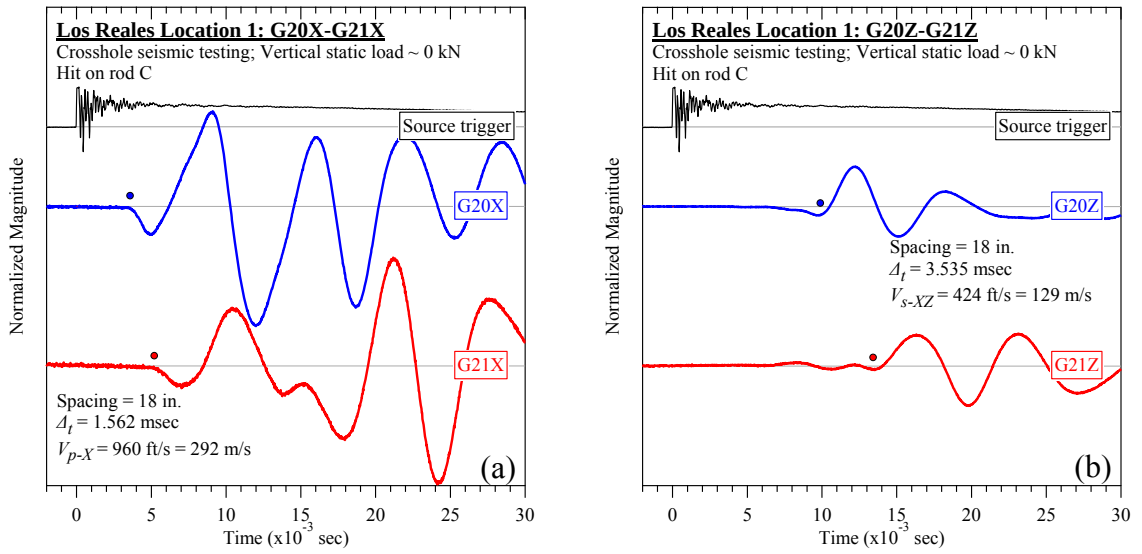

Figure C-17. Los Reales Landfill #1 (rod C): Crosshole seismic testing at vertical load of 0 kN: (a) $V_{p\text{-}X}$ and (b) $V_{s\text{-}XZ}$.

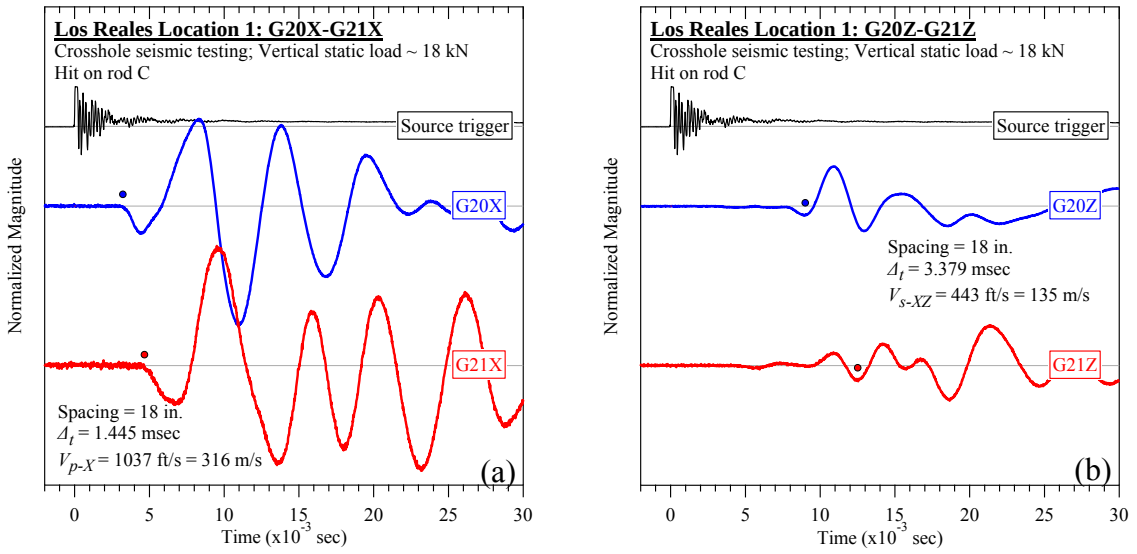

Figure C-18. Los Reales Landfill #1 (rod C): Crosshole seismic testing at vertical load of 18 kN: (a) $V_{p\text{-}X}$ and (b) $V_{s\text{-}XZ}$.

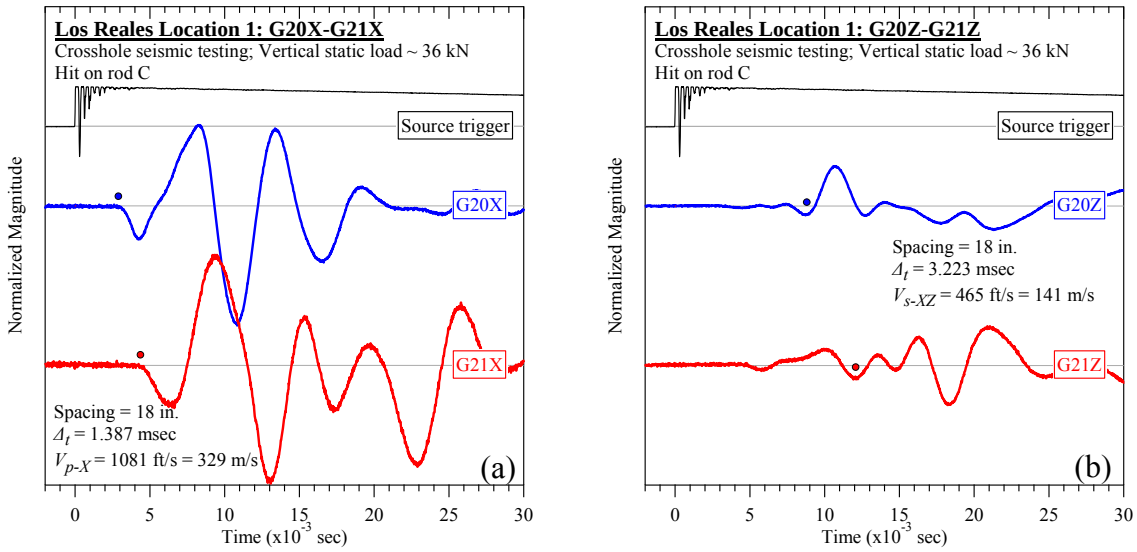

Figure C-19. Los Reales Landfill #1 (rod C): Crosshole seismic testing at vertical load of 36 kN: (a) $V_{p\text{-}X}$ and (b) $V_{s\text{-}XZ}$.

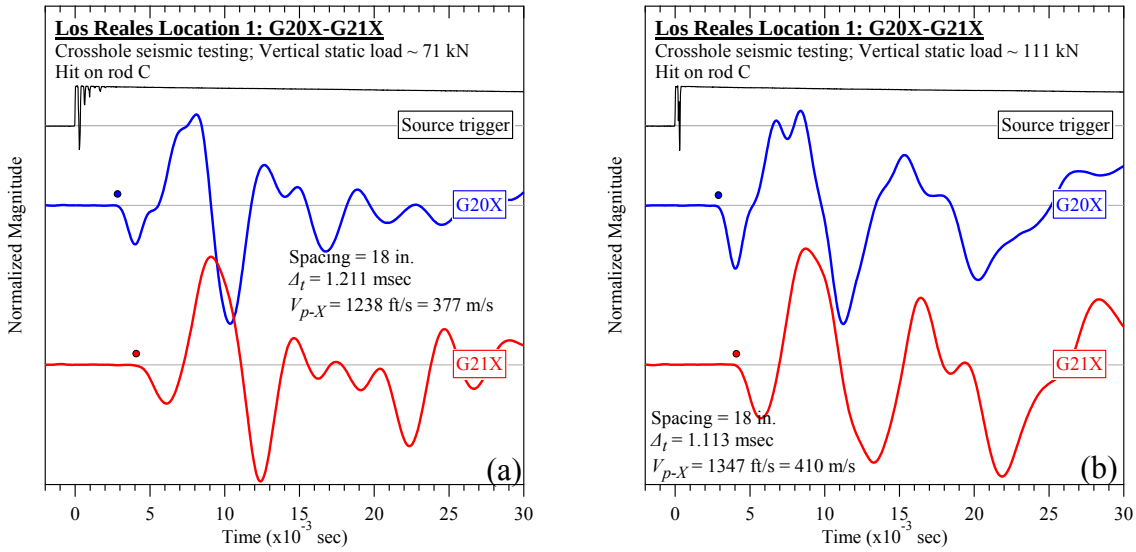

Figure C-20. Los Reales Landfill #1 (rod C): Crosshole seismic testing at vertical loads of (a) 71 kN and (b) 111 kN: $V_{p\text{-}X}$.

C.1.3 Steady-state Dynamic Testing

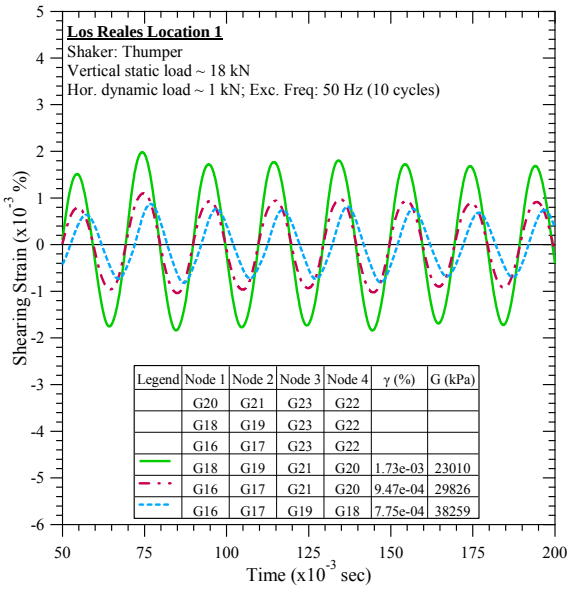

Legend	Node 1	Node 2	Node 3	Node 4	γ (%)	G (kPa)
	G20	G21	G23	G22		
	G18	G19	G23	G22		
	G16	G17	G23	G22		
	G18	G19	G21	G20	1.73e-03	23010
	G16	G17	G21	G20	9.47e-04	29826
	G16	G17	G19	G18	7.75e-04	38259

Figure C-21. Los Reales Landfill #1: Steady-state dynamic testing at vertical load of 18 kN and horizontal dynamic load of 1 kN.

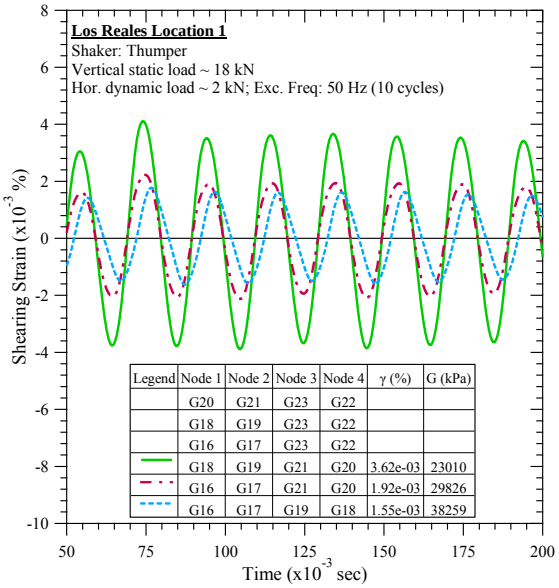

Figure C-22. Los Reales Landfill #1: Steady-state dynamic testing at vertical load of 18 kN and horizontal dynamic load of 2 kN.

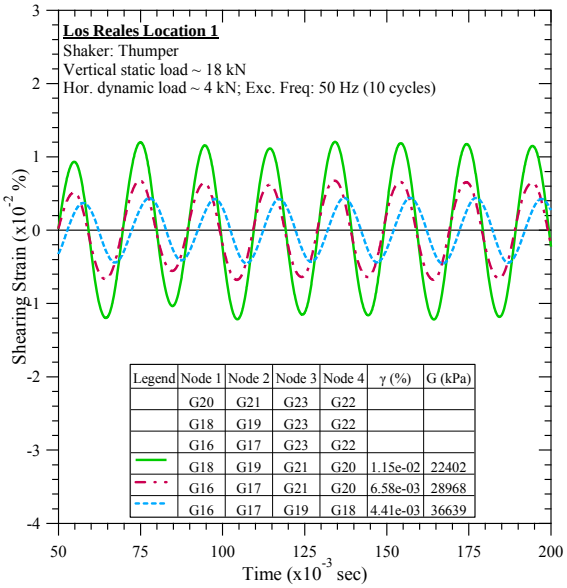

Figure C-23. Los Reales Landfill #1: Steady-state dynamic testing at vertical load of 18 kN and horizontal dynamic load of 4 kN.

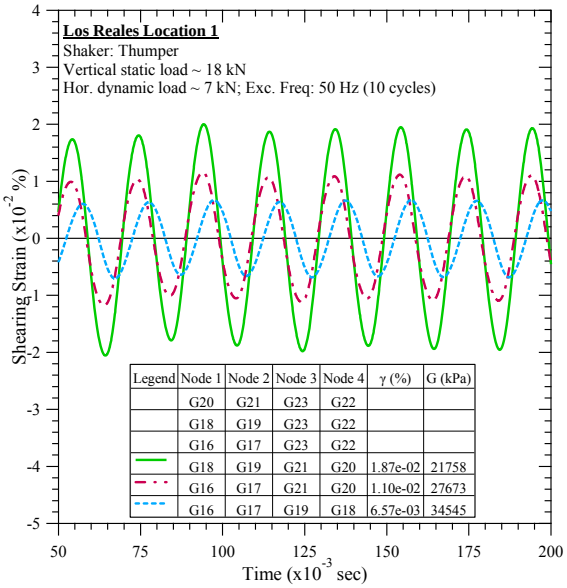

Figure C-24. Los Reales Landfill #1: Steady-state dynamic testing at vertical load of 18 kN and horizontal dynamic load of 7 kN.

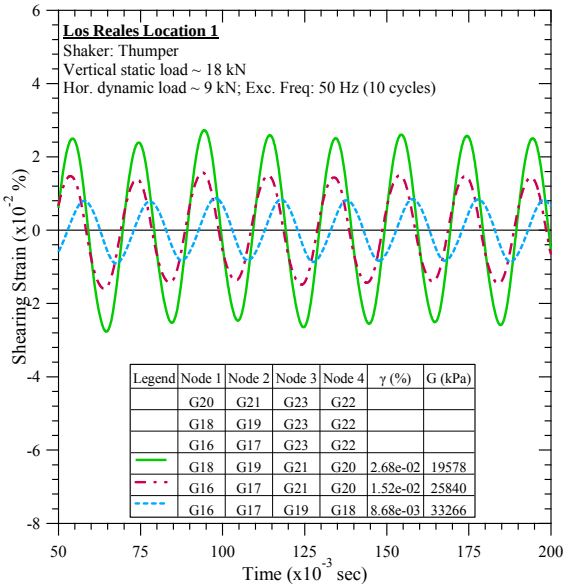

Figure C-25. Los Reales Landfill #1: Steady-state dynamic testing at vertical load of 18 kN and horizontal dynamic load of 9 kN.

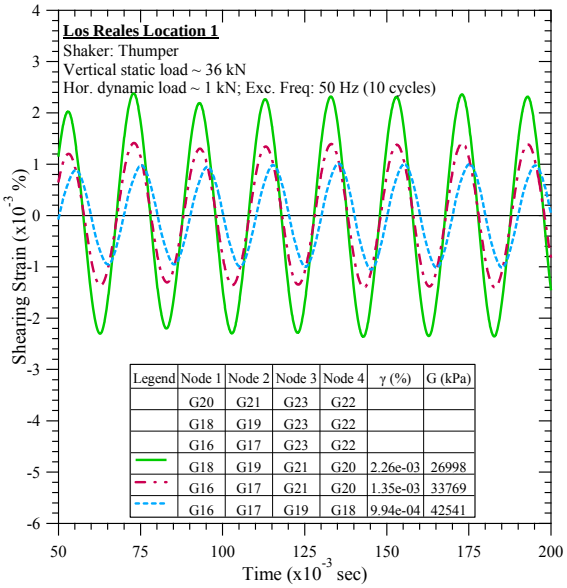

Figure C-26. Los Reales Landfill #1: Steady-state dynamic testing at vertical load of 36 kN and horizontal dynamic load of 1 kN.

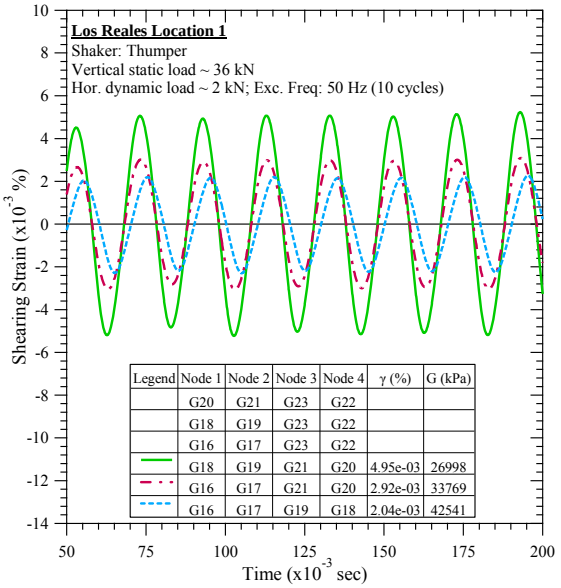

Figure C-27. Los Reales Landfill #1: Steady-state dynamic testing at vertical load of 36 kN and horizontal dynamic load of 2 kN.

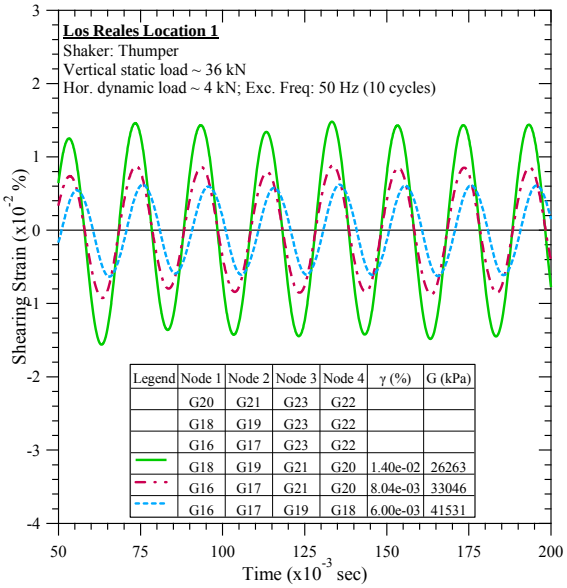

Figure C-28. Los Reales Landfill #1: Steady-state dynamic testing at vertical load of 36 kN and horizontal dynamic load of 4 kN.

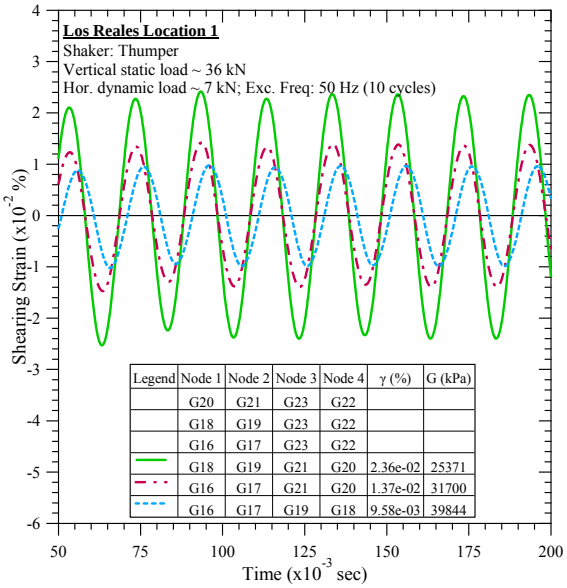

Figure C-29. Los Reales Landfill #1: Steady-state dynamic testing at vertical load of 36 kN and horizontal dynamic load of 7 kN.

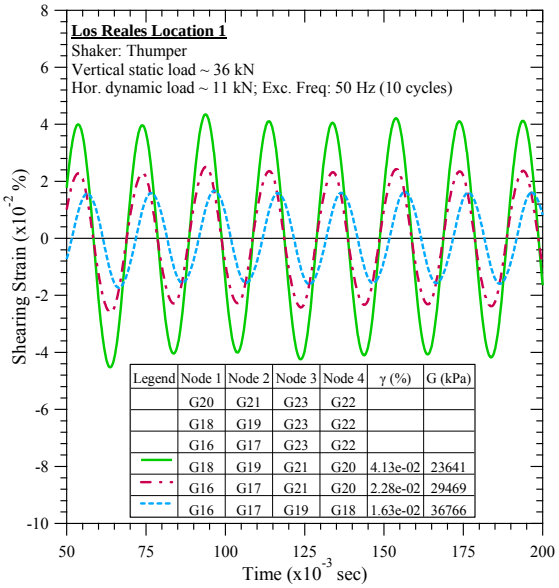

Figure C-30. Los Reales Landfill #1: Steady-state dynamic testing at vertical load of 36 kN and horizontal dynamic load of 11 kN.

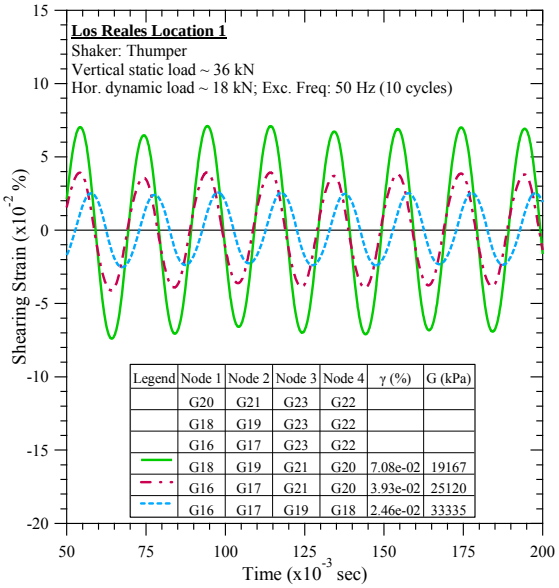

Figure C-31. Los Reales Landfill #1: Steady-state dynamic testing at vertical load of 36 kN and horizontal dynamic load of 18 kN.

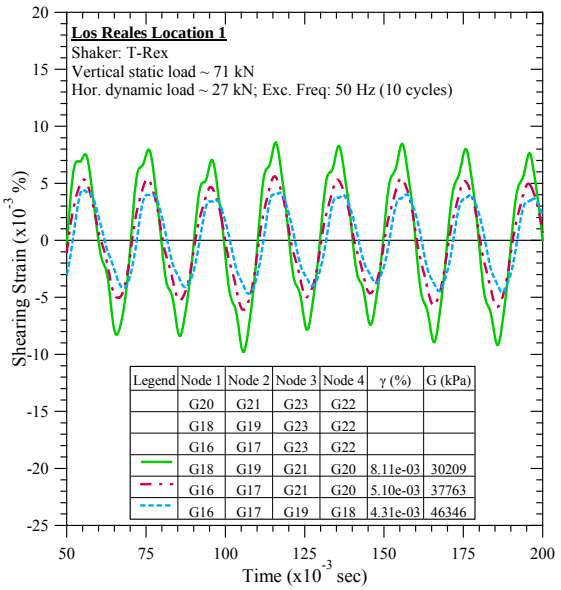

Figure C-32. Los Reales Landfill #1: Steady-state dynamic testing at vertical load of 71 kN and horizontal dynamic load of 27 kN.

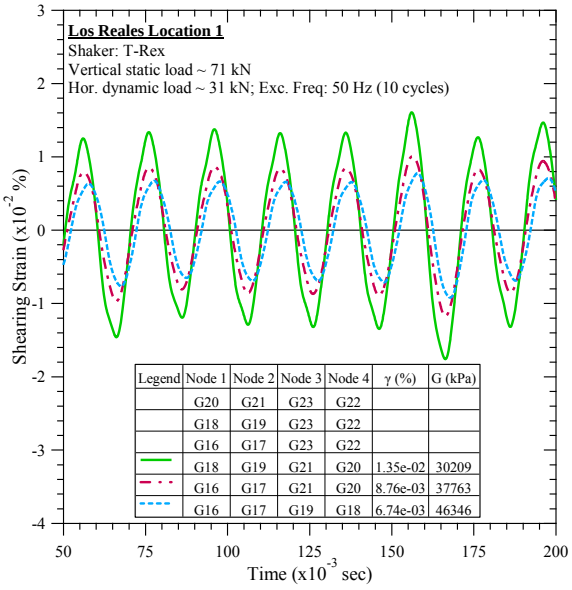

Figure C-33. Los Reales Landfill #1: Steady-state dynamic testing at vertical load of 71 kN and horizontal dynamic load of 31 kN.

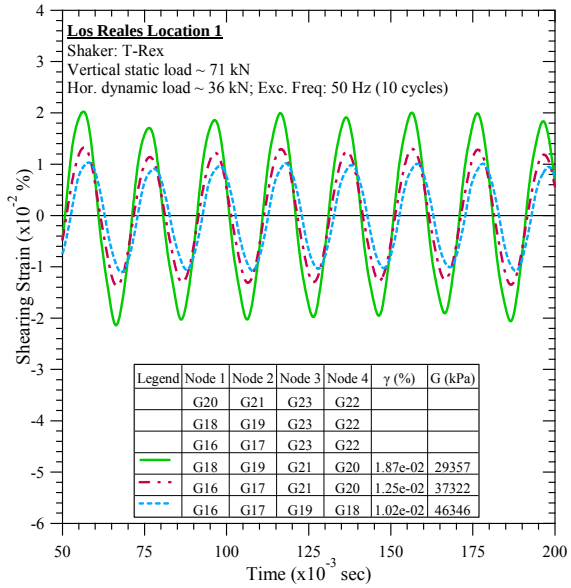

Figure C-34. Los Reales Landfill #1: Steady-state dynamic testing at vertical load of 71 kN and horizontal dynamic load of 36 kN.

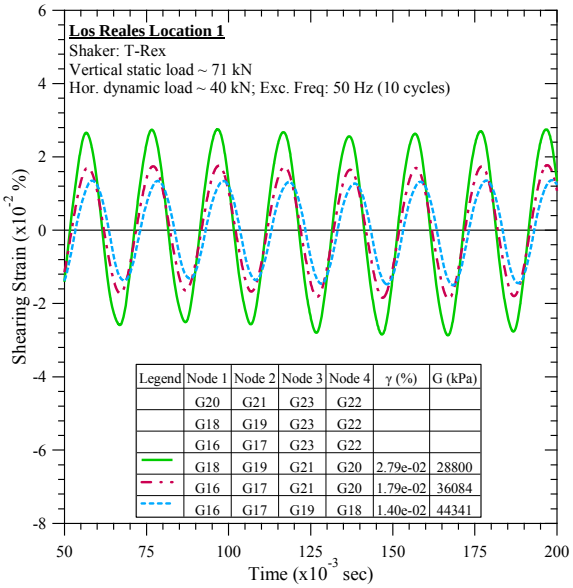

Figure C-35. Los Reales Landfill #1: Steady-state dynamic testing at vertical load of 71 kN and horizontal dynamic load of 40 kN.

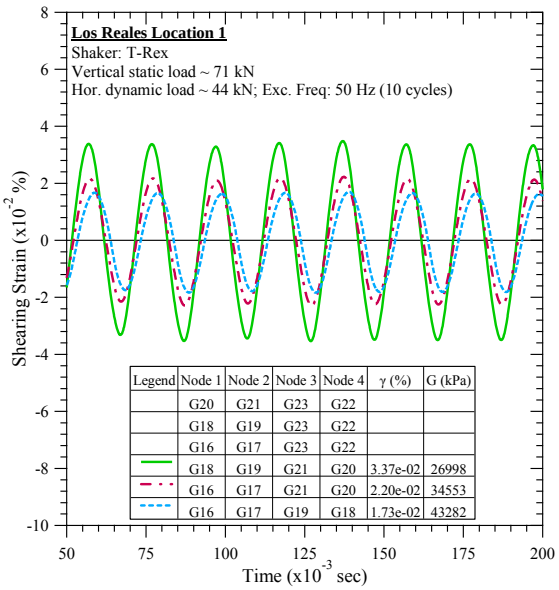

Figure C-36. Los Reales Landfill #1: Steady-state dynamic testing at vertical load of 71 kN and horizontal dynamic load of 44 kN.

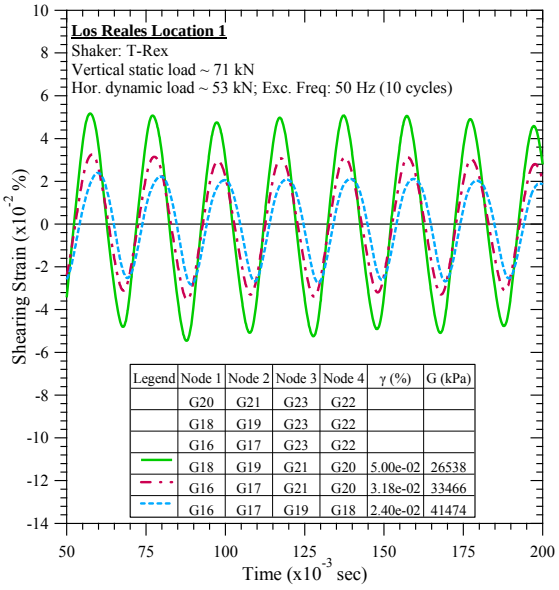

Figure C-37. Los Reales Landfill #1: Steady-state dynamic testing at vertical load of 71 kN and horizontal dynamic load of 53 kN.

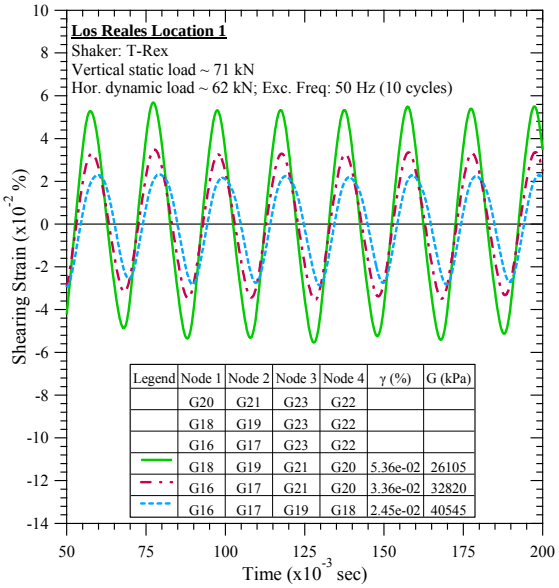

Figure C-38. Los Reales Landfill #1: Steady-state dynamic testing at vertical load of 71 kN and horizontal dynamic load of 62 kN.

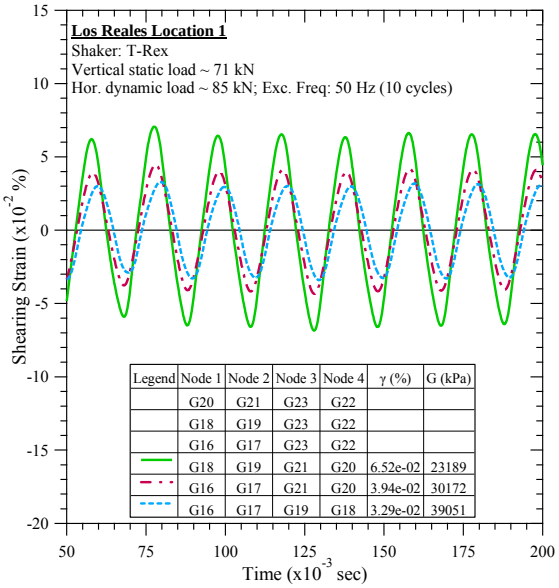

Figure C-39. Los Reales Landfill #1: Steady-state dynamic testing at vertical load of 71 kN and horizontal dynamic load of 85 kN.

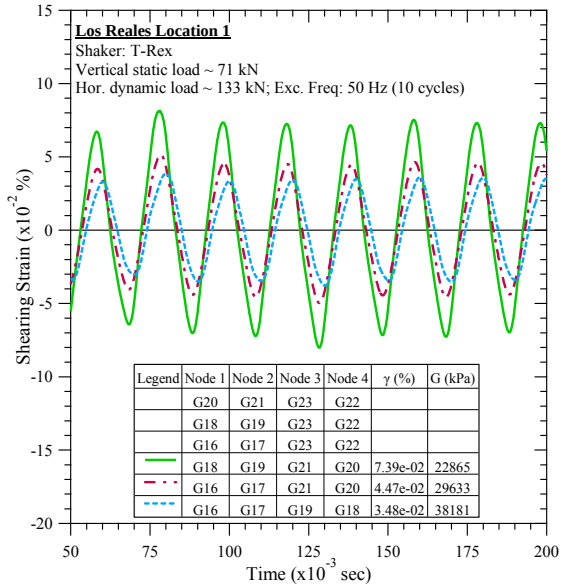

Figure C-40. Los Reales Landfill #1: Steady-state dynamic testing at vertical load of 71 kN and horizontal dynamic load of 133 kN.

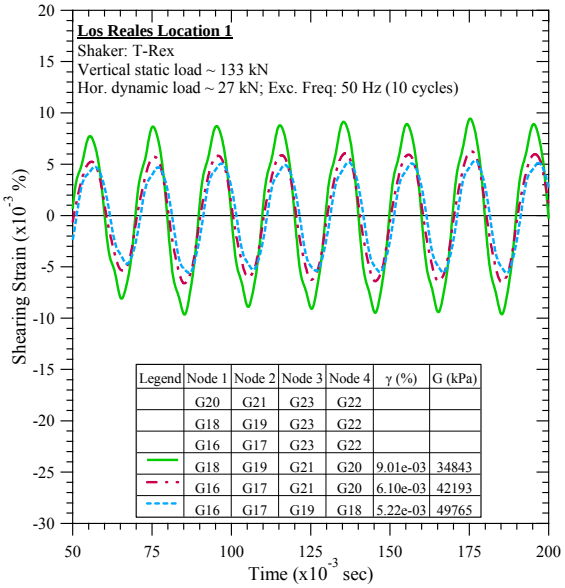

Figure C-41. Los Reales Landfill #1: Steady-state dynamic testing at vertical load of 133 kN and horizontal dynamic load of 27 kN.

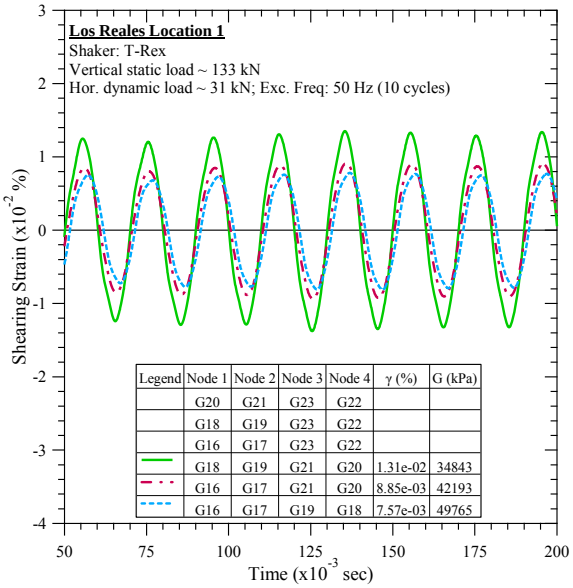

Figure C-42. Los Reales Landfill #1: Steady-state dynamic testing at vertical load of 133 kN and horizontal dynamic load of 31 kN.

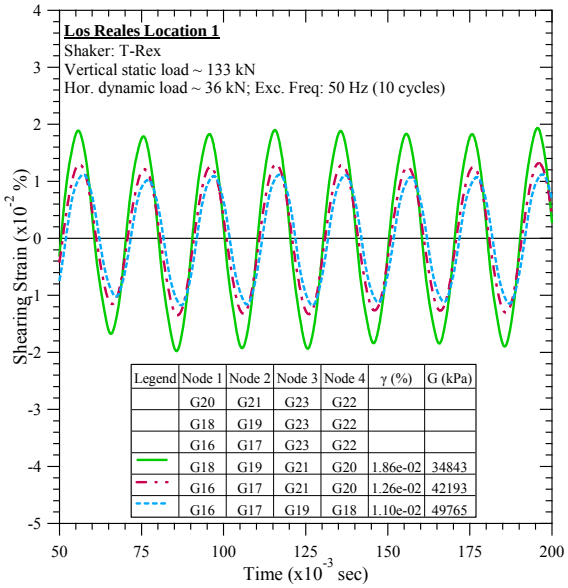

Figure C-43. Los Reales Landfill #1: Steady-state dynamic testing at vertical load of 133 kN and horizontal dynamic load of 36 kN.

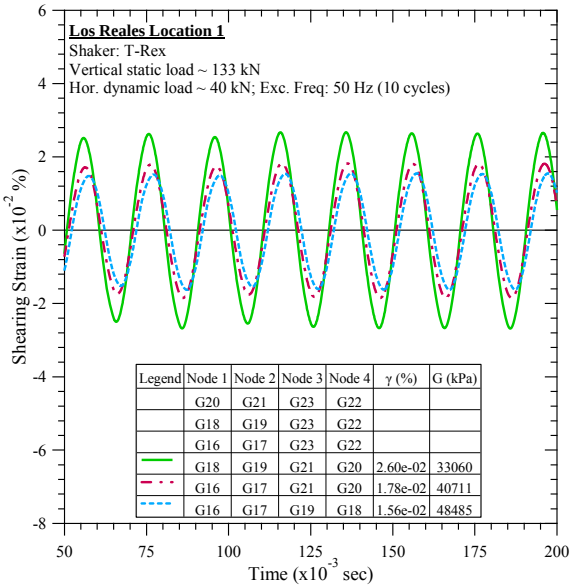

Figure C-44. Los Reales Landfill #1: Steady-state dynamic testing at vertical load of 133 kN and horizontal dynamic load of 40 kN.

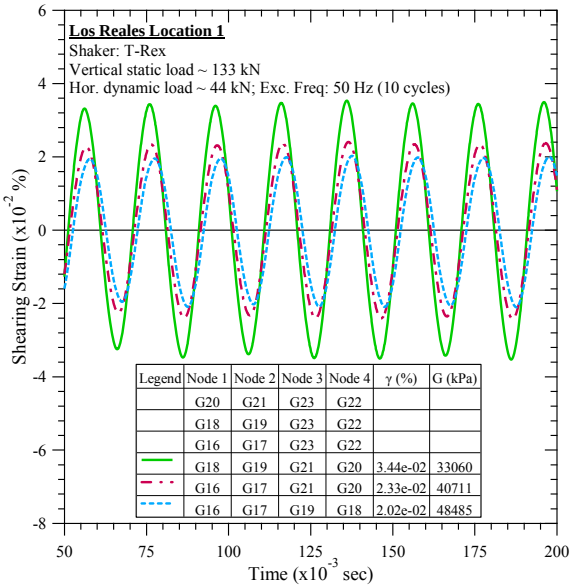

Figure C-45. Los Reales Landfill #1: Steady-state dynamic testing at vertical load of 133 kN and horizontal dynamic load of 44 kN.

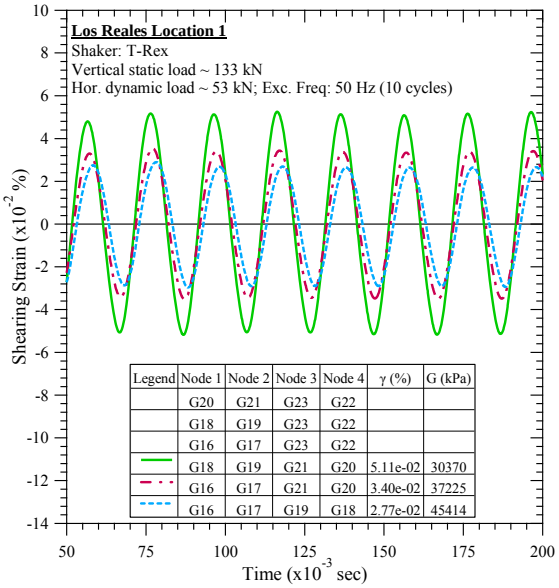

Figure C-46. Los Reales Landfill #1: Steady-state dynamic testing at vertical load of 133 kN and horizontal dynamic load of 53 kN.

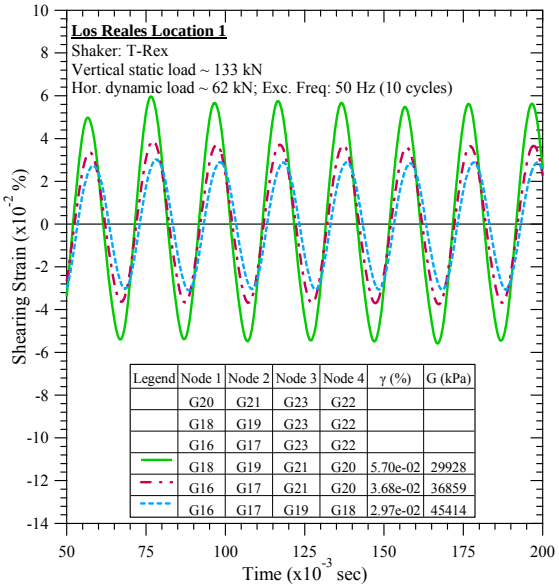

Figure C-47. Los Reales Landfill #1: Steady-state dynamic testing at vertical load of 133 kN and horizontal dynamic load of 62 kN.

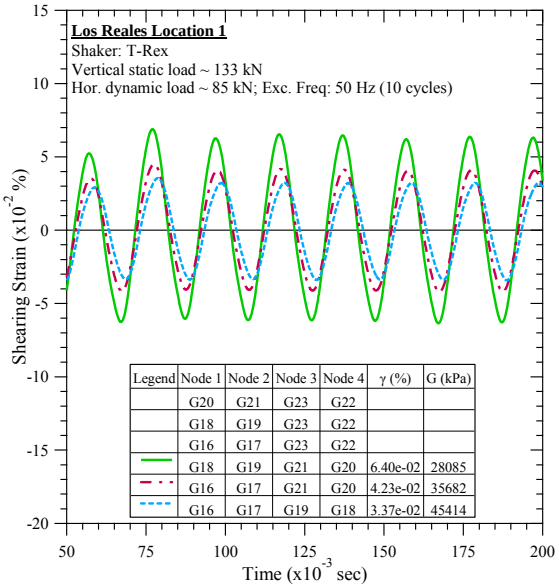

Figure C-48. Los Reales Landfill #1: Steady-state dynamic testing at vertical load of 133 kN and horizontal dynamic load of 85 kN.

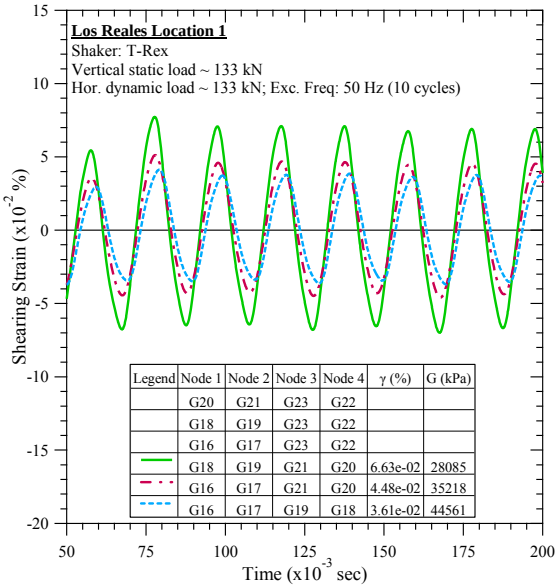

Figure C-49. Los Reales Landfill #1: Steady-state dynamic testing at vertical load of 133 kN and horizontal dynamic load of 133 kN.

C.2 Los Reales Landfill Location 2

C.2.1 Downhole Seismic Testing

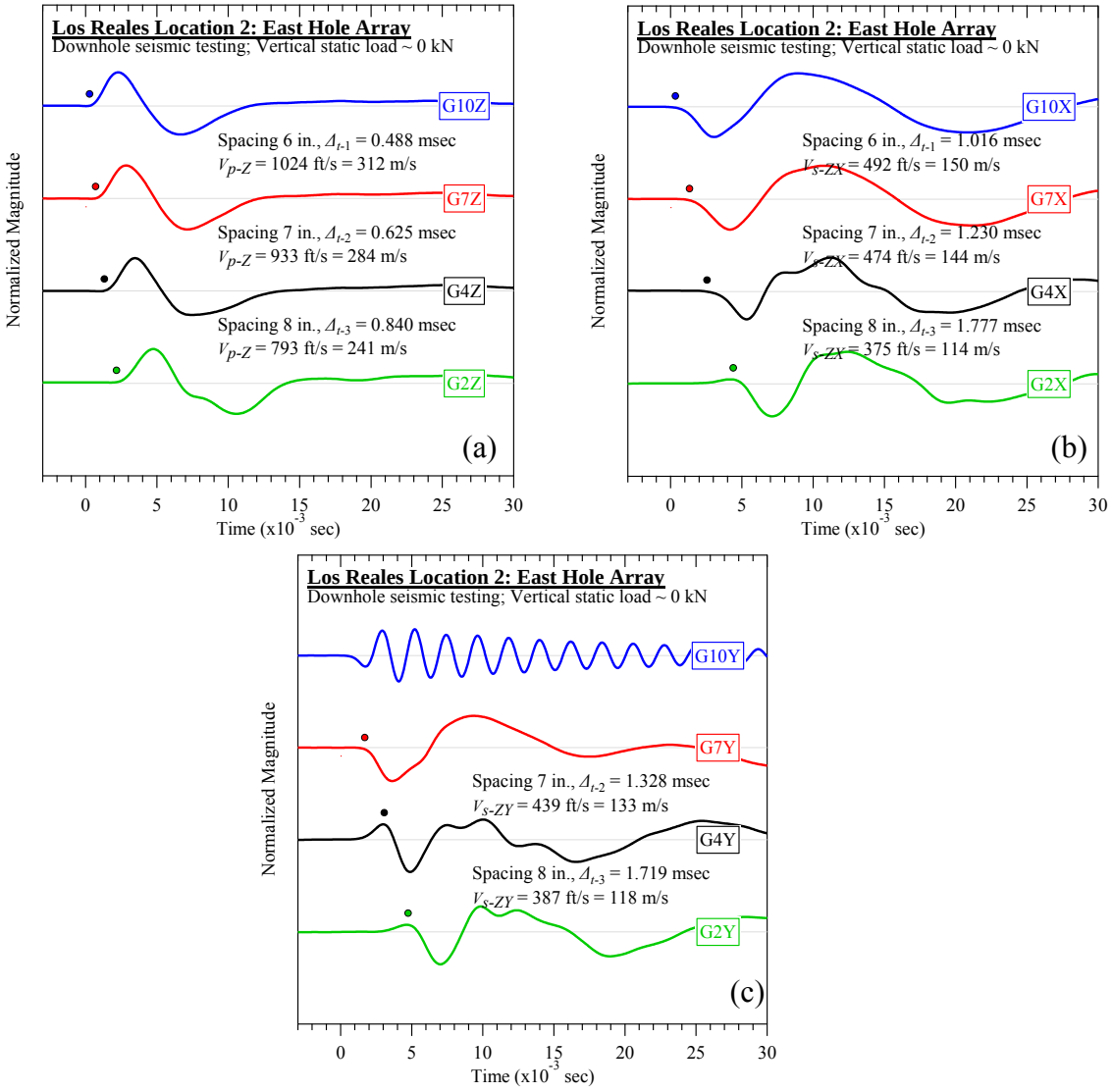

Figure C-50. Los Reales Landfill #2 (east hole): Downhole seismic testing at vertical load of 0 kN: (a) V_{p-Z}, (b) V_{s-ZX}, and (c) V_{s-ZY}.

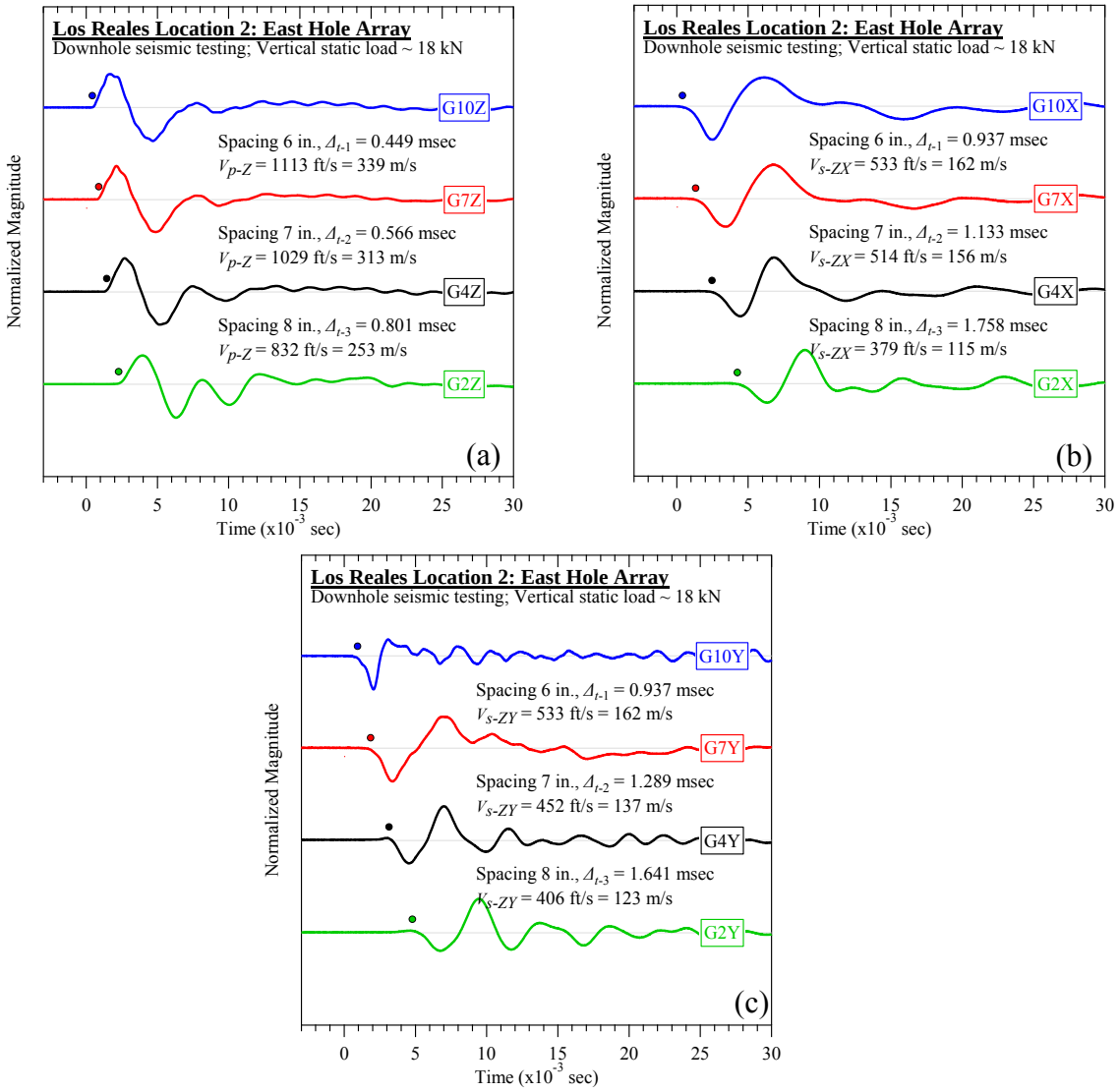

Figure C-51. Los Reales Landfill #2 (east hole): Downhole seismic testing at vertical load of 18 kN: (a) V_{p-Z}, (b) V_{s-ZX}, and (c) V_{s-ZY}.

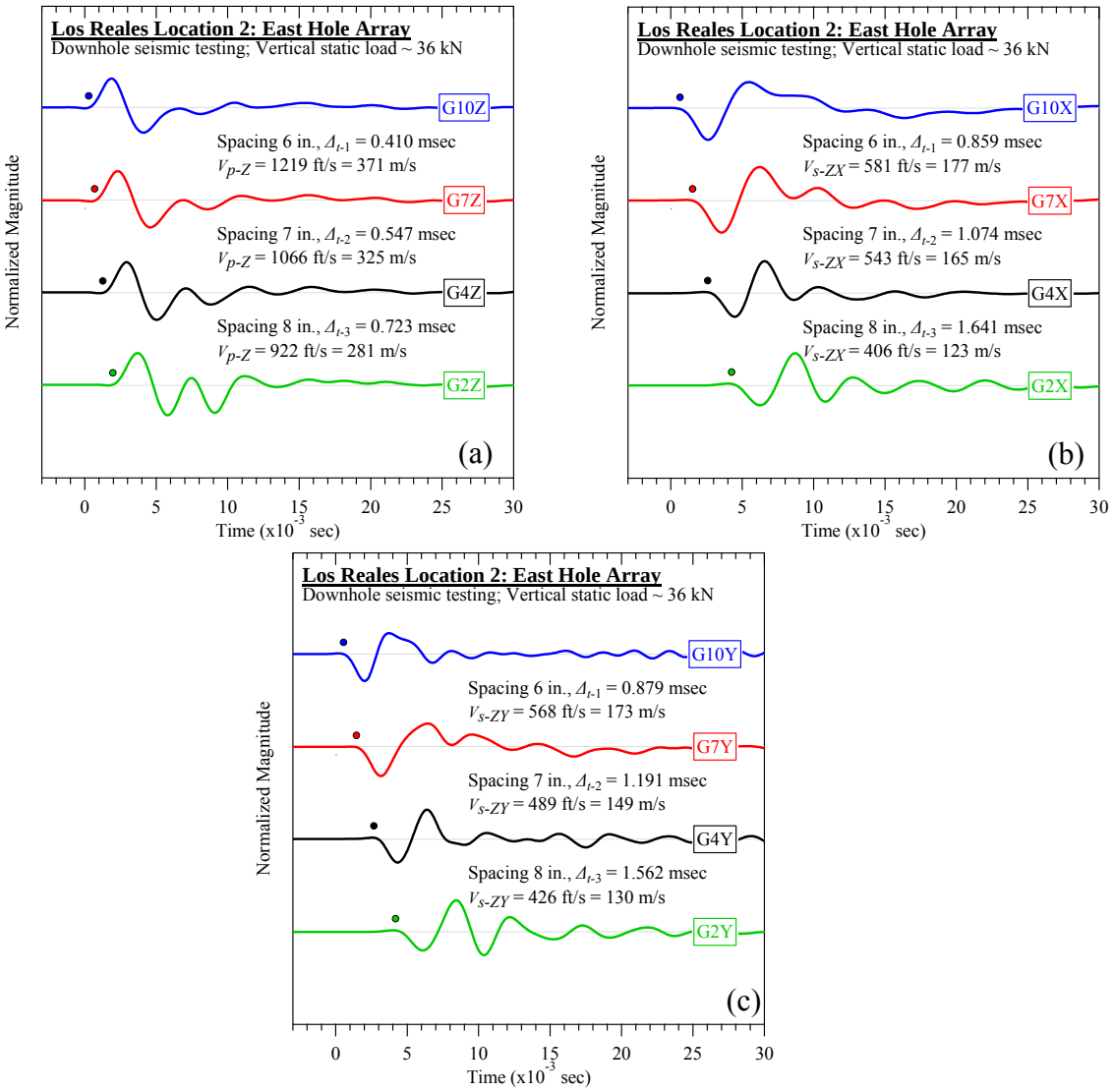

Figure C-52. Los Reales Landfill #2 (east hole): Downhole seismic testing at vertical load of 36 kN: (a) V_{p-Z}, (b) V_{s-ZX}, and (c) V_{s-ZY}.

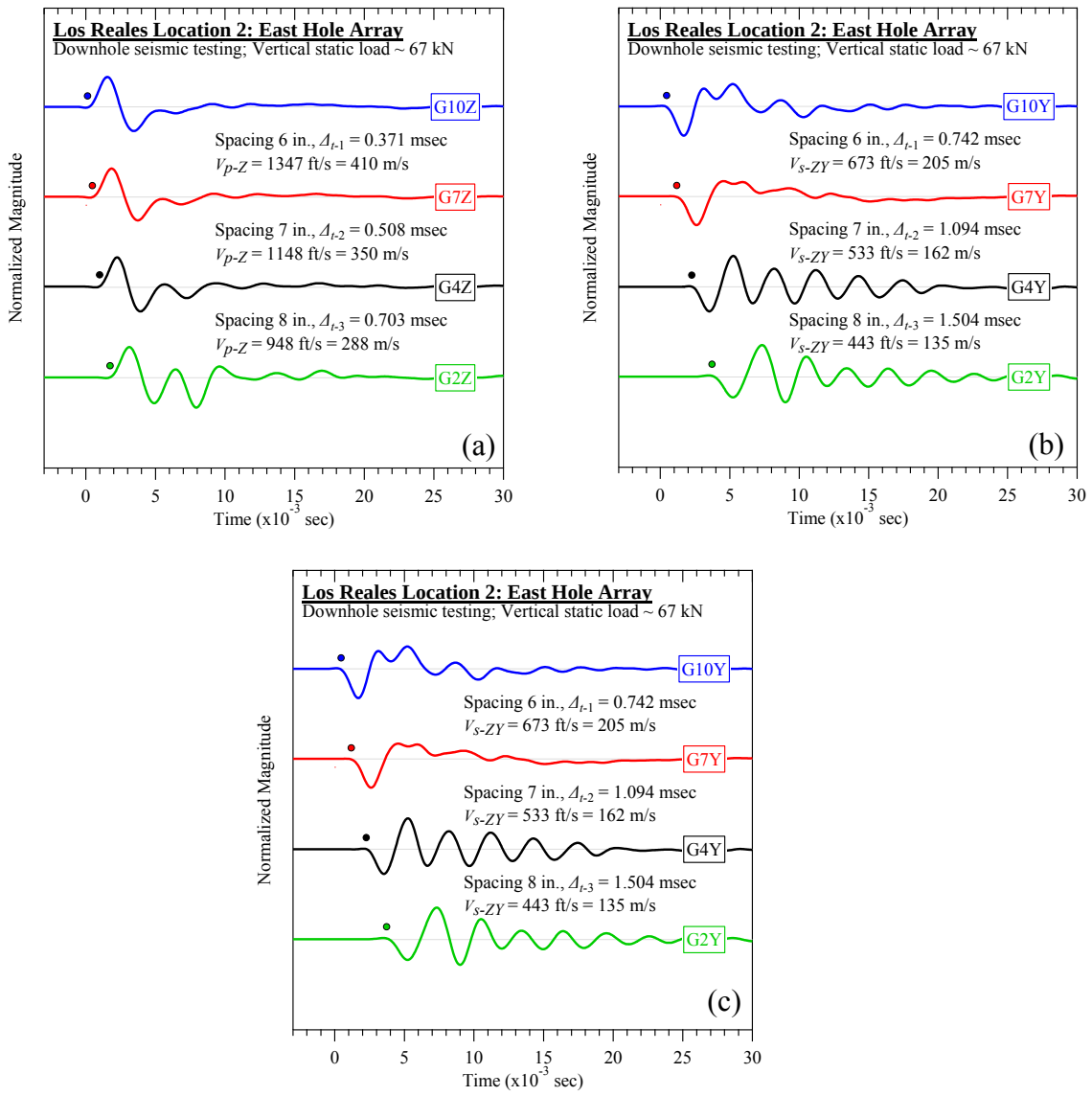

Figure C-53. Los Reales Landfill #2 (east hole): Downhole seismic testing at vertical load of 67 kN: (a) $V_{p\text{-}Z}$, (b) $V_{s\text{-}ZX}$, and (c) $V_{s\text{-}ZY}$.

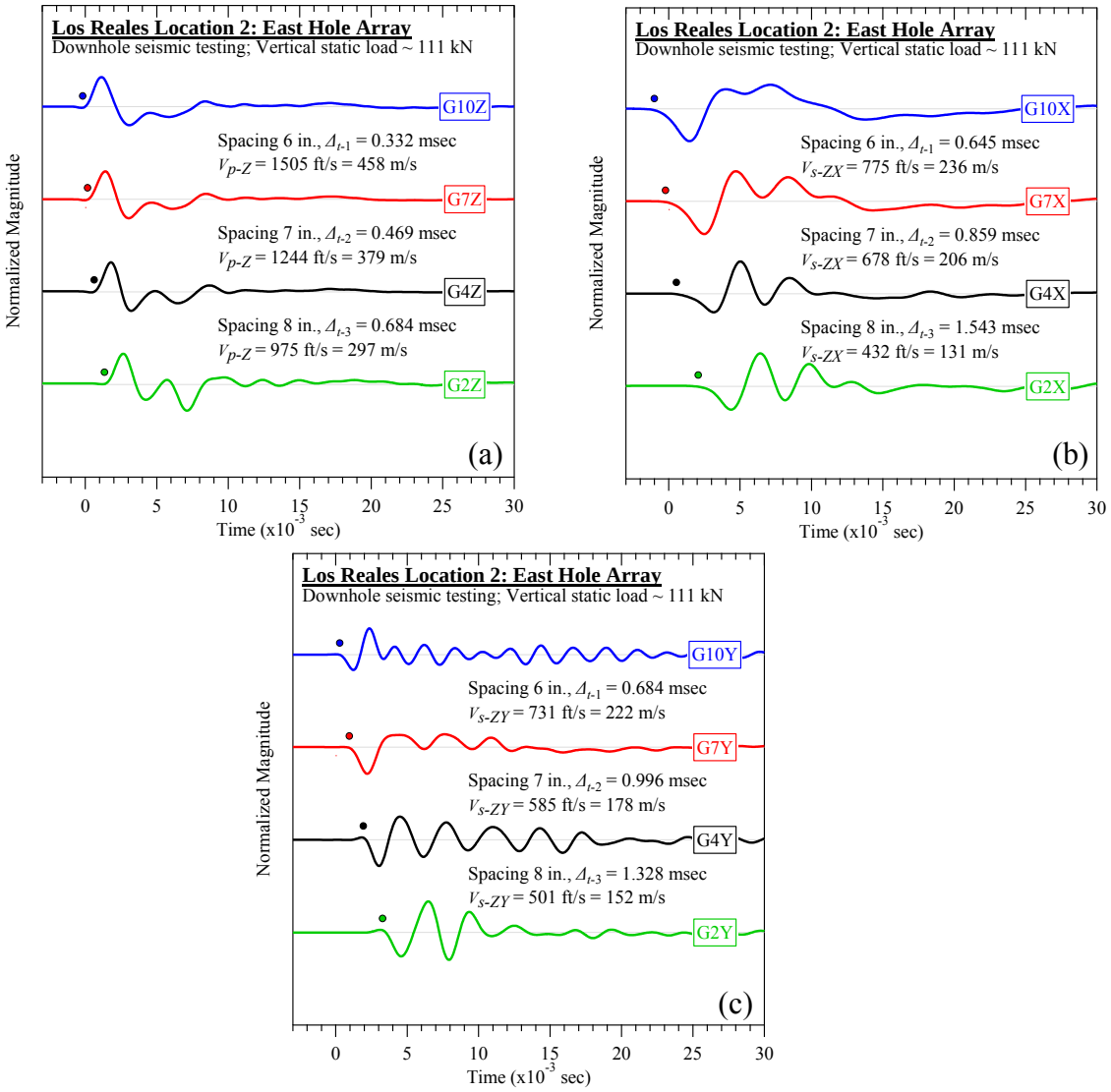

Figure C-54. Los Reales Landfill #2 (east hole): Downhole seismic testing at vertical load of 111 kN: (a) V_{p-Z}, (b) V_{s-ZX}, and (c) V_{s-ZY}.

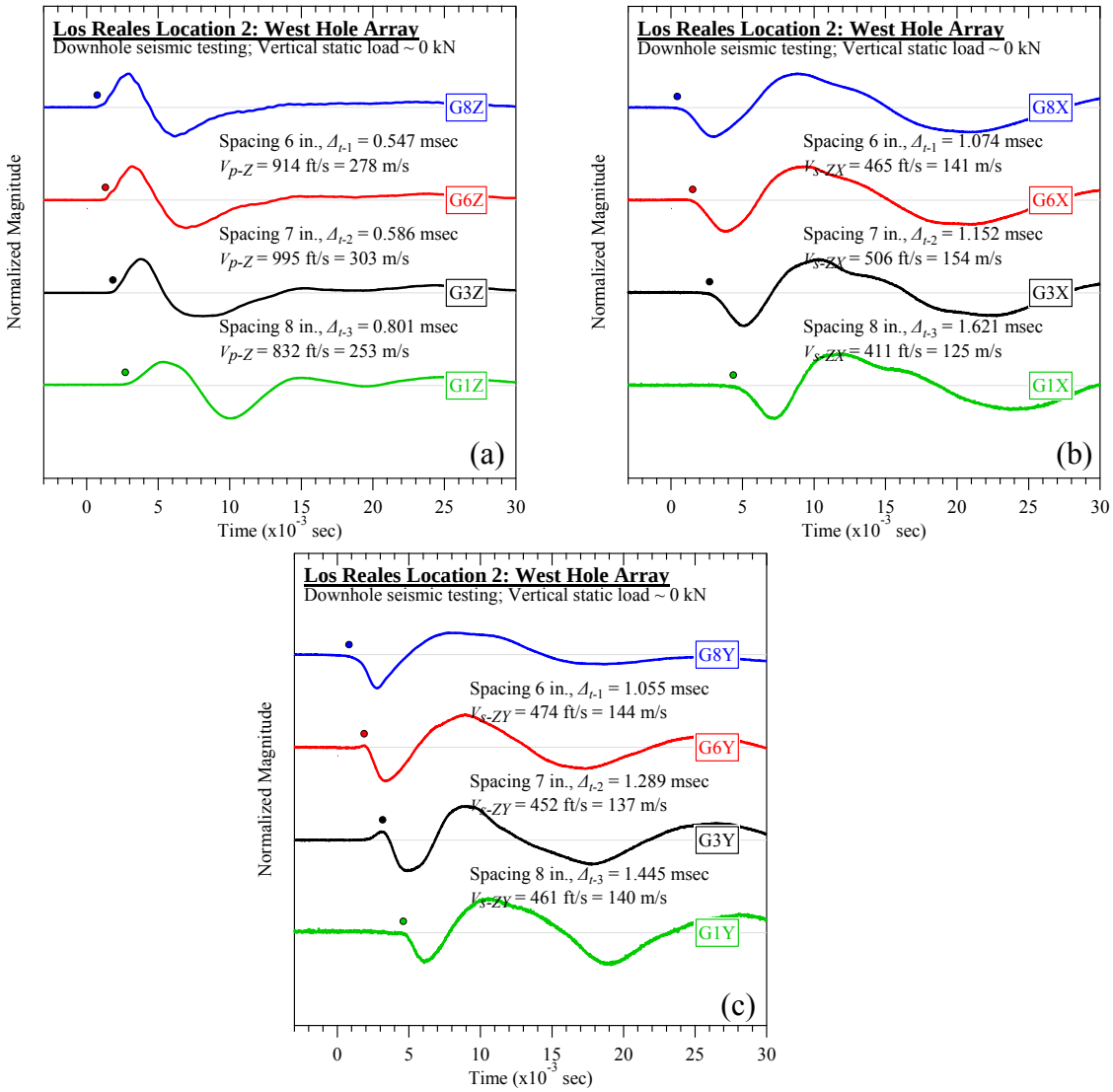

Figure C-55. Los Reales Landfill #2 (west hole): Downhole seismic testing at vertical load of 0 kN: (a) $V_{p\text{-}Z}$, (b) $V_{s\text{-}ZX}$, and (c) $V_{s\text{-}ZY}$.

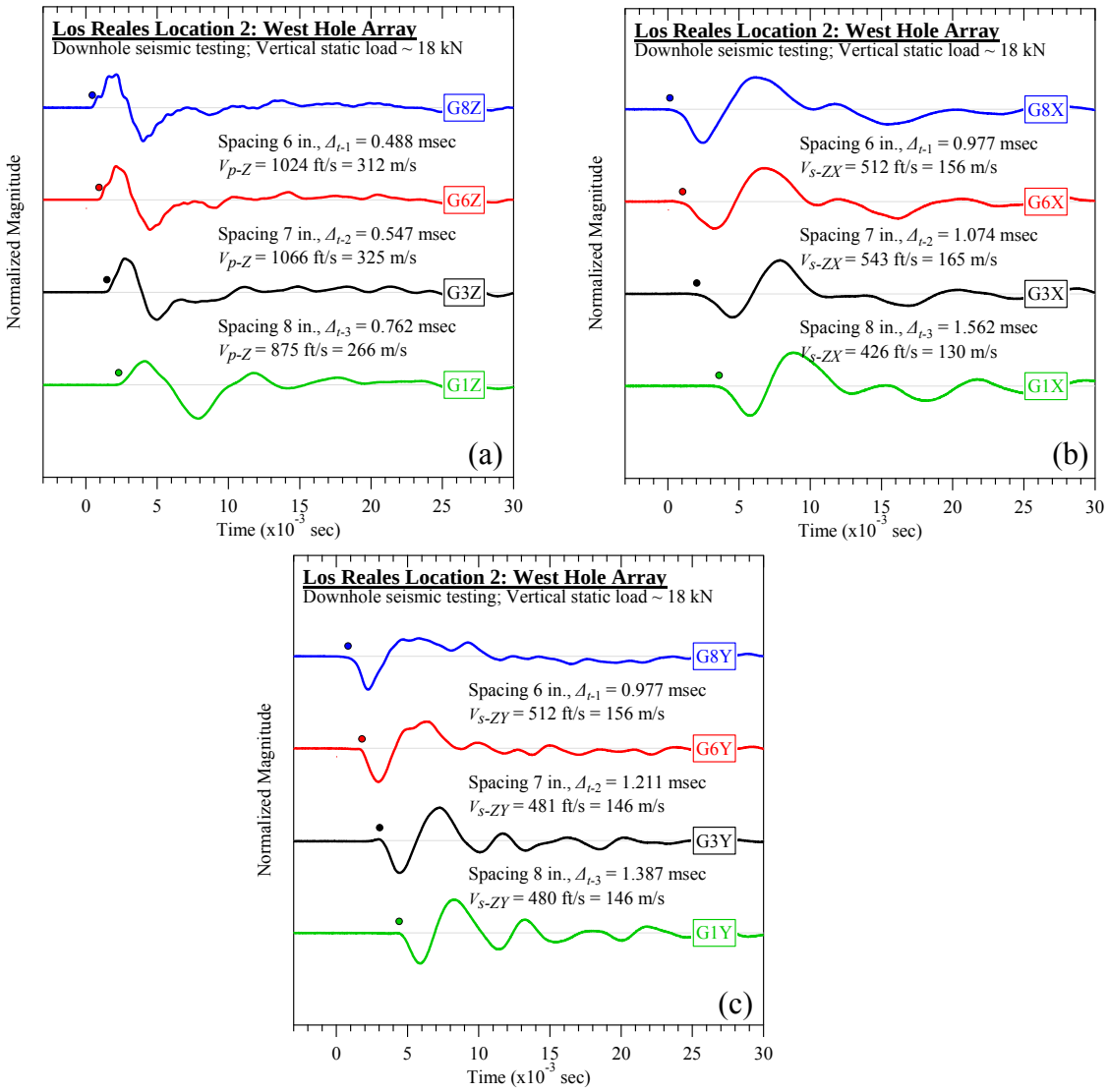

Figure C-56. Los Reales Landfill #2 (west hole): Downhole seismic testing at vertical load of 18 kN: (a) V_{p-Z}, (b) V_{s-ZX}, and (c) V_{s-ZY}.

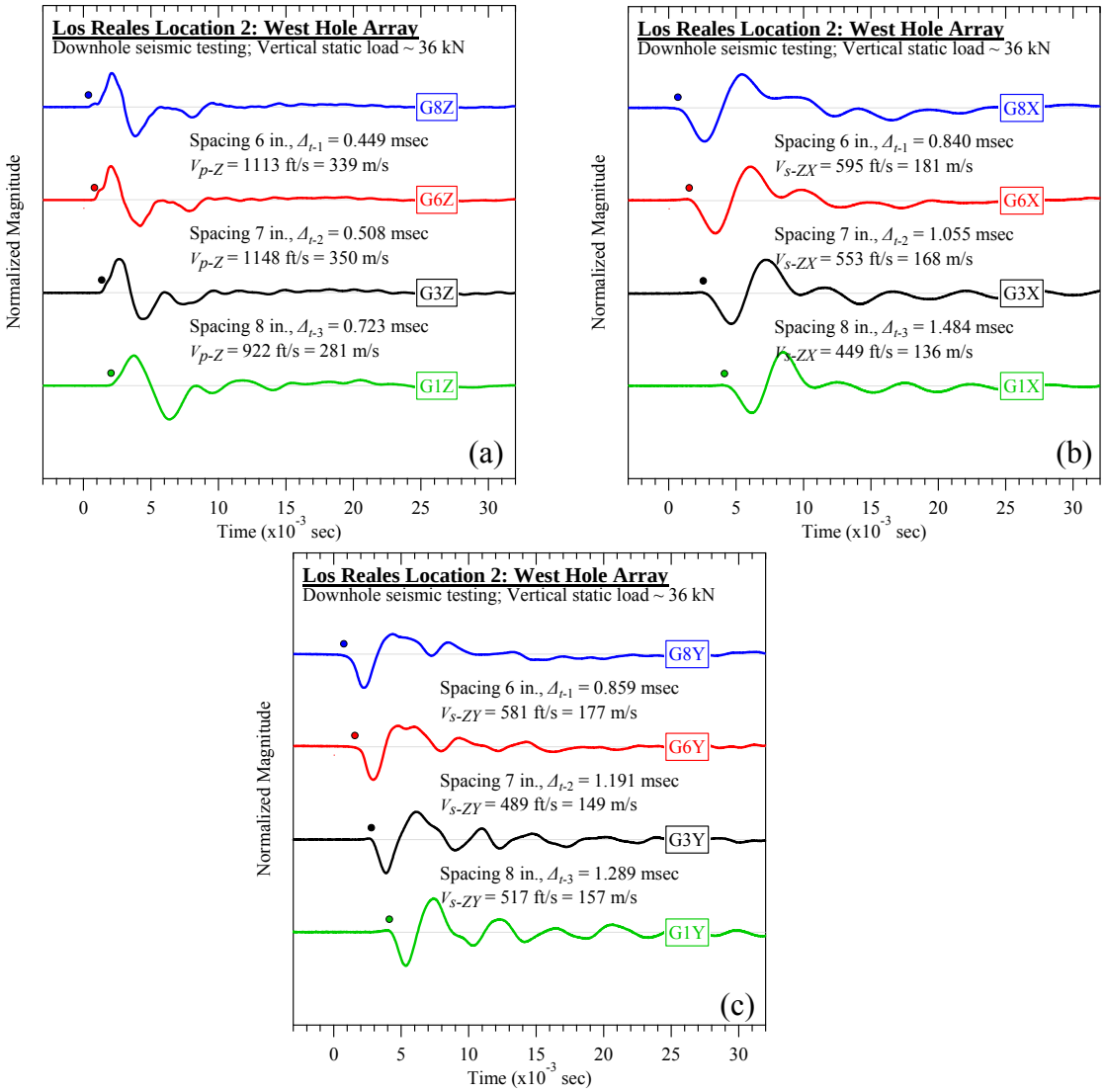

Figure C-57. Los Reales Landfill #2 (west hole): Downhole seismic testing at vertical load of 36 kN: (a) $V_{p\text{-}Z}$, (b) $V_{s\text{-}ZX}$, and (c) $V_{s\text{-}ZY}$.

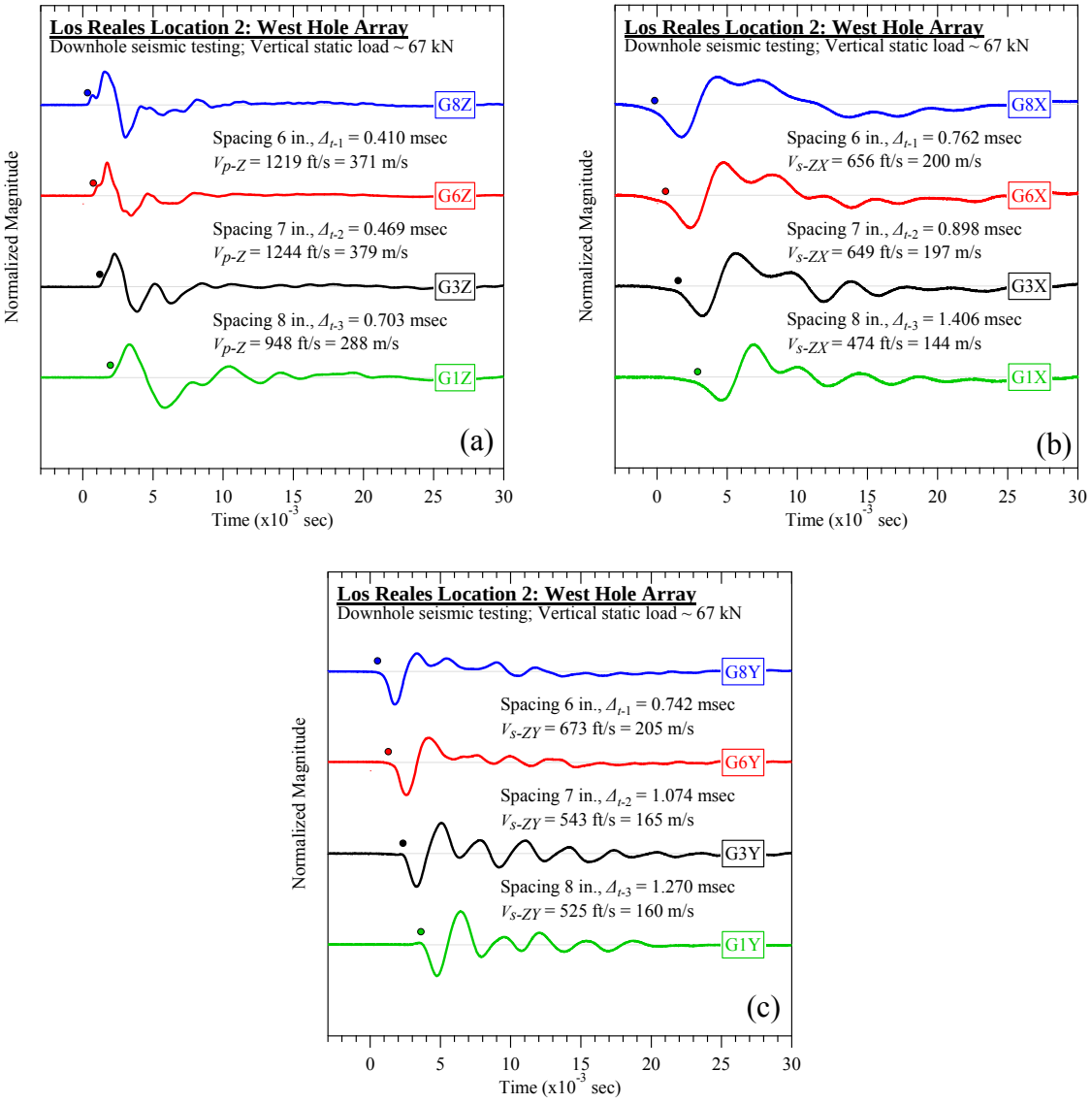

Figure C-58. Los Reales Landfill #2 (west hole): Downhole seismic testing at vertical load of 67 kN: (a) V_{p-Z}, (b) V_{s-ZX}, and (c) V_{s-ZY}.

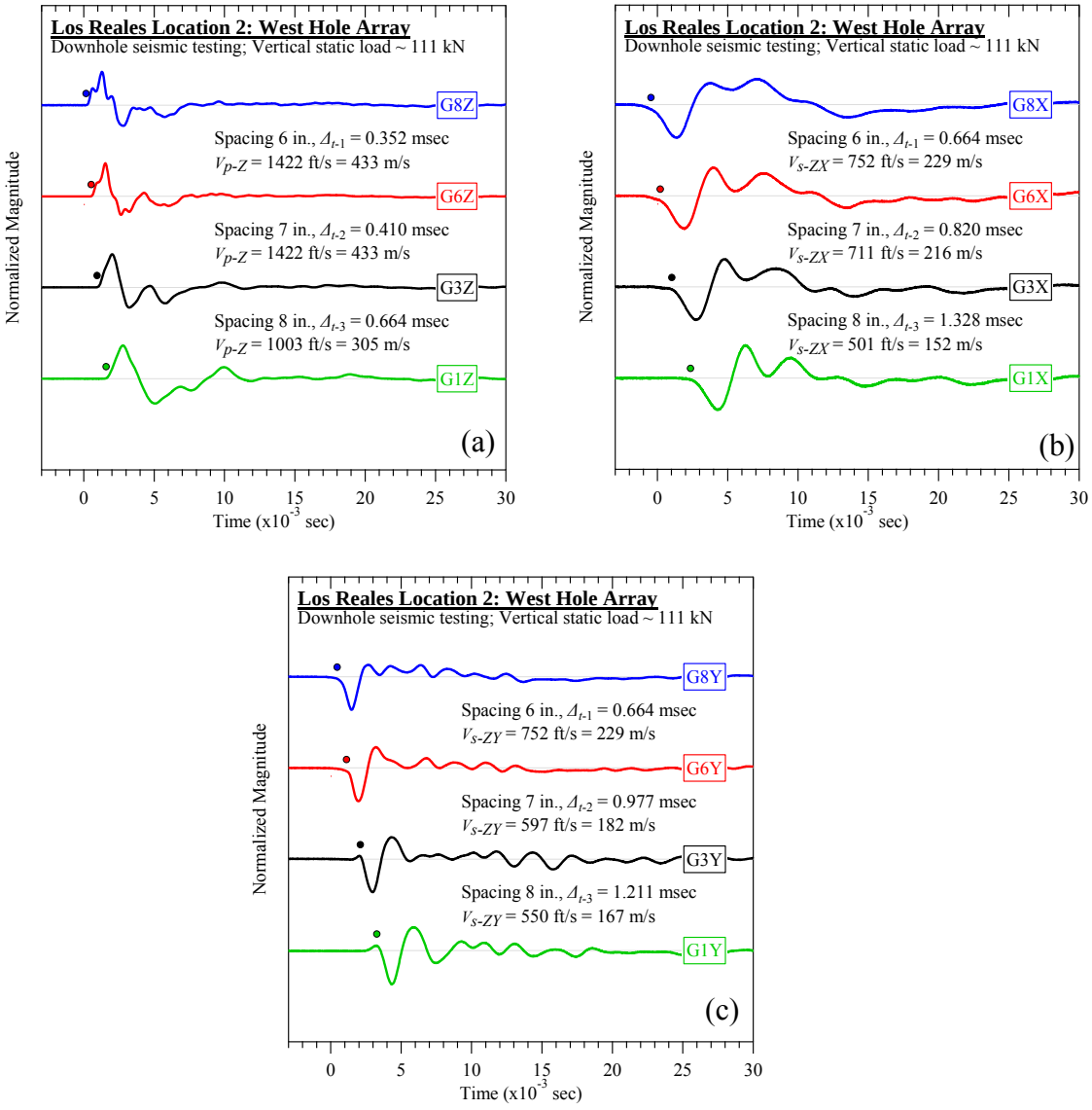

Figure C-59. Los Reales Landfill #2 (west hole): Downhole seismic testing at vertical load of 111 kN: (a) V_{p-Z}, (b) V_{s-ZX}, and (c) V_{s-ZY}.

C.2.2 Crosshole Seismic Testing

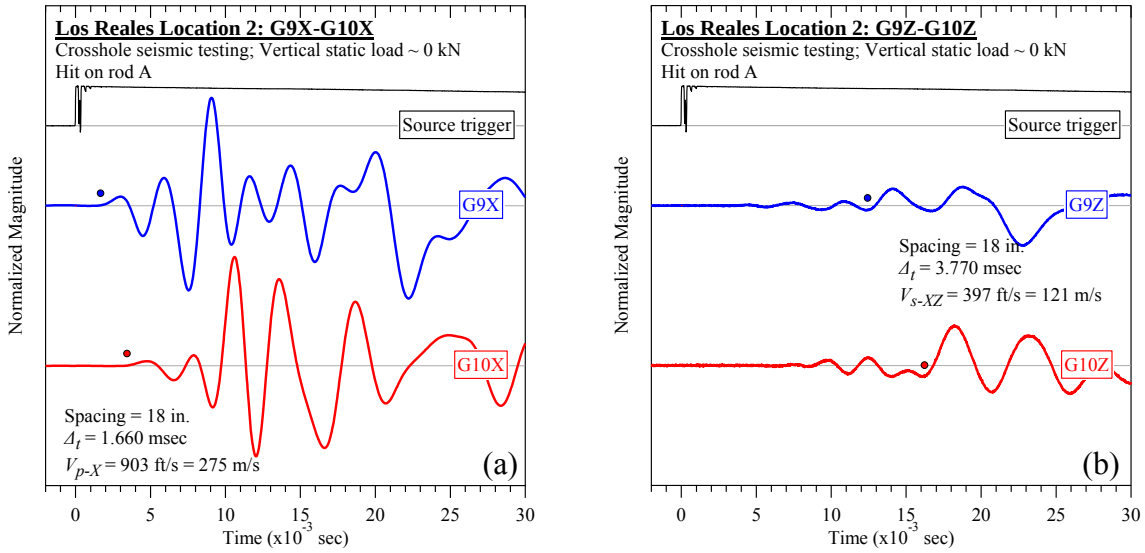

Figure C-60. Los Reales Landfill #2 (rod A): Crosshole seismic testing at vertical load of 0 kN: (a) $V_{p\text{-}X}$ and (b) $V_{s\text{-}XZ}$.

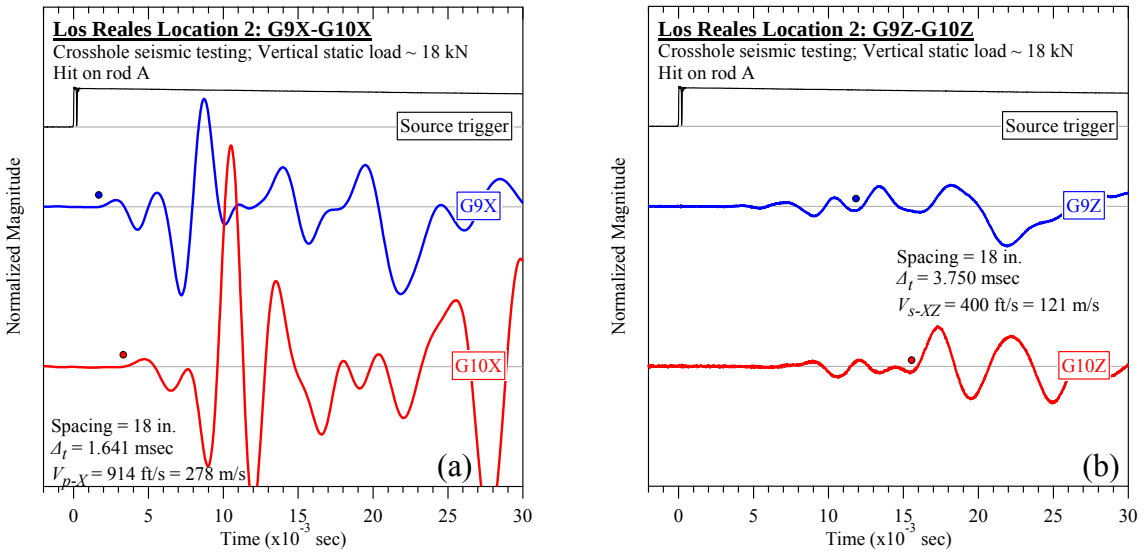

Figure C-61. Los Reales Landfill #2 (rod A): Crosshole seismic testing at vertical load of 18 kN: (a) $V_{p\text{-}X}$ and (b) $V_{s\text{-}XZ}$.

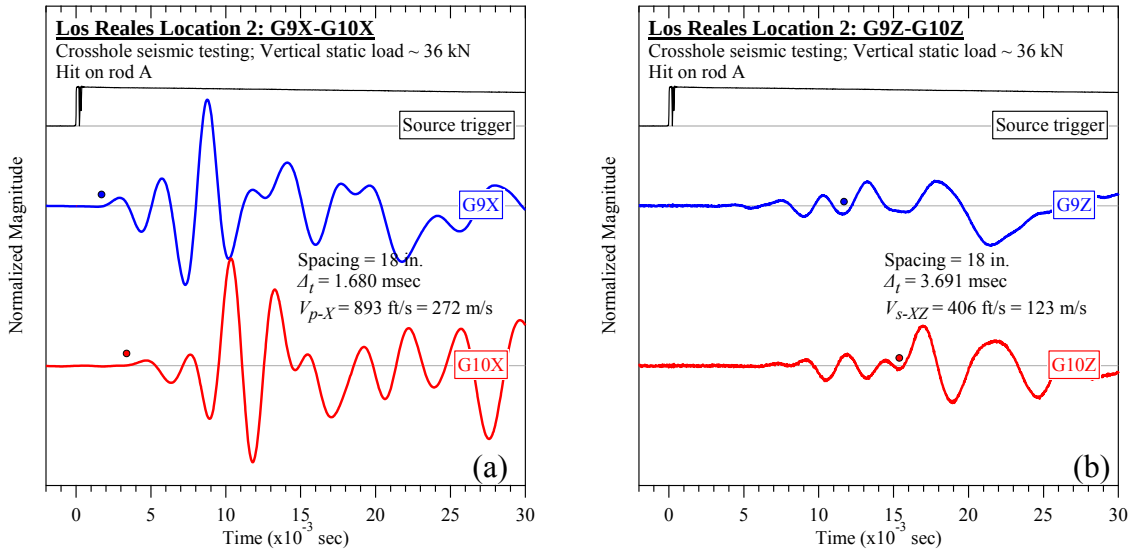

Figure C-62. Los Reales Landfill #2 (rod A): Crosshole seismic testing at vertical load of 36 kN: (a) $V_{p\text{-}X}$ and (b) $V_{s\text{-}XZ}$.

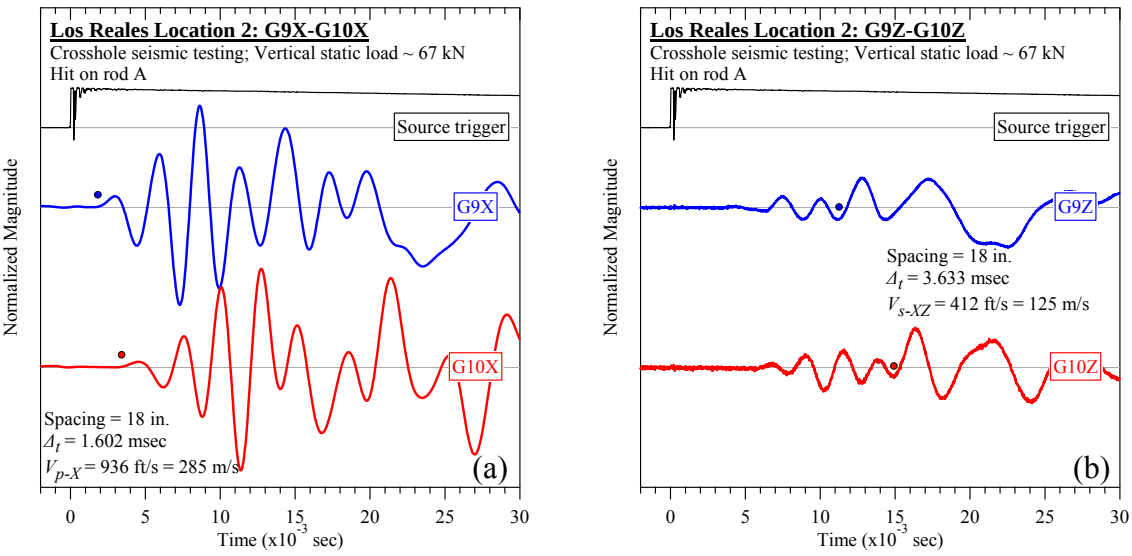

Figure C-63. Los Reales Landfill #2 (rod A): Crosshole seismic testing at vertical load of 67 kN: (a) $V_{p\text{-}X}$ and (b) $V_{s\text{-}XZ}$.

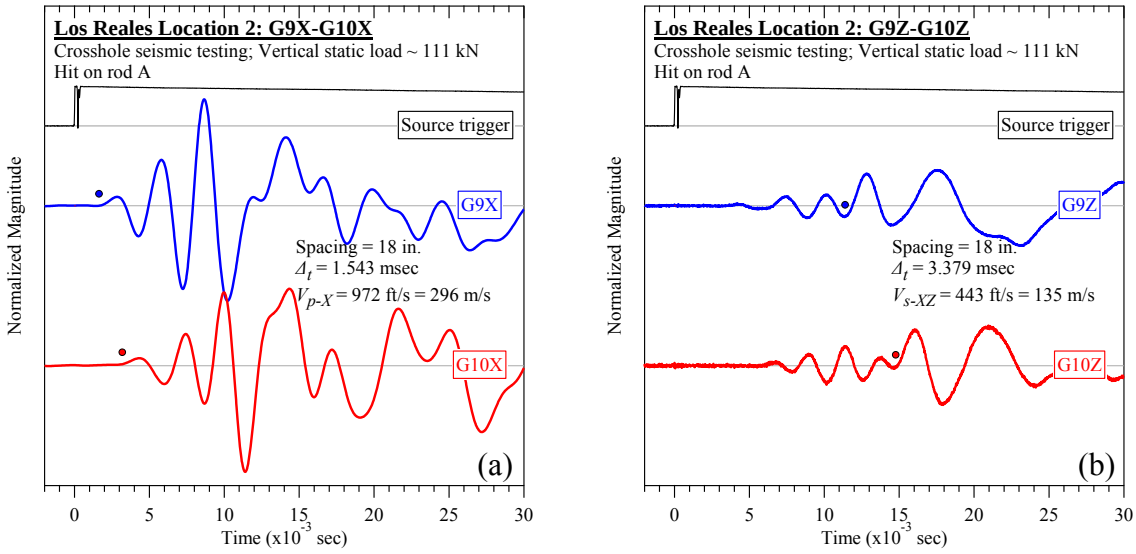

Figure C-64. Los Reales Landfill #2 (rod A): Crosshole seismic testing at vertical load of 111 kN: (a) $V_{p\text{-}X}$ and (b) $V_{s\text{-}XZ}$.

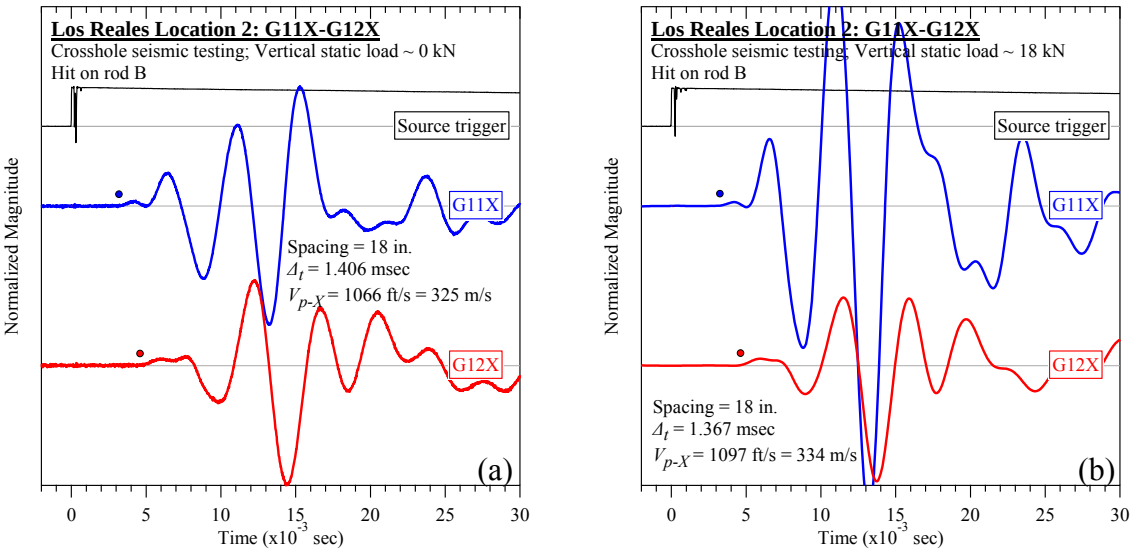

Figure C-65. Los Reales Landfill #2 (rod B): Crosshole seismic testing at vertical loads of (a) 0 kN and (b) 18 kN: $V_{p\text{-}X}$.

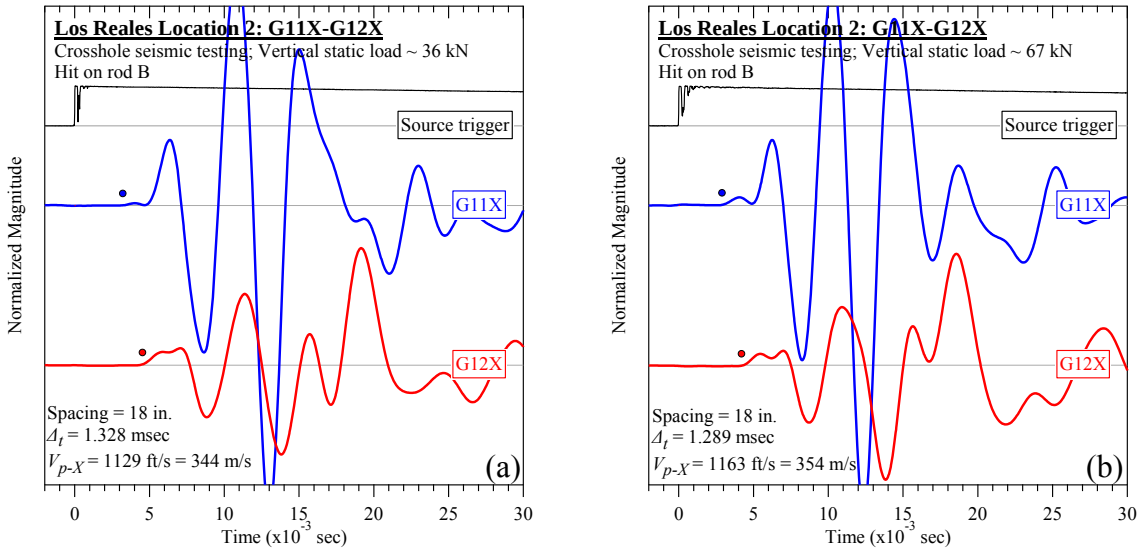

Figure C-66. Los Reales Landfill #2 (rod B): Crosshole seismic testing at vertical loads of (a) 36 kN and (b) 67 kN: $V_{p\text{-}X}$.

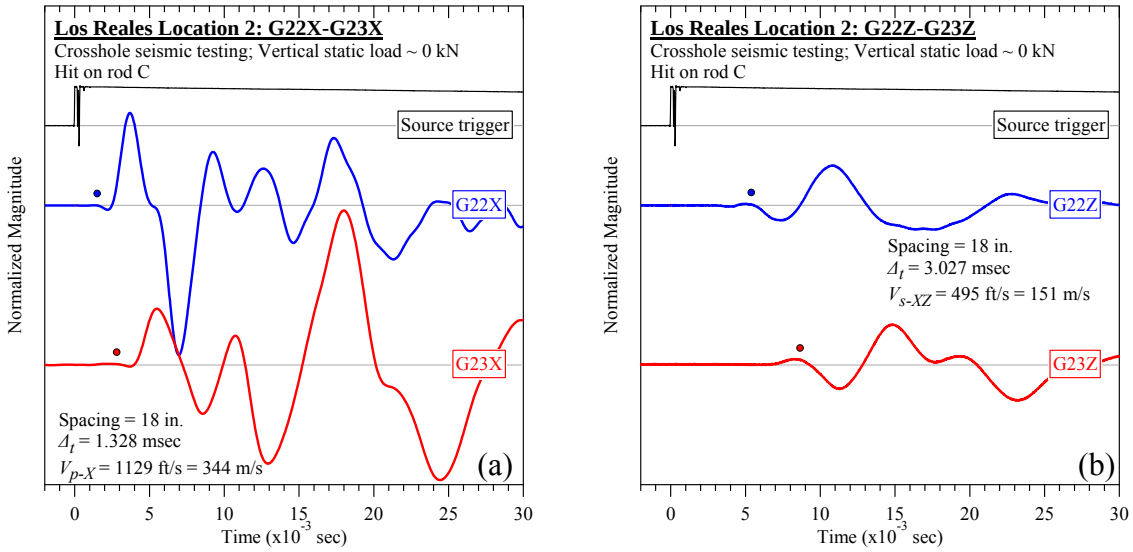

Figure C-67. Los Reales Landfill #2 (rod C): Crosshole seismic testing at vertical load of 0 kN: (a) $V_{p\text{-}X}$ and (b) $V_{s\text{-}XZ}$.

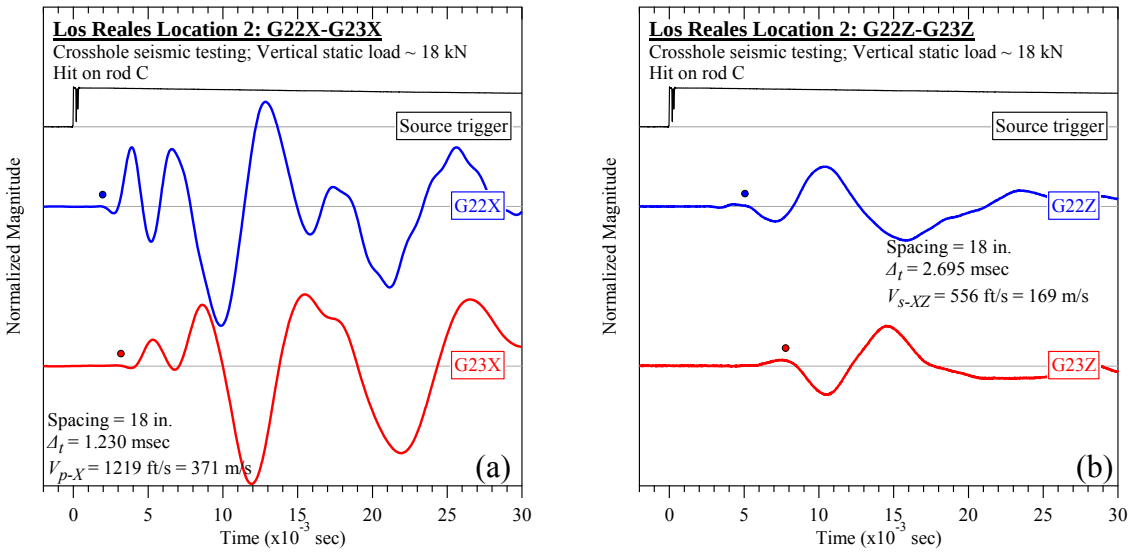

Figure C-68. Los Reales Landfill #2 (rod C): Crosshole seismic testing at vertical load of 18 kN: (a) $V_{p\text{-}X}$ and (b) $V_{s\text{-}XZ}$.

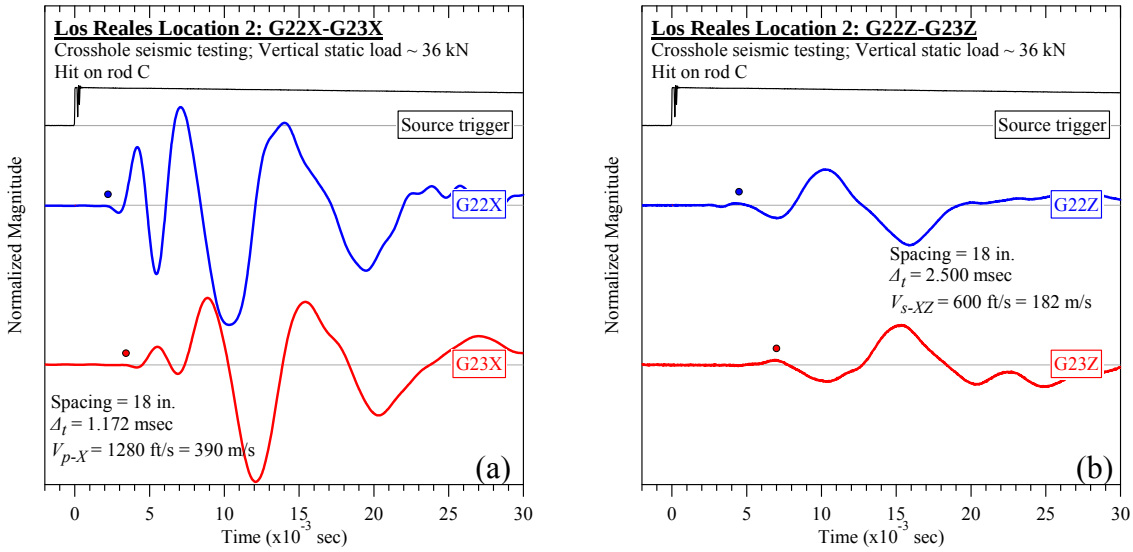

Figure C-69. Los Reales Landfill #2 (rod C): Crosshole seismic testing at vertical load of 36 kN: (a) $V_{p\text{-}X}$ and (b) $V_{s\text{-}XZ}$.

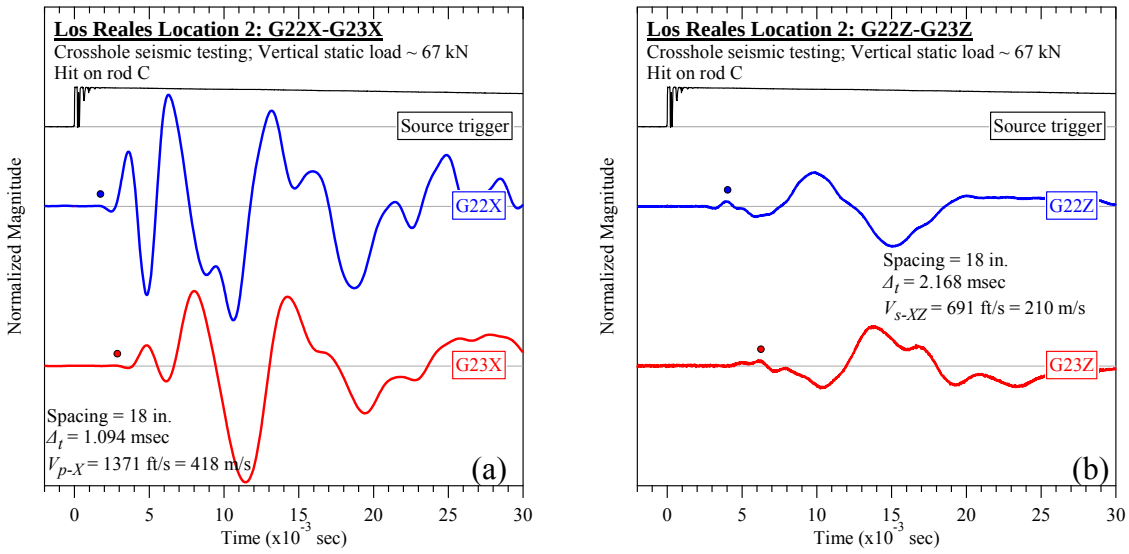

Figure C-70. Los Reales Landfill #2 (rod C): Crosshole seismic testing at vertical load of 67 kN: (a) $V_{p\text{-}X}$ and (b) $V_{s\text{-}XZ}$.

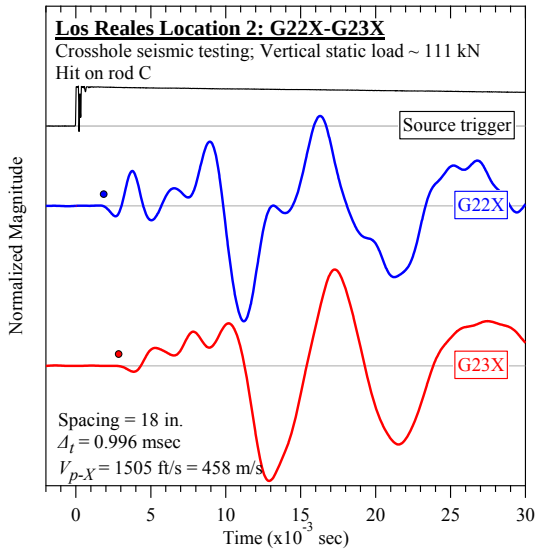

Figure C-71. Los Reales Landfill #2 (rod C): Crosshole seismic testing at vertical load of 111 kN: $V_{p\text{-}X}$.

C.2.3 Steady-state Dynamic Testing

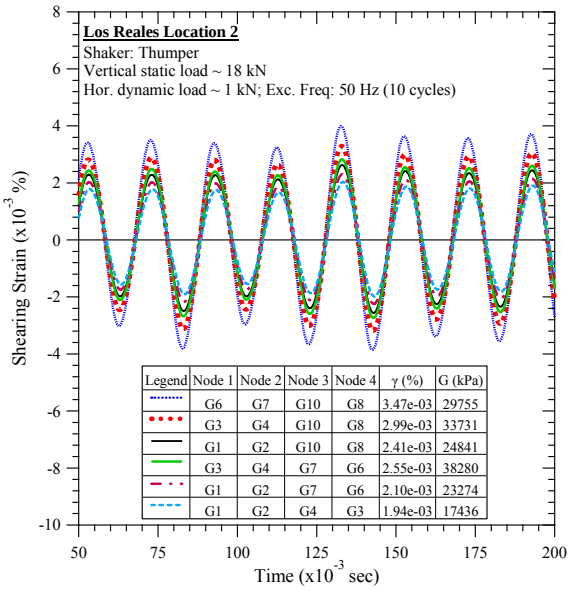

Figure C-72. Los Reales Landfill #2: Steady-state dynamic testing at vertical load of 18 kN and horizontal dynamic load of 1 kN.

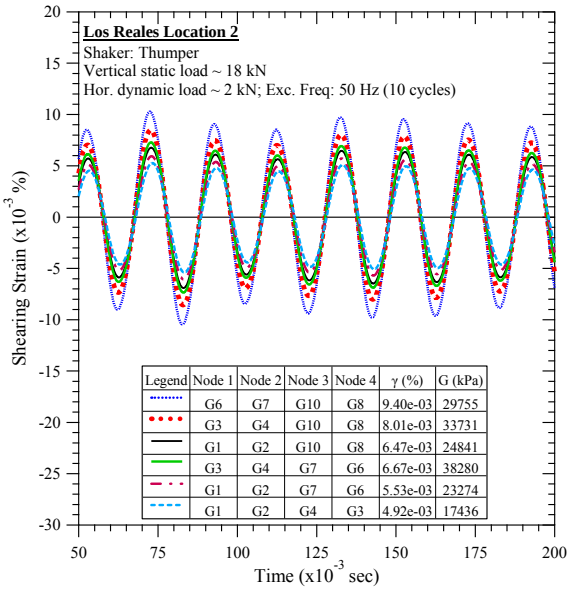

Figure C-73. Los Reales Landfill #2: Steady-state dynamic testing at vertical load of 18 kN and horizontal dynamic load of 2 kN.

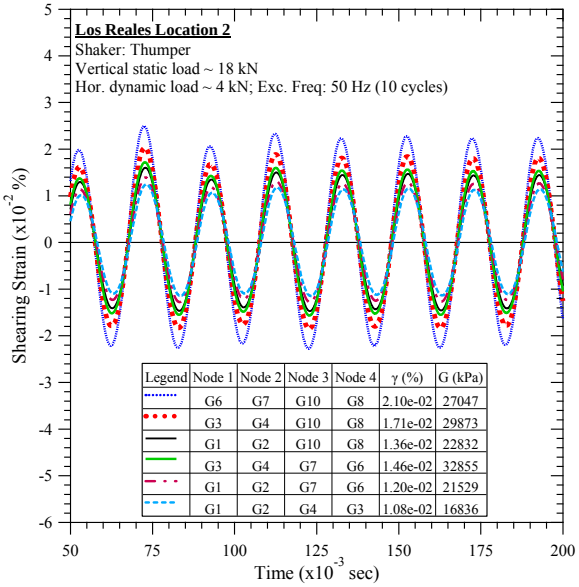

Figure C-74. Los Reales Landfill #2: Steady-state dynamic testing at vertical load of 18 kN and horizontal dynamic load of 4 kN.

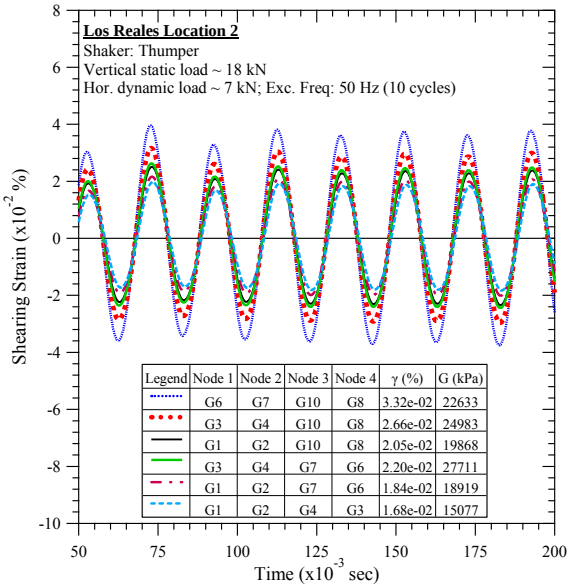

Figure C-75. Los Reales Landfill #2: Steady-state dynamic testing at vertical load of 18 kN and horizontal dynamic load of 7 kN.

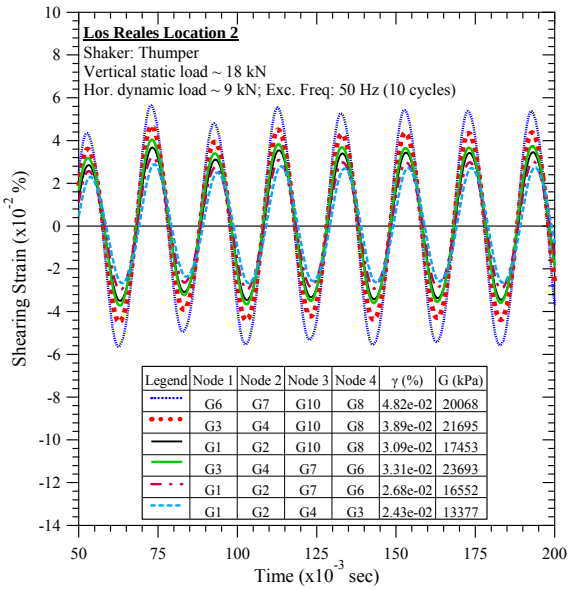

Figure C-76. Los Reales Landfill #2: Steady-state dynamic testing at vertical load of 18 kN and horizontal dynamic load of 9 kN.

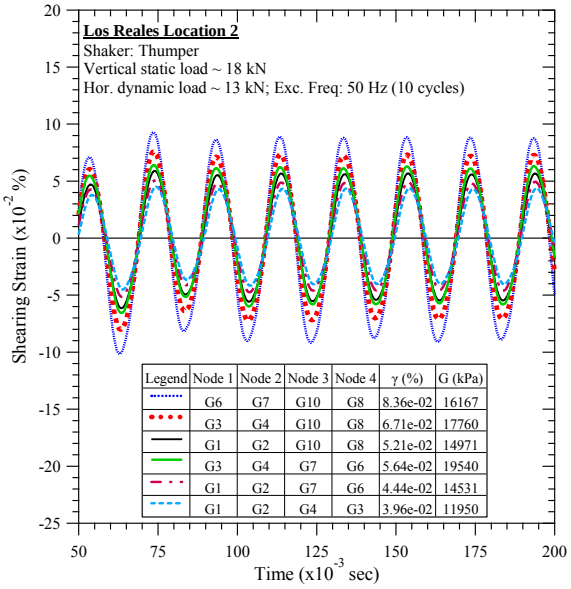

Figure C-77. Los Reales Landfill #2: Steady-state dynamic testing at vertical load of 18 kN and horizontal dynamic load of 13 kN.

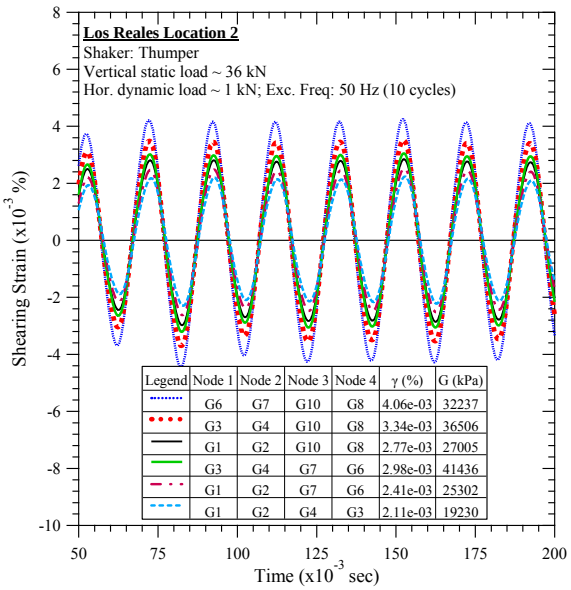

Figure C-78. Los Reales Landfill #2: Steady-state dynamic testing at vertical load of 36 kN and horizontal dynamic load of 1 kN.

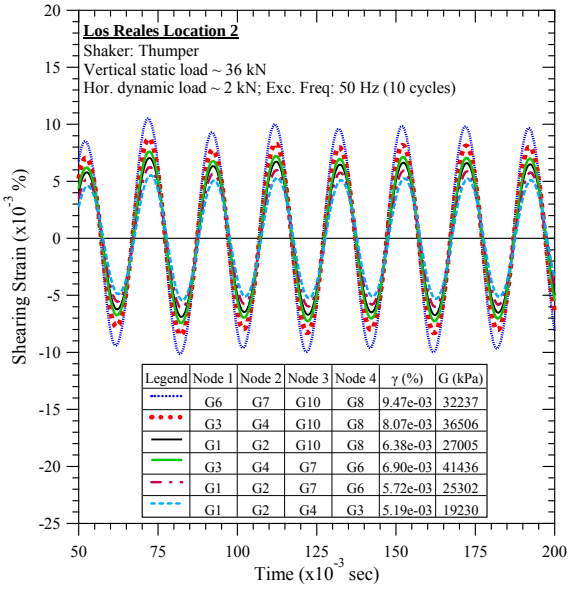

Figure C-79. Los Reales Landfill #2: Steady-state dynamic testing at vertical load of 36 kN and horizontal dynamic load of 2 kN.

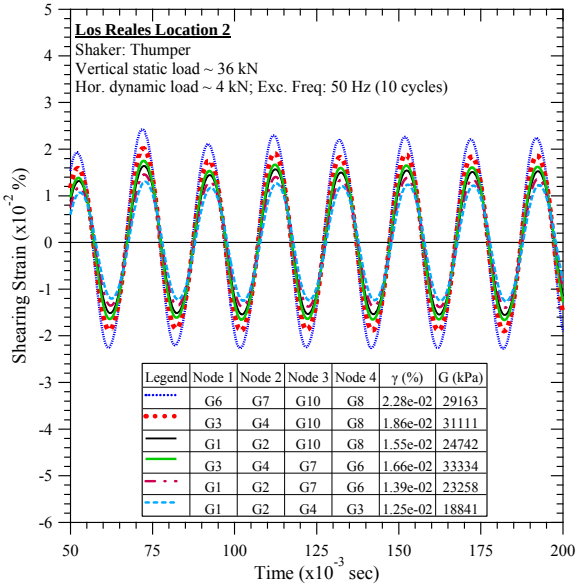

Figure C-80. Los Reales Landfill #2: Steady-state dynamic testing at vertical load of 36 kN and horizontal dynamic load of 4 kN.

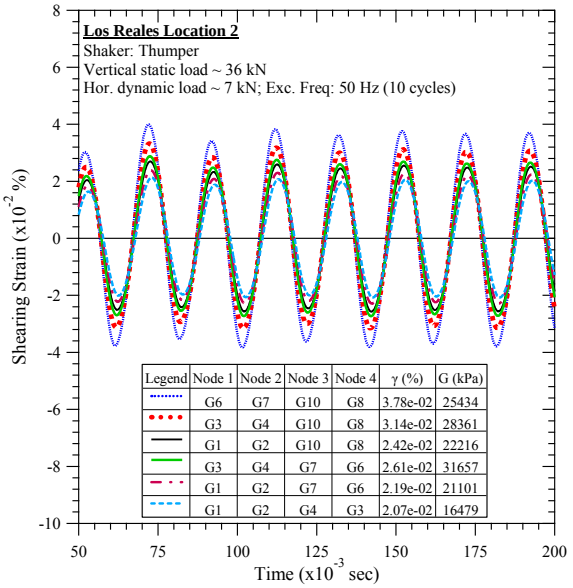

Figure C-81. Los Reales Landfill #2: Steady-state dynamic testing at vertical load of 36 kN and horizontal dynamic load of 7 kN.

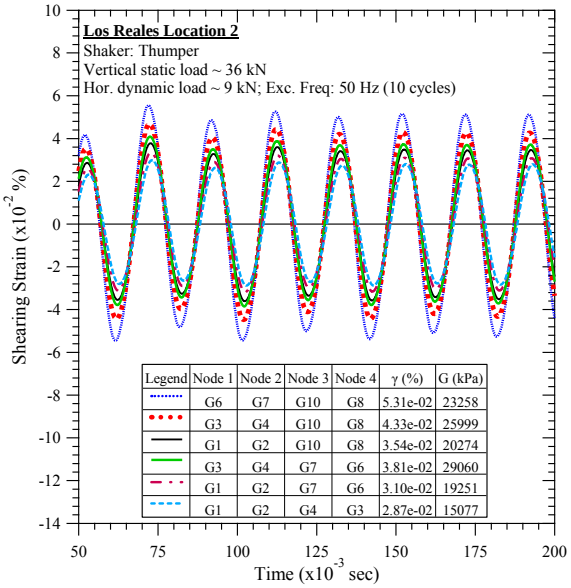

Figure C-82. Los Reales Landfill #2: Steady-state dynamic testing at vertical load of 36 kN and horizontal dynamic load of 9 kN.

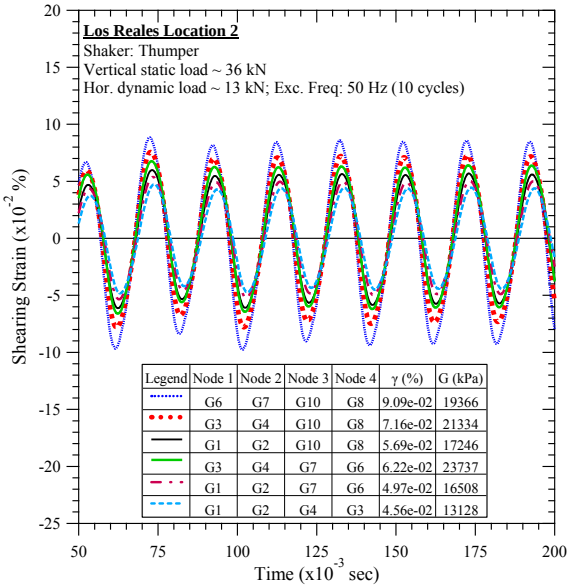

Figure C-83. Los Reales Landfill #2: Steady-state dynamic testing at vertical load of 36 kN and horizontal dynamic load of 13 kN.

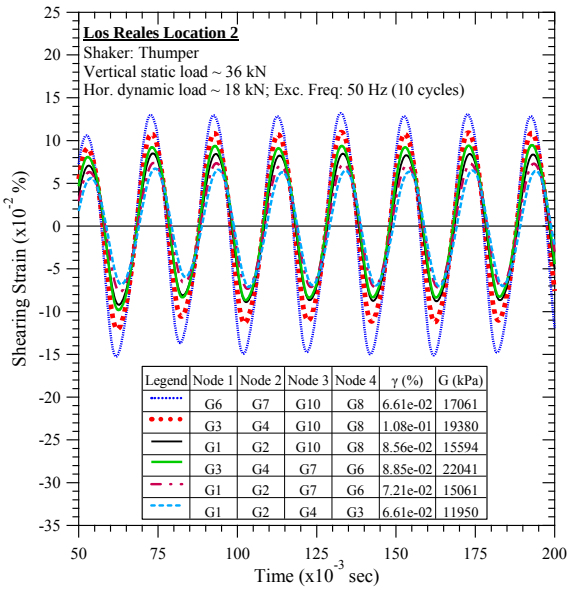

Figure C-84. Los Reales Landfill #2: Steady-state dynamic testing at vertical load of 36 kN and horizontal dynamic load of 18 kN.

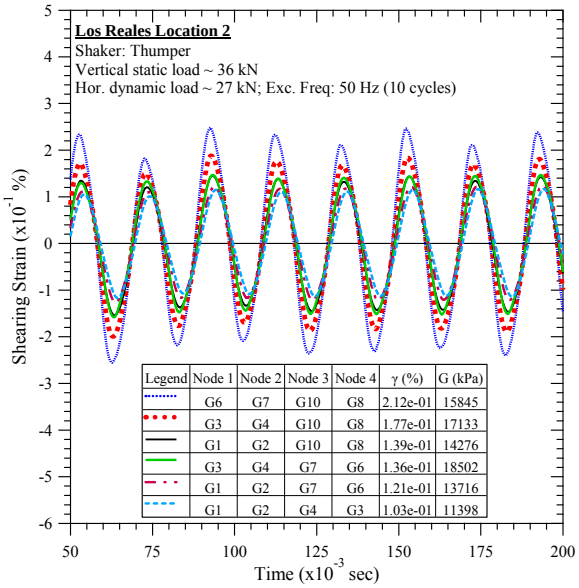

Figure C-85. Los Reales Landfill #2: Steady-state dynamic testing at vertical load of 36 kN and horizontal dynamic load of 27 kN.

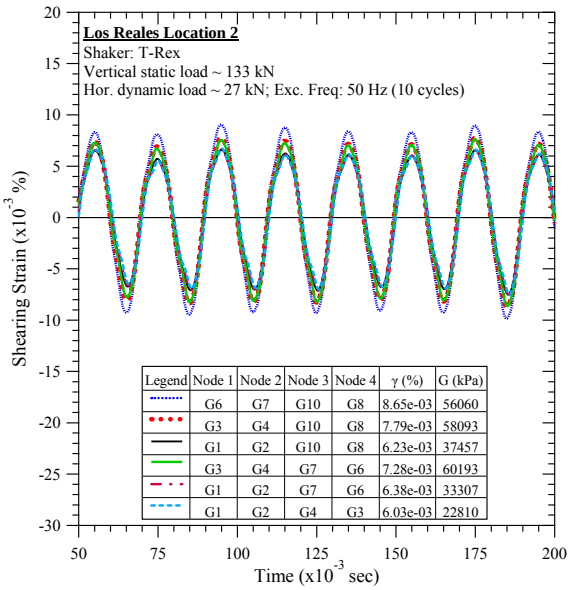

Figure C-86. Los Reales Landfill #2: Steady-state dynamic testing at vertical load of 133 kN and horizontal dynamic load of 27 kN.

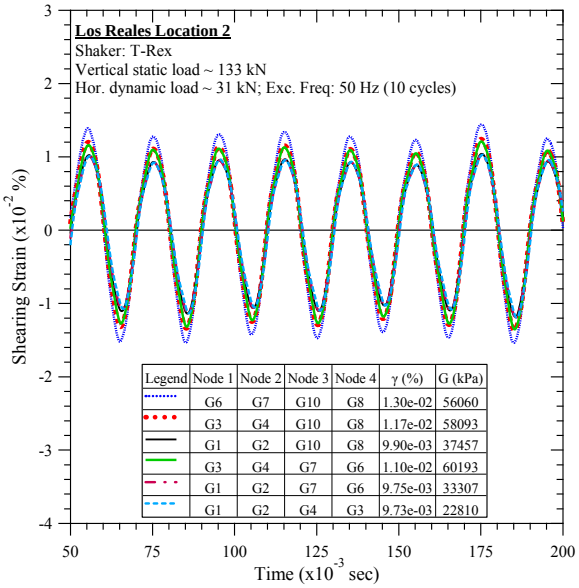

Figure C-87. Los Reales Landfill #2: Steady-state dynamic testing at vertical load of 133 kN and horizontal dynamic load of 31 kN.

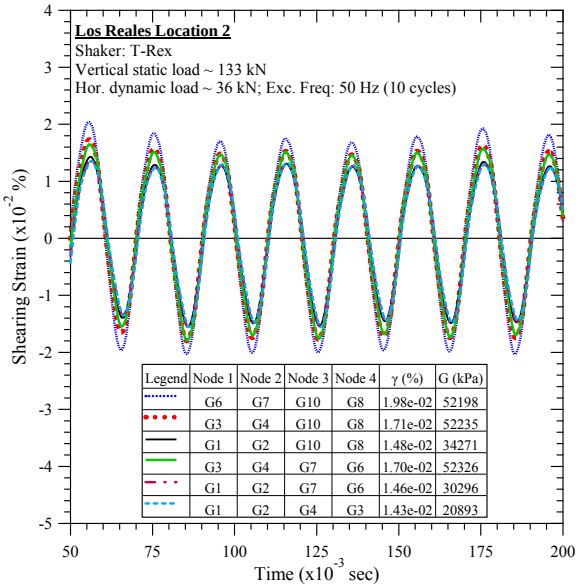

Figure C-88. Los Reales Landfill #2: Steady-state dynamic testing at vertical load of 133 kN and horizontal dynamic load of 36 kN.

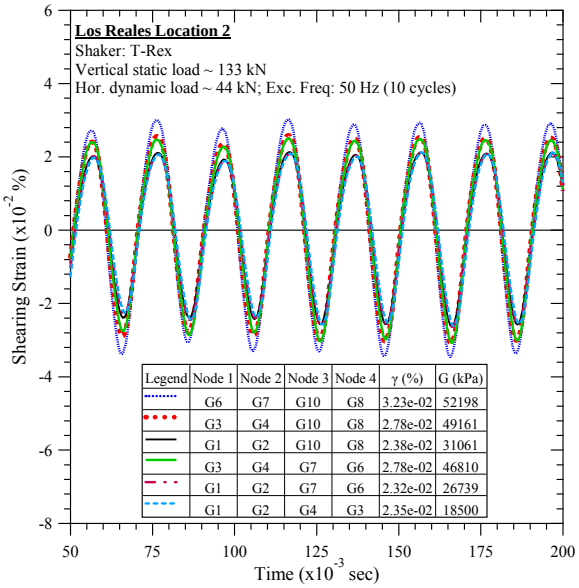

Figure C-89. Los Reales Landfill #2: Steady-state dynamic testing at vertical load of 133 kN and horizontal dynamic load of 44 kN.

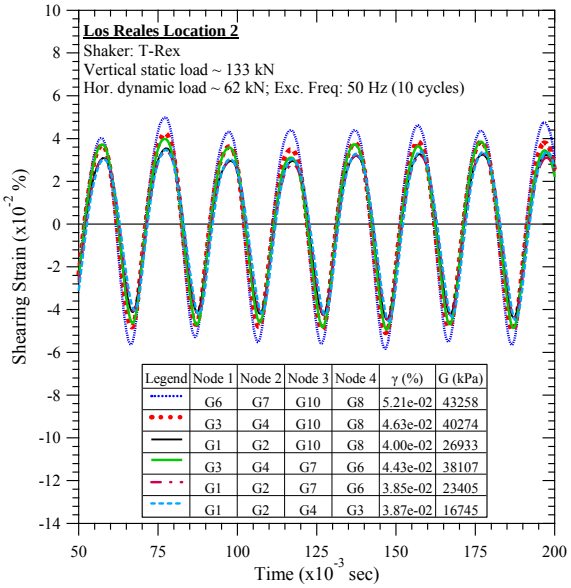

Figure C-90. Los Reales Landfill #2: Steady-state dynamic testing at vertical load of 133 kN and horizontal dynamic load of 62 kN.

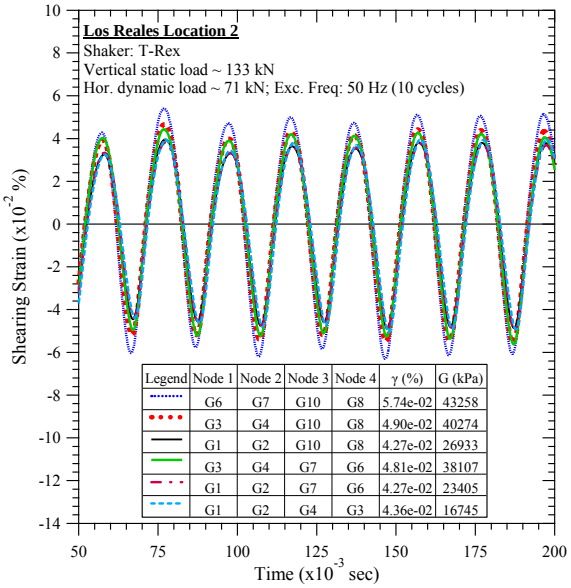

Figure C-91. Los Reales Landfill #2: Steady-state dynamic testing at vertical load of 133 kN and horizontal dynamic load of 71 kN.

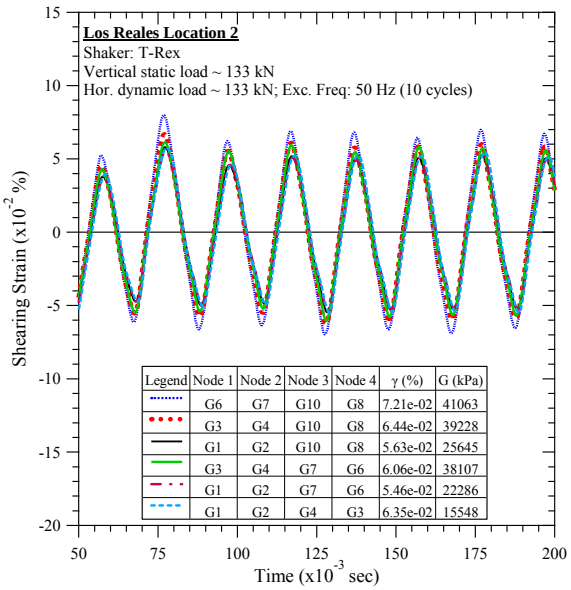

Figure C-92. Los Reales Landfill #2: Steady-state dynamic testing at vertical load of 133 kN and horizontal dynamic load of 133 kN.

C.3 Los Reales Landfill Location 3

C.3.1 Downhole Seismic Testing

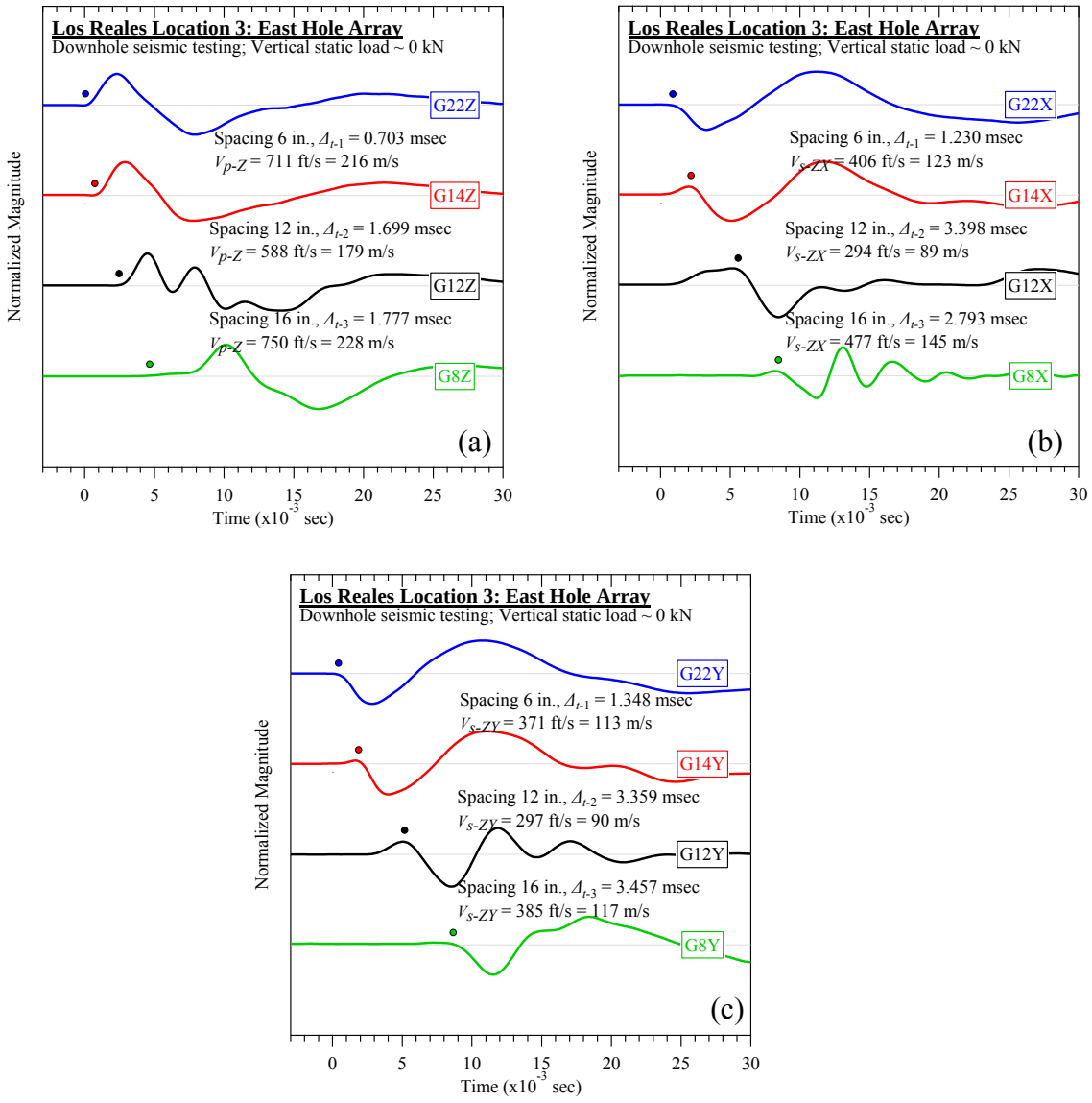

Figure C-93. Los Reales Landfill #3 (east hole): Downhole seismic testing at vertical load of 0 kN: (a) $V_{p\text{-}Z}$, (b) $V_{s\text{-}ZX}$, and (c) $V_{s\text{-}ZY}$.

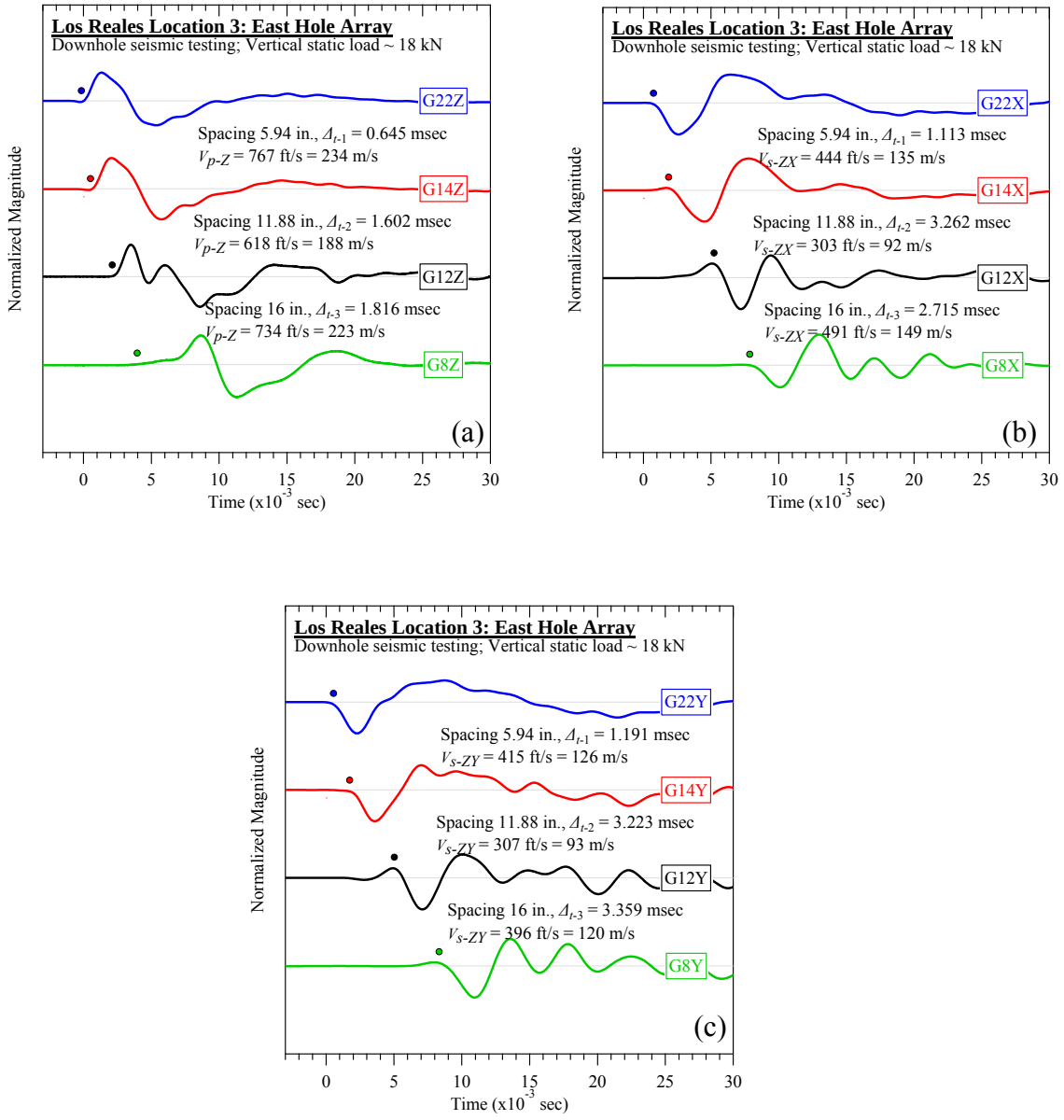

Figure C-94. Los Reales Landfill #3 (east hole): Downhole seismic testing at vertical load of 18 kN: (a) V_{p-Z}, (b) V_{s-ZX}, and (c) V_{s-ZY}.

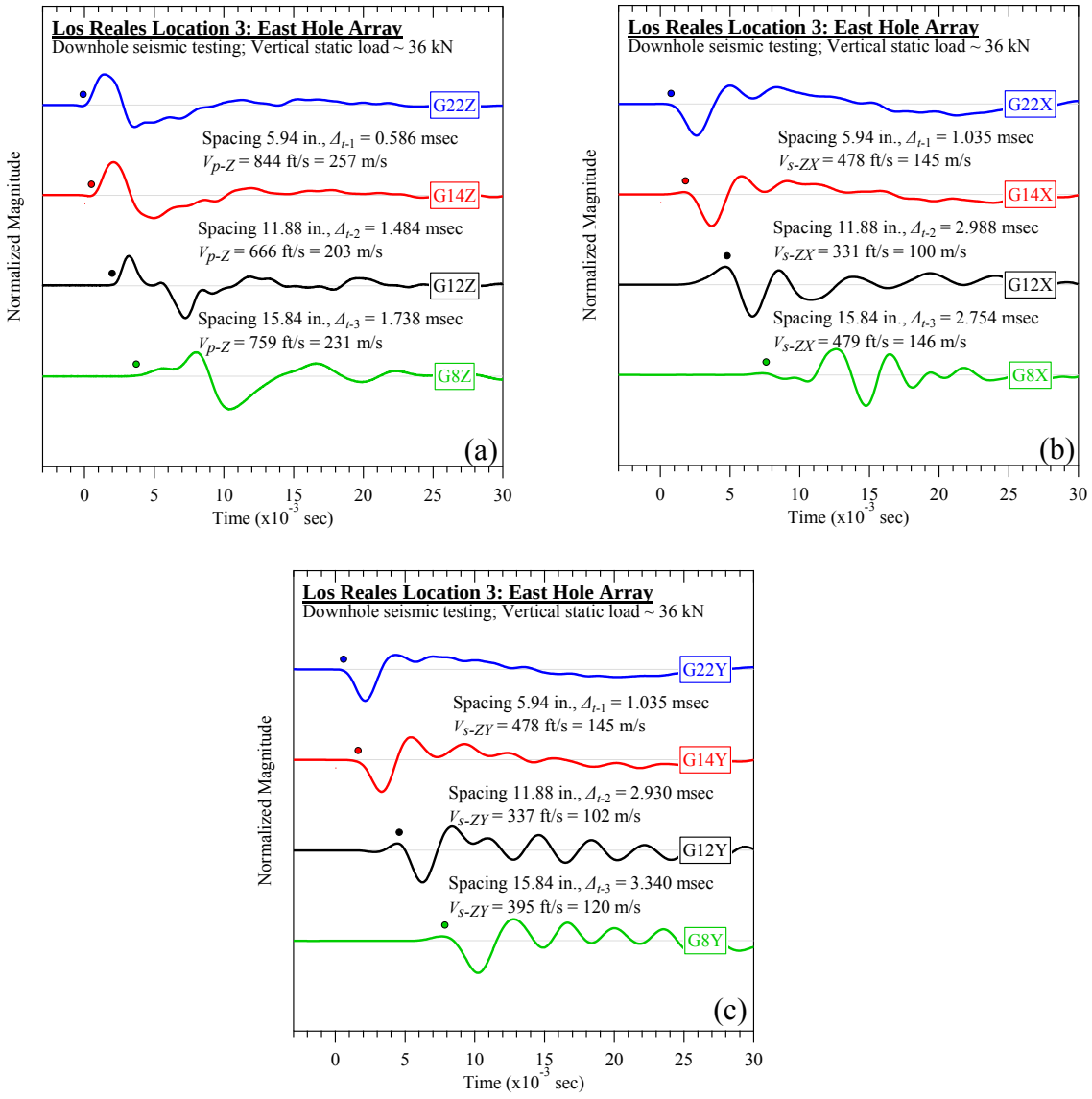

Figure C-95. Los Reales Landfill #3 (east hole): Downhole seismic testing at vertical load of 36 kN: (a) V_{p-Z}, (b) V_{s-ZX}, and (c) V_{s-ZY}.

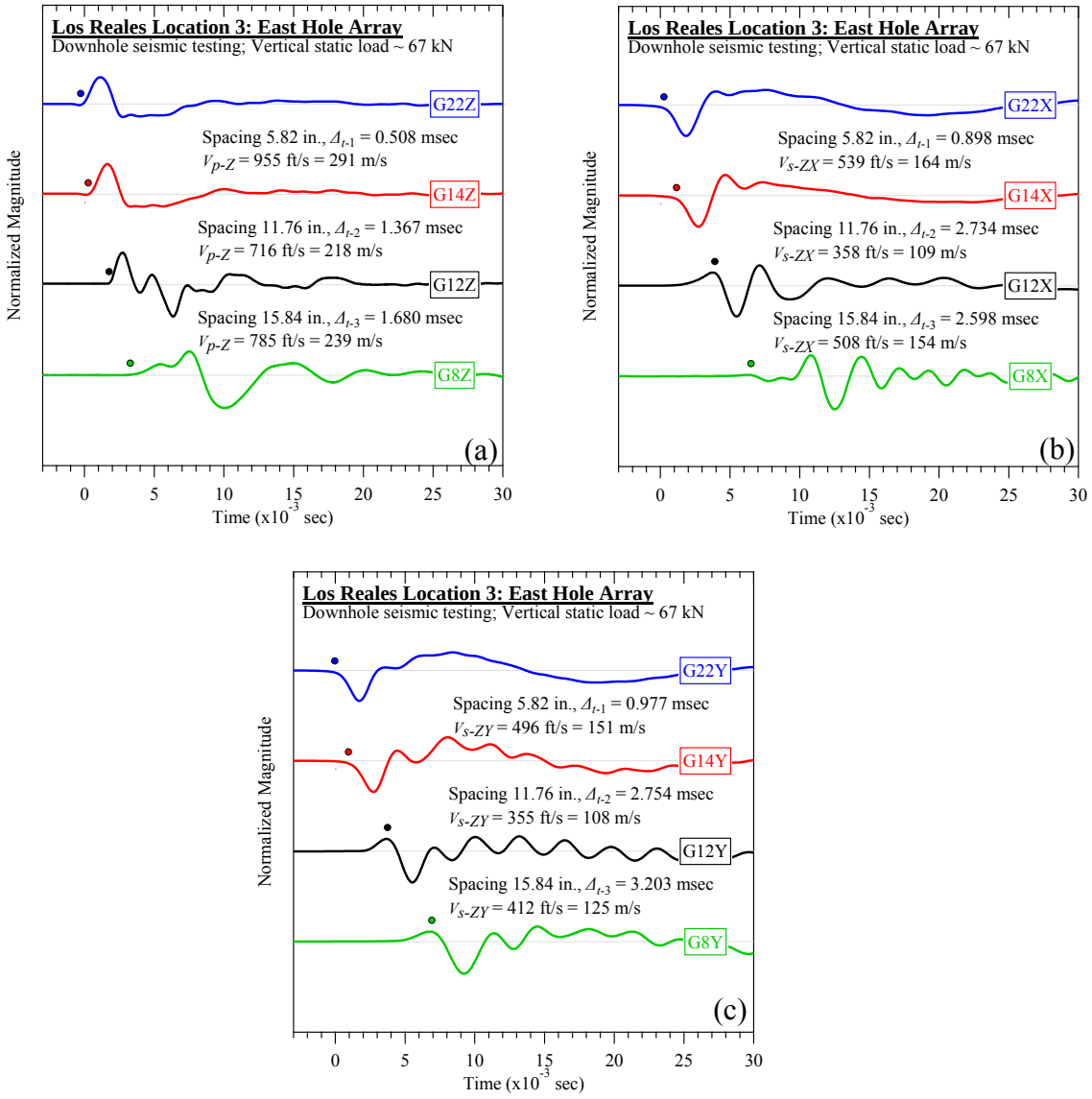

Figure C-96. Los Reales Landfill #3 (east hole): Downhole seismic testing at vertical load of 67 kN: (a) V_{p-Z}, (b) V_{s-ZX}, and (c) V_{s-ZY}.

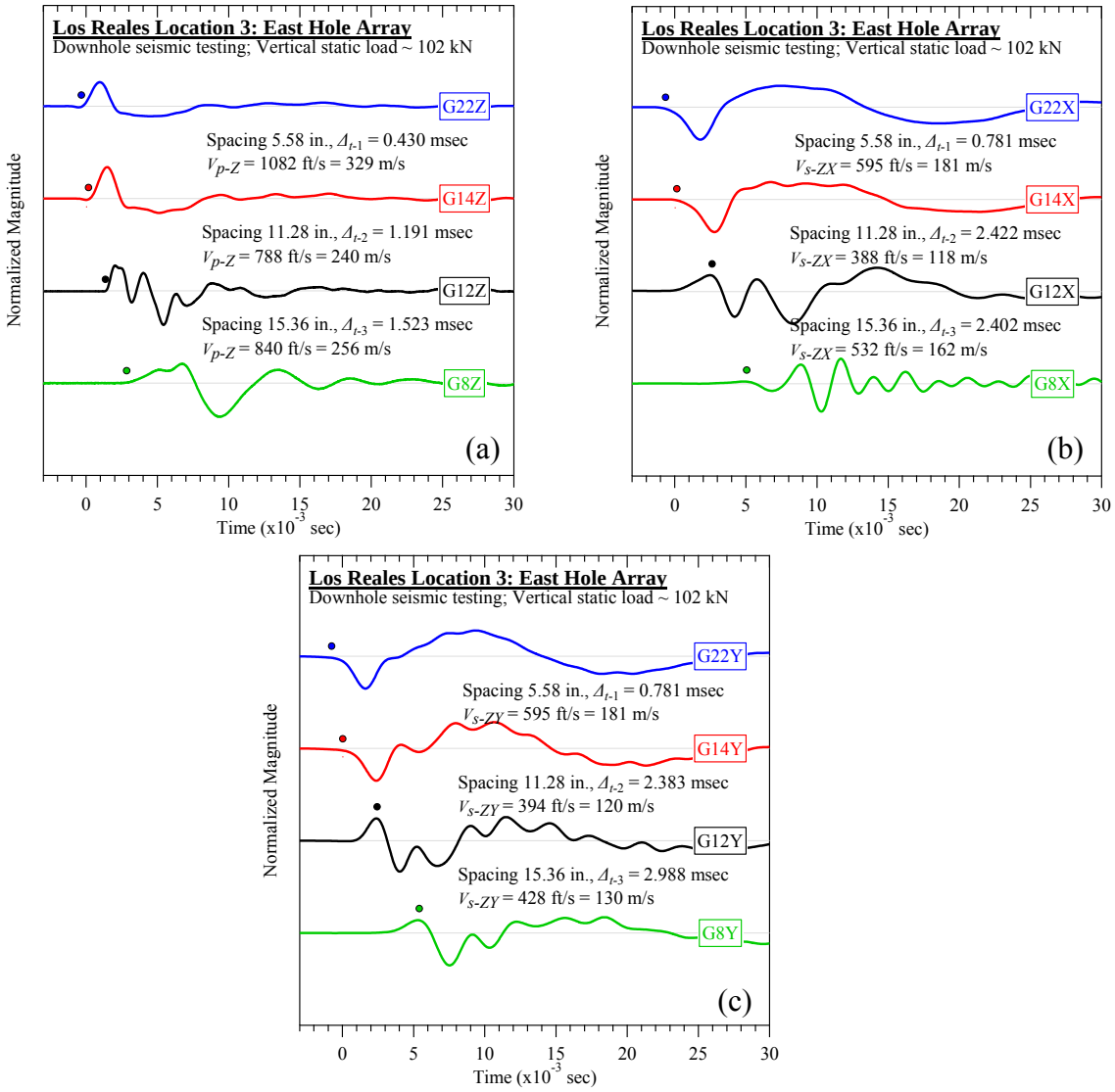

Figure C-97. Los Reales Landfill #3 (east hole): Downhole seismic testing at vertical load of 102 kN: (a) $V_{p\text{-}Z}$, (b) $V_{s\text{-}ZX}$, and (c) $V_{s\text{-}ZY}$.

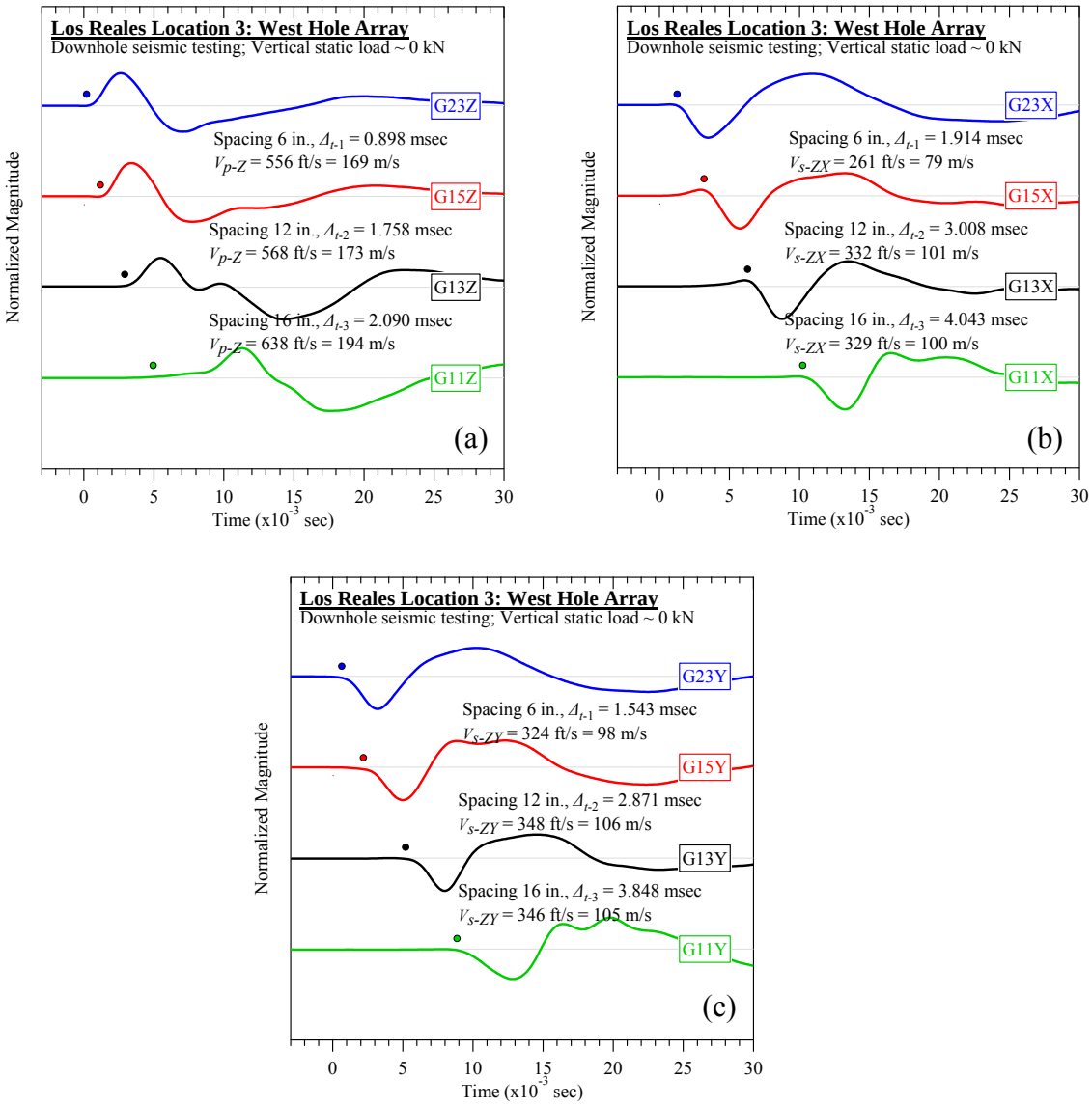

Figure C-98. Los Reales Landfill #3 (west hole): Downhole seismic testing at vertical load of 0 kN: (a) V_{p-Z}, (b) V_{s-ZX}, and (c) V_{s-ZY}.

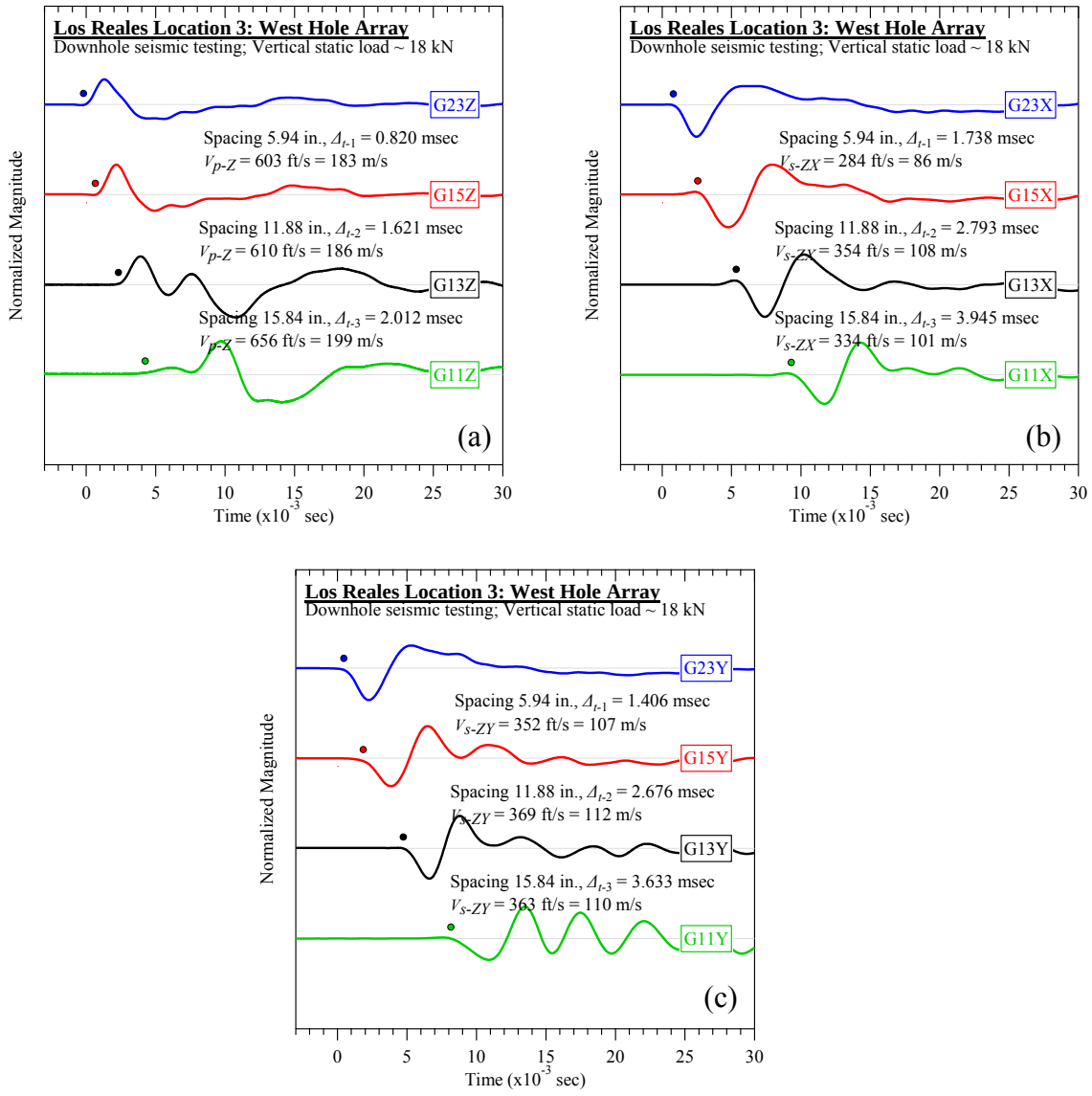

Figure C-99. Los Reales Landfill #3 (west hole): Downhole seismic testing at vertical load of 18 kN: (a) V_{p-Z}, (b) V_{s-ZX}, and (c) V_{s-ZY}.

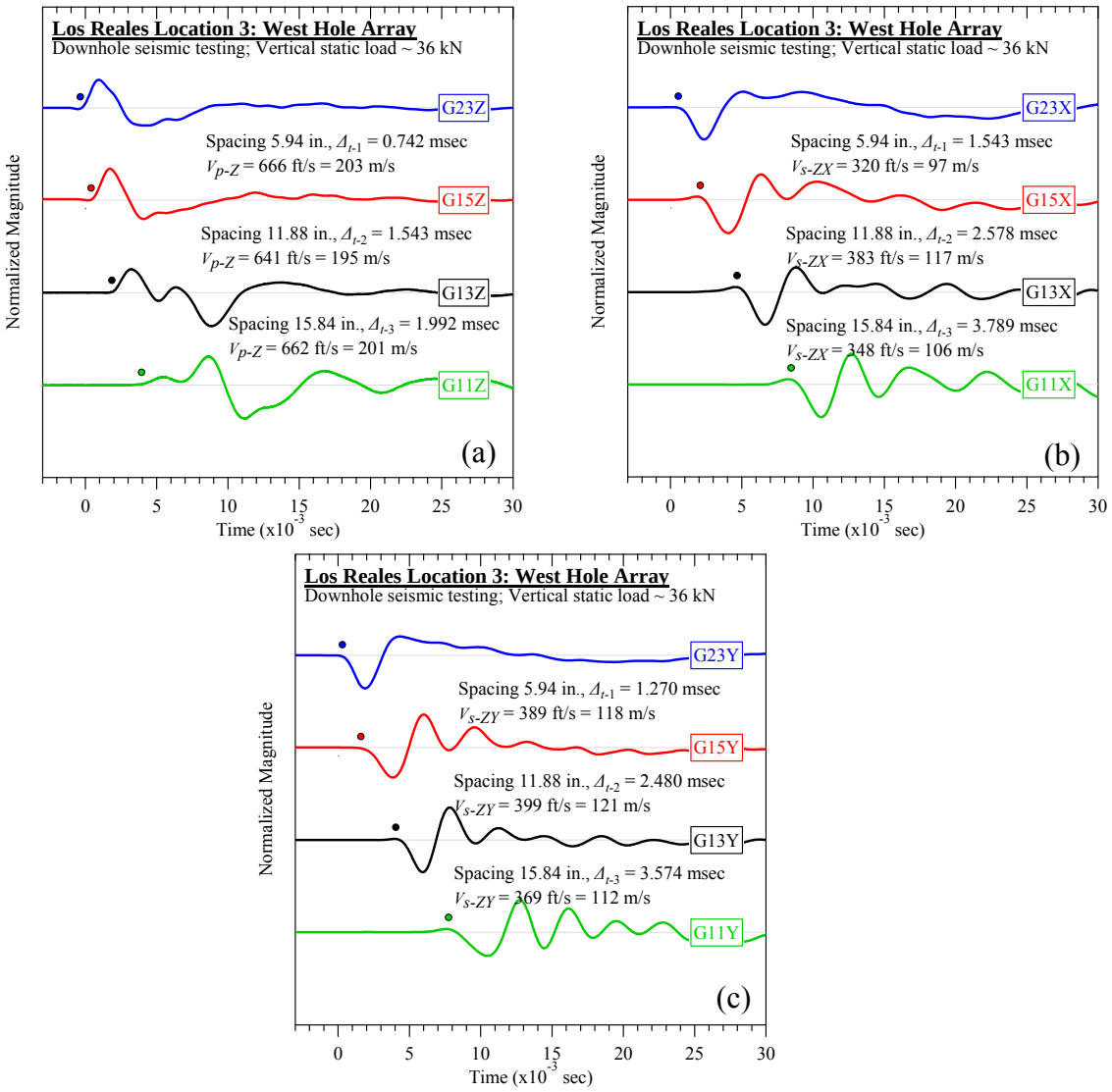

Figure C-100. Los Reales Landfill #3 (west hole): Downhole seismic testing at vertical load of 36 kN: (a) $V_{p\text{-}Z}$, (b) $V_{s\text{-}ZX}$, and (c) $V_{s\text{-}ZY}$.

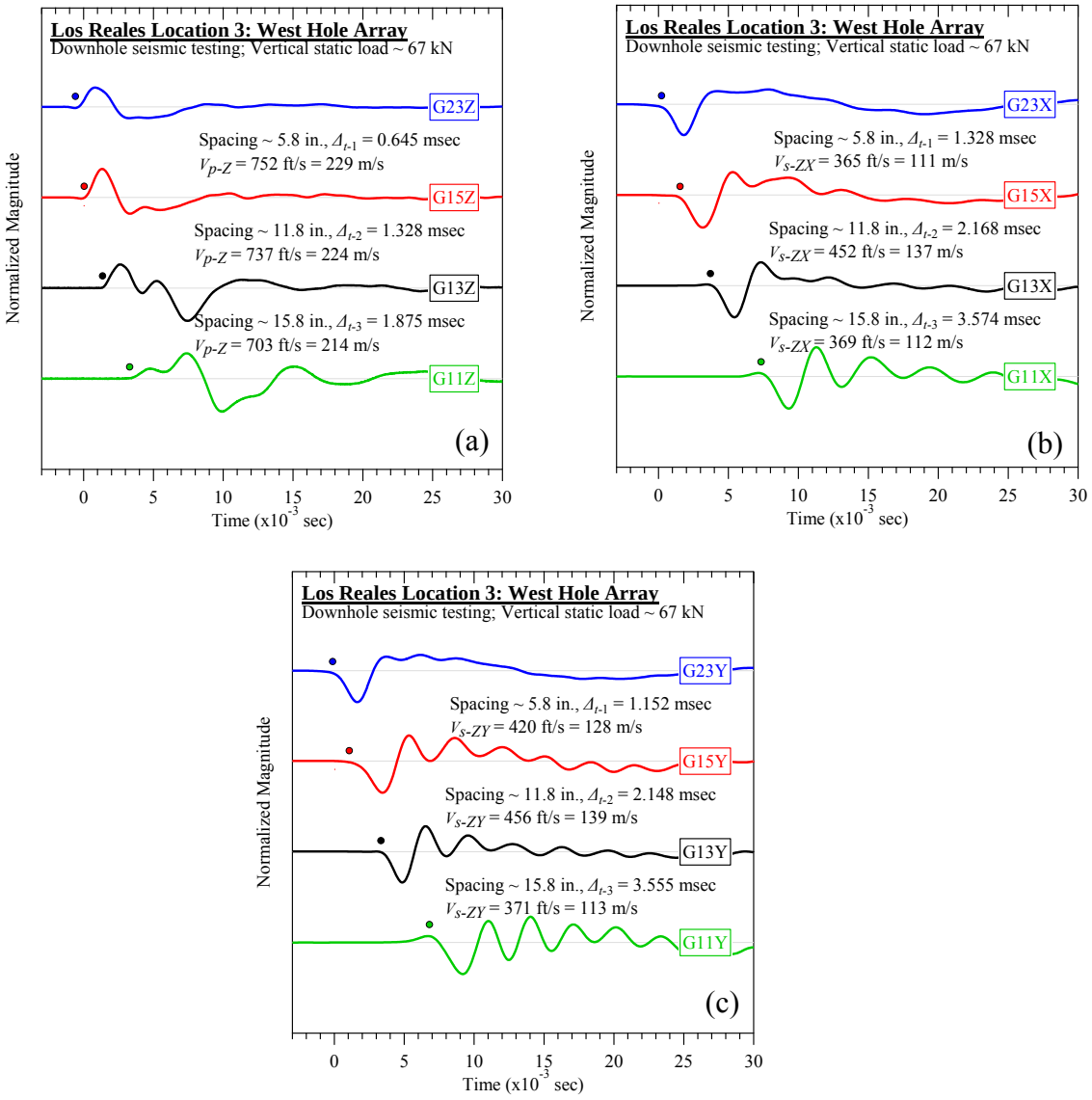

Figure C-101. Los Reales Landfill #3 (west hole): Downhole seismic testing at vertical load of 67 kN: (a) V_{p-Z}, (b) V_{s-ZX}, and (c) V_{s-ZY}.

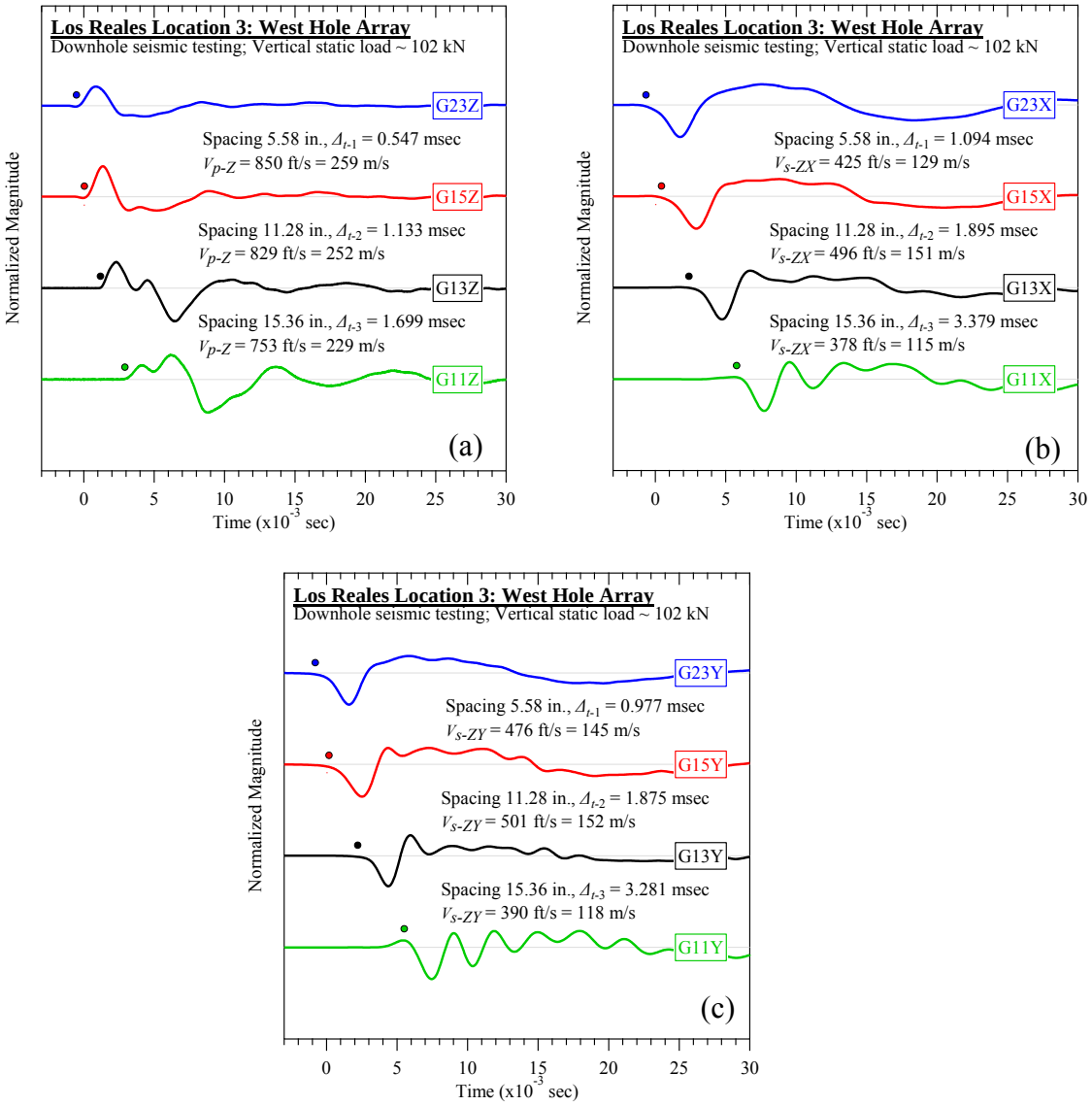

Figure C-102. Los Reales Landfill #3 (west hole): Downhole seismic testing at vertical load of 102 kN: (a) V_{p-Z}, (b) V_{s-ZX}, and (c) V_{s-ZY}.

C.3.2 Crosshole Seismic Testing

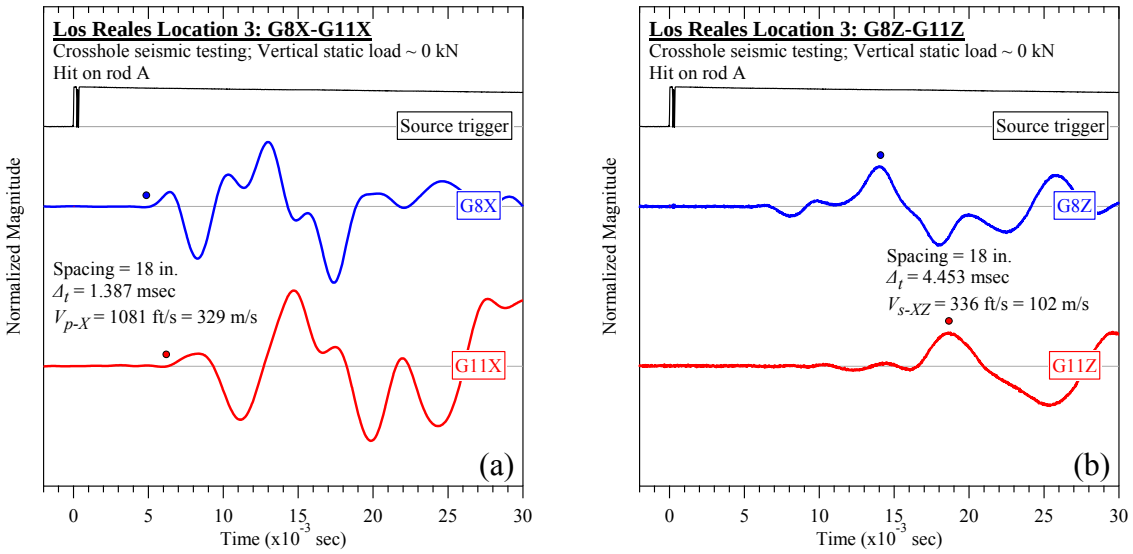

Figure C-103. Los Reales Landfill #2 (rod A): Crosshole seismic testing at vertical load of 0 kN: (a) $V_{p\text{-}X}$ and (b) $V_{s\text{-}XZ}$.

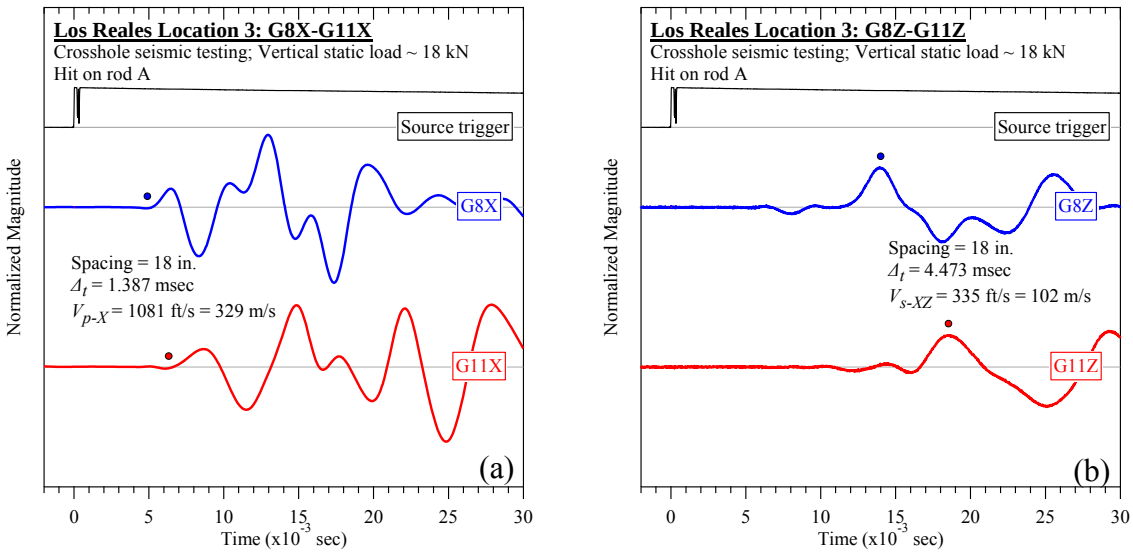

Figure C-104. Los Reales Landfill #2 (rod A): Crosshole seismic testing at vertical load of 18 kN: (a) $V_{p\text{-}X}$ and (b) $V_{s\text{-}XZ}$.

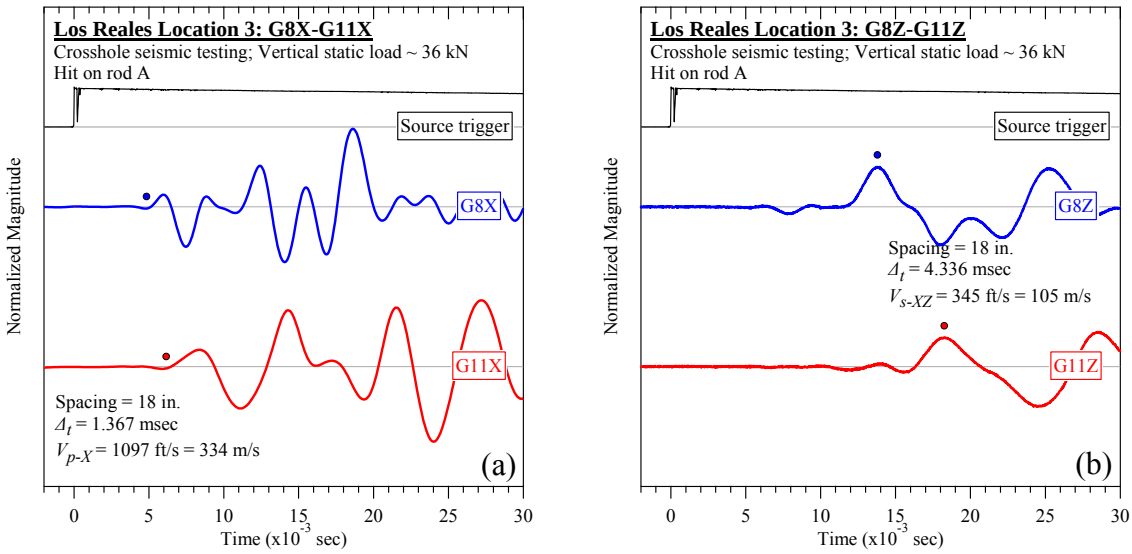

Figure C-105. Los Reales Landfill #2 (rod A): Crosshole seismic testing at vertical load of 36 kN: (a) $V_{p\text{-}X}$ and (b) $V_{s\text{-}XZ}$.

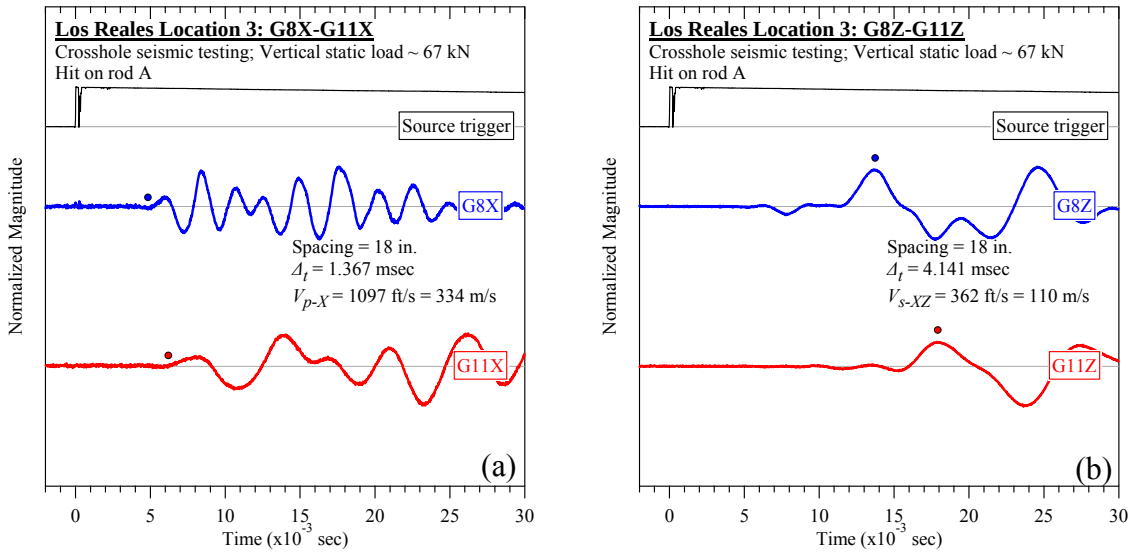

Figure C-106. Los Reales Landfill #2 (rod A): Crosshole seismic testing at vertical load of 67 kN: (a) $V_{p\text{-}X}$ and (b) $V_{s\text{-}XZ}$.

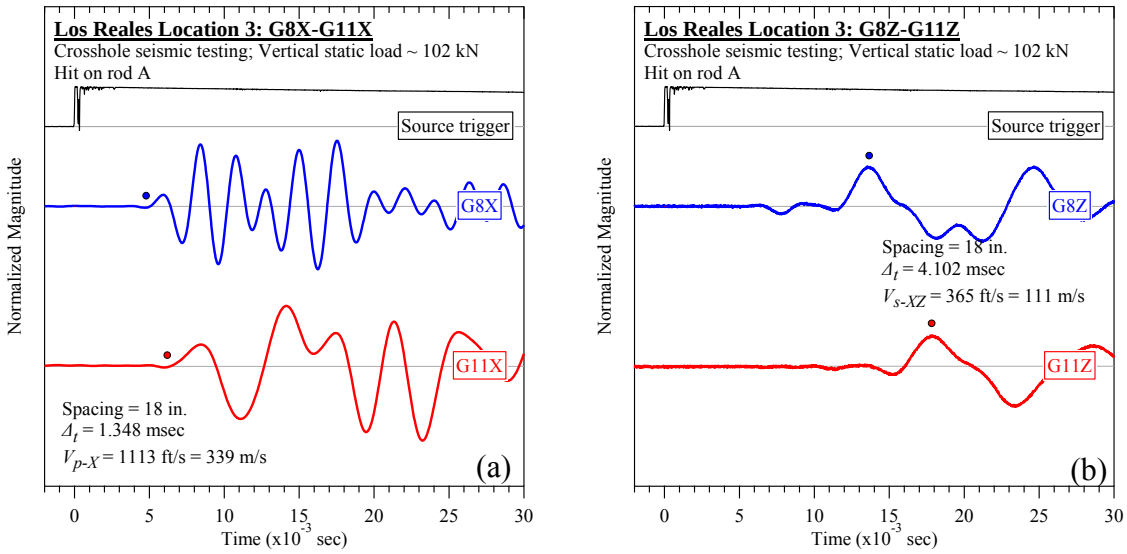

Figure C-107. Los Reales Landfill #2 (rod A): Crosshole seismic testing at vertical load of 102 kN: (a) $V_{p\text{-}X}$ and (b) $V_{s\text{-}XZ}$.

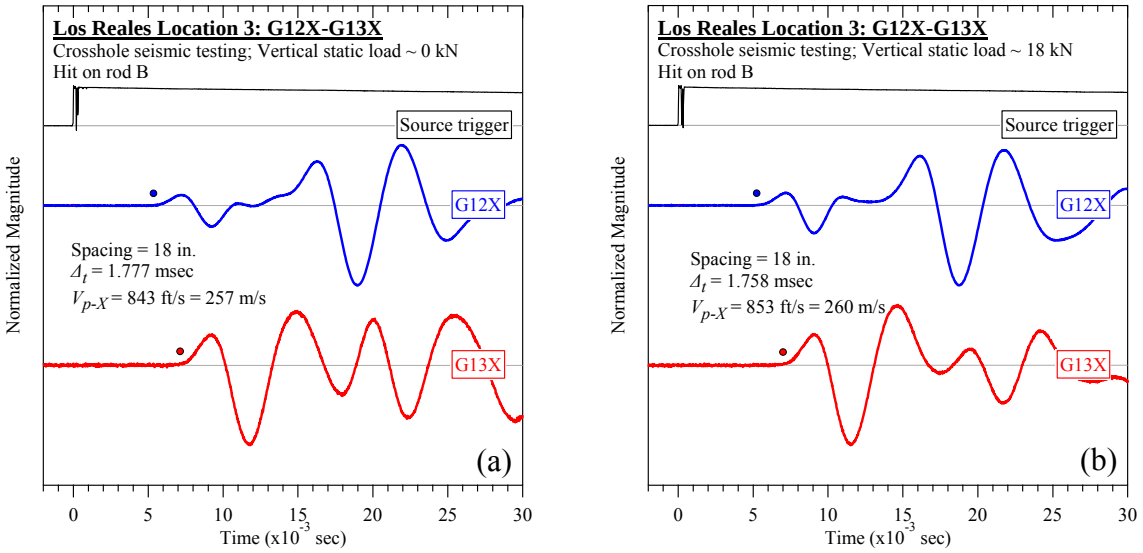

Figure C-108. Los Reales Landfill #2 (rod B): Crosshole seismic testing at vertical loads of (a) 0 kN and (b) 18 kN: $V_{p\text{-}X}$.

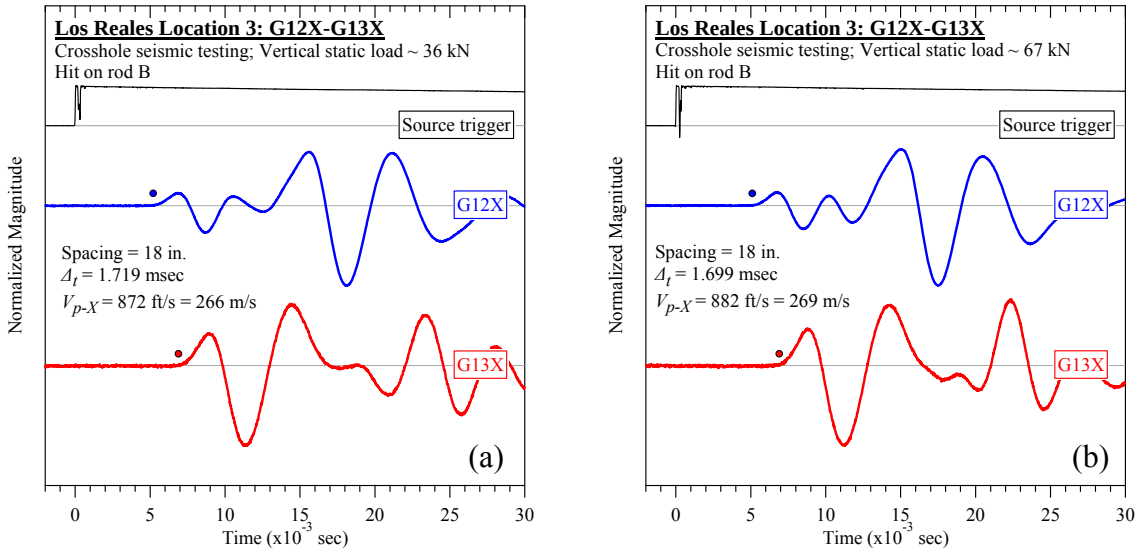

Figure C-109. Los Reales Landfill #2 (rod B): Crosshole seismic testing at vertical loads of (a) 36 kN and (b) 67 kN: $V_{p\text{-}X}$.

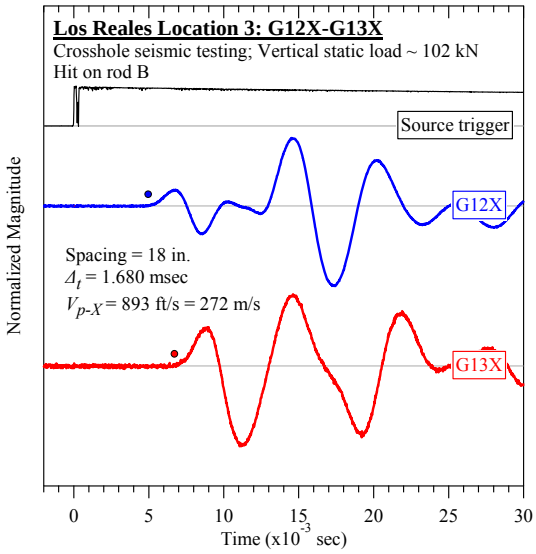

Figure C-110. Los Reales Landfill #2 (rod B): Crosshole seismic testing at vertical load of 102 kN: $V_{p\text{-}X}$.

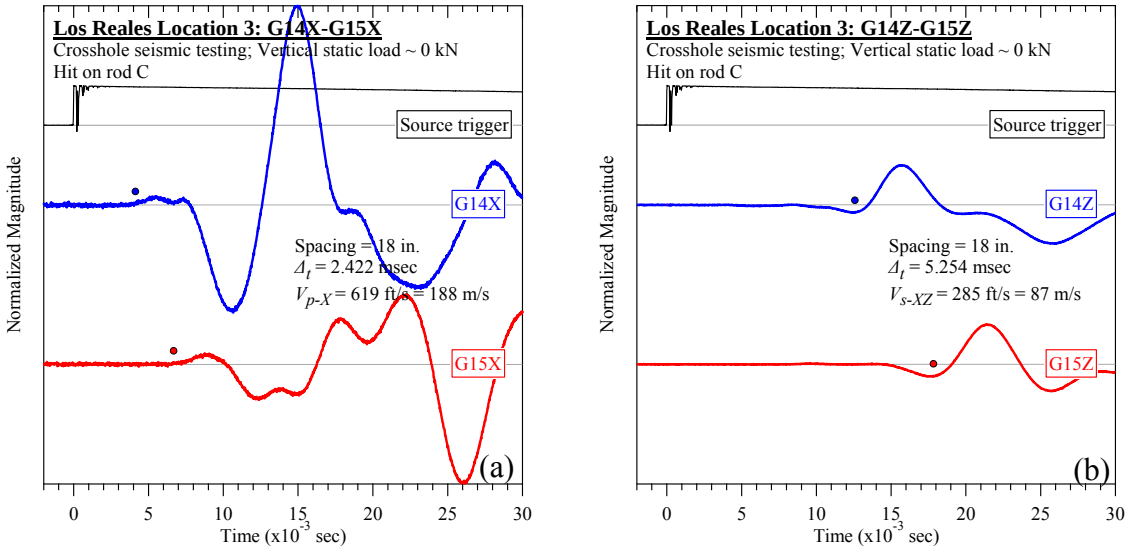

Figure C-111. Los Reales Landfill #2 (rod C): Crosshole seismic testing at vertical load of 0 kN: (a) $V_{p\text{-}X}$ and (b) $V_{s\text{-}XZ}$.

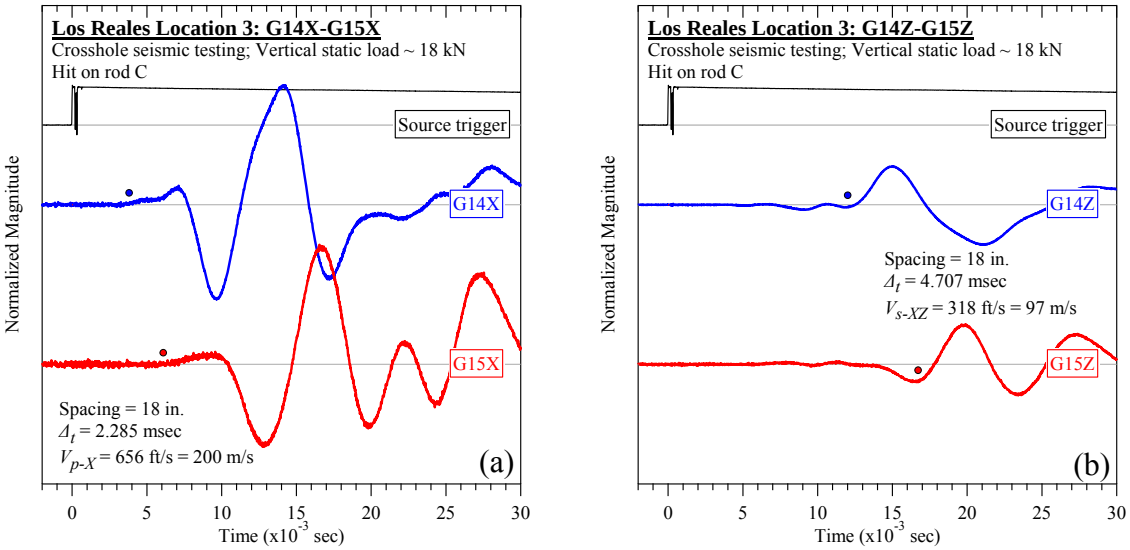

Figure C-112. Los Reales Landfill #2 (rod C): Crosshole seismic testing at vertical load of 18 kN: (a) $V_{p\text{-}X}$ and (b) $V_{s\text{-}XZ}$.

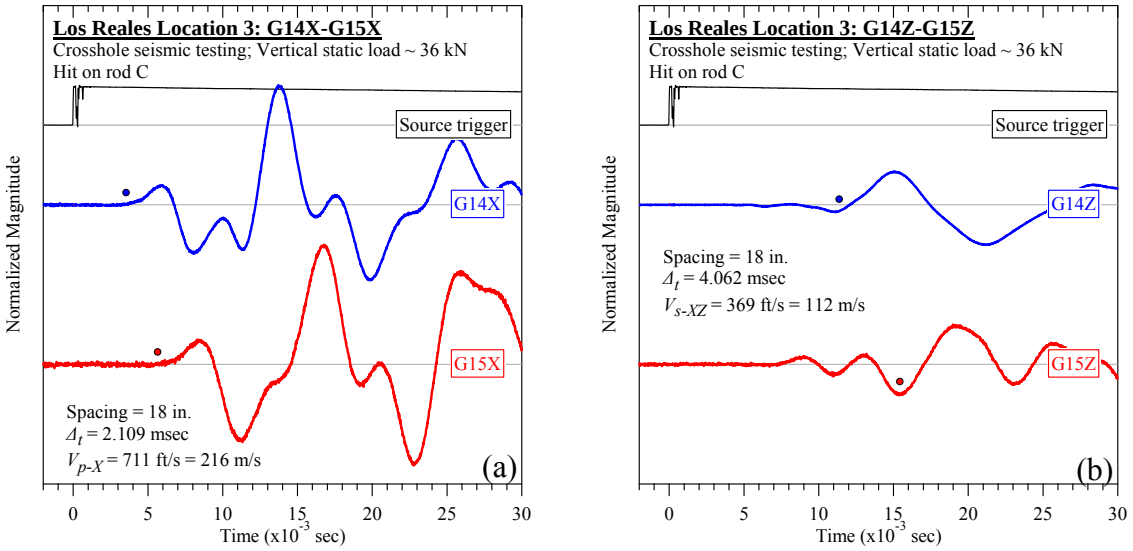

Figure C-113. Los Reales Landfill #2 (rod C): Crosshole seismic testing at vertical load of 36 kN: (a) $V_{p\text{-}X}$ and (b) $V_{s\text{-}XZ}$.

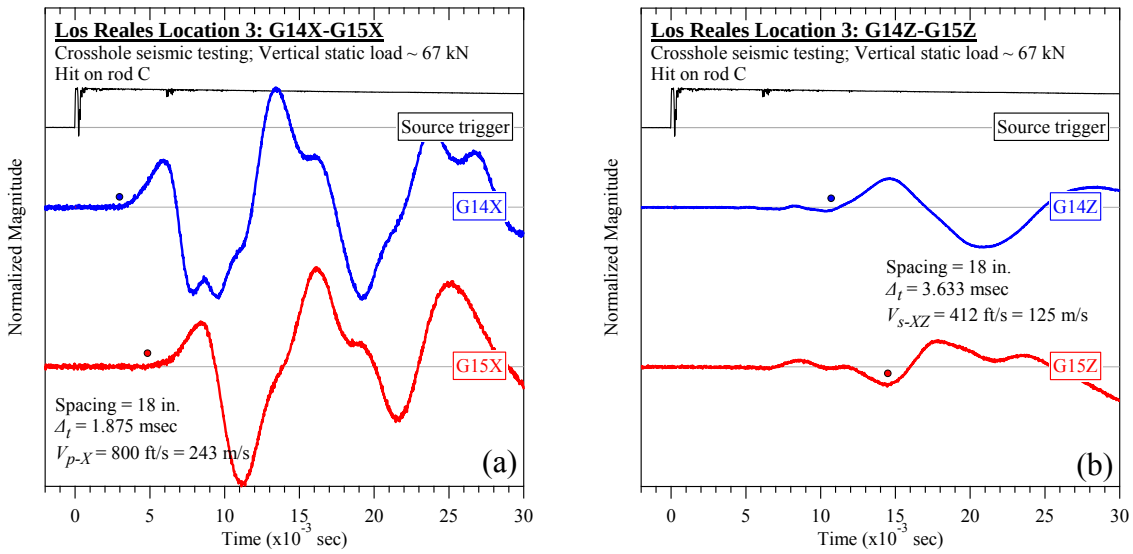

Figure C-114. Los Reales Landfill #2 (rod C): Crosshole seismic testing at vertical load of 67 kN: (a) $V_{p\text{-}X}$ and (b) $V_{s\text{-}XZ}$.

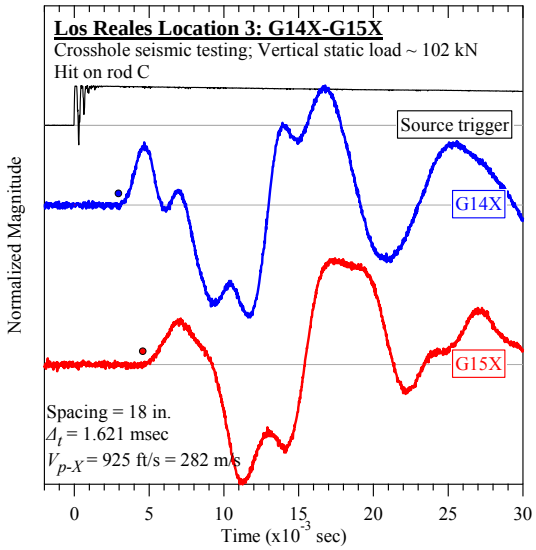

Figure C-115. Los Reales Landfill #2 (rod C): Crosshole seismic testing at vertical load of 102 kN: $V_{p\text{-}X}$.

C.3.3 Steady-state Dynamic Testing

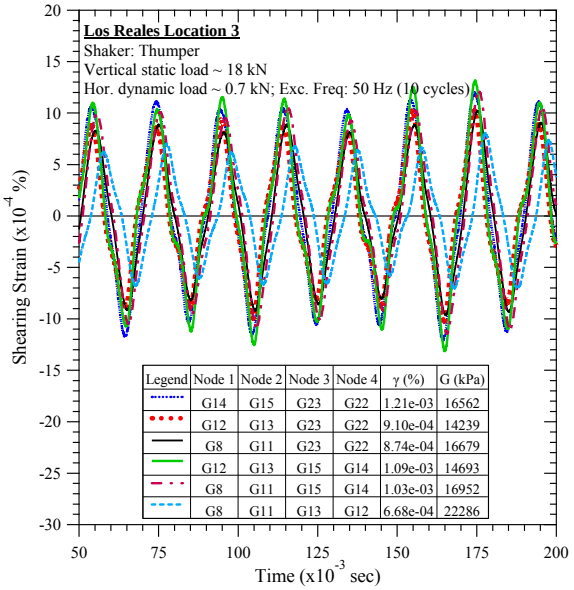

Figure C-116. Los Reales Landfill #3: Steady-state dynamic testing at vertical load of 18 kN and horizontal dynamic load of 0.7 kN.

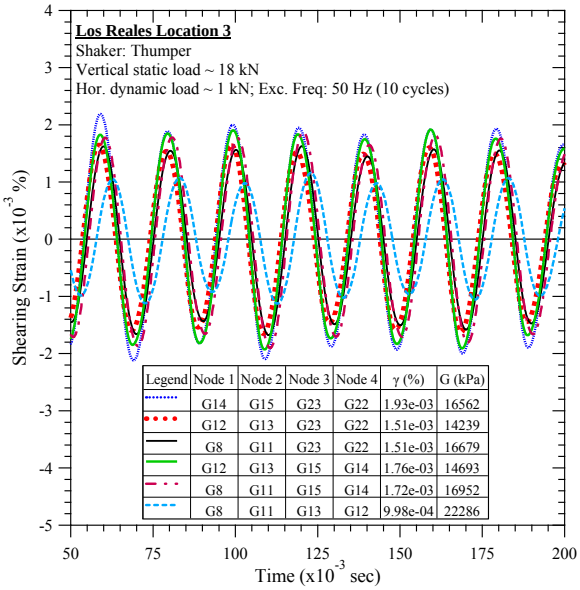

Figure C-117. Los Reales Landfill #3: Steady-state dynamic testing at vertical load of 18 kN and horizontal dynamic load of 1 kN.

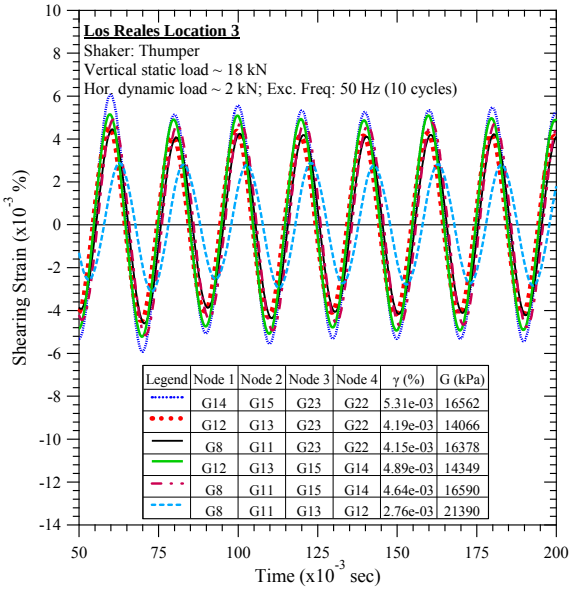

Figure C-118. Los Reales Landfill #3: Steady-state dynamic testing at vertical load of 18 kN and horizontal dynamic load of 2 kN.

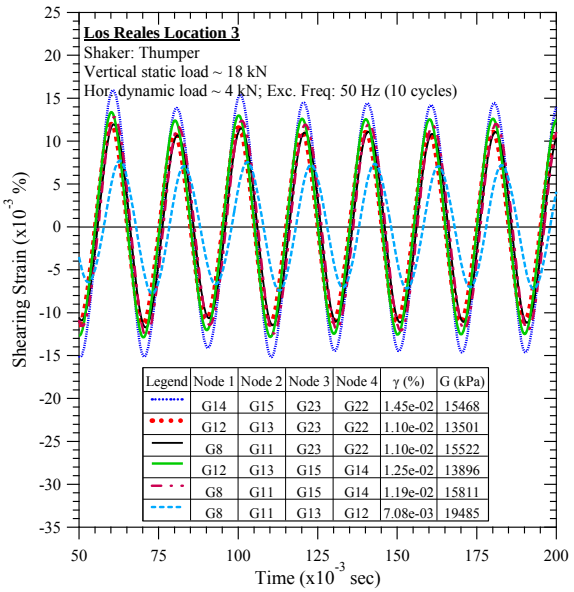

Figure C-119. Los Reales Landfill #3: Steady-state dynamic testing at vertical load of 18 kN and horizontal dynamic load of 4 kN.

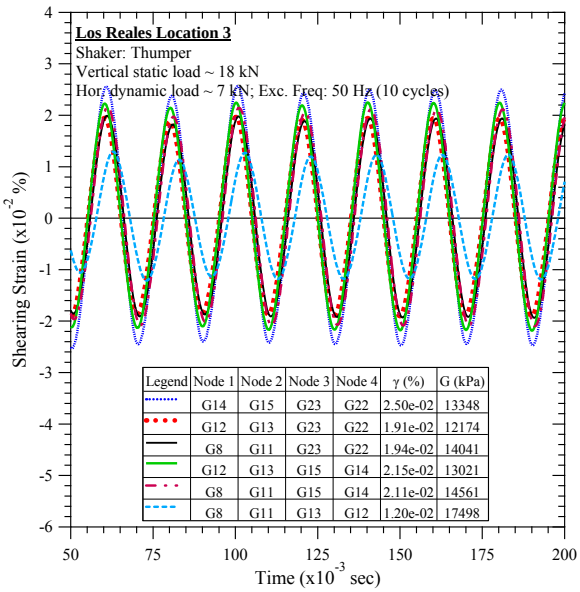

Figure C-120. Los Reales Landfill #3: Steady-state dynamic testing at vertical load of 18 kN and horizontal dynamic load of 7 kN.

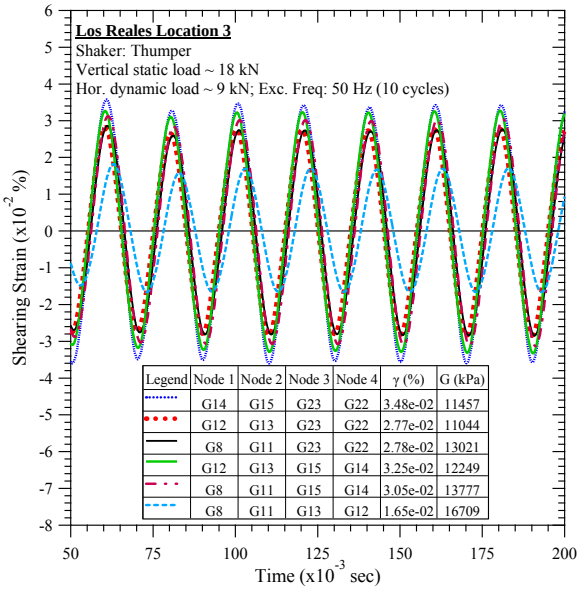

Figure C-121. Los Reales Landfill #3: Steady-state dynamic testing at vertical load of 18 kN and horizontal dynamic load of 9 kN.

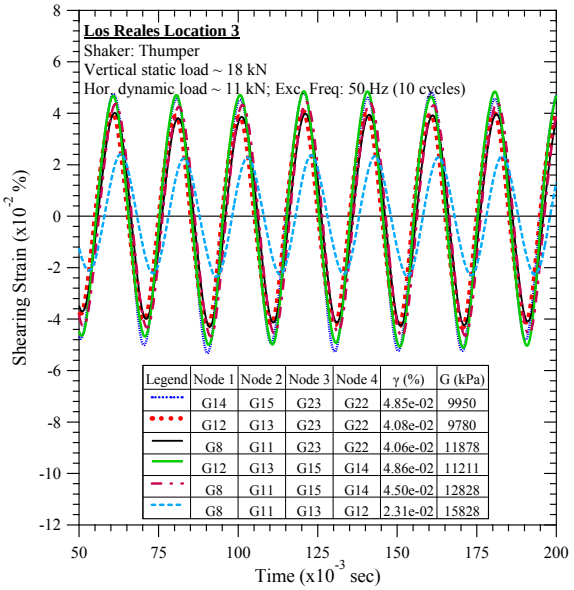

Figure C-122. Los Reales Landfill #3: Steady-state dynamic testing at vertical load of 18 kN and horizontal dynamic load of 11 kN.

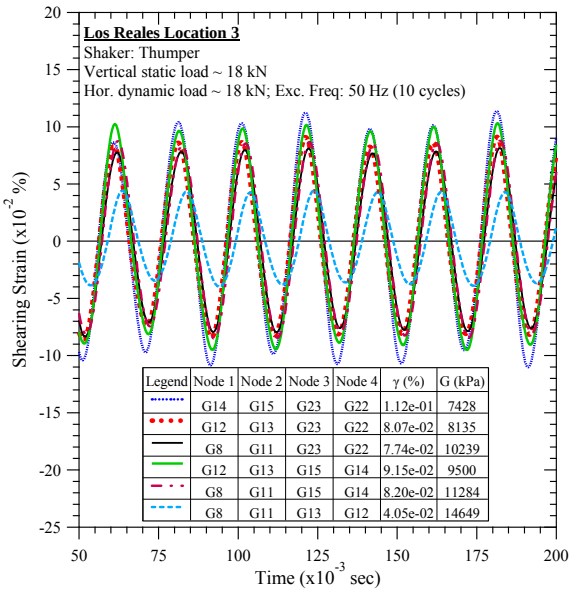

Figure C-123. Los Reales Landfill #3: Steady-state dynamic testing at vertical load of 18 kN and horizontal dynamic load of 18 kN.

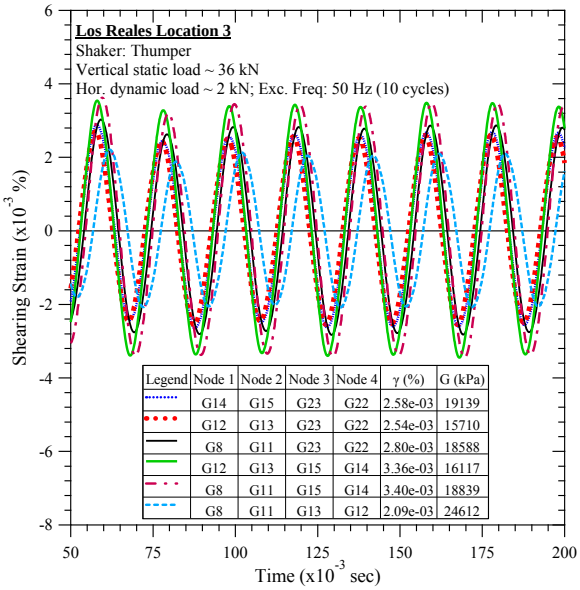

Figure C-124. Los Reales Landfill #3: Steady-state dynamic testing at vertical load of 36 kN and horizontal dynamic load of 2 kN.

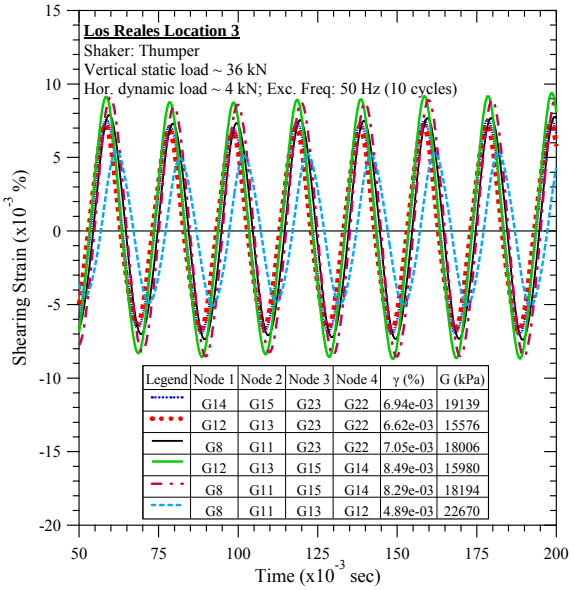

Figure C-125. Los Reales Landfill #3: Steady-state dynamic testing at vertical load of 36 kN and horizontal dynamic load of 4 kN.

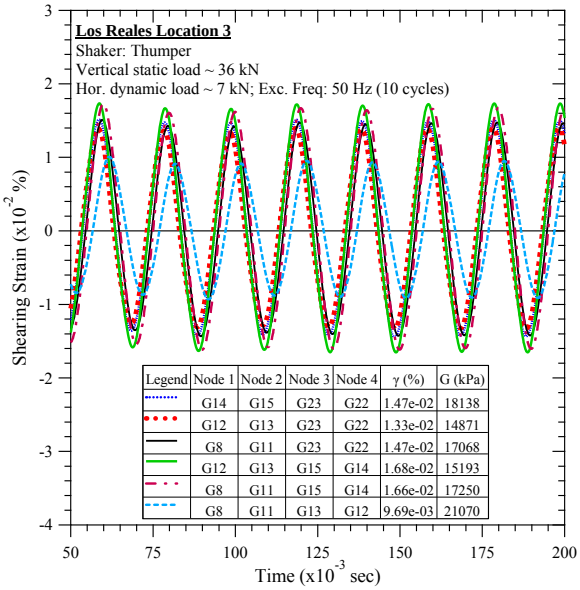

Figure C-126. Los Reales Landfill #3: Steady-state dynamic testing at vertical load of 36 kN and horizontal dynamic load of 7 kN.

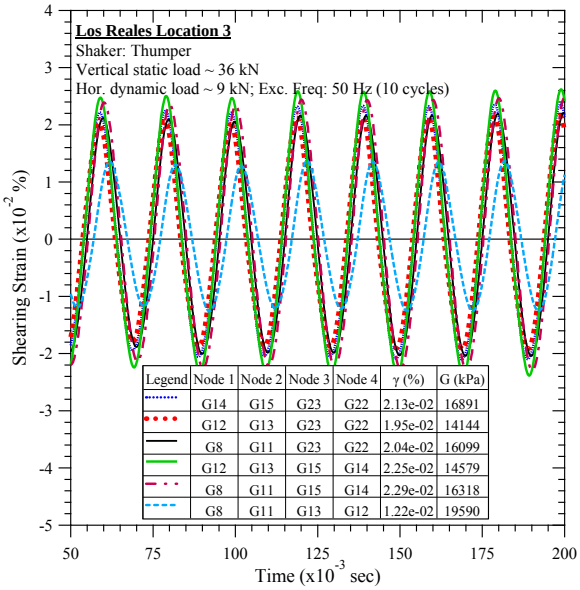

Figure C-127. Los Reales Landfill #3: Steady-state dynamic testing at vertical load of 36 kN and horizontal dynamic load of 9 kN.

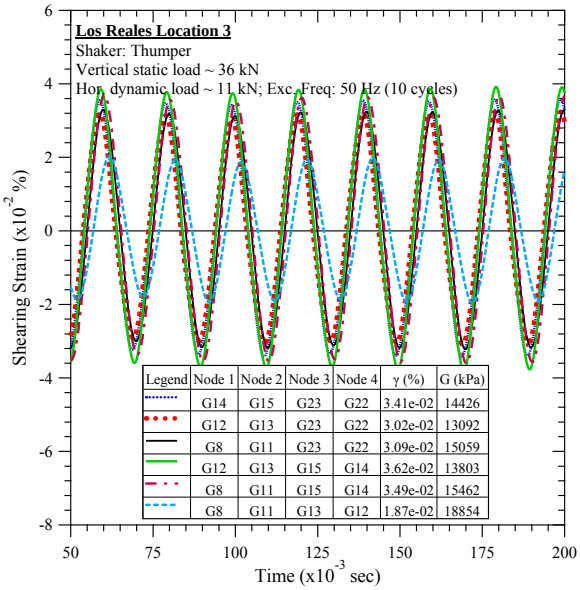

Figure C-128. Los Reales Landfill #3: Steady-state dynamic testing at vertical load of 36 kN and horizontal dynamic load of 11 kN.

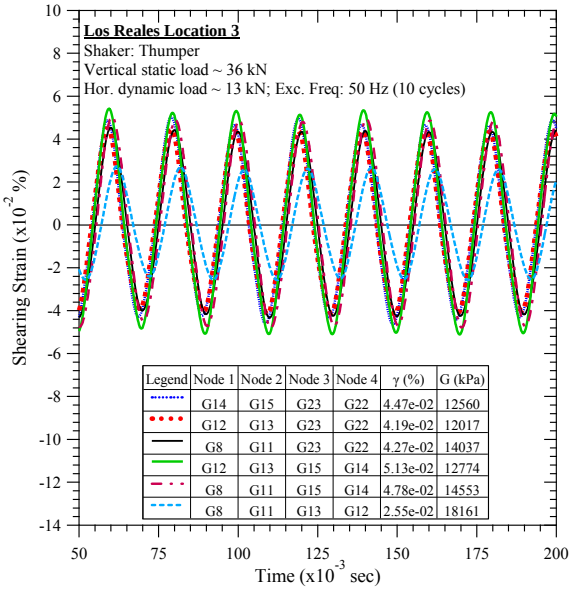

Figure C-129. Los Reales Landfill #3: Steady-state dynamic testing at vertical load of 36 kN and horizontal dynamic load of 13 kN.

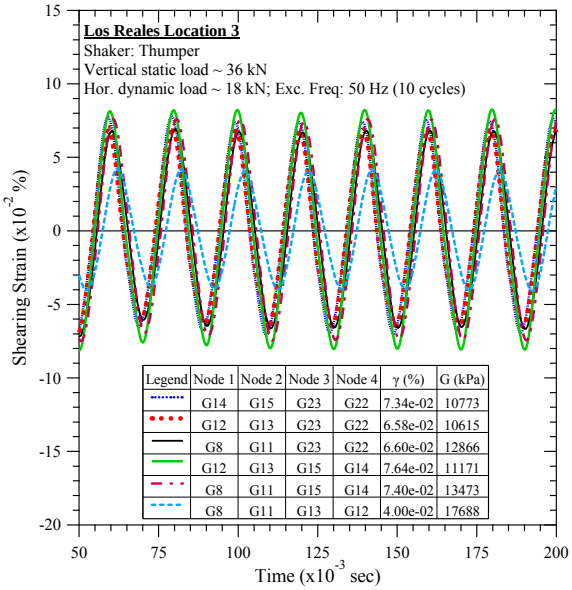

Figure C-130. Los Reales Landfill #3: Steady-state dynamic testing at vertical load of 36 kN and horizontal dynamic load of 18 kN.

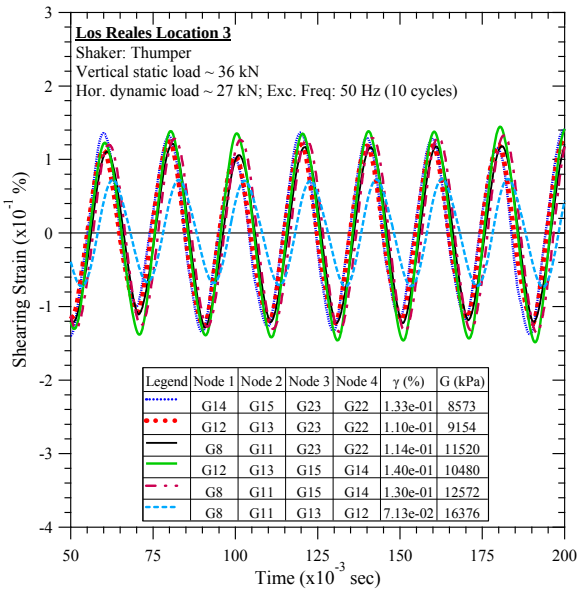

Figure C-131. Los Reales Landfill #3: Steady-state dynamic testing at vertical load of 36 kN and horizontal dynamic load of 27 kN.

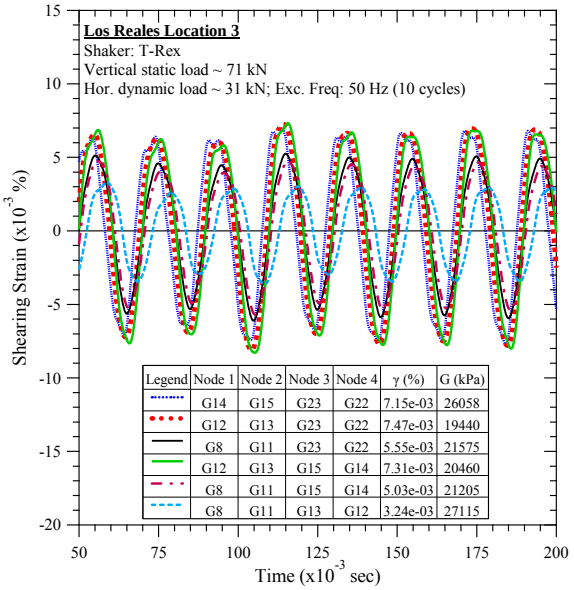

Figure C-132. Los Reales Landfill #3: Steady-state dynamic testing at vertical load of 71 kN and horizontal dynamic load of 31 kN.

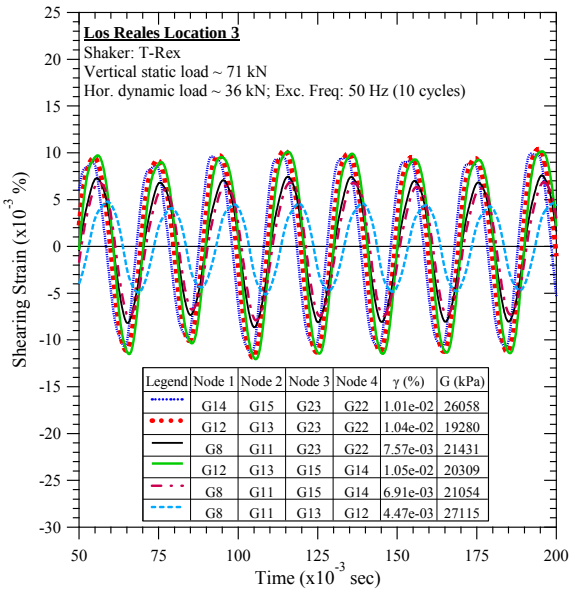

Figure C-133. Los Reales Landfill #3: Steady-state dynamic testing at vertical load of 71 kN and horizontal dynamic load of 36 kN.

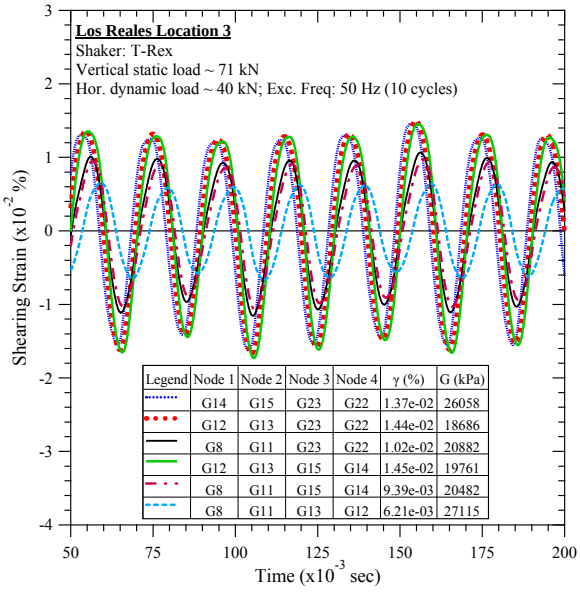

Figure C-134. Los Reales Landfill #3: Steady-state dynamic testing at vertical load of 71 kN and horizontal dynamic load of 40 kN.

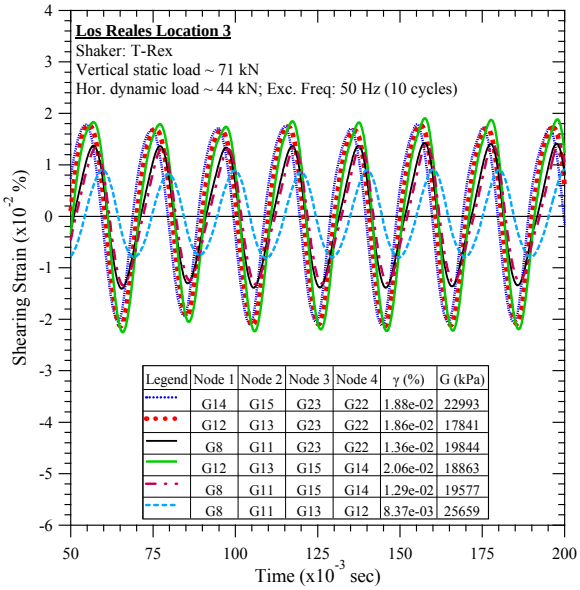

Figure C-135. Los Reales Landfill #3: Steady-state dynamic testing at vertical load of 71 kN and horizontal dynamic load of 44 kN.

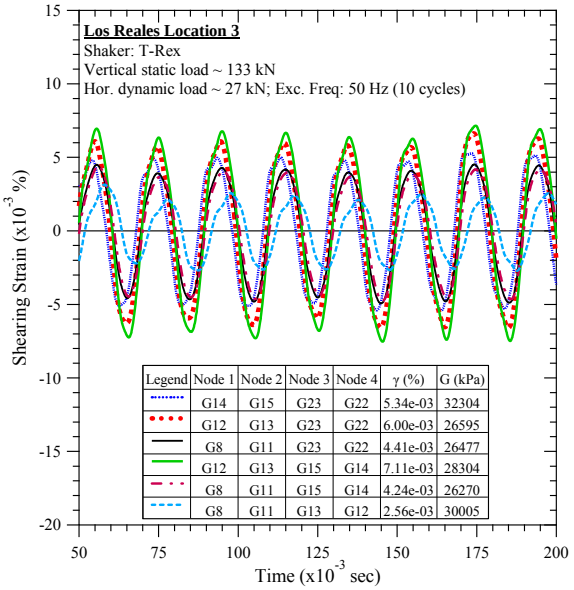

Figure C-136. Los Reales Landfill #3: Steady-state dynamic testing at vertical load of 133 kN and horizontal dynamic load of 27 kN.

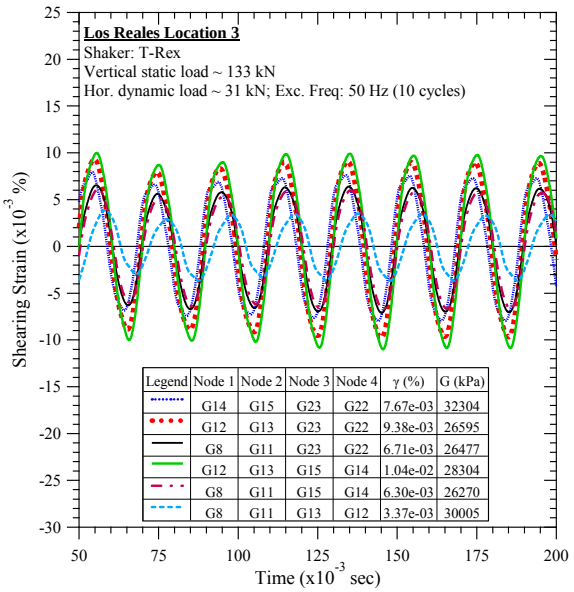

Figure C-137. Los Reales Landfill #3: Steady-state dynamic testing at vertical load of 133 kN and horizontal dynamic load of 31 kN.

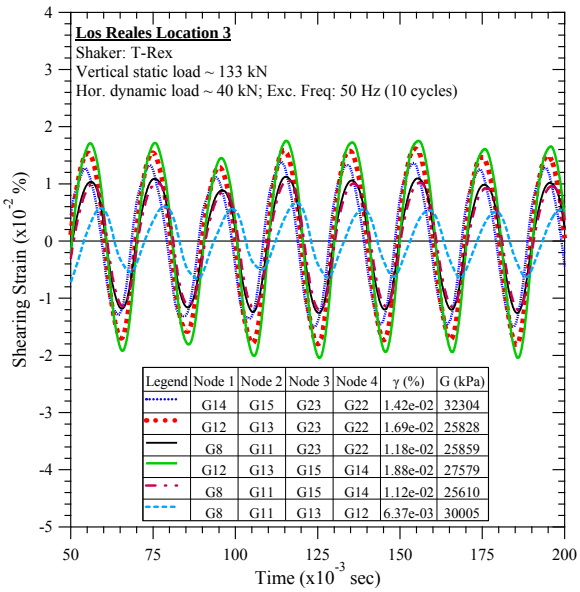

Figure C-138. Los Reales Landfill #3: Steady-state dynamic testing at vertical load of 133 kN and horizontal dynamic load of 40 kN.

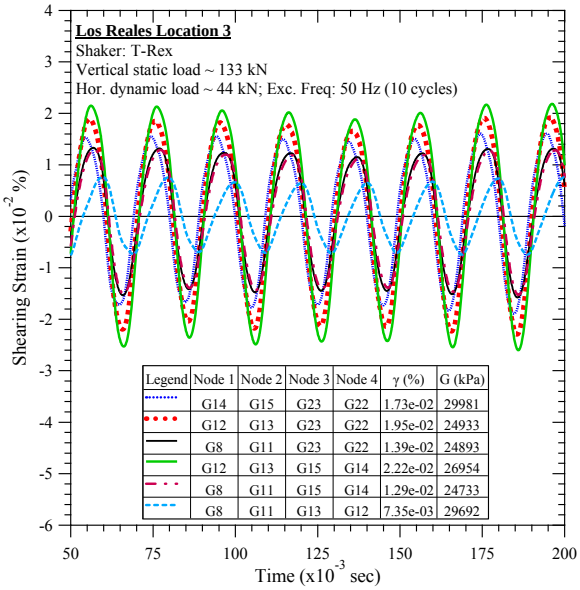

Figure C-139. Los Reales Landfill #3: Steady-state dynamic testing at vertical load of 133 kN and horizontal dynamic load of 44 kN.

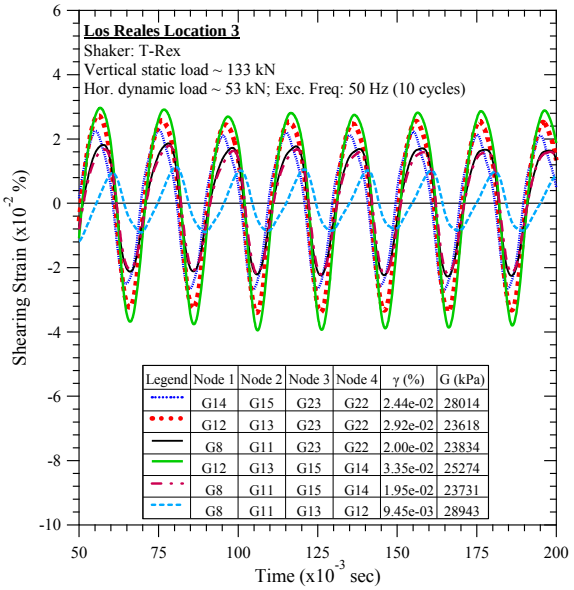

Figure C-140. Los Reales Landfill #3: Steady-state dynamic testing at vertical load of 133 kN and horizontal dynamic load of 53 kN.

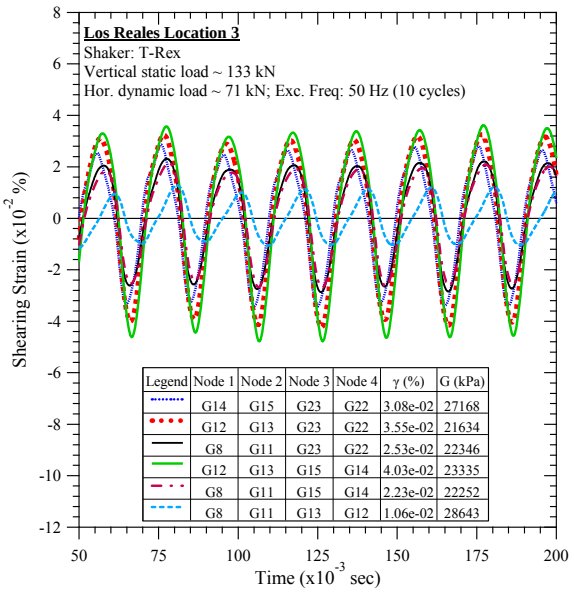

Figure C-141. Los Reales Landfill #3: Steady-state dynamic testing at vertical load of 133 kN and horizontal dynamic load of 71 kN.

D BKK Landfill Testing Results

D.1 BKK Landfill Location 1

D.1.1 Downhole Seismic Testing

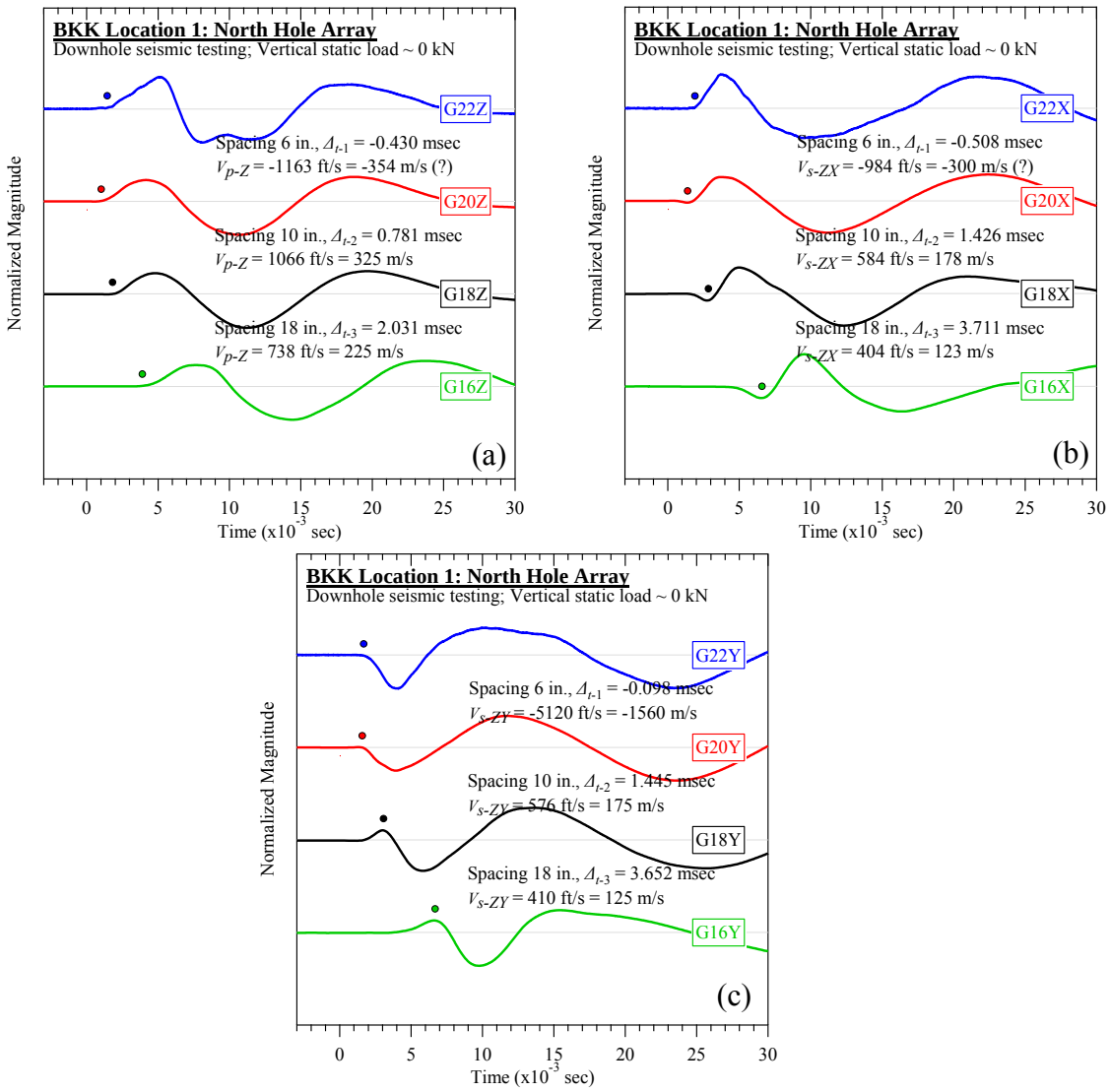

Figure D-1. BKK Landfill #1 (north hole): Downhole seismic testing at vertical load of 0 kN: (a) V_{p-Z}, (b) V_{s-ZX}, and (c) V_{s-ZY}.

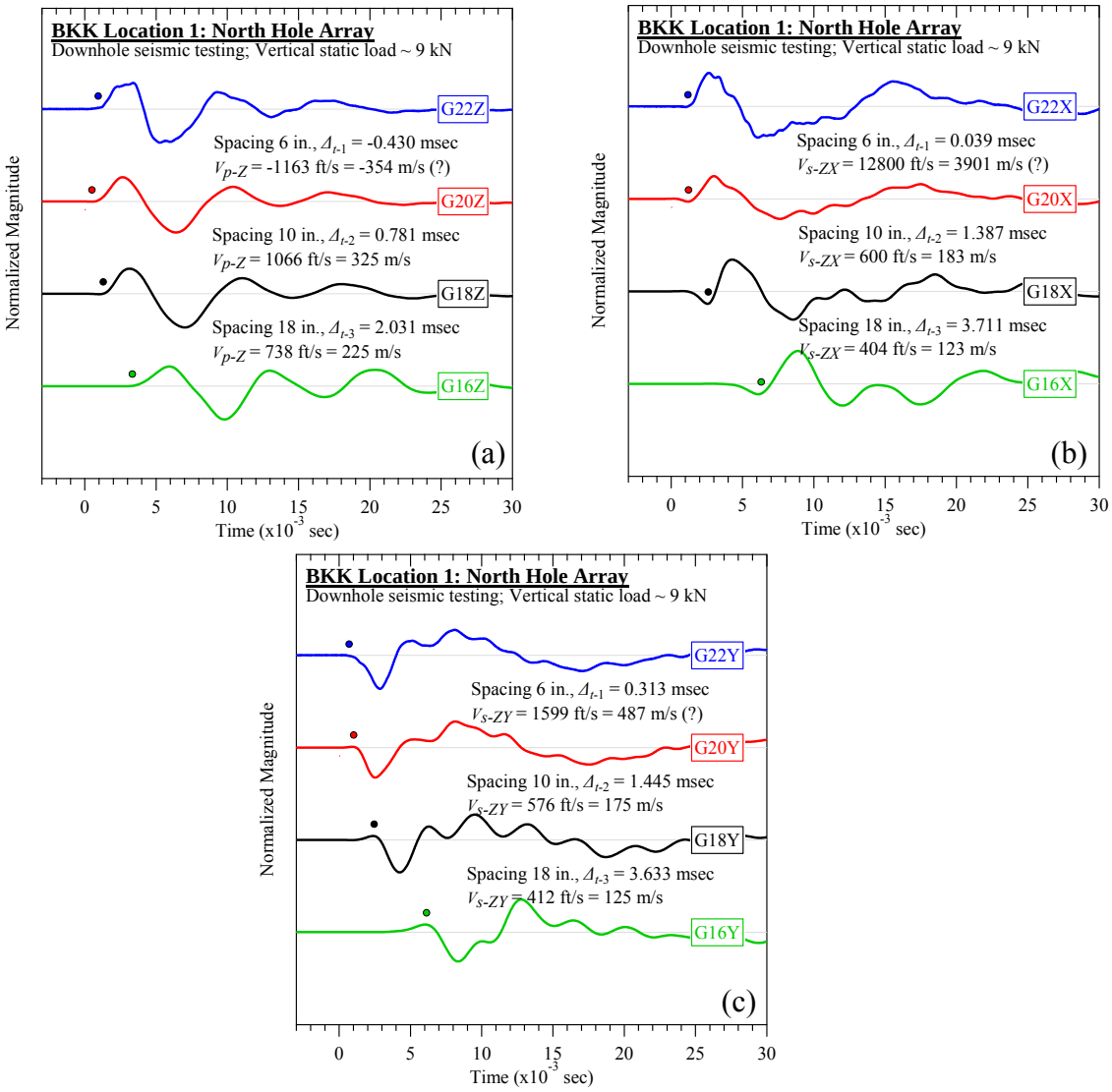

Figure D-2. BKK Landfill #1 (north hole): Downhole seismic testing at vertical load of 9 kN: (a) $V_{p\text{-}Z}$, (b) $V_{s\text{-}ZX}$, and (c) $V_{s\text{-}ZY}$.

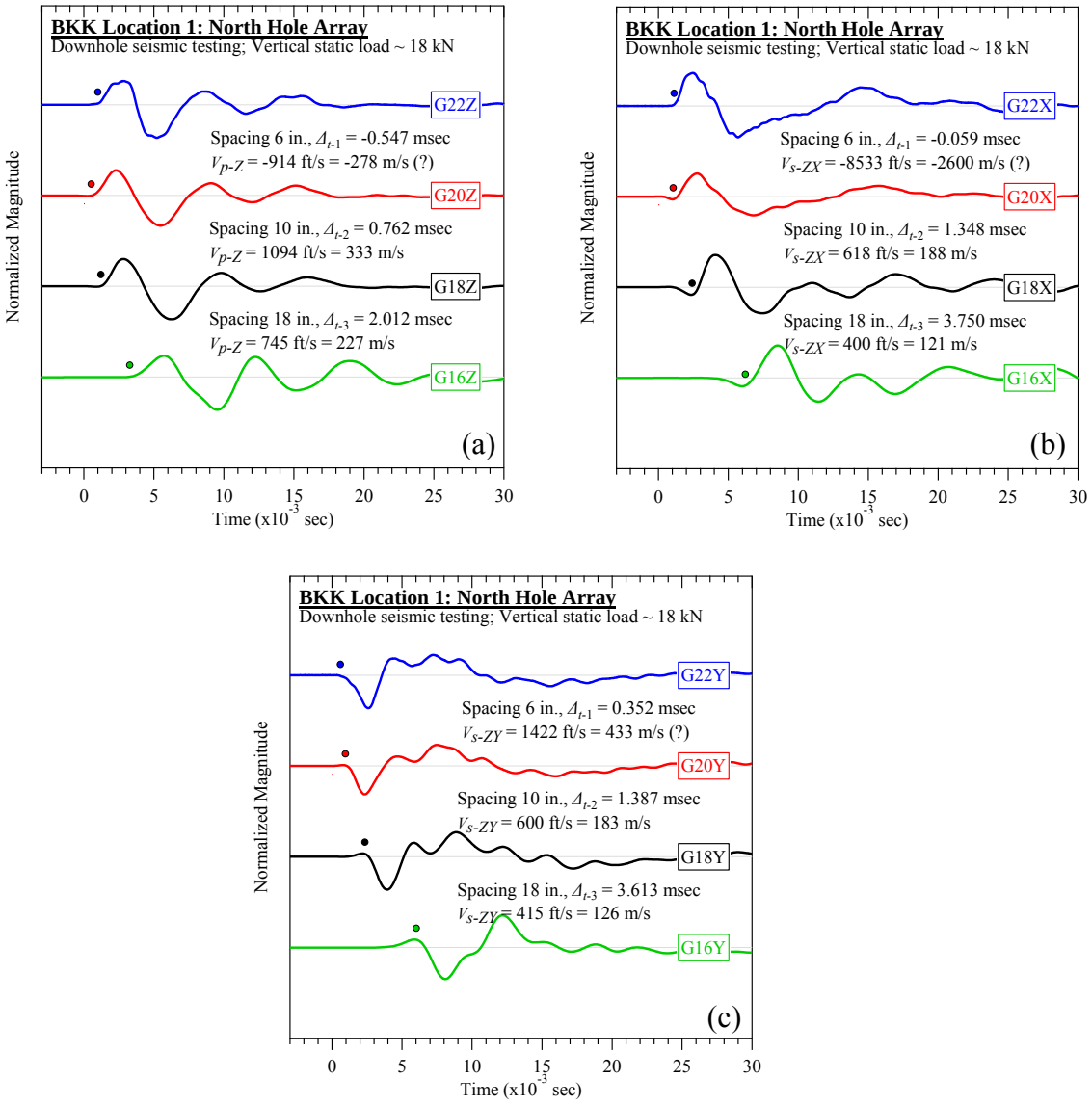

Figure D-3. BKK Landfill #1 (north hole): Downhole seismic testing at vertical load of 18 kN: (a) V_{p-Z}, (b) V_{s-ZX}, and (c) V_{s-ZY}.

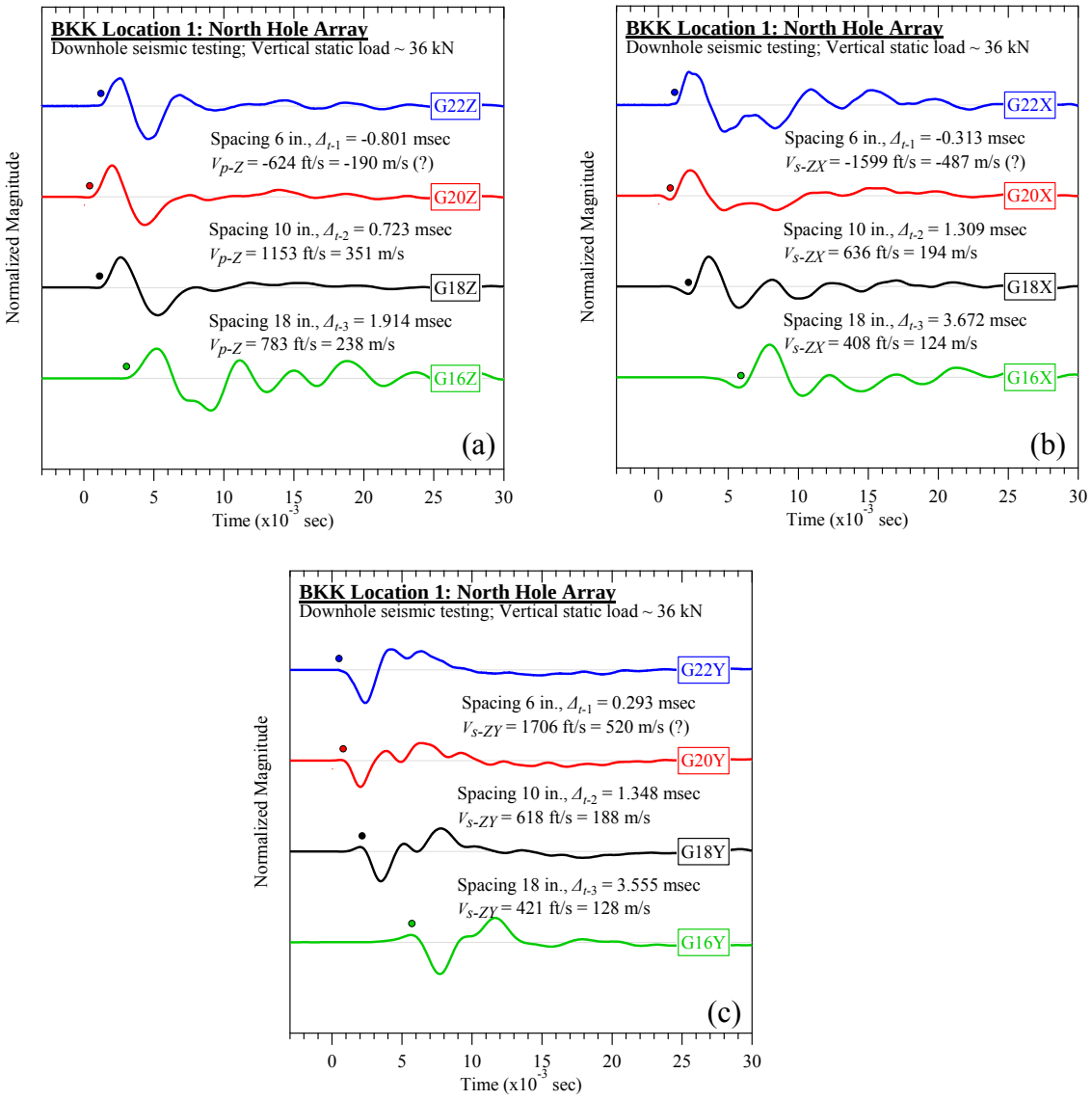

Figure D-4. BKK Landfill #1 (north hole): Downhole seismic testing at vertical load of 36 kN: (a) V_{p-Z}, (b) V_{s-ZX}, and (c) V_{s-ZY}.

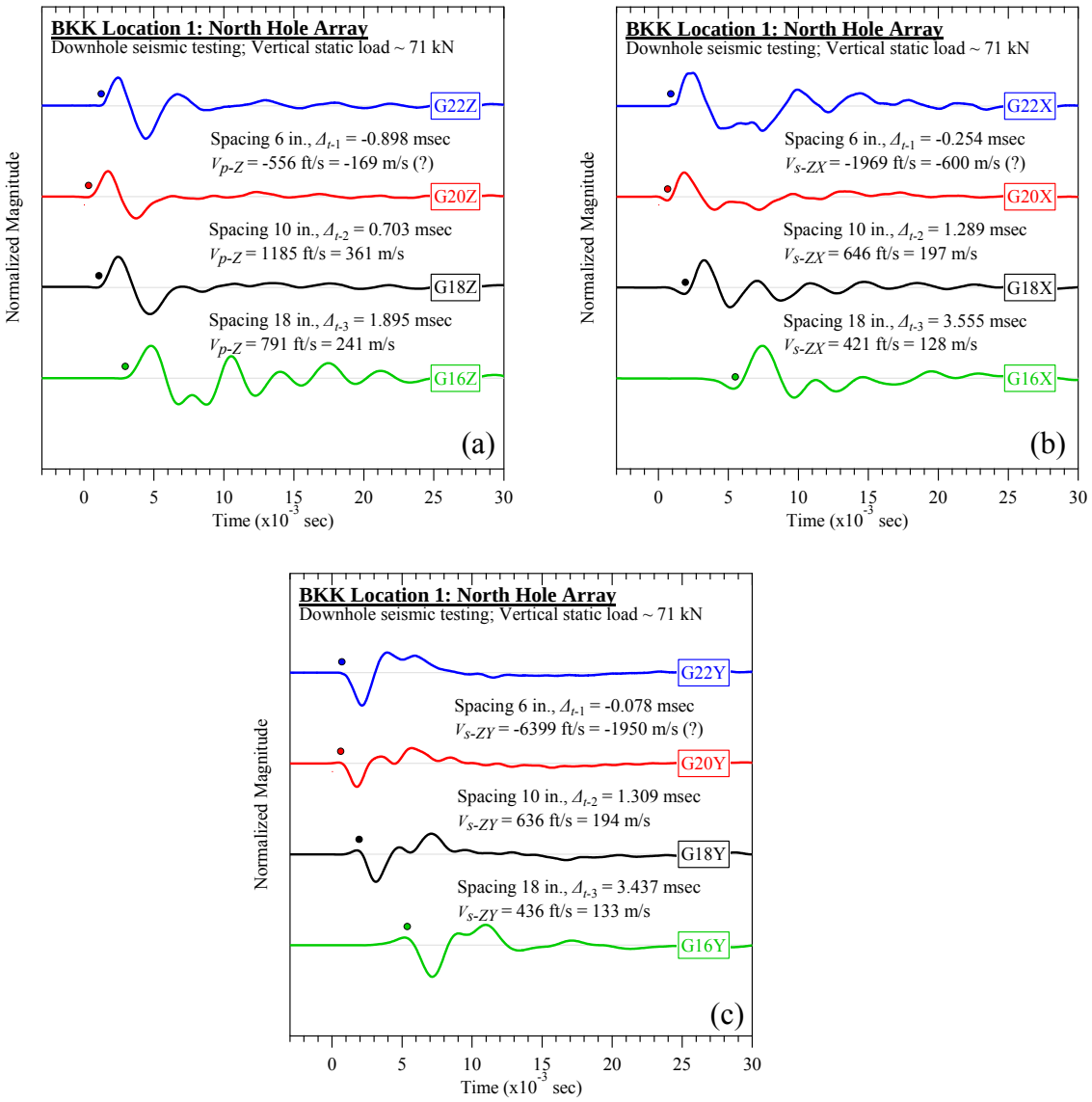

Figure D-5. BKK Landfill #1 (north hole): Downhole seismic testing at vertical load of 71 kN: (a) $V_{p\text{-}Z}$, (b) $V_{s\text{-}ZX}$, and (c) $V_{s\text{-}ZY}$.

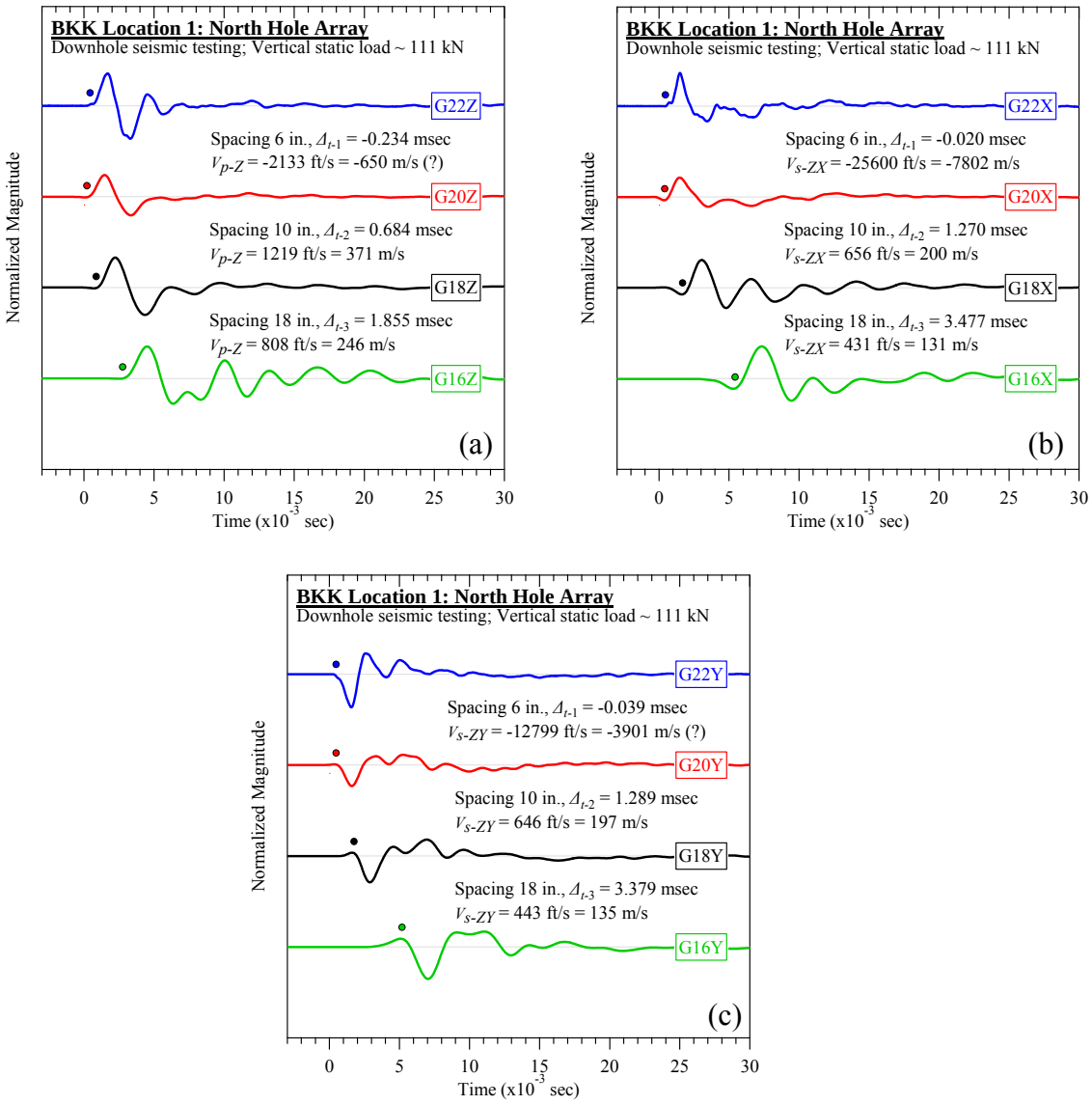

Figure D-6. BKK Landfill #1 (north hole): Downhole seismic testing at vertical load of 111 kN: (a) V_{p-Z}, (b) V_{s-ZX}, and (c) V_{s-ZY}.

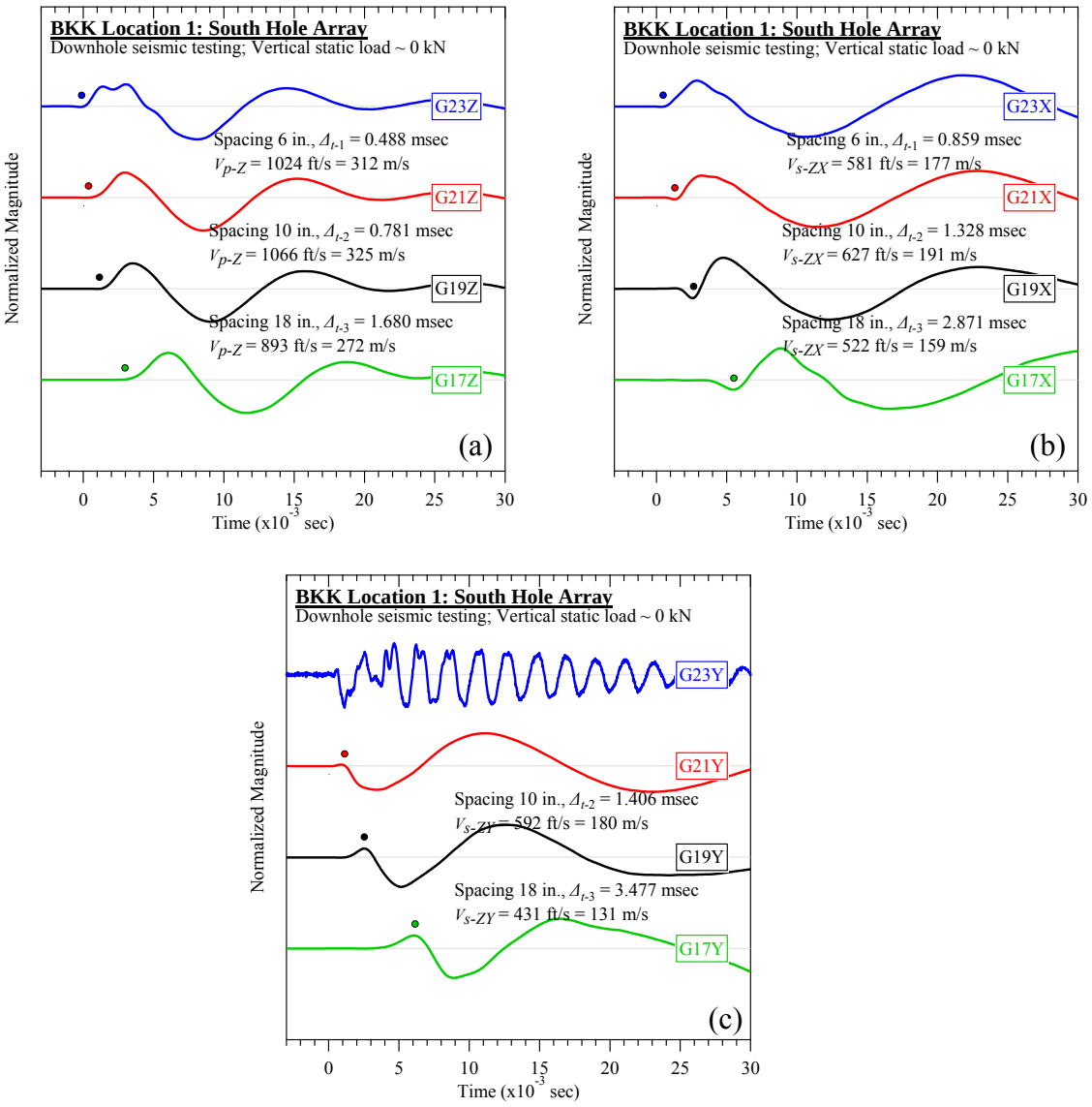

Figure D-7. BKK Landfill #1 (south hole): Downhole seismic testing at vertical load of 0 kN: (a) $V_{p\text{-}Z}$, (b) $V_{s\text{-}ZX}$, and (c) $V_{s\text{-}ZY}$.

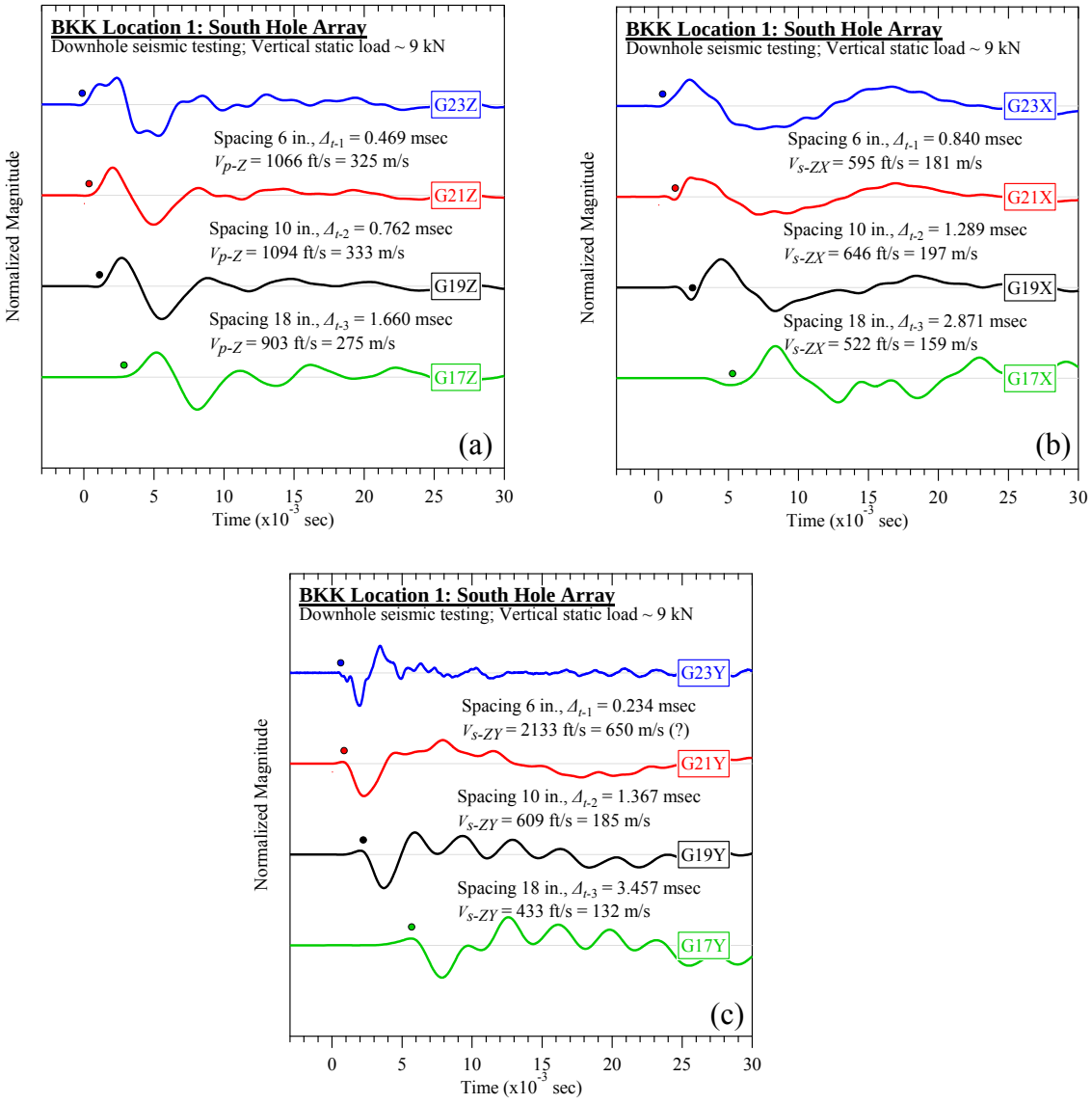

Figure D-8. BKK Landfill #1 (south hole): Downhole seismic testing at vertical load of 9 kN: (a) $V_{p\text{-}Z}$, (b) $V_{s\text{-}ZX}$, and (c) $V_{s\text{-}ZY}$.

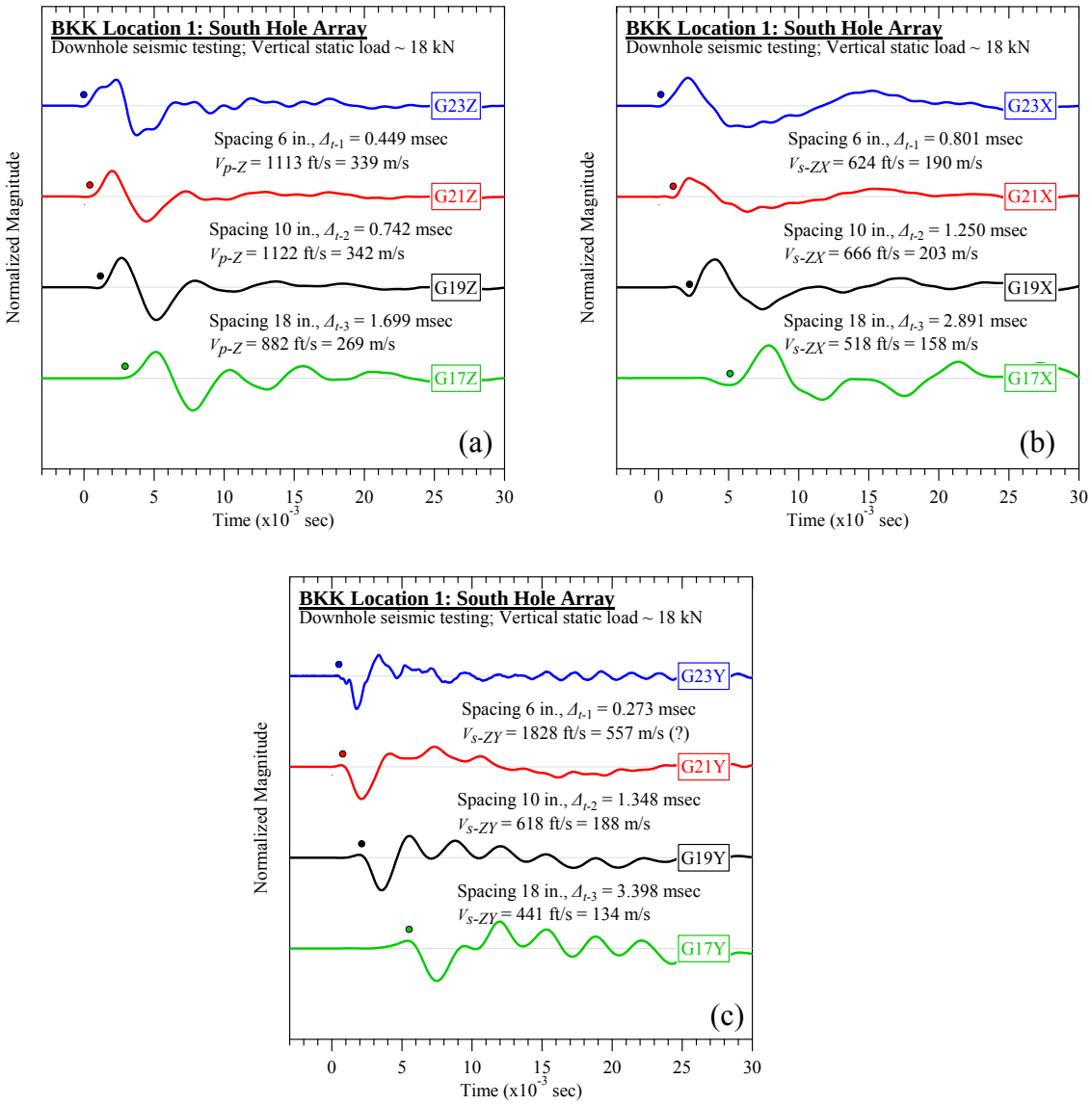

Figure D-9. BKK Landfill #1 (south hole): Downhole seismic testing at vertical load of 18 kN: (a) V_{p-Z}, (b) V_{s-ZX}, and (c) V_{s-ZY}.

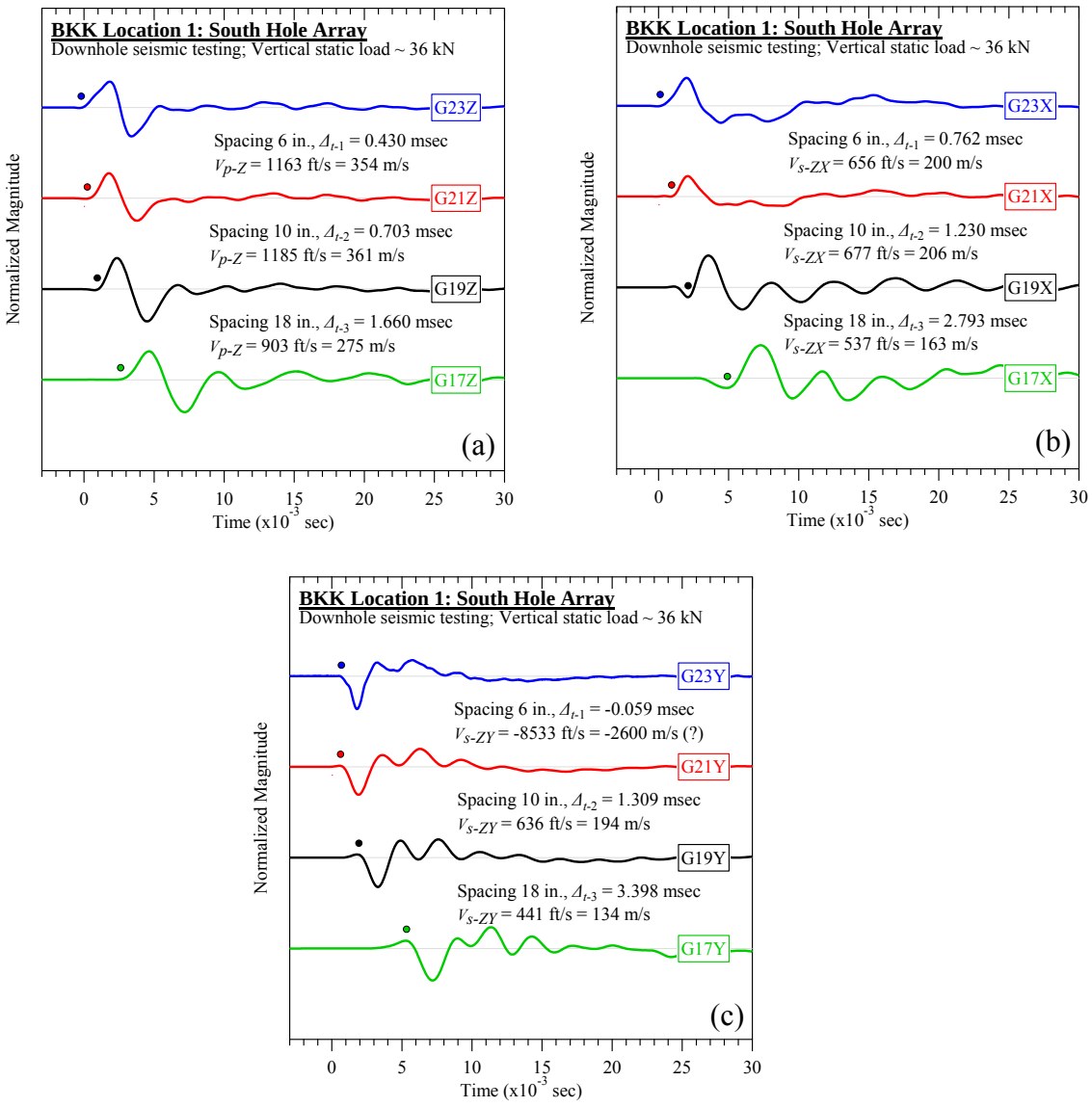

Figure D-10. BKK Landfill #1 (south hole): Downhole seismic testing at vertical load of 36 kN: (a) V_{p-Z}, (b) V_{s-ZX}, and (c) V_{s-ZY}.

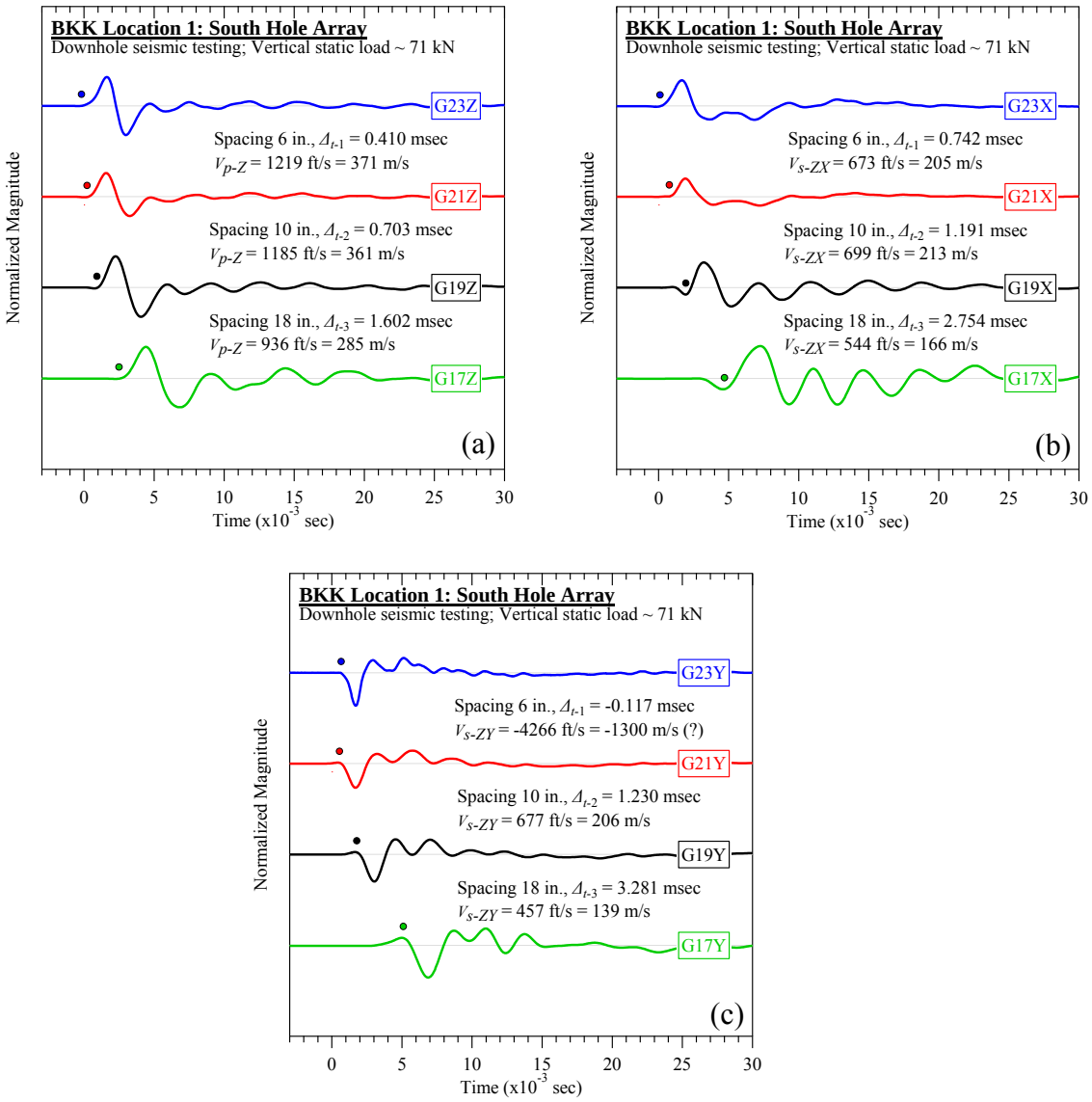

Figure D-11. BKK Landfill #1 (south hole): Downhole seismic testing at vertical load of 71 kN: (a) V_{p-Z}, (b) V_{s-ZX}, and (c) V_{s-ZY}.

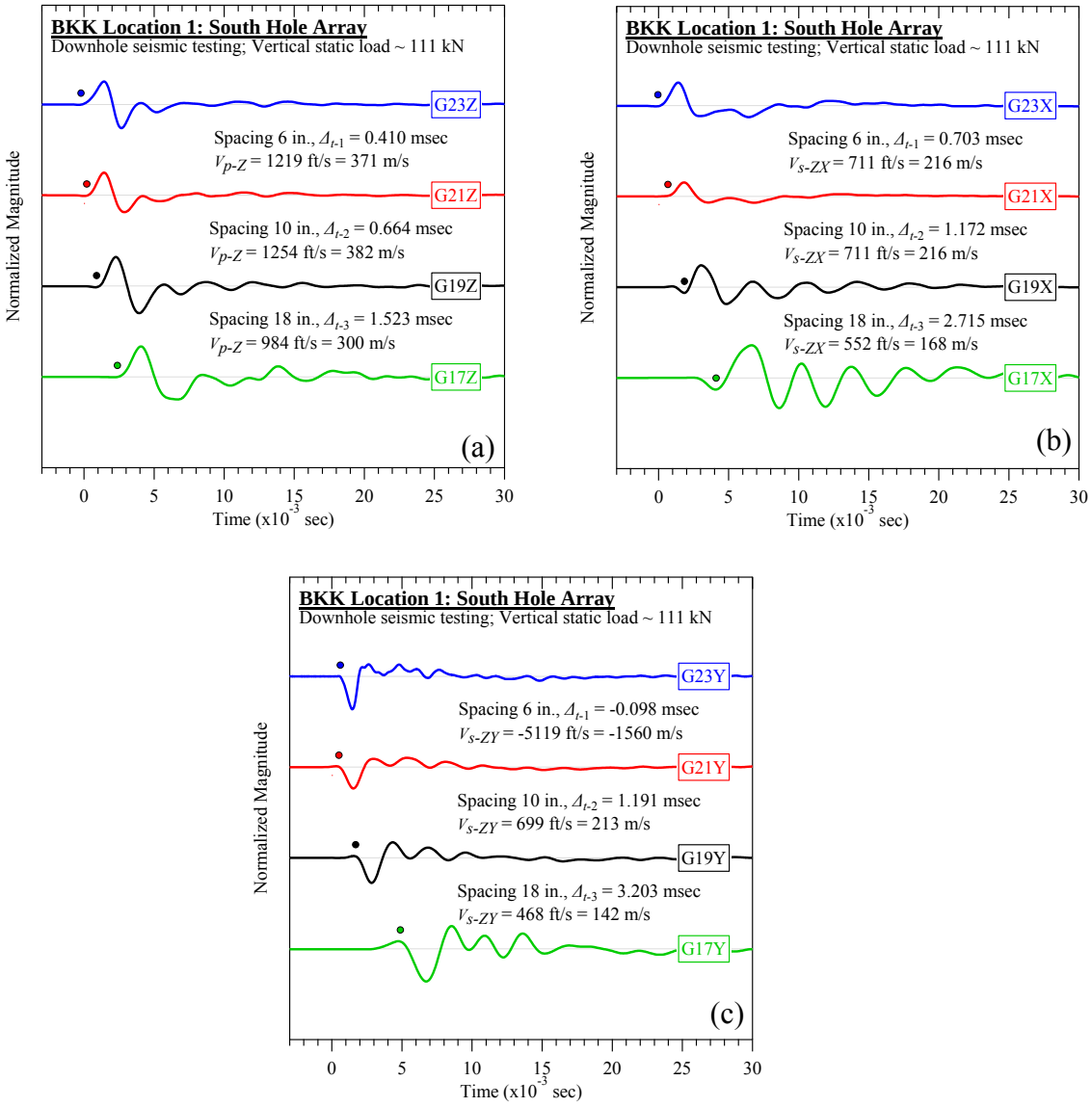

Figure D-12. BKK Landfill #1 (south hole): Downhole seismic testing at vertical load of 111 kN: (a) V_{p-Z}, (b) V_{s-ZX}, and (c) V_{s-ZY}.

D.1.2 Crosshole Seismic Testing

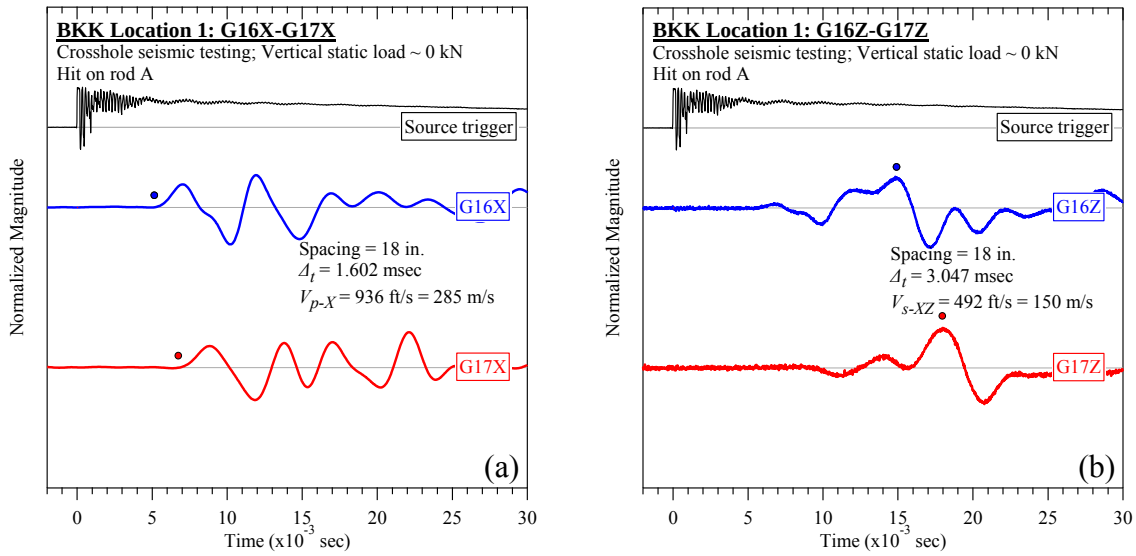

Figure D-13. BKK Landfill #1 (rod A): Crosshole seismic testing at vertical load of 0 kN: (a) $V_{p\text{-}X}$ and (b) $V_{s\text{-}XZ}$.

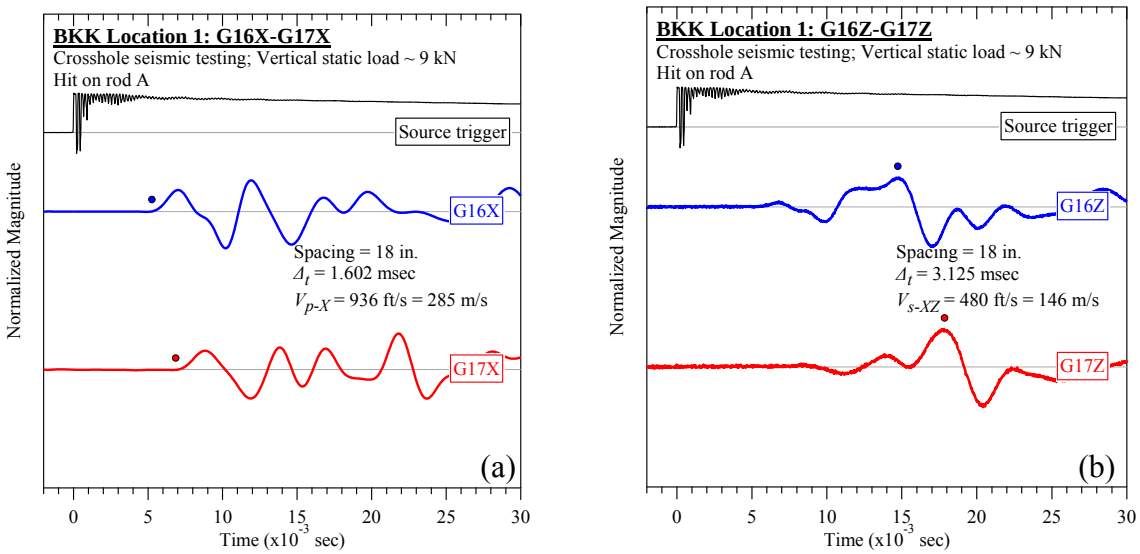

Figure D-14. BKK Landfill #1 (rod A): Crosshole seismic testing at vertical load of 9 kN: (a) $V_{p\text{-}X}$ and (b) $V_{s\text{-}XZ}$.

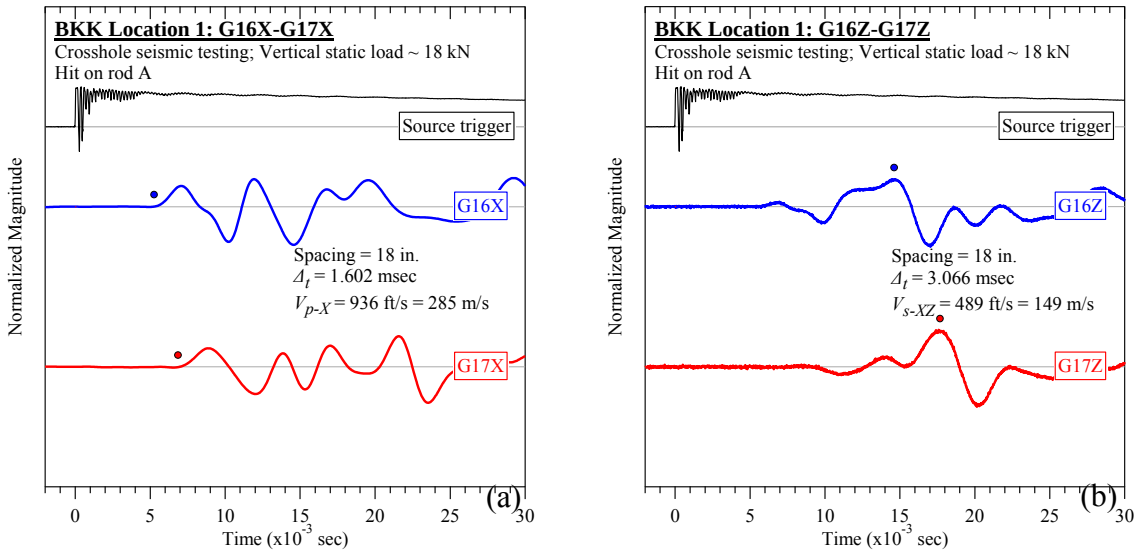

Figure D-15. BKK Landfill #1 (rod A): Crosshole seismic testing at vertical load of 18 kN: (a) $V_{p\text{-}X}$ and (b) $V_{s\text{-}XZ}$.

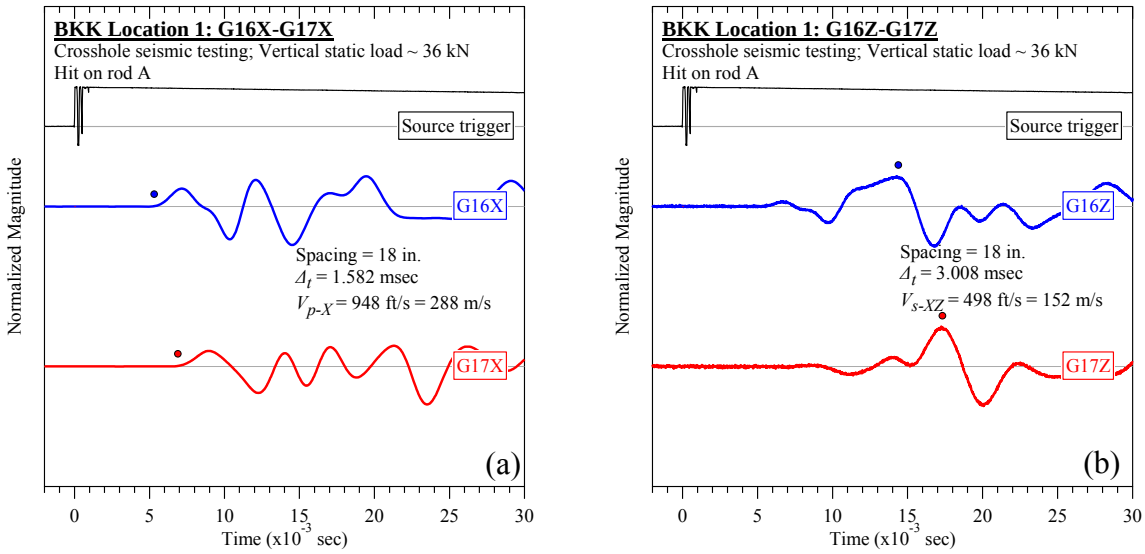

Figure D-16. BKK Landfill #1 (rod A): Crosshole seismic testing at vertical load of 36 kN: (a) $V_{p\text{-}X}$ and (b) $V_{s\text{-}XZ}$.

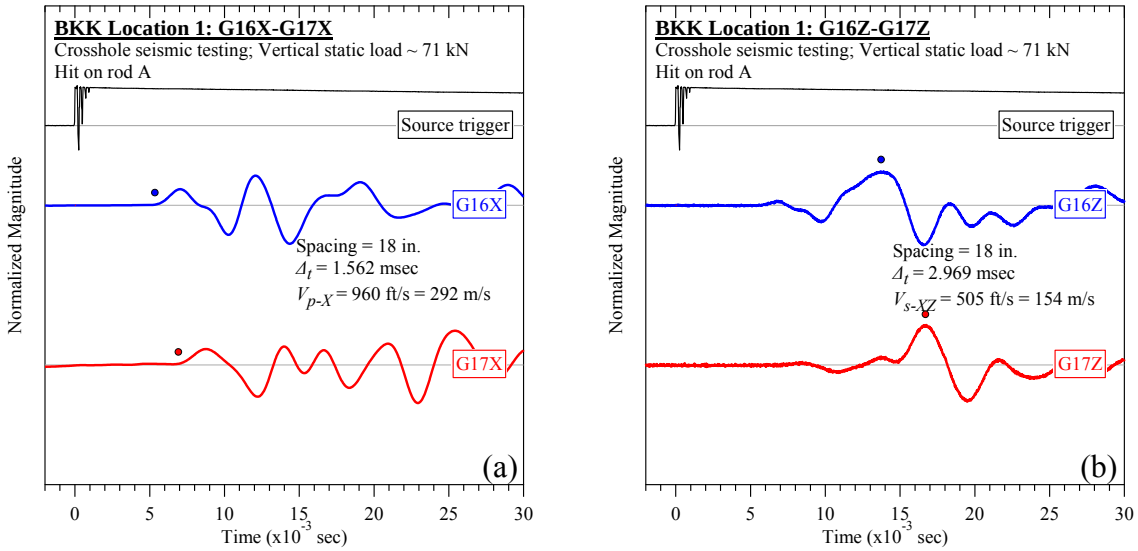

Figure D-17. BKK Landfill #1 (rod A): Crosshole seismic testing at vertical load of 71 kN: (a) $V_{p\text{-}X}$ and (b) $V_{s\text{-}XZ}$.

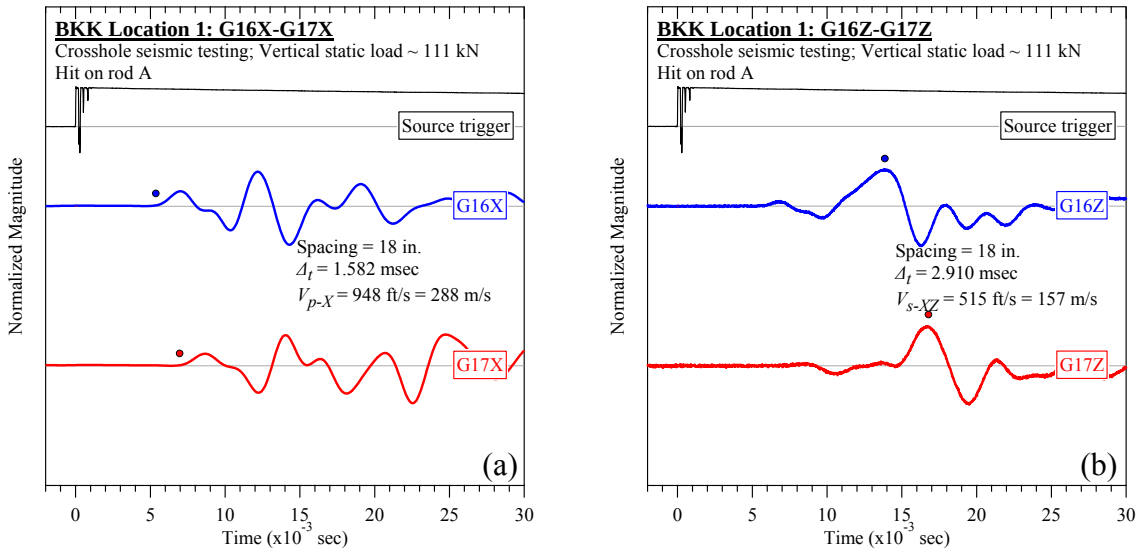

Figure D-18. BKK Landfill #1 (rod A): Crosshole seismic testing at vertical load of 111 kN: (a) $V_{p\text{-}X}$ and (b) $V_{s\text{-}XZ}$.

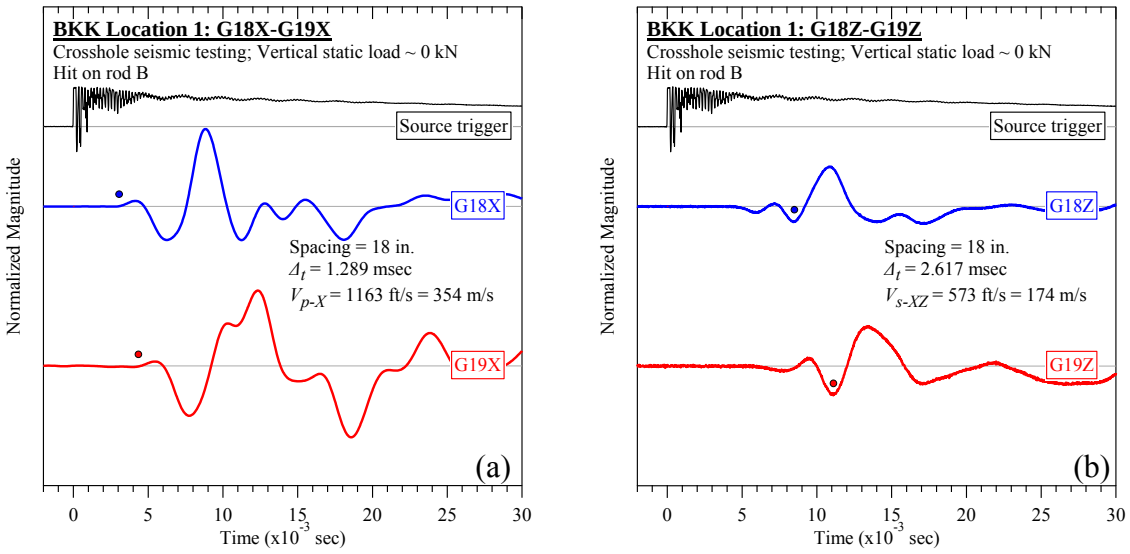

Figure D-19. BKK Landfill #1 (rod B): Crosshole seismic testing at vertical load of 0 kN: (a) $V_{p\text{-}X}$ and (b) $V_{s\text{-}XZ}$.

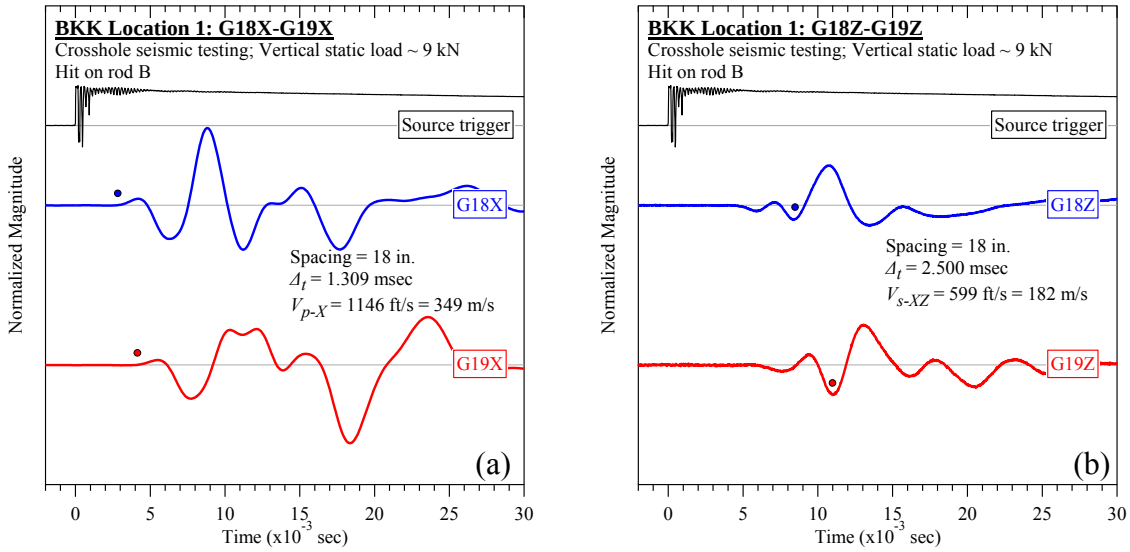

Figure D-20. BKK Landfill #1 (rod B): Crosshole seismic testing at vertical load of 9 kN: (a) $V_{p\text{-}X}$ and (b) $V_{s\text{-}XZ}$.

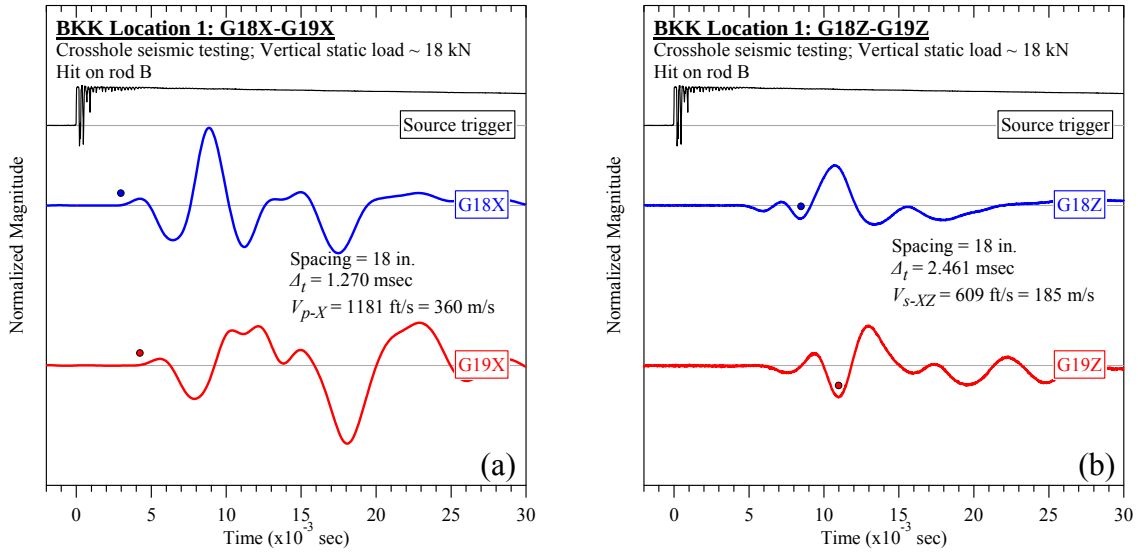

Figure D-21. BKK Landfill #1 (rod B): Crosshole seismic testing at vertical load of 18 kN: (a) $V_{p\text{-}X}$ and (b) $V_{s\text{-}XZ}$.

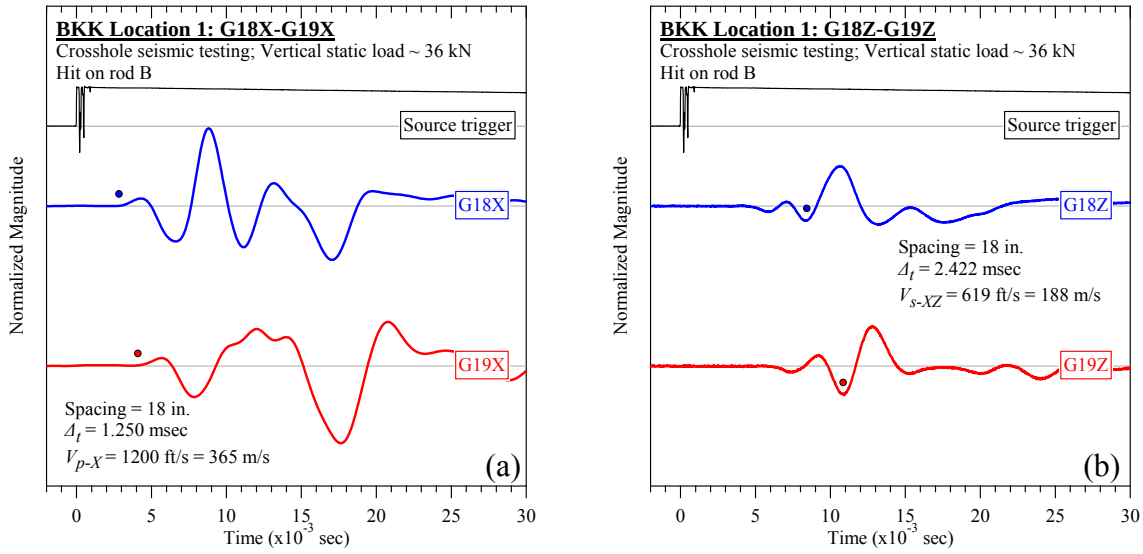

Figure D-22. BKK Landfill #1 (rod B): Crosshole seismic testing at vertical load of 36 kN: (a) $V_{p\text{-}X}$ and (b) $V_{s\text{-}XZ}$.

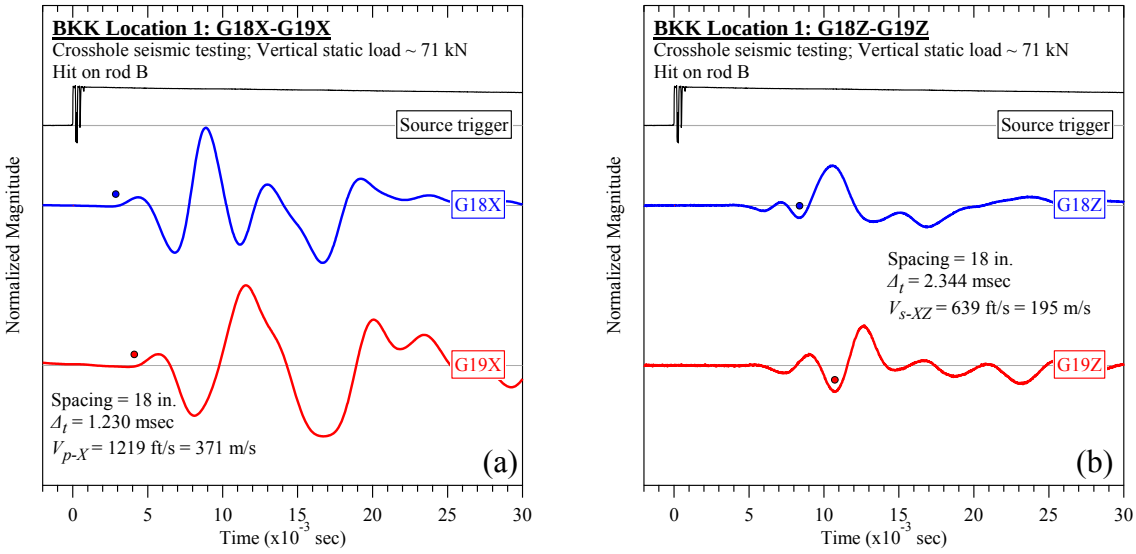

Figure D-23. BKK Landfill #1 (rod B): Crosshole seismic testing at vertical load of 71 kN: (a) $V_{p\text{-}X}$ and (b) $V_{s\text{-}XZ}$.

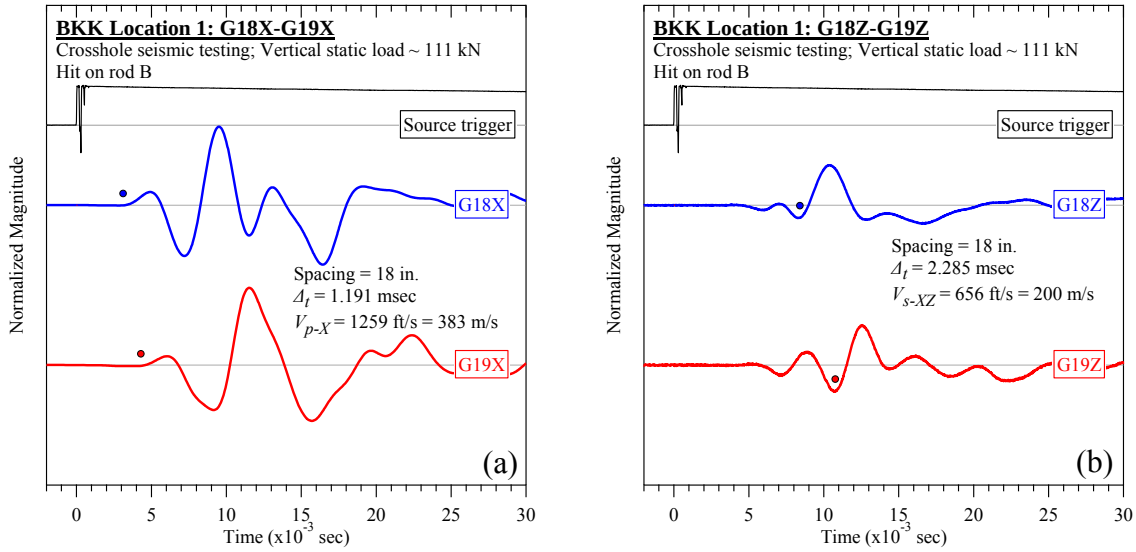

Figure D-24. BKK Landfill #1 (rod B): Crosshole seismic testing at vertical load of 111 kN: (a) $V_{p\text{-}X}$ and (b) $V_{s\text{-}XZ}$.

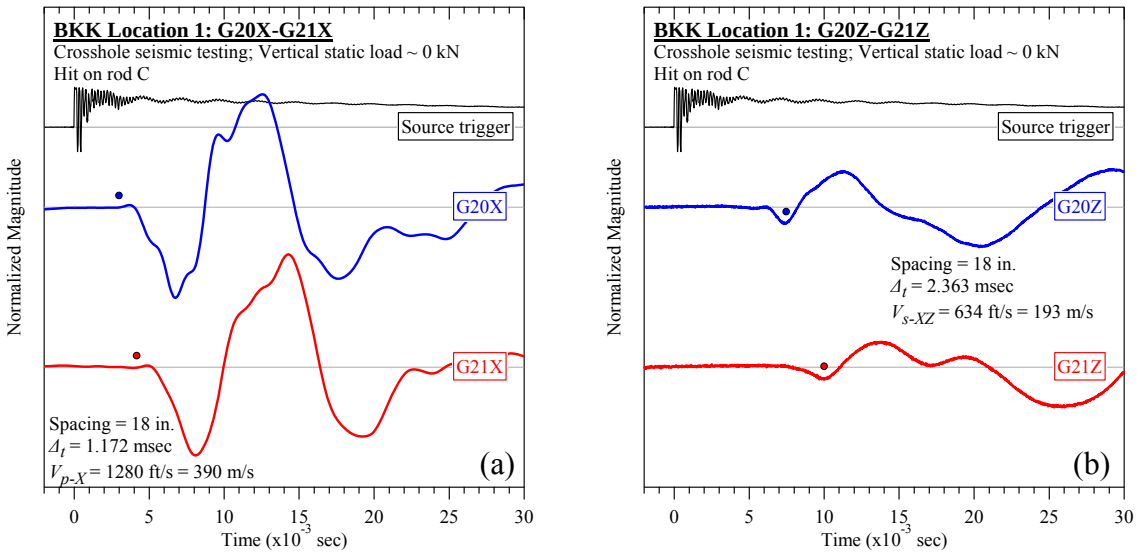

Figure D-25. BKK Landfill #1 (rod C): Crosshole seismic testing at vertical load of 0 kN: (a) $V_{p\text{-}X}$ and (b) $V_{s\text{-}XZ}$.

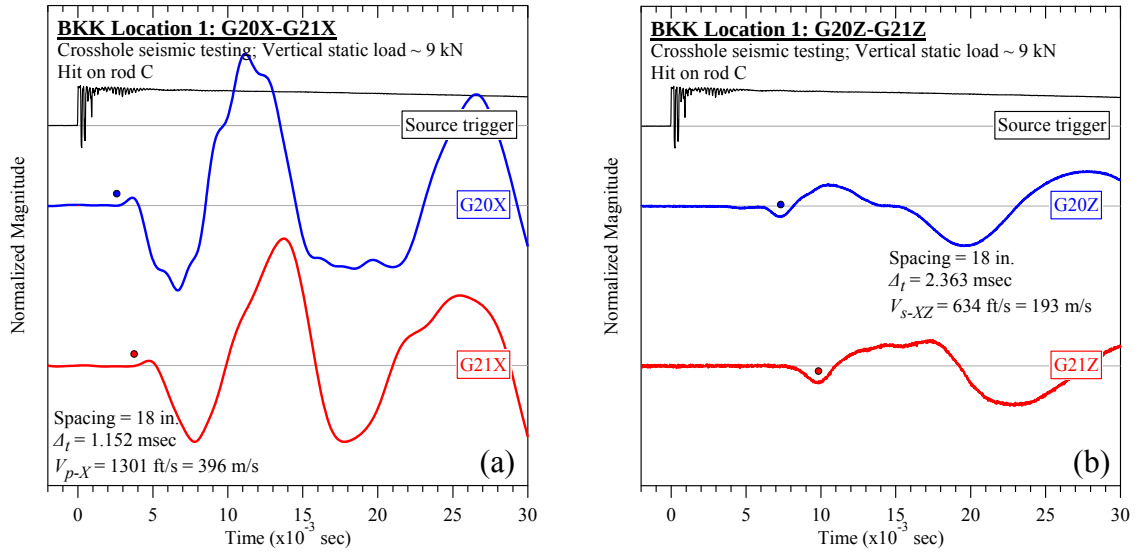

Figure D-26. BKK Landfill #1 (rod C): Crosshole seismic testing at vertical load of 9 kN: (a) $V_{p\text{-}X}$ and (b) $V_{s\text{-}XZ}$.

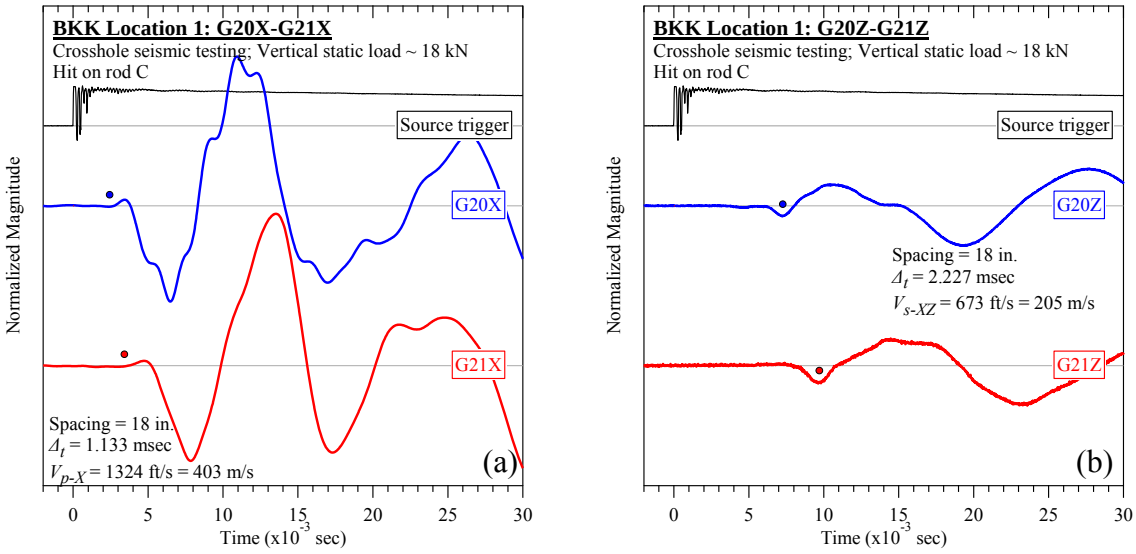

Figure D-27. BKK Landfill #1 (rod C): Crosshole seismic testing at vertical load of 18 kN: (a) $V_{p\text{-}X}$ and (b) $V_{s\text{-}XZ}$.

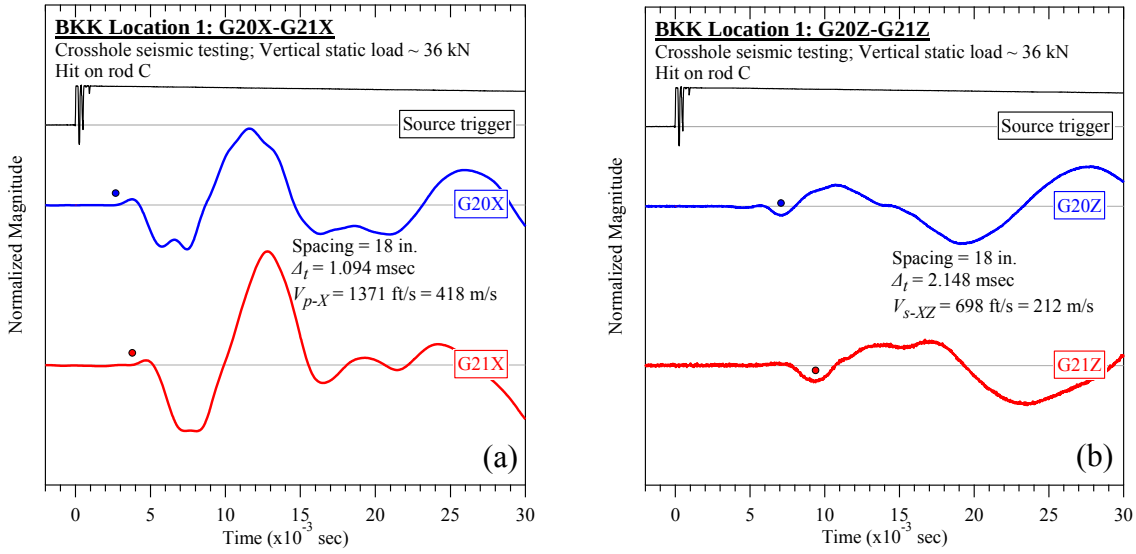

Figure D-28. BKK Landfill #1 (rod C): Crosshole seismic testing at vertical load of 36 kN: (a) $V_{p\text{-}X}$ and (b) $V_{s\text{-}XZ}$.

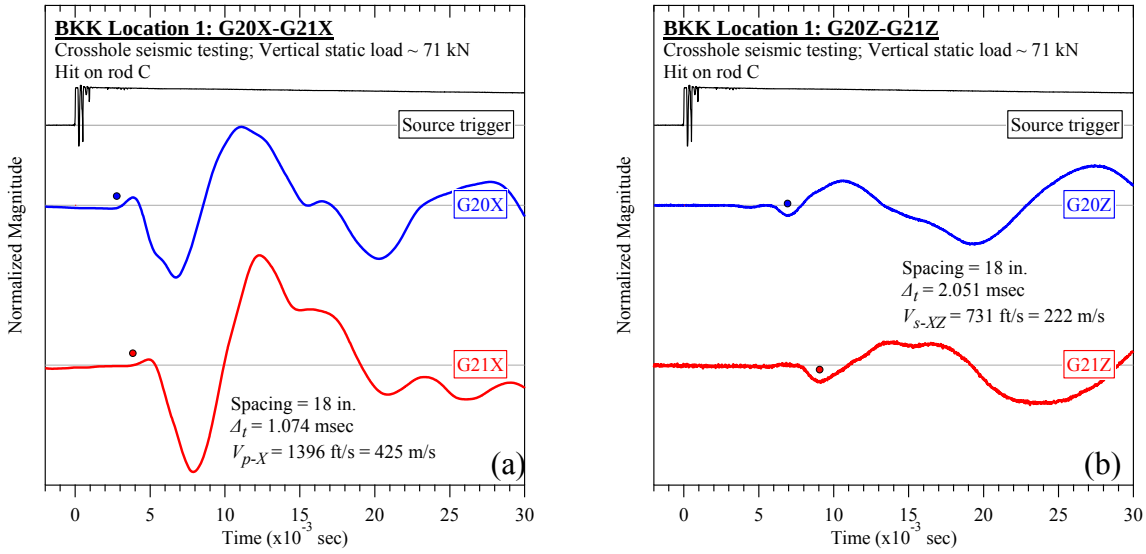

Figure D-29. BKK Landfill #1 (rod C): Crosshole seismic testing at vertical load of 71 kN: (a) $V_{p\text{-}X}$ and (b) $V_{s\text{-}XZ}$.

D.1.3 Steady-state Dynamic Testing

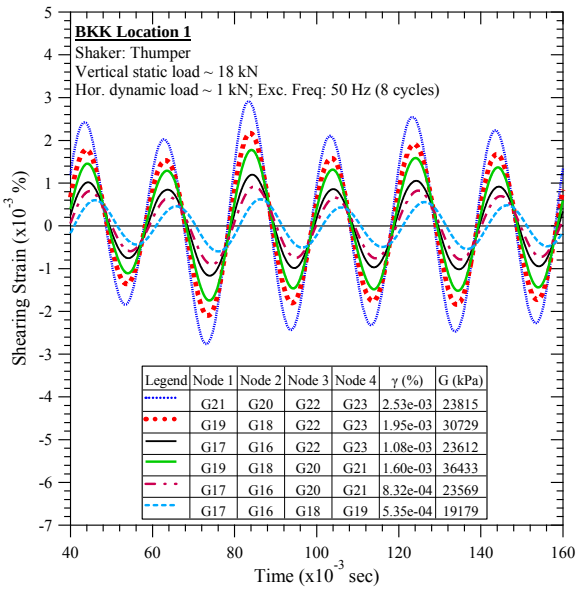

Figure D-30. BKK Landfill #1: Steady-state dynamic testing at vertical load of 18 kN and horizontal dynamic load of 1 kN.

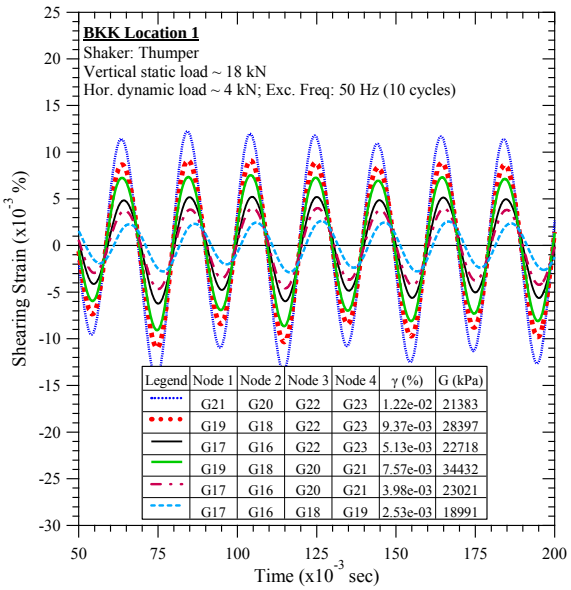

Figure D-31. BKK Landfill #1: Steady-state dynamic testing at vertical load of 18 kN and horizontal dynamic load of 4 kN.

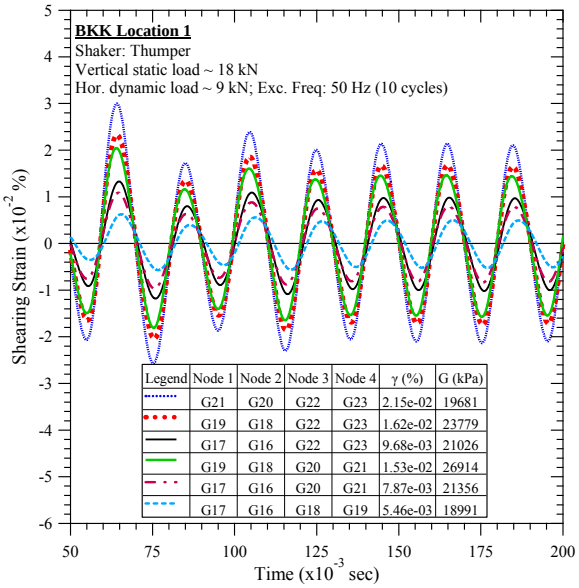

Figure D-32. BKK Landfill #1: Steady-state dynamic testing at vertical load of 18 kN and horizontal dynamic load of 9 kN.

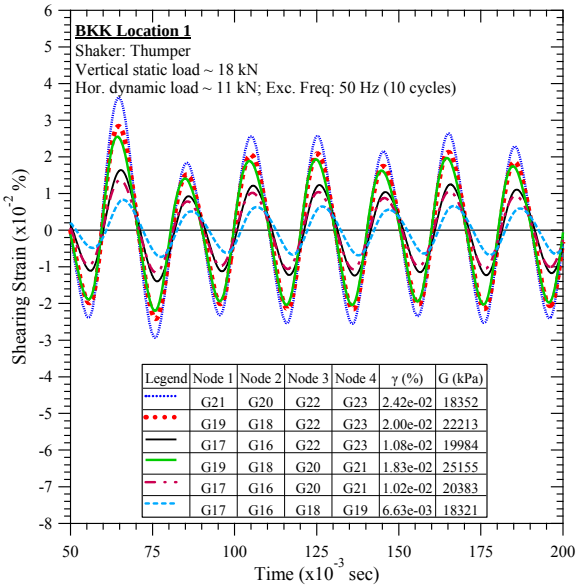

Figure D-33. BKK Landfill #1: Steady-state dynamic testing at vertical load of 18 kN and horizontal dynamic load of 11 kN.

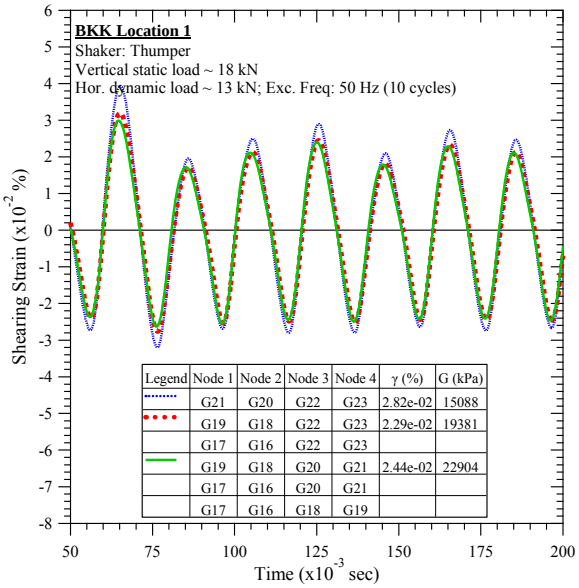

Figure D-34. BKK Landfill #1: Steady-state dynamic testing at vertical load of 18 kN and horizontal dynamic load of 13 kN.

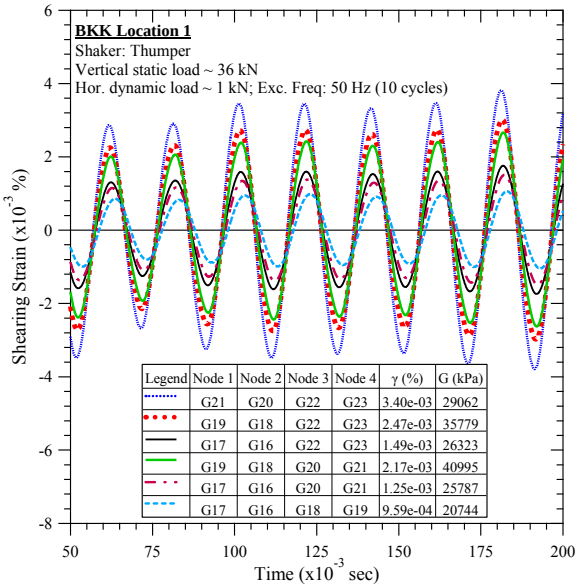

Figure D-35. BKK Landfill #1: Steady-state dynamic testing at vertical load of 36 kN and horizontal dynamic load of 1 kN.

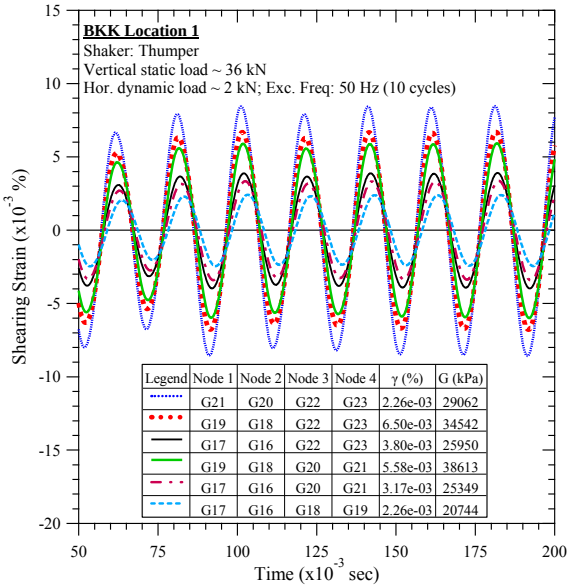

Figure D-36. BKK Landfill #1: Steady-state dynamic testing at vertical load of 36 kN and horizontal dynamic load of 2 kN.

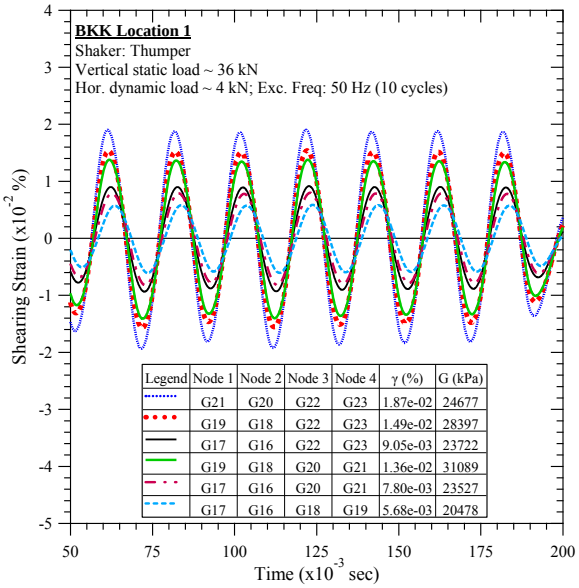

Figure D-37. BKK Landfill #1: Steady-state dynamic testing at vertical load of 36 kN and horizontal dynamic load of 4 kN.

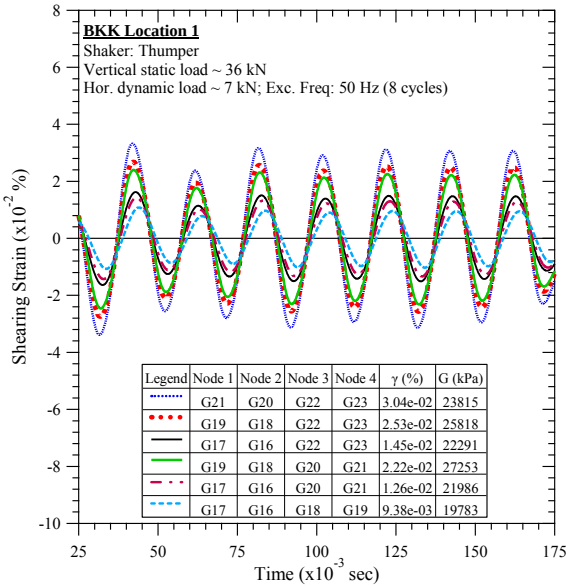

Figure D-38. BKK Landfill #1: Steady-state dynamic testing at vertical load of 36 kN and horizontal dynamic load of 7 kN.

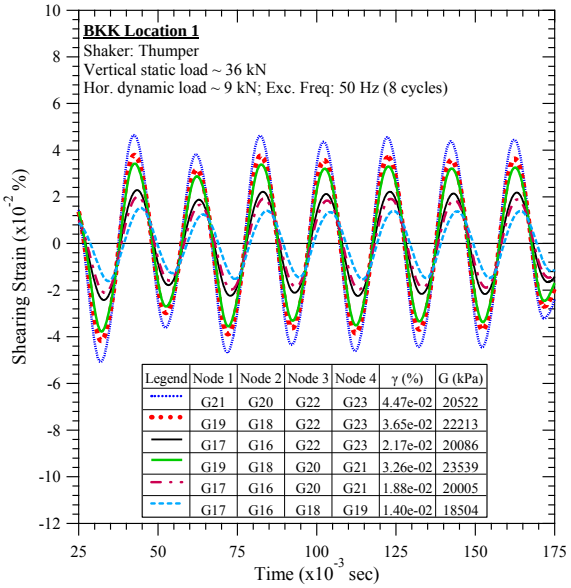

Figure D-39. BKK Landfill #1: Steady-state dynamic testing at vertical load of 36 kN and horizontal dynamic load of 9 kN.

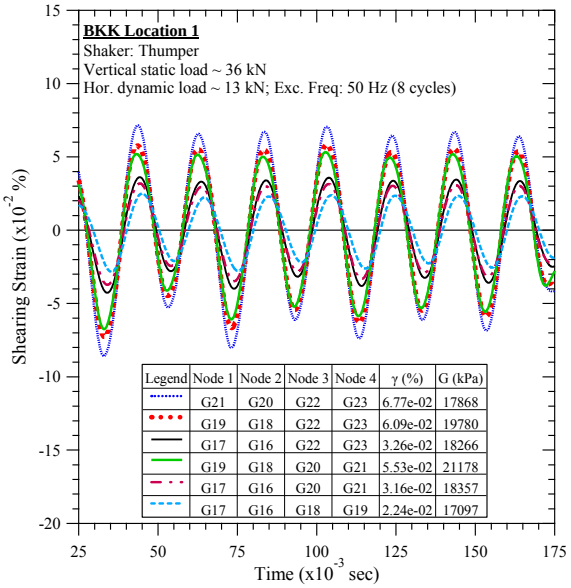

Figure D-40. BKK Landfill #1: Steady-state dynamic testing at vertical load of 36 kN and horizontal dynamic load of 13 kN.

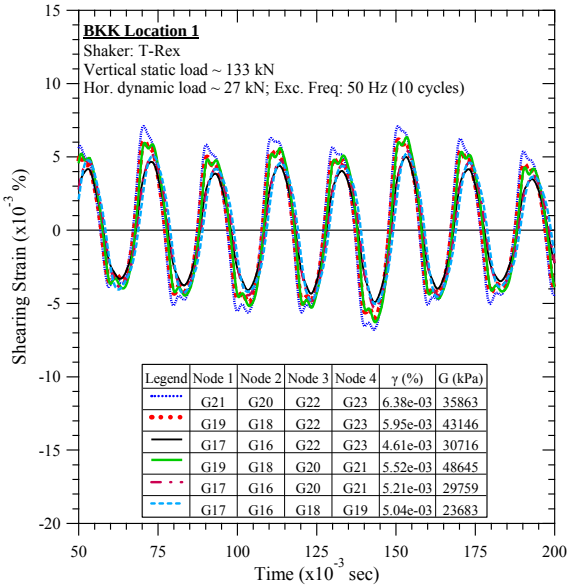

Figure D-41. BKK Landfill #1: Steady-state dynamic testing at vertical load of 133 kN and horizontal dynamic load of 27 kN.

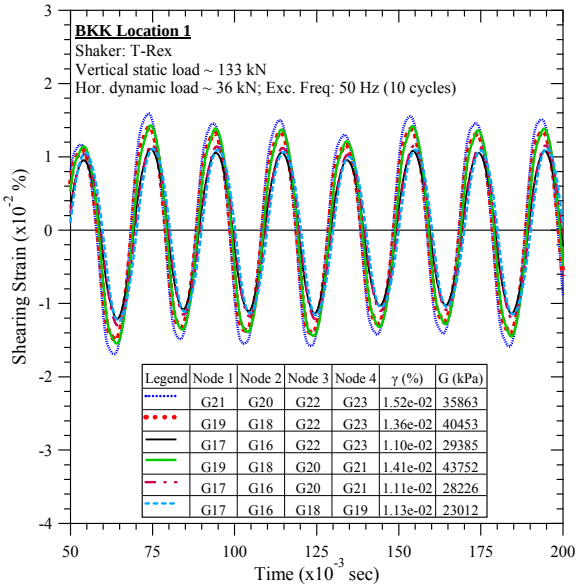

Figure D-42. BKK Landfill #1: Steady-state dynamic testing at vertical load of 133 kN and horizontal dynamic load of 36 kN.

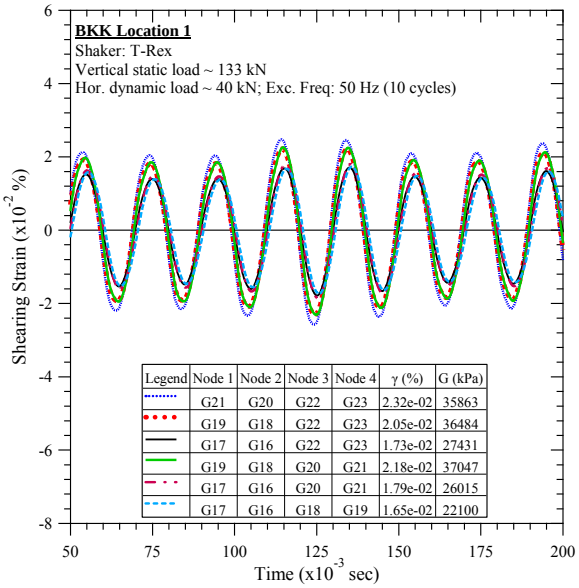

Figure D-43. BKK Landfill #1: Steady-state dynamic testing at vertical load of 133 kN and horizontal dynamic load of 40 kN.

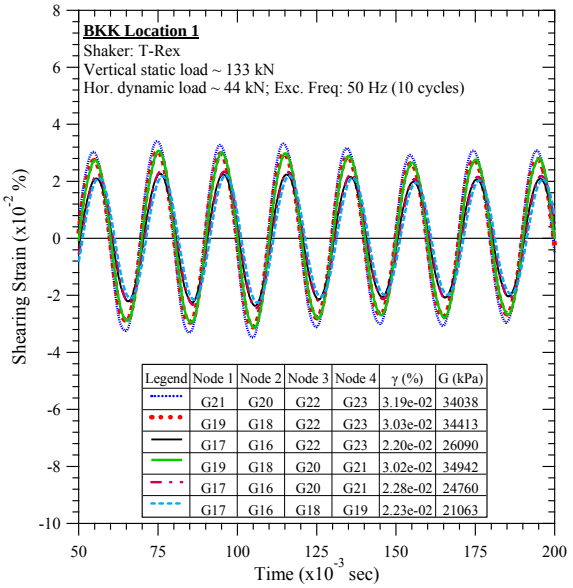

Figure D-44. BKK Landfill #1: Steady-state dynamic testing at vertical load of 133 kN and horizontal dynamic load of 44 kN.

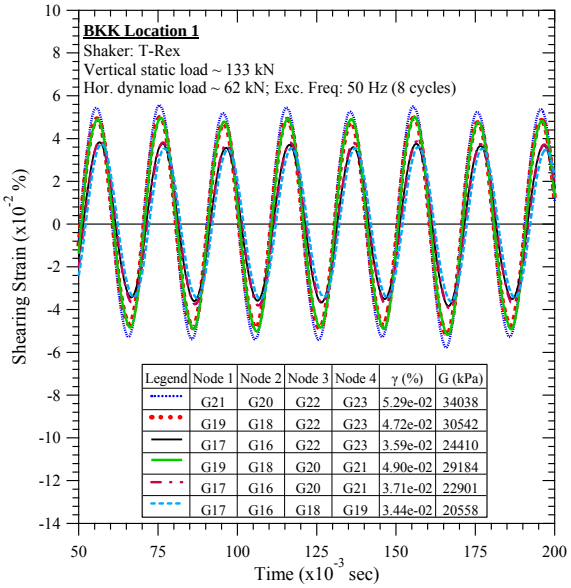

Figure D-45. BKK Landfill #1: Steady-state dynamic testing at vertical load of 133 kN and horizontal dynamic load of 62 kN.

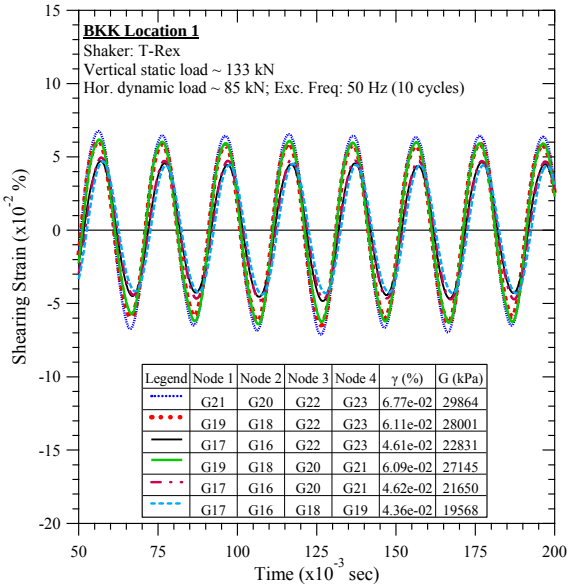

Figure D-46. BKK Landfill #1: Steady-state dynamic testing at vertical load of 133 kN and horizontal dynamic load of 85 kN.

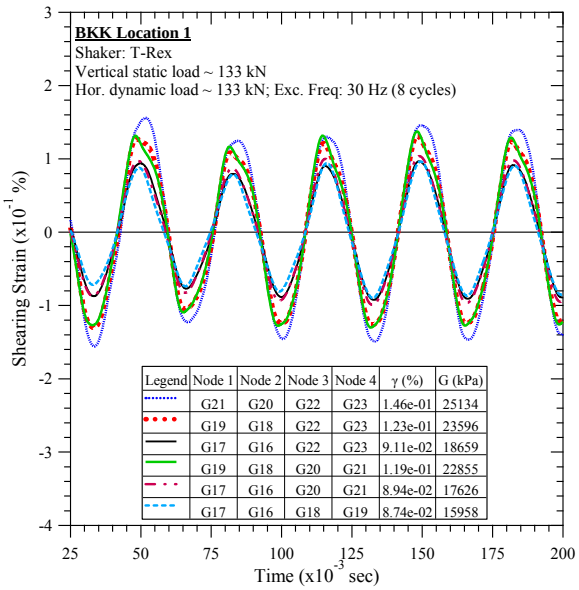

Figure D-47. BKK Landfill #1: Steady-state dynamic testing at vertical load of 133 kN and horizontal dynamic load of 133 kN.

D.2 BKK Landfill Location 2

D.2.1 Downhole Seismic Testing

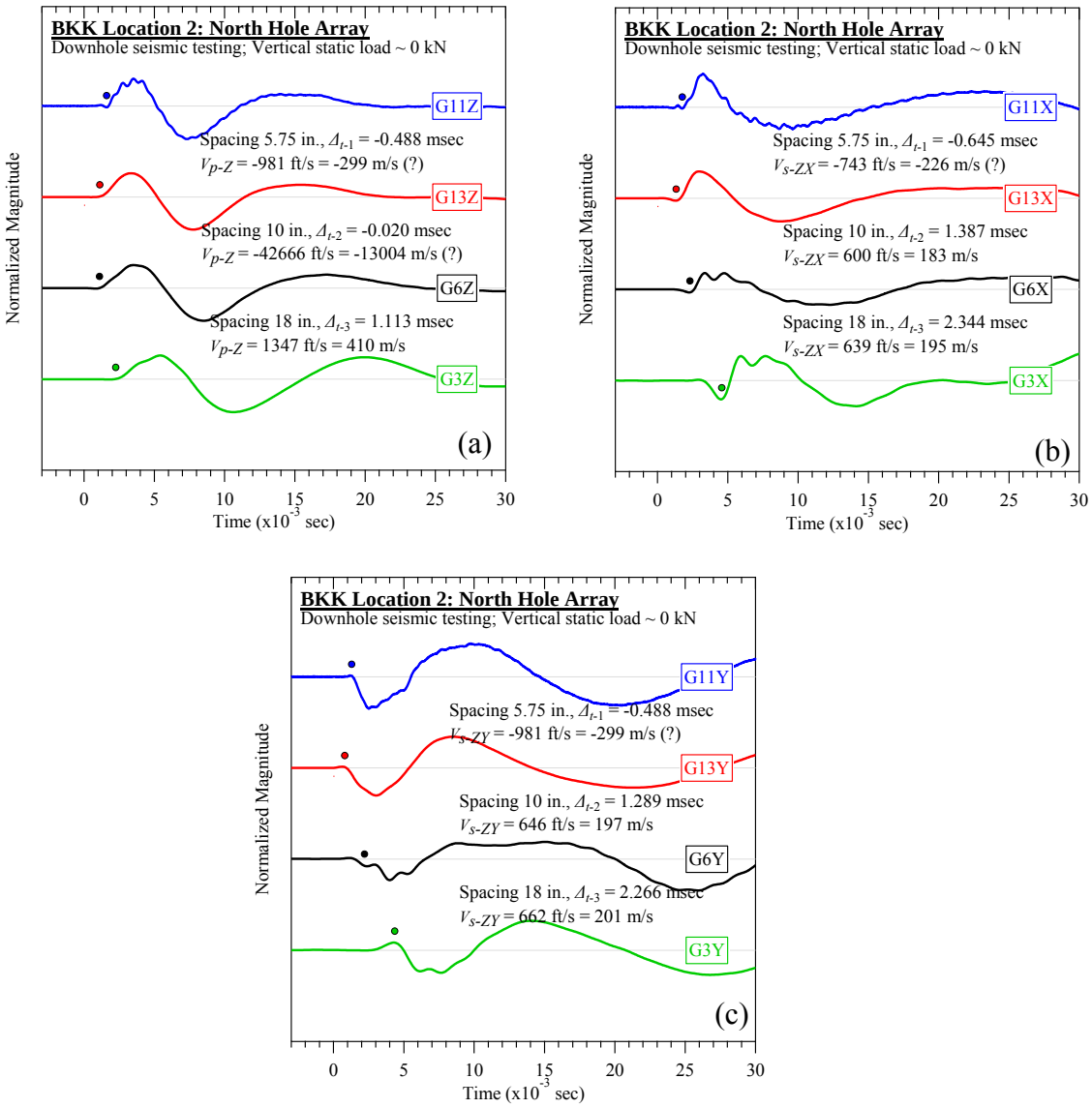

Figure D-48. BKK Landfill #2 (north hole): Downhole seismic testing at vertical load of 0 kN: (a) $V_{p\text{-}Z}$, (b) $V_{s\text{-}ZX}$, and (c) $V_{s\text{-}ZY}$.

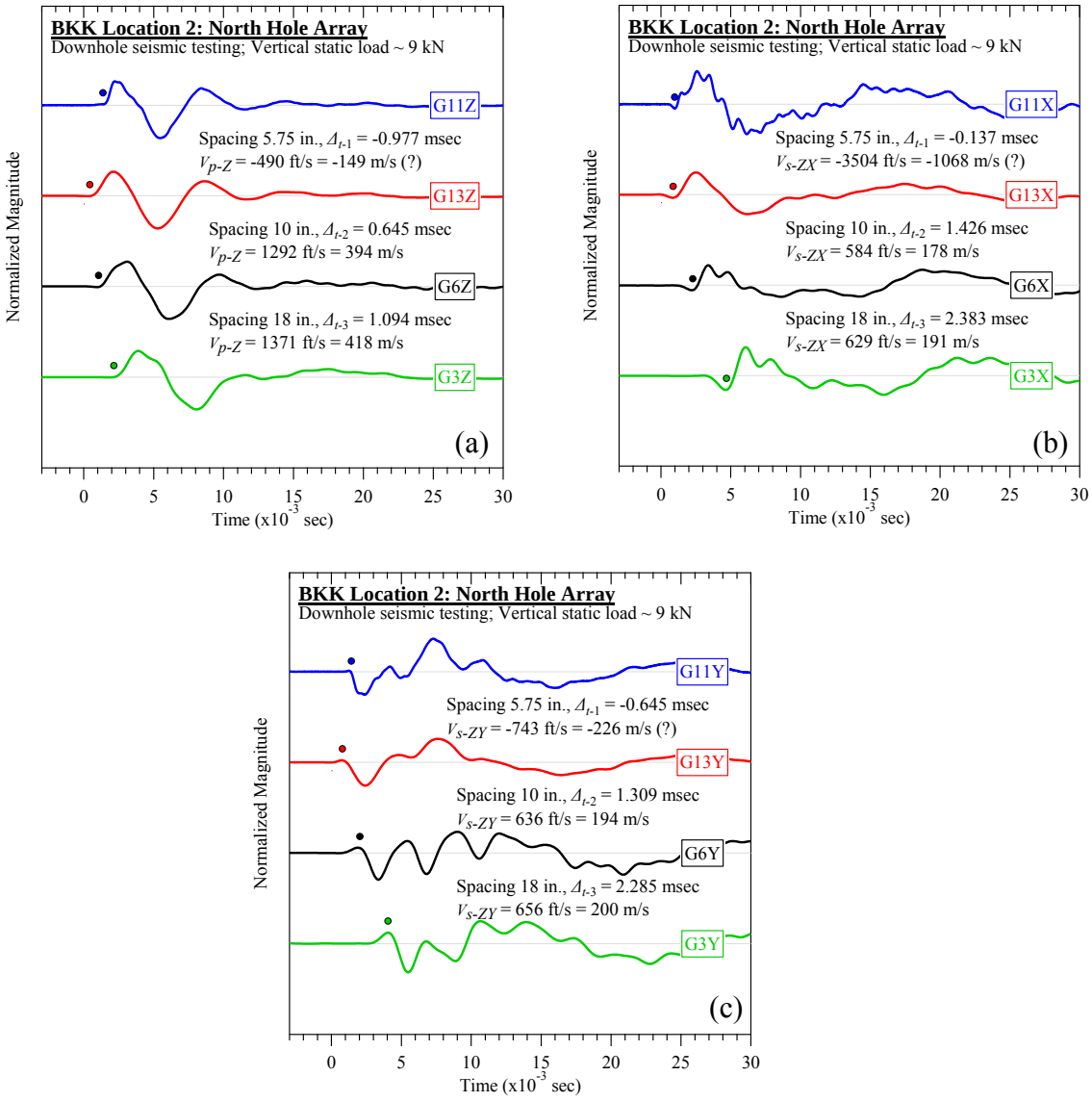

Figure D-49. BKK Landfill #2 (north hole): Downhole seismic testing at vertical load of 9 kN: (a) V_{p-Z}, (b) V_{s-ZX}, and (c) V_{s-ZY}.

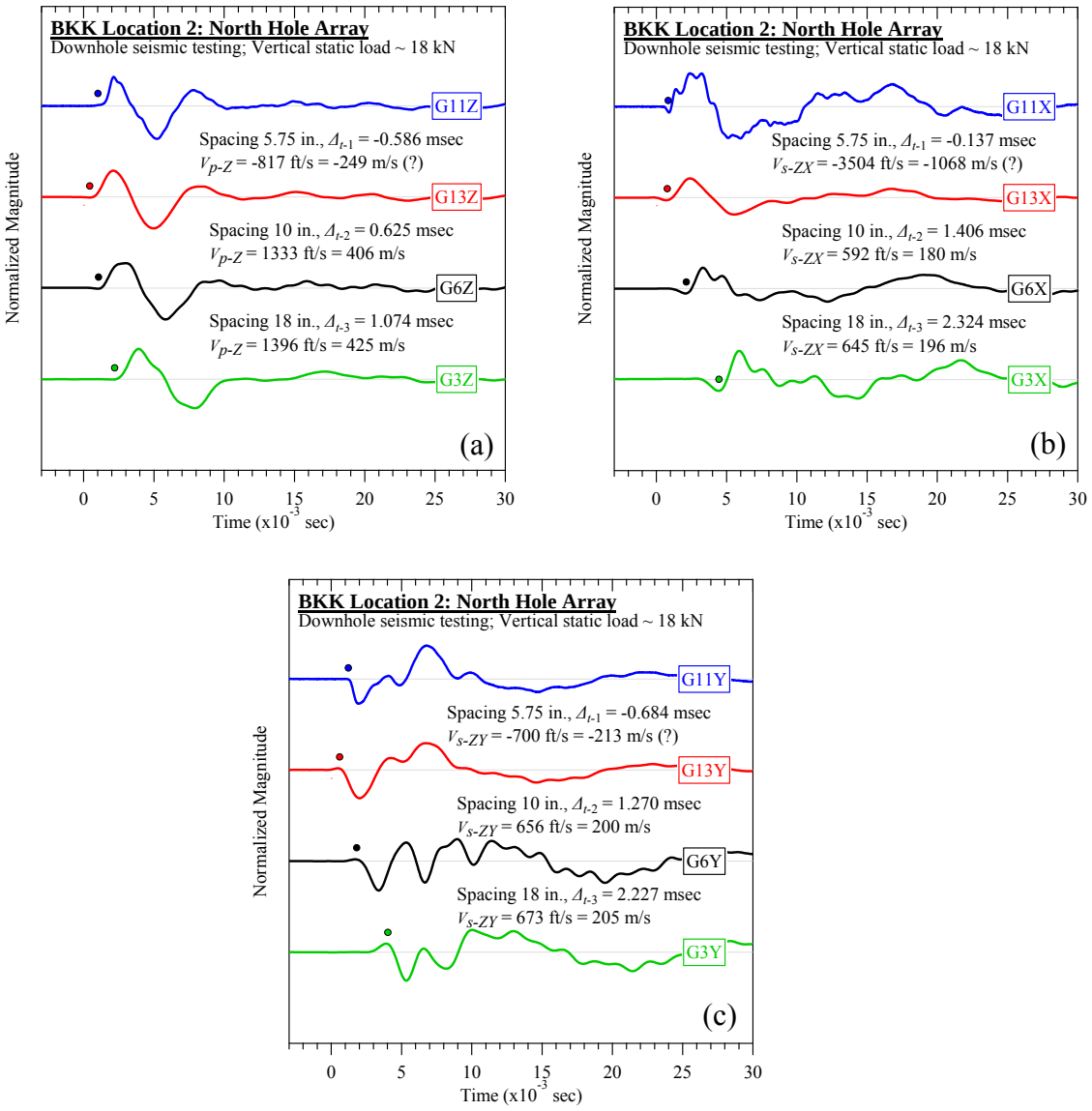

Figure D-50. BKK Landfill #2 (north hole): Downhole seismic testing at vertical load of 18 kN: (a) $V_{p\text{-}Z}$, (b) $V_{s\text{-}ZX}$, and (c) $V_{s\text{-}ZY}$.

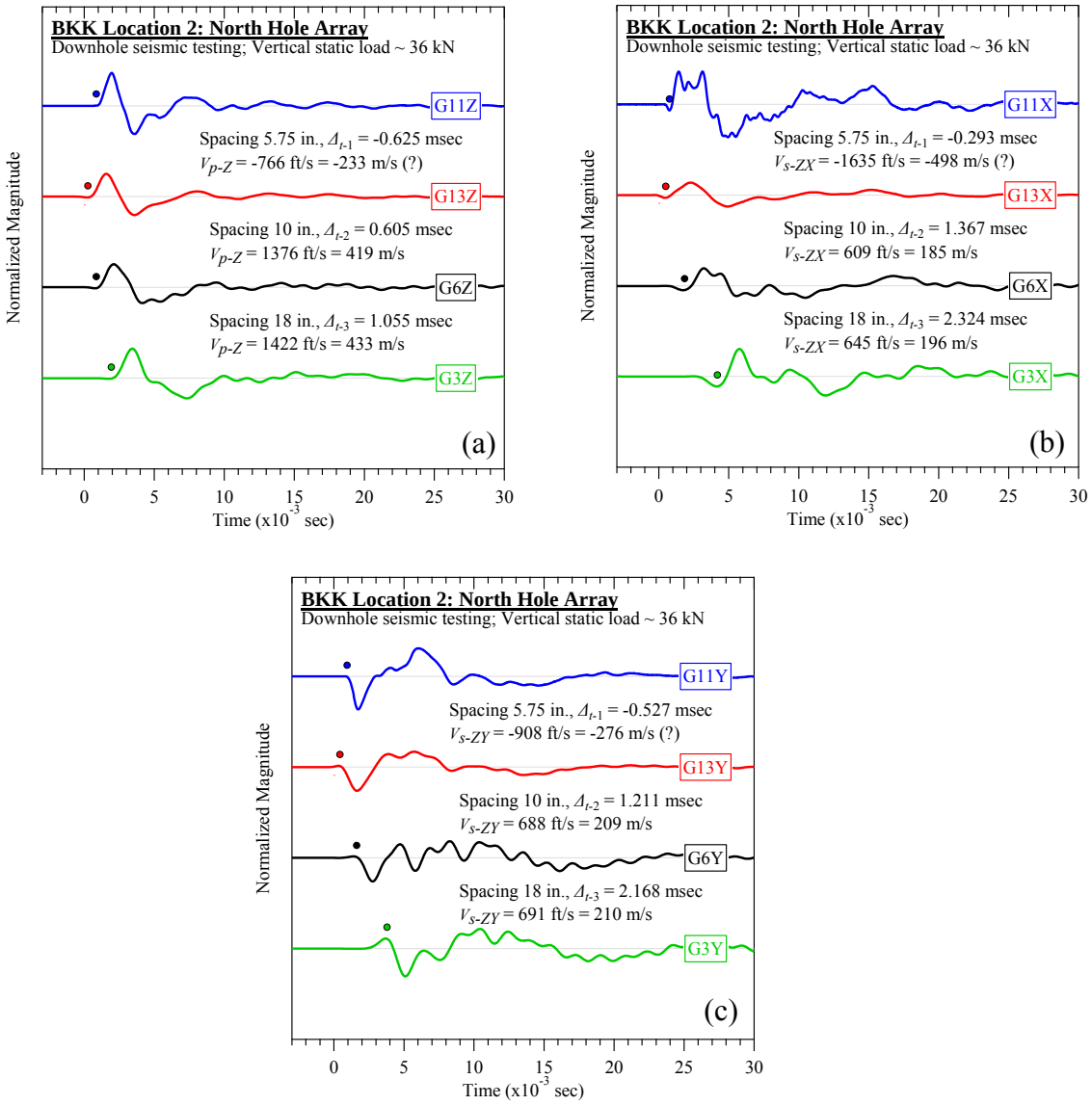

Figure D-51. BKK Landfill #2 (north hole): Downhole seismic testing at vertical load of 36 kN: (a) $V_{p\text{-}Z}$, (b) $V_{s\text{-}ZX}$, and (c) $V_{s\text{-}ZY}$.

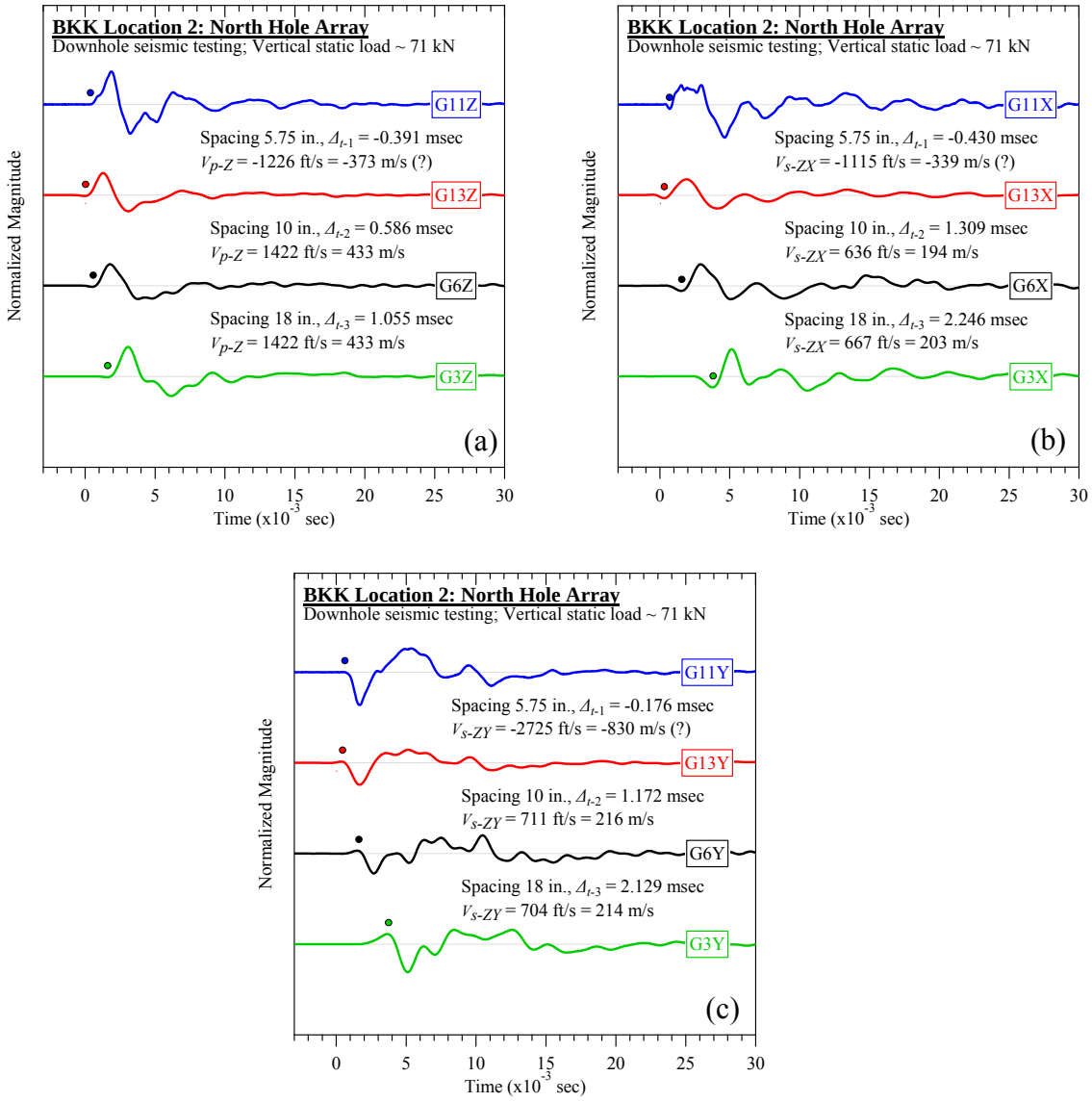

Figure D-52. BKK Landfill #2 (north hole): Downhole seismic testing at vertical load of 71 kN: (a) V_{p-Z}, (b) V_{s-ZX}, and (c) V_{s-ZY}.

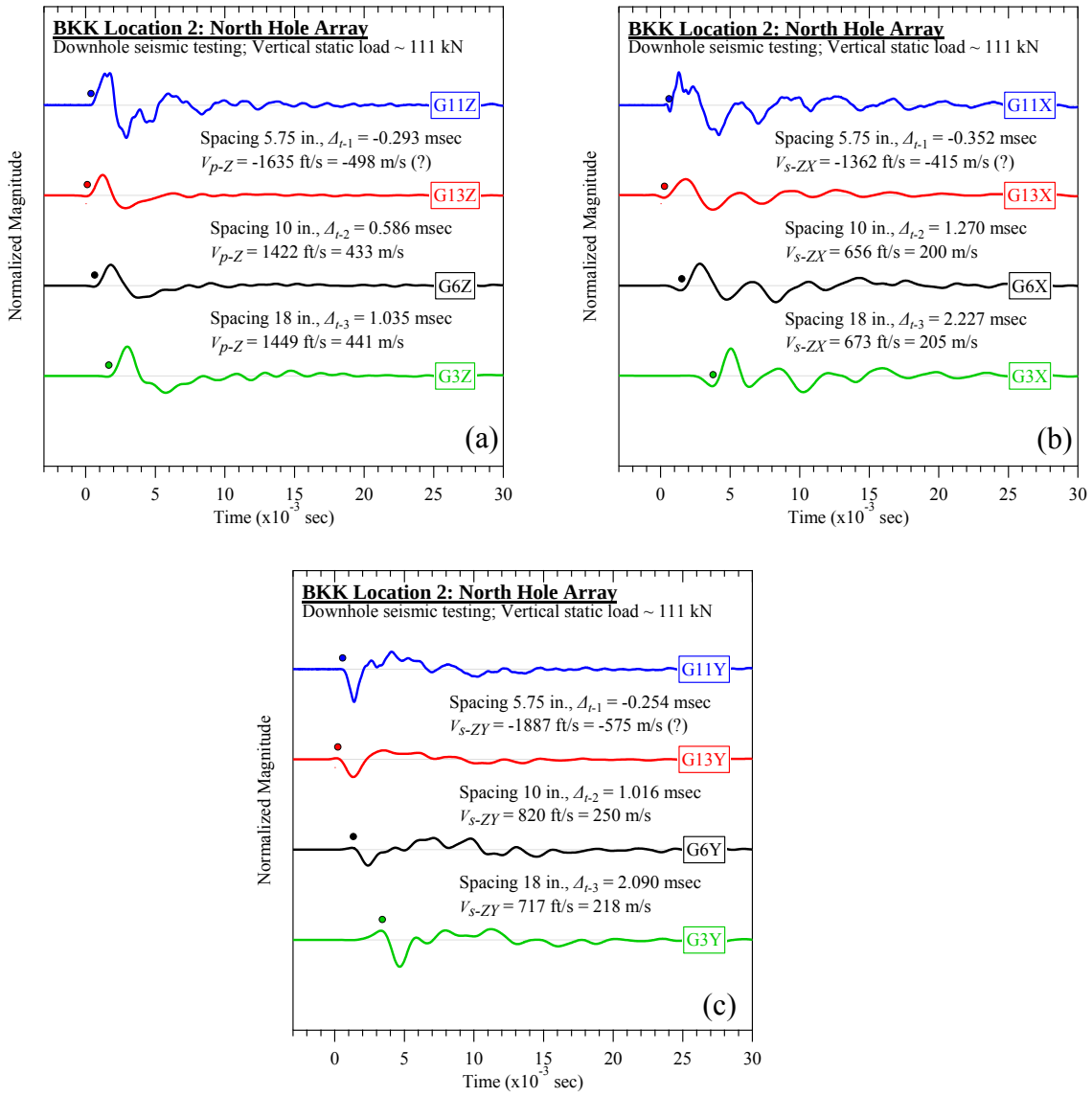

Figure D-53. BKK Landfill #2 (north hole): Downhole seismic testing at vertical load of 111 kN: (a) V_{p-Z}, (b) V_{s-ZX}, and (c) V_{s-ZY}.

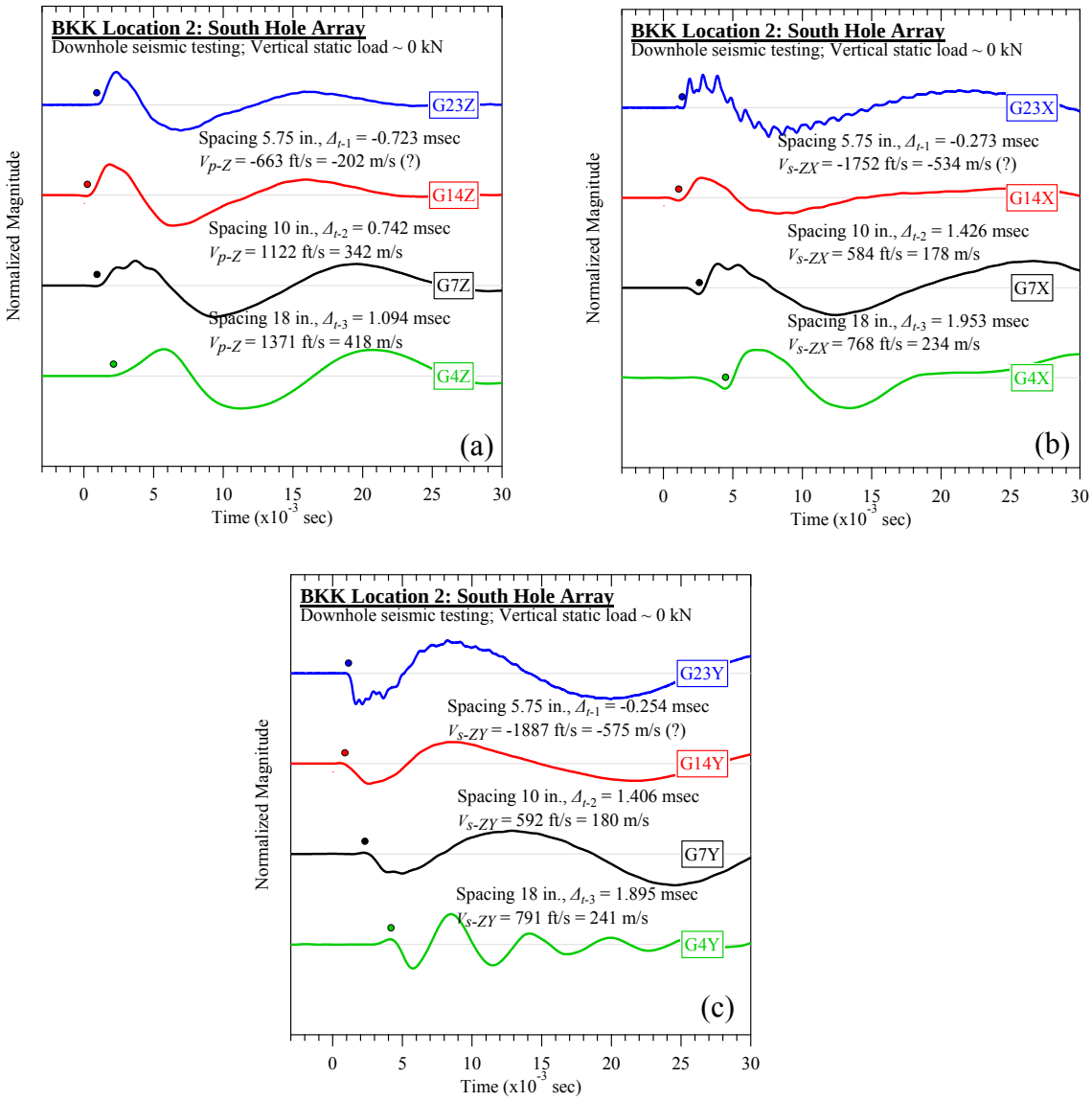

Figure D-54. BKK Landfill #2 (south hole): Downhole seismic testing at vertical load of 0 kN: (a) V_{p-Z}, (b) V_{s-ZX}, and (c) V_{s-ZY}.

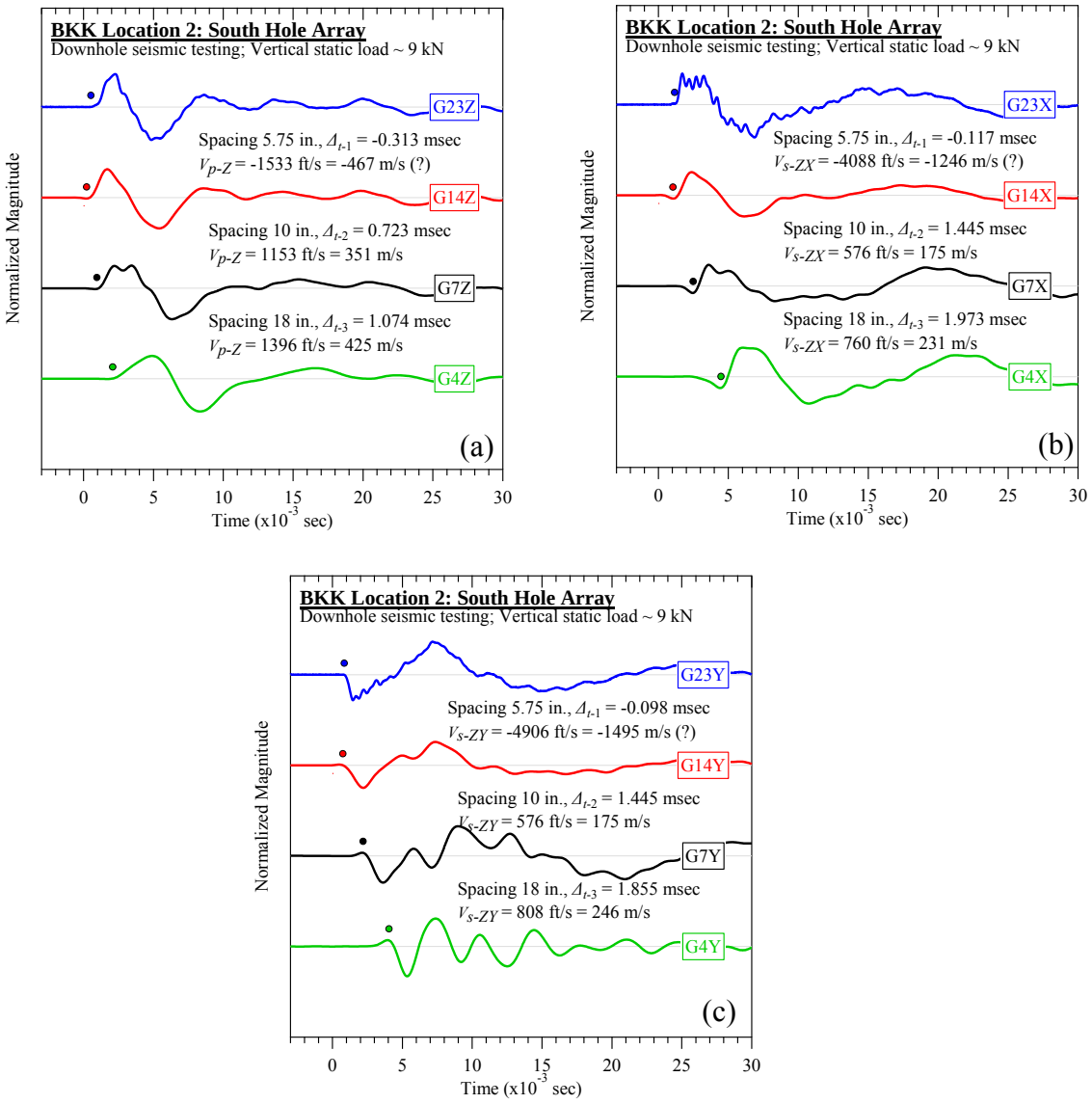

Figure D-55. BKK Landfill #2 (south hole): Downhole seismic testing at vertical load of 9 kN: (a) V_{p-Z}, (b) V_{s-ZX}, and (c) V_{s-ZY}.

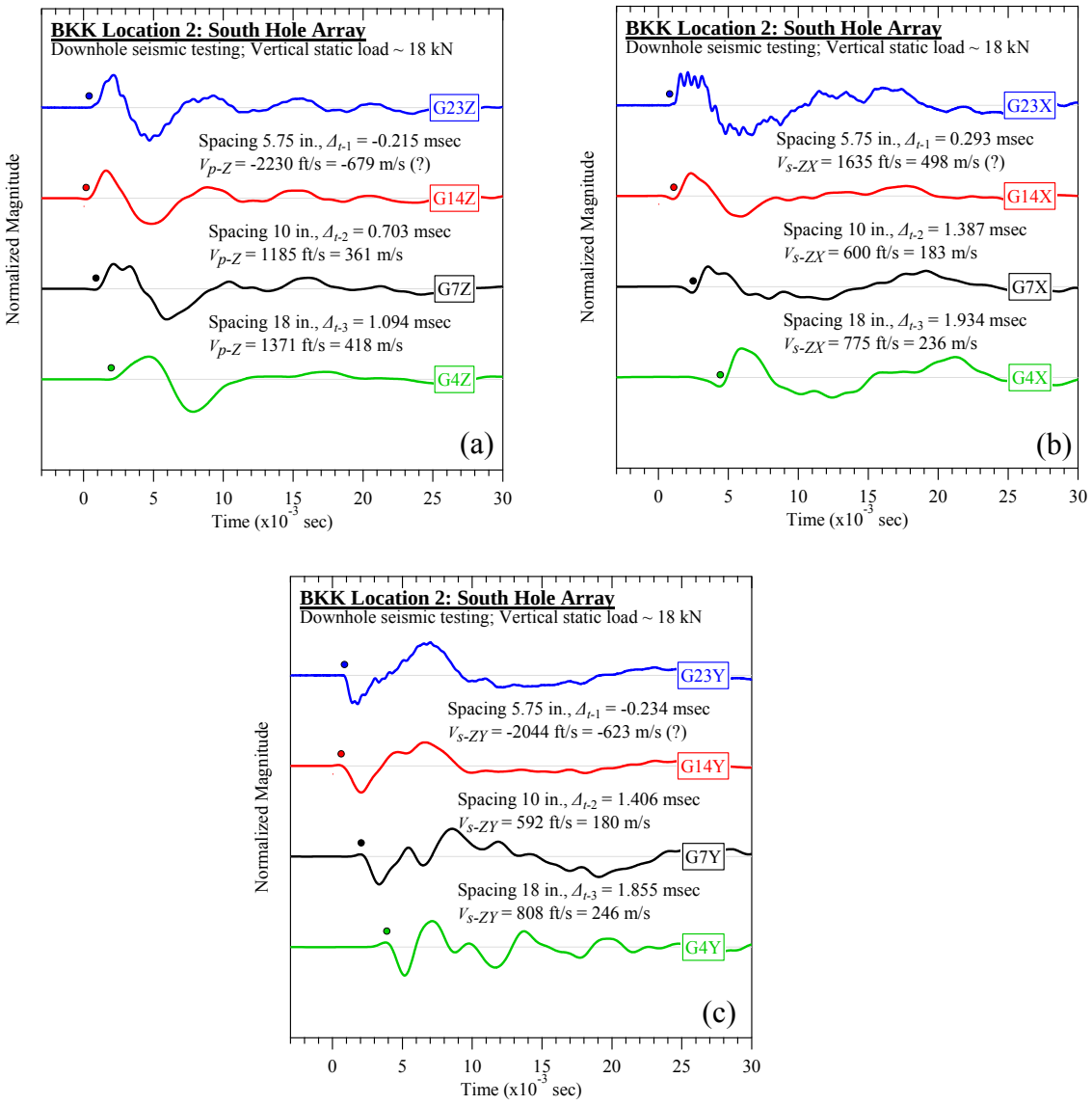

Figure D-56. BKK Landfill #2 (south hole): Downhole seismic testing at vertical load of 18 kN: (a) $V_{p\text{-}Z}$, (b) $V_{s\text{-}ZX}$, and (c) $V_{s\text{-}ZY}$.

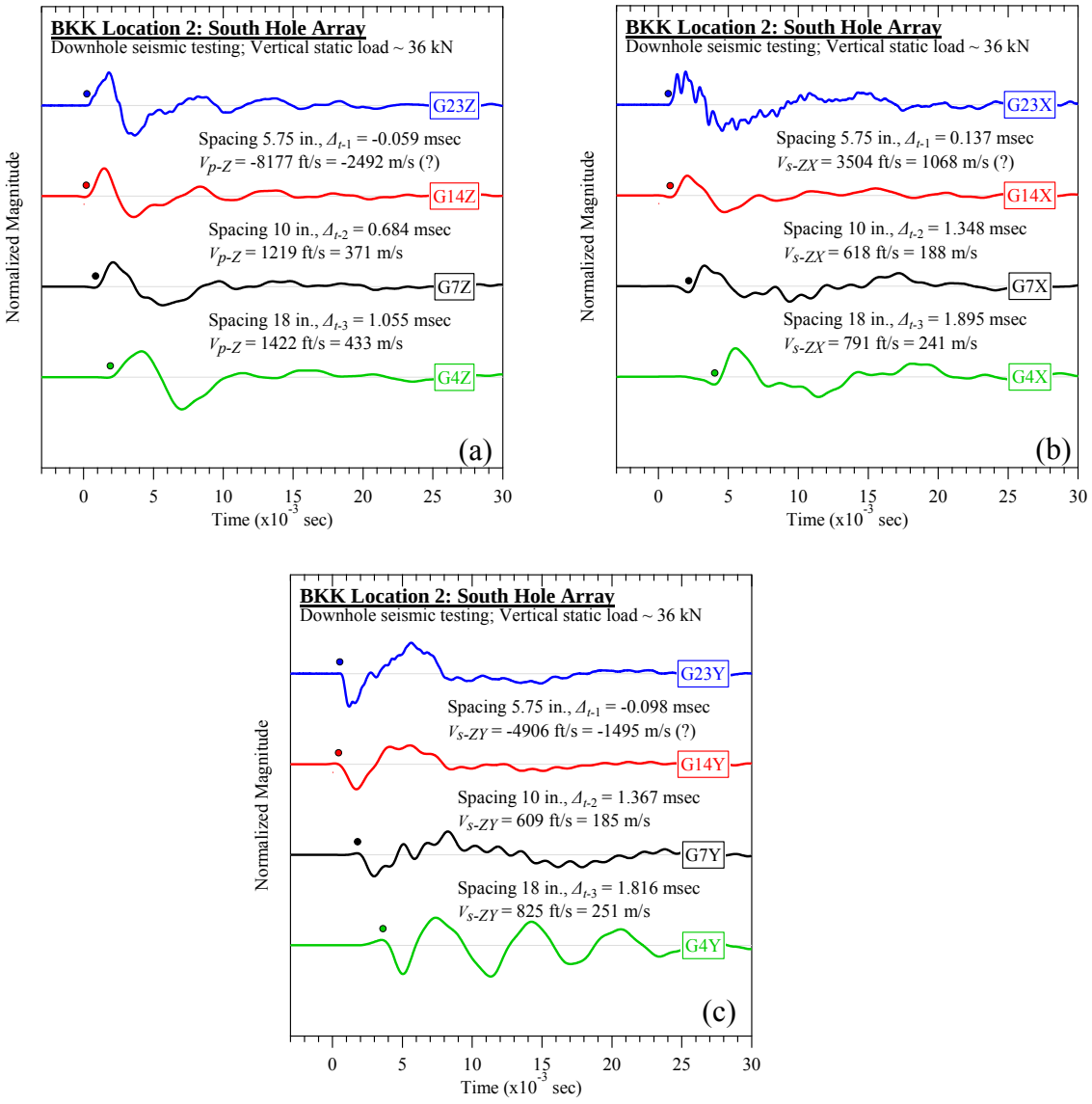

Figure D-57. BKK Landfill #2 (south hole): Downhole seismic testing at vertical load of 36 kN: (a) $V_{p\text{-}Z}$, (b) $V_{s\text{-}ZX}$, and (c) $V_{s\text{-}ZY}$.

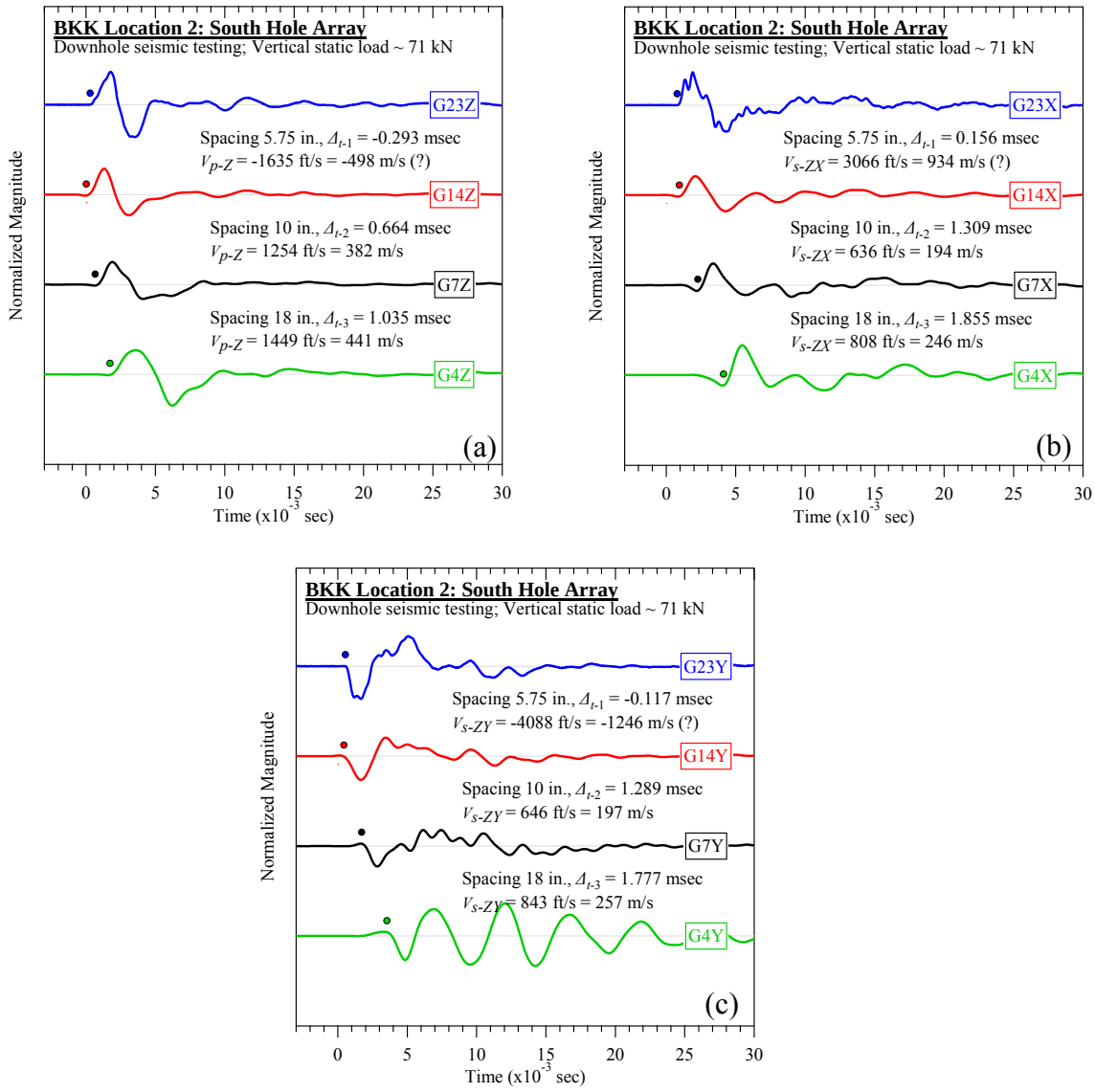

Figure D-58. BKK Landfill #2 (south hole): Downhole seismic testing at vertical load of 71 kN: (a) V_{p-Z}, (b) V_{s-ZX}, and (c) V_{s-ZY}.

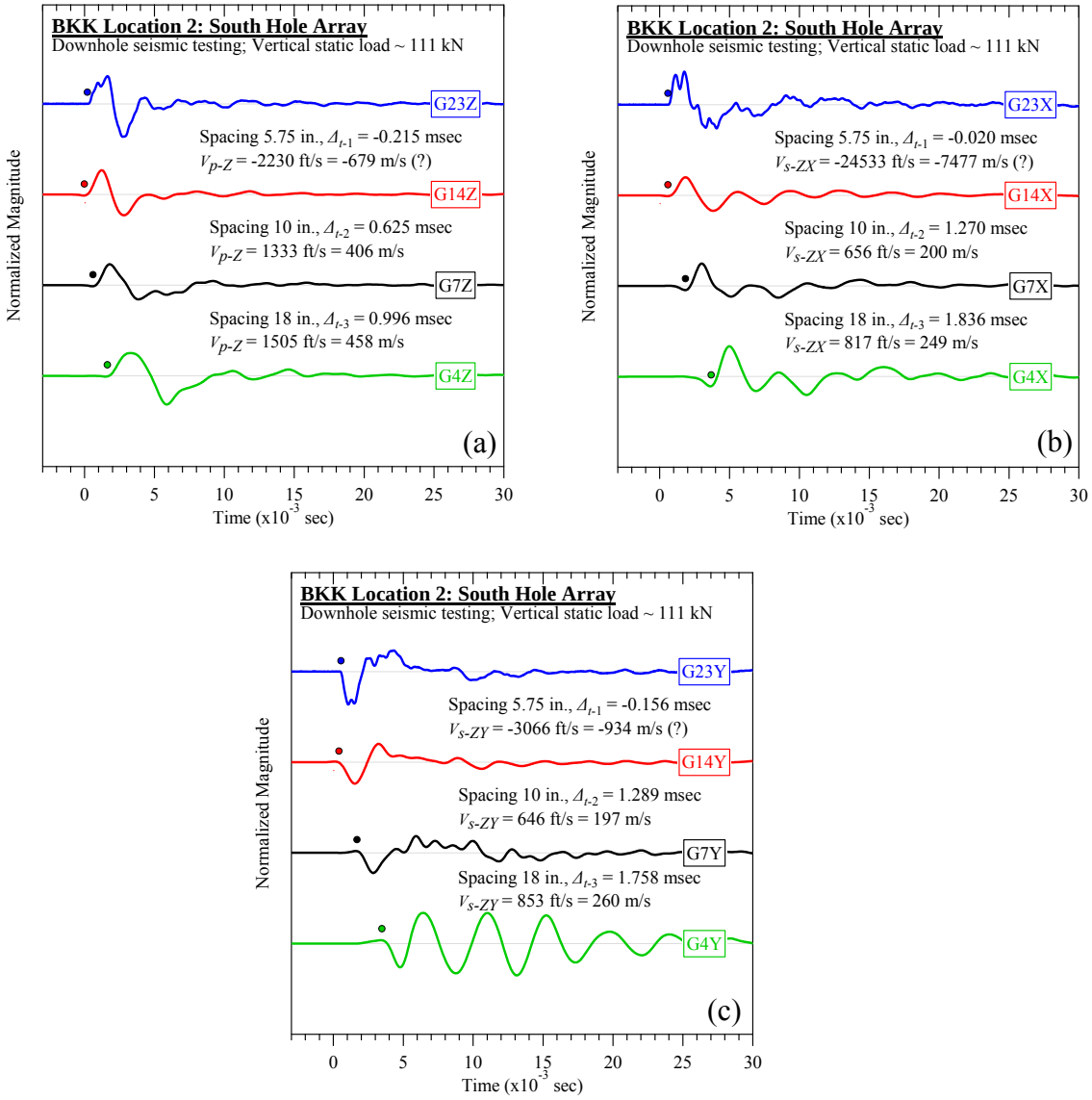

Figure D-59. BKK Landfill #2 (south hole): Downhole seismic testing at vertical load of 111 kN: (a) V_{p-Z}, (b) V_{s-ZX}, and (c) V_{s-ZY}.

D.2.2 Crosshole Seismic Testing

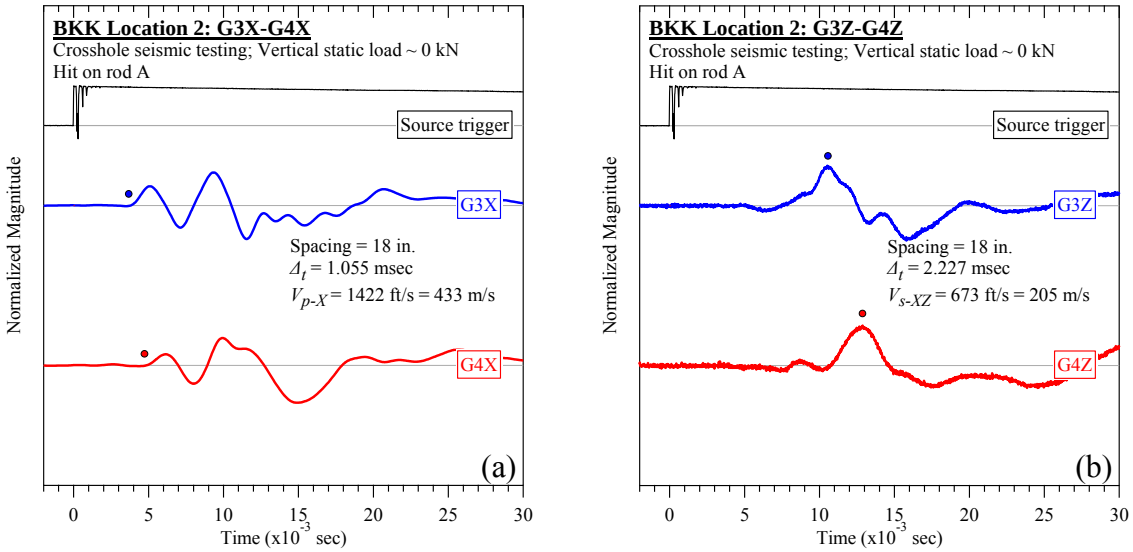

Figure D-60. BKK Landfill #2 (rod A): Crosshole seismic testing at vertical load of 0 kN: (a) $V_{p\text{-}X}$ and (b) $V_{s\text{-}XZ}$.

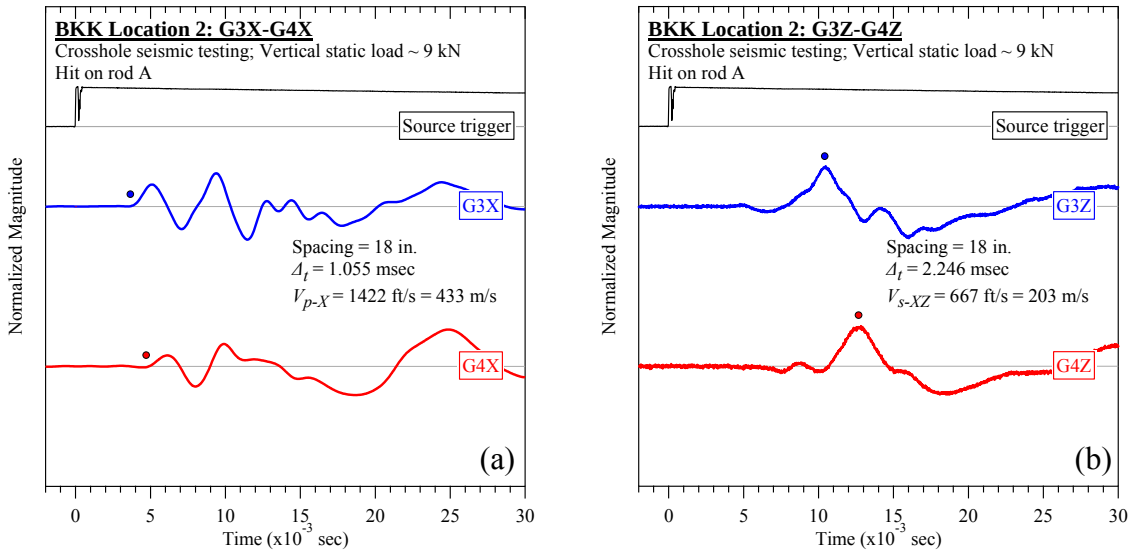

Figure D-61. BKK Landfill #2 (rod A): Crosshole seismic testing at vertical load of 9 kN: (a) $V_{p\text{-}X}$ and (b) $V_{s\text{-}XZ}$.

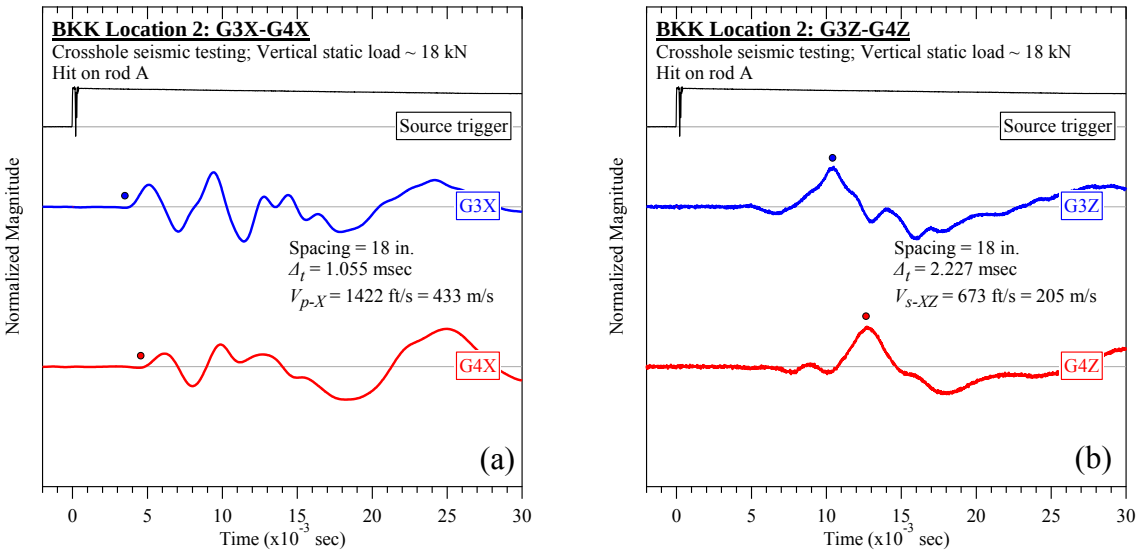

Figure D-62. BKK Landfill #2 (rod A): Crosshole seismic testing at vertical load of 18 kN: (a) $V_{p\text{-}X}$ and (b) $V_{s\text{-}XZ}$.

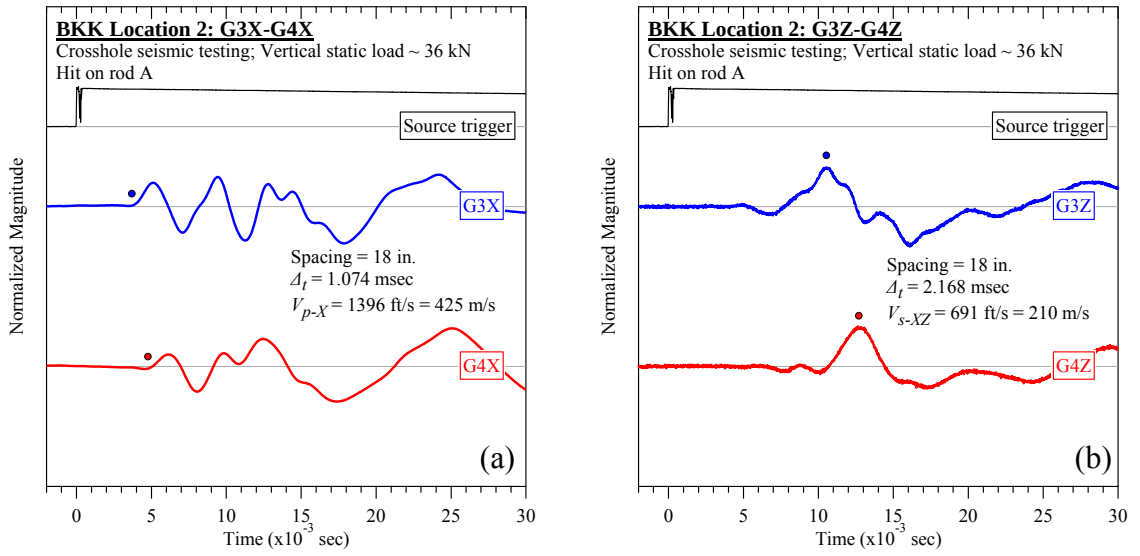

Figure D-63. BKK Landfill #2 (rod A): Crosshole seismic testing at vertical load of 36 kN: (a) $V_{p\text{-}X}$ and (b) $V_{s\text{-}XZ}$.

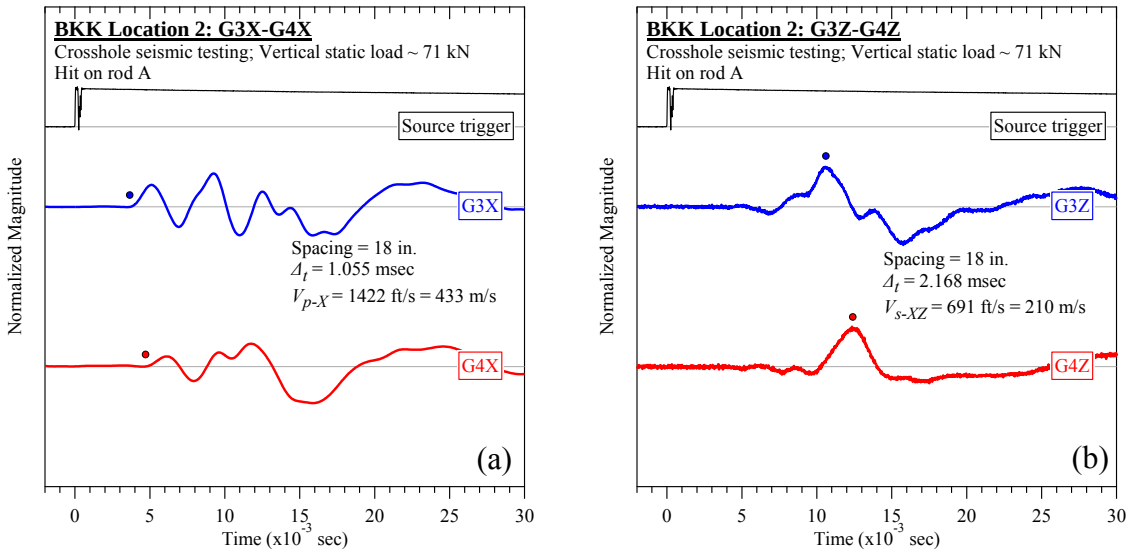

Figure D-64. BKK Landfill #2 (rod A): Crosshole seismic testing at vertical load of 71 kN: (a) $V_{p\text{-}X}$ and (b) $V_{s\text{-}XZ}$.

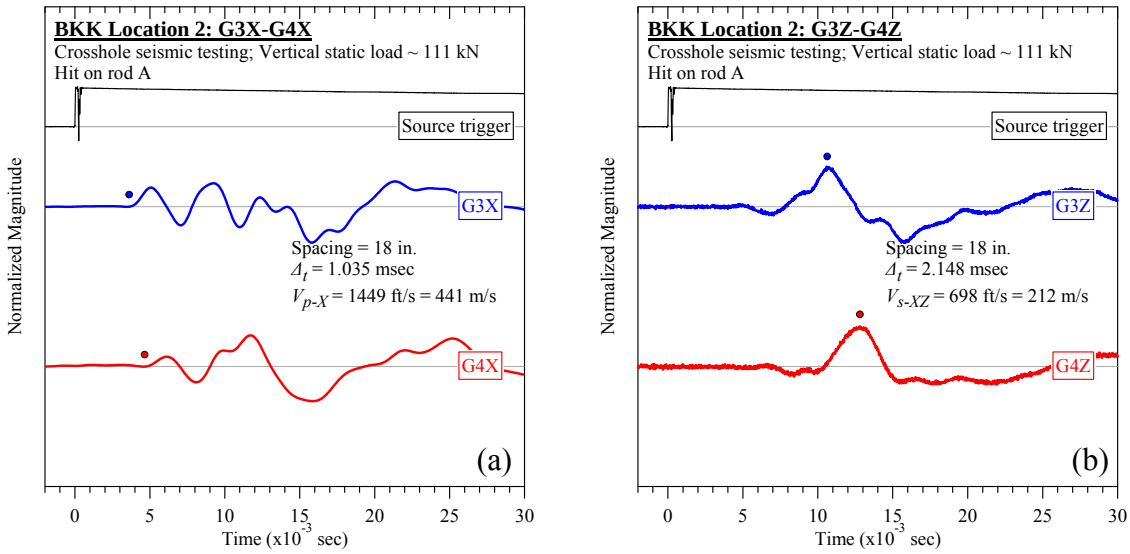

Figure D-65. BKK Landfill #2 (rod A): Crosshole seismic testing at vertical load of 111 kN: (a) $V_{p\text{-}X}$ and (b) $V_{s\text{-}XZ}$.

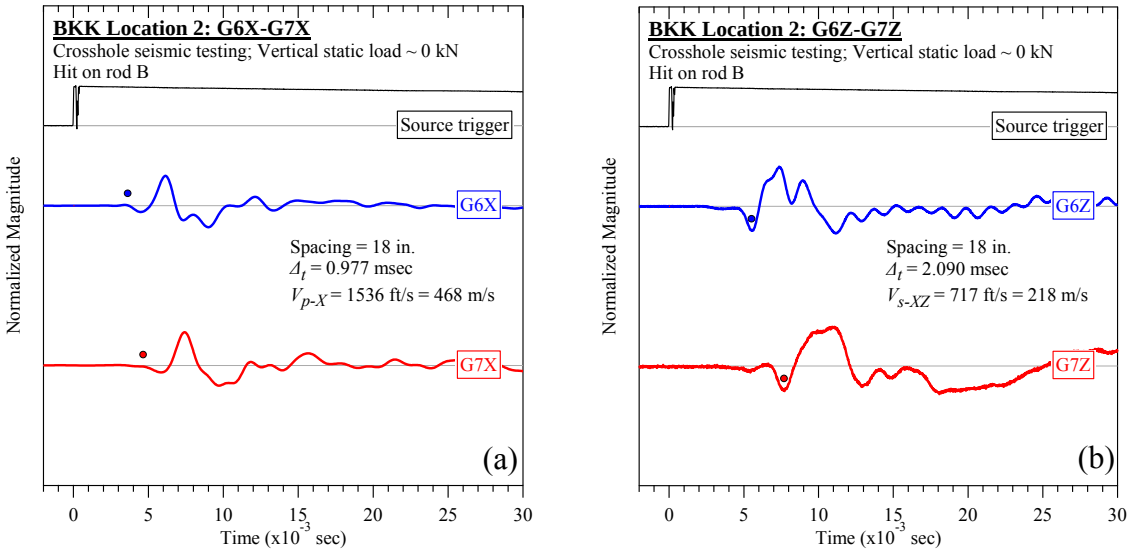

Figure D-66. BKK Landfill #2 (rod B): Crosshole seismic testing at vertical load of 0 kN: (a) $V_{p\text{-}X}$ and (b) $V_{s\text{-}XZ}$.

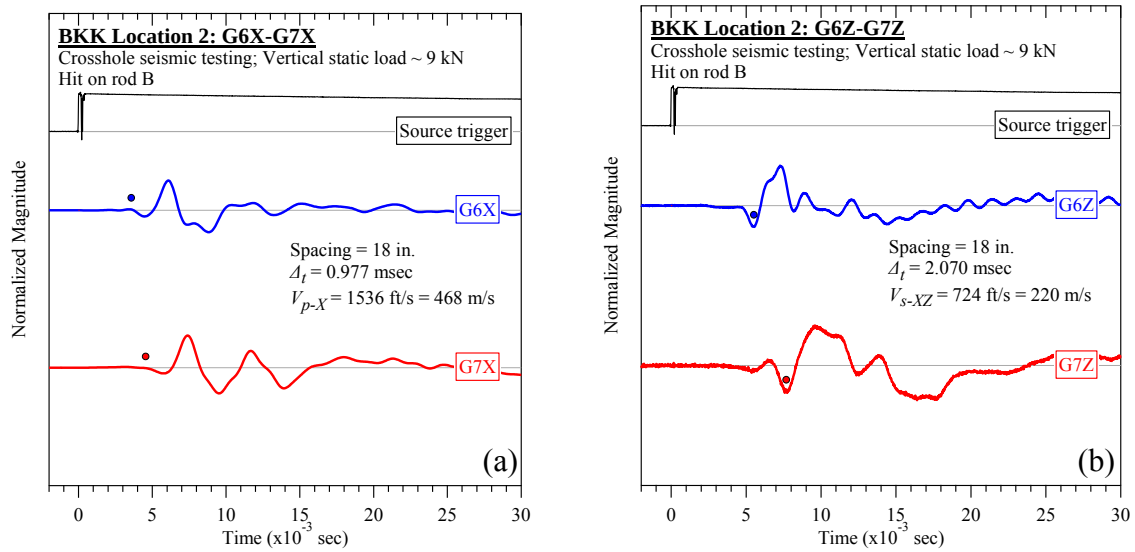

Figure D-67. BKK Landfill #2 (rod B): Crosshole seismic testing at vertical load of 9 kN: (a) $V_{p\text{-}X}$ and (b) $V_{s\text{-}XZ}$.

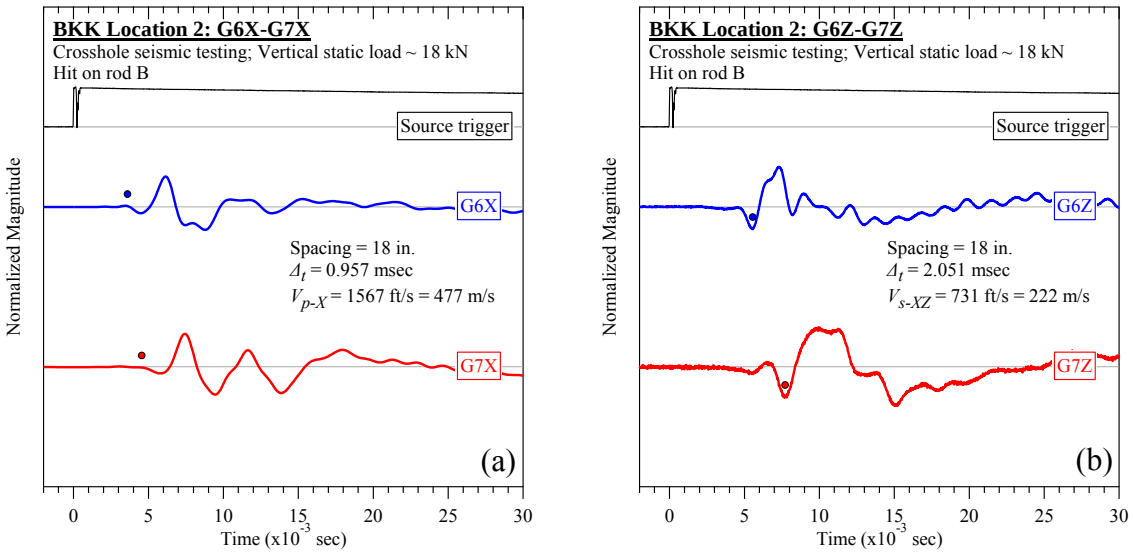

Figure D-68. BKK Landfill #2 (rod B): Crosshole seismic testing at vertical load of 18 kN: (a) $V_{p\text{-}X}$ and (b) $V_{s\text{-}XZ}$.

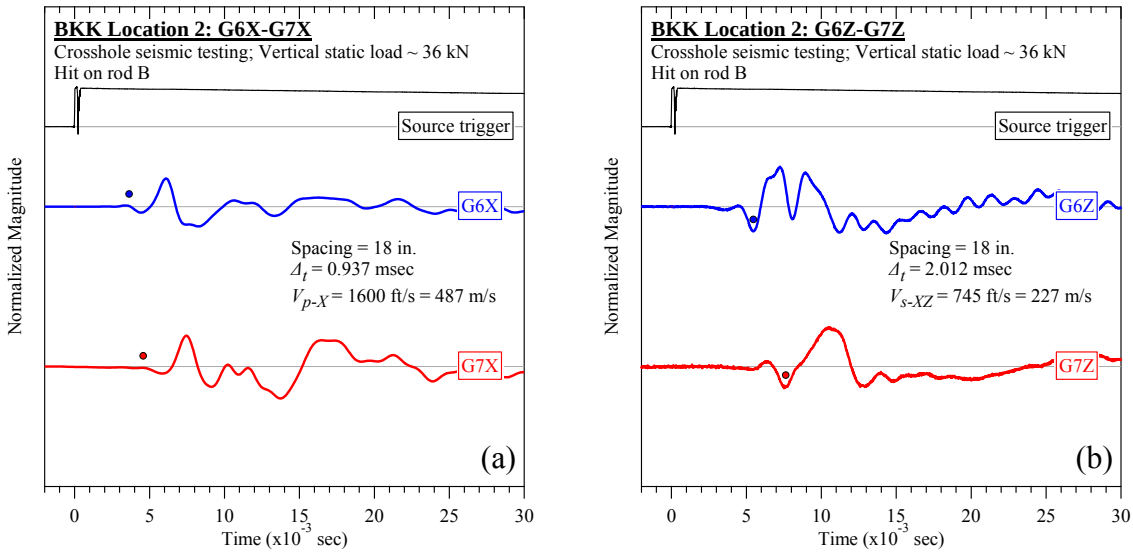

Figure D-69. BKK Landfill #2 (rod B): Crosshole seismic testing at vertical load of 36 kN: (a) $V_{p\text{-}X}$ and (b) $V_{s\text{-}XZ}$.

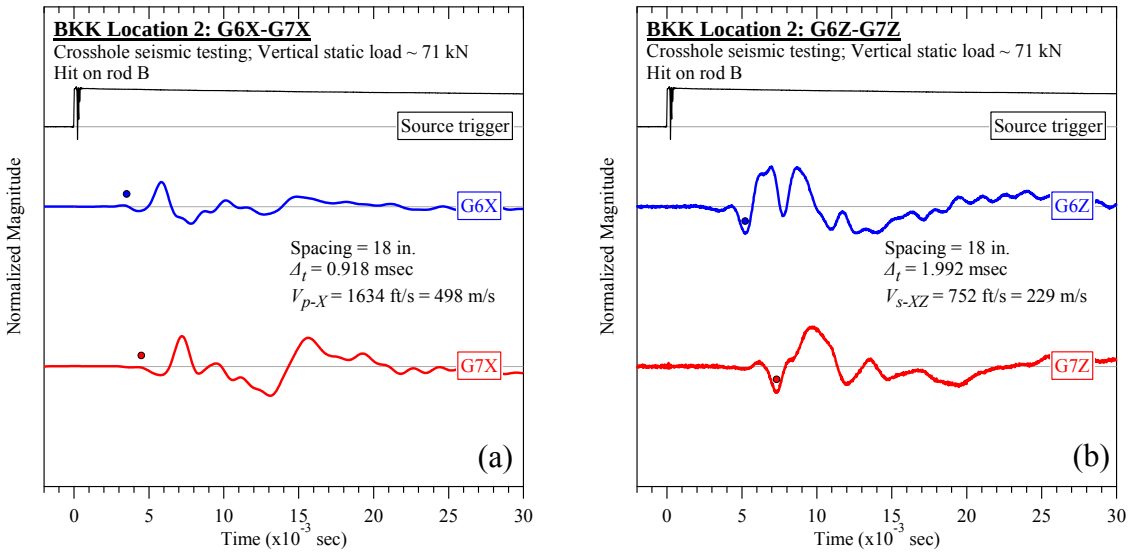

Figure D-70. BKK Landfill #2 (rod B): Crosshole seismic testing at vertical load of 71 kN: (a) $V_{p\text{-}X}$ and (b) $V_{s\text{-}XZ}$.

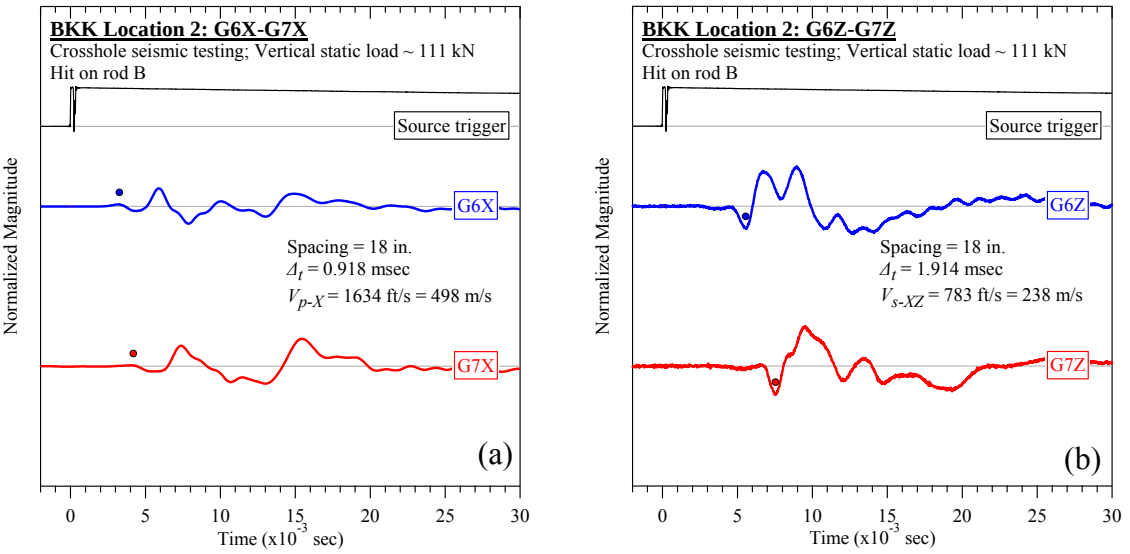

Figure D-71. BKK Landfill #2 (rod B): Crosshole seismic testing at vertical load of 111 kN: (a) $V_{p\text{-}X}$ and (b) $V_{s\text{-}XZ}$.

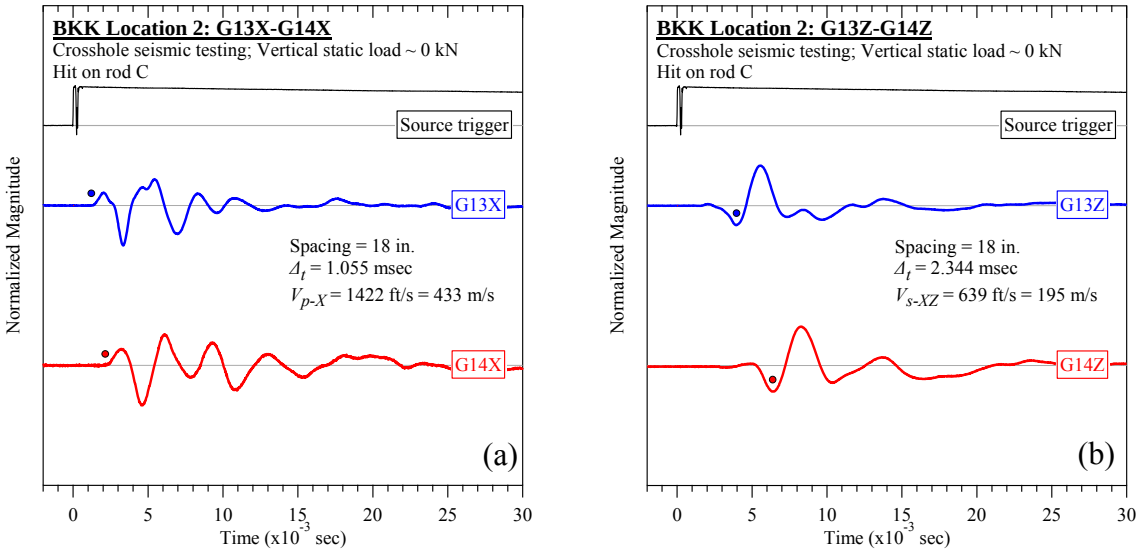

Figure D-72. BKK Landfill #2 (rod C): Crosshole seismic testing at vertical load of 0 kN: (a) $V_{p\text{-}X}$ and (b) $V_{s\text{-}XZ}$.

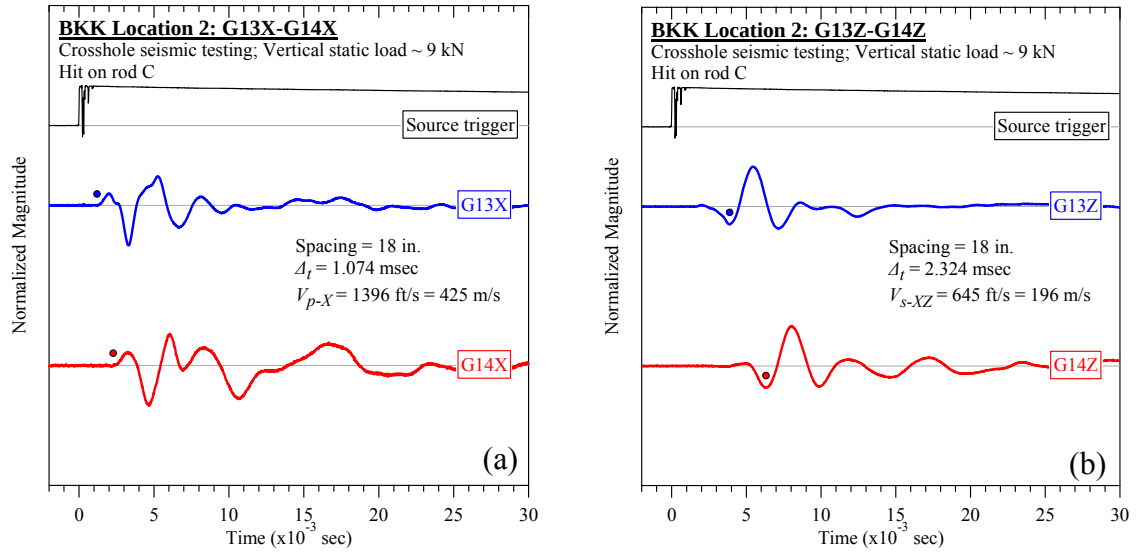

Figure D-73. BKK Landfill #2 (rod C): Crosshole seismic testing at vertical load of 9 kN: (a) $V_{p\text{-}X}$ and (b) $V_{s\text{-}XZ}$.

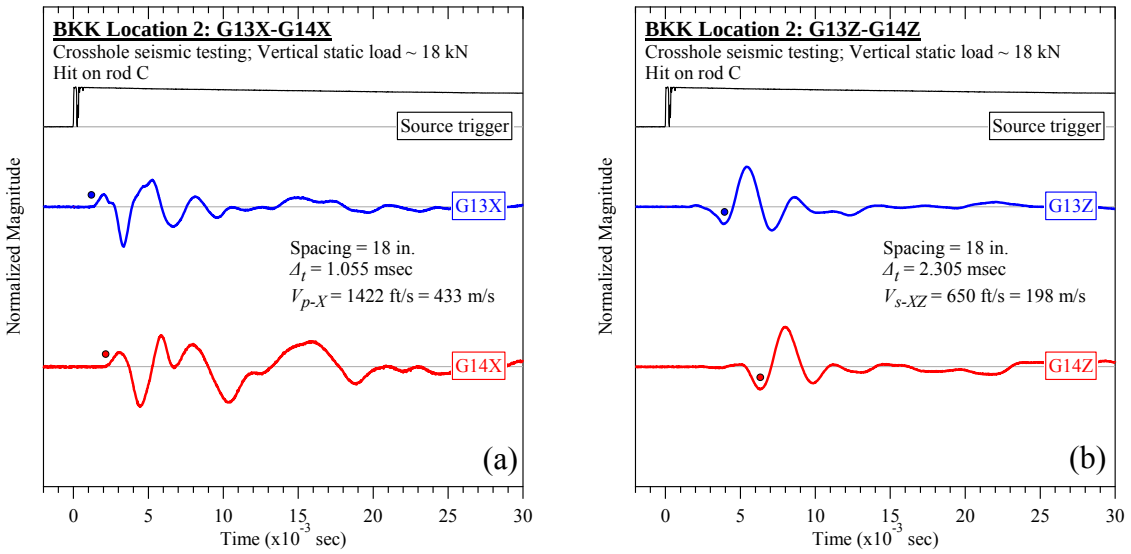

Figure D-74. BKK Landfill #2 (rod C): Crosshole seismic testing at vertical load of 18 kN: (a) $V_{p\text{-}X}$ and (b) $V_{s\text{-}XZ}$.

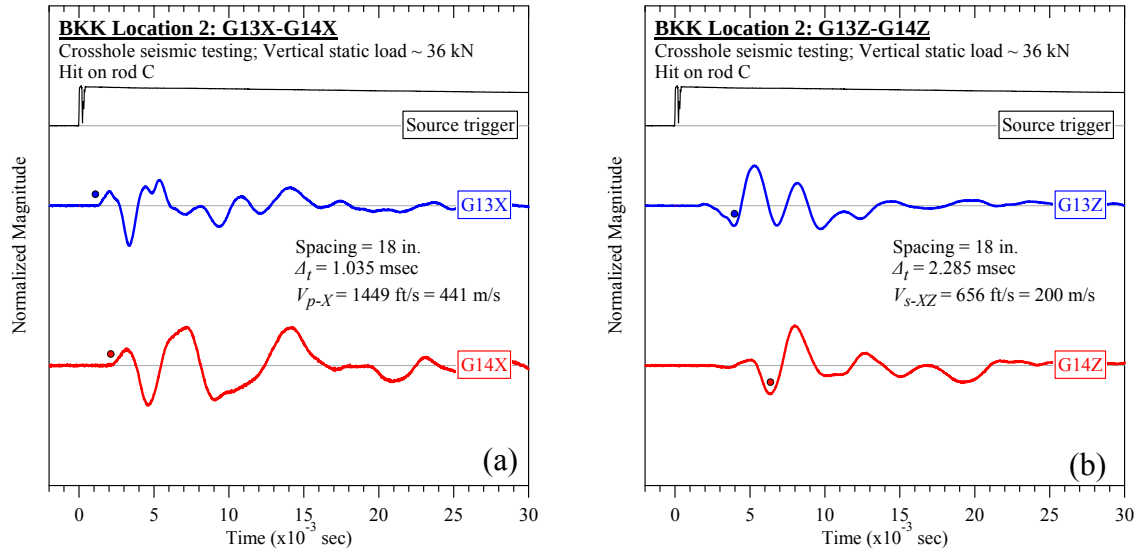

Figure D-75. BKK Landfill #2 (rod C): Crosshole seismic testing at vertical load of 36 kN: (a) $V_{p\text{-}X}$ and (b) $V_{s\text{-}XZ}$.

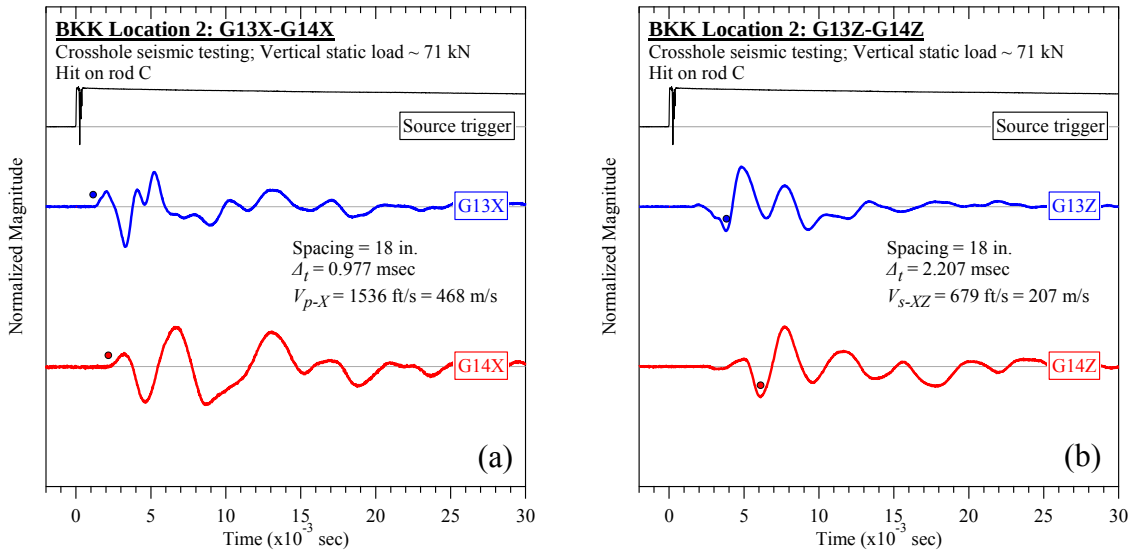

Figure D-76. BKK Landfill #2 (rod C): Crosshole seismic testing at vertical load of 71 kN: (a) $V_{p\text{-}X}$ and (b) $V_{s\text{-}XZ}$.

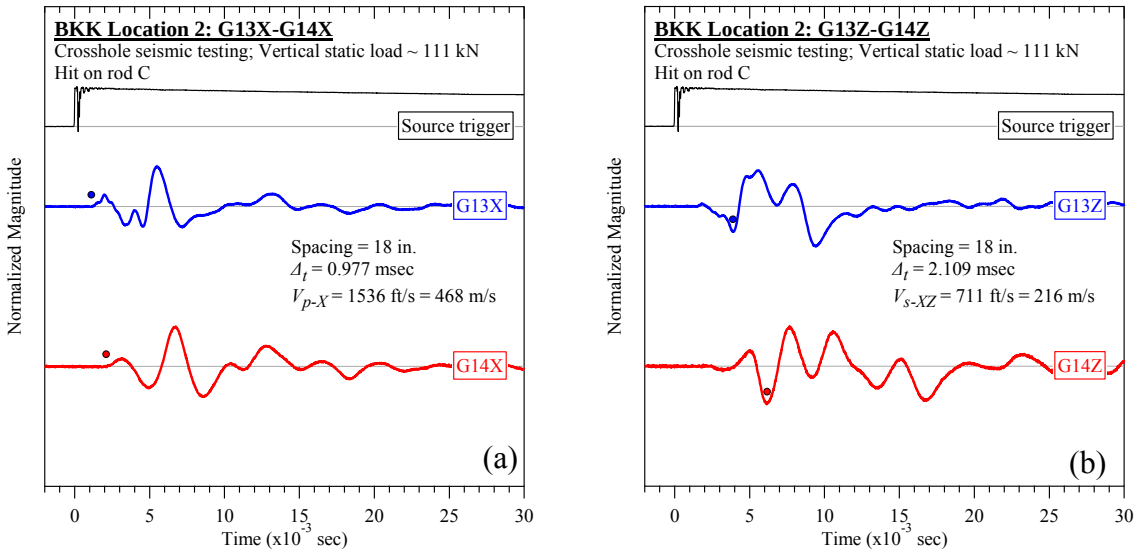

Figure D-77. BKK Landfill #2 (rod C): Crosshole seismic testing at vertical load of 111 kN: (a) $V_{p\text{-}X}$ and (b) $V_{s\text{-}XZ}$.

D.2.3 Steady-state Dynamic Testing

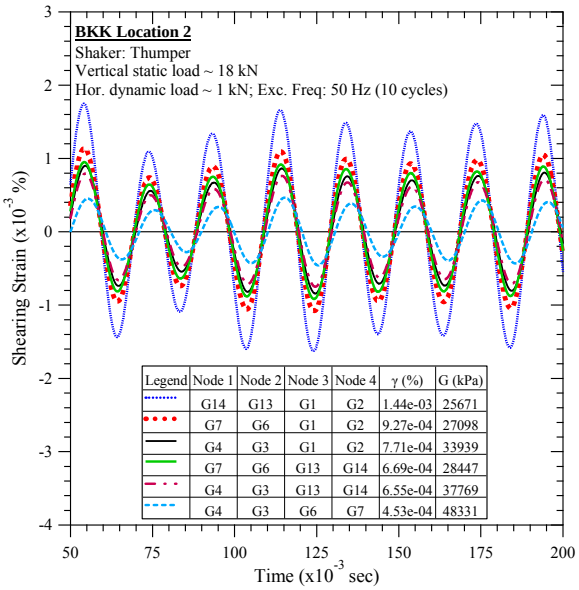

Figure D-78. BKK Landfill #2: Steady-state dynamic testing at vertical load of 18 kN and horizontal dynamic load of 1 kN.

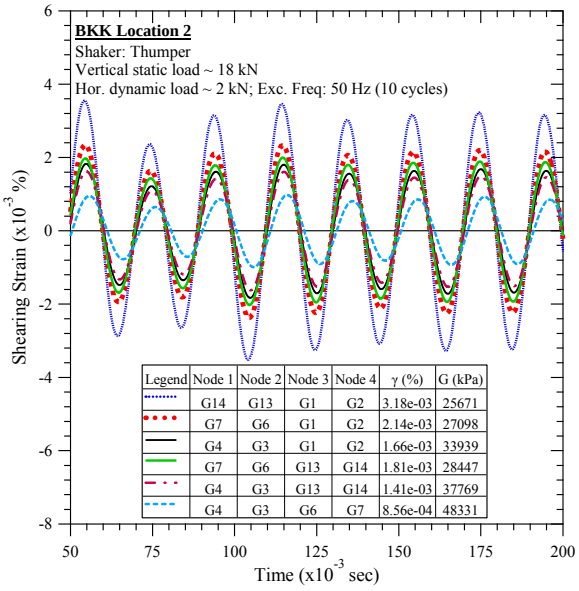

Figure D-79. BKK Landfill #2: Steady-state dynamic testing at vertical load of 18 kN and horizontal dynamic load of 2 kN.

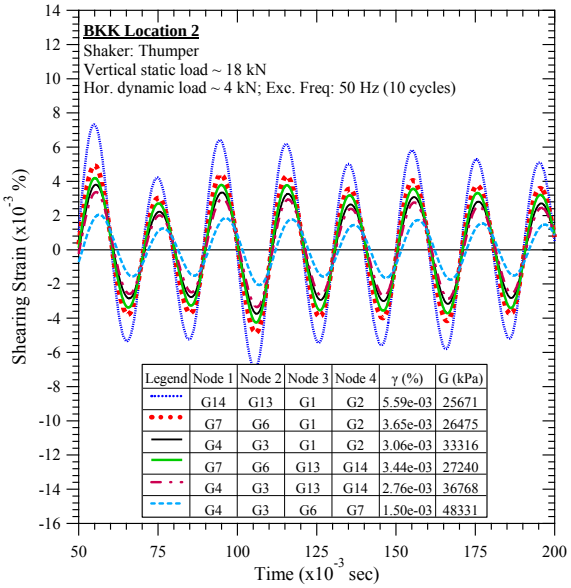

Figure D-80. BKK Landfill #2: Steady-state dynamic testing at vertical load of 18 kN and horizontal dynamic load of 4 kN.

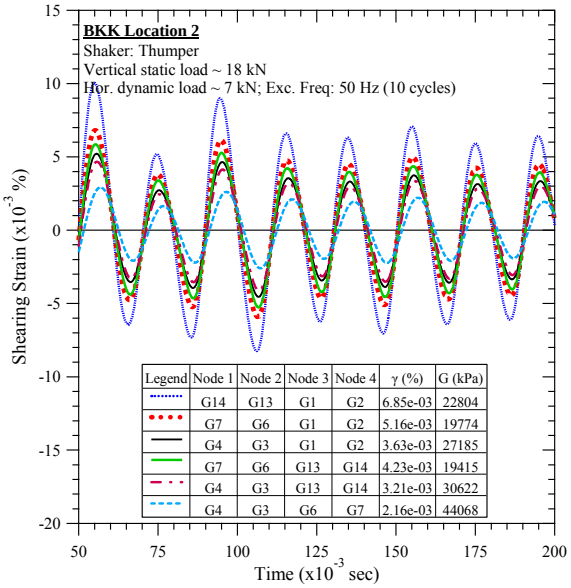

Figure D-81. BKK Landfill #2: Steady-state dynamic testing at vertical load of 18 kN and horizontal dynamic load of 7 kN.

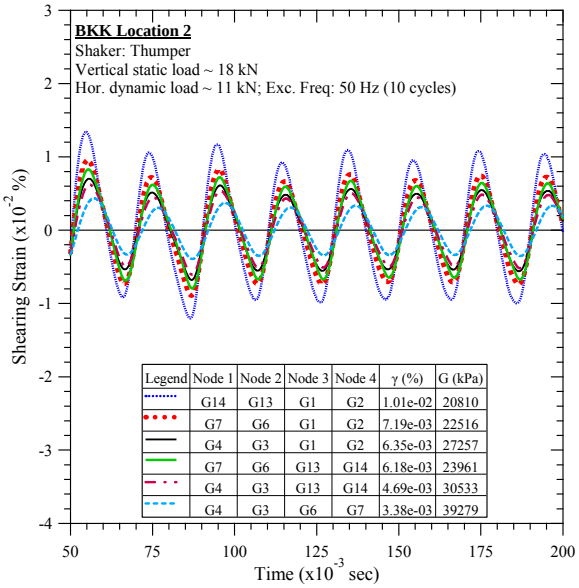

Figure D-82. BKK Landfill #2: Steady-state dynamic testing at vertical load of 18 kN and horizontal dynamic load of 11 kN.

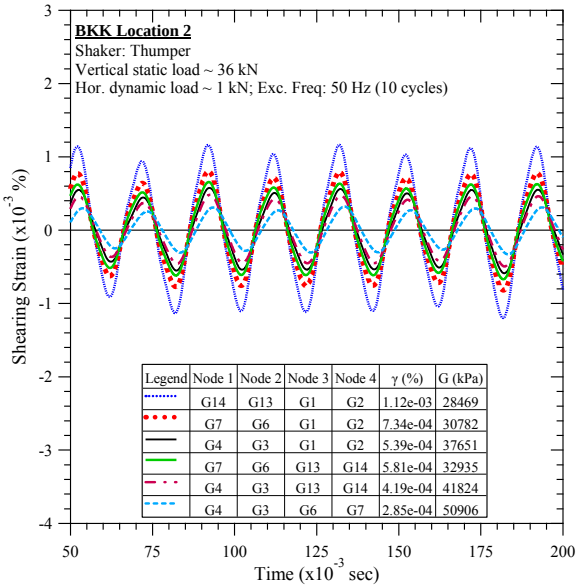

Figure D-83. BKK Landfill #2: Steady-state dynamic testing at vertical load of 36 kN and horizontal dynamic load of 0.6 kN.

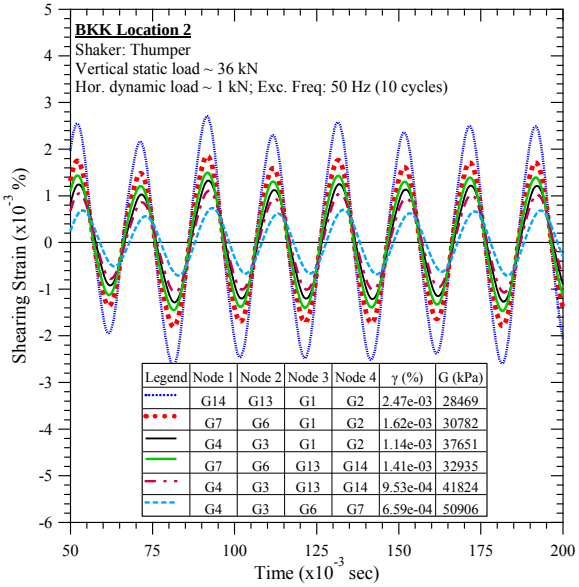

Figure D-84. BKK Landfill #2: Steady-state dynamic testing at vertical load of 36 kN and horizontal dynamic load of 1.24 kN.

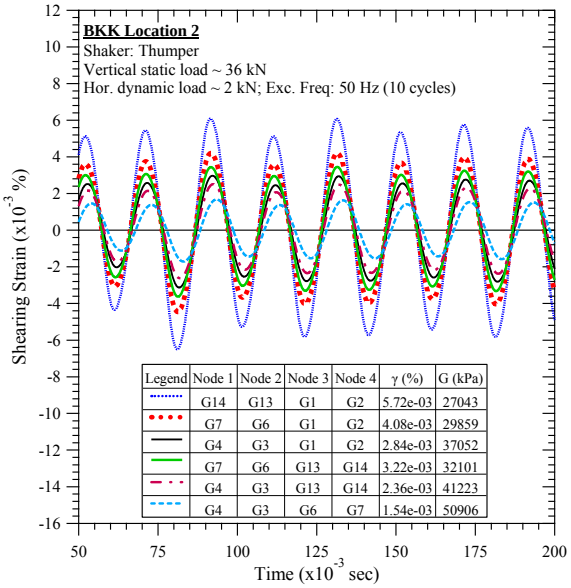

Figure D-85. BKK Landfill #2: Steady-state dynamic testing at vertical load of 36 kN and horizontal dynamic load of 2 kN.

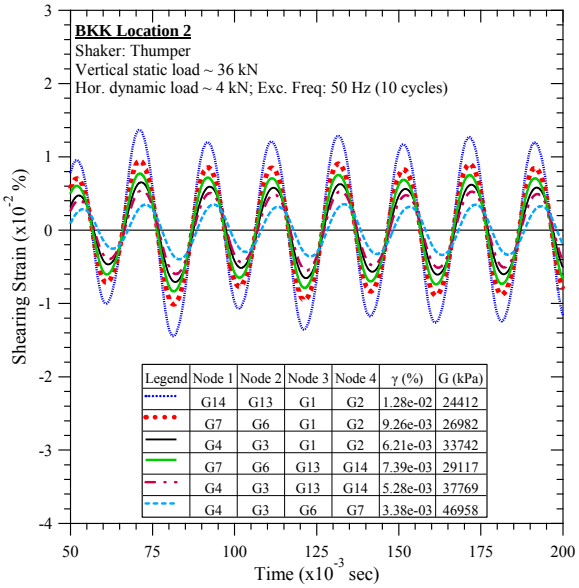

Figure D-86. BKK Landfill #2: Steady-state dynamic testing at vertical load of 36 kN and horizontal dynamic load of 4 kN.

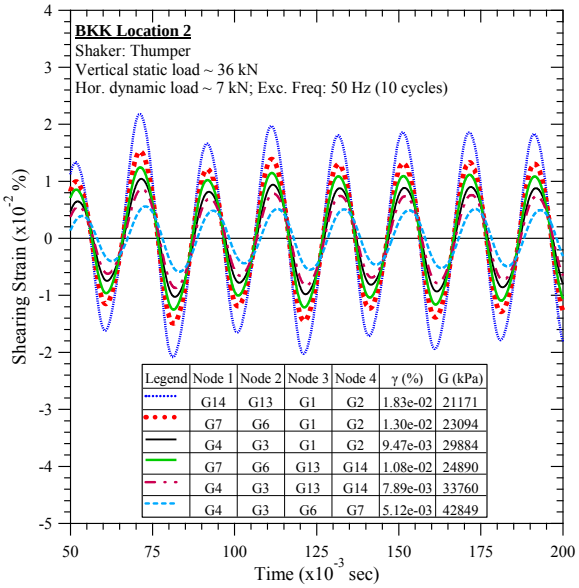

Figure D-87. BKK Landfill #2: Steady-state dynamic testing at vertical load of 36 kN and horizontal dynamic load of 7 kN.

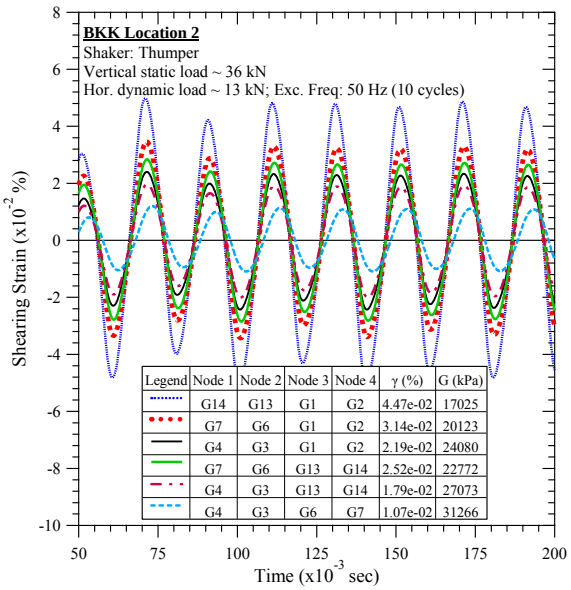

Figure D-88. BKK Landfill #2: Steady-state dynamic testing at vertical load of 36 kN and horizontal dynamic load of 13 kN.

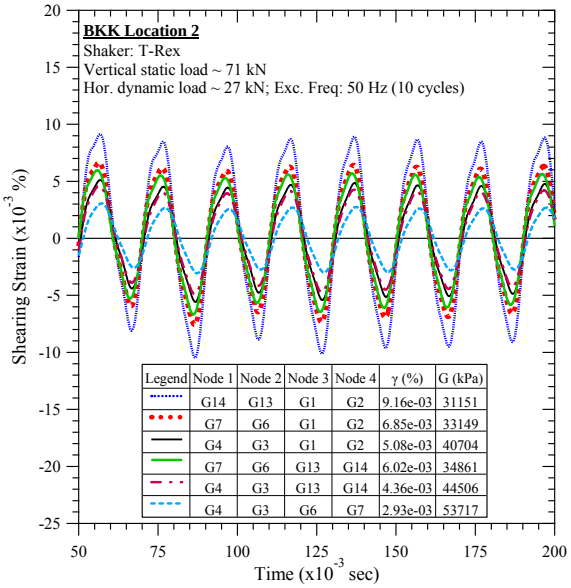

Figure D-89. BKK Landfill #2: Steady-state dynamic testing at vertical load of 71 kN and horizontal dynamic load of 27 kN.

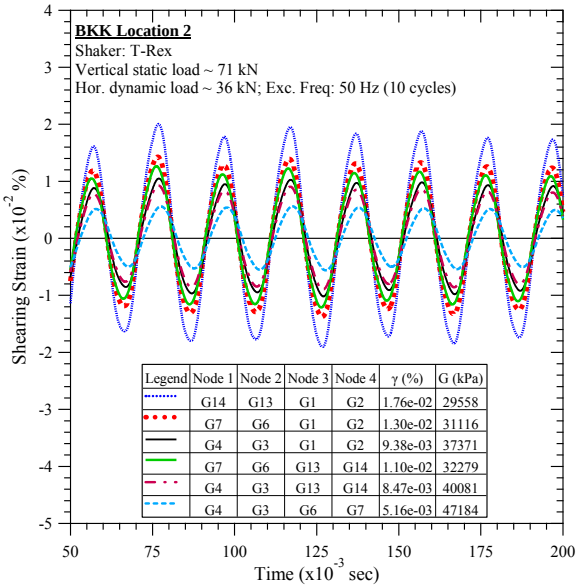

Figure D-90. BKK Landfill #2: Steady-state dynamic testing at vertical load of 71 kN and horizontal dynamic load of 36 kN.

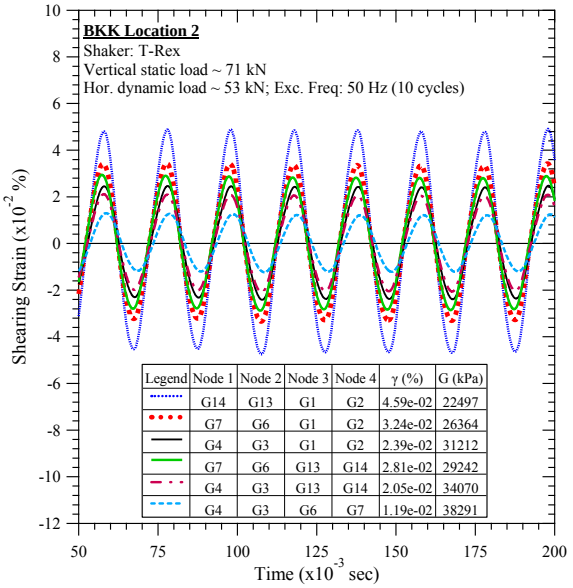

Figure D-91. BKK Landfill #2: Steady-state dynamic testing at vertical load of 71 kN and horizontal dynamic load of 53 kN.

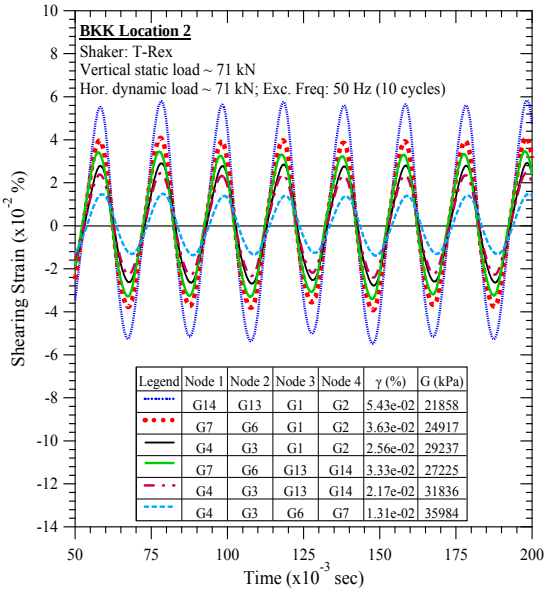

Figure D-92. BKK Landfill #2: Steady-state dynamic testing at vertical load of 71 kN and horizontal dynamic load of 71 kN.

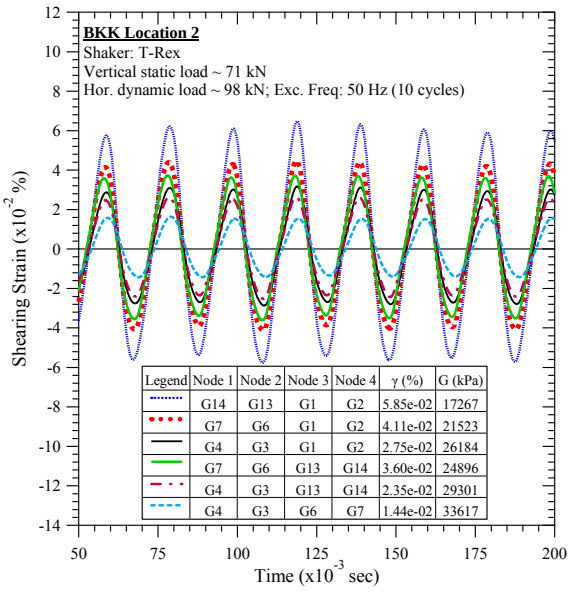

Figure D-93. BKK Landfill #2: Steady-state dynamic testing at vertical load of 71 kN and horizontal dynamic load of 98 kN.

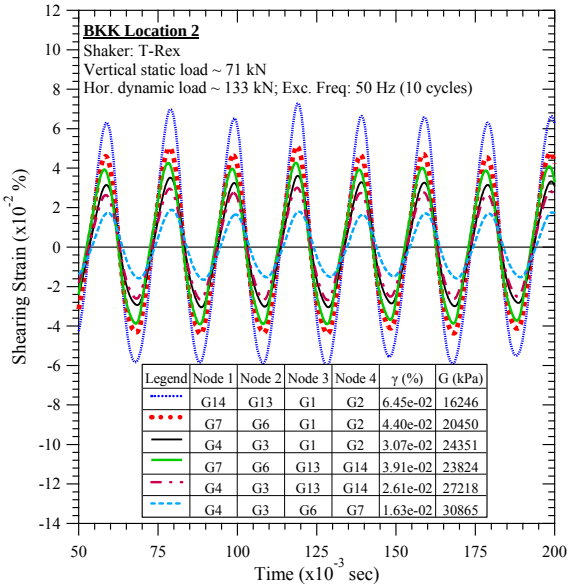

Figure D-94. BKK Landfill #2: Steady-state dynamic testing at vertical load of 71 kN and horizontal dynamic load of 133 kN.

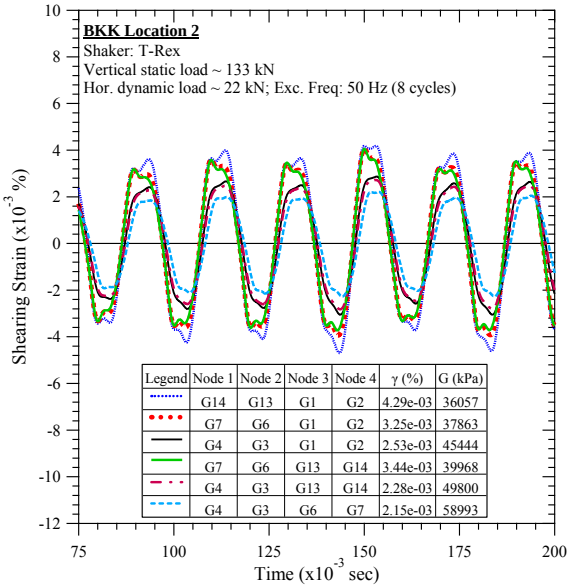

Figure D-95. BKK Landfill #2: Steady-state dynamic testing at vertical load of 133 kN and horizontal dynamic load of 22 kN.

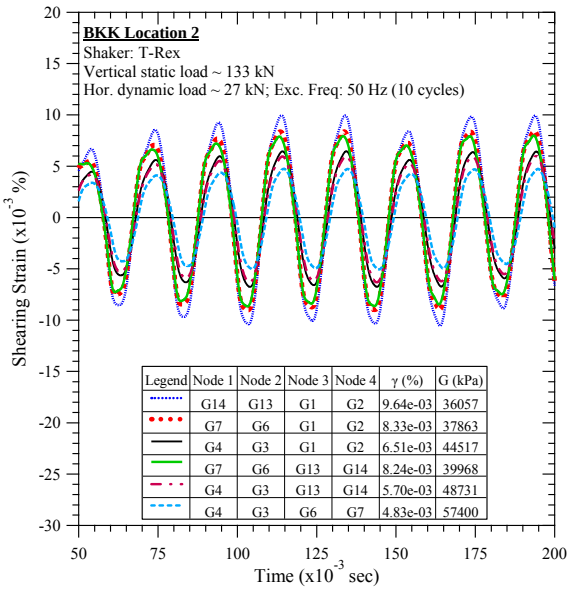

Figure D-96. BKK Landfill #2: Steady-state dynamic testing at vertical load of 133 kN and horizontal dynamic load of 27 kN.

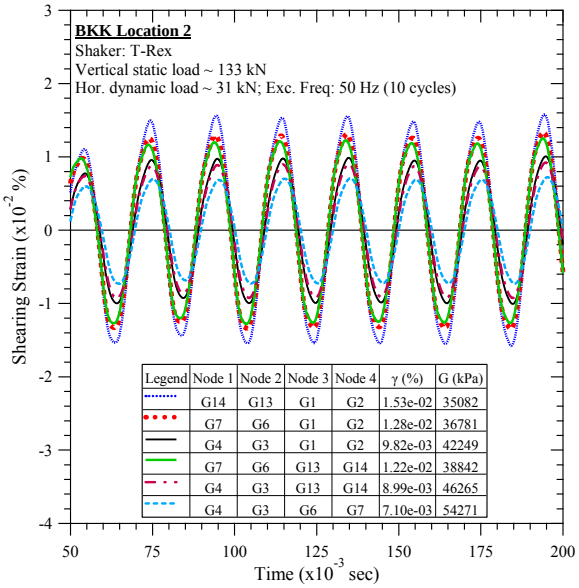

Figure D-97. BKK Landfill #2: Steady-state dynamic testing at vertical load of 133 kN and horizontal dynamic load of 31 kN.

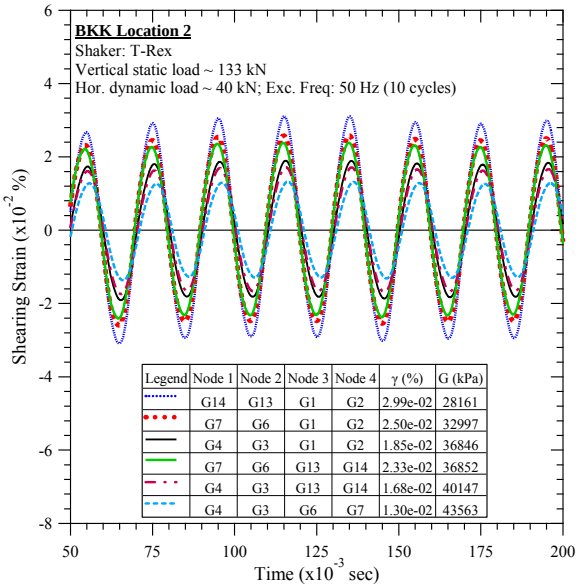

Figure D-98. BKK Landfill #2: Steady-state dynamic testing at vertical load of 133 kN and horizontal dynamic load of 40 kN.

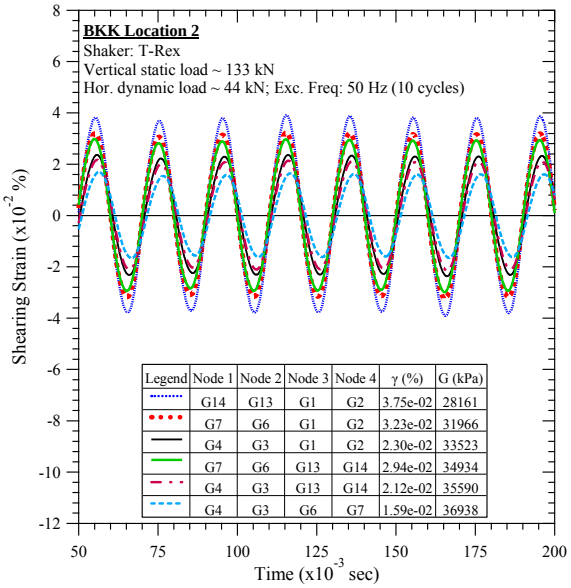

Figure D-99. BKK Landfill #2: Steady-state dynamic testing at vertical load of 133 kN and horizontal dynamic load of 44 kN.

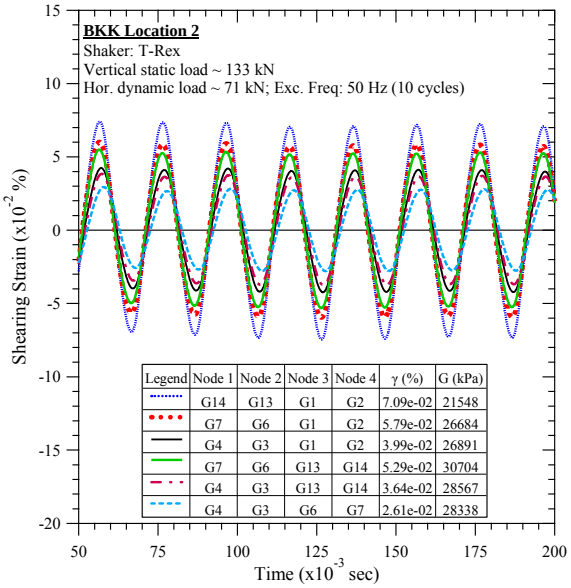

Figure D-100. BKK Landfill #2: Steady-state dynamic testing at vertical load of 133 kN and horizontal dynamic load of 71 kN.

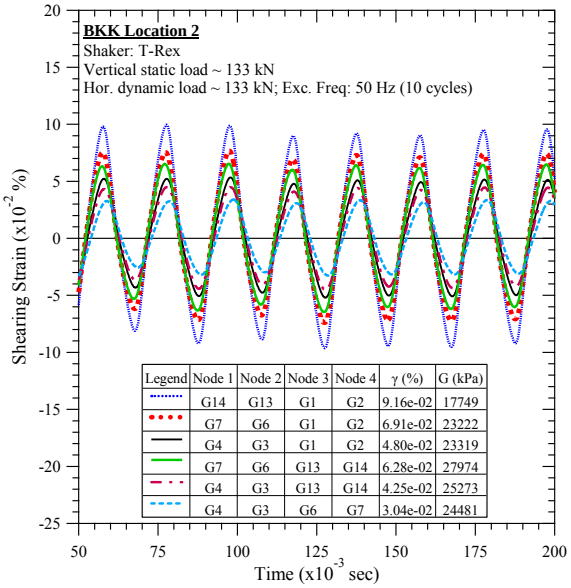

Figure D-101. BKK Landfill #2: Steady-state dynamic testing at vertical load of 133 kN and horizontal dynamic load of 133 kN.

D.3 BKK Landfill Location 3

D.3.1 Downhole Seismic Testing

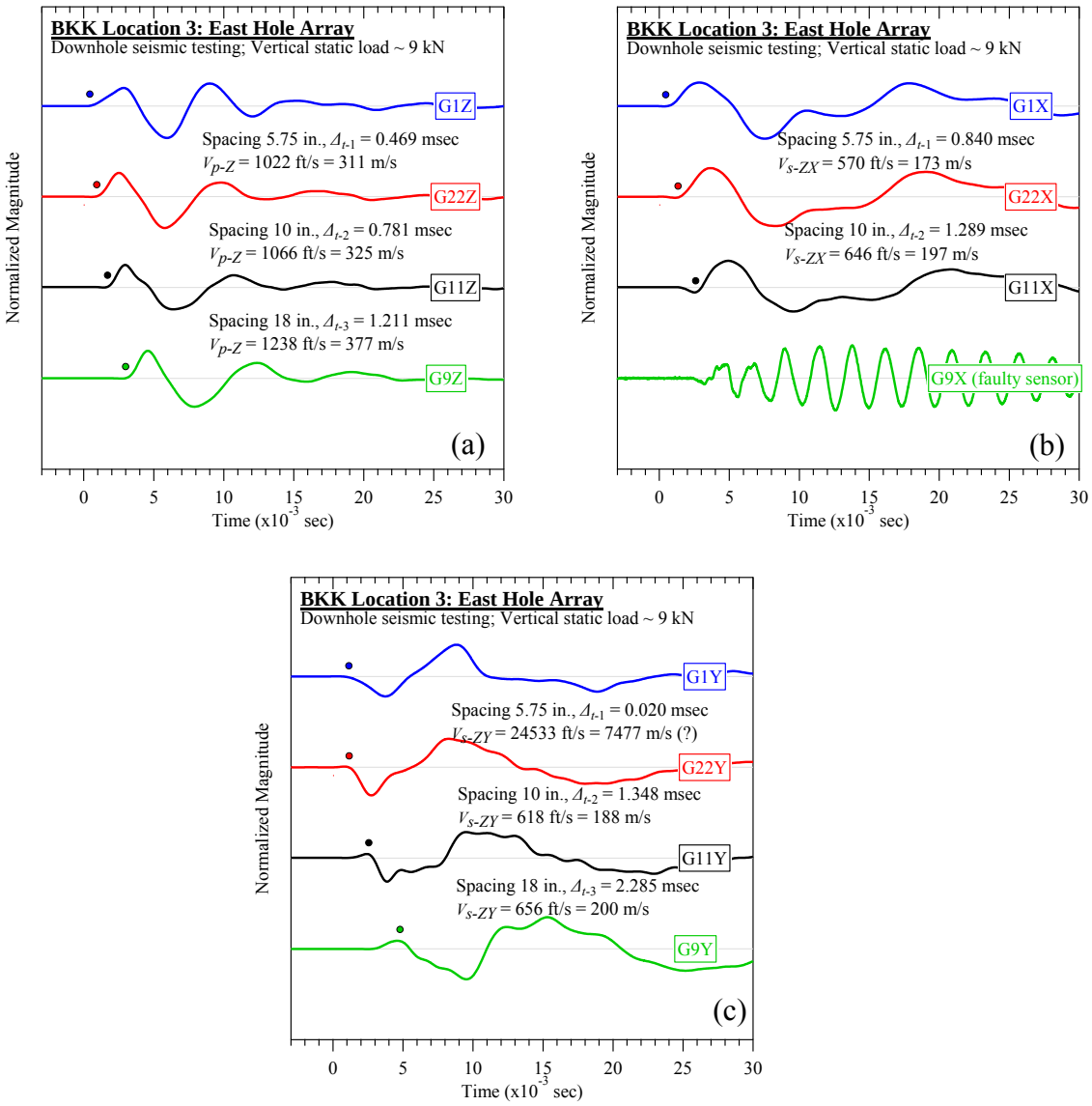

Figure D-102. BKK Landfill #3 (east hole): Downhole seismic testing at vertical load of 9 kN: (a) V_{p-Z}, (b) V_{s-ZX}, and (c) V_{s-ZY}.

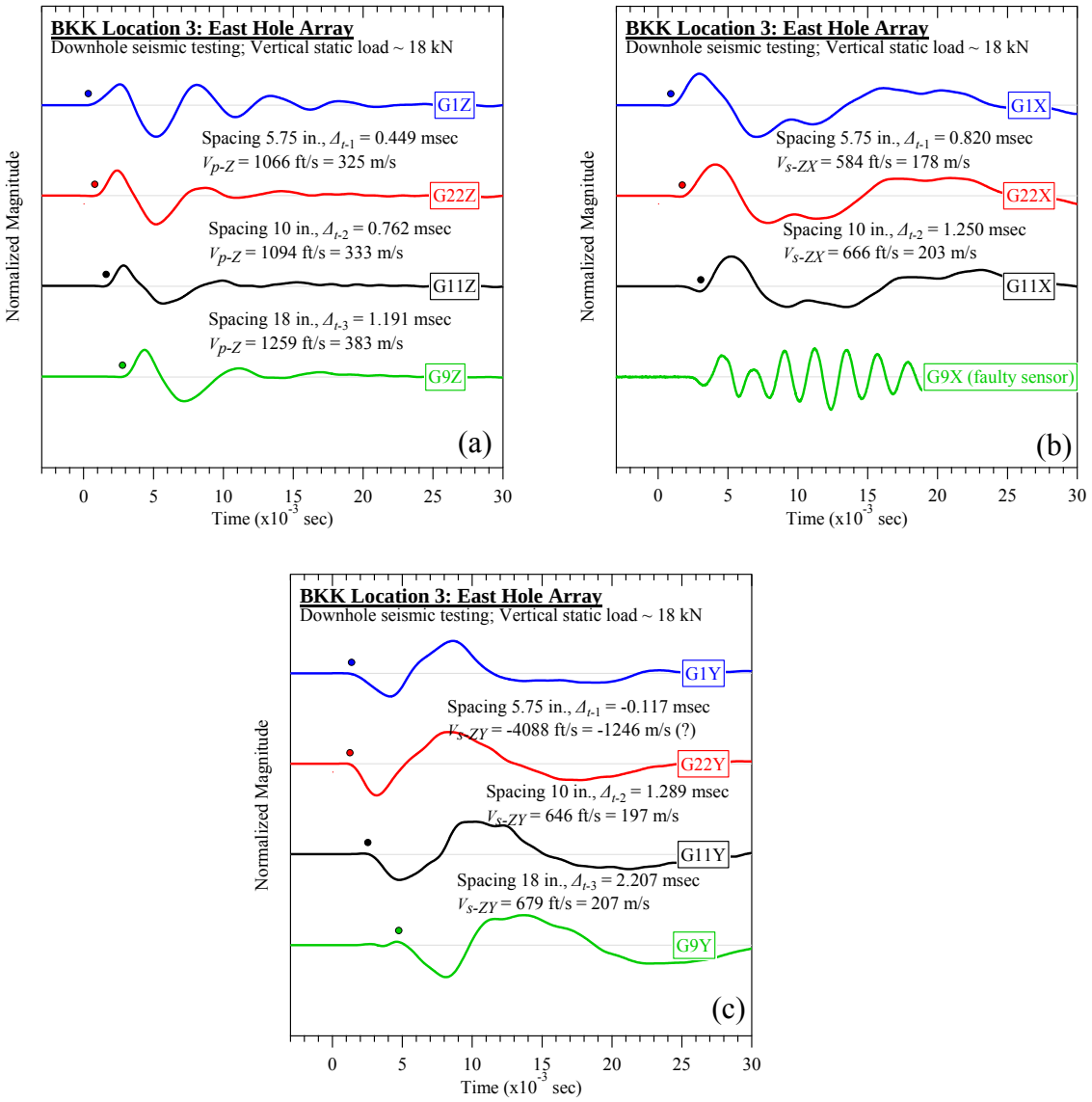

Figure D-103. BKK Landfill #3 (east hole): Downhole seismic testing at vertical load of 18 kN: (a) V_{p-Z}, (b) V_{s-ZX}, and (c) V_{s-ZY}.

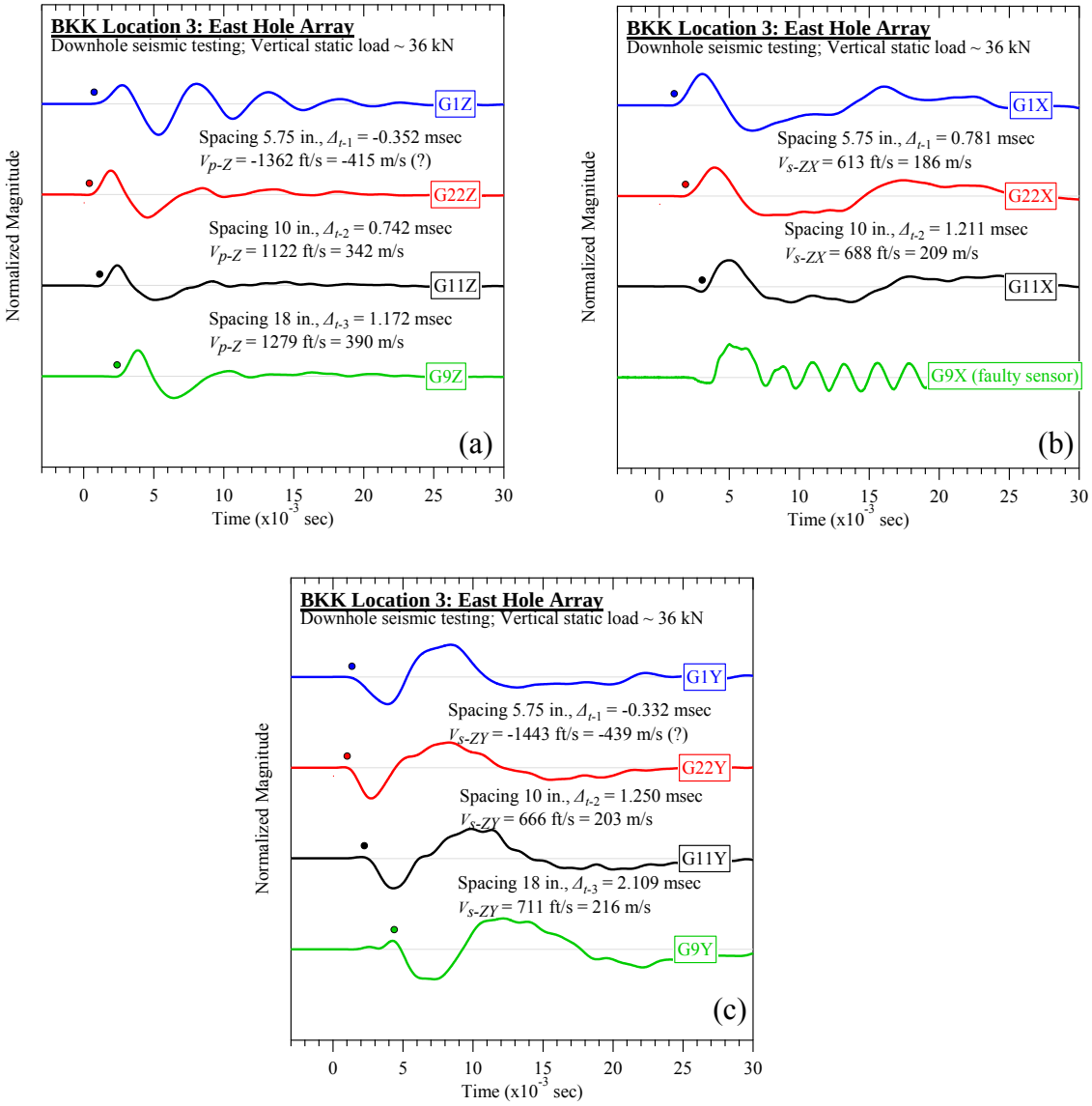

Figure D-104. BKK Landfill #3 (east hole): Downhole seismic testing at vertical load of 36 kN: (a) V_{p-Z}, (b) V_{s-ZX}, and (c) V_{s-ZY}.

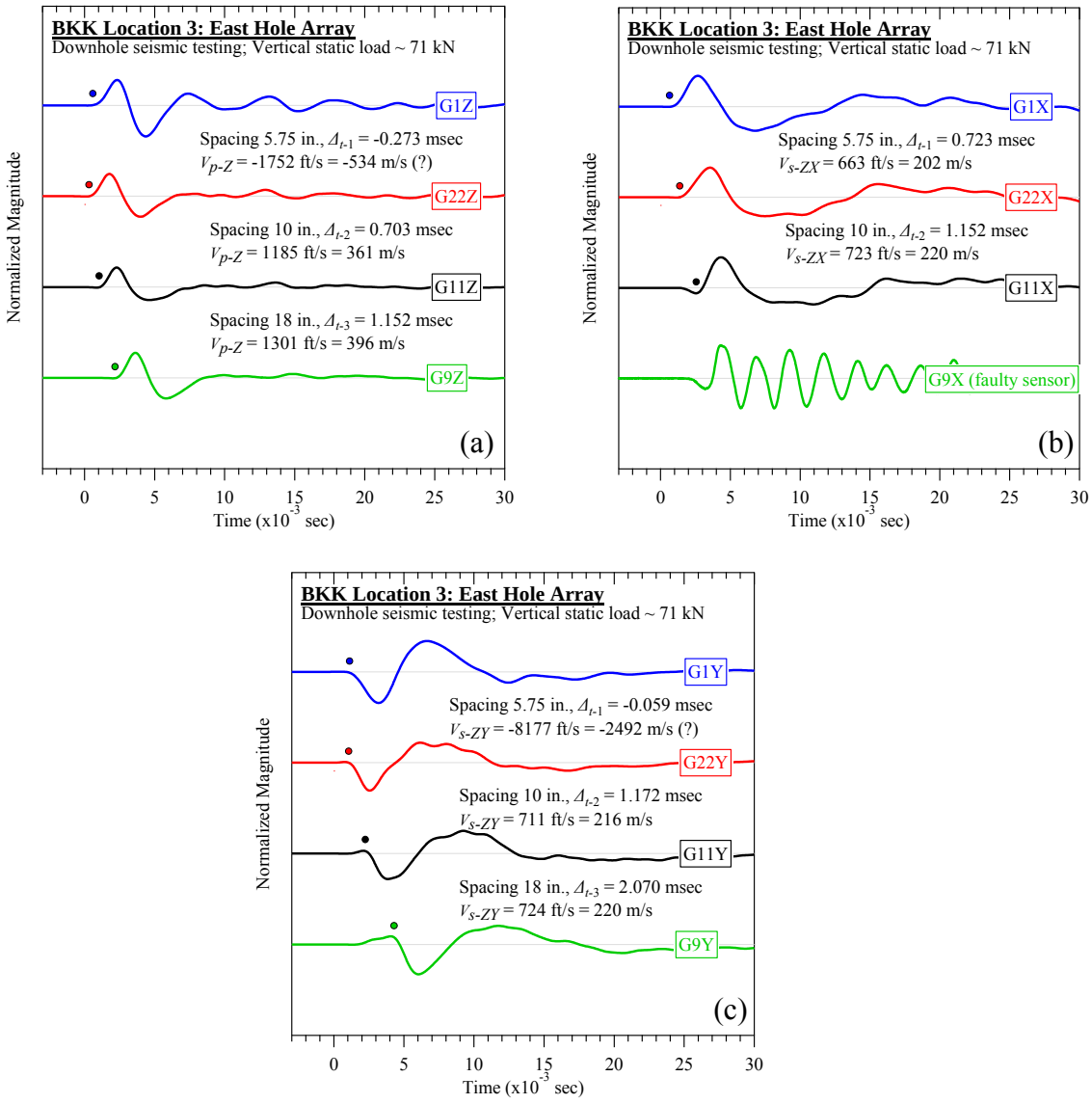

Figure D-105. BKK Landfill #3 (east hole): Downhole seismic testing at vertical load of 71 kN: (a) V_{p-Z}, (b) V_{s-ZX}, and (c) V_{s-ZY}.

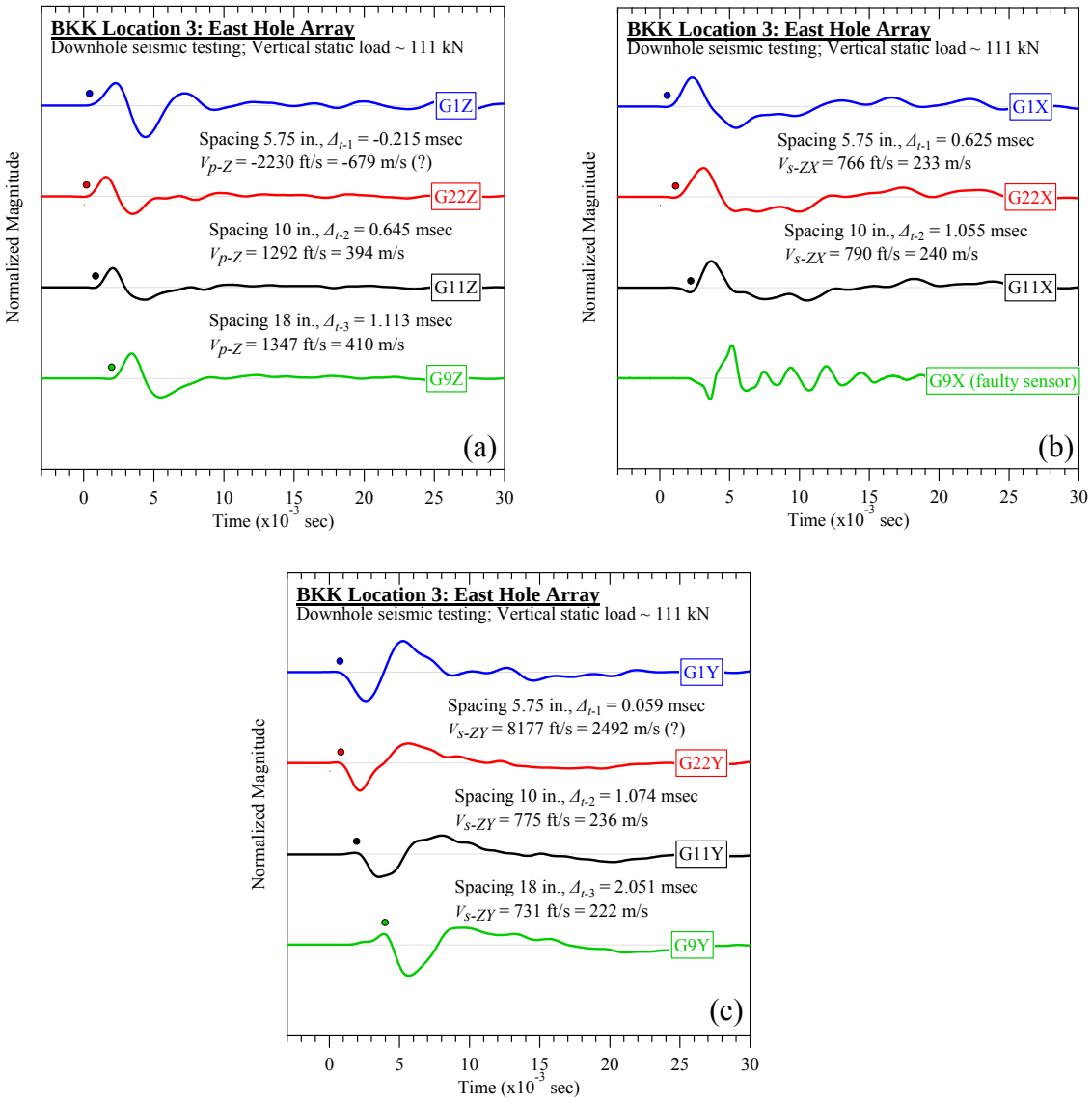

Figure D-106. BKK Landfill #3 (east hole): Downhole seismic testing at vertical load of 111 kN: (a) V_{p-Z}, (b) V_{s-ZX}, and (c) V_{s-ZY}.

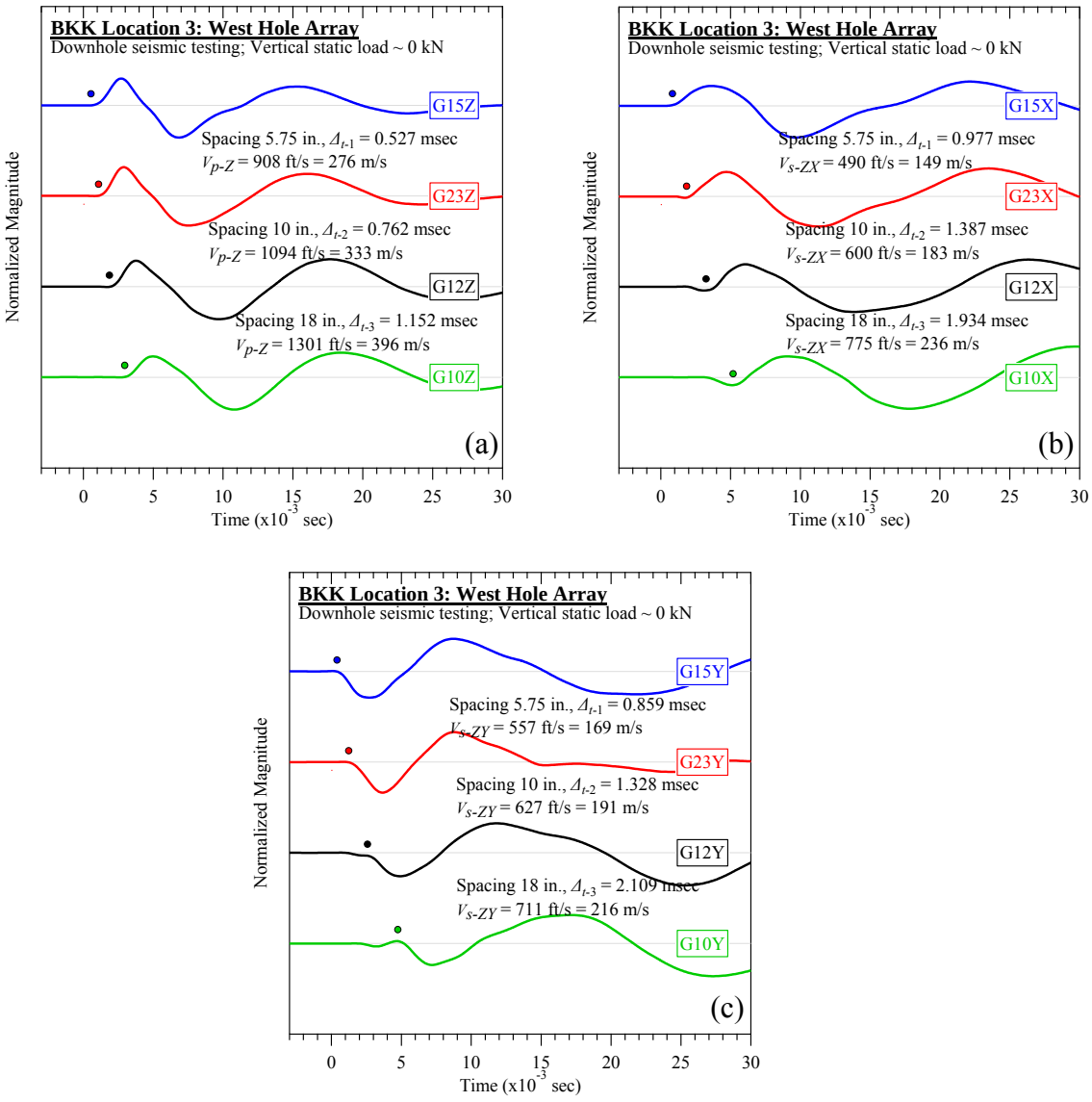

Figure D-107. BKK Landfill #3 (west hole): Downhole seismic testing at vertical load of 0 kN: (a) V_{p-Z}, (b) V_{s-ZX}, and (c) V_{s-ZY}.

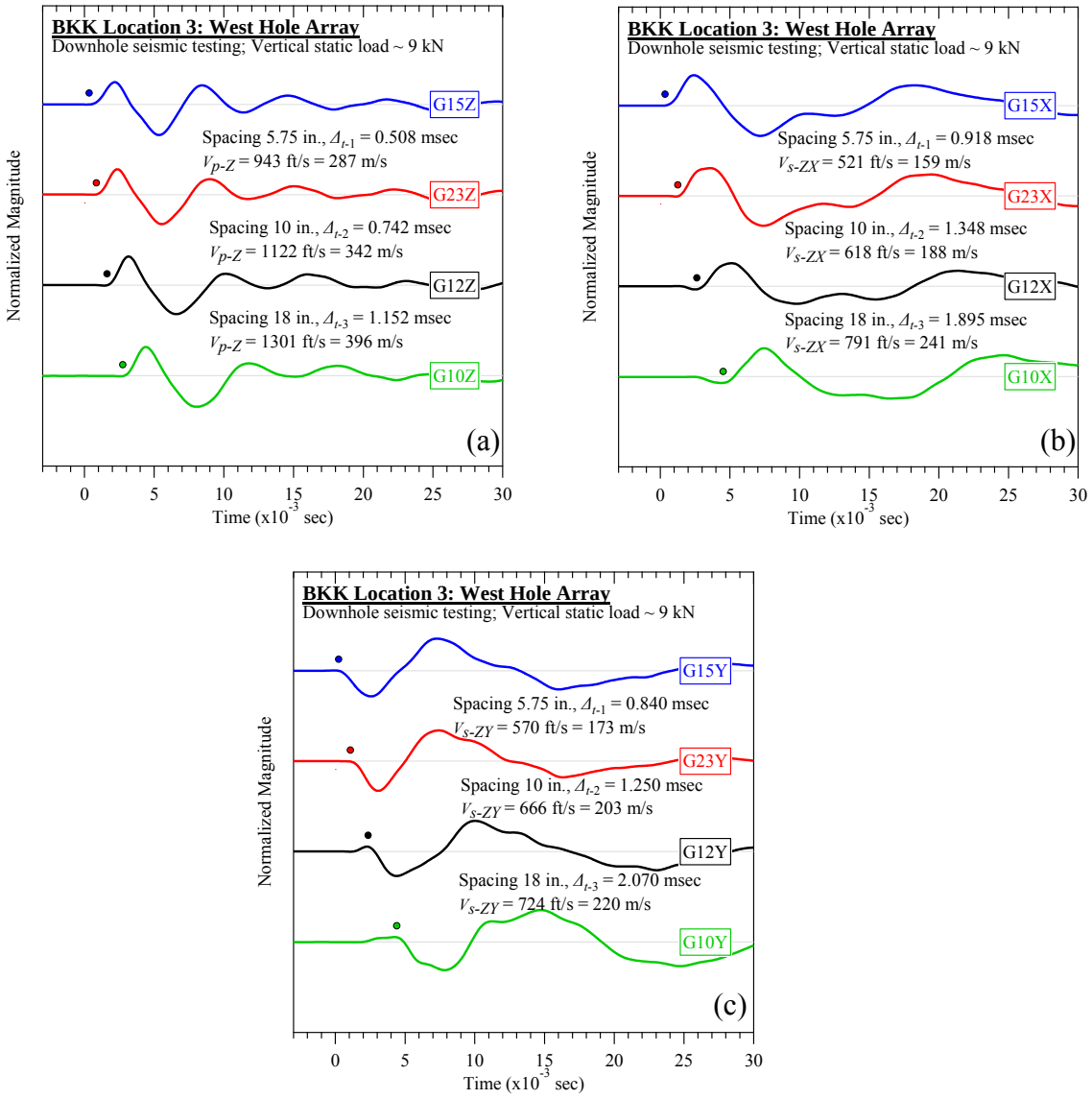

Figure D-108. BKK Landfill #3 (west hole): Downhole seismic testing at vertical load of 9 kN: (a) V_{p-Z}, (b) V_{s-ZX}, and (c) V_{s-ZY}.

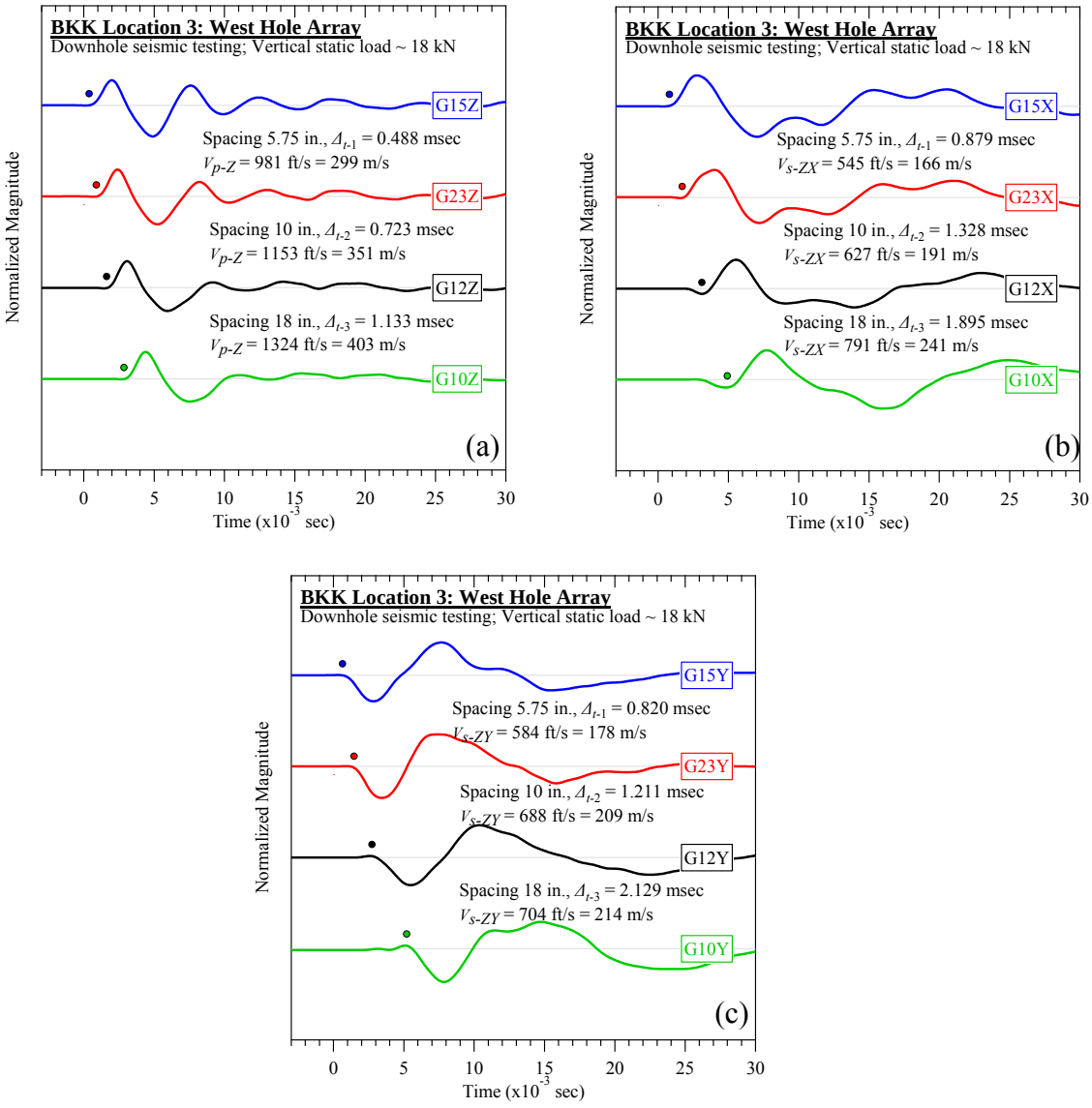

Figure D-109. BKK Landfill #3 (west hole): Downhole seismic testing at vertical load of 18 kN: (a) V_{p-Z}, (b) V_{s-ZX}, and (c) V_{s-ZY}.

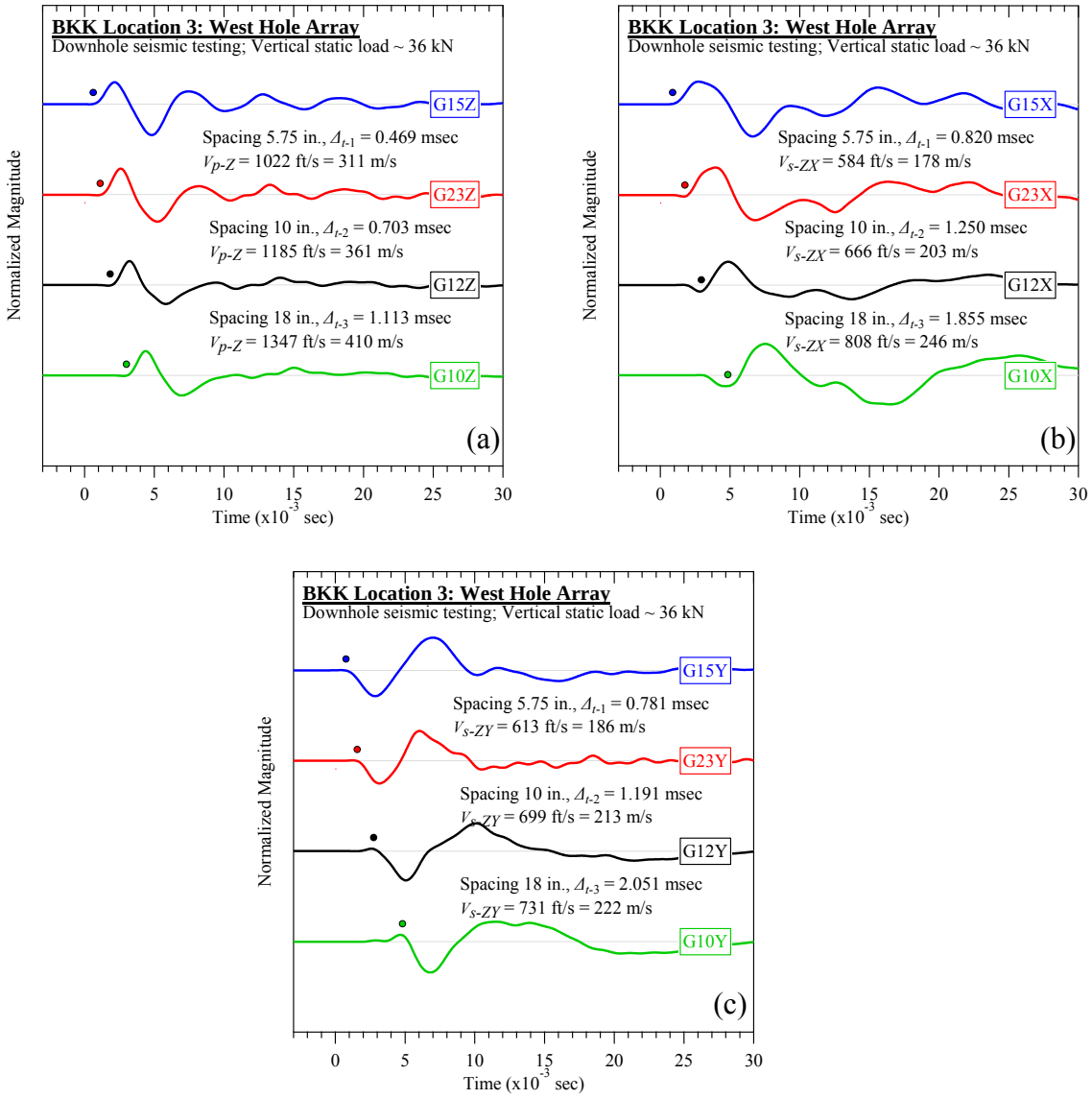

Figure D-110. BKK Landfill #3 (west hole): Downhole seismic testing at vertical load of 36 kN: (a) V_{p-Z}, (b) V_{s-ZX}, and (c) V_{s-ZY}.

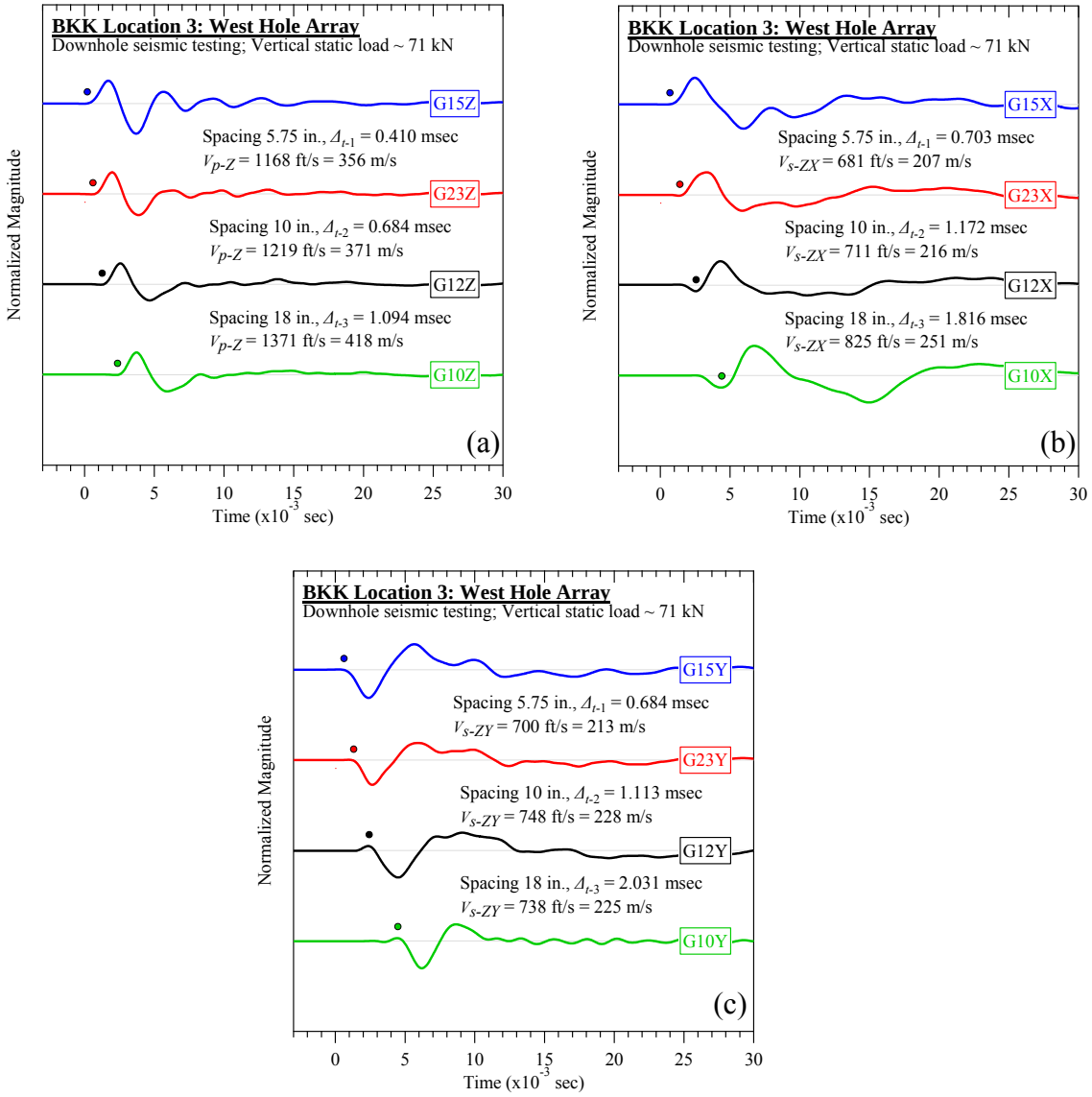

Figure D-111. BKK Landfill #3 (west hole): Downhole seismic testing at vertical load of 71 kN: (a) V_{p-Z}, (b) V_{s-ZX}, and (c) V_{s-ZY}.

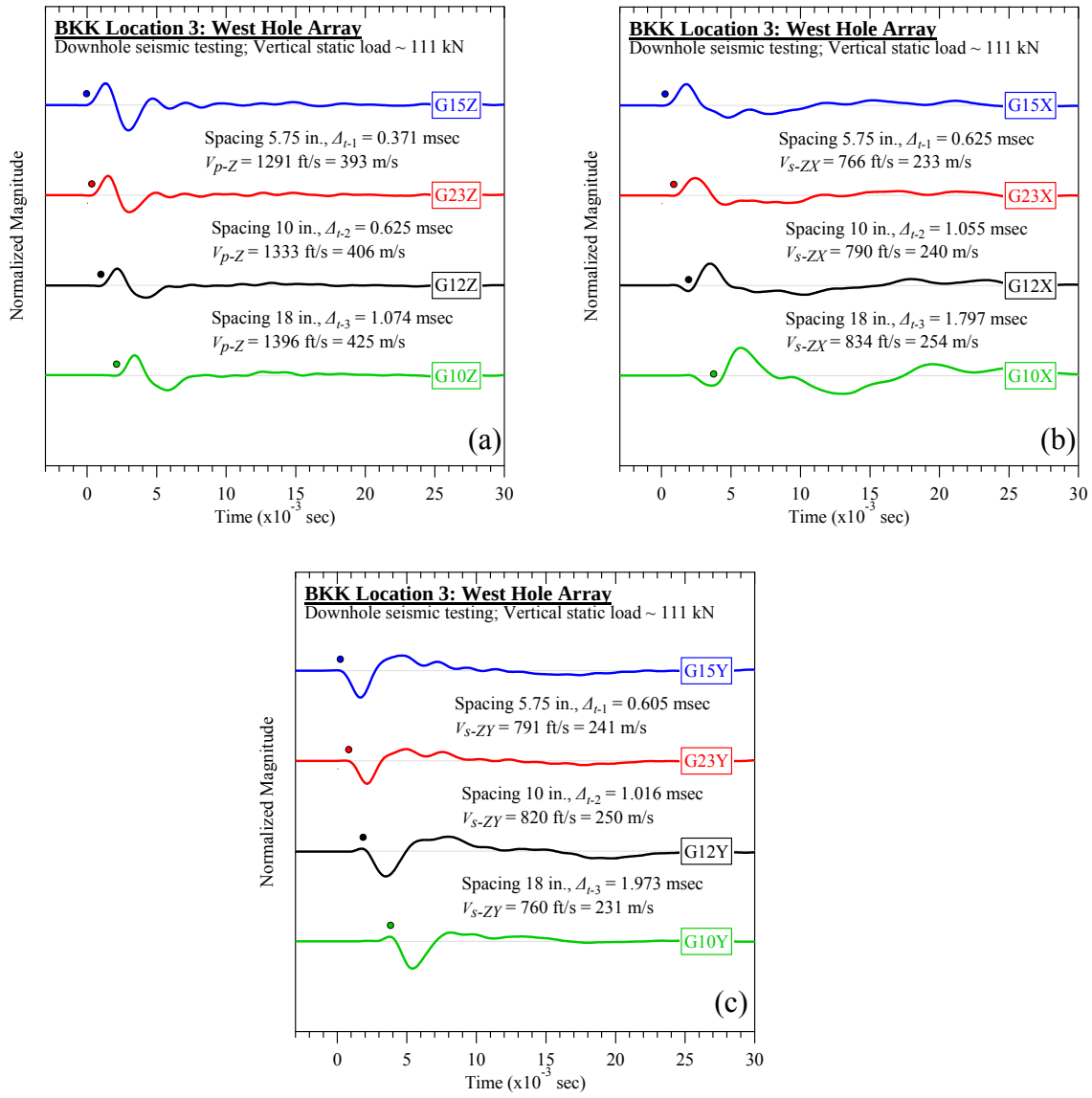

Figure D-112. BKK Landfill #3 (west hole): Downhole seismic testing at vertical load of 111 kN: (a) V_{p-Z}, (b) V_{s-ZX}, and (c) V_{s-ZY}.

D.3.2 Crosshole Seismic Testing

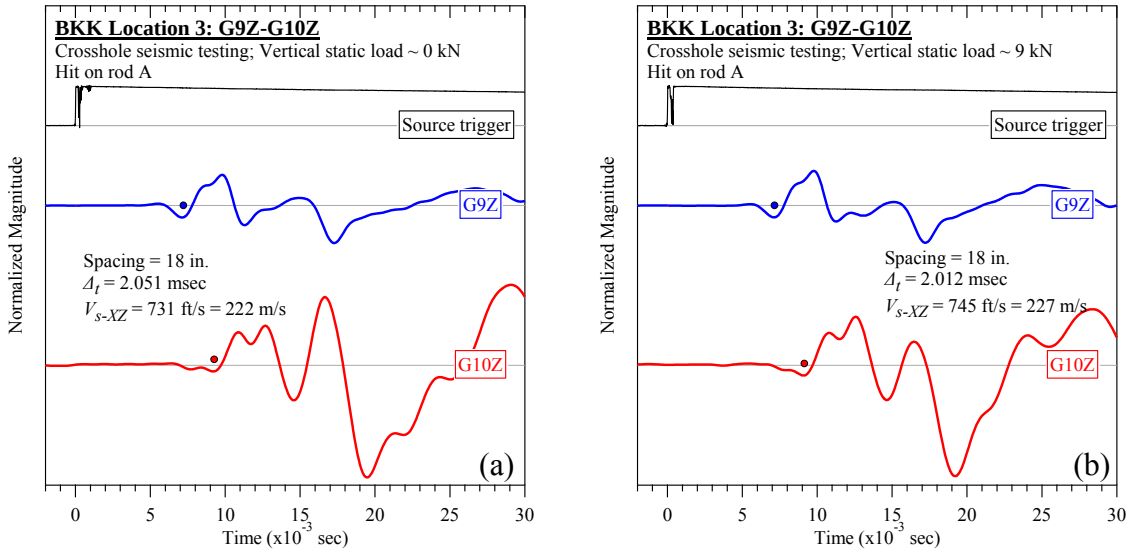

Figure D-113. BKK Landfill #3 (rod A): Crosshole seismic testing at vertical loads of (a) 0 kN and (b) 9 kN: $V_{s\text{-}XZ}$.

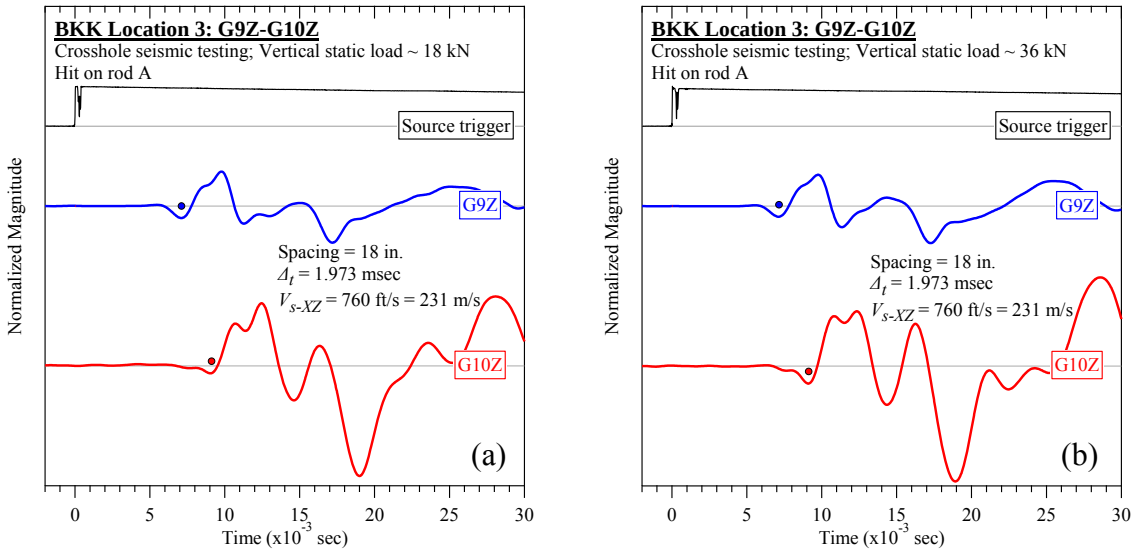

Figure D-114. BKK Landfill #3 (rod A): Crosshole seismic testing at vertical loads of (a) 18 kN and (b) 36 kN: $V_{s\text{-}XZ}$.

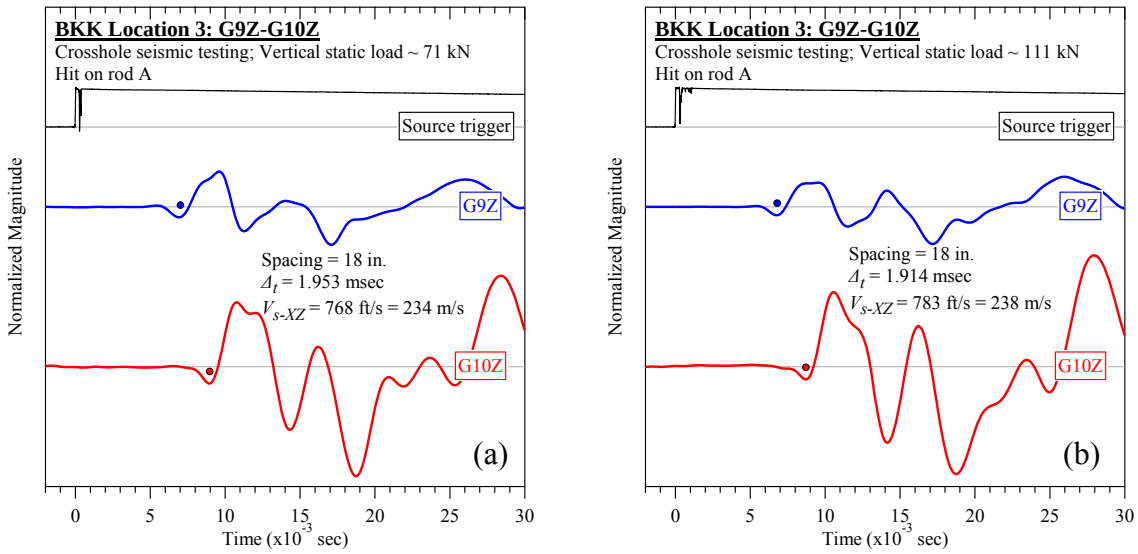

Figure D-115. BKK Landfill #3 (rod A): Crosshole seismic testing at vertical loads of (a) 71 kN and (b) 111 kN: $V_{s\text{-}XZ}$.

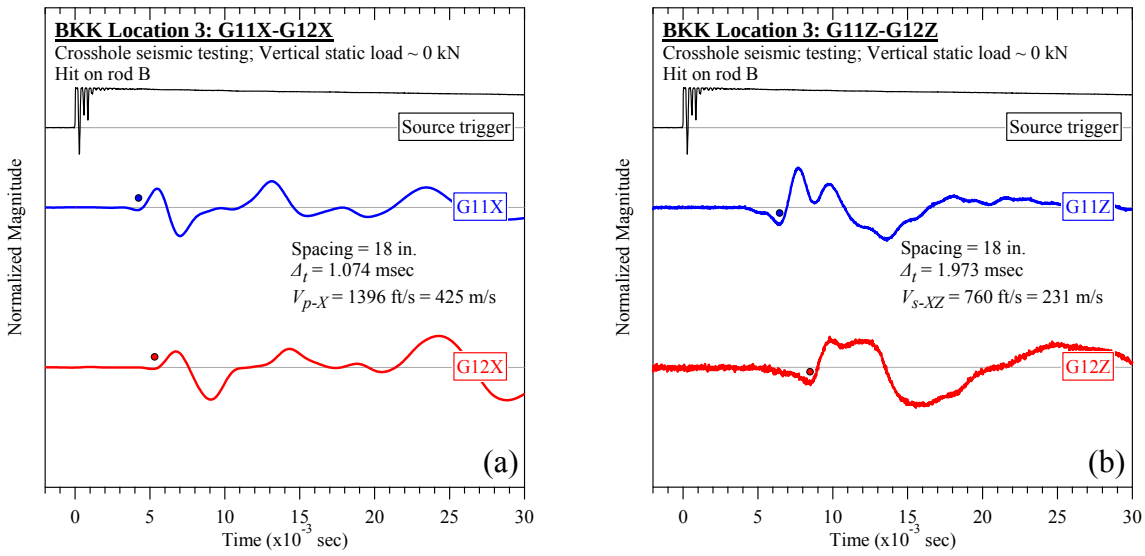

Figure D-116. BKK Landfill #3 (rod B): Crosshole seismic testing at vertical load of 0 kN: (a) $V_{p\text{-}X}$ and (b) $V_{s\text{-}XZ}$.

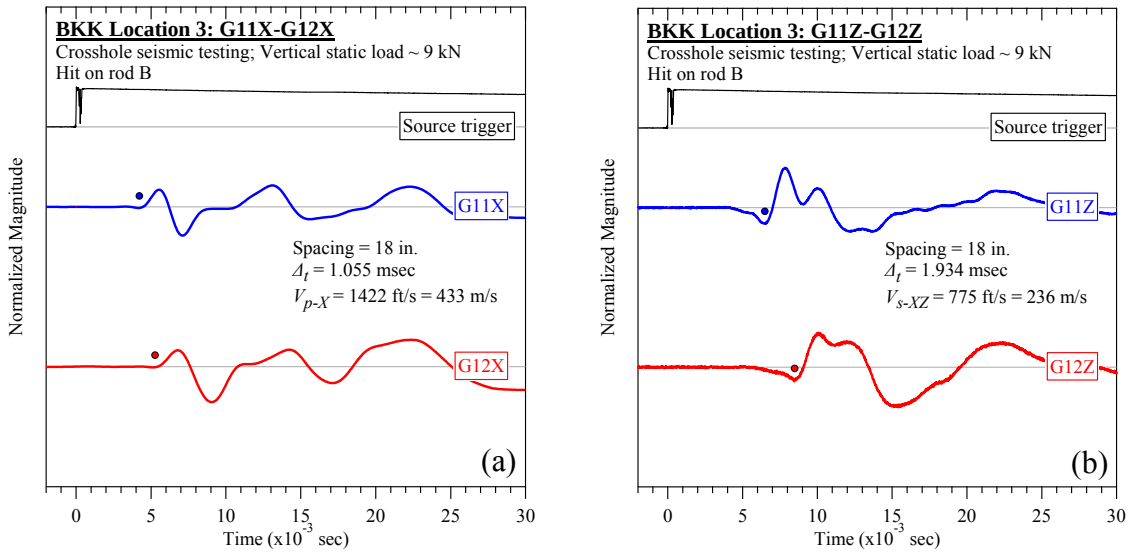

Figure D-117. BKK Landfill #3 (rod B): Crosshole seismic testing at vertical load of 9 kN: (a) $V_{p\text{-}X}$ and (b) $V_{s\text{-}XZ}$.

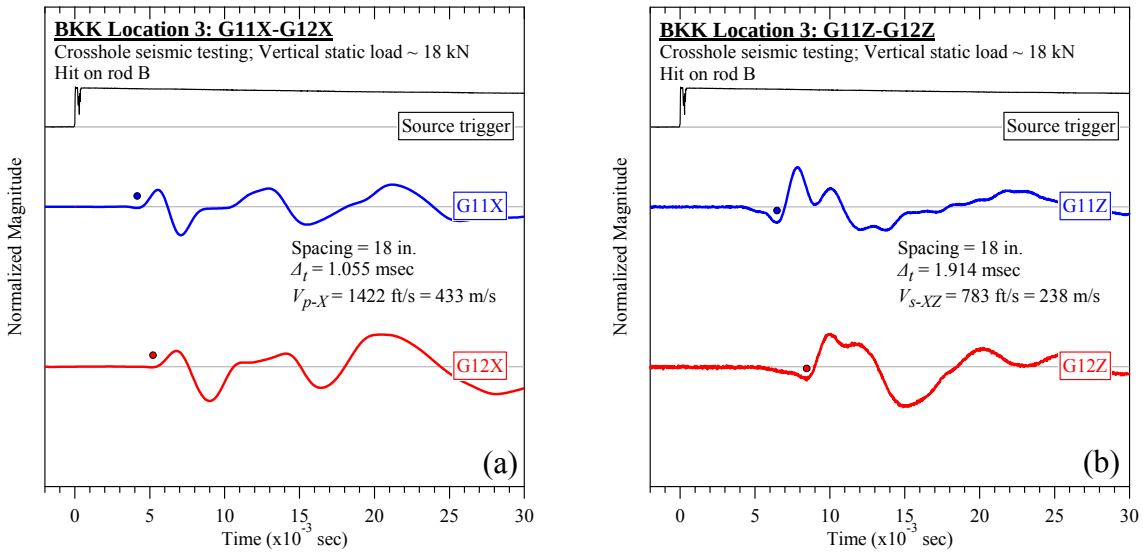

Figure D-118. BKK Landfill #3 (rod B): Crosshole seismic testing at vertical load of 18 kN: (a) $V_{p\text{-}X}$ and (b) $V_{s\text{-}XZ}$.

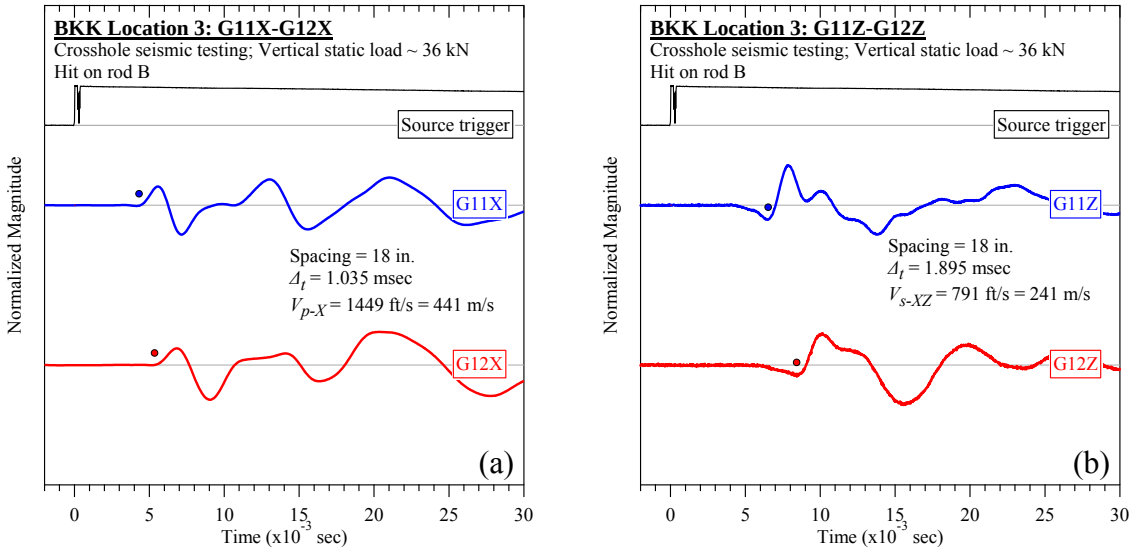

Figure D-119. BKK Landfill #3 (rod B): Crosshole seismic testing at vertical load of 36 kN: (a) $V_{p\text{-}X}$ and (b) $V_{s\text{-}XZ}$.

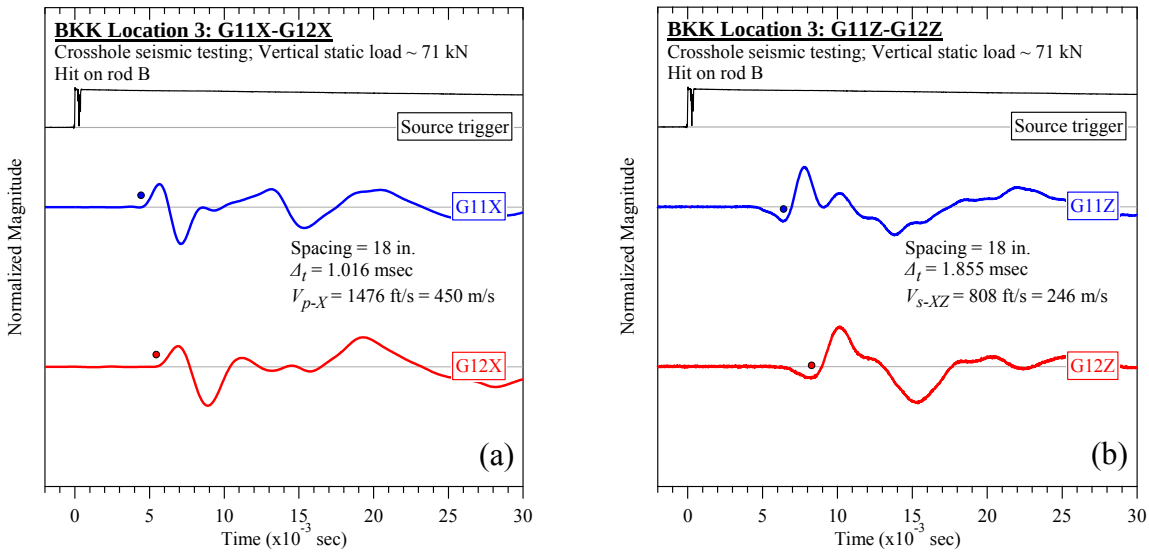

Figure D-120. BKK Landfill #3 (rod B): Crosshole seismic testing at vertical load of 71 kN: (a) $V_{p\text{-}X}$ and (b) $V_{s\text{-}XZ}$.

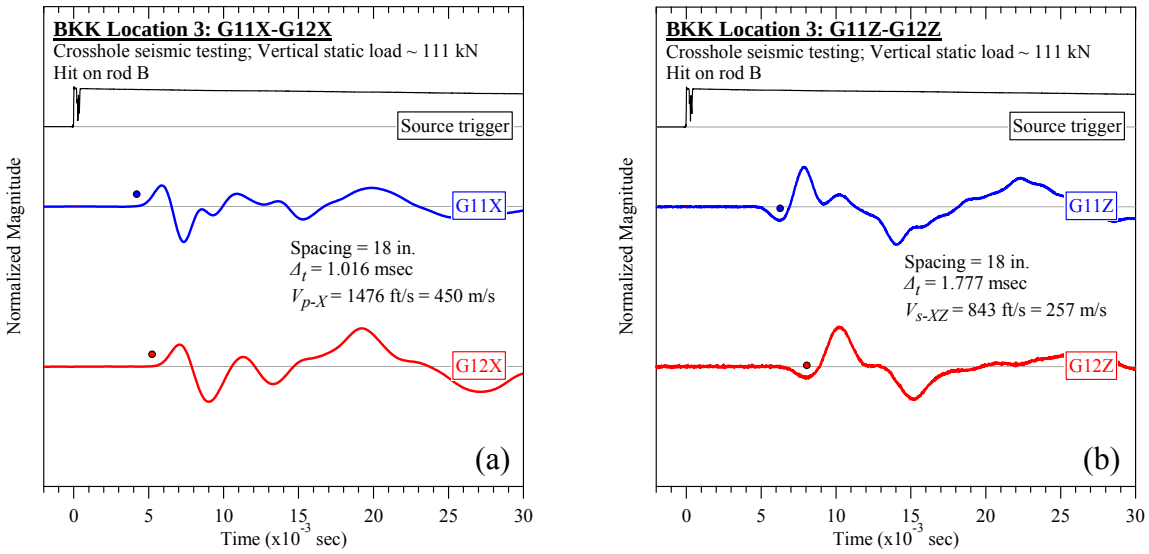

Figure D-121. BKK Landfill #3 (rod B): Crosshole seismic testing at vertical load of 111 kN: (a) $V_{p\text{-}X}$ and (b) $V_{s\text{-}XZ}$.

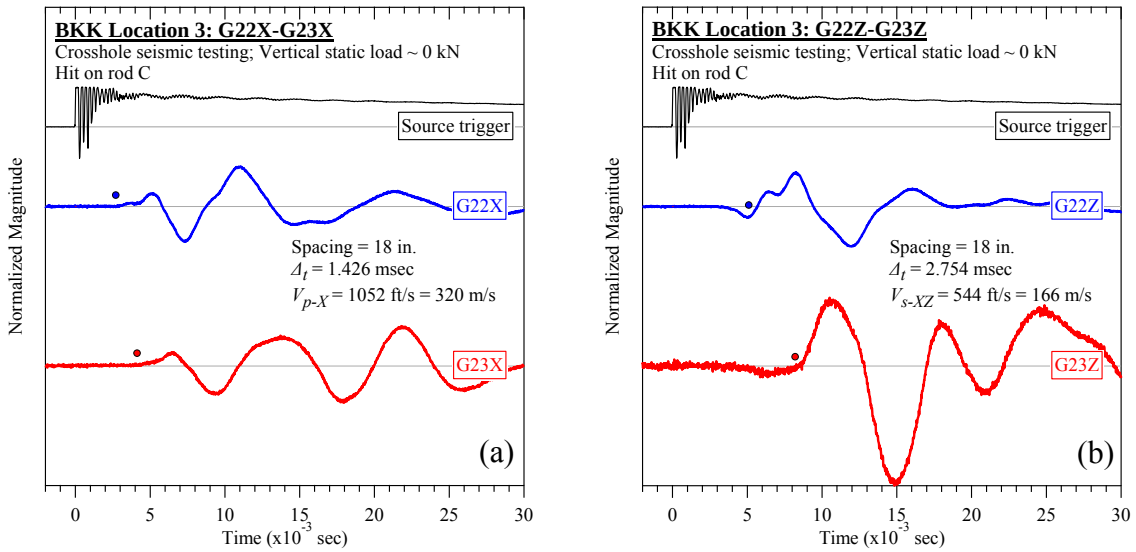

Figure D-122. BKK Landfill #3 (rod C): Crosshole seismic testing at vertical load of 0 kN: (a) $V_{p\text{-}X}$ and (b) $V_{s\text{-}XZ}$.

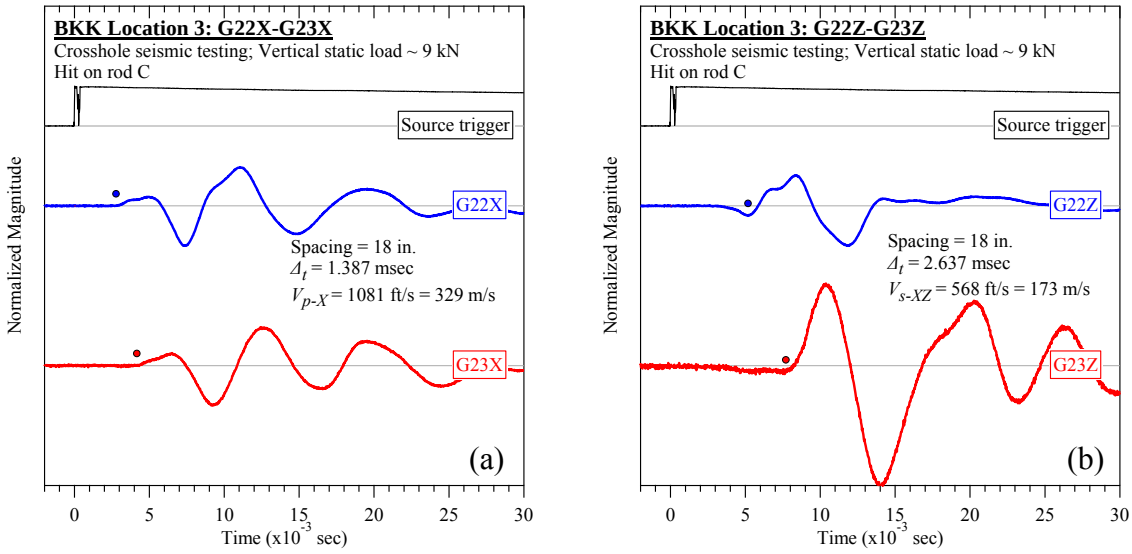

Figure D-123. BKK Landfill #3 (rod C): Crosshole seismic testing at vertical load of 9 kN: (a) $V_{p\text{-}X}$ and (b) $V_{s\text{-}XZ}$.

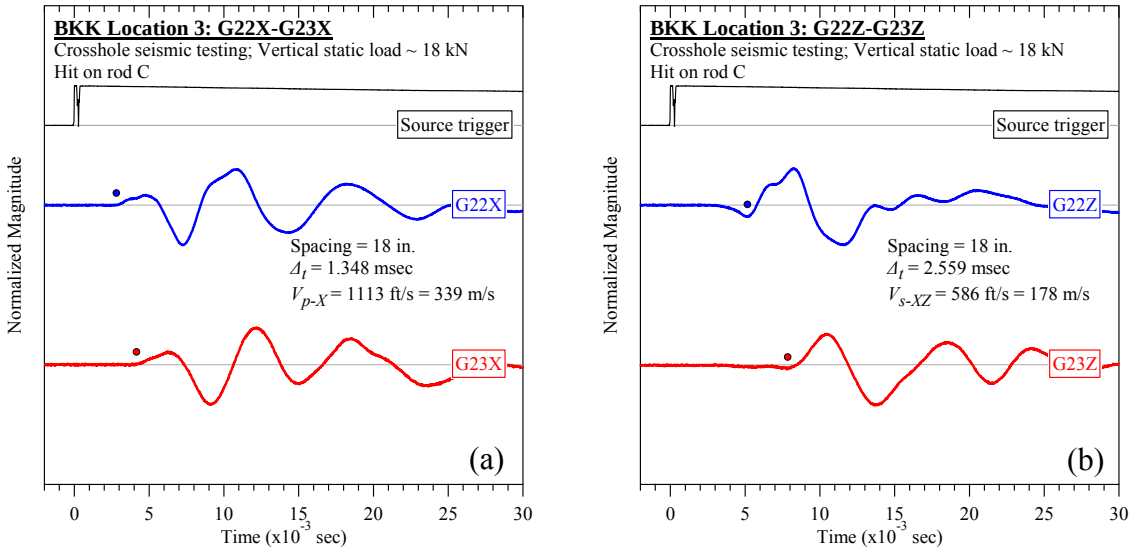

Figure D-124. BKK Landfill #3 (rod C): Crosshole seismic testing at vertical load of 18 kN: (a) $V_{p\text{-}X}$ and (b) $V_{s\text{-}XZ}$.

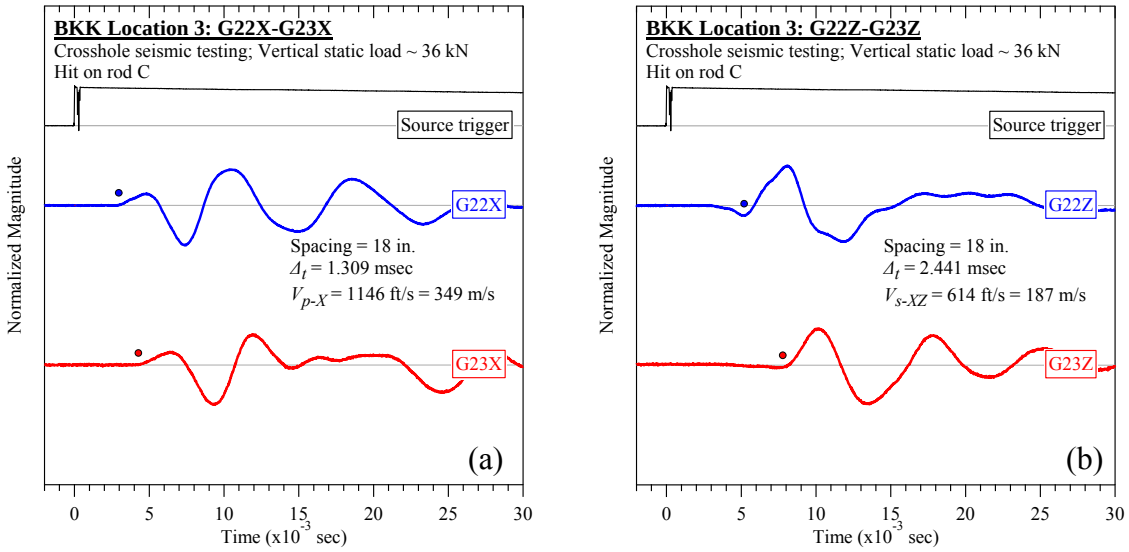

Figure D-125. BKK Landfill #3 (rod C): Crosshole seismic testing at vertical load of 36 kN: (a) $V_{p\text{-}X}$ and (b) $V_{s\text{-}XZ}$.

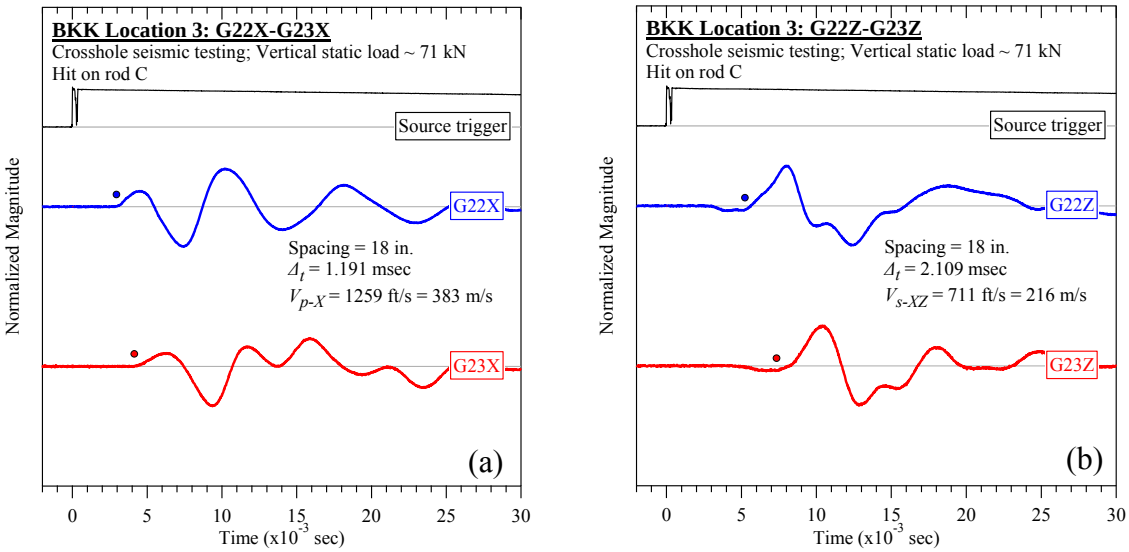

Figure D-126. BKK Landfill #3 (rod C): Crosshole seismic testing at vertical load of 71 kN: (a) $V_{p\text{-}X}$ and (b) $V_{s\text{-}XZ}$.

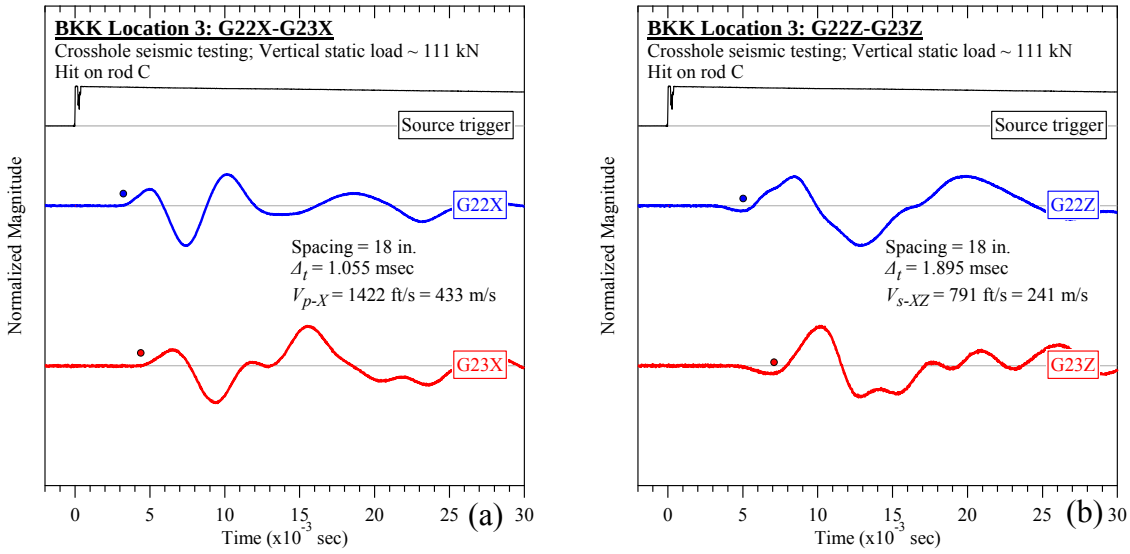

Figure D-127. BKK Landfill #3 (rod C): Crosshole seismic testing at vertical load of 111 kN: (a) $V_{p\text{-}X}$ and (b) $V_{s\text{-}XZ}$.

D.3.3 Steady-state Dynamic Testing

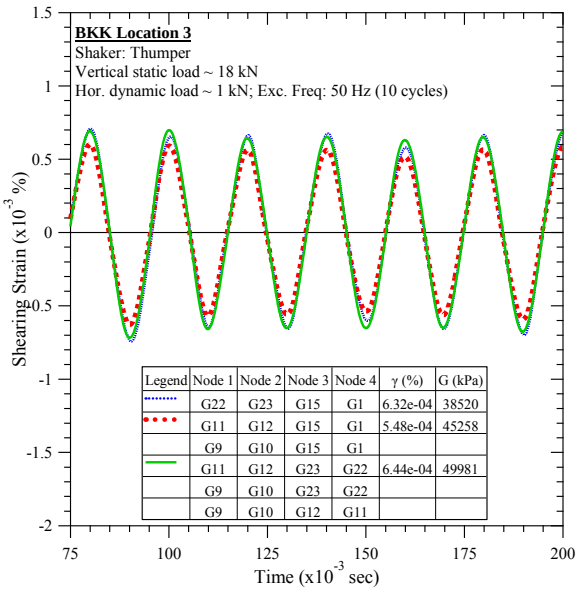

Figure D-128. BKK Landfill #3: Steady-state dynamic testing at vertical load of 18 kN and horizontal dynamic load of 1 kN.

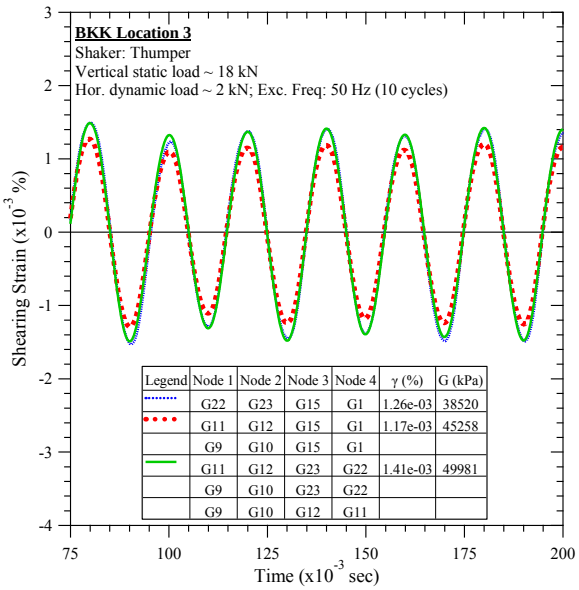

Figure D-129. BKK Landfill #3: Steady-state dynamic testing at vertical load of 18 kN and horizontal dynamic load of 2 kN.

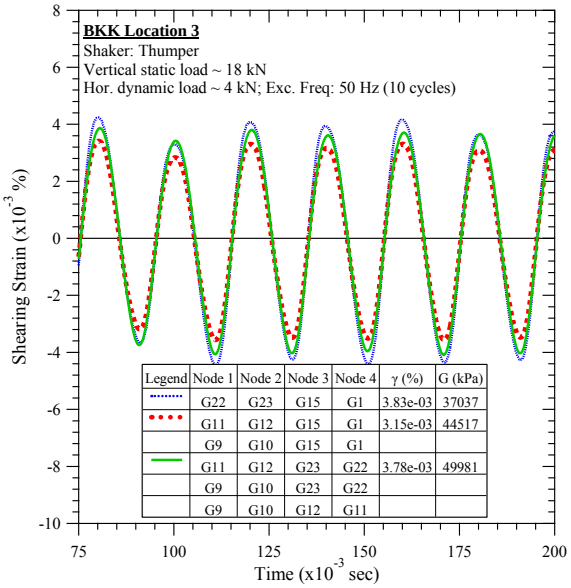

Figure D-130. BKK Landfill #3: Steady-state dynamic testing at vertical load of 18 kN and horizontal dynamic load of 4 kN.

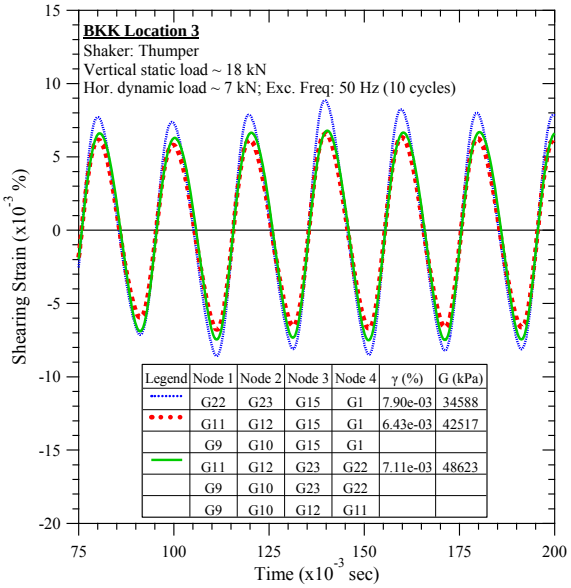

Figure D-131. BKK Landfill #3: Steady-state dynamic testing at vertical load of 18 kN and horizontal dynamic load of 7 kN.

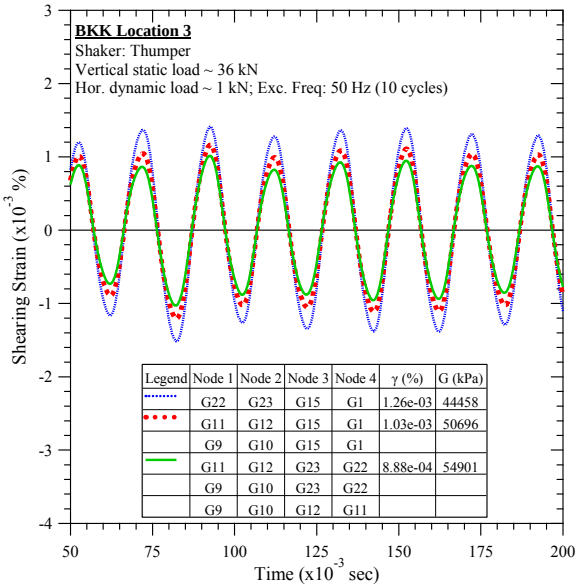

Figure D-132. BKK Landfill #3: Steady-state dynamic testing at vertical load of 36 kN and horizontal dynamic load of 0.56 kN.

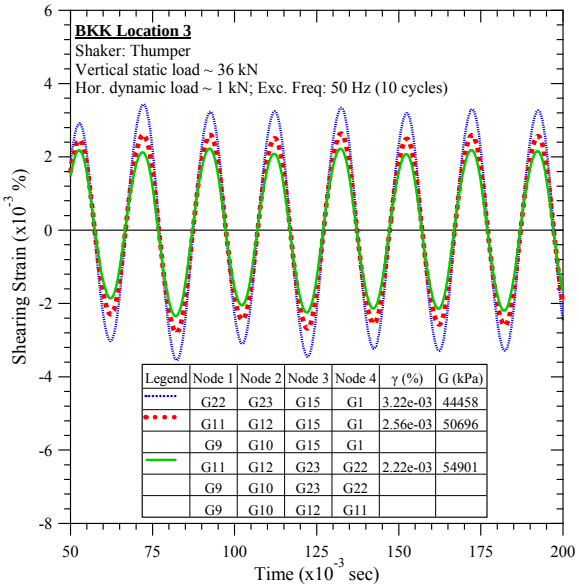

Figure D-133. BKK Landfill #3: Steady-state dynamic testing at vertical load of 36 kN and horizontal dynamic load of 1 kN.

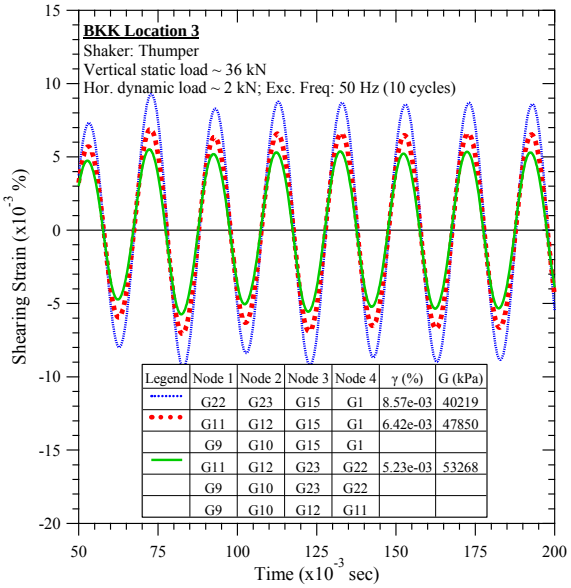

Figure D-134. BKK Landfill #3: Steady-state dynamic testing at vertical load of 36 kN and horizontal dynamic load of 2 kN.

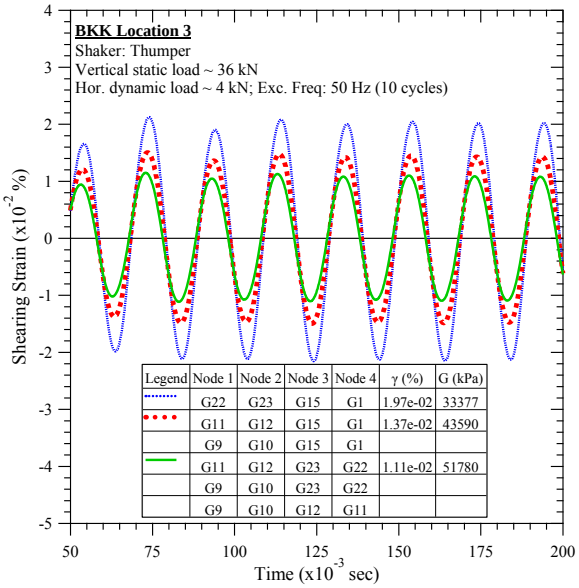

Figure D-135. BKK Landfill #3: Steady-state dynamic testing at vertical load of 36 kN and horizontal dynamic load of 4 kN.

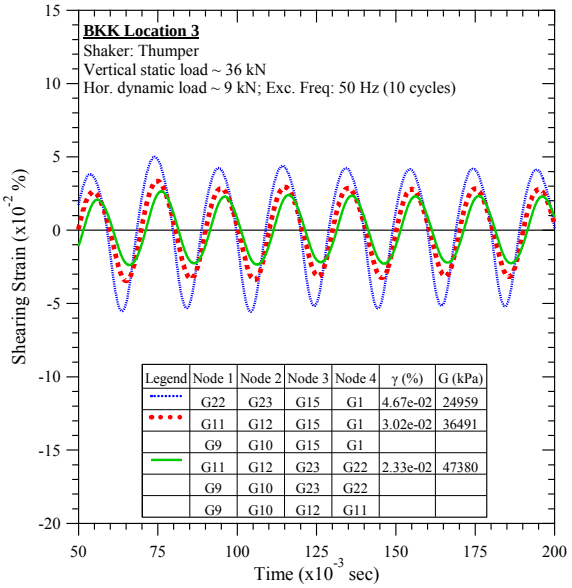

Figure D-136. BKK Landfill #3: Steady-state dynamic testing at vertical load of 36 kN and horizontal dynamic load of 9 kN.

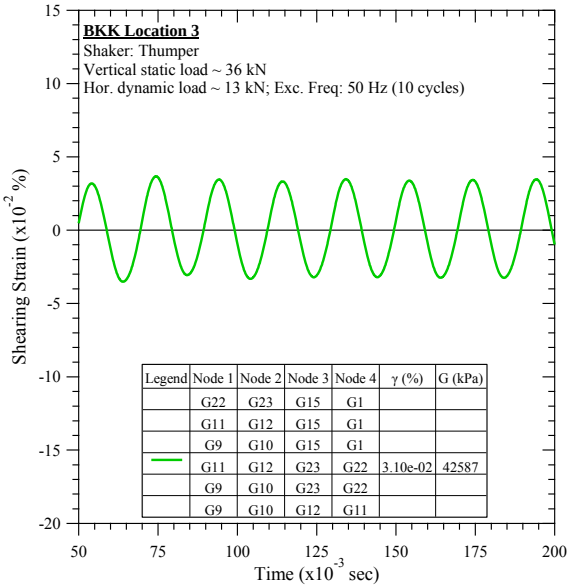

Figure D-137. BKK Landfill #3: Steady-state dynamic testing at vertical load of 36 kN and horizontal dynamic load of 13 kN.

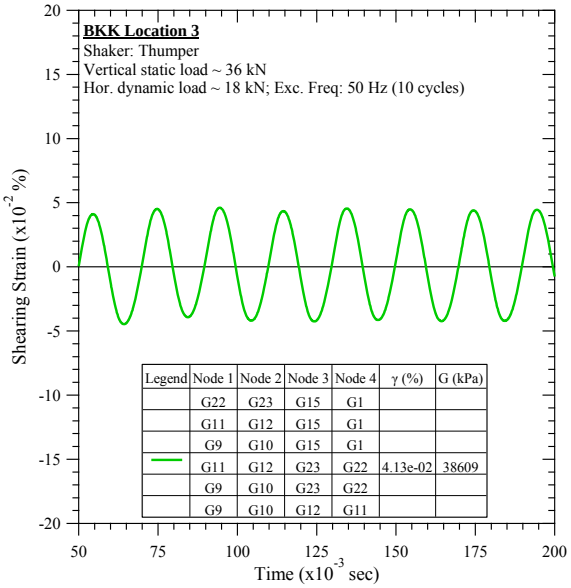

Figure D-138. BKK Landfill #3: Steady-state dynamic testing at vertical load of 36 kN and horizontal dynamic load of 18 kN.

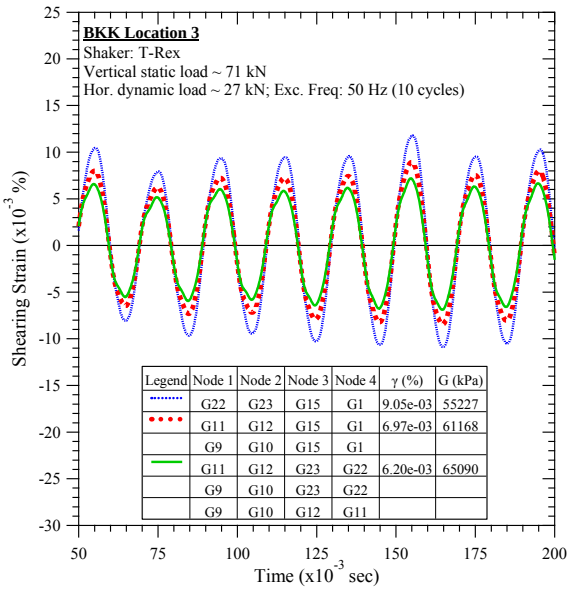

Figure D-139. BKK Landfill #3: Steady-state dynamic testing at vertical load of 71 kN and horizontal dynamic load of 27 kN.

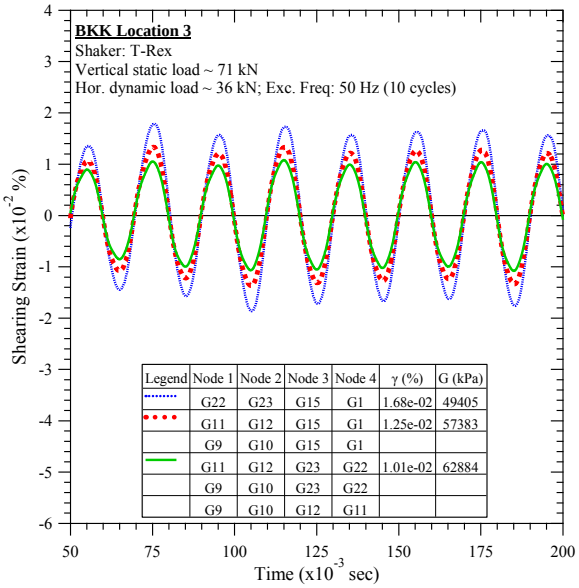

Figure D-140. BKK Landfill #3: Steady-state dynamic testing at vertical load of 71 kN and horizontal dynamic load of 36 kN.

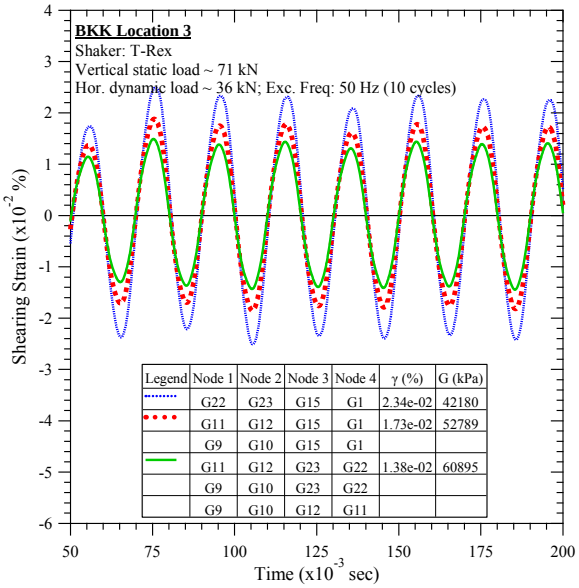

Figure D-141. BKK Landfill #3: Steady-state dynamic testing at vertical load of 71 kN and horizontal dynamic load of 36 kN.

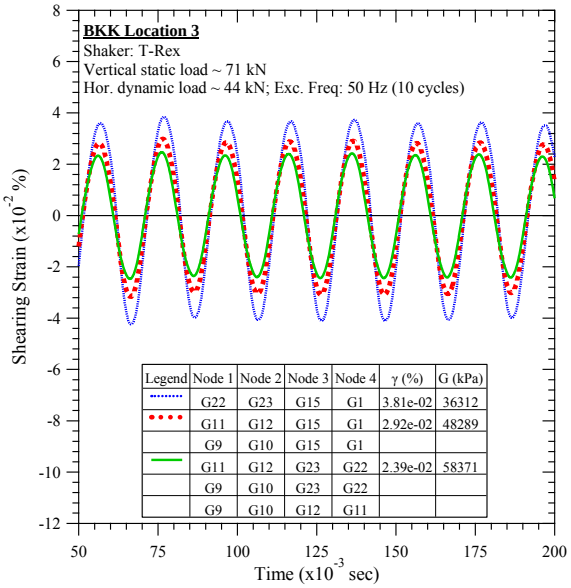

Figure D-142. BKK Landfill #3: Steady-state dynamic testing at vertical load of 71 kN and horizontal dynamic load of 44 kN.

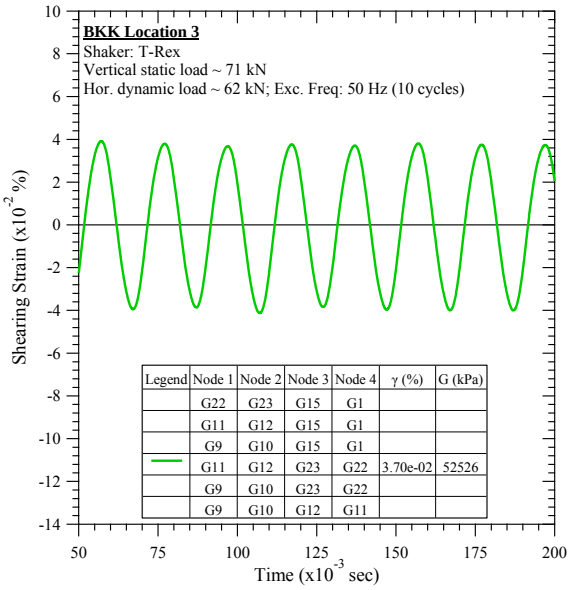

Figure D-143. BKK Landfill #3: Steady-state dynamic testing at vertical load of 71 kN and horizontal dynamic load of 62 kN.

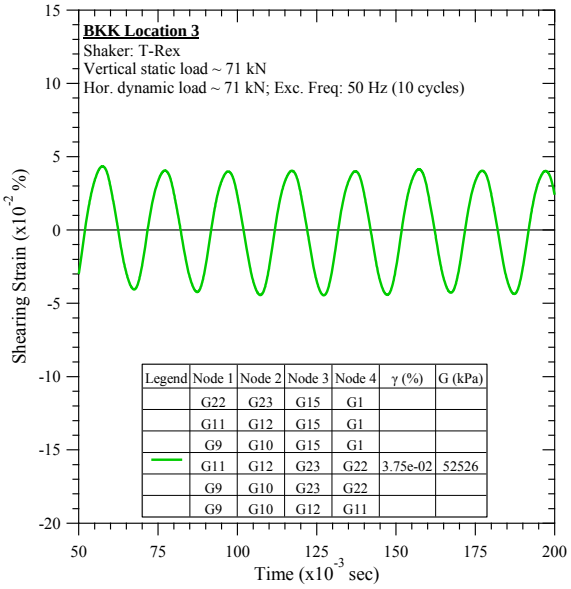

Figure D-144. BKK Landfill #3: Steady-state dynamic testing at vertical load of 71 kN and horizontal dynamic load of 71 kN.

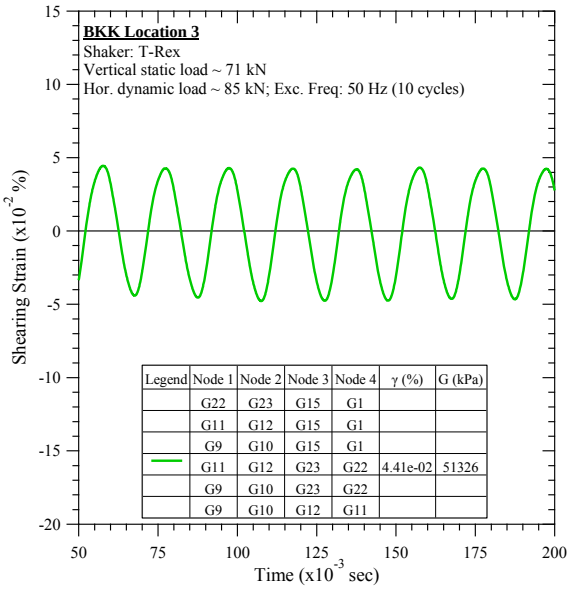

Figure D-145. BKK Landfill #3: Steady-state dynamic testing at vertical load of 71 kN and horizontal dynamic load of 85 kN.

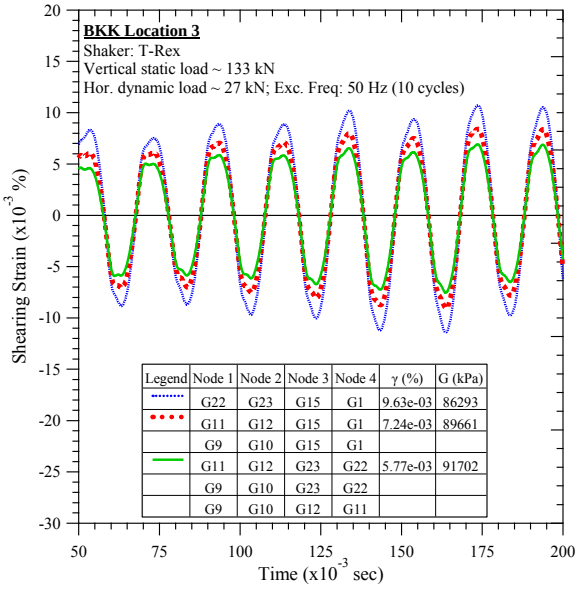

Figure D-146. BKK Landfill #3: Steady-state dynamic testing at vertical load of 133 kN and horizontal dynamic load of 27 kN.

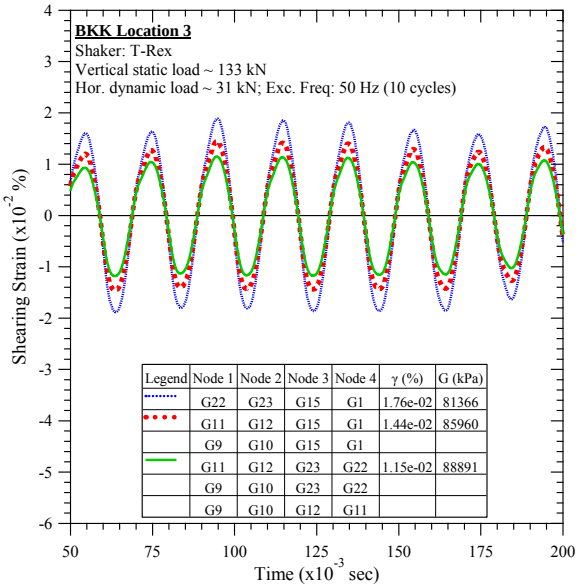

Figure D-147. BKK Landfill #3: Steady-state dynamic testing at vertical load of 133 kN and horizontal dynamic load of 31 kN.

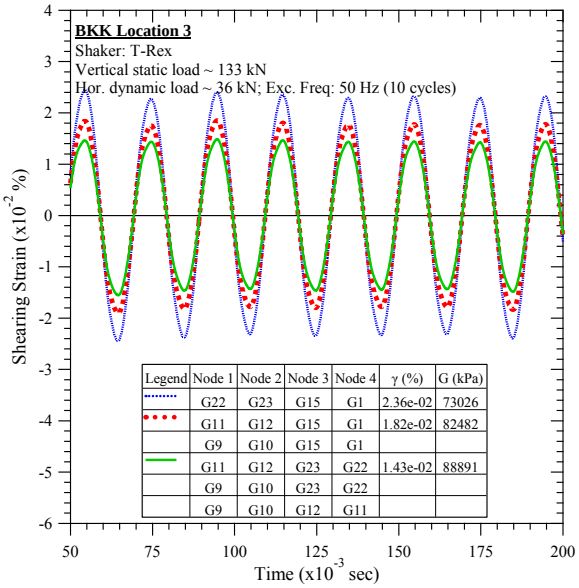

Figure D-148. BKK Landfill #3: Steady-state dynamic testing at vertical load of 133 kN and horizontal dynamic load of 36 kN.

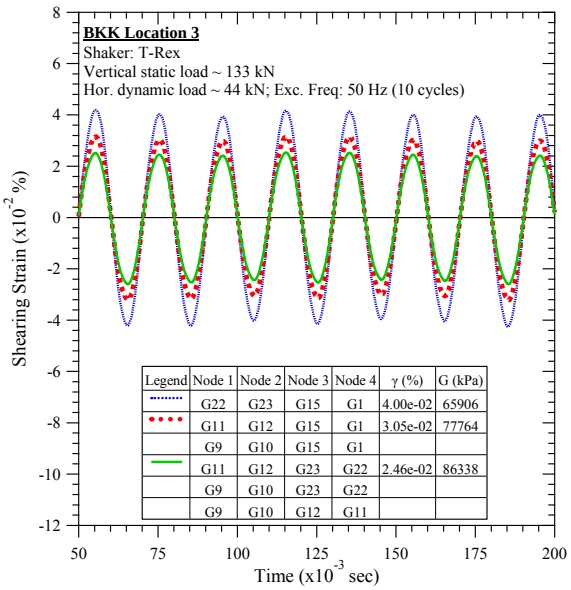

Figure D-149. BKK Landfill #3: Steady-state dynamic testing at vertical load of 133 kN and horizontal dynamic load of 44 kN.

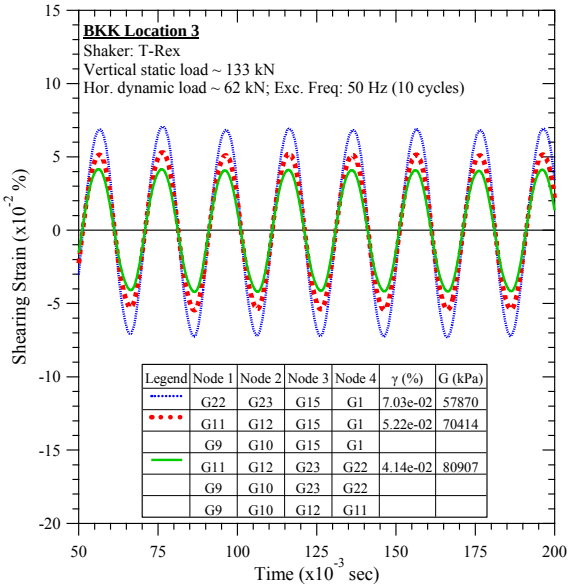

Figure D-150. BKK Landfill #3: Steady-state dynamic testing at vertical load of 133 kN and horizontal dynamic load of 62 kN.

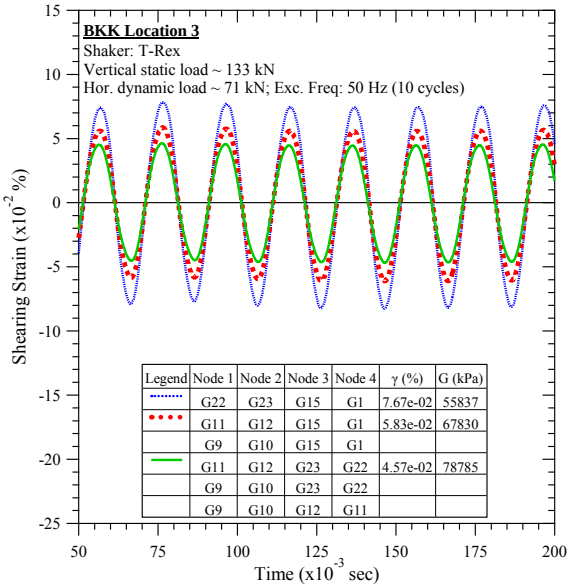

Figure D-151. BKK Landfill #3: Steady-state dynamic testing at vertical load of 133 kN and horizontal dynamic load of 71 kN.

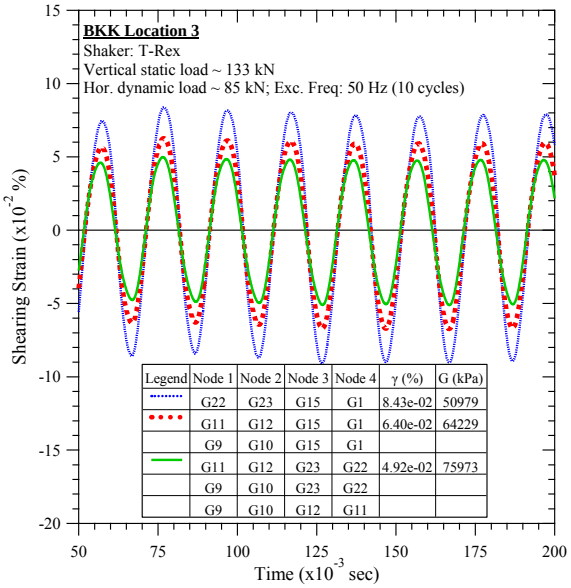

Figure D-152. BKK Landfill #3: Steady-state dynamic testing at vertical load of 133 kN and horizontal dynamic load of 85 kN.

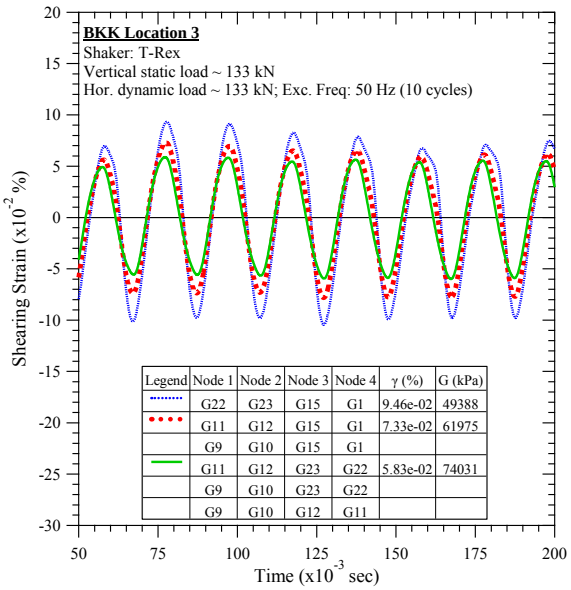

Figure D-153. BKK Landfill #3: Steady-state dynamic testing at vertical load of 133 kN and horizontal dynamic load of 133 kN.

REFERENCES

Aki, K., 1957, “Space and Time Spectra of Stationary Stochastic Waves with Special Reference to Microtremors,” Bull. Earthq. Res. Inst., v. 35: 415-456.

Amat A. S., 2007, "Elastic stiffness moduli of Huston sand," Project report. Department of Civil Engineering, University of Bristol, UK

Anderson, D. G. and Kavazanjian, E. Jr., 1995, "Performance of landfills under seismic loading," Proc. 3rd International Conference on Recent Advances in Geotechnical Earthquake Engineering and Soil Dynamics, St. Louis, Missouri, 3, 277-306.

Anderson, R. L., 1995, "Earthquake related damage and landfill performance," In: Earthquake Design and Performance of Solid Waste Landfills, ASCE Geotechnical Special Publication No. 54, 1-16.

Andrus, R. D., and Stokoe, K. H., II., 2000, “Liquefaction resistance of soils from shear-wave velocity,” J. Geotech. Geoenviron. Eng., 126(11), 1015–1025.

Andrus, R. D., Zhang, J., Ellis, B. S., and Juang, C. H., 2003, “Guide for estimating the dynamic properties of South Carolina soils for ground response analysis.” Rep. No. FHWA-SC-03-07, South Carolina Department of Transportation, Columbia, S.C.

Argrwal TK, Ishibashi I, 1991, "Multi-directional wave velocity by piezoelectric crystals". In: Bhatia, Blaney (eds) Proceedings, recent advances in instrumentation, data acquisition and testing in soil dynamics, Orlando, FL. ASCE, pp 102–117

Arroyo, M., Muir Wood, D., Greening, P.D., Medina, L., and Rio, J. 2006, "Effects of sample size on bender-based axial G_0 measurements," Geotechnique, 56(1): 39–52.

Arulnathan R., Boulanger R. W., Riemer M. F., 1998, "Analysis of bender element tests," Geotech Testing J ASTM 21(2): 120–131

Asten M. W., 1983., “Discussion on Seismic Array Noise Studies at Roosevelt Hot Springs, Utah Geothermal Area.” Geophysics v. 48: 1560–1561

Asten,M. W., Dhu, T., and Lam, N., 2004 ”Optimised array design for microtremor array studies applied to site classification; observations, results and future use” Paper 2903, Conference Proceedings of the 13th World Conference of Earthquake Engineering, Vancouver, Aug 1-6.

ASTM D1140-00(2006) “Standard Test Methods for Amount of Material in Soils Finer than No. 200 (75-μm) Sieve”

ASTM D1556 - 07 “Standard Test Method for Density and Unit Weight of Soil in Place by the Sand-Cone Method”

ASTM D2487-11 “Standard Practice for Classification of Soils for Engineering Purposes (Unified Soil Classification System)”

ASTM D422-63(2007) “Standard Test Method for Particle-Size Analysis of Soils”

ASTM D4318-10 “Standard Test Methods for Liquid Limit, Plastic Limit, and Plasticity Index of Soils”

Athanasopoulos, G., Grizi, A., Zekkos, D., Founta P., Zisimatou, E., 2008, "Municipal Solid Waste as a Reinforced Soil: Investigation Using Synthetic Waste", ASCE-Geoinstitute Geocongress 2008, The challenge of sustainability in the geoenvironment, March 9-12 2008, New Orleans, Geotechnics of Waste Management and Remediation, Geotechnical Special Publication (GSP) #177, pp. 168-175.

Athanasopoulos-Zekkos, A., Zekkos, D., and Matasovic, N., 2008, "Validation of generic municipal solid waste material properties for seismic design of landfills", 4th Geotechnical Earthquake Engineering and Soil Dynamics Conference, Sacramento, CA, May 18-22, 2008.

Augello, A. J., Bray, J. D., Leonards, G. A., Repetto, P. C., Byrne, R. J., 1995, "Response of landfills to seismic loading", Geoenvironment 2000, ASCE Geotechnical Special Publication No. 46, Vol. 2, pp. 1050-1065.

Augello, A. J., Bray, J. D., Seed, R. B., Matasovic, N., and Kavazanjian, E., Jr., 1998b, "Performance of solid-waste landfill during the Northridge earthquake," Proc., NEHRP Conf. and Workshop on Research on the Northridge, California Earthquake of January 17, 1994, II-71–II-80.

Augello, A. J., Matasovic, N., Bray, J. D., Kavazanjian, E. Jr., and Seed, R. B., 1995,"Evaluation of Solid Waste Landfill Performance During the Northridge Earthquake," Earthquake Design and Performance of Solid Waste Landfills, ASCE Geotechnical Special Publication No. 54, pp. 17-50.

Augello, A.J., Bray, J.D., Abrahamson, N.A., Seed, R.B., 1998a, "Dynamic properties of solid waste based on back-analysis of OII landfill", ASCE Journal of Geotechnical and Geoenvironmental Engineering, Vol. 124, No.3, March, 1998.

Axtell, P.J., Stokoe, K.H., II, Rathje, E.M. and Chang, W.-J., 2002, "Development of methods to measure nonlinear properties and liquefaction characteristics of near surface soils," Report No. GR02-4, Geotechnical Engineering Center, The University of Texas at Austin, U.S.A.

Ballard, R. F., Jr., 1964, "Determination of Soil Shear Moduli at Depth by In-situ Vibratory Techniques," WES, Misc. Paper No. 4-691, Dec.

Barrows, A. G., 1975, "Surface effects and related geology of the San Fernando earthquake in the Foothill region between Little Tujunga and Wilson Canyons," In: Oakeshott, Gordon B., Ed., San Fernando, California Earthquake of 9 February 1971, California Division of Mines and Geology Bulletin 19, Sacramento, California, 97-117.

Bartake P. P., Patel A., Singh D. N., 2008, "Instrumentation for bender element testing of soils," Int J Geotech Eng 2(4):395–405

Bartake P. P., Singh D. N., 2007, "Studies on the determination of shear wave velocity in sands," Geomech Geoeng 2(1):41–49

Bates, C. R., 1989. "Dynamic soil property measurement during triaxial testing," Geotechnique, 39(4): 721–726.

Belloti, R., Jamiolkowski, M., Lo Presti, D. C. F., and O'Neill, D. A. 1996 "Anisotropy of small-strain stiffness of Ticino Sand," Geotechnique, Vol. 46, No. 1, pp. 115-131.

Bjerrum, L. and Landva, A. 1966, "Direct Simple-Shear Tests on a Norwegian Quick Clay." Geotechnique, Vol. 16 (1): 1-20.

Blewett, J., Blewett, I. J., and Woodward, P. K., 2000, "Phase and amplitude responses associated with the measurements of shear wave velocity in sand by bender elements," Canadian Geotechnical Journal, 37(6): 1348–1357.

Bolt, B.A. 1976. "Nuclear Explosions and Earthquakes," San Francisco, CA: W.H. Freeman

Bray, J. D., Zekkos, D., Kavazanjian, E., Jr., Athanasopoulos, G. A., Riemer, M. F., 2009, "Shear strength of Municipal Solid Waste", Journal of Geotechnical and Geoenvironmental Engineering, ASCE, June 2009, Vol. 135, No. 6, pp. 709-722.

Brignoli, E.G.M., Gotti, M., and Stokoe, K.H., II. 1996, "Measurement of shear waves in laboratory specimens by means of piezoelectric transducers." Geotechnical Testing Journal, 19(4): 384– 397.

Brocanelli D, Rinaldi V., 1998, "Measurement of low-strain material damping and wave velocity with bender elements in the frequency domain." Can Geotech J 35(6):1032–1040.

Buranek, D. and Prasad, S., 1991, "Sanitary landfill performance during the Loma Prieta earthquake," Proc. 2nd International Conference on Recent Advances in Geotechnical Earthquake Engineering and Soil Dynamics, St. Louis, Missouri, 1655-1660.

Carvalho, M.de F., Vilar, O.M., 1998, "In situ tests in urban waste sanitary landfill, Environmental" Geotechnics, editor Seco e Pinto, 1998, Balkema, Rotterdam, pp. 121-126.

Cascante G, Santamarina J. C., 1996 "Interparticle contact behavior and wave propagation," ASCE Geotech J 122(10):831–839.

Chang, C.Y., Mok, C.M. and Tang, H.T. 1996. "Interface of dynamic shear modulus from Lotung downhole data," J. Geotech. Engrg., ASCE, 122(8), 657-665.

Chang, W. J., 2002, "Development of an In-Situ Dynamic Liquefaction Test," Ph.D. Dissertation, the University of Texas, Austin, TX, 316 pp.

Christian, J. T., and Beacher, G. B., 1999 "Point-Estimate Method as Numerical Quadrature" J. Geotech. Geoenviron. Eng. 125 (9).

Cowland, J. W., Tang, K. Y., and Gabay, 1993. "Density and strength properties of Hong Kong refuse." Proc., Sardinia, 93, 4th Int. Landfill Symp., 1433–1446.

Cox, B., 2006, "Development of a direct test method for dynamically assessing the liquefaction resistance of soil in situ," Ph.D. Dissertation, The University of Texas at Austin. U.S.A. 497 pp.

Cox, B. R., and Beekman, A. N., 2011, "Intramethod Variability in ReMi Dispersion Measurements and Vs Estimates at Shallow Bedrock Sites." Journ. of Geotech. and Geoenviro. Eng. v. 137, no. 4.

Cox, B., Stokoe, K. H., II., Rathje, E. M., 2009, "An in-situ test method for evaluating the coupled pore pressure generation and nonlinear shear modulus behavior of liquefiable soils," ASTM Geotechnical Testing Journal, Vol. 32, No. 1, pp. 11-21.

Cuellar, V., Monte, J.L., Valerio, J. 1998, “Static and dynamic elastic moduli for waste landfills”, 570 Proceedings of the third international congress on Environmental Geotechnics, Lisboa, Portugal, 571 Vol.1: 325-329.

Darendeli, B. M. 2001, “Develop of a new Family of Normalized Modulus Reduction and Material Damping Curves,” Ph.D. Dissertation, The University of Texas at Austin.

Dixon, N., and Jones, D. R. V. 2005, "Engineering properties of Municipal Solid Waste, Geotextiles and Geomembranes," 23, pp. 205-233.

Dixon, N., and Langer, U. 2006, “Development of a MSW classification system for the evaluation of mechanical properties.” Waste Manage., 263, 220–232.

"Dixon, N., Jones, D. R. V., Whittle, R. W. 1999, “Mechanical properties of household waste: In situ assessment using pressuremeters,” Proceedings Sardinia 99, Seventh International Waste Management and Landfill Symposium."

Dixon, N., Ng'ambi, S., Jones, D.R.V. 2004, "Structural performance of a steep slope landfill lining system, Proceedings of the Institution of Civil Engineers, Geotechnical Engineering," 157, July 2004, Issue GE3, pp. 115-125

Dobry, R. and Vucetic, M. 1987, “State of the art report: Dynamic properties and response of soft clay deposits.” Proc. Int. Symp on Geotechnical Engineering of Soft Soils, Vol. 2, 51-87.

Drnevich, V. P. 1977. "Resonant Column Testing - Problems and Solutions," Dynamic Geotechnical Testing, ASTM, STP 654, pp.384-398.

Drnevich, V. P., Hardin, B. O., and Shippy, D. J. 1977, "Modulus and Damping Ratio of Soils by Resonant Column Method," Dynamic Geotechnical Testing, ASTM, STP 654, pp.91-125.

Dyvik, R., and Madshus, C. 1985, Lab measurement of G_{max} using bender elements. Norwegian Geotechnical Institute, Oslo, Norway. pp. 186–196. Publication No. 161.

Eid, H. T, Stark, T. D, Douglas, W. D., and Sherry, P. E., 2000 “Municipal Solid waste slope failure 1. Waste and foundation properties.” Journal of Geotechnical and Geoenvironmental Engineering, ASCE, Vol.126, No.5, pp.397-407.

Elgamal, A., Lai, T., Gunturi, R., Zeghal, M. 2004, “System identification of landfill seismic response, Journal of earthquake engineering,” Vol. 8, No. 4, pp. 545-5666, Imperial College Press.

ESI, 1995 "Geophysical Measurements for Seismic Analysis," Rep. No. TM-14, Environmental Solutions, Inc (ESI), Irvine, California.

Fam, M. A., and Santamarina, J. C., 1995, “Study of geoprocesses with complementary wave measurements in an oedometer.” Geotech. Test. J., 19(4), 307–314.

Fernandez, A. L. 2000, “Tomographic imaging the state of stress.” PhD thesis Civil Engineering, Georgia Institute of Technology, Atlanta.

Fioravante, V., and Capoferri, R. 2001. "On the use of multi-directional piezoelectric transducers in triaxial testing." Geotechnical Testing Journal, 24(3): 243–255.

Fioravante, V., Jamiolkowski, M., and LoPresti, D. C. F. 1998. “Assessment of the coefficient of earth pressure at rest from shear wave velocity.” Geotechnique, 48(5), 657–666.

Foti S., Comina C., Boiero D., and Socco L.V., 2009, “Non uniqueness in surface wave inversion and consequences on seismic site response analyses,” Soil Dynamics and Earthquake Engineering vol. 29, pp. 982-993.

Fu L., 2004, "Application of piezoelectric sensors in soil property determination." PhD Thesis, Department of Civil Engineering, Case Western Reserve University, USA

Gajo A, Fedel A, Mongiovi L, 1997, "Experimental analysis of the effects of fluid–solid coupling on the velocity of elastic waves in porous media." Geotechnique 47(5):993–1008

Geosyntec. 1996, “Waste mass field investigation, Operating Industries Inc. landfill, Monterey Park, California.” Rep. No. SWP-2, Geosyntec Consultants, Huntington Beach, California.

GeoSyntec. 2003, “Waste characterization report.” Cherry Island Landfill Expansion Project, Wilmington, Del., GeoSyntec Consultants Project Number ME0250, Columbia, Md.

Ghayamghamian, M. R. and Kawakami, H., 2000, "On-site nonlinear hysteresis curves and dynamic soil properties," J. Geotech. Engrg., ASCE, 126(6), 543-555.

Gomes, C., Ernesto, A., Lopes, M. L., and Moura, C. 2002, “Sanitary landfill of Santo Tirso-municipal waste physical, chemical and mechanical properties.” Proc., 4th Int. Congress on Environmental Geotechnics, Brazil, Vol. 1, 255–261.

Greening P. D., Nash D. F. T., 2004, "Frequency domain determination of G0 using bender elements." Geotech Testing J 27(3):1–7.

Grisolia, M., Napoleoni, Q., and Tangredi, G. 1995 “Contribution to a technical classification of municipal solid waste,” Proc., 5th Int. Landfill Symp., Sardinia ’95, Vol. 2, CISA, Cagliari, Italy, 703–710.

Gucunski, N., and Woods, R. D., 1992, “Numerical simulation of the SASW tests”, Soil Dynamics and Earthquake Engineering, Vol. 11, No. 4, Aug., 1216-1233.

Hanson, J. L., Yesiller, N., Oettle, N. K. 2010, “Spatial and Temporal Temperature Distributions in Municipal Solid Waste Landfills, Journal of Environmental Engineering, Vol. 136, No. 8, August 1, 2010, pp. 804-814.

Hardin, B. O. 1978, “The nature of stress-strain behavior for soils,” Proc. ASCE Geotech. Eng. Div. Specialty Conf. on Earthquake Engineering and Soil Dynamics, Vol. 1 3-90.

Hardin, B. O., and Dmevich, V. P., 1972b, “Shear modulus and damping in soils: design equations and curves,” Journal of Soil Mechanics and Foundation Division, ASCE, Vol. 98, 667-692.

Hardin, B. O., and Black, W. L.. 1968. "Vibrations on Modulus of Normally Consolidated Clays," J. Soil Mech. Found. Div., Am. Soc. Civ. Eng. 94(SM-2), 353-369.

Hardin, B. O., and Drnevich, V. P., 1972a, "Shear Modulus and Damping in Soil, Measurement and Parameter Effects", J. Soil Mech. Found. Div., Am. Soc. Civ. Eng. 98(SM-6), pp. 603-624.

Hardin, B.O., and Richart Jr. F. E., 1963, “Elastic wave velocities in granular soils. Journal of the Soil Mechanic and Foundations Division, ASCE 89 (1), pp. 33–65.

Hayashi, K., 2012, "Analysis of Surface-wave Data Including Higher Modes Using the Genetic Algorithm." Geotechnical Special Publication 225 GeoCongress 2012, Oakland, California, 2776 - 2785

Henke, R., and Henke, W., 1993, "Laboratory evaluation of in situ geotechnical torsional cylindrical impulse shear test for earthquake resistant design," Bull. Seism. Soc. Am., 83(1): 245-263.

Henke, R. and Henke, W. 2002, "In situ nonlinear inelastic shearing deformation characteristics of soil deposits inferred using the torsional cylindrical impulse shear test," Bull. Seism. Soc. Am., 92(5), 1970-1983.

Houston, W.N., Houston, S.L., Liu, J.W., Elsayed, A., Sanders, C.O., 1995, “In-situ testing methods for dynamic properties of MSW landfills”, Earthquake Design and performance of solid waste landfills, ASCE Geotechnical Special Publication No.54: 73-82.

Hryciw, R. D., and Thomann, T. G., 1993, “Stress-history-based model for Ge of cohesionless soils. Journal of Geotech Eng, ASCE;119(7):1073–93.

Hushmand B., Anderson, D. G., Crouse, C. B. and Robertson, R. J., 1990, Seismic monitoring and evaluation of a solid waste landfill, Proc. 4th U. S. National Conference on Earthquake Engineering, Palm Springs, California, 3, 855-863.

Husmand Associates, 1994, "Landfill Response to Seismic Events: Report Prepared for the USEPA Region IX," Husmand Associates, Laguna Niguel, California.

Idriss, I. M., Dobry, R., and Singh, R. D., 1978, “Nonlinear behavior of soft clays during cyclic loading.” J. Geotech. Engrg. Div. , ASCE, 104 GT12, 1427–1447.

Idriss, I. M., Fiegel, G., Hudson, M. B., Mundy, P. K., and Herzig, R. 1995, “Seismic Response of the Operating Industries Landfill,” Earthquake Design and Performance of Solid Waste Landfills, M. K. Yegian and W. D. L. Finn, eds., ASCE Geotech. Spec. Publ., No. 54, ASCE, Reston, VA., pp. 83-118.

Ishihara, K., 1996, “Soil Behavior in Earthquake Geotechnics,” Clarendon Press, Oxford, U.K.

Iwasaki, T., and Tatsuoka, F., 1977, "Effects of grain size and grading on dynamic shear moduli of sands." Soils and Found., 17(3), 19-35.

Jessberger, H. L., Kockel, R. 1993, “Determination and assessment of the mechanical properties of waste materials,” Waste Disposal by landfill-Green ’93, Sarsby (ed.), 1995 Balkema, Rotterdam, pp.313-322.

Johnson, M. E., Lundy, J., Lew, M. and Ray, M. E., 1991, “Investigation of sanitary landfill slope performance during strong ground motion from the Loma Prieta earthquake of October 17, 1989,” Proc. 2nd International Conference on Recent Advances in Geotechnical Earthquake Engineering and Soil Dynamics, St. Louis, Missouri, 1701-1706.

Jones, R., 1955, "A vibration method for measuring the thickness of concrete road slabs in situ," Magazine of Concrete Research, 7(20), 97–102.

Jones, R., 1962, "Surface wave technique for measuring the elastic properties and thickness of roads: Theoretical development," British Journal of Applied Physics, 13, 21-29

Jovicic, V., Coop, M. R., and Simic, M., 1996, "Objective criteria for determining G_{max} from bender element tests." Geotechnique, 46(2): 357–362.

Kavazanjian, E. Jr., 1999, "Seismic design of solid waste containment facilities," Proceedings of the Eight Canadian Conference on Earthquake Engineering, Vancouver, BC, June 1999: 51-89.

Kavazanjian, E. Jr., and Matasovic, N., 1995, "Seismic Analysis of Solid Waste Landfills," Proceedings of GeoEnvrionment, 2000, ASCE Geotechnical Special Publication, No. 46, Vol. 2, 1066-1080.

Kavazanjian, E. Jr., Snow, M.S., Matasovic, N, Poran, C., Satoh, T., 1994, "Non-intrusive Rayleigh wave investigations at solid waste landfills," Proceedings, 1st International Conference on Environmental Geotechnics, Edmonton, Alberta, BiTech Publishers, Richmond, B. C.

Kavazanjian, E., Jr., Matasovic, N., Bonaparte, R., and Schmertmann, G. R. 1995, "Evaluation of MSW properties for seismic analysis." Geoenvironment 2000, Vol. 2, 1126–1141.

Kavazanjian, E., Jr., Matasovic, N., Stokoe, K. H. II, Bray, J.D. 1996, "In situ shear wave velocity of solid waste from surface wave measurements," Environmental Geotechnics, Kamon, (editor), Balkema, Vol. 1, pp. 97-102.

Kawaguchi, T., Mitachi, T., Shibuya, S., 2001 "Evaluation of shear wave travel time in laboratory bender element test," In: Proceedings of the 15th international conference on soil mechanics and geomechanics engineering, pp 155–158.

Khosravi, A., and McCartney, J. S., 2009, "Impact of Stress State on the Dynamic Shear Moduli of Unsaturated, Compacted Soils." 4th Asia Pacific Conference on Unsaturated Soils. Newcastle, Australia. Nov. 23-25, 2009

Koelsch, F., Fricke, K., Mahler, C., Damanhuri, E., 2005, "Stability of landfills – The Bandung dumpsite disaster", Proceedings Sardinia 2005, Tenth International Waste Management and Landfill Symposium

Kokusho, T., Aoyagi, T., and Wakunami, A., 2005, "In situ soil-specific nonlinear properties back-calculated from vertical array Records during the 1995 Kobe earthquake," J. Geotech. Geoenviron. Eng., ASCE 131(12), 1509-1521.

Kokusho, T., Yoshida, Y., and Essahi, Y. 1982. "Dynamic Soil Properties of Soft Clay for Wide Strain Range," Soils and Foundations, JSSMFE, Vol. 22, No. 4, Dec, pp. 1-18.

Kramer, S. L., 1994, "Geotechnical earthquake engineering," Prentice Hall, NJ.

Kurtulus, A., 2006, "Field measurement of the linear and nonlinear shear moduli of soils using drilled shafts as dynamic cylindrical sources," Ph.D. Dissertation, The University of Texas at Austin, U.S.A. 492 pp.

Lai, C. G., and Rix, G. J., 1998, "Simultaneous Inversion of Rayleigh Phase Velocity and Attenuation for Near-Surface Site Characterization," Georgia Institute of Technology, Atlanta, USA.

Landva, A. O., and Clark, J. I., 1986, "Geotechnical testing of wastefill." Proc., 39th Canadian Geotechnical Conf. Ottawa, 371–385.

Landva, A. O., and Clark, J. I., 1990, "Geotechnics of waste fill, theory and practice," STP 1070, A. Landva and G. D. Knowles, ed., ASTM, West Conshohocken, Pa., 86–103.

Landva, A. O., Valsangkar, A. J., and Pelkey, S.G., 2000, "Lateral Earth Pressure at Rest and Compressibility of Municipal Solid Waste," Canadian Geotechnical Journal, Volume 37, Number 6, December, pp. 1157-1165.

Lawrence, F.V., 1963, "Propagation of ultrasonic waves through sand," Massachusetts Institute of Technology, Cambridge, Mass. Research Report R63–08.

Lawrence, F. V., 1965. "Ultrasonic shear wave velocity in sand and clay," Massachusetts Institute of Technology, Cambridge, Mass. Research Report R65–05.

LeBlanc M. T., 2013, "Field Measurements of the Linear and Nonlinear Constrained Moduli of Granular Soil," Ph.D. Dissertation, The University of Texas at Austin, U.S.A.

Lee, J. J., 2007, "Dynamic characteristics of Municipal Solid Waste (MSW) in the linear and nonlinear strain ranges," Ph.D. Dissertation, The University of Texas at Austin.

Lee, J. S., and Santamarina, J. C., 2005, "Bender elements: performance and signal interpretation," Journal of Geotechnical and Geoenvironmental Engineering, 131(9): 1063–1070. doi:10. 1061/(ASCE)1090-0241(2005)131:9(1063).

Leong E. C., Cahyadi, J., Rahardjo, H., 2009 "Measuring shear and compression wave velocities of soil using bender–extender elements." Can Geotech J 46(7):792–812.

Leong, E. C., Yeo, S.H., and Rahardjo, H. 2005. Measuring shear wave velocity using bender elements. Geotechnical Testing Journal, 28(5): 488–498.

Lin, Y.-C., Rosenblad, B., and Stokoe, K. H., II., 2004, "Data report on shear wave velocity profiles determined by SASW method at: Altamont landfill, Redwood landfill, and Tri-Cities landfill," Geotechnical Engineering Center, Civil and Environmental Engineering Department, The University of Texas at Austin, 29 October 2004, Geotechnical Engineering Report GR04-3.

Lings, M. L., and Greening, P. D., 2001, "A novel bender/extender element for soil testing," Geotechnique, 51(8): 713–717.

Louie, J. N., 2001, "Faster, better: shear-wave velocity to 100 meters depth from refraction microtremor arrays"; Bull. of the Seis. Soc. of Am, v. 91, n. 2: 347-364.

Love, A. E. H., 1911 "Some Problems of Geodynamics," Cambridge University Press.

Mari, J. L., 1984, "Estimation of static correction for shear-wave profiling using the dispersion properties of Love waves," Geophysics, 49, 1169–1179.

Masing, G. 1926, "Eigenspannungen und Verfestigung beim Messing." Proceedings of te 2nd International Congress on Applied Mechanics, Zurich, Switzerland, pp. 332-335.

Matasovic, N., and Kavazanjian, E., Jr.. 1998. "Cyclic characterization of OII landfill solid waste." J. Geotech. Geoenviron. Eng., 124 3, 197–210.

Matasovic, N., and Kavazanjian, E., Jr. 2006 "Seismic Response of a Composite Landfill Cover" J. Geotech. Geoenviron. Eng., 132(4), 448-455.

Matasovic, N., and Vucetic, M.. 1993, "Cyclic Characterization of Liquefiable Sands," Journal of Geotechnical Engineering, Vol. 119, No. 11, November, pp. 1805-1822.

Matasovic, N., Kavazanjian, E. Jr., and Abourjeily, F., 1995, "Dynamic Properties of Solid Waste from Field Observations," Proc., 1st Int. Conf. on Earthquake Geotech. Engrg., 1, pp. 549-554.

Matasovic, N., Kavazanjian, E. Jr., and Anderson, R., 1998, "Performance of solid waste landfills in earthquakes," Earthquake Spectra, Issue #2, Vol. 14, p. 319-334.

Matasovic, N., Kavazanjian, E., Jr., Augello, A. J., Bray, J. D., and Seed, R. B., 1995 "Solid Waste Landfill Damage Caused by 17 January 1994 Northridge Earthquake", In: Woods, M. C. and Seiple, W. R., eds., The Northridge California Earthquake of 17 January 1994, California Department of Conservation, Division of Mines and Geology Special Publication 116, pp. 61-69.

Menq, F.-Y. 2003, "Dynamic Properties of Sandy and Gravelly Soils," Doctoral thesis, the University of Texas at Austin.

Menq, F.-Y., Stokoe, K.H., II, Park, K., Rosenblad, B. and Cox, B. R., 2008, "Performance of Mobile Hydraulic Shakers at NEES@UTexas for Earthquake Studies," 14th World Conference of Earthquake Engineering, October 12-17, Beijing, China.

Merry, S. M., Kavazanjian, E. Jr, Fritz, W. U. 2005, "Reconnaissance of the July 10, 2000, Payatas Landfill Failure", ASCE Journal of Performance of Constructed Facilities, May 2005, 100-107.

Morochnik, V., Bardet, J. P., Hushmand, B. 1998, "Identification of Dynamic Properties of OII Landfill," Journal of Geotechnical and Geoenvironmental Engineering, Vol. 124, No. 3, March, pp. 186-222.

Nazarian, S., 1984, "In situ Determination of Elastic Moduli of Soil Deposits and Pavement Systems by Spectralanalysis- of-surface-waves method," Ph.D. dissertation, The University of Texas at Austin.

Nazarian, S. and Stokoe, K. H., II. 1984, "In situ Shear Wave Velocities from Spectral Analysis of Surface Waves," Proc. Eighth World Conf. Earthquake Eng., San Fransisco, CA, Vol. III, 31-38.

Oakeshoff, G. B., 1975, Geology of the epicentral area, In: Oakeshott, Gordon B., Ed., San Fernando, California Earthquake of 9 February 1971, California Division of Mines and Geology Bulletin 19, Sacramento, California, 19-30.

Orr, W. R. and Finch, M. O., 1990, "Solid waste landfill performance during Loma Prieta earthquake, Geotechnics of Waste Fills - Theory and Practice," ASTM STP 1070, 22-30.

Okada, H. 2003. "The Microtremor Survey Method," Geophysical Monograph Series no. 12. Society of exploration geophysicists: 135.

Oweis, I. S., and Khera, R. P., 1998, "Geotechnology of waste management," PWS, Boston.

Park W., 2010, " Field Measurements of the linear and nonlinear shear moduli of cemented alluvium using dynamically loaded surface footings", Ph.D. Dissertation, The University of Texas at Austin, U.S.A.

Park, C. B., and Miller, R. D., 2008. "Roadside Passive Multichannel Analysis of Surface Waves (MASW)." Journ. of Env. & Eng. Geophys, v.13, no 1: 1-11.

Park, C. B., Miller, R. D., Laflen, D., Cabrillo, N., Ivanov, J., Bennett, B., and Huggins, R. 2004, "Imaging Dispersion Curves of Passive Surface Waves" [Exp. Abs.]: Soc. Expl. Geophys.: 1357-1360.

Park, C. B., Miller, R. D., and Xia, J. 1999a. Multichannel Analysis of Surface Wave, Geophysics, 64: 800-808.

Park, C. B., Miller, R. D., Ryden, N., Xia, J., and Ivanov, J., 2005, "Combined Use of Active and Passive Surface Waves," Journal of Environmental & Engineering Geophysics; September 2005; v. 10 : 323-334.

Park, C. B., Miller, R. D., Xia, J., 1999b. "Multimodal Analysis of High Frequency Surface Wave," Proceedings of the Symposium on the Application of Geophysics to Engineering and Environmental Problems (SAGEEP 99), Oakland, CA, March 14-18. Environmental and Engineering Geophysical Society, Wheat Ridge, Colorado, USA: 115–122.

Park, C. B., Miller, R. D., and Miura, H., 2002. "Optimum field parameters of a MASW survey [Exp. Abs.]," Soc. Explor. Geophys.- Japan, Tokyo, May 22-23.

Patel, A, Singh, D. N., Singh, K. K., 2010, "Performance Analysis of Piezo-Ceramic Elements in Soils" Geotech Geol Eng 28:681–694.

Peacock, W. H. and Seed, H. B. 1968, "Sand Liquefaction Under Cyclic Loading Simple Shear Conditions," J. Soil. Mech. Found. Div., Am., Soc. Civ. Eng. 94(SM-3), 689-708.

Pelekis, P. C., and Athanasopoulos, G. A., 2011, "An overview of surface wave methods and a reliability study of a simplified inversion technique", Soil Dynamics and Earthquake Engineering 31 (2011) 1654–1668.

Pennington, D.S., Nash, D.F.T., and Lings, M.L. 2001. Horizontally mounted bender elements for measuring anisotropic shear moduli in triaxial clay specimens. Geotechnical Testing Journal, 24(2): 133–144.

Pereira, A.G.H., Sopena, L., Mateos, T.G., 2002, “Compressibility of a municipal solid waste landfill”, Proceedings of the Fourth International Congress on Environmental Geotechnics, Brazil: 201-206.

Pezeshk, S., and Zarrabi, M. 2005, "A New Inversion Procedure for Spectral Analysis of Surface Waves Using a Genetic Algorithm," The Bulletin of the Seismological Society of America (BSSA), Vol. 95, No. 5, October 2005; v. 95; no. 5; p. 1801-1808.

Phillips, R.D., 2000, “Initial design and implementation of an in situ test measurement of nonlinear soil properties,” M.S. Thesis, The University of Texas at Austin, TX.

Rathje, E.M., Chang, W-J., Stokoe, K.H., II and Cox, B.R., 2004, “Evaluation of ground strain from in situ dynamic testing,” Paper No. 3099, 13th World Conf. on Earthquake Engrg., Vancouver, Canada, August.

Rayleigh, L., 1885, "On waves propagated along the plane surface of an elastic solid," Proc. Lond. Math. Soc., 17, 4.

Richardson, G., Reynolds, D. 1991, "Geosyntetic considerations in a landfill on compressible clays," Proceedings of Geosynthetics '91, Vol.2, Industrial Fabrics Association International, St. Paul, MN.

Richart, F. E. Jr., 1975 “Some effects of dynamic soil properties on soil-structure interaction.” Journal of Geotech. Eng. Div, ASCE, 101 (12), pp. 1193–1240.

Richart, F. E., Jr., Hall, J. R., and Woods, R. D. 1970, "Vibrations of Soils and Foundations," Prentice-Hall, Englewood Cliffs, New Jersey.

Rio, J. F. M. E., 2006, "Advances in laboratory geophysics using bender elements," Ph.D. dissertation, University College London, UK.

Rix, G. J., Lai, C. G., Foti, S., Zywicki, D., 1998, “Surface wave tests in landfills and embankments,” Geotechnical Earthquake Engineering and Soil Dynamics III, ASCE Geotechnical Special Publication No. 75, Volume 2, 1008-1019.

Roberston, P. K., Sasitharan, S., Cunning, J. C., Sego, D. C., 1995 "Shear-wave Velocity to Evaluate In-situ State of Ottawa Sand", Journal of Geotechnical Engineering, Vol. 121, No.3.

Roblee, C. J., and Riemer, M. F., 1998, "The downhole freestanding shear device concept, Geotechnical Earthquake Engineering and Soil Dynamics III," Seattle, Washington, 3-6 August, American Society of Engineers, 200-212.

Rosenblad, B. L., Li, J., Menq, F-Y., and Stokoe, K.H., II, 2007. "Deep Shear Wave Velocity Profiles from Surface Wave Measurements in the Mississippi Embayment," Earthquake Spectra, EERI, v. 23, no. 4: 791-809.

Rosenblueth, E. 1975, ‘‘Point estimates for probability moments.’’ Proc., Nat. Acad. of Sci., 72(10), 3812–3814.

Rosenblueth, E. 1981, ‘‘Two-point estimates in probabilities.’’ Appl. Math. Modelling, 5(2), 329–335.

Safaqah, O.A., Riemer, M. F., and Grizzle, C. 2003, “Development and implementation of the donwhole freestanding shear device”. Proceeding at 6th International Symposium on Field Measurements in Geomechanics, FMGM 2003, Oslo, Norway 15-18 September.

Sahadewa, A., Zekkos, D., and Woods R. D., 2012, “Observations from the Implementation of a Combined Active and Passive Surface Wave Based Methodology”, Geocongress 2012 State of the Art and Practice in Geotechnical Engineering Conference, 25-28 March 2012, Oakland, California, pp. 2786-2795.

Sahadewa, A., Zekkos, D., Lobbestael, A. B., and Woods, R. D., 2011, “Shear Wave Velocity Measurements at Municipal Solid Waste Landfills in Michigan.” Pan-Am CGS Geotechnical Conf. 2011, Toronto.

Salgado, R., Drnevich, V. P., Ashmawy, A., Grant, W. P. and Vallenas, P. 1997, "Interpretation of large-strain seismic cross-hole tests," J. Geotech. Engrg., ASCE, 123(4): 382-388.

Sanchez-Salinero, I., Rosset, J. M., and Stokoe, K. H. II. 1986. “Analytical studies of body wave propagation and attenuation.” Rep. No. GR-86-15, Univ. of Texas, Austin, Tex.

Santamarina J. C., Fam M. A., 1995 "Changes in dielectric permittivity and shear wave velocity during concentration diffusion." Can. Geotech J 32:647–659.

Santamarina J. C., Klein K. A., Fam M. A., 2001, "Soils and waves—particulate materials behavior, characterization and process monitoring." Wiley, New York.

Sawangsuriya, A., 2012, "Wave Propagation Methods for Determining Stiffness of Geomaterials," Wave Processes in Classical and New Solids, Prof. Pasquale Giovine (Ed.), ISBN: 978-953-51-0821-4, InTech.

Sawangsuriya A., Biringen E., Fratta D., Bosscher P. J. , Edil T. B., 2006, "Wave Propagation Methods for Determining Stiffness of GeomaterialsGeoShanghai Conference, Site and Geomaterial Characterization," ASCE, Geotechnical Special Publication149 Shanghai, China, 160166.

Schultheiss, P. J., 1981. “Simultaneous measurements of P & S wave velocities during conventional laboratory soil testing procedures,” Marine Geotechnology, 4(4): 343–367.

Seed, H. B. and Idriss, I. M. 1970. "Soil Moduli and Damping Factors for Dynamic Response of Analyses," Report No. EERC 70-10, Earthquake Engineering Research Centre, University of California.

Sharma, H. D., Dukes, M. T., Olsen, D. M., 1990, “Field Measurements of Dynamic Moduli and Poisson’s Ratio of Refuse and Underlying Soils at a Landfill Site, Geotechnics of Waste Fills – Theory and Practice, STP 1070, Landva and Knowles (ed.), ASTM, pp. 57-70.

Sheehan, A. J., Olson, R., E., Park, K. and Stokoe, II, K. H., 2010, “Estimation of Settlement of Footings Under Working Loads using Equivalent-Linear Elasticity,” GeoFlorida 2010: Advances in Analysis, Modeling & Design (GSP 199), February 20-24 2010, West Palm Beach, Florida, pp. 1708-1717 (in cd-rom).

Shirley, D. J., and Hampton, L. D., 1978, “Shear wave measurements in laboratory sediments,” J. Acoust. Soc. Am., 63 (2), 607–613.

Shirley, D. J., 1978, “An improved shear wave transducer,” The Journal of the Acoustical Society of America, 63(5): 1643–1645.

Siegel, R. A., Robertson, R. J., and Anderson, D. G., 1990, “Slope stability investigation at a landfill in southern California, Geotechnics of Waste Fills-Theory and Practice,” ASTM STP 1070, Philadelphia, Pennsylvania, 259-284.

Singh, S. and Murphy, B. J. 1990, “Evaluation of the Stability of Sanitary Landfills”, 444 Geotechnics of Waste Fills – Theory and Practice, ASTM STP 1070, A. Landva and G.D. Knowles, eds., American Society of Testing and Materials, pp.240-258.

Song, Y. Y., Castagna, J. P., Black, R. A., and Knapp, R. W., 1989, "Sensitivity of near-surface shear-wave velocity determination from Rayleigh and Love waves," 59th Ann. Internat Mtg., Meeting, Soc. Expl. Geophys., Expanded Abstracts, 509–512.

Stokoe K. H., II., Axtell, P. J., Rathje, E. M., and Valle Celestino, 2005 "In Situ Measurement of Small-Strain Stiffnesses in Soil Beneath a Footing with Varying Static Loads" GSP 134 Proceedings of Geo-Frontiers 2005, Austin, Texas.

Stokoe, K. H. II., Santamarina, J. C. 2000, “Seismic-wave-based testing in geotechnical engineering”, GeoEng 2000, International Conference on Geotechnical and Geological Engineering, 19-24 November 2000, Melbourne, Australia, Vol. 1: Invited Papers, pp. 1490-1536.

Stokoe, K. H. II., Wright, S. G., Bay, J. A., and Roesset, J. M., 1994, “Characterization of geotechnical sites by SASW method.” In Geophysical Characterization of Sites, R. Woods (ed.), pp. 15-26, International Science, New York.

Stokoe, K. H. II., Hwang S.K., Lee, J. N. K., and Andrus R.D., 1995, "Effect of Various Parameters on the Stiffness and Damping of Soils at Small to Medium Strains" Keynote Lecture 2, IS Hokaido. 2: 785-816 Balkema.

Stokoe, K. H., II., and Woods, R. D., 1972. "In-situ Shear Waves Velocity by Cross-Hole Method," J. Soil Mech. Found. Div. Am. Soc. Civ. Eng. 98(SM-5), 443-460.

Stokoe, K. H., II., Darendeli, M. B., Andrus, R. D., and Brown, L. T. 1999. “Dynamic soil properties: laboratory, field and correlation studies,” Proceedings o f 2nd International Conference on Earthquake Geotechnical Engineering, Lisbon, Portugal, Vol. 3, 811-845.

Stokoe, K. H., II., Kurtulus, A., and Park, K., 2006 “Development of Field Methods to Evaluate Nonlinear Shear and Compression Moduli of Soil,” Proceedings of New Zealand Earthquake Geotechnical Engineering Workshop, November, Canterbury University, Christchurch, New Zealand, pp. 56-70.

Stokoe, K. H., II., Lee, J. N.-K., and Lee, S. H.-H. 1991, “Characterization of soil in calibration chambers with seismic waves,” Proceedings, 1st International Symposium on Calibration Chamber Testing, Potsdam, New York.

Stokoe, K. H., II., Menq, F.-Y., Wood, S. L., Park, K., Rosenblad, B. and Cox, B. R., 2008, “Experience with NEES@UTexas large-scale mobile shakers in earthquake engineering

studies," Third International Conference on Site Characteristic, April 1-4, Taipei, Taiwan, 6 pp.

Stokoe, K. H., II., Wright, G. W., James, A. B., and Jose, M. R., 1994, "Characterization of Geotechnical Site by SASW Method." in Woods, R. D., Ed., Geophysical characterization of sites: Oxford.

Stokoe, K. H., II., Zalachoris, G., Cox, B., and Park, K., 2011 "Field Evaluations of the Effects of Stress State, Strain Amplitude and Pore Pressure Generation on Shear Moduli of Geotechnical and MSW Materials," International Symposium on Deformation Characteristics of Geomaterials, September 1-3, Seoul, South Korea, pp. 120-140.

Stokoe, K. H., II., Axtell, P. J., and Rathje, E.M., 2001, "Development of an in situ method to measure nonlinear soil behavior," 3rd International Conference on Earthquake Resistant Engineering Structures, September, Malaga, Spain, pp. 561-570.

Stokoe, K. H., II., Hwang, S. K., and Lee, J. N.- K., 1995, "Effects of Various Parameters on the Stiffness and Damping of Soils at Small to Medium Strains." Proceedings of 1st International Symp. On Pre-failure Deformation Characteristics of Geomaterials. Vol. 2, 785-816.

Stokoe, K. H., II., Rathje, E. M., Wilson, C. R., Rosenblad, B. L.. and Menq, F. Y.. 2004, "Development of the NEES large-scale mobile shakers and associated instrumentation for in situ evaluation of nonlinear characteristics and liquefaction resistance of soils," 13th World Conference on Earthquake Engineering, Paper No. 535. Vancouver, Canada, August.

Strobia, C., and Cassiani, G., 2011, "Refraction microtremors: Data analysis and diagnostics of key hypotheses", Geophysics, Vol. 76, No. 3 (May-June 2011), MA11-MA20.

Tatsuoka, F., Lo Presti, D. C. F.. and Kohata,Y., 1995, "Deformation characteristics of soils and soft rocks under monotonic and cyclic loads and their relationships." SOA Report, Proc. of the 3rd Int. Conf. on Recent Advances in Geotechnical Earthquake Engineering and Soil Dynamics, St Louis. Prakash ed. Vol. 2, pp. 851-879.

Thomann, T. G. & Hryciw, R. D., 1990, "Laboratorymeasurement of small strain shear modulus under K_0 conditions," ASTM Geotechnical Testing Journal 13(2): 97–105.

Tokimatsu, K., Tamura, S., and Kojima, H., 1992, "Effects of Multiple Modes of Rayleigh Wave Dispersion Characteristics", Journal of Geotechnical Engineering, 118: 1529-1543.

Towhata, I., Kawano, Y., Yonai, Y., Koelsh, F. 2004, "Laboratory tests on dynamic properties of Municipal Wastes," 11th Conference in Soil Dynamics and Earthquake Engineering and 3rd International Conference on Earthquake Geotechnical Engineering, Vol.1, pp.688-693.

Tran, K. T. and Hiltunen, D. R. 2008. "A Comparison of Shear Wave Velocity Profiles from SASW, MASW, and ReMi Techniques", Geotechnical Earthquake Engineering and Soil Dynamics IV, GSP 181 © 2008 ASCE (in cd-rom).

Turner, M. A., 1990, "Near-surface velocity reconstruction using surface wave inversion," M.S. thesis, University of Utah, USA.

Van der Poel C., 1951, "Dynamic testing of road constructions," Journal of Applied Chemistry, 1, 281-290.

Viggiani, G., and Atkinson, J. H., 1995, “Interpretation of bender element tests,” Geotechnique, 45(1), 149–154.

Vucetic, M. and Dobry, R. 1991. "Effect of soil plasticity on cyclic response," J. Geotech. Eng., ASCE, 117, 89-107.

Wang Y. H., Lo K. F., Yan WM, Dong X. B., 2007, "Measurement biases in the bender element test." J Geotech Geoenv Eng 133(5):564–574.

Woods, R. D. 1978. "Measurement of Dynamic Soil Properties," State of The Art. Proc. ASCE. Spec. Conf. Earthquake Eng. Soil Dyn., Pasadena, Ca, Vol. 1, 91-180.

Woods, R. D., 1968, “Screening of Surface Waves in Soils,” Journal of the Soil Mechanics and Foundations Division, American Society of Civil Engineers, Vol. 94, No. SM4, pp. 951–979.

Xia, J., Miller, R. D., and Park, C. B., 1999. “Estimation of Near-surface Shear-wave Velocity by Inversion of Rayleigh Waves,” Geophysics, 64: 691-700.

Yoon, S., and Rix, J. G., 2009 “Near-Field Effects on Array-Based Surface Wave Methods with Active Sources” J. Geotech. Geoenviron. Eng., 135(3), 399-406.

Youd, T. L., Idriss, I. M., Andrus, R. D., Arango I., Castro G., Christian J. T., Dobry R., Finn, W. D. L., Harder L. F. Jr., Hynes, M. E., Ishihara K., Koester, J. P., Liao . S. C., Marcuson, W. F. III, Martin G. R., Mitchell, J. K., Moriwaki, Y., Power, M. S., Robertson P. K., Seed R. B., and Stokoe, K. H. II (2001) Liquefaction Resistance of Soils: Summary Report from the 1996 NCEER and 1998 NCEER⁄NSF Workshops on Evaluation of Liquefaction Resistance of Soils” J. Geotech. Geoenviron. Eng. 127(10), 817-333.

Yuan, P., Kavazanjian, E. Jr., Chen, and W., Seo, B., 2011, “Compositional effects on the dynamic properties of municipal solid waste,” Waste Management, Vol. 31, pp. 2380-2390.

Zalachoris, G., 2010, “Field Measurements of Linear and Nonlinear Shear Moduli of Solid Municipal Waste using a Dynamically Loaded Surface Footing,” Master Thesis, The University of Texas at Austin. U.S.A.

Zeghal, M., Elgamal, A.W., Tang, H.T. and Stepp, J. C., 1995, "Lotung downhole array. II: Evaluation of soil nonlinear properties," J. Geotech. Eng., ASCE, 121(4), 363- 378.

Zekkos, D., 2013 "Experimental Evidence of Anisotropy in Municipal Solid Waste," Proc., Coupled Phenomena in Environmental Geotechnics, Politecnico di Torino, Italy, 1 – 3 July 2013, 69-79.

Zekkos, D. Bray, J. D., Kavazanjian, E. Jr., Matasovic, N., Rathje, E. M., Riemer, M. F., Stokoe, K. H., II., 2006a, "Unit weight of Municipal Solid Waste", ASCE Journal of Geotechnical and Geoenvironmental Engineering, Vol. 132, No. 10, October 2006 pp. 1250-1261.

Zekkos, D. P. 2005, “Evaluation of Static and Dynamic Properties of Municipal Solid- Waste,” Ph.D. The University of California at Berkeley.

Zekkos, D. P., Bray, J. D., Riemer, M. F. 2006b, "Shear modulus reduction and material damping relationships for Municipal Solid-Waste", Proceedings of the 8th U.S. National Conference on Earthquake Engineering, April 18-22, 2006, San Francisco, California, USA, Paper No. 1324.

Zekkos, D., and Flanagan, M. 2011 "Case Histories-based Evaluation of the Deep Dynamic Compaction Technique on Municipal Solid Waste Sites." Adv. in Geotech. Eng. Geofrontiers 2011, 13-16 March 2011.

Zekkos, D., Bray, J. D., and Riemer, M. F., 2008 "Shear Modulus and Material Damping of Municipal Solid Waste Based on Large-Scale Cyclic Triaxial Testing," Canadian Geotechnical Journal, Vol. 45, No. 1, 2008, pp. 45-58.

Zekkos, D., Kavazanjian, E. Jr., Bray, J. D., Matasovic, N., Riemer, M. F., 2010, "Physical Characterization of Municipal Solid Waste for Geotechnical Purposes", Journal of Geotechnical and Geoenvironmental Engineering, ASCE, September 2010, Vol. 136, 9, pp. 1231-1241.

Zekkos, D., Matasovic, N., El-Sherbiny, R., Athanasopoulos-Zekkos, A., Towhata, I., Maugeri, M. 2011 "Chapter 4: Dynamic Properties of Municipal Solid Waste." In Geotechnical characterization, field measurement, and laboratory testing of Municipal Solid Waste." Proceedings of the 2008 International Symposium on Waste Mechancis, , ASCE Geotechnical Special Publication No. 209, Zekkos D. (ed), pp. 112-134.

Zekkos, D., Sahadewa, A., and Carlson, C., 2012, "In-situ Shear Wave Velocity Measurement in a Hazardous Landfill", Geotechnical Engineering Research Report UMGT#2012-1, University of Michigan, Ann Arbor, USA.

Zekkos, D., Sahadewa, A., Woods, R., and Stokoe, K. H., II., 2013 "Development of a Model for Shear Wave Velocity of Municipal Solid Waste. J. Geotech. Geoenviron. Eng. 140 (3).

Zhang, J., Andrus, R. D., and Juang, C. H., 2005, "Normalized Shear Modulus and Material Damping Ratio Relationships" J. Geotech. Geoenviron. Eng. 131 (4).

Zhou, Y., and Chen, Y., 2005, "Influence of seismic cyclic loading history on small strain shear modulus of saturated sands," Soil Dynamics and Earthquake Engineering 25, pp. 341–353.

Zywicki, D. J., 1999, "Advanced Signal Processing Methods Applied to Engineering Analysis of Seismic Waves," Ph.D. thesis, Georgia Institute of Technology: 357.